

Universidad de Granada
Programa de Doctorado en Farmacia



**GLYCOSYL AND ALKYL MODIFICATIONS ON POTENTIAL
THERAPEUTIC DRUGS TARGETING PARASITIC, CANCER
AND NEURODEGENERATIVE DISEASES**

Tesis Doctoral

Efres Belmonte Reche

20 Marzo 2018



Universidad de Granada
Programa de Doctorado en Farmacia



CONSEJO SUPERIOR DE INVESTIGACIONES CIENTÍFICAS
INSTITUTO DE PARASITOLOGÍA Y BIOMEDICINA LÓPEZ NEYRA

Memoria presentada por el licenciado
Efres Belmonte Reche
para optar al grado de Doctor en Farmacia

Dirigida por

Dr. Juan Carlos Morales Sánchez

Dr. Pablo Peñalver Puente

Editor: Universidad de Granada. Tesis Doctorales
Autor: Efres Belmonte Reche
ISBN: 978-84-9163-898-8
URI: <http://hdl.handle.net/10481/51849>

Agradecimientos

Se el cambio que quieres ver en el mundo

Mohandas K. Gandhi

Siendo franco, estos años dedicados a la investigación no habrían sido posibles si no fuera por un grupo selecto de personas a las que estaré siempre agradecido:

Muy especialmente mis padres, Efres y Angelina cuyo apoyo moral y económico han sustentado a este proyecto de investigador. Muchas gracias por estar incondicionalmente a mi lado. Espero que algún día os sintáis tan orgullosos de mí como yo me siento de vosotros.

A Bruno, mi hermano, futuro farmacéutico-médico (pero siempre farmacéutico primero). Muchas gracias por los buenos momentos, las buenas conversaciones y los buenos consejos. La cita de este capítulo va por ti, fue uno de los consejos que me diste como conclusión a tu punto de vista, tenías toda la razón.

A mis tíos Aurelia y Domingo que me han ofrecido su casa y su apoyo como si fuera un hijo más. A mi tío Carlos, que con sus particulares razonamientos acabaron por convencerme para emprender este camino. Al resto de los miembros de mi estupenda familia que no han dudado en ayudarme cuando lo he necesitado. Muchas gracias.

A Juan Carlos, por ofrecerme tantas oportunidades. Gracias a tu maestría y liderazgo a través del trabajo duro, de los buenos y malos momentos me has hecho crecer como persona, aprendiendo y recapitando sobre lo que quiero y deseo conseguir.

A Pablo, que me trajo al CSIC, fuente de consejos, de diplomacia y de tacto. Por las largas horas haciendo columnas, ensayos con neuronas, ratones... y por los buenos momentos dentro y fuera del laboratorio.

¡Muchas gracias directores!

A la pequeña Mati, que me ha acompañado en esta etapa de mi vida. Su forma de ser, sus palabras de aliento, su conocimiento técnico; han hecho mucho más agradable y llevadero mi día a día.

A la Fundación “World Wide Cancer Research”, por el apoyo de económico y confianza para llevar a cabo la investigación relacionada con los ligandos de quadruplex.

A la gente del López: Marta, Irene, Marta, Raquel, Clara, Norma..., los técnicos que han trabajado con nosotros: Ismael, María, Marisa, Sonia, Natascha, Vincente y muchas personas más que hacen del Instituto un lugar agradable en el que trabajar

A Claudia, Gracias por todo.

A los que no están: Augusto, Angelina, Rodrigo, Ignacio y Justo.

*Para los que están,
Para los que no están.*

*Never give in. Never give in.
Never, never, never -
in nothing, great or small,
large or petty.
Never give in
except to convictions of honor and good sense.
Never yield to force,
never yield to the apparent overwhelming might of the enemy.*

Sir Winston Churchill

Abbreviations and Chemical Formulas

5-FU:	5- fluorouracil
A:	adenine
A549:	adenocarcinomic human alveolar basal epithelial cells
AD:	Alzheimer's disease
Ac:	acetyl
ACN:	acetonitrile
AIDS:	acquired immune deficiency syndrome
AKT:	Akt murine thymoma viral oncogene
ALS:	Amyotrophic lateral sclerosis
ATP:	adenosine triphosphate
BBB:	blood brain barrier
BCL2:	B-cell lymphoma
BLM:	Bloom Syndrome Protein
C:	cytosine
CAT:	catalase
Carb-NDI:	carbohydrate NDI conjugate
CC₅₀:	concentration with 50% of cytotoxic growth effect
CD:	circular dichroism
CDCl₃:	chloroform
cKIT:	stem cell growth factor receptor
CNS:	central nervous system
COX:	Cyclooxygenase
CuAAC:	Cu-catalyzed alkyne azide cycloaddition
d:	doublet
Da:	Dalton
D₂O:	deuterium oxide
DBU:	2,3,4,6,7,8,9,10-Octahydropyrimidol[1,2-a]azepine
DCQAs:	dicafeoylquinic acids
dd:	double doublet
DMAP:	4-dimethylaminopyridine
DMEM:	Dulbecco's Modified Eagle Medium
DMF:	dimethylformamide
DMSO:	dimethyl sulfoxide

DNA:	deoxyribonucleic acid
dsDNA:	double-stranded DNA
EGFP:	enhanced green fluorescent protein
EGFR:	epidermal growth factor receptor
ESI:	electrospray ionization
ESI-MS:	electrospray Ionization Mass Spectrometry
EtOAc:	ethyl acetate
FAD:	flavin adenine dinucleotide
FRET:	Förster resonance energy transfer
G:	guanine
G4:	G-quadruplex
Gal:	galactose
Glc:	glucose
GLUT:	glucose transporter
GPx:	glutathione peroxidase
GTP:	guanosine triphosphate
GSH:	glutathione
GST:	glutathione S-transferase
HD:	Huntington's disease
HDL:	high density lipoproteins
Hex:	hexane
HFF:	human foreskin fibroblasts
HIF:	hypoxia inducible factor
HIV:	human immunodeficiency virus
HPLC:	high performance liquid chromatography
HRMS:	high-resolution mass spectrometry
Hsp90:	heat shock protein 90
HT:	hydroxytyrosol
HT-29:	human colorectal adenocarcinoma
hTel:	human telomeric sequence
hTERT:	human telomerase reverse transcriptase
IC₅₀:	concentration with 50% of inhibitory growth effect.
iFBS:	inactivated fetal bovine serum
IL:	interleukin
IM:	intramuscular
IPBLN:	Instituto de Parasitología y Biomedicina "López Neyra"
ITAG:	ionic-liquid as soluble functional supports
IV:	intravenous

Kd:	dissociation equilibrium constant
LC₅₀:	median lethal dose
LDL:	low density lipoproteins
LGT:	<i>Leishmania</i> glucose transporter
LOEC:	lowest observed effect concentration
LPS:	lipopolysaccharide
LRMS:	low resolution mass spectrometry
LTR:	long terminal repeat
m:	multiplet
m:	meta
MDA-MB-435:	melanoma breast cancer xenograft model
Me:	methyl
MeOH:	methanol
mer:	a synonym for repeat unit in chemistry
MIA-PaCa-2:	pancreatic cancer cell line
mRNA:	messenger RNA
MW:	microwave
Mw:	molecular weight
MET:	tyrosine-protein kinase MET
NADH:	reduced form of nicotinamide adenine dinucleotide
NCI:	National Cancer Institute
NCp:	nucleocapsid protein
NDI:	naphthalene diimide
NMR:	nuclear magnetic resonance
NOEC:	no observed effect concentration
Nts:	nucleotides
PDB:	protein data bank
PDH:	pyruvate dehydrogenase
Pf:	<i>Plasmodium falciparum</i>
PfHT:	<i>Plasmodium falciparum</i> hexose transporter
PI3K:	phosphoinositide 3-kinase
PKM2:	pyruvate kinase isozyme M2
ppm:	part per million
PQS:	putative quadruplex sequences
r.t.:	room temperature
Rap1:	transcriptional repressor/activator protein 1
RES:	resveratrol
RNA:	ribonucleic acid

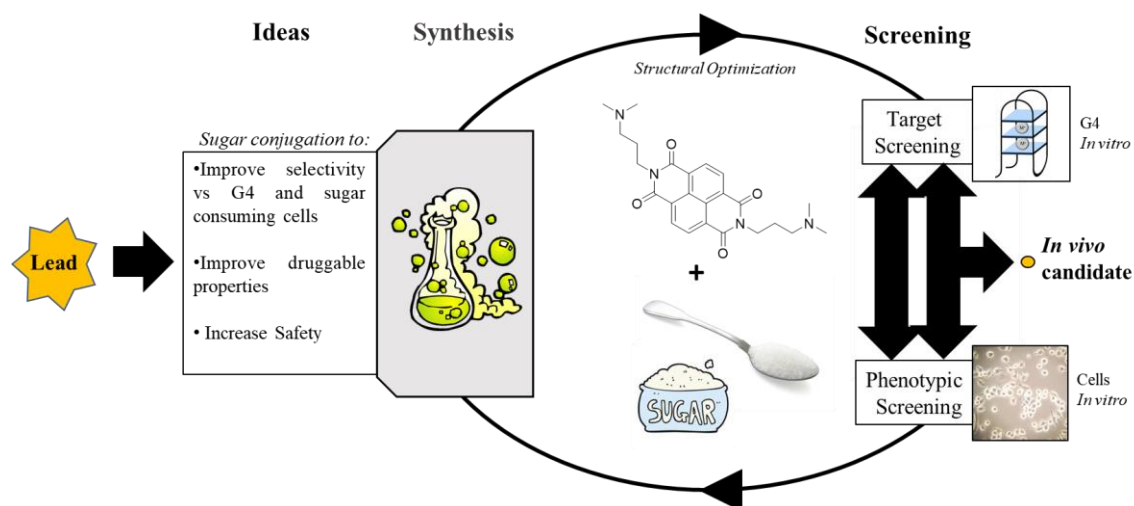
ROS:	reactive oxygen species
RRE:	rev response element
RTTEL1:	Regulator of Telomere elongation helicase 1
RU:	response unit
SDS:	sodium dodecyl sulfate
sFv:	intracellular single-chain antibody
SGLT:	sodium-dependent glucose transporter
SI:	selectivity index
SIRT:	sirtuin
siRNA:	small interfering RNA
SOD:	superoxide dismutase
ssDNA:	single-stranded DNA
T:	thymine
t:	triplet
TAMRA:	tetramethylrhodamine
TAR:	transactivation responsive element region
Tb:	<i>Trypanosoma brucei</i>
TBAF:	Tetra-n-butylammonium fluoride
TBTA:	Tris[(1-benzyl-1H-1,2,3-triazol-4-yl)methyl]amine
TDS:	thermal difference spectra
TEA:	triethylamine
TERRA:	RNA transcript from DNA human telomeric sequence
TFA:	trifluoroacetic acid
THF:	tetrahydrofuran
THT:	<i>Trypanosoma</i> hexose transporter
THP-1:	monocytic cell line
TIN2:	TRF1 interacting protein 2
T_m:	melting temperature
TMAA:	trimethylammonium acetate
TMSN₃:	trimethylsilyl azide
TNFα:	tumor necrosis factor alpha
TNP:	transdominant negative protein
TRAP:	telomeric repeat amplification protocol
TRF1:	telomeric repeat binding factor 1
TRF2:	telomeric repeat binding factor 2
TSS:	transcription start site
Tyr:	tyrosol
U:	uracil

UPLC:	ultra performance liquid chromatography
UV:	ultraviolet
VEGF:	vascular endothelial growth factor
WHO:	World Health Organization
WI38:	lung normal human cell line
WSP:	Werner Syndrome Protein
ΔT_m:	change in melting temperature

Resumen

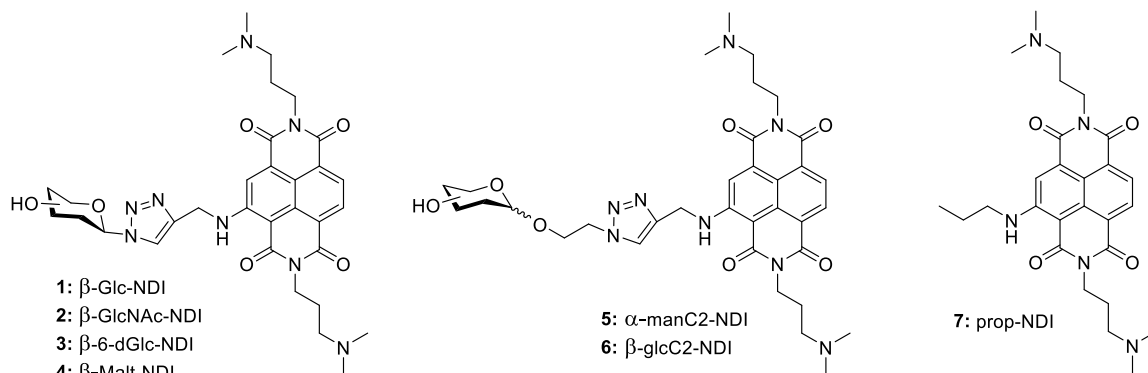
La presente tesis doctoral está centrada en el desarrollo de conjugados de potenciales fármacos con carbohidratos y cadenas lipófilas. Estos compuestos que se han considerado “Lead” a optimizar se basan en ligandos de ADN en G-quadruplex (G4) (véase la siguiente ilustración) y en tres fenoles naturales, tirosol (Tyr), hidroxitirosol (HT) y resveratrol (RES).

En primer lugar, hemos diseñado y sintetizado conjugados de azúcares y ligandos de G4 como posibles agentes anticancerígenos y antiparasitarios. La idea es obtener compuestos con mejores propiedades farmacológicas, mejor afinidad hacia sus dianas terapéuticas y mejor selectividad hacia células tumorales y parásitos protozoarios.



La diana terapéutica son los ADN en G-quadruplex (G4), estructuras secundarias que se forman en secuencias del ADN y ARN ricas en guaninas vinculadas a la regulación de importantes procesos biológicos, incluidos la replicación y la transcripción de determinados genes.

Se ha sintetizado la nueva familia de ligandos de G-quadruplex basadas en las **naftalen-diimidias (NDI)** en colaboración con el Prof. Mauro Freccero (Universidad de Pavia, Italia).

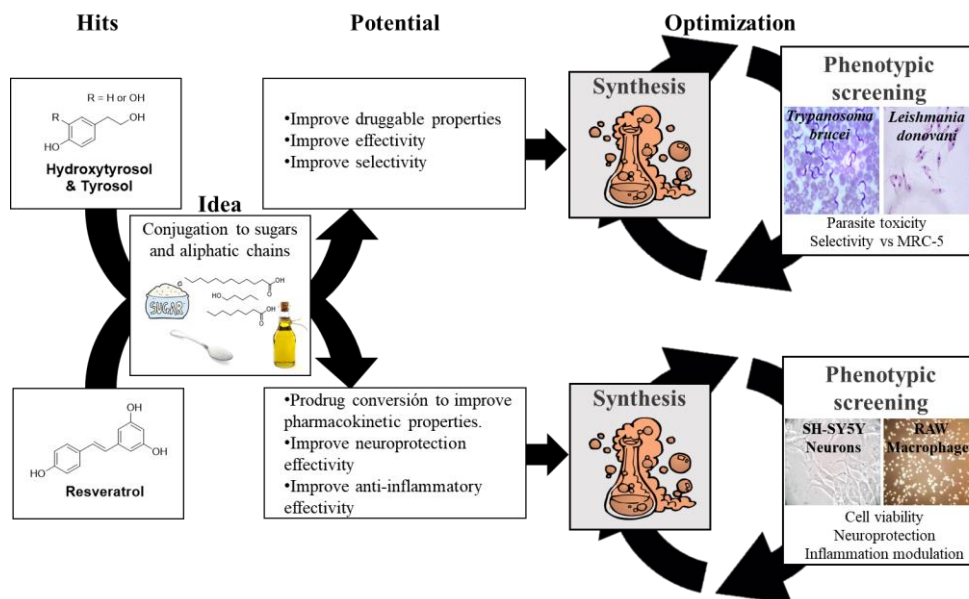


La preparación de los conjugados se realizó por medio de la cicloadición 1,4- de Huisgen (click chemistry) usando como precursores azidoazúcares y un NDI modificado con un alquino. Los carb-NDI se unen fuertemente a sus dianas y muestran selectividad frente a dúplex de ADN. La presencia del carbohidrato reduce ligeramente la afinidad por las dianas si se compara con el control aglicona-NDI pero aún así también son buenos ligandos de las secuencias mayoritarias de *Trypanosoma brucei* y *Leishmania major*, encontradas mediante una búsqueda *in silico* de la incidencia y función biológica de G4 en sus respectivos genomas, y de la secuencia del telomero humano. Se han realizado estudios de entrada celular de los ligandos carb-NDI mediante citometría de flujo y espectroscopía de fluorescencia en diferentes líneas cancerígenas y no tumorales. Pudimos observar diferencias importantes entre el control sin azúcar, que se localizan en el núcleo de manera casi instantánea independientemente de la temperatura, y los conjugados carb-NDI, que también se acumulan en el núcleo pero más lentamente. En este último casi su entrada depende de la temperatura, tiempo de incubación y del tipo de unión del carbohidrato. Empleando incubaciones con diferentes inhibidores de GLUT (transportadores de glucosa), se observó que para la entrada de los carb-NDI en las células se producía, al menos parcialmente, mediante GLUT4. Se observó una correlación entre entrada celular y viabilidad de las células tumorales tras incubación con los derivados NDI. El control aglicona-NDI que entra más rápidamente es el más citotóxico, pero no el más selectivo hacia las líneas cancerígenas. Los carb-NDI mostraron actividad antiproliferativa en el rango submicromolar y son potenciales candidatos a ser ensayados *in vivo*.

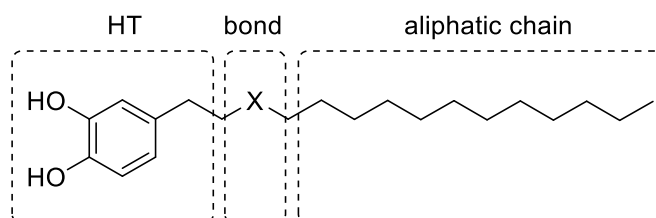
La actividad antiparasitaria de los carb-NDI fue destacable en los diferentes parásitos, en especial en *Trypanosoma brucei* y *Leishmania major* donde se observaron algunas diferencias dependiendo del carbohidrato y del tipo de unión. En todos los casos, la fluorescencia inherente en los compuestos permitió localizar los conjugados principalmente en el núcleo y el kinetoplasto usando microscopía confocal.

Los ensayos de toxicidad *in vivo* en un modelo de pez cebra demostraron que los compuestos con carbohidrato eran menos tóxicos que el control aglicona-NDI.

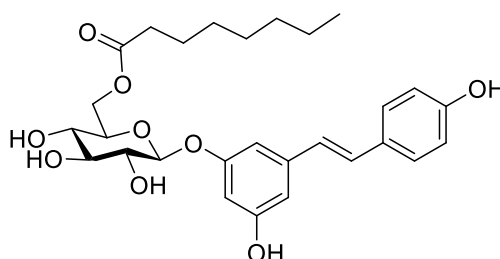
En segundo lugar, se sintetizaron diferentes derivados glicosilados y alquilados de **hidroxitirosol, tirosol y resveratrol** (ver siguiente esquema).



Los derivados de HT y Tyr fueron evaluados como potenciales agentes antiparasitarios mostrando una interesante actividad y selectividad especialmente frente a *Trypanosoma brucei*. El estudio de la relación estructura-actividad de los compuestos determinó que la longitud óptima de la cadena alifática es de entre 10 y 12 carbonos. Por otro lado, la forma de unión de la cadena alifática al HT parece menos importante, al menos según los resultados obtenidos en el modelo *in vitro* utilizado.



Los derivados alquilados y glicosilados de RES fueron evaluados como potenciales agentes neuroprotectores y anti-inflamatorios. Algunos de estos compuestos demostraron una actividad mejor que el propio RES *in vitro*. Esta mejora también fue observada en dos modelos *in vivo*, uno de pez cebra y otro murino. El compuesto 3-O-(6'-O-octanoil)- β -D-glucopiranosido resveratrol (véase debajo) demostró la mejor actividad neuroprotectora y anti-inflamatoria, señalándolo como un potencial fármaco para enfermedades neurodegenerativas.



Index

1. General Introduction	- 1 -
1.1. Drugs vs Diseases	- 3 -
1.1.1. Drug discovery and development	- 3 -
1.1.2. Lead Optimization Strategies	- 9 -
1.2. G-Quadruplex as targets	- 28 -
1.2.1. Structure	- 28 -
1.2.2. Relevance of G-Quadruplex in humans	- 30 -
1.2.3. Relevance of G-Quadruplex in other biological systems	- 31 -
1.2.4. G-Quadruplex as targets in cancer	- 32 -
1.3. Natural phenols	- 36 -
1.3.1. Tyrosol and Hydroxytyrosol	- 36 -
1.3.2. Resveratrol	- 39 -
2. Hypothesis and Objectives	- 44 -
3. Results	- 46 -
3.1. Synthesis, binding properties and difference in cell uptake of G-Quadruplex Ligands based on carbohydrate naphthalene diimide conjugates	- 46 -
3.2. G-Quadruplex identification in the genome of protozoan parasites points to naphthalene diimide ligands as new antiparasitic agents.	- 55 -
3.3. Tyrosol and hydroxytyrosol derivatives as antitrypanosomal and antileishmanial agents.	- 65 -
3.4. Alkylated resveratrol prodrugs and metabolites as potential therapeutics for neurodegenerative diseases.	- 83 -
4. Conclusions	- 130 -
5. Tools developed	- 131 -
1.1. High-resolution mass finder	- 131 -
1.2. Cellular viability analyzer	- 133 -
6. Bibliography	- 135 -
Annex 1: Supplementary material of <i>Chem. Eur. J.</i> 2017	- 149 -
Annex 2: Supplementary material of <i>J. Med. Chem.</i> 2018	- 193 -
Annex 3: Supplementary material of <i>E. J. Med. Chem.</i> 2016	- 203 -
Annex 4: Supplementary material of <i>E. J. Med. Chem.</i> 2018	- 214 -

A

ñade el hombre conocimientos a conocimientos: nunca el saber es bastante. Si tanto es uno más hombre cuanto más sabe, el más noble empleo será el aprender.

Baltasar Gracián y Morales

1. General Introduction

This thesis is a contribution to the design, synthesis and screening of novel compounds as potential drugs to treat cancer, protozoan parasitic infections and neurodegenerative diseases following several non-standard approaches.

In the introduction, the drug discovery process -used to search for new compounds as therapeutics- will be explained. Non-standard approaches for lead optimization through glycosylation and aliphatic modifications to gain selectivity and efficacy will follow, and will introduce prodrugs as possible outcomes of these conjugations.

Then, these approaches will be investigated for G-quadruplexes as potential new targets in cancer and parasites. Secondary metabolites present in beneficial dietary products such as olive oil and wine will also be modified and examined as antiparasitic, neuroprotector and anti-inflammatory potential drugs.

All this work has resulted in 4 publications:

I. M. Arévalo-Ruiz, F. Doria, **E. Belmonte-Reche**, A. De Rache, J. Campos-Salinas, R. Lucas, E. Falomir, M. Carda, J. M. Pérez-Victoria, J.-L. Mergny, J. C. Morales, *Chemistry - A European Journal* **2017**, *23*, 2157–2164;

II. **E. Belmonte-Reche**, M. Martínez-García, A. Guédin, M. Zuffo, M. Arévalo-Ruiz, F. Doria, J. Campos-Salinas, M. Maynadier, J. J. López-Rubio, M. Freccero, J. L. Mergny, J. C. Morales, *Journal of Medicinal Chemistry* **2018**, *61*, 3, 1231-1240;

III. **E. Belmonte-Reche**, M. Martínez-García, P. Peñalver, V. Gómez-Pérez, R. Lucas, F. Gamarro, J. M. Pérez-Victoria, J. C. Morales, *European Journal of Medicinal Chemistry* **2016**, *119*, 132–140;

IV. P. Peñalver*, **E. Belmonte-Reche***, N. Adán, M. Caro, M. L. Mateos-Martín, M. Delgado, E. González-Rey, J. C. Morales, *European Journal of Medicinal Chemistry* **2018**, *146*, 123-138. (* These authors contributed equally)

and exposure in several international scientific reunions including:

- **Efres Belmonte** et al. “G-Quadruplex identification in the genome of protozoan parasites points to naphthalene diimide ligands as new antiparasitic agents”. Poster. 16th Iberian peptide meeting/ 4th Chemical biological group meeting, 5th – 7th of February 2018;

- **Efres Belmonte** et al. “Synthesis, binding properties, cell uptake and cytotoxicity of G-quadruplex ligands modified with carbohydrates”. Poster. 6th international meeting on Quadruplex Nucleic Acids, (G4thering in Prague), 31st of May – 3rd of June 2017;

- Pablo Peñalver Puente, **Efres Belmonte** et al. “New Resveratrol derivatives induce neuroprotection in retinal degeneration of mice model”. Flash communication. 6th EuChMS Chemistry Congress, 11th – 15th September 2016;

- Pablo Peñalver Puente, **Efres Belmonte** et al. “Resveratrol and hydroxytyrosol derivatives: Neuroprotection and antiparasitic activities”. Flash Communication. III Biennial Meeting of the Chemical Biology Group, 14th – 16th March 2016;

- Pablo Peñalver, Marisa Mateos, Ricardo Lucas, **Efres Belmonte**, Juan Carlos Morales. “A library of new resveratrol derivatives: Improved neuroprotection and anti-inflammation activities”. Flash communication. XXXV Bienal RSEQ, 19th – 23rd July 2015.

In addition, during my PhD I completed several training courses which facilitated the completion of this thesis and complemented my formation. These are:

- Neurohacking in R, Johns Hopkins University, 2017;
- Cuidado, eutanasia y realización de procedimientos con animales de experimentación, Universidad de Granada, 2016;
- R Programming, Johns Hopkins University. 2016;
- Organic Chemistry, Universidad Autónoma de Madrid. 2015;
- The Scientist Toolbox, Johns Hopkins University. 2015;
- Prevention of workplace risks, Universidad de Granada. 2014;
- Medicinal Chemistry, Davidson College - Novartis. 2014;
- Strategies for effective research publication, Universidad de Granada. 2014.

Todo tiene remedio, menos la muerte

Spanish saying

1.1. Drugs vs Diseases

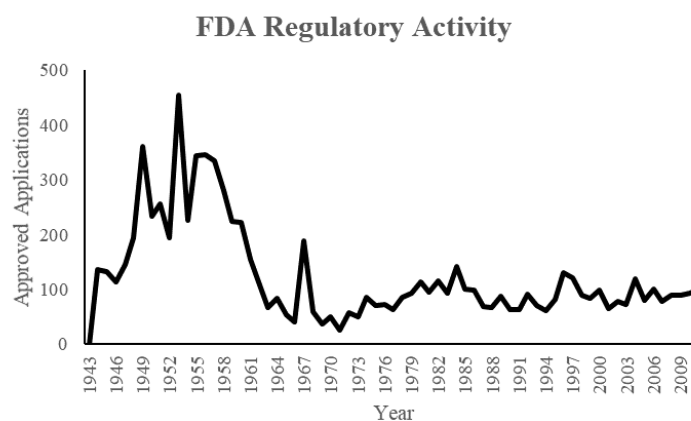
Drugs are one of the main tools we have to treat diseases. They are developed through pharmaceutical and medicinal chemistry technology which is a discipline that lies in the intersection between chemistry and biology with a focus on health-related applications. It involves the design and chemical synthesis of bioactive molecules in a synergic combination of the biological, chemical and physical sciences.

Most drugs are based on carbon (organic) and fit into the classification criteria of small organic molecules or biologics -which include a wide range of products such as vaccines, somatic cells, gene therapy, tissues, oligonucleotides, monoclonal antibodies and recombinant therapeutic proteins. A smaller number of drugs are inorganic and organometallic compounds such as lithium and platinum derivatives.

1.1.1. Drug discovery and development

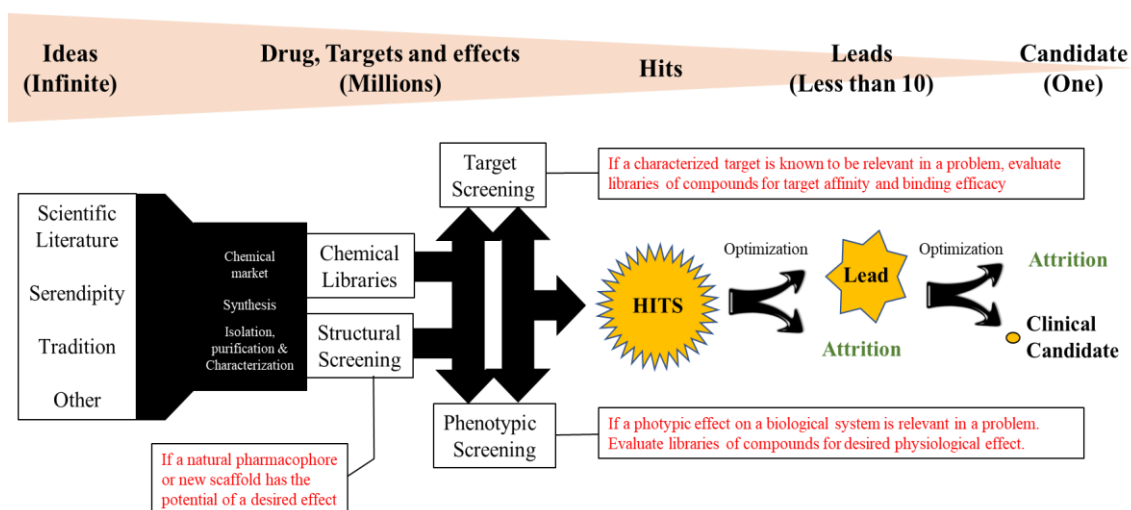
In the last decades, advances in pharmacological and medicinal chemistry, in addition to other biomedical, areas have undergone exponential growth.^[1] This progress is fueled by technological breakthroughs such as high throughput screening^[2] and advances in the genomic and proteomic fields.^[3] However, this has not lead into a higher number of drugs available for the patients (Figure 1).

Figure 1: United States Food and Drug Administration (FDA) regulatory activity since 1944.
Source: <https://www.fda.gov/> accessed January 2018.



This inconsistency is the result of several factors: lack of new chemical entities, difficulties to find new targets, complexity of the nature of certain diseases, and increasing costs due to the man hours needed to discover and develop a drug under the actual regulatory environment.^[4,5] In average, the complete drug discovery process can involve up to 15 years of work with an investment of over 2000 million €. ^[6,7] This long discovery process is divided in several steps (Figure 2).

Figure 2: Drug discovery path, which gets narrower and more demanding as it is completed.



Hit Screening

Two main approaches are used in drug discovery that can be undertaken independently or combined (Figure 3).

I. **Target based drug discovery:** It accepts the paradigm that a specific drug binding to a target (usually a protein) can activate or inhibit the target's action and hence, modulate a (patho)physiological response.^[8,9] This approach has yielded most of the commercial drugs available in the pharmaceutical market because of its popularity during the 20th century. This was motivated by the explosion of technological advances -mainly in genomics and molecular biology-, the simplicity of the validation required (measuring interactions between a purified and isolated target and a drug) and the huge amounts of possible targets. Discovery effort starts from a specific known druggable protein (or another target) to which a selective and effective candidate must be identified. The candidate must show that it interacts with the target and modify the disease in a safe and effective manner. Additionally, the drug must have tractability, and allow further optimization to gain more selectivity and efficacy. Complementary

to this validation, *in silico* methods based on target -or target family- data have been used as fast and cheap ways to determine the binding of the drug to the target.

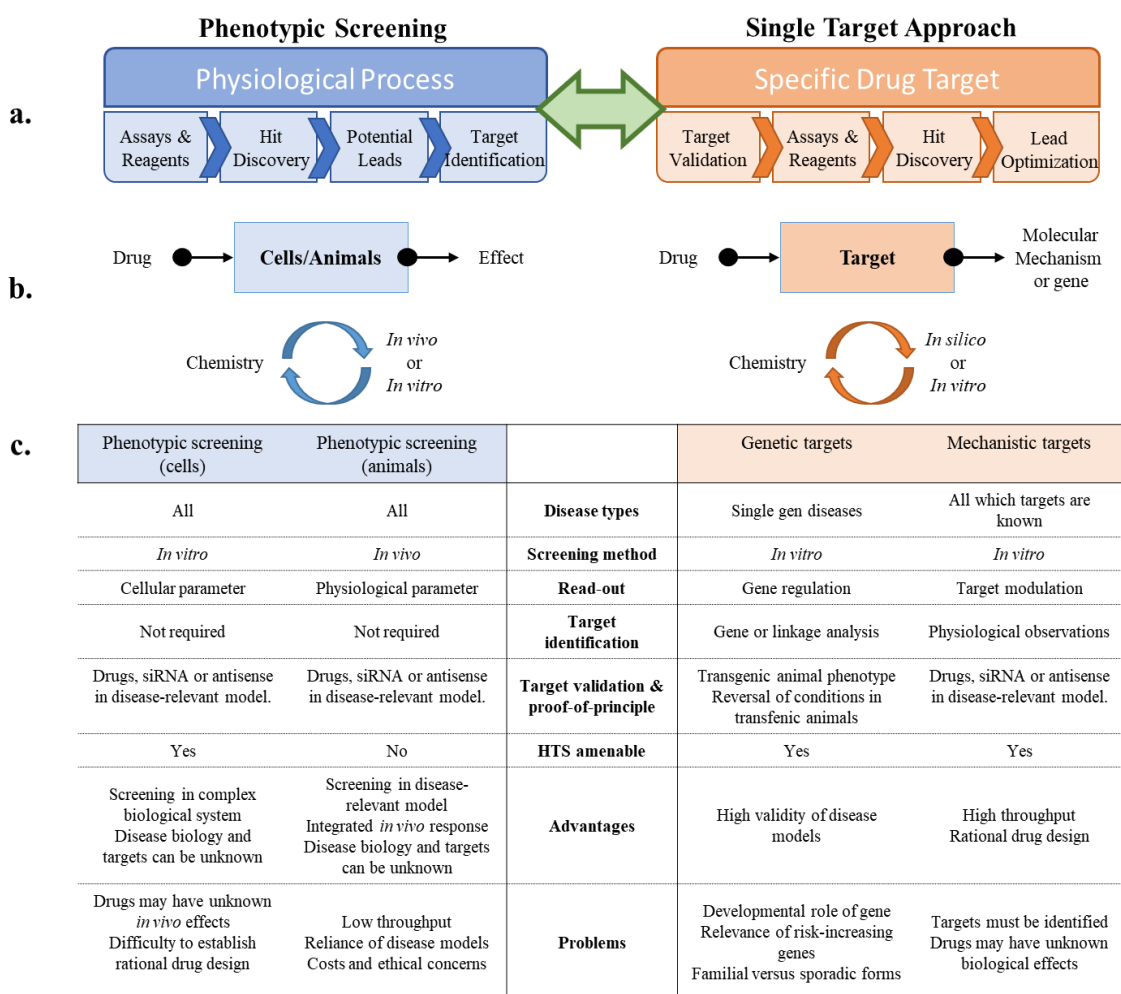
The main drawback to this screening process comes from the need to: have extensive knowledge of the target at hand, to be able to relate the modulation effect of the target to the disease and to extrapolate the results obtained to more complex biological systems.^[10,11]

Figure 3: The main approaches to drug discovery.

Section a. Steps involved in each approach from the starting hypothesis.

Section b. The efficacy evaluation system of each approach, including iterations of a small number of chemical modifications for hit identification and validation.

Section c. Differences between the approaches.



II. **Phenotypic / physiological screening approach:** Rather than starting from a single target, this approach initiates the discovery sequences from a more complex biological system such as cell cultures or laboratory animals,^[12,13] and measure physiological changes to the system. This wider perspective allows a better translation of the observed results to *in vivo* systems, normally providing better leads. This approach does not require understanding of the

biology and etiology of the disease nor the mechanism of action of the drug. However, it makes it more difficult to analyze the results and extrapolate the structure-activity relationships. Hence, the exclusive use of this approach can result in less rational and effective lead optimization pathway. Additionally, special attention must be placed to the results as the observed effects can be due (at least partially) to non-specific actions of the drugs, such as toxicity. This effect can cause false positive results.

A possible start to the process, if the target is known, can be a target-focused screening of effective drugs in similar targets (for example amongst a protein family) which however can end up giving selectivity problems. Alternatively, **High throughput screening (HTS)** can be used to find interesting molecules by examining rapidly of thousands of compounds. Large HTS libraries have been developed – by the conjunction of the very large number of structures supplied by chemical dealers (over 20 million^[14]) and combinatorial chemistry- which has expanded the possible chemical space for novel pharmacophore identification. The diversity within this chemical space is not random and often uses highly contrasted chemical libraries. The main drawback of this methodology is the high investment required, and thus, to gain process efficiency, observation of certain rules is advisable. These are:

- a) Chemical properties: meeting Lipinski rules,^[15]
- b) Chemical diversity: spreading the pharmacophore and scaffold diversity,^[16]
- c) Chemical quality: minimum of purity, stability, reactivity and solubility,^[17]
- d) Selectivity: promiscuity to other known targets,
- e) Costs of acquiring, maintaining and dispensing the compounds.

An interesting approach which can further enlarge the coverage of chemical space and maximize resources and times is known as **fragment based drug discovery**. This approach uses small pieces of molecules (with molecular weights of less than 200 Da) in relative high concentrations to find the ones that can bind to the target or cause the desired effect.^[18,19] This allows a relative small number of compounds and evaluations to provide wide and interesting results which can help further select and optimize a hit.

The next step involves **hit validation**, to avoid any artifacts or minor contaminants which could have tempered with any results.^[20-22] Related structures should also be tested to confirm the activity. New stocks or even re-synthesis of the hits might also be necessary to certify that the results are not due to the chemical structure decomposition products. Then, dose response testing can be used to select the hit candidates and structure-activity patterns (SAR) examined.

Hit to lead

Hits are then selected and converted to leads when some -if not all- requested conditions are met. For example, candidates are usually those that show evident familiar-SAR patterns, affinity and selectivity, that have strong binding, proper chemical properties including solubility, chemical tractability, can be protected under the scope of patents and which have shown no drawbacks that can cause future failure. These leads must be a reduced number of interesting compounds which will then be submitted to an evaluation of available analogues and simple synthetic modifications in a process called lead optimization.

Lead Optimization

Once a lead series meets all the criteria, iterative cycles of chemical optimization driven by biological measurements/evaluation should result in a single candidate for clinical use. Such modifications should focus primarily on finding alternatives which increase efficacy and safety (or at least increase the therapeutic window) since the two main reasons for drug candidate failure are inadequate effectiveness and safety concerns. Secondly, some chemical modifications can improve other innate properties of the structure of the drug and its biological effects. These properties include pharmacokinetic properties such as ADME-TOX (absorption, distribution, metabolism, excretion and toxicology of a drug in a biological system).

The data from many high-throughput technologies have been processed to construct virtual models capable of predicting structural properties that identifies the lead's potential problems. The simplicity and cost-effectiveness of these processes makes of them a very popular and interesting starting point for lead optimization. These studies can reduce the iterations needed of the "redesign-synthesize-evaluate cycle" and hence, the time needed to develop a clinical candidate. Current popular models include:

- a) Intestinal Absorption,
- b) Blood-Brain Barrier permeability,
- c) Cytochrome metabolism predictions,
- d) Toxicity predictions,
- e) Physicochemical predictions,

which are available -usually free- online. Overview with programs/web services was reviewed by Romero et al.^[23] ADME models were reviewed by Moroy et al.^[24] and Stepensky,^[25] Physicochemical properties by Nieto-Draghi et al.^[26] and toxicological by Raeies et al.^[27]

However, *in silico* evaluations needs to be corroborated by *in vitro* or *in vivo* results. These can be done in cellular or animal models. For example, determining if a compound

trespasses a biophysical barrier and how it achieves so, where it accumulates and how the compound gets metabolized. These studies require sensitive chromatographic tools such as HPLC to quantify the small quantities of the compound and metabolites in the biological system. Yet, implementing *in silico* pharmacokinetic predictions corroborated with *in vitro* and especially *in vivo* validation of its pharmacokinetic properties can accelerate development of the potential drug.

1.1.2. Lead Optimization Strategies

After yielding a potential lead, the drug discovery process continues its optimization to increase potency, reduce off-target activities and improve its physicochemical/metabolic properties in order to obtain a clinical candidate. Many modifications can be applied for further optimizing its structure and druggability. In this work, we will focus primarily on three approaches: glycosylation, lipophilic conjugation and prodrug conversion.

1.1.2.1. Drug glycosylation

The conjugation of a carbohydrate to a potential drug has been recurrently used in medicinal chemistry in order to improve several drug properties:

I. **Increase druggability.** Carbohydrate conjugation will increase the overall solubility and polarity of a compound, making of the conjugate usually a better drug.^[28] A highly lipophilic drug dissolves poorly in aqueous solutions -like blood- to concentrate in lipophilic environments, but by conjugating it with a sugar the conjugate increases its hydrophilicity and improves its solubility in the biological media. This approach is used naturally by some cells as a metabolism pathway to detoxify lipophilic xenobiotics. For instance, UDP-Glucuronosyltransferase and UDP-glycosyltransferase carry out sugar conjugations to increase aqueous solubility and favor the conjugate elimination in a process called phase II metabolism.^[29] This conjugation is favored by the extensive availability of sugars in the system.

Additionally, carbohydrate conjugation can increase drug-target interactions by the glycan moiety potentially forming hydrogen bonds with the target and/or polymeric structures.

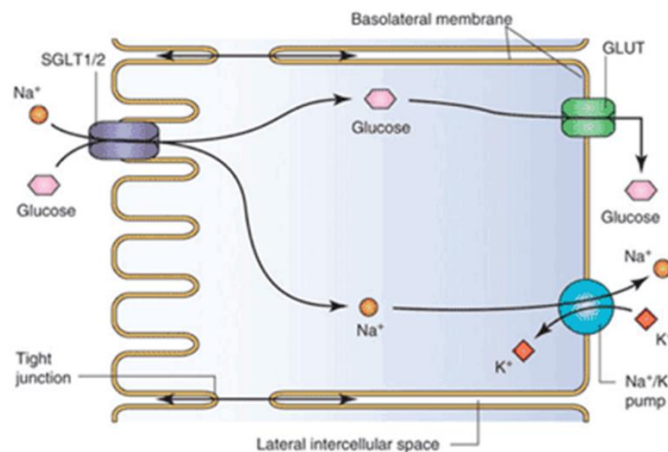
II. **Increase drug distribution to cells/tissues.** As sugars are of paramount importance for life, carbohydrate conjugation can help the drug translocate physical barriers such as cell membranes via specific transporters. These transporters are a family of trans-membranal proteins called GLUT that translocate, regulate the movement and concentration of sugar through the cell membrane. Each protein member has different affinities for a variety of hexoses and pentoses, and is expressed differently in the body's cells and organs. Hence, the GLUT family is categorized primarily by the way the sugar is transferred and also by its physical location, the sugar affinity and its biological function.

A. Sugar Transporters in humans

SGLT - Sodium dependent glucose transporters

SGLT: are proteins responsible for the forced intake of carbohydrates during absorption and reabsorption processes in the kidneys and gastrointestinal system. Since solvated sugars tend to distribute equally in the solvent, SGLT are in charge of using energy to internalize carbohydrates into the cell when the sugar gradient is negative (there is more sugar inside than outside the cell) by simultaneously taking advantage of the positive gradient of internalizing Na^+ . However, this causes an ion unbalance in the cell, which is then forced to employ energy in the form of ATP through the Na^+/K^+ pump to restore it (Figure 4).

Figure 4: GLUT role in sugar distribution, involved in the absorption of sugars from the outside (SGLT) and distribution in between cells and blood (GLUT).



Only 2 out of the 6 known SGLT are properly characterized in the literature.

SGLT1 reabsorbs glucose and galactose at the cost of 2 Na^+ and has been found to be pivotal for intestinal glucose absorption and glucose-dependent incretin secretion in the intestine and kidney,^[30] where it relates to meal ingestion and insulin regulation.^[31] They are also expressed in trachea, heart, brain, testis and prostate.

SGLT2 is a glucose selective symport transporter with an internalization ratio of only 1 Na^+ per glucose. It is through this mechanism that 90% of the glucose reabsorption in the kidney is achieved,^[32] yet the transporter is also expressed in liver, thyroid, muscle and heart.

GLUT – glucose transporters

These transporters maintain sugar homeostasis within the body and within tissues. The natural tendency for solvated sugars in tissue is to move between and within cells as these are consumed for energy. This flow is enabled by an energy-free GLUT facilitated transport service. There are 14 isoforms of GLUT, categorized in 3 families based on sequence similarity which distribute along all cells and organs. Only the majority of the first family of GLUT are well characterized. These are GLUT 1, 2, 3 and 4.

GLUT1: The principal substrate of GLUT1 is glucose, but mannose, galactose, glucosamine and ascorbate can also be transported. To do so, GLUT1 suffers a conformational change when linked to its substrate which enables internalization of the sugar. This change is the rate limiting step for the transport to occur.^[33] The transporter is distributed ubiquitously throughout the body yet it is specially concentrated in cells that require higher sugar internalization rates. For example, in erythrocytes, up to 10% of the protein wall is constituted by GLUT1.^[34] Additionally, in the endothelial cells of the BBB^[35] and in astrocytes^[36] glucose is taken up and then distributed in the brain to feed and maintain neuronal activity by GLUT1 and 3 activity. The embryo and fetus survival^[37] and development also depends on GLUT1.^[38] Likewise, some cancers depend on overexpression of GLUT1 transporters to intake the required fuel for tumor growth and expansion.^[39]

GLUT2: The principal substrate of GLUT2 is glucosamine, with 20 times more affinity than glucose, and 70 times more than galactose, mannose and fructose.^[40] It is highly expressed in hepatocytes, in intestinal absorptive cells, in kidney and in pancreatic beta cells,^[41] plus neurons and astrocytes. Due to the relationship of GLUT2 with the glucose sensing mechanisms and glucagon secretion in response to hypoglycemia, it is thought that their main function is as part of a sugar regulatory mechanism.^[42]

GLUT3: Can be found mainly in the brain and testis with an extremely high affinity for glucose.^[43] They are the main supplier of carbohydrates to neurons with the assistance of GLUT1, and are also found resting in the storage vesicles of white blood cells until the correct stimuli is sent.^[44]

GLUT4: Located in adipocytes, skeletal muscle and cardiomyocytes and working as insulin-dependent transporters, this protein can also be widely overexpressed by cancerous cells.^[45] During low blood-insulin levels (hence low sugar in blood), GLUT4 is saved in intracellular compartments in the Golgi network, but as insulin levels increase, a protein cascade commands these compartments to distribute on the cellular membrane via fusion with phospholipids or endosomal action for fast internalization of external sugars.^[46] This is especially useful for the cell's (punctual or not) sugar uptake increase. A defect in this mechanism is related

to Diabetes type 2.^[47] In neurons, especially cholinergic ones, sugars are internalized in response to higher energy demands through GLUT4 association with GLUT3.

B. Sugar Transporters in Parasites

Carbohydrates are of paramount importance not only for humans but also for some parasites. *Leishmania major*, *Plasmodium falciparum* and *Trypanosoma brucei* depend on carbohydrates to live, replicate and invade the host. Glucose transporters play a central role in the nutrition and metabolism of these organisms, both in vectors and hosts, and are essential for their viability. The life cycle and morphology of the parasites determine the type of sugars and the consumption process they exhibit. In fact, the carbohydrate supply between the intracellular and extracellular environments is so different that, in order to adapt, the parasites express different transporters in each situation.

The promastigotes of *Leishmania* feed off the sugars of the mosquito's plant nectar meals when in its gut.^[48] In the host's macrophage phagolysosome, the amastigotes express several sugar transporters to internalize carbohydrates as food, despite the low sugar availability.^{[49][50][51]} Known as the LGT family,^[52] these proteins relate to the human GLUT1 in sequence and structure having even higher glucose affinity than its human counterpart,^[53] plus a possible role for proton symport to force intracellular sugar transport at the cost of energy.^{[54][55][56]} Additionally, they have been found to be critical for parasite survival as LGT null mutants are more susceptible to oxidative killing, have reduced viability at elevated temperatures and with nutrient deficits.^{[53][57][58]}

Plasmodium falciparum in the mammalian host is totally dependent upon the hosts sugar reservoir to survive. As it replicates within the host's erythrocytes, the consumed nutrients travel easily through the GLUT1-rich red cell wall, the parasitophorous vacuole membrane (which presents a high-capacity and low-specificity channel),^[59] and the parasite plasma membrane procured by the PfHT1 protein. This protein has significant sequence identity to the human GLUT1^[60] and broad specificity for hexoses. The result is that during malaria infections, parasitized erythrocytes can consume up to 50% more glucose than normal ones.

Lastly, the trypanomastigote of *Trypanosoma brucei* that lives extracellularly within the bloodstream of the host also feeds exclusively on the host's supply. The main transporter identified in this form is THT1 which is a low-affinity and high-capacity facilitative transporter that takes advantage of the high concentration of glucose at its disposal.^[61] By the contrary, THT2 is a high-affinity low-capacity protein adapted for the vector environment, which may function

as a proton symporter at low concentrations and as a facilitative transporter at high disposition of substrate.^[62]

III. **Reduce toxicity of drugs.** Carbohydrate conjugation to a drug can lower the intrinsic toxicity of the drug by up to 5 times, depending on the drug and sugar.^[28] This is because sugars can be converted to energy to endure damage.^[63] Inside the cell, several glycoside hydrolases separate the monomers of carbohydrates for energy production to eventually release the aglycone.

IV. **Gain selectivity against sugar dependent diseases.** Taking into account points II and III, drug selectivity can be gained by conjugating a drug with a sugar which acts as a vector for cellular uptake. Diseases with high energy requirements such as cancer and some parasitic diseases usually present high expression of sugar transporters. Therefore, a carb-drug may potentially be better internalized than over its aglycone counterpart.

Cancer and the Warburg effect

Cancer cells overexpress GLUT transporters and glycolytic enzymes to consume up to 200 times more glucose than normal cells.^{[64][65]} This can allow them to rely exclusively on the energy and biomass obtained from glycolysis alone,^{[66][67][68]} and hence surpass the regulated ROS-generating mitochondrial trap.^[69] This is known as the Warburg effect.^[70] Even though it is unknown if these metabolic transformations are merely a secondary side effect of cancer or whether it is a direct initiator of tumorigenesis, this effect has been successfully exploited to obtain cancer selectivity by sugar conjugation.^{[71][72]} The German physiologist Otto H. Warburg (1883 – 1970) discovered that cancer tissue fermented glucose into lactate through anaerobic respiration even in the presence of an excess of oxygen. Thus, glycolysis (2 ATPs) supported by anaerobic respiration is used preferentially to the aerobic pathway (≈ 34 ATPs). To compensate the lower efficiency of glycolysis, cancer cells increase sugar intake (through GLUT overexpression) and metabolism (by increasing glycolytic enzymes). There are several reasons for this:

1. **Because the amount of energy per glucose obtained is sufficient** to proliferate faster than normal cells if the glucose supply is sufficient. In cancer cells, the overexpression of GLUTs and glycolytic enzymes by oncogenes and other factors allows increased sugar internalization and metabolism to cope for the poorer ATP yields of glycolysis. These oncogenes and factors include mainly phosphoinositide 3-kinase (PI3K),^[73] serine-threonine kinase AKT,^[74] MYC,^[75] hTERT, T antigen, H-Ras and other tyrosine kinases.^[76,77]

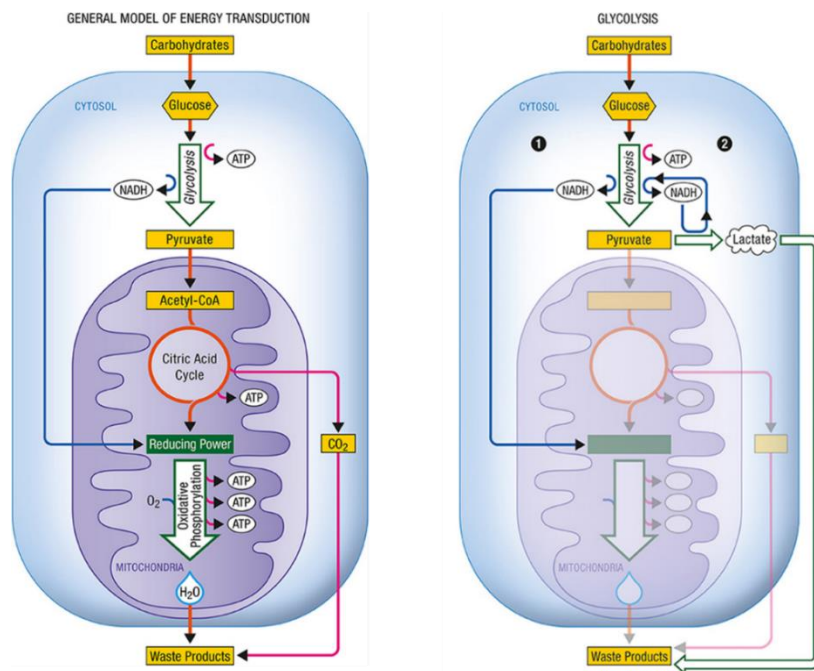
2. **Because cancer cells need biomass to replicate** and not only energy. When cells catabolize sugars by glycolysis they obtain energy and pyruvate residues. These residues can be converted into lactate and used for further anabolic construction of -for example- phospholipids for the cellular membrane. Total anabolism through the Krebs cycle yields energy but no carbon units for catabolic construction. In a recent experiment using ¹³C-marked glucose and alanine, glioblastoma cells converted up to 90% of glucose and 60% glutamine into lactate and alanine.^[67] These species were then used as C and N building blocks for organelle construction during cellular replication. In opposite conditions, with: lack of biomass, energetic species such as NAD⁺ (required for glycolysis) and lactate dehydrogenase results in the cells incapacity to proliferate.^[78]

3. **Because cancer cells can avoid using the mitochondria.** The mitochondria function is heavily regulated by tumor-suppressive proteins since oxidative phosphorylation produces ROS side-products.^[69] Furthermore, too much ROS can damage the cell and/or promote dangerous mutations. Hence, even if these events can help the cancer cell to become more aggressive, it can

also force it to die. So avoiding the use of the mitochondria through anaerobic glycolysis is the fastest and more reliable method of obtaining energy for cancer cells (Figure 5).

Figure 5: Metabolism differences between a normal and a cancer cells or some parasites. Normal cells use the mitochondria to generate water, carbon dioxide and energy whilst cancer cells primarily use glycolysis for energy extraction and biomass. This is known as the Warburg effect.

Source: Demetrius, L. A.; Magistretti, P. J.; Pellerin, L. *Frontiers in Physiology* **2015**, 5.



4. **Because cancer cells can avoid using oxygen.** As cancer cells grow one on top of the other, the tumorous environment will also be exposed to reduced quantities of oxygen and acidity (from the lactate residues). Even when cancer cells use glycolytic metabolism before hypoxia exposure, it actually is a major contributor to the metabolism.^[74,79,80] When the cells suffer high O₂ depletion, the hypoxia-induced factor (HIF) is activated and contributes to the angiogenesis - to create new capillaries to feed the tumor- and stimulates glycolysis through the activation of glycolytic enzymes.^[81] Other oncogenes also get activated such as the tyrosine-protein kinases and H-Ras which are involved in cell division.^[82]

The Warburg effect is the most commonly accepted theory but others have been proposed such as the reverse-Warburg effect.^[83] These alternative theories are out of the scope of this thesis.

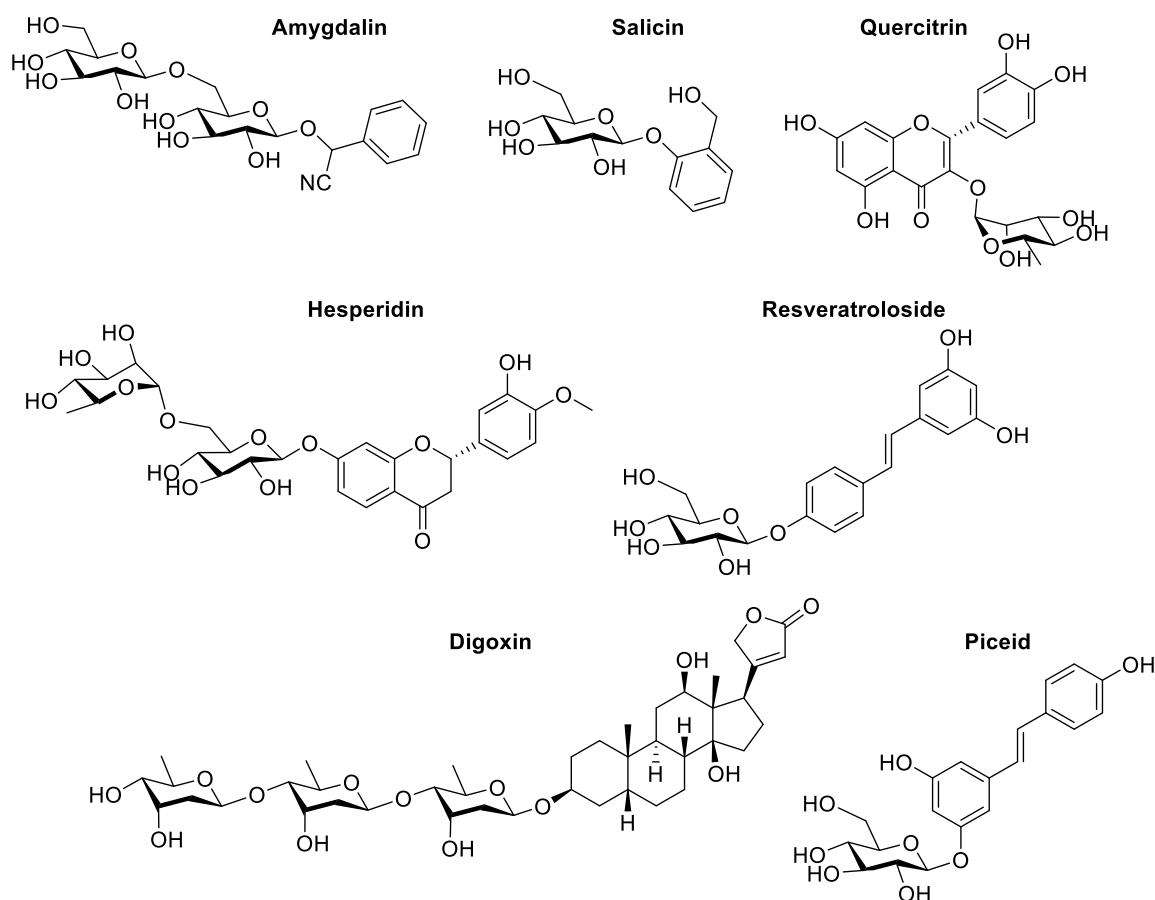
Parasitic diseases and carb-drug conjugation

Both cancer cells and the parasites under study need sugars to survive. They have specific transporters to internalize and consume carbohydrates exclusively by glycolysis, and hence, both have the potential of increasing the selectivity of a drug by carbohydrate conjugation. In any case, most approaches related to the high consumption of sugars by parasites have focused on the transport and metabolism inhibition. Various 3-*O*-methyl glucose analogues have proven to be potent inhibitors of glucose transporter proteins in *Plasmodium* and very poor for the human GLUT1.^[84] In *Trypanosoma brucei*, several attempts targeting transporter inhibition have been made.^{[85][86][87]} In fact, the commonly used drugs used to treat the disease such as Suramin and Melarsoprol directly work by interfering the metabolism of sugars, similarly to what the antimonials and alopurinol do in *Leishmania*.

Carbohydrate drug conjugates

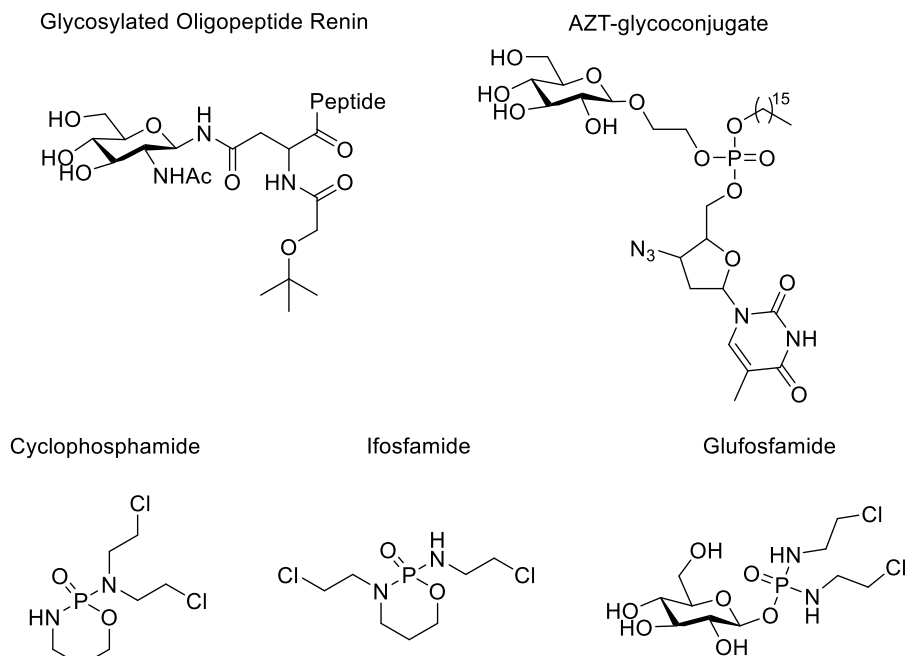
Many natural products with interesting biological properties contain sugar moieties in their structure. The first carb-drug to be discovered was Amygdalin (Figure 6), found in 1830 by Pierre Robiquet.^[88] Since then, many others have been revealed, usually presenting similar effect than the aglycone but with better druggability. For example, the carb-conjugate salicin, found in the barks of the *Salix* genus trees and precursor of the aspirin, is converted into salicylic acid in the body causing analgesic, antipyretic and anti-inflammatory effects.^[89] Flavonoids glycosides such as hesperidin and quercitrin have been found to be beneficiary for health because of their antioxidants and anti-inflammatory properties,^[90,91] and cardiovascular protection.^[92] Similarly, steroid glycosides -such as Digoxin found in *Digitalis* plant genera- are commonly used in heart diseases and failure,^[93] whilst phenolic derivatives such as piceid and resveratrolside have been described as potential neuroprotective agents.^[94-96]

Figure 6: Natural glycosides mentioned



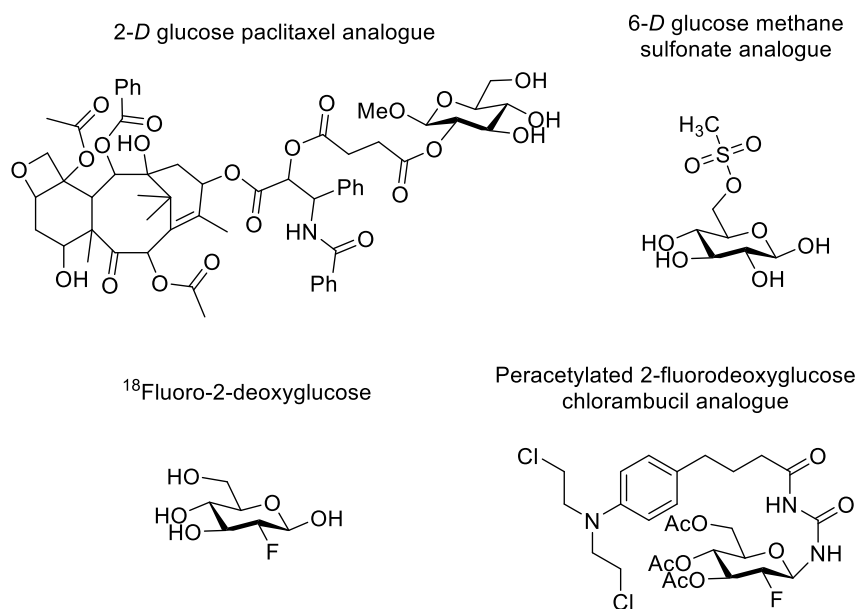
Conscious conjugation of carbohydrates to drugs started in 1991, when Renin -a peptide uses to treat hypertension- was linked to mannose and *N*-acetyl-glucosamine (Figure 7) to increase its pharmacokinetic properties.^[97] In the same year, the anti-retroviral 3-azido-3-deoxythymidine (AZT) was also conjugated with glucose and mannose to improve the drug's CNS absorption mediated by GLUT transporters.^[98,99] The first carb-drug conjugate as an anticancer drug was reported in 1995. Ifosfamide was modified to incorporate glucose to take advantage of the Warburg effect and named glufosfamide.^[28] The mode of action of both compounds are similar, but the intrinsic toxicity of glufosfamide was reduced by 2-5 fold when compared to ifosfamide. *In vitro* co-treatment with GLUT inhibitors also interfered with their antiproliferative activity, demonstrating -at least partial- GLUT uptake. Furthermore, radioactive glufosfamide showed that the compound mainly localizes in the cancerous tissue and less abundantly in insulin independent high carbohydrate consuming organs.^[100,101] In 1997, clinical trials of glufosfamide started evaluating the drug in humans.^[102] Other clinical trials followed showing modest but positive results in several types of cancer, including pancreatic and non-small lung cell tumors, with less side effects than the aglycone.^[103-105]

Figure 7: Glycoconjugates and active drugs mentioned.



Since then, many other chemotherapeutics has been conjugated with sugars. For instance, Taxols such as paclitaxel, have been linked to glucose (Figure 8) and glucuronic acid to improve their water solubility and selectivity against tumorous cells.^[106,107] Additionally, efficacy of these drugs increased fivefold over the aglycone. The busulfan core and other nitrogen mustards such as the chlorambucil core, have also been widely studied.^[108,109] A peracetylated fluoro-2-deoxyglucose chlorambucil conjugate demonstrated to be 25 times more toxic in cancer cells than the aglycone and 6 times less toxic in mice.^[110] ¹⁸fluoro-2-deoxyglucose (FDG) has also been extensively used to visualize tumors and metastases.^[111] In all these cases, conjugates usually get uptaken by the cell through GLUT1.

Figure 8: Examples of lead structures tested as chemotherapy



1.1.2.2. Lipophilic conjugation

Another possible approach for lead optimization is the addition of lipophilic moieties to the drug. This can be easily accomplished by the conjugation of fatty acid residues to free alcohol or amine groups within the drug. Other covalent modifications include introduction of more resistant bonds such as ethers and thioethers which can evade -or at least delay- enzymatic activity. These fatty acids and analogues can be classified by their chain length (short < 7, medium 7 – 12 or long chain fatty acids >12 carbons), by the linearity of the chain (linear or branched) and by the number and location of unsaturations (saturated, mono and polyunsaturated). Similarly to the glycoconjugation, this approach may bring several advantages to the drug, which are:

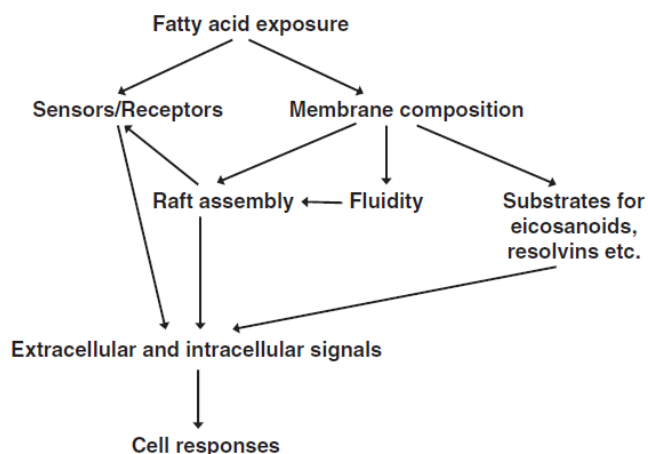
I. **Alternative energy source** since fatty acids are a source of energy for cells. Through a process called beta-oxidation in the mitochondria, long chains are broken down to generate acetyl-CoA, NADH and FADH₂. This energy can be used by the cell to endure damage. Short chain fatty acids usually undergo bacterial fermentation in the gut where they are converted to glucose. When cells do not require energy, fatty acids are conjugated with glycerol and stored as triglycerides for posterior use.

II. **Increase conjugate distribution.** For highly hydrophilic drugs, administration and distribution in the body and through cells is extremely complicated due to passive diffusion impairment. The alternative for this kind of compounds is facilitated protein transport, which complicates the lead optimization process as transport specificity and affinity must be considered.

A way to solve this problem is through lipophilic conjugation to the drug's polar functional groups. This reduces the molecules overall hydrophilicity and potentially increases its bioavailability. Furthermore, the appropriate alkyl chain can specifically be chosen to obtain the desired overall lipophilicity for precise passage through problematic physical barriers, such as transdermal or ocular passage.^[112] Similarly, oral bioavailability of the conjugate can increase due to specific uptake of apical transport proteins located in the intestines. Once in the blood, the lipophilic conjugate will preferentially bind to albumin which will further stabilizes and increases the circulatory half-life of the complex.^[113,114] Alternatively, the conjugate can associate with other lipoproteins, which can transport the conjugate to high energy consuming cells such as tumorous cells. Thus, LDL and HDL have both been successfully used with hydrophobic chemotherapy as a mean to obtain distribution selectivity in cancer tissues.^[115-117] Once reached the final tissue destination and after protein dissociation, the fatty acid can be cleaved off from the drug by the glutathione reductive activity, by a peptidase or by an esterase.

III. **Potential intrinsic effects of a fatty acid.** If the lipophilic drug conjugate ends up liberating the fatty acid, this molecule may have an intrinsic effect. (Figure 9).

Figure 9: Overview of the mechanisms by which fatty acids can influence inflammation.
 Source: P. C. Calder, *European Journal of Pharmacology* 2011, 668, S50–S58.

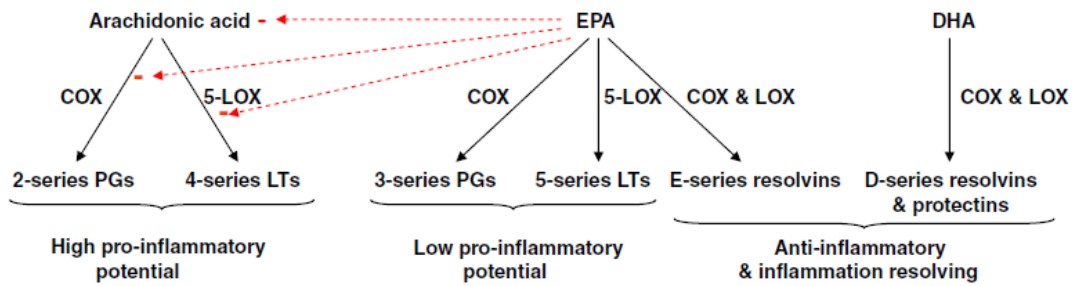


Liberated free fatty acids may interact with several G protein-coupled receptors called free fatty acid receptors (FFAR). Four variants have been reported (FFAR 1-4) to detect exterior stimulus, internal signal transduction and cellular response.^[118,119] FFAR 2 and 3 are activated by short alkyl chains and FFAR 1 and 4 by medium and long ones.^[120,121] Their action mainly involve energetic control and hence, can be found in the gastrointestinal and endocrine system's regulatory hormones.^[120,122,123] However, they can also play a role in inflammation,^[124,125] neurodevelopment and neurogenesis,^[126] and cancer.^[127–129]

In fact, the relationship between inflammation and fatty chains is widely known. Non-esterified fatty acids can influence the complex metabolite and nutrient factors within an inflammatory cell which in turn can promote the inflammation reaction. These chains can be incorporated as phospholipids to the cell membranes where they can play important roles assuring function, order and lipid raft formation.^[130] They can also act as precursors for biosynthesis of essential molecules for inflammation. For example, eicosanoids are synthesized from the arachidonic acid under demand, and yield prostaglandins, thromboxanes and leukotrienes (Figure 10). These are all involved in modulation of the inflammatory response with opposing effects,^[131,132] with an overall result that depends on the nature of the stimulus and concentration of each one within the inflammatory cell. Eicosapentaenoic acid (EPA) and docosahexaenoic acid

(DHA) also give rise to resolvins and protectins which act as inflammation resolvers and are obtained via cyclooxygenase (COX) and lipoxygenase (LOX) activities.^[133–135]

*Figure 10: General overview of synthesis and actions of lipid mediators produced from arachidonic acid, EPA and DHA. COX, cyclooxygenase; LOX, lipoxygenase; LT, leukotriene; PG, prostaglandin.
Source: P. C. Calder, European Journal of Pharmacology 2011, 668, S50–S58.*



Fatty acids can also interact with transcription factors modulators, such as the peroxisome proliferator-activated receptor (PPAR) which acts in an anti-inflammatory manner.^[136] PPAR is associated with a reduction of TNF- α and IL-6 values upon LPS stimulus and certain gene modifications in the inflammatory mechanism.

1.1.2.3. Prodrugs

The prodrug concept is based on masking the lead activity of a compound by conjugation with a chemical moiety until enzymatic or chemical cleavage within the body activates the lead compound (Figure 11). This masking moiety can potentially be any chemical, and commonly include carbohydrate, aminoacid, phosphate or lipophilic conjugations (Figure 12).

Figure 11: Concept of a prodrug.

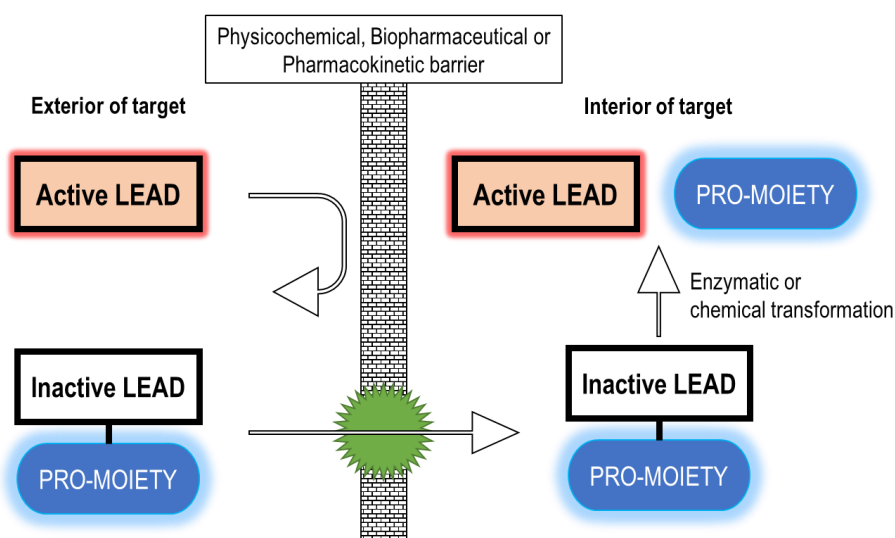
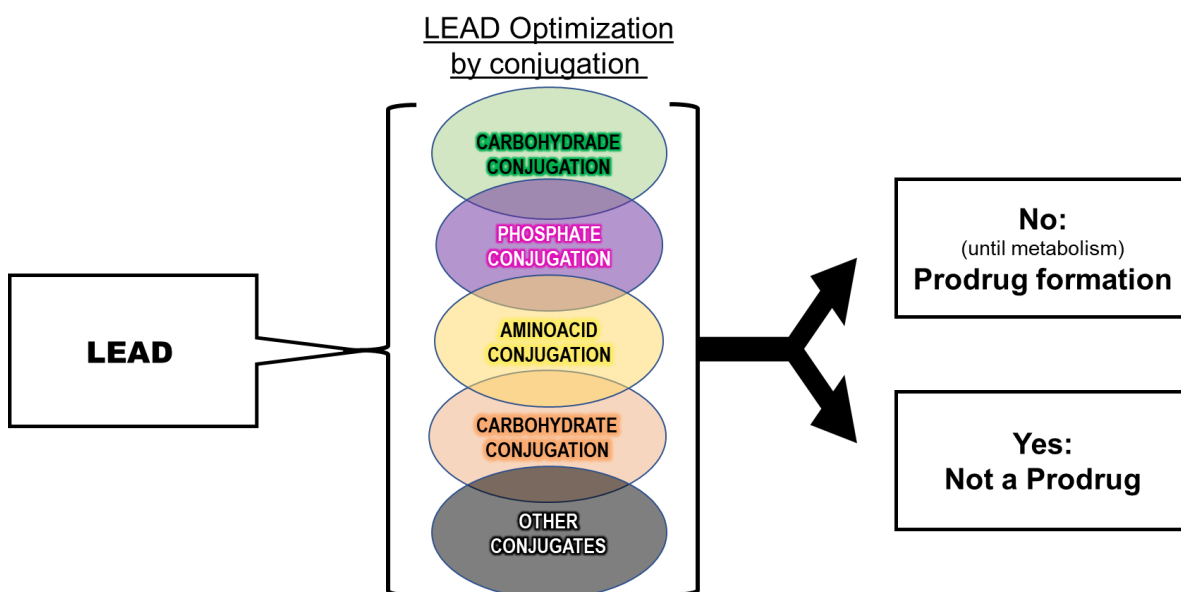


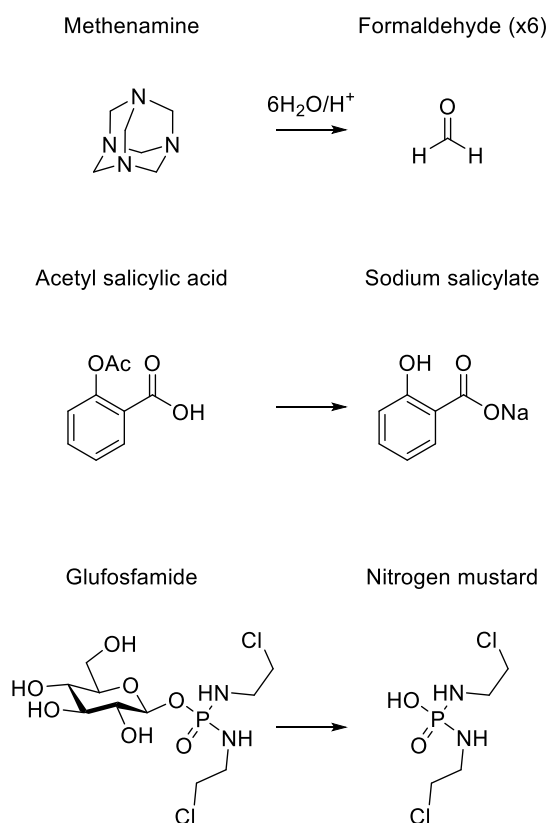
Figure 12: Lead optimization strategies include many possible chemical modifications. These can give rise to a prodrug conversion of the conjugate if the activity is masked until metabolism of the compound liberates the active moiety.



Preparation of a prodrug is a strategy used to increase the pharmacokinetic properties and the selectivity for a target/tissue of a drug and to reduce its toxicity. Hence, due to its potential, prodrugs have become of interest in medicinal chemistry, making up for about a third of all recent approved small-molecules and up to 10 % of all marketed drugs in 2010.^[137,138] This interest started around 1960, and by the year 2000 it became a constant in drug discovery.^[139] By 2009, 15% of the 100-best-selling small-molecules were prodrugs,^[138] including Vyvanse (the L-lysine prodrug of amphetamine with less abuse potential) and omeprazole and derivatives (which activate in the acidic parietal cells of the stomach).

The first intentional conversion to a prodrug was methenamine by Schering in 1899, which was able to release 6 equivalents of formaldehyde (antibacterial) and 4 of ammonium ions selectively (Figure 13).^[140,141] Bayer's aspirin (acetylsalicylic acid) shortly followed, as a less irritating form of anti-inflammatory sodium salicylate. Since then, many other prodrugs have also been prepared including glufosfamide, mentioned previously which requires hydrolysis for its activation. Around 36 % of glufosfamide is enzymatically transformed and half of that is activated to the active compound nitrogen mustard which can accumulate in cancerous tissue for over 24 h.

Figure 13: Prodrugs activated by metabolism mentioned in this section



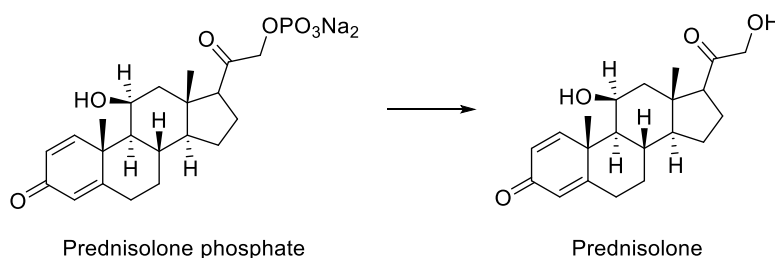
Prodrug benefits

Preparation of a prodrug can add several beneficial properties to a drug, similar to the sugar and lipophilic conjugation. These are:

I. **Improve drug solubility, bioavailability and absorption.** Prodrugs can increase the drug's solubility, bioavailability and absorption by improving dissolution rates via ionizable or polar neutral groups, such as phosphates, amino acids and -of course- sugar moieties. These conjugations can potentially transport drugs to the target tissue through passage of several lipid membranes.^[142] As the requirements for membrane passive diffusion permeability are far from being ideal for a drug, lipophilic prodrug modifications have also been extensively used in literature. These are specially relevant for oral, transdermal and ocular administration,^[112] which requires ubiquitous esterases to activate the drug.^[143]

Phosphate esters can improve both solubility and bioavailability of drugs which suffer from these issues.^[141] These conjugates get so rapidly metabolized by endogenous phosphatases that the parent drug permeability is not affected. An example is Prednisolone sodium phosphate prodrug (Figure 14), which is 30 times more soluble than the immunosuppressant parent drug and is rapidly hydrolyzed by the gut epithelial alkaline phosphatases during absorption to give almost exclusively the active compound in circulation.^[144]

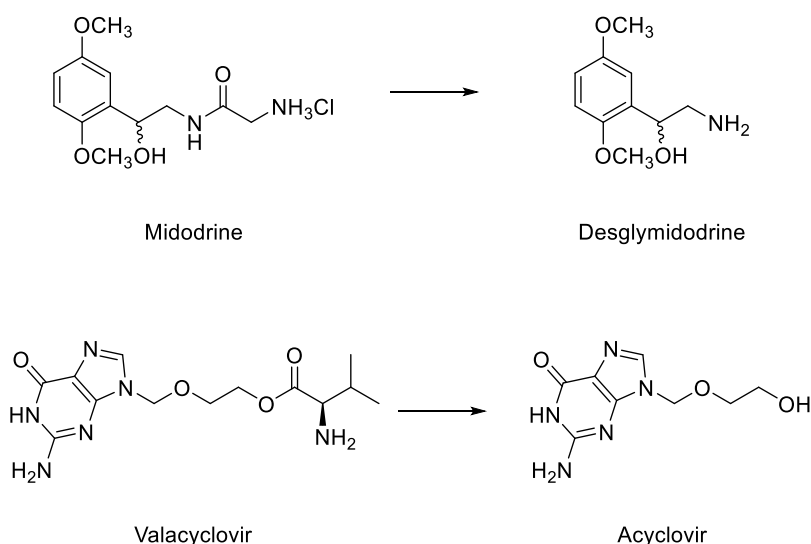
Figure 14: Prednisolone prodrug and metabolism to active compound



Similarly, amino acid esters or amides can be conjugated to -OH, -SH, -NH₂ and -COOH groups of the parent drug to increase solubility.^[145] Additionally, absorption and bioavailability are enhanced due to the presence of specific transporters in the intestinal epithelium.^[146,147] Several esterases, amidases and peptidases can bio-convert the prodrug to the active parent drug after absorption. An example is Midodrine (Figure 15), a glycine prodrug of desglymidodrine used in orthostatic hypotension which has shown increased absorption through the proton-coupled

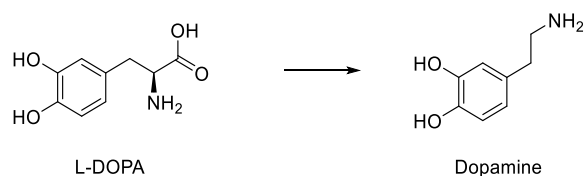
peptide transporter. This increased the bioavailability up to 93 %.^[148,149] Similarly, valacyclovir, a prodrug resulting of the conjugation of L-valyl residue with the purine nucleoside antiviral acyclovir, increased the bioavailability of the drug from 20 to 40%.^[150]

Figure 15: Midodrine and valacyclovir prodrug and metabolism to active compounds



II. **Modifying the drug distribution** to achieve site-selective drug delivery. The prodrug approach is a promising technique which can exploit specific enzymes and transporters to gain selectivity.^[145] The effect is similar to that seen previously with the carbohydrate and lipophilic conjugation. An example is dopamine, which is too hydrophilic to surpass the BBB and distribute to the brain when trying to treat Parkinson's disease. However, by conjugation with an L-amino acid to form the prodrug L-DOPA (Figure 16), it can accumulate in the brain through L-type amino acid transporter 1 and being activated by the decarboxylase to yield dopamine.^[151]

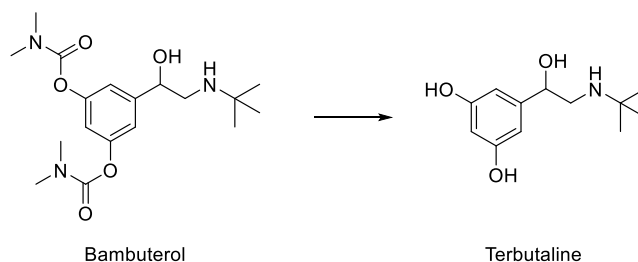
Figure 16: L-DOPA prodrug and metabolism to active compound



III. **Reduction of drug metabolism and excretion.** Many drugs suffer the first-pass effect in the gastrointestinal tract and liver, followed by fast elimination due to the efficient kidney elimination of water-soluble substances. This can decrease the hydrophilic and/or easily metabolizable drug therapeutic action. Prodrug conjugation can help to protect the parent drug

from such events, by masking the metabolically labile but pharmacological essential functional groups of the molecule. For instance, terbutaline, a β_2 -agonist used to treat asthma, suffers rapid metabolism through modification of its phenolic groups. In contrast, the prodrug bambuterol is slowly converted into terbutaline,^[152] provoking less side effects and a more distended dose administration protocol (it needs to be used less times to give the same effect - Figure 17).

Figure 17: Bambuterol prodrug and metabolism to active compound



IV. **Less Toxicity.** Prodrug conjugation can inactivate the molecule until it reaches its target, where it will get activated and exert its action, lowering its toxicity and side effects in non-target areas.^[137,153] An example is glufosfamide, the inactive carb-conjugate prodrug of the nitrogen mustard which is 5 fold less toxic and has less side effects than the aglycone (Figure 13). However, the global distribution of most of the enzymes responsible for bioactivation can reduce the benefits. So administration of exogenous activators such as enzymes guided by antibodies or modified genes which transcribe the activators have been used to further reduce overall toxicity.^[154,155]

*E*l hombre propone y Dios dispone

Spanish saying

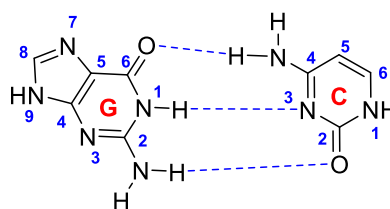
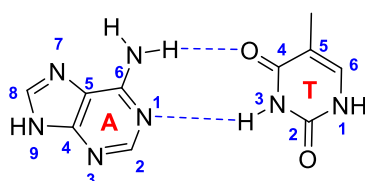
1.2. G-Quadruplex as targets

1.2.1. Structure

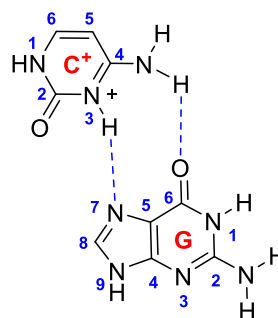
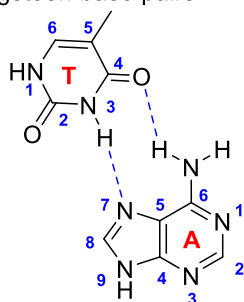
G-quadruplexes (G4) are DNA and RNA non-canonical guanine-rich sequences that form a unique four stranded morphology and follow the pattern $G_{\geq 3} X_n G_{\geq 3} X_o G_{\geq 3} X_p G_{\geq 3}$ (where G is guanine, X is any nucleotide and n, o and p are lengths between 2 and 20).^[156] This is accomplished by the formation of “Hoogsteen” hydrogen bonds (Figure 18).^[157]

Figure 18: Interaction between nucleic acid bases. A. Classical Watson-Crick base pair. B. Alternative Hoogsteen base pair.

A. Watson-Crick base pairs



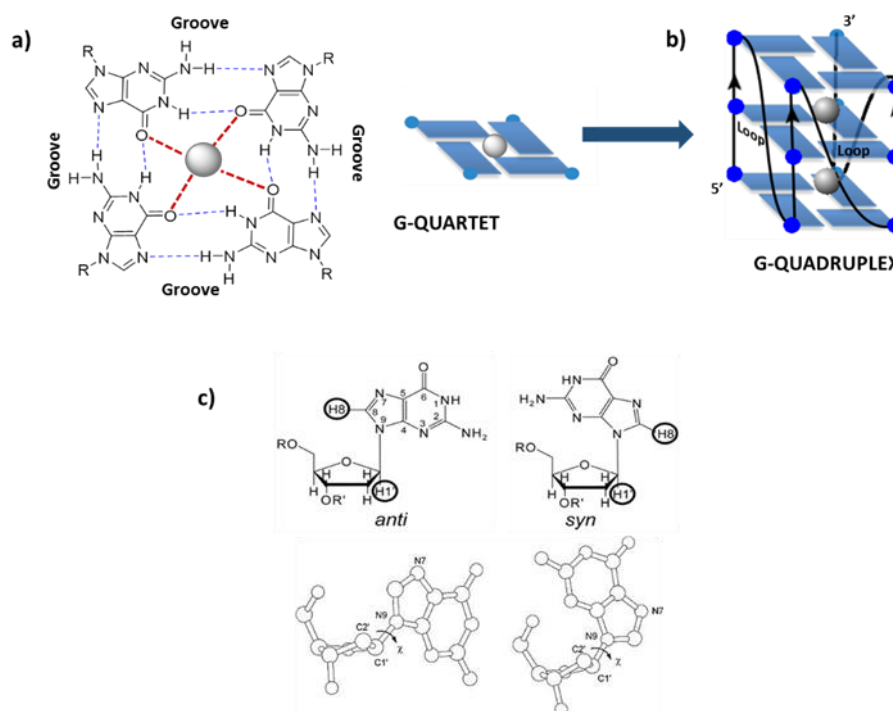
B. Hoogsteen base pairs



The basic unit of the G4 is the tetrad (or quartet), composed by four associated guanines in a planar structure stabilized by “Hoogsteen” hydrogen bonds (Figure 19, part a). Several tetrads can then superimpose and stack by π - π interactions to form the G4 (Figure 19, part b). Most of these structures require the stabilization effect of a cation hosted in the central cavity of the

G4.^[158,159] The ion's stabilization effect depends on the size and charge of the cation, being potassium usually the best stabilizer followed by sodium and ammonium.

Figure 19: a) G-quartet and the interaction network with the gray ball representing the cation and blue dashed lines representing the hydrogen bonds. b) Resultant quadruplex from three G-quartets stacking. c) anti and syn guanine glycosidic bond conformation..



The many possible different three-dimensional topologies of a G4 arise as a consequence of the nature of the grooves and loops of the structure, as well as of the glycosidic angle of the sequence (Figure 19, part c), the strand orientation (parallel if all strands have the same direction, antiparallel if half have opposing directions and hybrid if they have a 3 to 1 disposition) and the stabilizing-effect of the cation. Thus, G4 can be classified according to:

<u>Strand number and type:</u>	<u>Strand orientation:</u>	<u>Loop Conformation:</u>
Intramolecular: 1 strand	Parallel	Lateral
Intermolecular: >1 strand	Antiparallel	Diagonal
	Hybrid	Parallel

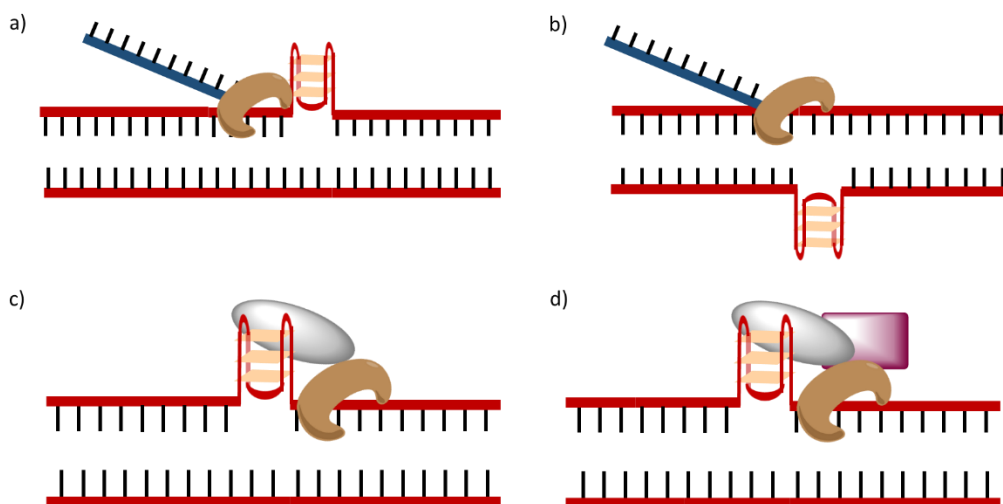
1.2.2. Relevance of G-Quadruplex in humans

It has been estimated that more than 375.000 possible quadruplex sequence (PQS) can be found in the human genome.^[160] They play an active role on the genomic transcription and replication processes. These structures mainly locate in the telomeric regions of the chromosomes under the repeating motif (GGGTTA)_n also called hTel, and near gene transcription start site regions (TSS). With smaller incidence, PQS have also been located near known human replication origins^[161] and in RNA sequences.^[162]

In the telomeres, the highly conserved telomeric sequence (hTel) is repeated several hundred to thousand times. They protect the end of the chromosome from degradation and fusion with neighboring chromosomes. During genomic replication, the DNA polymerase is unable to encode the telomere endings as a natural mechanism for regulating division in somatic cells. Hence, each replication cycle shortens the telomere until the genome becomes nonfunctional, causing cell death by senescence and apoptosis.^[163] In highly replicant cells -such as cancerous cells- telomerase enzymes reconstructs the telomere and prevents this mechanism from happening.^[164] To do so, it requires the unfolding of any formed intramolecular hTel-G4.^[165] Hence, stabilization of the G4 can eventually force the cell to activate senescence and die. The mechanism which regulates this folding and unfolding equilibrium is unresolved, but the protein-complex Shelterin^[166] and the telomere binding proteins (hPOT1) seem to play important and opposite roles in the complex process.^[167]

Regarding the possible prevalence of G4 in other areas of the human genome, around 50% of the regulatory genes and oncogenes in humans have PQS near their promoter regions.^[168,169] This suggests a possible role for G4 in their genomic expression, but the mechanism and biological effects are yet unknown. One theory suggests that G4 formation downstream the TSS promotes transcription but formation in further-along segments blocks transcription by hindering RNA-polymerase II (Figure 20, part a and b).^[170] A second theory indicates that G4s hinder normal nucleosome formation and duplex-DNA binding to proteins which, in turn, block transcription (Figure 20, part c and d).^[171,172]

Figure 20: Possible roles of DNA G-quadruplex in transcription by RNA-polymerase (brown). a) Blocking transcription: transcription is inhibited due to the formation of a stable G-quadruplex. b) Facilitating transcription: formation of a stable G4 in the complementary strand enhances transcription. c) Stimulating transcription: proteins (gray) bind to G-quadruplexes and stimulate the transcription process. d) Repressing transcription: Proteins binds G-quadruplexes and repress transcription directly (gray) or via other proteins (purple).



Given that the DNA must be unwound to a single strand for the potential formation of the G4, helicases may be a regulating factor in this process.^[172–174] However the actual mechanism of the interaction of helicases with G4 is unknown and it has not been demonstrated *in vivo*.

1.2.3. Relevance of G-Quadruplex in other biological systems

Besides humans, different searches have located G4s in the genome of other animals (including other mammals), and lower organisms such as yeasts, bacteria and viruses. These results have accentuated the interest on G4 as therapeutic targets. Examples include: *Saccharomyces cerevisiae*,^[175] *Escherichia coli*,^[176,177] *Herpes Simplex 1*,^[178] *papilloma*^[179] and *Epstein-Bar* viruses.^[180] For parasites however, G4s have been scarcely studied except in *Plasmodium falciparum*.^[181,182]

1.2.4. G-Quadruplex as targets in cancer

Human telomerase is overexpressed in more than 80 % of cancers,^[183] and the stabilization of the hTel has been proposed as a potential target against it.^[184] Additionally, many oncogenes such as c-MYC,^[185] c-KIT,^[186,187] HIF,^[188,189] BCL-2,^[190,191] RET,^[192] k-RAS,^[193] h-RAS,^[194] HSP90,^[195] b-RAF,^[196] the androgen receptor,^[197] VEGF^[191] and MET,^[198] possess sequences that form G4 structures. The effect that these quadruplexes exert depends on both the specific G4 and the gene, being the relationship between G4 stability and growth inhibition positive and direct in most cases. For example, the c-MYC expression is downregulated when its G4s structures are stabilized.^[185,199,200] Hence, in this thesis we will study the use of a carb-NDI conjugate family as ligands for G4-targets within cancer cells. We will study their effectiveness, selectivity and distribution patterns *in vitro* in attempts to find ligands capable of stabilizing G4s which can selectively interfere with the replication of cancerous tissues.

1.2.4.1. G4 Ligands

G4's potential involvement in the expression and replication of the DNA makes of them very interesting therapeutic targets. Thus, many DNA binders have been reported as G4 ligands with probable antiproliferative activity.^[201]

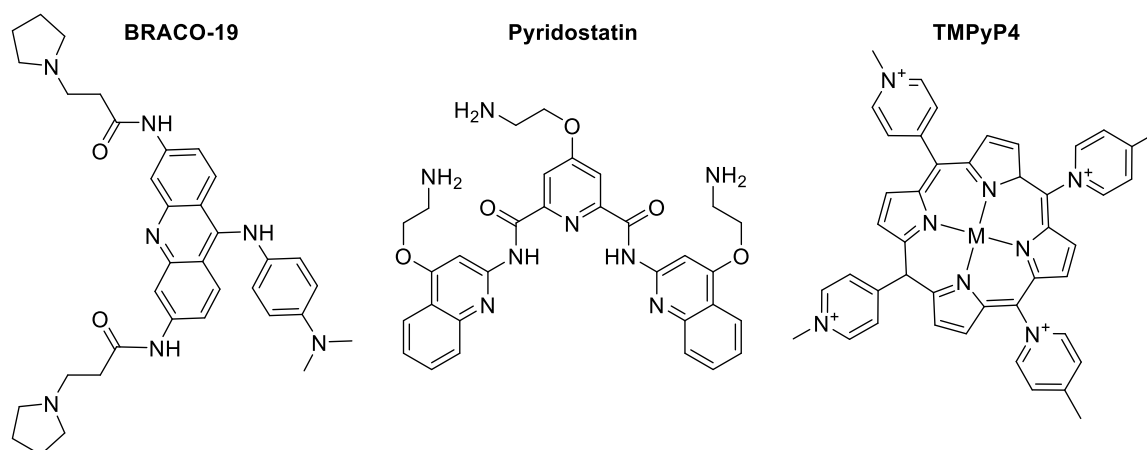
An ideal G4 ligand should present G4 vs duplex DNA selectivity in order to avoid side-effects and excessive toxicity. The ligand should also present selectivity against different G4s, although this feature is not trivial to achieve due to the similarity amongst the structures of the different G4 topologies.^[202]

Regarding chemical characteristics, G4 ligands usually include large aromatic cores to stack via π - π interactions over the last quartet of the quadruplex,^[203] and flexible cationic side chains to interact with the phosphates in the grooves.

The first G4 ligands developed were designed as telomerase inhibitors using porphyrin,^[204] triazine,^[205] anthraquinone^[206] and acridine cores.^[207,208] The best example is the acridine derivative BRACO-19 (Figure 21),^[209] which has demonstrated activity against several types of cancers in the sub-micromolar concentration range,^{[210][211]} and which displays the typical mechanism of actions involving acridine stacking and side chains interactions with the G4 grooves.^[212] Another family of ligands are synthetic macrocycles based on cores such as quinacridine,^[213] oxazole^[214] and quinolone.^[215] For example Pyridostatin, a flat and flexible pyridine G4-binder, causes DNA damage in PQS-location sites.^[216] Polycyclic aromatic

compounds with coordinated metals such as Pt^{II} , Mn^{II} , Cu^{II} and Zn^{II} are considered as the metal complex family. The cation configures the polyaromatic core in the optimal conformation for stacking interactions with the tetrad.^[217,218] TMPyP4 is an example of a polycyclic aromatic complex based on porphyrin which shows high affinity but poor selectivity for G4.^[219]

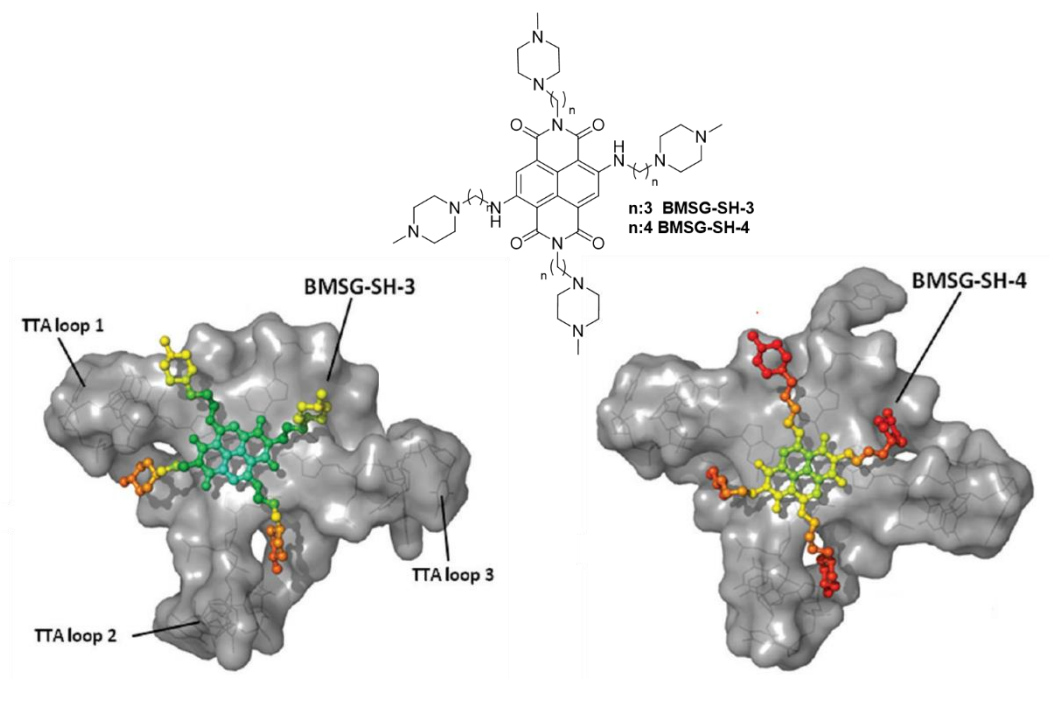
Figure 21: Structures of BRACO-19, Pyridostatin and TMPyP4, known G4 Ligands.



1.2.4.2. Naphtalene diimides (NDIs)

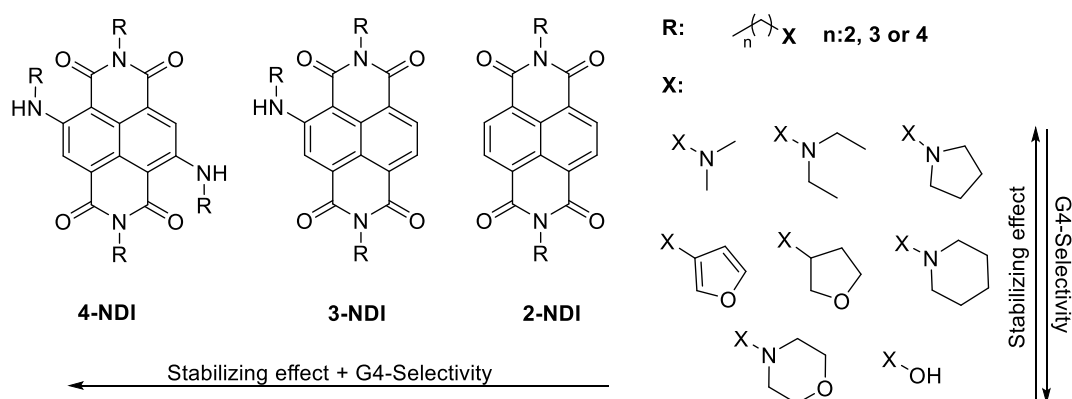
Aromatic diimides are a relevant family of G4 ligands which bind G4-structures in a similar way as the reported ligands.^[220,221] They usually present poor solubility in most solvents due to their structure so several modifications have been made to increase both the solubility in lipophilic and aprotic polar solvents,^[222] and in water.^[223] NDIs are fluorescent molecules as they undergo reversible one-electron reduction to form stable radical anions when solvated. They usually give intense red and near-infrared absorption bands. However, the color range depends on the core's substituents^[224] and environmental pH.^[225] Using this innate fluorescence properties, NDIs have been used as: DNA-sensors and DNA-discriminators between double and single strands,^[226] as molecular-based optoelectronics in solar energy conversion,^[227] as biomimetic of transmembrane channel systems,^[228–230] and as guest host systems where they have been used as intercalators, foldamers, ion channels, catenanes and rotaxanes.^[231] Recently a common use for the NDI core has been as G4 ligands because of its aromatic and planar structure which allows them to stack to the G4-tetrads (Figure 22).^[220]

Figure 22: BMSG-SH-3 and BMSG-SH-4 NDI ligands to the terminal G-quartets of the hTel22 quadruplex. Source: Collie et al., Journal of the American Chemical Society 2012, 134, 2723–2731.



NDIs can effectively stabilize G4 at low concentrations *in vitro* yet are poor clinical candidates due to their core's lipophilicity and structure. To overcome this problem, modifications to the core can be easily achieved through straight forward chemical approaches to add functionalized substituents.^{[232][233]} These include bi, tri and tetra substitutions with different lateral chains that interact with the G4-grooves (Figure 23). In general, the tetra-substituted NDIs (4-NDI) show the best hTel stabilization effect as the four side chains can interact with all the grooves.^[233] By the contrary, bi-substituted NDIs (2-NDI) show the poorest stabilization and selectivity towards G4-structures.^[234,235] Regarding the terminal functional group of the substituents, dimethylamino, diethylamino and pyrrolidine show the highest G4-stabilization effect yet present low selectivity versus duplex DNA. By the contrary, morpholine and hydroxy groups display the opposite traits, lower effect with higher selectivity.

Figure 23: Structure and substituents of NDIs tested as G4-ligands.



The high G4-stabilization effect and G4-selectivity of certain NDI derivatives makes them promising anticancer drugs. Their activity measured by 50 % inhibition concentration (IC_{50}) lies between the nanomolar (for dimethylamine and *N*-methyl piperazine derivatives) and the micromolar (morpholine derivatives) range.^[233,235,236]

Using the intrinsic fluorescence of the NDI-core incubation with MRC-7 breast cancer cells showed up to 50 % telomerase activity inhibition and an accumulation in the cell nucleus.^{[235][237]} However these results do not apply to all NDIs as some can localize in the cytoplasm or interact with different onco-related G4s.^{[221][238]} *In vivo* experiments with NDIs are scarce because the pharmacokinetic properties of the molecules are not ideal. Yet, the results show noticeable tumor growth reduction (between 50 to 80 %) after IV administration in a murine model of cancer.^{[239][240]}

A ceite y vino, bálamo divino.

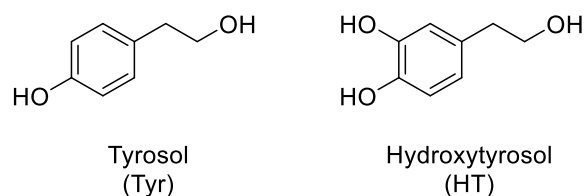
Spanish saying

1.3. Natural phenols

1.3.1. Tyrosol and Hydroxytyrosol

Tyrosol (Tyr) and hydroxytyrosol (HT) are phenolic secondary metabolites synthesized by plants -as for example *Olea europaea* (olive) and *Vitis vinifera* (grape vine)- to act as a defensive mechanism against external pathogens and herbicides.^[241] We ingest these compounds from fruits and their derivatives (olive oil and wine),^[242–244] or acquire it from the degradation of dopamine. The phenolic core (Figure 24) provides strong redox and antioxidant properties to these compounds which can mitigate ROS damage in cells.^[245] However, Tyr and HT are actually involved in many other roles besides radical scavenging.^[246]

Figure 24: Structures of the natural phenols Tyrosol and Hydroxytyrosol.



HT and Tyr have similar pharmacokinetic profiles. During digestion they are transported by passive bidirectional diffusion mechanism which quantitatively absorbs them.^[247] However, they have an extremely poor bioavailability due to extensive first-pass metabolism in the gut and liver.^[248,249] In plasma, free forms are usually undetectable but several organs (such as muscles, lungs, liver, brain and kidneys) intake the phenols in a fast manner,^[250] where they accumulate in a dose-dependent way.^[251] HT is very rapidly metabolized in blood and tissue mainly to its glucuronide derivative.^[252] *O*-methylated analogues,^[249] aldehydes and acids from the aliphatic alcohol oxidation,^[250] sulfates^[253] and acetylated derivatives^[254] have also been detected as metabolites. Finally, these metabolites are excreted through the urine around 6 h after consumption.

1.3.1.1. Tyrosol and Hydroxytyrosol biological effects

The main ability of Tyr and HT is to scavenge ROS,^[255,256] but considering the fast metabolism of both, it is very possible that part of its biological effect is due to active metabolites. The phenolic groups of Tyr, HT and their metabolites are able to donate protons and efficiently stabilize electrons to neutralize charged and unstable molecules. These derivatives include the species formed by UV radiation and peroxy nitrite exposure, where HT was able to prevent DNA damage.^[257,258] Due to its structure, HT can also chelate metals and interact with several genes related to the antioxidant defense system.^[259] Its cellular presence can promote antioxidant response like DNA-repair proteins and phase II detoxifying enzymes.^[260–262] Besides, superoxide dismutase (SOD), glutathione peroxidase (GPx), glutathione reductase and catalase activities improve in the presence of HT.^[256,263] In the mitochondria, HT promotes its biogenesis^[264] and protects it by reducing age-related intracellular ROS as well as activating SOD expression.^[265] Tyr also displays similar biological effects.^[266]

These properties make Tyr and HT potential candidates for many disorders. As neuroprotector, oral administration of HT in mice improved the brain cells survival against oxidative stress.^[267] Similarly, in a hypoxia–re-oxygenation model, they display cell protection in the brain by reducing damaging ROS and NOS species.^[268,269]

As cardioprotector, HT is associated with increasing HDL content^[270] and protecting LDL from oxidation.^[271,272] HT can decrease the formation of atherosclerotic plaques and reduce the plasmatic levels of cholesterol and lipids.^[273–275] Additionally, it is an antithrombotic agent capable of inhibiting platelet synthesis.^[276] Tyr has also demonstrated cardioprotection effects *in vivo*.^[277]

HT has showed anti-inflammatory effects by activation of several genes related to inflammatory profiles in peripheral blood mononuclear cells.^[278] In LPS-challenged THP-1 cells, HT was able to decrease cytokine formation as well as nitric oxide and TNF- α .^[279,280] COX1 and COX2 are also inhibited by HT with the same efficacy as ibuprofen.^[281]

Furthermore, HT is an antitumoral compound^[282,283] effective with dosage between 10 to 17 mg/g.^[284] Several different action mechanisms have been proposed for this effect, including blockade of the cyclin-dependent kinases, inhibition of the messengers involved in cell proliferation -such as ROS-^[285] and cell cycle arrest with apoptosis induction.

HT demonstrated antimicrobial activity against *Vibrio cholerae*, *Salmonella typhi*, *Haemophilus influenza* and *Staphylococcus aureus*.^[286] HT has also been reported as anti-parasitic agent against *Leishmania spp.*^[287] HT-rich olive oil extracts have similarly demonstrated activity

against *Escherichia coli*, *Candida albicans*, *Clostridium perfringens*, *Streptococcus mutans* and *Salmonella enterica*.^[288,289]

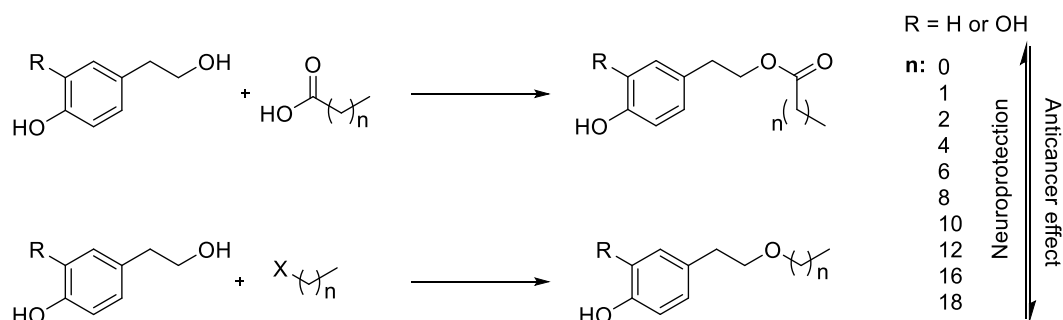
1.3.1.2. Modifications to Tyrosol and Hydroxytyrosol

The main goal modifying Tyr and HT is to improve its pharmacokinetic properties whilst improving or at least preserving its activity. Usually, this approach involves modifications to its primary alcohol in order to change its solubility and lipophilicity and hence increase its bioavailability and plasma half-life (Figure 25).^[290] The modifications can be classified as:

Esters, where lipases and esterases cleave the fatty chain liberating Tyr and HT. Acetate derivatives can be found naturally in olive oil together with Tyr and HT but other esters have also been synthesized and evaluated.^[291–293] The alkyl chain length relates to the neuroprotection power as it grows, especially for short and medium lengths chains. These derivatives have antioxidant capacities in the range of the parent phenol, with slightly better results due to the slight increase in lipophilicity which facilitates its internalization and use as antioxidant by the cell. However, as the chain length grows over 12 carbons, this effect decreases,^[294,295] because excessive lipophilicity hinders easy diffusion of the esters into the cells and causes entrapment into the plasma-membrane where they interact with the long phospholipids.

As anti-tumoral agents, esters have higher toxicity than the parent drug. For example, HT-acetate and other esters show better activity in several cancer cell lines than HT by arresting the cell cycle.^[290,296] Additionally, HT-esters can up-regulate pro-apoptotic proteins.

Figure 25: Tyr and HT ester and ether formation, and activity potential regarding the chain length.



Ethers. Ethers have only been studied in HT. These HT derivatives are lipophilic analogues with increased enzymatic resistance against cleavage. Short chain ethers of HT reduce ROS *in vitro* in a dose dependent manner and also reduces GSH depletion better than HT.^[297]

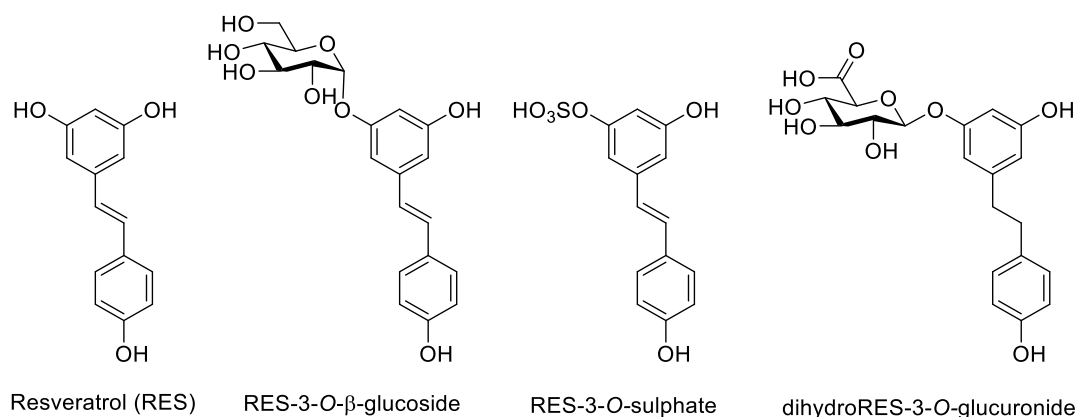
These effects were also found *in vivo* (in rat brain slices).^[294] Again, as the chain increases length, its antioxidant effect decreases.

As anti-cancer drugs, the HT-ethers show better activity than the esters and HT itself. Its activity is in the low and medium micromolar range and the length of the chain affects inversely to its antiproliferative effects. In this case, shorter carbon lengths have less activity than the longer versions of the analogue.^[297-299]

1.3.2. Resveratrol

Resveratrol (RES) is a polyphenol which was first discovered in the roots of *Veratrum grandflirum O. Loes* in 1940 (Figure 26).^[300] Other sources such as *Vitis vinifeora* (vine), the *Morus* genus (mulberries), *Arachis hypogaea* (peanuts) and *Polygonum cuspidatum* (used in traditional oriental medicine) have also been identified.^[301-303] In these plants, RES is a secondary metabolite used as biosynthetic countermeasure against pathogenic attacks and adverse environmental conditions.^[304] Its biosynthetic pathway is derived from the conversion of *p*-coumaric acid though the phenylpropanoid pathway and hence, it can be considered a natural phenol.^[305]

Figure 26: Structures of Resveratrol (RES) and other RES metabolites



In 1992, RES was proposed as the responsible of the cardioprotective effect of red wine.^[306] Since then, many other potential beneficial effects have been proposed (see next section).

The main drawback of RES is its pharmacokinetic profile. However, the information on this aspect is in many cases contradictory and very variable. It is estimated that RES is highly

absorbed after oral consumption and rapidly metabolized (in less than 15 min) to its metabolites.^[307,308] Actually, only trace amount of free RES can be found in urine.^[309] RES-monosulphate and dihydro-RES monosulphate are the predominant metabolites in humans (around 40% of total RES), followed by isomeric forms of RES monoglucuronide and dihydro-RES monoglucuronide (around 20% of the administered RES). The rest of RES is converted to other metabolites. In general RES-metabolites have a much longer half-life than the parent molecule (9 vs 0.5 hours) and hence, they can be partially responsible for the effect of RES *in vivo*.

High doses of RES are usually well tolerated in most animal studies concluding that RES is benign even at a gram scale.^[310] However in humans, mild adverse effects can happen after administration of large quantities of RES (> 400 mg /day) including blood electrolyte changes, nasopharyngitis, rashes,^[311] increased blood bilirubin, headaches, diarrhea and acute nephrotoxicity.^[312]

1.3.2.1. Resveratrol biological effect

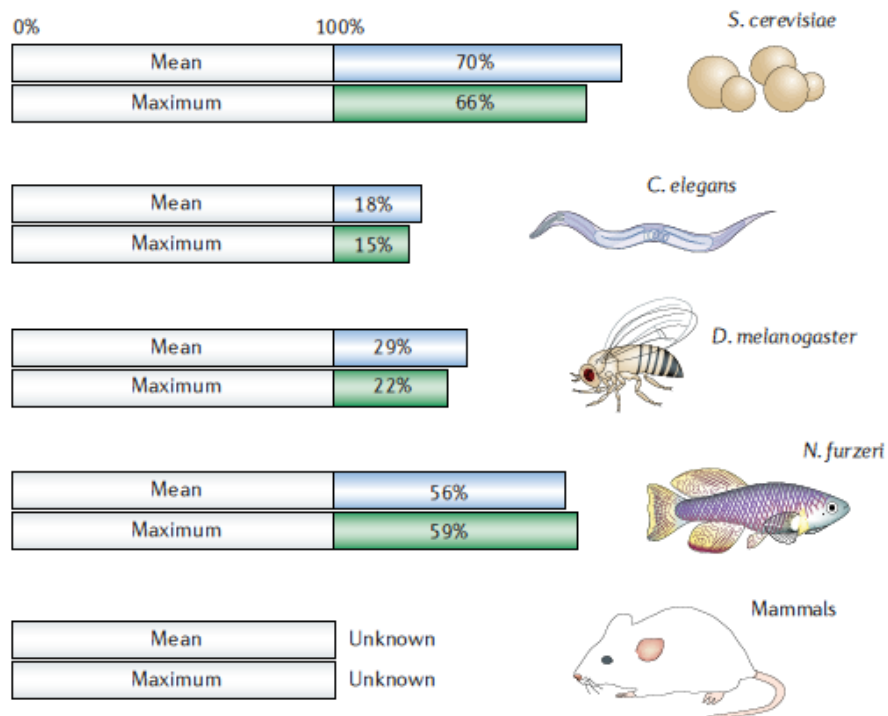
Similarly to other phenolic compounds, RES can scavenge ROS and neutralize them with hydrogen and/or electron transfers. The resulting phenoxy radicals are stabilized by the delocalization of electrons within the phenyl rings and the conjugated alkene bond.^[313] Thus, RES inhibits lipid peroxidation and preserves the cellular integrity under oxidative stress. RES has been found to reduce superoxide ions and hemoglobin oxidation,^[314,315] prevent LDL^[316] and copper-mediated oxidations,^[317] and the formation of toxic oligomers in neurodegenerative models.^[318] Furthermore, RES can relieve overwhelmed cells by allowing them time to replenish their natural ROS-countermeasures (such as GPx, GST, GR, SOD and CAT) and hence, avoid further oxidative stress damage.^[319,320]

The biological activity of RES goes much further than its antioxidant properties. Even though its implications are not fully understood, a wide range of signaling transduction pathways are affected by RES. These include modifications in the biological activities of cells such as cell growth and differentiation, apoptosis, angiogenesis and metastasis.^[321–323] RES also activates SIRT-1 and hence, it modulates essential metabolic regulatory transcription factors,^[324–327] inflammation response,^[328] and it prolongs the life span of several animals (Figure 27).^[329–331] RES is also able to protect neurons by reducing the toxicity of glutamate^[332] and calcium over exposure.^[333,334] The general neuronal state is also improved by RES through the modulation of the glucose metabolism^[335] and distribution in the CNS.^[336,337]

All these beneficiary effects have been confirmed to exert a positive effect over a wide range of pathologies including: cancer,^[338] cardiovascular diseases including antiplatelet blood-related disorders,^[301] inflammatory^[339] and neurodegenerative diseases such as Alzheimer disease (AD), Huntington’s disease (HD), Parkinson’s disease (PD) and amyotrophic lateral sclerosis (ALS).^[340]

In HD, RES has been reported to inhibit COX I in a 3-nitropropionic HD model,^[341] to protect neurons from toxicity via SIRT1 activation,^[342] to hinder p53 expression and apoptosis by modulating its acetylation^[343,344] and to reduce overall neuronal ROS damage.

Figure 27: Largest reported increases in mean and maximal lifespan for various species treated with RES. Source: J. A. Baur, D. A. Sinclair, Nature Reviews Drug Discovery 2006, 5, 493–506.



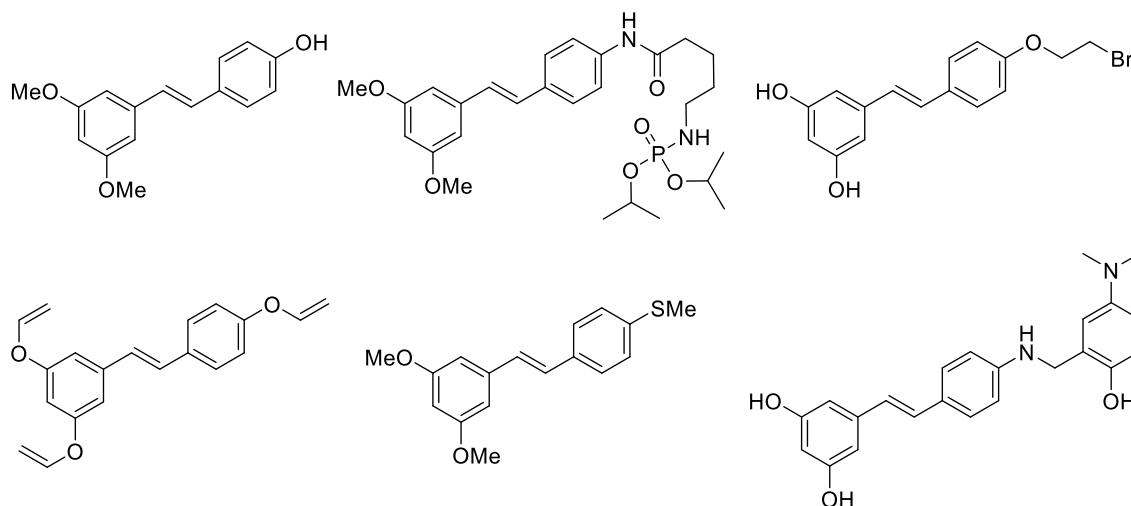
1.3.2.2. Modifications to Resveratrol

Many modifications have been applied to RES to gain effectivity, selectivity and to improve its pharmacokinetic properties. These can be classified depending on whether the modifications are made on the phenolic functional groups or over other parts of the structure.

Modifications at the phenolic groups: Modifications at the hydroxyl groups can transform the compound into a prodrug, delaying its general metabolism and improving its distribution. This is especially relevant for modifications at the 4'-OH group, which is more acidic and reactive than the other two *m*-OH groups (and used mainly for its free radical scavenging activity).^[345]

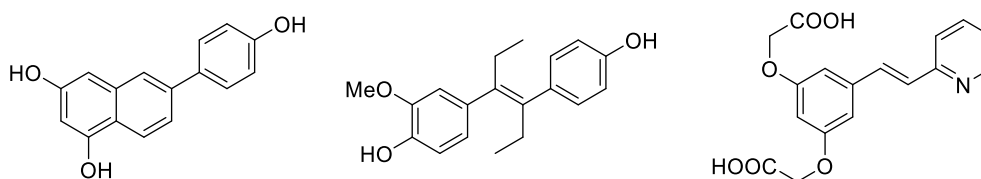
RES metabolites and other natural occurring RES derivatives - like Pterostilbene (Figure 28, compound 1)- have shown better activity than RES itself.^[346,347] *N*-phosphoryl amino acid,^[348] bromoethoxy,^[349] and allyl^[350] modifications (Figure 28) have shown to effectively improve RES anticancer properties. Methoxide and thio-methoxide modifications have been used to improve the pharmacokinetic properties and antiproliferative activity of RES.^[351] Other modifications such as 4-dimethylamino phenols are able to inhibit Cu (II) and self-induced β -amyloid protein aggregation.^[352] This last compound was able to cross the BBB *in vitro* and did not exert any acute toxicity in mice with dosages of 2000 mg/kg making it a promising candidate for *in vivo* evaluation.

Figure 28: Modifications to RES phenolic groups



Modifications of the stilbene structure: These include alterations to the aromatic cycles or the double bond of RES. Examples include rigidification of the alkene, by using a naphthalene core instead of the phenyl and alkenes groups,^[353] and the substitution of the alkene protons with ethyl groups (Figure 29).^[354] Changes to the phenolic ring with a pyridine ring also yielded improved performance than RES in several phenotypic responses.^[355]

Figure 29: Modifications to RES's phenyl and alkene groups



2. Hypothesis and Objectives

NDIs are known G4-ligands with cytotoxic effect on cancer cells. However, their target/tissue selectivity and pharmacokinetic properties can limit their use *in vivo*. To improve these properties, we have conjugated carbohydrates to the NDI core. We expected the new conjugates to display less intrinsic toxicity, improved selectivity towards cancerous cells lines and better G4-binding due to the potential sugar-groove interactions.

In parasites, especially those in the Trypanosomatide order, the relevance and incidence of G4 is unknown. Besides, a carbohydrate-drug conjugation has never been examined with the aim of taking advantage of the avidity of parasites for glucose. Thus, we have investigated the existence of G4 in the genome of several parasites and the use of the carb-NDI family as potential antiparasitic agents.

Resveratrol (RES), tyrosol (Tyr) and hydroxytyrosol (HT) are three natural products with a phenolic group in their structure which are found in different foods and plants. The three entities can be considered lead compounds due to their promising biological properties. However, they present poor bioavailability and ADME properties and therefore, further lead optimization is needed. Here, we have optimized RES, Tyr and HT to overcome their drawbacks and to improve their neuroprotective (for RES) and antiparasitic properties (for Tyr and HT). Glycosyl- and alkyl- modifications on RES, Tyr and HT have been investigated in order to improve their efficacy and druggability.

Figure 30: General scheme of the approach for the optimization of the NDI G4-ligands. The conjugates will be evaluated in phenotypic and in target based screening.

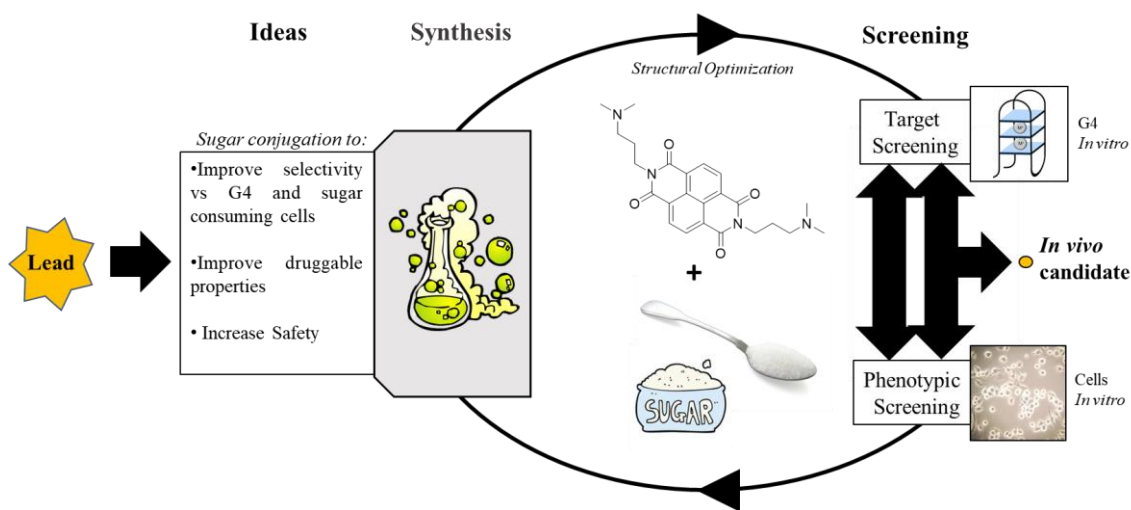
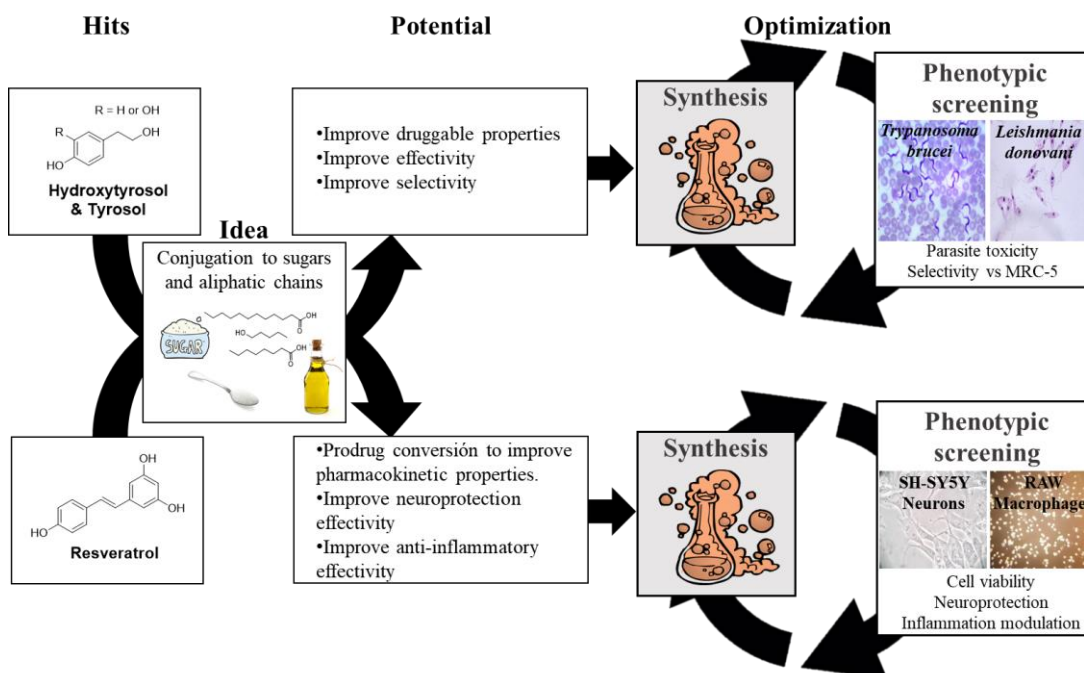


Figure 31: General scheme of the approach for the natural phenol conjugations to carbohydrates and lipophilic moieties. Hits will be optimized by iterations of chemical modifications and phenotypic screening.



The aims of this thesis are:

3. To design and synthesize:
 - a) carbohydrate conjugates of NDI G4 ligands (carb-NDIs).
 - b) glycosyl and alkyl derivatives of RES, Tyr and HT.
4. Identify new potential G-quadruplex forming sequences in the genome of parasites.
5. To measure the binding of carb-NDIs to different G4 structures.
6. To evaluate the *in vitro* biological activity of:
 - a) carb-NDIs as antiproliferative agents.
 - b) carb-NDIs as antiparasitic agents.
 - c) RES derivatives as neuroprotective agents.
 - d) Tyr and HT derivatives as antiparasitic agents.
7. To study the cellular uptake and localization of carb-NDIs within cells and parasites.
8. To evaluate the *in vivo* biological activity of RES derivatives in a Huntington's disease murine model.

3. Results

3.1. Synthesis, binding properties and difference in cell uptake of G-Quadruplex Ligands based on carbohydrate naphthalene diimide conjugates

Reference:

M. Arévalo-Ruiz, F. Doria, E. Belmonte-Reche, A. De Rache, J. Campos-Salinas, R. Lucas, E. Falomir, M. Carda, J. M. Pérez-Victoria, J.-L. Mergny, M. Freccero, J. C. Morales, *Chemistry - A European Journal* **2017**, 23, 2157–2164.

DOI:

[10.1002/chem.201604886](https://doi.org/10.1002/chem.201604886)

Supporting information:

<http://onlinelibrary.wiley.com/doi/10.1002/chem.201604886/suppinfo>

Glycoconjugates

Synthesis, Binding Properties, and Differences in Cell Uptake of G-Quadruplex Ligands Based on Carbohydrate Naphthalene Diimide Conjugates

Matilde Arévalo-Ruiz⁺,^[a] Filippo Doria⁺,^[b] Efres Belmonte-Reche,^[a] Aurore De Rache,^[c] Jenny Campos-Salinas,^[a] Ricardo Lucas,^[a] Eva Falomir,^[d] Miguel Carda,^[d] José María Pérez-Victoria,^[a] Jean-Louis Mergny,^[c] Mauro Freccero,^{*,[b]} and Juan Carlos Morales^{*,[a]}

Abstract: The G-quadruplexes (G4s) are currently being explored as therapeutic targets in cancer and other pathologies. Six carbohydrate naphthalene diimide conjugates (carb-NDIs) have been synthesized as G4 ligands to investigate their potential selectivity in G4 binding and cell penetration. Carb-NDIs have shown certain selectivity for G4 structures against DNA duplexes, but different sugar moieties do not induce a preference for a specific G4 topology. Interestingly, when monosaccharides were attached through

a short ethylene linker to the NDI scaffold, their cellular uptake was two- to threefold more efficient than that when the sugar was directly attached through its anomeric position. Moreover, a correlation between more efficient cell uptake of these carb-NDIs and their higher toxicity in cancerous cell lines has been observed. Carb-NDIs seem to be mainly translocated into cancer cells through glucose transporters (GLUT), of which GLUT4 plays a major role.

Introduction

The G-quadruplexes (G4s) are noncanonical higher-order nucleic acid structures that form on repeats of short guanine (G) tracts. Their recurrent structural motif is made by a planar arrangement of four strands of G bases stacked upon one another with a monovalent cation between them.^[1] Currently, G4s are viewed as emerging therapeutic targets in cancer,^[2] as well as in neurological disorders^[3] and viral infections.^[4] The central hypothesis of the field is that stabilizing a promoter G4

through small-molecule binding results in inhibition of the transcriptional machinery and downregulation of expression of the target gene.^[5] However, several important challenges remain if G4 ligands are to be therapeutically useful compounds, including selectivity against much more abundant double-stranded DNA, selectivity between different G4 structures, and/or topologies and selectivity towards cellular targets.

We previously studied carbohydrate–DNA interactions in double helices and in G4 by using carbohydrate oligonucleotide conjugates.^[6] We found that carbohydrate–thrombin-binding aptamer conjugates showed stacking interactions between the sugar and a DNA guanine tetrad together with hydrogen bonding and hydrophobic contacts.^[7] Di Antonio et al. explored this possibility by conjugation of neutral carbohydrates to G4 ligands, resulting in the identification of stronger and more selective DNA G4 binders.^[8] Similarly, isoflavones, such as glycosidic daidzin, were reported as G4 ligands capable of inducing a structural change of the polymorphic human telomeric (hTel) G4 into its antiparallel conformation.^[9] Recently, *N*-phenanthroline glycosylamine copper(II) complexes have been reported to bind hTel with an important contribution of groove and/or loop contacts.^[10] Amino sugars, such as neomycin, have also been attached to different aromatic rings to prepare G4 ligands.^[11]

In the last decade, a large number of studies have exploited the naphthalene diimide (NDI) moiety as a G4-binding motif, taking advantage of its synthetic accessibility, optoelectronic,^[12] G4 binding,^[13] and sensing properties.^[14] Tri- and tetrasubstituted NDIs have been broadly explored NDIs due to their potency

[a] M. Arévalo-Ruiz,⁺ E. Belmonte-Reche, Dr. J. Campos-Salinas, Dr. R. Lucas, Dr. J. M. Pérez-Victoria, Dr. J. C. Morales
Department of Biochemistry and Molecular Pharmacology
Instituto de Parasitología y Biomedicina, CSIC
Parque Tecnológico Ciencias de la Salud
Avenida del Conocimiento, s/n, 18016 Armilla, Granada (Spain)
E-mail: jcmorales@ipb.csic.es

[b] Dr. F. Doria,⁺ Prof. M. Freccero
Department of Chemistry, University of Pavia
V.le Taramelli 10, 27100 Pavia (Italy)
E-mail: mauro.freccero@unipv.it

[c] Dr. A. De Rache, Dr. J.-L. Mergny
Institut Européen de Chimie Biologie (IECB)
ARNA Laboratory, Université de Bordeaux
Inserm U1212, CNRS UMR5320, 2, rue Robert Escarpit, Pessac (France)

[d] Dr. E. Falomir, Dr. M. Carda
Department of Inorganic and Organic Chemistry
University Jaume I, 12071 Castellón (Spain)

[*] These authors contributed equally to this work.

Supporting information and the ORCID identification numbers for the authors of this article can be found under <http://dx.doi.org/10.1002/chem.201604886>.

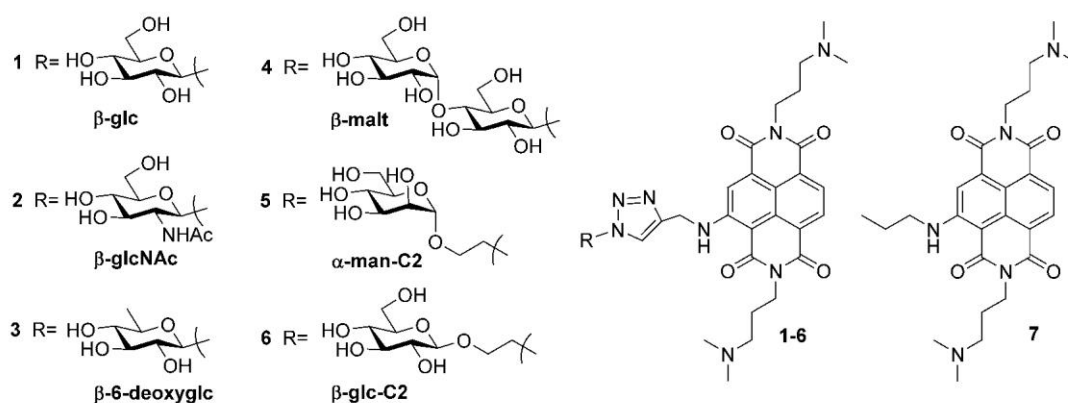


Figure 1. Carb-NDI conjugates 1–6 prepared and investigated in this work together with the aglycone NDI 7.

and duplex versus G4 selectivity, and have proven to be effective cores for multimodal reactive^[15] and photoreactive NDI conjugates,^[16] and even targeting human medullary thyroid cancer.^[17] Tetrasubstituted NDIs have shown bimodal fluorescence and photocytotoxicity,^[18] high affinity for hTel G4 DNA,^[19] antiproliferative potency in pancreatic cancer cells^[13c,20] and inhibition of telomerase activity.^[21]

Herein, we have designed and synthesized a family of carbohydrate–G4 ligand conjugates based on a substituted naphthalene diimide scaffold (carb-NDIs; Figure 1). By sugar conjugation to discharged substituted NDIs, we reduced the overall positive charge in comparison to that of previously investigated tri- and tetracharged substituted NDIs, preserving their solubility and the fluorescence emission of the NDI core, with absorbance and emission maxima centered at 595 and 661 nm, respectively.^[12a] We selected to attach glucose in different presentations (β -glc, β -glcC2, and β -malt) and three other monosaccharides (β -glcNAc, β -6deoxyglc, and α -manC2) to discharged substituted NDIs to explore their potentially different binding to G4 targets and their different capacities to be transported through glucose transporters (GLUTs).

From this conjugation, we expected to increase compound solubility and bioavailability, improve G4 binding through sugar-mediated interactions to the phosphates and G4 DNA grooves, and finally promote selective entrance into tumor cells through overexpressed GLUT. This approach has been explored in other cytotoxic drugs by taking advantage of the Warburg effect and energy requirements for rapid growth displayed by aggressive cancerous cells.^[22] Examples include glucose–paclitaxel,^[23] 2-amino-2-deoxyglucose adriamycin,^[24] glucose–lactate dehydrogenase inhibitors,^[25] glucose–platinum conjugates,^[26] and glufosfamide,^[27] which has recently advanced to metastatic pancreatic cancer phase III clinical trials.

Results and Discussion

Design and synthesis of NDI carbohydrate conjugates

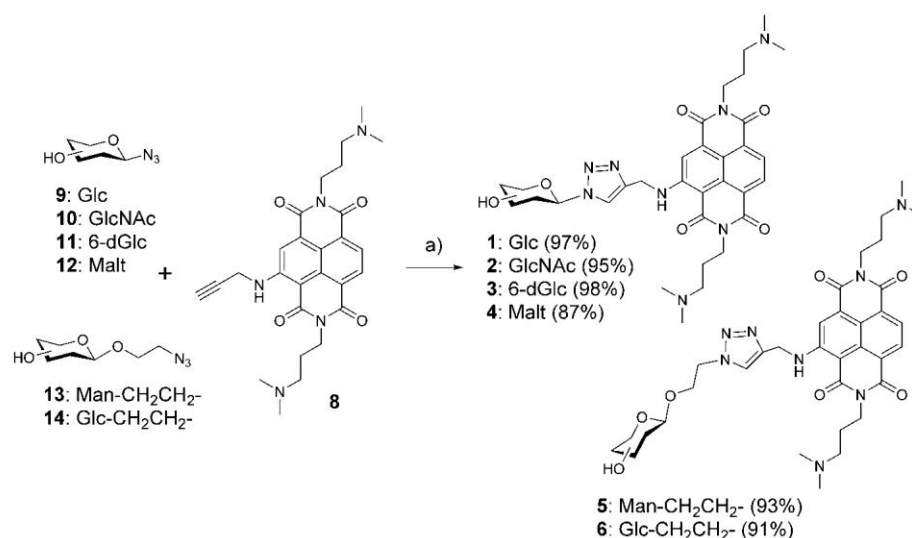
The syntheses of new carbohydrate–triazole–NDI conjugates 1–6 were carried out by using copper(I)-catalyzed azide–alkyne cycloaddition (CuAAC) click chemistry. A series of azido glyco-

sides building blocks with focused structural diversity were initially synthesized and then clicked onto 2-*N*-propargyl naphthalene diimide **8** (Scheme 1). The preparation of **8** relies on the imidation of commercially available 2,6-dibromo-1,4,5,8-naphthalenetetracarboxylic dianhydride by *N,N*-dimethyl-1,3-propanediamine, giving quantitatively the *N,N*-bis[(dimethylamino)propylamino]-2,6-di-bromo-1,4,5,8-naphthalenetetracarboxylic bisimide (Scheme S1 in the Supporting Information). Subsequent nucleophilic aromatic substitution (S_NAr) in the presence of an excess (2.5 equiv) of propargylamine (CH_3CN as solvent, 75 °C, 4.5 h) afforded **8** as the only product with quantitative conversion. Azido glycosides and 2-azidoethyl glycosides were synthesized as described previously.^[28] Briefly, acetobromo sugars reacted with sodium azide and subsequent removal of protecting groups under basic conditions yielded the corresponding azido glycosides. The 2-azidoethyl glycosides were obtained through glycosylation with 2-bromoethanol, followed by reaction with sodium azide, and treatment with sodium methoxide.^[29] Carb-NDIs 1–6 were synthesized by copper(I)-catalyzed Huisgen 1,3-dipolar cycloaddition between **8** and azide building blocks 9–14 (Scheme 1). The click reaction was performed under standard conditions by using $CuSO_4 \cdot 5H_2O$ and sodium ascorbate in a mixture of $tBuOH/H_2O$ (1:1) with stirring for 2 h at RT under a nitrogen atmosphere. The reactions proceeded smoothly and the final carb-NDI derivatives were purified by preparative HPLC. Aglycone NDI **7** was prepared as a reference ligand to compare the biophysical and biological properties of the new carb-NDI conjugates with a sugar-free NDI analogue (see Scheme S2 in the Supporting Information).

G4 binding studies

FRET melting assays

The binding of ligands 1–7 to the G4 structures was first investigated by using FRET-based melting assays on the F21T human DNA telomeric oligonucleotide^[30] in the presence of K^+ (Figure 2a). All ligands induced an increase of the melting temperature ($T_{1/2}$) of the G4 structure. This stabilization is expressed as the difference in melting temperature with and without ligand ($\Delta T_{1/2}$). The NDI–sugar conjugates had an



Scheme 1. Synthesis of the new carb-NDI conjugates **1–6** through the CuAAC reaction: a) sodium ascorbate, CuSO₄, tBuOH/H₂O (1:1), RT.

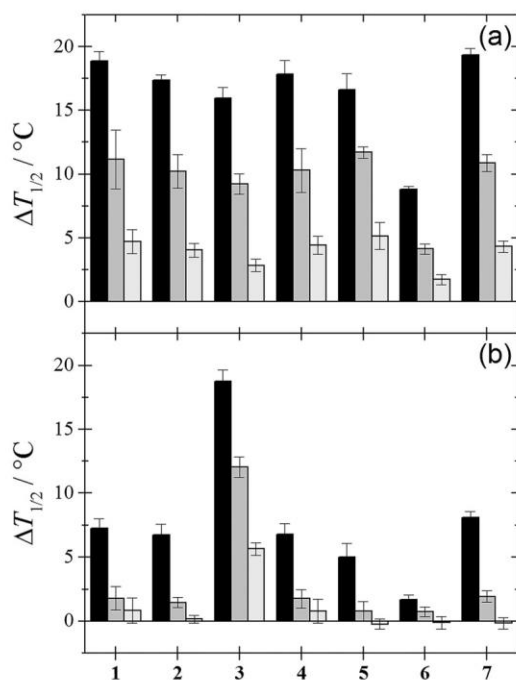


Figure 2. FRET melting competition assay results. Thermal stabilization induced by the tested compounds (2 μM) on the hTel quadruplex F21T (0.2 μM) in 10 mM lithium cacodylate pH 7.2 containing: a) 10 mM KCl and 90 mM LiCl, or b) 100 mM NaCl. The duplex competitor (ds26) strand concentrations were 0 (black), 3 (gray), and 10 μM (light gray).

important stabilization effect on the F21T G4, with $\Delta T_{1/2}$ values close to 20 °C at 2 μM compound concentration, which was almost identical to stabilization induced by control ligand **7** lacking a carbohydrate in its structure. Therefore, with the exception of compound **6**, the sugar moiety did not introduce any detrimental effects on G4 stabilization. Carb-NDI $\Delta T_{1/2}$ values were slightly lower than the $\Delta T_{1/2}$ values reported previously for trisubstituted NDIs with a conjugated Mannich base ($\Delta T_{1/2} = 22$ °C)^[31] or charged tertiary amines under physiological

conditions ($\Delta T_{1/2} = 26$ °C). Nevertheless, a direct comparison of our $\Delta T_{1/2}$ values and literature results can be misleading because different ligand and K⁺ concentrations have been used.

In the presence of 3 μM duplex competitor (15 equiv), the induced stabilization dropped by approximately 6 °C for all ligands. With 10 μM competitor (50 equiv), the induced stabilization was even lower, but remained significant. These results demonstrate some selectivity of the ligands for G4 against DNA duplexes. This selectivity was confirmed by using a variety of labeled oligonucleotides (see below).

The hTel sequence is known to adopt different conformations in Na⁺ (antiparallel)^[32] and K⁺ media (parallel,^[33] antiparallel,^[34] hybrid, or [3+1]^[35]). Hence, G4 stabilization values were also calculated in the presence of Na⁺ as an initial indication of ligand G4 topology selectivity (Figure 2b). All ligands showed significantly lower Na⁺ $\Delta T_{1/2}$ values than those observed in K⁺, which suggested that the compound-induced stabilization depended on the G4 topology.

To provide further insight into the structural dependencies of ligand binding, FRET melting selectivity profiles (Figure 3) were built from the $\Delta T_{1/2}$ values obtained with a set of sequences that included a duplex and five G4s (Table 1 and Figure S1 in the Supporting Information).^[36] The choice of oligonucleotide sequences aimed to represent the structural and topological diversity of G4. Duplex sequence (FdxT) stabilization was negligible for all ligands, in comparison to that of the studied G4, which was in agreement with the results obtained in the competitive assay. No clear selectivity was observed for a given target, although compounds **1–6** showed higher stabilization of the polymorphic human telomere G4 structures.

Circular dichroism (CD) titrations

FRET melting experiments showed the highest thermal stabilization was observed on the polymorphic hTel sequence F21T. To assess whether the observed stabilization was due to an

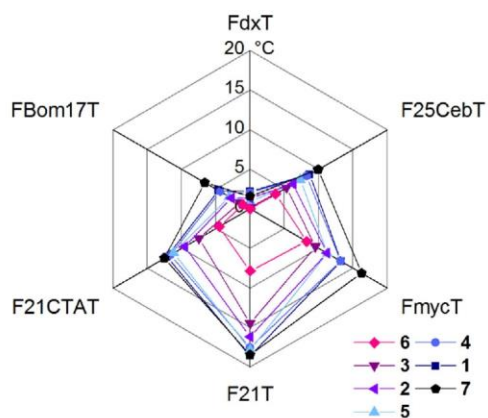


Figure 3. Selectivity profile results determined by FRET melting stabilization induced by the tested compounds (2 μM) on G4s of various topologies in 10 mM lithium cacodylate, pH 7.2, containing 10 mM KCl and 90 mM LiCl. Details of the sequences and structures of G4s used are provided in Table S1 in the Supporting Information.

Compound	Cell line		
	HT-29	MCF-7	MRC-5
1	453 \pm 65 (30%)	526 \pm 120 (28%)	236 \pm 53 (13%)
5	1093 \pm 159 (73%)	439 \pm 159 (23%)	545 \pm 176 (30%)
6	988 \pm 121 (66%)	762 \pm 241 (41%)	778 \pm 269 (43%)
7	1492 \pm 508 (100%)	1858 \pm 239 (100%)	1773 \pm 98 (100%)

[a] 225 000 cells were incubated with 5 μM of each NDI compound in medium (750 μL) for 2 h at 37 $^{\circ}\text{C}$. After centrifugation, supernatant removal, and washing, the cell pellet was resuspended in 0.4% sodium dodecyl sulfate (SDS; 750 μL) and homogenized. Fluorescence values were normalized through a protein quantification assay by using Pierce BCA tests (ThermoFisher Scientific) and concentration values were extrapolated from a fluorescence–NDI concentration calibration curve.

interaction with G4 (and not to the fluorescent dyes), we performed CD titrations on the unlabeled 21g sequence (d-(GGGTTA)₃GGG) with ligands **1**, **4**, **6**, and **7** (Figure 4). In all four cases, the interaction of the ligand with 21g was evidenced by an intensity increase of the $\lambda = 287$ nm positive band (typical of [3+1] topology), without any change in G4 folding. This is an interesting aspect that differentiates carb-NDIs from other NDIs, such as trisubstituted NDIs embedding amines, because the latter had a tendency to induce partial refolding into a parallel topology.^[31] Furthermore, no free-ligand CD signature was observed at this wavelength (Figure S2 in the Supporting Information), which confirmed that the observed CD changes reflected an interaction between the ligands and G4 structure formed by the 21g sequence.

Biological studies

Cell uptake studies

We selected three structurally different NDI derivatives—**1**, with a sugar directly attached to the azide unit; **5**, with a man-

nose linked through a spacer; and **7**, with no attached carbohydrate—to study their entrance within two cancer cell lines (human colon adenocarcinoma HT-29 and breast adenocarcinoma MCF-7) and a noncancerous cell line (human lung fibroblast MRC-5). We took advantage of the red fluorescent emission of NDI derivatives **1–7** to monitor their cell entry. By using flow cytometry and incubating these cell lines at different NDI–ligand concentrations (1 and 5 μM), different times (5 min, 1 h, 2 h, and 4 h), and two temperatures (4 and 37 $^{\circ}\text{C}$), we detected the quick entrance of sugar-free NDI **7** in all cell lines, independent of the temperature and times assayed (similar uptake at 4 $^{\circ}\text{C}$ after 5 min and at 37 $^{\circ}\text{C}$ after 4 h; Figure 5 and Figures S3–S6 in the Supporting Information); this suggested uptake by passive diffusion or facilitated transport. In contrast, at 4 $^{\circ}\text{C}$, NDI **1** barely penetrated into the cells, whereas **5** was incorporated slightly better because it was more efficient in its cellular transport. When the temperature was increased to 37 $^{\circ}\text{C}$, ligands **1** and **5** were incorporated much more efficiently than at 4 $^{\circ}\text{C}$; this indicated a temperature-dependent mechanism of cell uptake operating in the process. Moreover, NDI **5** seems to enter the cells more efficiently than NDI **1**.

We carried out intracellular quantification of **1**, **5**, **6**, and **7** to confirm the apparent differences observed in cellular uptake among the three ligands. Fluorescence spectroscopy measurements were made directly by irradiating the red dye at $\lambda = 485$ nm and recording its emission at $\lambda = 535$ nm after incubation with the compounds (5 μM) for 2 h (Table 1). As expected from the flow cytometry studies, we observed higher intracellular concentrations of control **7** than those of **1**, **5**, and **6** in all three cell lines examined. At the same time, cellular uptake of **5** and **6** was considerably more efficient (two- to threefold) than that for **1**. Compounds **5** and **6** both comprise a monosaccharide linked through an ethylene glycol spacer to the azide–NDI scaffold, whereas **1** has glucose directly linked to the azide–NDI structure; this confirms the tendency observed by flow cytometry on HT-29 and MRC-5 cells, but not on MCF-7 cells (0.8- to 1.4-fold). Our results are in contrast with recent studies by Patra et al.,^[26b] who used glucose–platinum conjugates. Contrary to our findings, they concluded that increasing the length of the linker decreased cell uptake. However, the different nature of the core and different dimensions may also influence the transport mechanism and could explain these divergent results.

GLUTs are likely to be proteins associated with the cellular transport of the carb-NDI ligands. Thus, we examined this possibility by quantifying the entrance of carb-NDIs (**1**, **5**, and **6**) and control **7** into cancerous HT-29 cells in the absence or presence of several GLUT inhibitors, including WZB117, a specific GLUT1 inhibitor;^[37] ritonavir, a specific GLUT4 inhibitor;^[38] and flavonoids quercetin and genistein, which are reported to be dual GLUT1 and GLUT4 inhibitors.^[39] We observed clear cell uptake inhibition for **1**, **5**, and **6** (35–64% inhibition) when quercetin was used as an inhibitor (Figure 6 and Figure S7 in the Supporting Information). A smaller but similar effect was also perceived with genistein, another GLUT1 and GLUT4 inhibitor, which decreased carb-NDI uptake by 43–44% for compounds **5** and **6**. This inhibition was not observed for

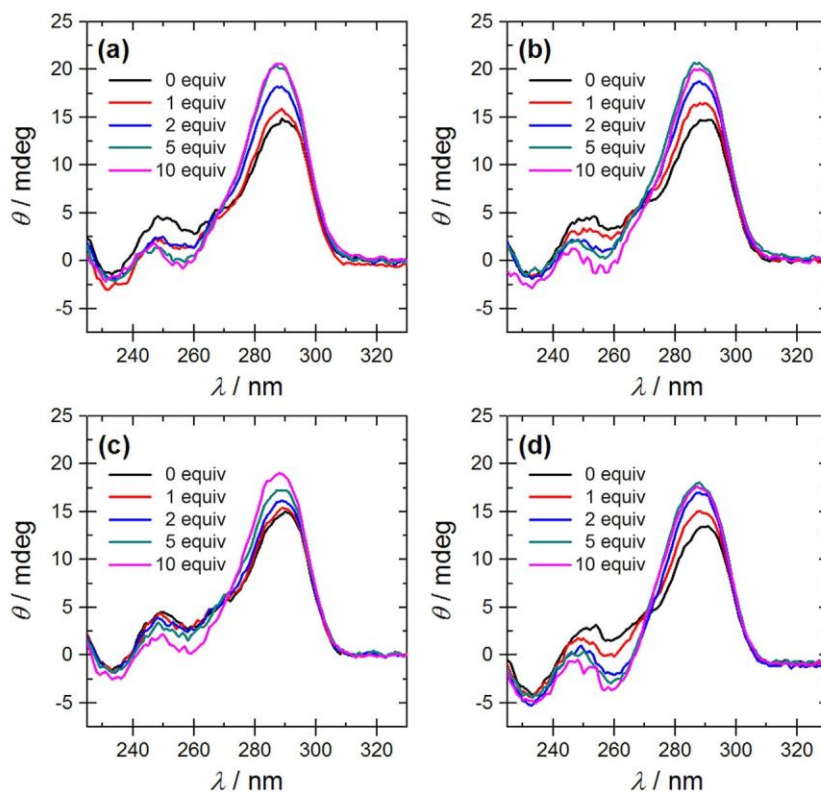


Figure 4. CD titration of 21g with compounds: a) 1, b) 4, c) 6, and d) 7. The oligonucleotide concentration was 4 μM .

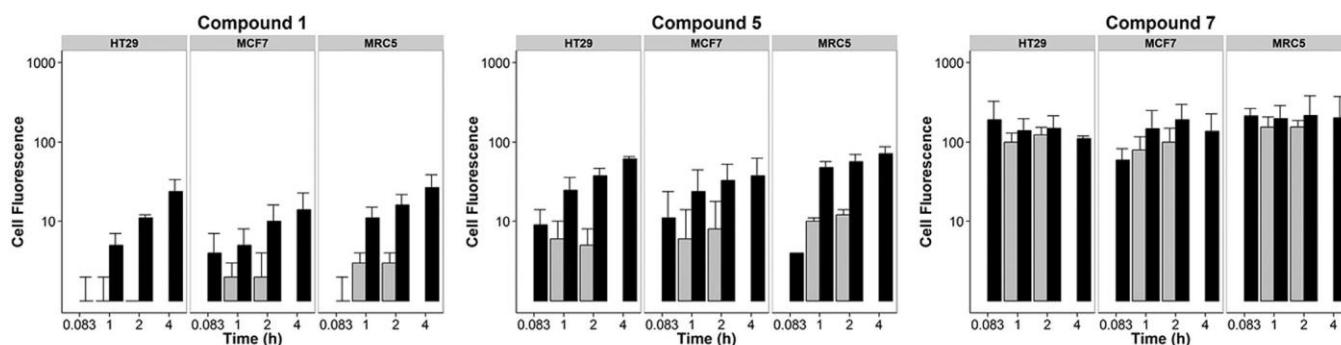


Figure 5. The mean fluorescence intensity of 1, 5, and 7 incubated at a concentration of 5 μM with various cancer and normal cell lines for 5 min, 1, 2, and 4 h, as measured by flow cytometry. Bars in gray, $T=4^\circ\text{C}$; bars in black, $T=37^\circ\text{C}$.

Inhibitor	Glut Target	HT29-uptake Inhibition (%)				Inhibition (%)	
		Prop-NDI 7	glc-NDI 1	manC2-NDI 5	glcC2-NDI 6		
ZWB117	Glut 1	○ 20	○ -19	○ 7	○ 18	% < 25	○ Small
Quercetin	Glut 1 & 4	○ 24	● 54	● 35	● 64	25 > % > 40	● Medium
Genistein	Glut 1 & 4	○ 9	○ 17	● 43	● 44	% > 40	● High
Ritonavir	Glut 4	○ 8	○ 0	● 28	● 59		

Figure 6. Cell uptake inhibition in HT-29 cancer cells of 1, 5, 6, and 7 in the presence of several GLUT inhibitors, as determined by intracellular concentration measured by means of fluorescence spectroscopy. Preincubation with inhibitors (100 μM) for 1 h was followed by incubation with NDI compounds (5 μM) for 2 h.

compound **1**, in which the carbohydrate is directly linked to the NDI-azide scaffold. Unexpectedly, the presence of the specific GLUT1 inhibitor WZB117 yielded no significant cell uptake differences, with inhibitor-free control for all carb-NDIs examined. In addition, NDI **7** showed a small cell uptake inhibition (8–24%) in the presence of the GLUT inhibitors examined. This small effect was previously reported for other aglycone drugs, such as cyclohexane-1,2-diamine platinum derivatives, when their cell uptake was assayed in the presence of phloretin or 4,5-*O*-ethylidene- α -D-glucose GLUT inhibitors.^[26b]

To confirm that GLUT4 played an important role in the cell uptake of **5** and **6**, we carried out cell uptake inhibition assays in the presence of the specific GLUT4 inhibitor ritonavir (Figure 6). Cellular uptakes of compounds **5** and **6**, in particular, decreased, without affecting either **1** or control **7**. Our results reveal the main role of GLUT4 translocating compounds **5** and **6**, which contain mannose and glucose, respectively, attached through a short linker to the azide-NDI scaffold. GLUT1, which was previously identified as the main GLUT involved in cellular uptake of other glucose-conjugated drugs, seemed to be playing a minor role, if any, in translocating **5** and **6**. It is important to note that the functional groups, as well as the size and shape of the attached drug, may also have a strong influence on the interaction with GLUT and its resulting translocation process. Moreover, other GLUT isoforms could also be involved in the cell uptake of these carbohydrate-conjugated G4 ligands; this is especially pertinent for **1**, which possesses glucose directly linked to the azide-NDI structure.

When we examined the influence of GLUT inhibitors in cell uptake of NDI derivatives **1**, **5**, **6**, and **7** in noncancerous MRC-5 cells (Figures S7 and S8 in the Supporting Information), we observed no inhibition with any of the GLUT inhibitors tested. The exception was **5**, which was partially inhibited by querce-

tin and genistein (28–37%). These results seem to correlate with the overexpression of GLUTs in cell membranes of cancerous cells, such as HT-29, in comparison to smaller expression in noncancerous cells, such as MRC-5.

Confocal microscopy analysis was used to determine the localization of NDI derivatives **1**, **5**, **6**, and **7** in HT-29 and MRC-5 cells. After incubation at 37 °C for 2 h, all four compounds were detected inside the cells and were mostly localized in the nucleus (see Figure 7 for **5** and Figures S8–S10 in the Supporting Information).

These experiments confirm that glycoconjugated NDIs may reach their DNA G4 target within the nuclear genome. Similar results were found with control **7**, in agreement with the location of other reported NDI derivatives, such as Neidle's tetra-charged NDI MM41.^[18,20] It is important to note that our carbohydrate-modified NDIs possess only two positively charged groups and still locate at the nucleus.

In vitro antiproliferative studies

The *in vitro* antiproliferative activity of compounds **1–7** was measured by using the 3-(4,5-dimethylthiazol-2-yl)-2,5-diphenyltetrazolium bromide (MTT) methodology against three cancer cell lines, HT-29, MCF-7, and HeLa (cervical cancer), together with a noncancerous cell line, MRC-5 (Table 2). NDI **7** with no carbohydrate in its structure displayed the lowest IC₅₀ values in all cancerous cell lines (0.13–0.29 μ M), closely followed by ethyl-linked mannose and glucose carb-NDIs **5** and **6** (0.15–0.42 μ M) and spacer-free 6-deoxyglucose carb-NDI **3** (0.35–0.69 μ M). Carb-NDIs (**1**, **3**, **5**, and **6**) and control **7** displayed less toxicity for the noncancerous cell line within a factor of 1.4- to 6.5-fold.

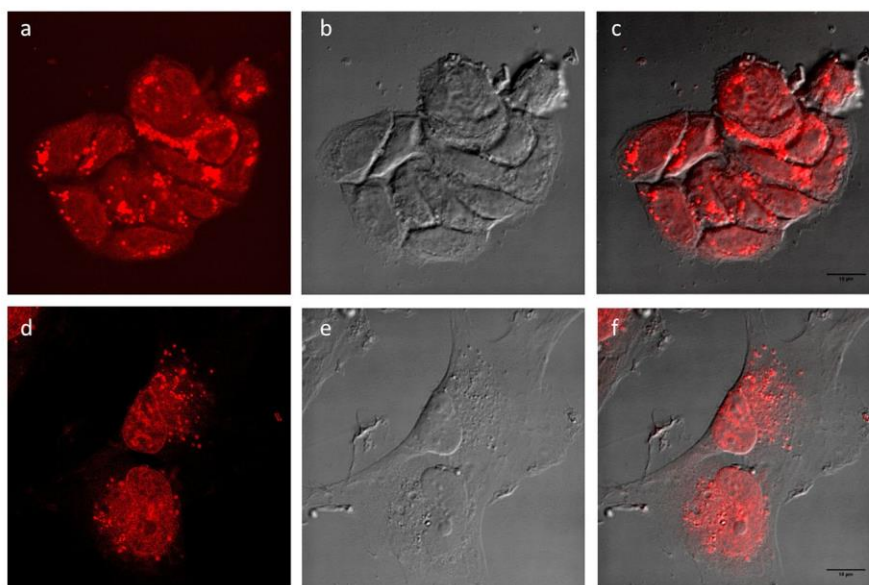


Figure 7. Confocal images of HT-29 and MRC-5 cells after co-incubation with **5** (5 μ M) for 2 h. HT-29 cells: a) fluorescence image of **5**, b) transmitted light image (differential interference contrast (DIC)), and c) merged image; MRC-5 cells: d) fluorescence image of compound **5**, e) transmitted light image (DIC), and f) merged image. Scale bar: 10 μ m.

Table 2. IC₅₀ values (μM ± standard deviation) of compounds 1–7 measured in different cell lines.

Compound	HT-29	MCF-7	HeLa	MRC-5
1	2.92 ± 0.48	1.19 ± 0.31	1.56 ± 0.70	1.15 ± 0.29
2	2.26 ± 1.03	1.06 ± 0.01	0.95 ± 0.76	0.51 ± 0.01
3	0.40 ± 0.08	0.69 ± 0.71	0.35 ± 0.05	0.91 ± 0.32
4	1.85 ± 0.19	1.42 ± 0.38	0.54 ± 0.34	2.04 ± 0.05
5	0.42 ± 0.05	0.15 ± 0.04	0.29 ± 0.14	0.81 ± 0.44
6	0.36 ± 0.13	0.24 ± 0.16	0.24 ± 0.03	0.71 ± 0.25
7	0.12 ± 0.02	0.13 ± 0.07	0.29 ± 0.18	0.36 ± 0.16

Moreover, the presence of the carbohydrate reduced the toxicity in MRC-5 cells (up to fivefold for **4**) compared with that of **7**, which was the most toxic compound of the series.

Whereas important cell uptake differences were observed between control **7** and glycoconjugated NDI derivatives **1–6**, there was no clear correlation with the IC₅₀ values. However, when comparing the sugar-derived NDIs, some correlation is observed. Cell uptake of **6** into HT-29 and MCF-7 cells, which was two- to threefold more efficient than that for **1**, correlated with the 5.7- to eightfold higher cytotoxicity IC₅₀ values.

Conclusions

Novel carb-NDIs **1–6** were designed and synthesized. We observed that the presence of the sugar in carb-NDIs was not detrimental to G4 binding and they showed some selectivity against DNA duplexes. However, no clear selectivity for a given G4 topology was observed, although compounds **1–6** showed higher stabilization of the polymorphic human telomere G4 structures. Moreover, different sugar units affected the global G4 stabilization, without changing the overall selectivity profile. Cell uptake studies revealed fast cell penetration of aglycone NDI **7** in a non-temperature-dependent manner, whereas the uptake mechanism of carb-NDIs was found to be very different; these compounds were mainly transported through GLUT and dependent on time, temperature, type of carbohydrate, and sugar accessibility. Additionally, carb-NDI cell uptake correlated to some extent with their cytotoxicity properties, as observed for **6**, which entered the cells more efficiently and was significantly more toxic in both HT-29 and MCF-7 cells than **1**. Selectivity towards cancerous cell lines also seemed to be dependent on sugar type and attachment, resulting in punctual selectivity gain compared with that of aglycone-NDI **7**. Notably, cell uptake studies in the presence of a variety of GLUT inhibitors showed that **5** and **6** were transported at least partially through GLUT4. Finally, confocal microscopy studies confirmed that carb-NDIs could reach the nucleus where their intended genomic G4 DNA targets were located.

Acknowledgements

Financial support from the Spanish Ministerio de Economía y Competitividad (CTQ2012-35360, CTQ2015-64275-P, and

SAF2016-80228-R), Junta de Andalucía (BIO1786), Worldwide Cancer Research Foundation (16-0290), Italian Association for Cancer Research (AIRC, IG2013-14708), Agence Nationale de la Recherche (ANR Quarpdiem, ANR-12-BSV8-0008-01), and FEDER funds from the EU are gratefully acknowledged. M.A.R. thanks the Ministerio de Educación for a FPU predoctoral fellowship. A.D.R. is the recipient of an ANRS postdoctoral fellowship. We also thank Aurore Guédin for helpful advice.

Keywords: cancer · carbohydrates · glycoconjugates · G-quadruplexes · structure–activity relationships

- [1] J. T. Davis, *Angew. Chem. Int. Ed.* **2004**, *43*, 668–698; *Angew. Chem.* **2004**, *116*, 684–716.
- [2] S. Balasubramanian, L. H. Hurley, S. Neidle, *Nat. Rev. Drug Discov.* **2011**, *10*, 261–275.
- [3] a) K. Zhang, C. J. Donnelly, A. R. Haeusler, J. C. Grima, J. B. Machamer, P. Steinwald, E. L. Daley, S. J. Miller, K. M. Cunningham, S. Vidensky, S. Gupta, M. A. Thomas, I. Hong, S. L. Chiu, R. L. Haganir, L. W. Ostrow, M. J. Matunis, J. Wang, R. Sattler, T. E. Lloyd, J. D. Rothstein, *Nature* **2015**, *525*, 56–61; b) A. Kovanda, M. Zalar, P. Sket, J. Plavec, B. Rogelj, *Sci. Rep.* **2015**, *5*, 17944.
- [4] a) R. Perrone, M. Nadai, I. Frasson, J. A. Poe, E. Butovskaya, T. E. Smithgall, M. Palumbo, G. Palu, S. N. Richter, *J. Med. Chem.* **2013**, *56*, 6521–6530; b) A. Rajendran, M. Endo, K. Hidaka, P. L. Tran, J. L. Mergny, R. J. Gorelick, H. Sugiyama, *J. Am. Chem. Soc.* **2013**, *135*, 18575–18585; c) S. Amrane, A. Kerkour, A. Bedrat, B. Vialet, M. L. Andreola, J. L. Mergny, *J. Am. Chem. Soc.* **2014**, *136*, 5249–5252; d) S. Artusi, M. Nadai, R. Perrone, M. A. Biasolo, G. Palu, L. Flamand, A. Calistri, S. N. Richter, *Antiviral Res.* **2015**, *118*, 123–131.
- [5] S. A. Ohnmacht, S. Neidle, *Bioorg. Med. Chem. Lett.* **2014**, *24*, 2602–2612.
- [6] a) R. Lucas, I. Gómez-Pinto, A. Aviñó, J. J. Reina, R. Eritja, C. González, J. C. Morales, *J. Am. Chem. Soc.* **2011**, *133*, 1909–1916; b) R. Lucas, E. Vengut-Climent, I. Gómez-Pinto, A. Aviñó, R. Eritja, C. González, J. C. Morales, *Chem. Commun.* **2012**, *48*, 2991–2993.
- [7] I. Gómez-Pinto, E. Vengut-Climent, R. Lucas, A. Aviñó, R. Eritja, C. González, J. C. Morales, *Chem. Eur. J.* **2013**, *19*, 1920–1927.
- [8] M. Di Antonio, G. Biffi, A. Mariani, E. A. Raiber, R. Rodríguez, S. Balasubramanian, *Angew. Chem. Int. Ed.* **2012**, *51*, 11073–11078; *Angew. Chem.* **2012**, *124*, 11235–11240.
- [9] J. L. Zhang, Y. Fu, L. Zheng, W. Li, H. Li, Q. Sun, Y. Xiao, F. Geng, *Nucleic Acids Res.* **2009**, *37*, 2471–2482.
- [10] K. Duskova, S. Sierra, M. S. Arias-Perez, L. Gude, *Bioorg. Med. Chem.* **2016**, *24*, 33–41.
- [11] a) M. Kaiser, A. De Cian, M. Sainlos, C. Renner, J. L. Mergny, M. P. Teulade-Fichou, *Org. Biomol. Chem.* **2006**, *4*, 1049–1057; b) L. Xue, N. Ranjan, D. P. Arya, *Biochemistry* **2011**, *50*, 2838–2849; c) N. Ranjan, E. Davis, L. Xue, D. P. Arya, *Chem. Commun.* **2013**, *49*, 5796–5798.
- [12] a) F. Doria, I. Manet, V. Grande, S. Monti, M. Freccero, *J. Org. Chem.* **2013**, *78*, 8065–8073; b) F. Doria, C. M. Gallati, M. Freccero, *Org. Biomol. Chem.* **2013**, *11*, 7838–7842.
- [13] a) F. Cuenca, O. Greciano, M. Gunaratnam, S. Haider, D. Munnur, R. Nanjunda, W. D. Wilson, S. Neidle, *Bioorg. Med. Chem. Lett.* **2008**, *18*, 1668–1673; b) R. Perrone, F. Doria, E. Butovskaya, I. Frasson, S. Botti, M. Scalabrin, S. Lago, V. Grande, M. Nadai, M. Freccero, S. N. Richter, *J. Med. Chem.* **2015**, *58*, 9639–9652; c) M. Micco, G. W. Collie, A. G. Dale, S. A. Ohnmacht, I. Pazitna, M. Gunaratnam, A. P. Reszka, S. Neidle, *J. Med. Chem.* **2013**, *56*, 2959–2974.
- [14] a) F. Doria, A. Oppi, F. Manoli, S. Botti, N. Kandoth, V. Grande, I. Manet, M. Freccero, *Chem. Commun.* **2015**, *51*, 9105–9108; b) M. Zuffo, F. Doria, V. Spalluto, S. Ladame, M. Freccero, *Chem. Eur. J.* **2015**, *21*, 17596–17600; c) F. Doria, M. Folini, V. Grande, G. Cimino-Reale, N. Zaffaroni, M. Freccero, *Org. Biomol. Chem.* **2015**, *13*, 570–576.
- [15] F. Doria, M. Nadai, M. Folini, M. Scalabrin, L. Germani, G. Sattin, M. Mella, M. Palumbo, N. Zaffaroni, D. Fabris, M. Freccero, S. N. Richter, *Chem. Eur. J.* **2013**, *19*, 78–81.

- [16] M. Nadai, F. Doria, L. Germani, S. N. Richter, M. Freccero, *Chem. Eur. J.* **2015**, *21*, 2330–2334.
- [17] A. Loperigolo, R. Perrone, M. Tortoreto, F. Doria, G. L. Beretta, V. Zuco, M. Freccero, M. Grazia Borrello, C. Lanzi, S. N. Richter, N. Zaffaroni, M. Folini, *Oncotarget* **2016**, *7*, 49649–49663.
- [18] E. Salvati, F. Doria, F. Manoli, C. D'Angelo, A. Biroccio, M. Freccero, I. Manet, *Org. Biomol. Chem.* **2016**, *14*, 7238–7249.
- [19] G. W. Collie, R. Promontorio, S. M. Hampel, M. Micco, S. Neidle, G. N. Parkinson, *J. Am. Chem. Soc.* **2012**, *134*, 2723–2731.
- [20] S. A. Ohnmacht, C. Marchetti, M. Gunaratnam, R. J. Besser, S. M. Haider, G. Di Vita, H. L. Lowe, M. Mellinas-Gomez, S. Diocou, M. Robson, J. Šponer, B. Islam, R. B. Pedley, J. A. Hartley, S. Neidle, *Sci. Rep.* **2015**, *5*, 11385.
- [21] M. Gunaratnam, M. de la Fuente, S. M. Hampel, A. K. Todd, A. P. Reszka, A. Schätzlein, S. Neidle, *Bioorg. Med. Chem.* **2011**, *19*, 7151–7157.
- [22] a) E. C. Calvaresi, P. J. Hergenrother, *Chem. Sci.* **2013**, *4*, 2319–2333; b) C. Granchi, S. Fortunato, F. Minutolo, *MedChemComm* **2016**, *7*, 1716–1729.
- [23] D. Z. Liu, S. Sinchaikul, P. V. Reddy, M. Y. Chang, S. T. Chen, *Bioorg. Med. Chem. Lett.* **2007**, *17*, 617–620.
- [24] J. Cao, S. Cui, S. Li, C. Du, J. Tian, S. Wan, Z. Qian, Y. Gu, W. R. Chen, G. Wang, *Cancer Res.* **2013**, *73*, 1362–1373.
- [25] E. C. Calvaresi, C. Granchi, T. Tuccinardi, V. Di Bussolo, R. W. Huigens, 3rd, H. Y. Lee, R. Palchaudhuri, M. Macchia, A. Martinelli, F. Minutolo, P. J. Hergenrother, *ChemBioChem* **2013**, *14*, 2263–2267.
- [26] a) P. Liu, Y. Lu, X. Gao, R. Liu, D. Zhang-Negrerie, Y. Shi, Y. Wang, S. Wang, Q. Gao, *Chem. Commun.* **2013**, *49*, 2421–2423; b) M. Patra, T. C. Johnstone, K. Suntharalingam, S. J. Lippard, *Angew. Chem. Int. Ed.* **2016**, *55*, 2550–2554; *Angew. Chem.* **2016**, *128*, 2596–2600; c) M. Patra, S. G. Awuah, S. J. Lippard, *J. Am. Chem. Soc.* **2016**, *138*, 12541–12551.
- [27] J. Pohl, B. Bertram, P. Hilgard, M. R. Nowrousian, J. Stuben, M. Wiessler, *Cancer Chemother. Pharmacol.* **1995**, *35*, 364–370.
- [28] a) H. Miyake, C. Otsuka, S. Nishimura, Y. Nitta, *J. Biochem.* **2002**, *131*, 587–591; b) E. D. Soli, A. S. Manoso, M. C. Patterson, P. DeShong, D. A. Favor, R. Hirschmann, A. B. Smith, *J. Org. Chem.* **1999**, *64*, 3171–3177.
- [29] P. Quagliotto, G. Viscardi, C. Barolo, D. D'Angelo, E. Barni, C. Compari, E. Duce, E. Fiscaro, *J. Org. Chem.* **2005**, *70*, 9857–9866.
- [30] A. De Cian, L. Guittat, M. Kaiser, B. Saccà, S. Amrane, A. Bourdoncle, P. Alberti, M.-P. Teulade-Fichou, L. Lacroix, J.-L. Mergny, *Methods* **2007**, *42*, 183–195.
- [31] F. Doria, M. Nadai, M. Folini, M. Di Antonio, L. Germani, C. Percivalle, C. Sissi, N. Zaffaroni, S. Alcaro, A. Artese, S. N. Richter, M. Freccero, *Org. Biomol. Chem.* **2012**, *10*, 2798–2806.
- [32] a) Y. Wang, D. J. Patel, *Structure* **1994**, *2*, 1141–1156; b) K. W. Lim, V. C. M. Ng, N. Martín-Pintado, B. Heddi, A. T. Phan, *Nucleic Acids Res.* **2013**, *41*, 10556–10562.
- [33] a) G. N. Parkinson, M. P. H. Lee, S. Neidle, *Nature* **2002**, *417*, 876–880; b) B. Heddi, A. T. Phan, *J. Am. Chem. Soc.* **2011**, *133*, 9824–9833.
- [34] K. W. Lim, S. Amrane, S. Bouaziz, W. Xu, Y. Mu, D. J. Patel, K. N. Luu, A. T. Phan, *J. Am. Chem. Soc.* **2009**, *131*, 4301–4309.
- [35] a) K. N. Luu, A. T. Phan, V. Kuryavyi, L. Lacroix, D. J. Patel, *J. Am. Chem. Soc.* **2006**, *128*, 9963–9970; b) A. T. Phan, V. Kuryavyi, K. N. Luu, D. J. Patel, *Nucleic Acids Res.* **2007**, *35*, 6517–6525.
- [36] A. De Rache, J. L. Mergny, *Biochimie* **2015**, *115*, 194–202.
- [37] Y. Liu, Y. Cao, W. Zhang, S. Bergmeier, Y. Qian, H. Akbar, R. Colvin, J. Ding, L. Tong, S. Wu, J. Hines, X. Chen, *Mol. Cancer Ther.* **2012**, *11*, 1672–1682.
- [38] A. K. Vyas, J. C. Koster, A. Tzekov, P. W. Hruz, *J. Biol. Chem.* **2010**, *285*, 36395–36400.
- [39] P. Strobel, C. Allard, T. Perez-Acle, R. Calderon, R. Aldunate, F. Leighton, *Biochem. J.* **2005**, *386*, 471–478.

Manuscript received: October 19, 2016

Accepted Article published: December 7, 2016

Final Article published: ■ ■ ■, 0000

3.2. G-Quadruplex identification in the genome of protozoan parasites points to naphthalene diimide ligands as new antiparasitic agents.

Reference:

E. Belmonte-Reche, M. Martínez-García, A. Guédin, M. Zuffo, M. Arévalo-Ruiz, F. Doria, J. Campos-Salinas, M. Maynadier, J.-J. Lopez-Rubio, M. Freccero, J. C. Morales, *Journal of Medicinal Chemistry* **2018**, *61* (3), 1231–1240.

DOI:

[10.1021/acs.jmedchem.7b01672](https://doi.org/10.1021/acs.jmedchem.7b01672)

Supporting information:

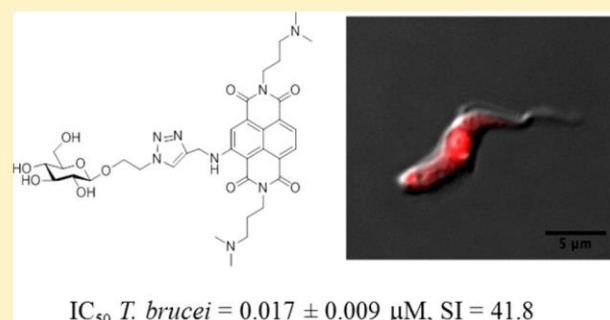
pubs.acs.org/doi/suppl/10.1021/acs.jmedchem.7b01672/suppl_file/jm7b01672_si_001.pdf

G-Quadruplex Identification in the Genome of Protozoan Parasites Points to Naphthalene Diimide Ligands as New Antiparasitic Agents

Efres Belmonte-Reche,[†] Marta Martínez-García,[†] Aurore Guédin,[‡] Michela Zuffo,[§] Matilde Arévalo-Ruiz,[†] Filippo Doria,[§] Jenny Campos-Salinas,[†] Marjorie Maynadier,^{||} José Juan López-Rubio,[⊥] Mauro Freccero,[§] Jean-Louis Mergny,^{‡, #} José María Pérez-Victoria,^{*, †} and Juan Carlos Morales^{*, †}[†]Department of Biochemistry and Molecular Pharmacology, Instituto de Parasitología y Biomedicina, CSIC, PTS Granada, Avda. del Conocimiento, 17, 18016 Armilla, Granada, Spain[‡]ARNA Laboratory, Université de Bordeaux, Inserm U1212, CNRS UMR5320, Institut Européen de Chimie Biologie (IECB), 2 Rue Robert Escarpit, 33607 Pessac, France[§]Department of Chemistry, University of Pavia, Via Taramelli 10, 27100 Pavia, Italy^{||}Dynamique des Interactions Membranaires Normales et Pathologiques, CNRS UMR 5235, Université de Montpellier, 34095 Montpellier, France[⊥]CNRS, 5290, IRD 224, University of Montpellier (UMR “MiVEGEC”), INSERM, 34394 Montpellier, France[#]Institute of Biophysics, AS CR, v.v.i. Kralovopolska 135, 612 65 Brno, Czech Republic

Supporting Information

ABSTRACT: G-quadruplexes (G4) are DNA secondary structures that take part in the regulation of gene expression. Putative G4 forming sequences (PQS) have been reported in mammals, yeast, bacteria, and viruses. Here, we present PQS searches on the genomes of *T. brucei*, *L. major*, and *P. falciparum*. We found telomeric sequences and new PQS motifs. Biophysical experiments showed that EBRI, a 29 nucleotide long highly repeated PQS in *T. brucei*, forms a stable G4 structure. G4 ligands based on carbohydrate conjugated naphthalene diimides (carb-NDIs) that bind G4's including hTel could bind EBRI with selectivity versus dsDNA. These ligands showed important antiparasitic activity. IC₅₀ values were in the nanomolar range against *T. brucei* with high selectivity against MRC-5 human cells. Confocal microscopy confirmed these ligands localize in the nucleus and kinetoplast of *T. brucei* suggesting they can reach their potential G4 targets. Cytotoxicity and zebrafish toxicity studies revealed sugar conjugation reduces intrinsic toxicity of NDIs.



INTRODUCTION

G-quadruplexes (G4) are secondary structures formed by guanine-rich DNA and RNA sequences. Their basic motif is a four-guanine tetrad linked through Hoogsteen hydrogen bonding that stacks on top of other G-tetrads helped by interactions with cations, such as Na⁺ or K⁺. G4 topologies are quite diverse and depend on base sequence, loop connectivity, and the *syn* or *anti* guanine configuration along the oligonucleotide folding.¹

G4 sequences are overrepresented in certain key regions of the genome² such as promoters, enhancers, insulators, origins of replications, and telomeres. These findings suggest that G4 have important functions in cellular and genetic processes. Visualization and genome mapping experiments³ suggest that G-quadruplex DNA can be formed when DNA single strands are exposed during replication or transcription. G4 structures pose challenges to replication, and G4 helicases are essential to unwind them and thus maintain genetic stability.⁴ Sarkies et al.

also suggested that G4 DNA are involved in the maintenance of epigenetic regulation of gene expression.⁵

Putative G-quadruplex sequences (PQS) have been found in organisms other than humans, such as other mammals,⁶ yeast,⁷ bacteria,⁸ and viruses.⁹ In contrast, few data have been reported of G4 in parasites.¹⁰ The malaria-causing parasite *Plasmodium falciparum* has an extremely AT rich DNA (>80%), which in principle lowers the possibilities of G4 formation.¹¹ Nevertheless, successive bioinformatic searches have identified several putative quadruplex sequences^{1e,12} that may play a role in antigenic variation and diversification.^{10,12a} Bottius et al.¹³ reported the existence of a common degenerate motif GGGTTYA (where Y is T or C, PFTel) in the DNA of *P. falciparum* and localized it mainly in the 1.3 kb (average) telomeric regions of the parasite chromosomes. This

Received: November 15, 2017

Published: January 11, 2018

Table 1. Most Frequent PQS Found in *L. major*, *T. brucei*, and *P. falciparum* Genomes and Number of Occurrences^{4a}

	PQS	name	frequency	
<i>L. major</i>	GGGTTAGGGTTAGGGTTAGGG	hTel	465	
	GGGAGGGAGGGAGGG		26	
	GGGTGAGCGGGTGGGGGTCAGTGGG		22	
	GGGGTGGGCCACGCGGGGACAGGACGGG		21	
	GGGCGTGGGTGTGGGTGTGGG		19	
	GGGCGAGGGGAGGGGGGTGCTGGG		17	
	GGGAAAAGAAGGGGAAGGGGTAGGG		16	
	GGGTGGGTGGGTGGG	T30693	16	
	<i>T. brucei</i>	GGGCAGGGGGTGATGGGGAGGAGCCAGGG	EBR1	33
		GGGTTAGGGTTAGGGTTAGGG	hTel	26
GGGAGAGGGAGAGGGAGAGGG			5	
<i>P. falciparum</i>	GGGTTTAGGGTTCAGGGTTTAGGG	PfTel	84	
	GGGTTTAGGGTTTAGGGTTTAGGG	PfTel	67	
	GGGTTTAGGGTTTAGGGTTTAGGG	PfTel	63	
	GGGTTTAGGGTTTAGGGTTTAGGG	PfTel	63	
	GGGTTTAGGGTTTAGGGTTTAGGG	PfTel	58	
	GGGTTTAGGGTTTAGGGTTTAGGG	PfTel	26	
	GGGTTTAGGGTTTAGGGTTTAGGG	PfTel	19	

^{4a}Frequency is the number of times the sequence occurs in the genome.

capacity facilitative protein that takes advantage of the high concentration of glucose in the blood.³⁷

In this work, we have made a genomic search of PQS for *T. brucei*, *L. major*, and *P. falciparum*. We have localized G4 sequences in their genomes and evaluated their possible importance for the parasite survival. We have evaluated a unique G4 sequence found in *T. brucei* (EBR1) for its ability to form stable G-quadruplex using biophysical methods. Furthermore, the carbohydrate-NDIs have been investigated as potential ligands of EBR1 and evaluated as antitrypanosomal, antileishmanial, and antimalarial agents together with their toxicity in human cells and in zebrafish embryo. Finally, location of carb-NDIs inside *T. brucei* was also studied.

RESULTS AND DISCUSSION

Putative G-Quadruplex Sequences (PQS) Search in *T. brucei*, *P. falciparum*, and *L. major* Genomes. The possibility of G-quadruplex formation was analyzed using the online algorithm software for PQS-search engine called QGRS Mapper since it is a user-friendly, commonly used algorithm.³⁸ The genomes were downloaded from tritrypDB (<http://tritrypdb.org> for *T. brucei*, version 5.1, accessed January 2016), the Sanger Institute (<http://www.sanger.ac.uk> for *L. major*, version 6.1, accessed June 2016), and plasmoDB (<http://plasmodb.org> for *P. falciparum*, version 3.0, accessed January 2016), and only the positive strands were included. The results were set to leave out overlapping PQS. Additional parameters were set to default (max length = 30, min G-group size = 3, loop size = 3–10). With these parameters, 466 PQS were found for *P. falciparum*, whereas Smargiasso et al.^{12b} reported 891 PQS when searching through the whole genome. The resulting variation is probably due to the differences in the parameter criteria (Smargiasso used a loop range of 0–11) and in the genome version. A similar number of PQS (433) was also detected in *T. brucei*, although its genome is larger than the one of *P. falciparum* (32 vs 23 Mbp) and its composition is more GC-rich (45% *T. brucei*, 20% *P. falciparum*). *L. major* displayed 4719 PQS, 10 times more than *T. brucei*, despite having similar genomic size and a composition of 57% GC. Both of these genomic parameters cannot explain the big

difference in PQS detection rates. These tendencies were better observed when comparing parasite PQS densities (number of PQS/10.000 bases) 0.15, 0.24, and 1.42 for *T. brucei*, *P. falciparum*, and *L. major*, respectively. Large differences were also observed between chromosomes. *L. major*'s chromosomes 4, 13, 17, 34, and 36 displayed very high PQS concentration, while chromosomes 12 and 14 of *P. falciparum* have a very low density of G4-prone sequences (Table S2 in Supporting Information). *T. brucei* displayed low PQS concentration in its entire genome.

The relevance of the PQS found can be estimated based on the G-score, a validation system on QGRS-mapper. The algorithm tends to emphasize shorter loops with equal size and higher number of guanine tetrads. However, false positives (where high G-score PQS are unable to form G4) and false negatives (where low G-score PQS are able to form stable G4) are given sometimes as results. To solve these potential errors, several other algorithms have been developed, such as G4-hunter.¹⁶ G4-hunter validates PQS ability to form G4 by taking into account G-richness (G in sequence) and skewness (G/C asymmetry with the complementary strand) of the PQS area and thus drastically reduces false results. We decided to validate PQS results simply by frequency. Higher frequencies are in principle less prone to be random nucleotide sequences without a biological role. At the same time, all highly frequent PQS found for the examined parasites are verified G4-forming sequences. For *L. major* and *T. brucei* these PQS include the hTel sequence, and for *P. falciparum* the variety of PfTel sequences (Table 1). In *T. brucei* we also found a highly frequent new nontelomeric sequence that however was given a poor G-score by the search engine. This sequence (EBR1) was found 33 times (Table 1).

When we checked the location of EBR1 in *T. brucei* genome, we found it was repeated 22 times between percentile 34.2 and 35.2 of chromosome 9, where it was located inside several genes coding, among others, for a purine nucleoside transporter (NT10), a calpain-like cysteine peptidase, an adenylosuccinate lyase, and other proteins with unknown function. The rest of the EBR1 sequences were found between percentile 6.6 and 6.9 of chromosome 11 and inside a gene coding for an iron/

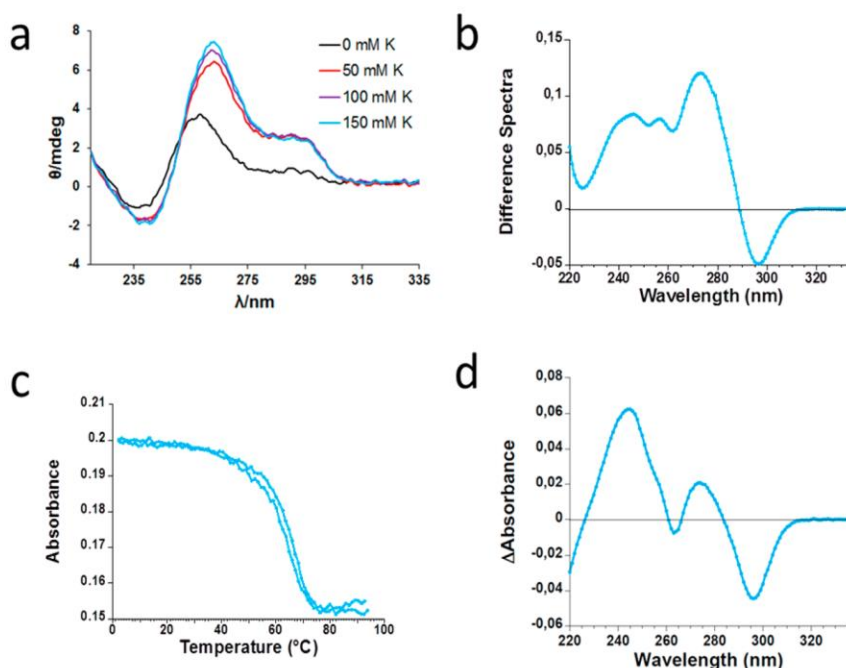


Figure 2. Characterization of EBR1 sequence: (a) CD spectra in the absence and presence of different concentrations of K^+ ; (b) thermal difference spectra (TDS); (c) UV-monitored thermal denaturation experiment at 295 nm; (d) isothermal difference spectra at 25 °C (IDS).

ascorbate oxidoreductase. The hTel sequences in *L. major* and *T. brucei* were mainly localized in the telomeric regions as expected. For *T. brucei*, some of these sequences were found to be in or in between VSG genes, yet also throughout nontelomeric areas affecting a trans-sialidase neuraminidase and several unknown proteins. PfTel sequences found in *P. falciparum* were mostly localized in the telomeric areas (percentile >99.9) and affecting PfEMP1 expressing genes as it was reported earlier.

G4 Formation by *T. brucei* EBR1 Sequence. Due to the novelty and frequency number in *T. brucei* genome, the EBR1 sequence (Table 1) was selected and analyzed for its ability to form G-quadruplex. Circular dichroism (CD) spectroscopy was first carried out in the absence and presence of increasing concentrations of K^+ to investigate G-quadruplex formation.³⁹ EBR1 CD spectra showed positive signals at 260 and 295 nm and a negative signal at 240 nm, suggesting a predominantly parallel G-quadruplex conformation (Figure 2a). When CD was recorded in sodium buffer conditions, the spectra were similar but with lower intensity (Figure S1). It is important to mention that G4 seems to be partially folded even in the absence of cations (Figure S1) and CD signals increase with accumulative amount of cations. Other examples have been reported of G4 formation in the absence or low concentration of monovalent cations.⁴⁰ A mutated EBR1 sequence (EBR1-mut) where several guanine residues were changed to adenine or thymine was also examined for comparison (Figure S2). In this case, no CD signals characteristic of G-quadruplex formation were detected and only small changes were observed after K^+ or Na^+ addition.

UV thermal difference spectroscopy (TDS)⁴¹ was recorded on EBR1 (Figure 2b) by subtracting spectra at 93.5 and 2.7 °C. Major positive peaks at 247, 257, and 274 nm, together with a negative peak at 296 nm, are a typical signature of G-quadruplex folding. UV melting⁴² of EBR1 monitored at 295 nm showed the usual negative sigmoidal curve for G-quadruplex with a T_m value of 65 °C (Figure 2c). The reverse

cooling experiment showed an almost overlapping curve (Figure 2c). IDS spectra on EBR1 were obtained by taking the difference between the absorbance spectra of folded and unfolded oligonucleotides. These spectra were respectively recorded before and after potassium cation addition (100 mM KCl) at 25 °C (Figure 2d). This signature is characteristic of a G4 structure, as in the case of the TDS spectra. The spectra showed major positive peaks at 244 and 274 nm with a negative peak at 296 nm.

Proton NMR experiments were run on the unlabeled EBR1 sequence at 25 and 60 °C, close to the T_m measured by UV melting. Both spectra displayed the characteristic imino peaks in the 10–12 ppm range and none at higher field (Figure S3), suggesting the exclusive folding into G4 structures.⁴³ However, the spectra displayed a complex mixture of signals, indicating the coexistence of more than one conformation. Even close to the melting temperature a favored one could not be identified, suggesting that they all have similar stability.

After validation of EBR1 folding into a G4 structure, we proceeded to test ligand binding. FAM and TAMRA fluorophores were attached to the 5'- and 3'-ends of EBR1 sequence (EBR1-FT; see Table S1) to run FRET experiments. Preliminary UV melting and CD experiments were carried out on EBR1-FT. The results demonstrated that the stability and folding topology are in good agreement with those obtained for the unlabeled EBR1 sequence (Figure S4).

Next, two of our G-quadruplex ligands, the carb-NDI 6 and the reference aglycone-NDI (7), were tested for binding to the EBR1 G4 structure using FRET. Carb-NDIs 1–6 and aglycone NDI 7 have previously shown binding to several G-quadruplex structures (hTel, c-myc, human minisatellite, and Bombyx telomere) with certain selectivity for quadruplexes over DNA duplexes.³¹ FRET-based melting assays were performed in the presence of 10 and 50 mM concentrations of K^+ , with 0.5, 1, and 2 μM of compound 6 or 7 and 0.2 μM of the oligonucleotide. Both compounds showed binding to EBR1, and ΔT_m values were higher for aglycone-NDI 7 than for

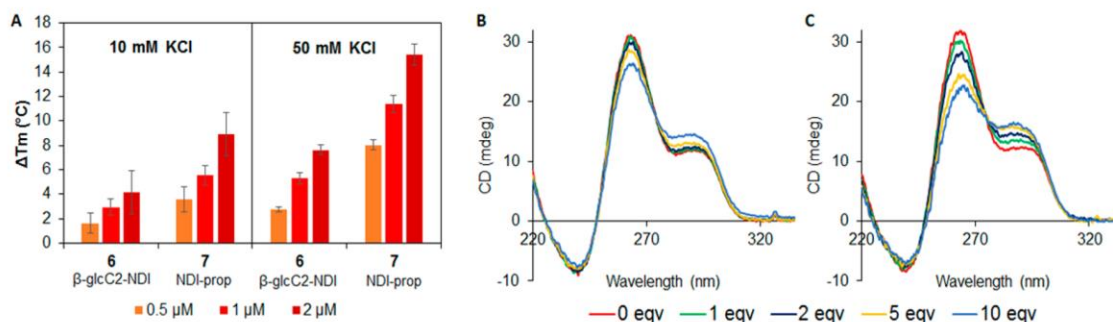


Figure 3. (A) FRET melting assay. Thermal stabilization induced by the tested compounds **6** and **7** (0.5, 1, and 2 μ M) on the EBR1-FT (fluorescently labeled) quadruplex (0.2 μ M) in 10 mM lithium cacodylate, pH 7.2, containing 10 mM KCl + 90 mM LiCl or 50 mM KCl + 50 mM LiCl. (B) CD titration of compound **6** on the EBR1-FT quadruplex (3 μ M) in 10 mM lithium cacodylate (pH 7.2) containing 100 mM KCl. (C) CD titration of compound **7** on the EBR1-FT quadruplex (3 μ M) in 10 mM lithium cacodylate (pH 7.2) containing 100 mM KCl.

Table 2. Compound Antiparasitic Activity against All Three Parasites and Cytotoxicity Values for MRC5 Control Cell Line of the G4 Ligands 1–7 plus Three Classical G4 Binders and Selectivity Values

	IC ₅₀ parasite (μ M)				SI ^a		
	<i>L. major</i>	<i>T. brucei</i>	<i>P. falciparum</i>	MRC-5 ^b	<i>L. major</i>	<i>T. brucei</i>	<i>P. falciparum</i>
1 β -glc-NDI	0.244 \pm 0.007	0.024 \pm 0.001	1.350 \pm 0.636	1.15 \pm 0.29	4.7	47.9	0.9
2 β -glcNAc-NDI	1.041 \pm 0.027	0.089 \pm 0.007	0.360 \pm 0.071	0.51 \pm 0.01	0.5	5.7	1.4
3 β -6dglc-NDI	0.184 \pm 0.009	0.017 \pm 0.007	0.225 \pm 0.120	0.91 \pm 0.32	4.9	53.5	4.0
4 β -malt-NDI	0.921 \pm 0.051	0.099 \pm 0.010	0.370 \pm 0.085	2.04 \pm 0.05	2.2	20.6	5.5
5 α -manC2-NDI	0.306 \pm 0.019	0.021 \pm 0.003	0.180 \pm 0.099	0.81 \pm 0.44	2.6	38.6	4.5
6 β -glcC2-NDI	0.537 \pm 0.030	0.017 \pm 0.009	0.275 \pm 0.191	0.71 \pm 0.25	1.3	41.8	2.6
7 NDI-prop	0.034 \pm 0.005	0.009 \pm 0.001	0.091 \pm 0.013	0.36 \pm 0.16	10.6	40.0	4.0
pyridostatin	5.00 \pm 0.01	7.82 \pm 0.20	2.65 \pm 1.77	5.38 \pm 0.07	1.1	0.7	2.0
BRACO-19	12.73 \pm 0.47	5.51 \pm 0.99	9.70 \pm 4.67	8.33 \pm 2.96	0.7	1.5	0.9
TMPyP4	20.82 \pm 4.86	>10	>25	>25	>1.7		
chloroquine			0.0096 \pm 0.003				
suramin		0.038 \pm 0.003					
miltefosine	6.07 \pm 0.37						

^aSI = selectivity index (IC₅₀(MRC-5)/IC₅₀(parasite)). ^bFrom ref 30.

glcC2-NDI **6** (Figure 3A and Figure S5). This tendency had been observed previously for the same ligands **6** and **7** when binding to other G4 structures. Yet, ΔT_m values obtained for EBR1 were lower than those seen with the hTel sequence (at 10 mM K⁺ and 2 μ M compound, 19 °C for compound **7**, and 10 °C for compound **6**). CD titrations with carb-NDIs **6** and **7** on EBR1 also confirmed binding (Figure 3B and Figure 3C). An increase in the 290 nm band and a decrease in the 265 nm band were clearly observed upon addition of increasing concentrations of the ligands. These binding results indicate that ligands **6** and **7** not only bind to the *T. brucei* telomeric sequence but also bind to other G4 structures found within the *T. brucei* genome.

Antiparasitic Activity and Toxicity of G4 Ligands. The in vitro antiparasitic activities of carb-NDI G4 ligands (**1–7**) were evaluated against bloodstream forms of *T. brucei brucei*, against promastigotes of *L. major*, and against *P. falciparum* (Table 2). Cytotoxicity values of these compounds against a human nontumoral lung cell line (MRC-5) were recently reported and are also included in the table.³¹ Selectivity indices (SI) were calculated according to the formula IC₅₀(MRC-5)/IC₅₀(parasite). Pyridostatin, BRACO-19, and TmPyP4 were used as alternative G-quadruplex ligands for comparison. Suramin, miltefosine, and chloroquine were used as positive drug controls for *T. brucei*, *L. major*, and *P. falciparum*, respectively.

Carb-NDI G4 ligands (**1–6**) presented the best antiparasitic activity against *T. brucei* with IC₅₀ values between 17 and 24 nM except for compounds **2** and **4** which were slightly less potent (89 and 99 nM, respectively). Compounds **1–6** were more effective against *T. brucei* than against HT-29, MCF-7, and HeLa cancer cells (IC₅₀ values from 0.1 to 2.9 μ M), with aglycone-NDI **7** displaying the lowest IC₅₀ of the series in a similar way to the tendency found in cancerous cells.³¹ IC₅₀ values for most of these G-quadruplex ligands are in the same range as that of the commercial drug suramin, used to treat sleeping sickness. At the same time, the selectivity indexes (IC₅₀(MRC-5)/IC₅₀(parasite)) for compounds **1–7** were quite high ranging from 38.6 to 53.5 except for compounds **2** and **4** (5.7 and 20.6, respectively). It is important to note that classical G-quadruplex ligands such as pyridostatin, BRACO-19, and TMPyP4 showed IC₅₀ values in the micromolar range, far higher than those obtained for compounds **1–7**. Differences in drug uptake and/or binding to specific G4 targets such as EBR1 may explain these data.

In the cases of *L. major* and *P. falciparum*, all IC₅₀ values for Carb-NDI G4 ligands (**1–6**) and aglycone NDI (**7**) were higher than those found for *T. brucei*, although most of them remain in the submicromolar range. This lower effect could be due to differences in drug uptake by the different parasites. Again, aglycone-NDI **7** showed the best antiparasitic activity of the series in both cases, with the carb-NDI presenting slightly

higher values (5- to 30-fold in *L. major* and 2- to 15-fold in *P. falciparum*). The selectivity index of ligands 1–7 was smaller for these two parasites ranging from 0.5 to 10.6 for *L. major* and from 0.9 to 5.5 for *P. falciparum*. We had previously observed differences in antitumor activity depending on how the carbohydrate was attached to the NDI core.³¹ For example, compound 6 where the glucose is attached through an ethyl spacer is approximately 10-fold more active than compound 1 where it is directly attached to the core. In the case of their antiparasitic activity, the sugar presentation in the carb-NDI did not show differences except for *P. falciparum* where compound 6 was 5-fold more active than compound 1. Lastly, the classical G-quadruplex ligands investigated in *L. major* and *P. falciparum* (pyridostatin, BRACO-19, and TMPyP4) displayed IC₅₀ values in the micromolar range, being quite less potent than ligands 1–7.

Next, taking advantage of the intrinsic fluorescence of NDI derivatives β -glcC2-NDI 6 ($\lambda_{em} = 578$ nm, exciting at the maximum absorbance, $\lambda_{exc} = 517$ nm, in buffered conditions at pH 7.4, Figure S6) and aglycone-NDI 7 ($\lambda_{em} = 598$ nm, $\lambda_{exc} = 538$ nm, Figure S6), we investigated their localization in *T. brucei* by confocal microscopy. After 30 min of incubation at 37 °C, both compounds were detected inside the parasites and aglycone-NDI 7 was mainly found in the nucleus and in the kinetoplast (Figure 4). When longer incubation times (150 min) were used, both compounds localized mainly in the nucleus and in the kinetoplast. We had previously observed a similar uptake trend in HT-29 colon cancer cells and MRC-5 noncancerous cells³¹ where aglycone-NDI 7 entered more rapidly into the cells than carb-NDI derivatives, but at longer times all compounds eventually localized within the nucleus. These results suggest that such G4-ligands could reach and possibly target G-quadruplex structures found in the parasite's genome, such as the telomeric sequence and/or EBR1 sequence.

As G-quadruplex ligands 1–7 have shown nanomolar activity against *T. brucei* and selectivity indexes higher than 40, we decided to perform preliminary toxicity assays in the zebrafish embryo model before future investigation in a mice model of the disease. High fecundity, rapid embryonic development, and high homology to mammalian species make zebrafish a cost-effective model for toxicity screening.⁴⁴ Moreover, the embryo is preferred to adult fish because it is predicted that early life stages feel less pain and distress than adult fish. Fast acute toxicity was measured by incubation of zebrafish embryos with increasing concentration of each compound and cumulative mortality/toxicity was observed after 96 hpf (hours postfertilization).⁴⁵ It is important to note that cumulative mortality/toxicity is due to both developmental impact and organotoxicity. This methodology is becoming more frequently used by medicinal chemists.⁴⁶

Table 3 shows NOEC, LOEC, and LC₅₀ values for acute toxicity on zebrafish embryos and calculated LD₅₀ values on mice for G-quadruplex ligands 1–7. Conversion of LC₅₀ values on zebrafish embryo to LD₅₀ values on mice was carried out by correlation as suggested by Ali et al.⁴⁷ after a large-scale comparison of toxicity in both animal models for 60 water-soluble compounds (Table 3). Interestingly, β -6dglc-NDI (3) and β -malt-NDI (4), two compounds with low toxicity on MRC-5 cells, were estimated to be the most toxic compounds in mice. On the contrary, glucose or mannose conjugation to the aglycone NDI-prop (such as in compounds 5 and 6) seems to mitigate the unspecific toxicity associated with these

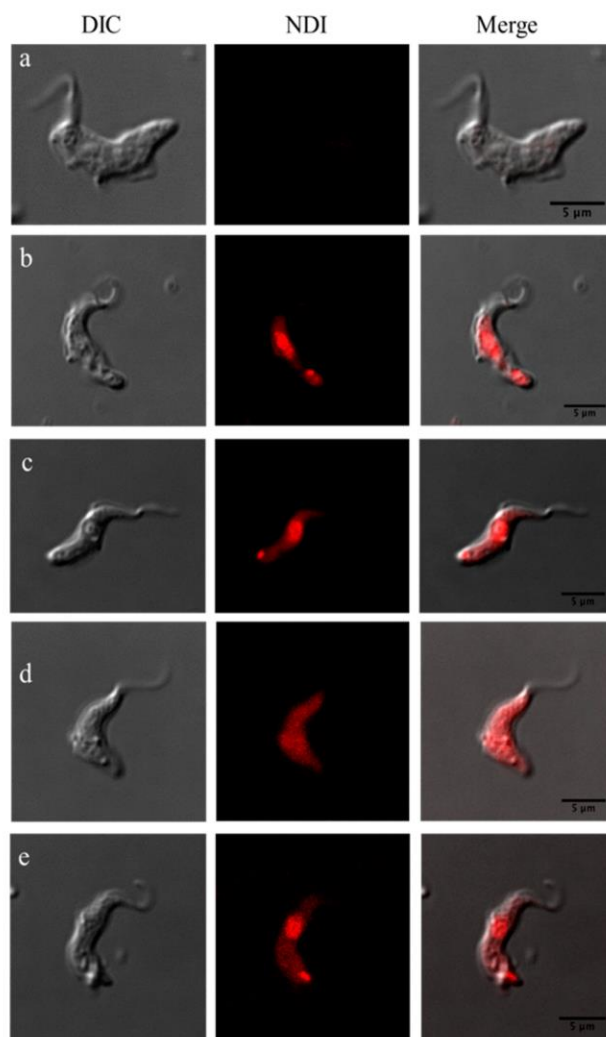


Figure 4. Confocal images of *T. brucei* parasites after incubation at 5 μ M concentration with aglycone-NDI 7 for 30 min (b) or 150 min (c) and with β -glcC2-NDI 6 for 30 min (d) or 150 min (e). Control parasites are shown in (a). Scale bar: 5 μ m.

naphthalene diimide ligands. These results point to the relevance that carbohydrate conjugation of G-quadruplex ligands may have on the final toxicity of the compound.

CONCLUSIONS

Increasing evidence suggests that G4 plays an important role in gene regulation in many organisms. Here, we completed PQS searches on the genome of *T. brucei*, *L. major*, and *P. falciparum*. Several interesting PQS were found, including EBR1 on *T. brucei*, which was also confirmed to form stable G4 structures through biophysical assays. The hTel sequences were also found abundantly in the trypanosomatid parasites in long islands of repetitions.

G-quadruplex ligands such as β -glcC2-NDI 6 and aglycone-NDI 7, which were previously reported to bind to several G4 structures including hTel, were also capable of binding EBR1 G4, found only in the genome of *T. brucei*. At the same time, the carb-NDI family and the aglycone NDI prop 7 showed antiparasitic activity against *T. brucei*, *L. major*, and *P. falciparum*. These G-quadruplex ligands were especially effective against *T. brucei* where they also showed a quite high selectivity versus the human control cell line MRC-5.

Table 3. NOEC, LOEC, and LC₅₀ Values for Acute Toxicity on Zebrafish Embryos and Calculated LD₅₀ Values on Mice for G-Quadruplex Ligands 1–7^a

compd	NOEC (μM)	LOEC (μM)	LC ₅₀ (mmol/L)	LD ₅₀ ^b (mmol/kg) mice	LD ₅₀ ^b (mg/kg) mice
(1) β-glc-NDI	100	NA	>1	>0.63	>580
(2) β-glcNAc-NDI	100	NA	>1	>0.63	>607
(3) β-6dglc-NDI	100	NA	0.17	0.17	154
(4) β-malt-NDI	100	NA	0.19	0.19	206
(5) β-manC2-NDI	100	NA	>1	>0.63	>609
(6) β-glcC2-NDI	100	NA	>1	>0.63	>609
(7) NDI-prop	100	1000	0.41	0.33	178

^aLC₅₀ (median lethal dose), calculated by fitting sigmoidal curve to mortality data ($y = \text{Bot} + (\text{Top} - \text{Bot}) / \{1 + 10^{[k(x_0 - \log(C))]\}$). Bot, minimum mortality; Top, maximum mortality; k , curve slope; x_0 , LC₅₀ estimated. NOEC: no observed effect concentration, with mortality score of >20% assumed as the effect. LOEC: lowest observed effect concentration, with mortality score of >20% assumed as the effect. ^bExtrapolated according to ref 43.

Confocal microscopy studies localized β-glcC2-NDI **6** and aglycone-NDI **7** in the nucleus and kinetoplast of *T. brucei* indicating that G4 structures could be their actual targets. Finally, glucose and mannose conjugation to toxic and potent G4-ligands could be an effective strategy in tuning down unspecific drug toxicity.

■ EXPERIMENTAL SECTION

Compound Synthesis and Purity. Compound synthesis was carried out as previously reported.³¹ The purity of all compounds tested was ≥95% and was confirmed by reverse phase HPLC by applying different elution systems and detecting the UV absorption.

Oligonucleotides. All oligonucleotides (Table S1) were purchased from Eurogentec (Belgium) and used without further purification for FRET and CD experiments. NMR samples were purified by centrifugation on 5 kDa filters. Oligonucleotide stock solutions (around 500 μM) were prepared in Milli-Q water and stored at –20 °C. The exact stock concentrations were determined from the absorbance at 260 nm. For FRET melting and CD experiments, the compounds were solubilized in Milli-Q water at concentrations of either 5 or 10 mM, depending on the solubility of the compound.

FRET Melting Assays. The ligand-induced thermal stabilizations ($\Delta T_{1/2}$) were determined from the difference between the temperature of mid-transition measured without and with the appropriate concentration of ligand, with a final oligonucleotide strand concentration of 0.2 μM. Three independent experiments were conducted on a Stratagene Mx3005P real-time PCR equipment using duplicate conditions in 96-well plates. The excitation wavelength was set to 492 nm and the emission recorded at 516 nm. The temperature profile consisted of an initial stabilization at 25 °C for 5 min followed by a 1 °C by minute increase until 95 °C. The induced stabilization was measured in 10 mM lithium cacodylate (pH 7.2) supplemented with 10 mM KCl and 90 mM LiCl.

Circular Dichroism (CD) Spectroscopy. CD spectra were recorded at 25 °C on a Jasco J-815 equipped with a Peltier temperature controller. Each spectrum corresponds to the average of three scans measured in 1 cm path length quartz cells at 100 nm min⁻¹ (bandwidth of 2 nm, data integration time of 1 s). The oligonucleotides were prefolded at 4 μM in 10 mM lithium cacodylate (pH 7.2) and with the relevant amount of KCl or NaCl. The ligand concentration was adapted to reach the desired ratio (between 1:0 and 1:10), in 100 mM KCl.

Cell Culture. MRC5 cells were maintained at 37 °C and 5% CO₂ in 100% of humidity in low glucose (1 g/L) DMEM supplemented with 10% heat-inactivated fetal bovine serum (hiFBS), 100 U/mL penicillin, and 100 mg/mL streptomycin.

In Vitro Antitrypanosomal Activity. Bloodstream forms (BSF) of *T. brucei brucei* “single marker” S427 (S16) were grown at 37 °C, 5% CO₂ in HMI-9 medium supplemented with 10% hiFBS. Drug susceptibility assay was performed as described in Carvalho et al.⁴⁸ Briefly, parasites (1 × 10⁴ BSF per mL) were incubated in 96-well

plates with increasing concentration of drugs/compounds for 72 h at 37 °C, 5% CO₂ in culture medium. Cell proliferation was determined using the alamarBlue assay⁴⁹ in vitro. Fluorescence was recorded with an Infinite F200 microplate reader (Tecan Austria GmbH, Austria) equipped with 550 and 590 nm filters for excitation and emission wavelengths, respectively.

In Vitro Antileishmanial Activity. The experiments of drug susceptibility on *L. major* (MHOM/IL/80/Friedlin) were carried out as described previously.⁵⁰ Briefly, 1 × 10⁶ promastigotes per mL were incubated for 72 h at 28 °C in 96-well plates in modified RPMI-1640 medium (Invitrogen, Carlsbad, CA) plus 10% hiFBS, containing increasing concentration of drugs. Cell proliferation was determined using a MTT-based assay.⁵¹ The absorbance was measured at a wavelength of 540 nm.

In Vitro Antimalarial Activity. Drug effects on in vitro *P. falciparum* growth were measured in microtiter plates according to Desjardins et al.⁵² The final volume in each well was 200 μL, consisting of 50 μL of complete medium (RPMI 1640 + 10% AB human serum) without (controls) or with drug and 150 μL of *P. falciparum* infected erythrocyte (3D7 strain) suspension (1.5% final hematocrit and 0.6% parasitemia). The drugs dissolved in DMSO were diluted in complete medium so that the final DMSO concentration never exceeded 0.25%. After 48 h incubation at 37 °C, 30 μL of complete medium containing 0.6 μCi [3H]-hypoxanthine were added to each well. After 18 h at 37 °C, cells were lysed using an automatic cell harvester, and the parasite macromolecules, including radioactive nucleic acids, were retained onto glass fiber filters. The filters were counted for radioactivity, after adding scintillation cocktail, in a liquid scintillation spectrometer. Radioactivity background was obtained from incubation of noninfected erythrocytes under the same condition and deduced. Parasitic viability was expressed as IC₅₀ which is the drug concentration leading to 50% parasite growth inhibition.

Cytotoxicity Assay. MRC5 cells were harvested by trypsinization (0.25%) and seeded in 96-well plates (5000 cells in 100 μL/well) in the presence of increasing concentrations of NDI-compounds. Cellular toxicity was determined using the colorimetric MTT-based assay after incubation at 37 °C for or 72 h.⁵¹ The results are expressed as the concentration of compound that reduces cell growth by 50% versus untreated control cells (IC₅₀).

Zebrafish Toxicity. Acute toxicity assay was carried out by Zeclinics (Barcelona, Spain). Lyophilized compounds were dissolved in 100% DMSO. DMSO volume was calculated for a 100 mM stock solution. To proceed to zebrafish embryo drug incubation, compounds were diluted in 1 mL of 0.1% DMSO/E3 medium to obtain 5 logarithmic concentrations: 0.01 μM, 0.1 μM, 1 μM, 10 μM, and 100 μM (for drugs 1, 2, 3, 4, 5, 6, 7) and 0.1 μM, 1 μM, 10 μM, 100 μM, and 1 mM (for drugs 8, 9, 10).

Zebrafish Embryos Preparation. Fertilized embryos of zebrafish (*Danio rerio*), strain AB, were collected in E3 medium in Petri dishes. At 3 h postfertilization (hpf), after abnormal or not fertilized embryos were discarded, 20 healthy embryos per condition were placed in wells of a 24-well plate. Once embryos were placed in each well, E3 medium

was replaced by the different dilutions prepared previously for every compound and concentration.

Acute Toxicity Assay. Embryos were grown from 3 hpf to 96 hpf at 28.5 °C. At 96 h⁵³ after treatment mortality LC₅₀ will be determined: LC₅₀ (median lethal dose), calculated by fitting sigmoidal curve to mortality data ($y = \text{Bot} + (\text{Top} - \text{Bot}) / (1 + 10^{[k(x_0 - \log(C))]}]$). Bot, minimum mortality; Top, maximum mortality; *k*, curve slope; *x*₀, LC₅₀ estimated.

Negative control:⁵⁴ 0.1% DMSO, in three replicates. Positive controls: 4-diethylaminobenzaldehyde (DEAB) at five different concentrations (0.1 μM, 1 μM, 10 μM, 100 μM, 1 mM). DEAB is a competitive inhibitor of aldehyde dehydrogenases known to generate toxic and teratogenic effects.

Absorption and Fluorescence Spectra. Absorption and emission spectra were recorded in $(1.0-1.5) \times 10^{-5}$ M aqueous solutions (buffered at pH 7.4, 1×10^{-3} M Tris-HCl) on a JASCO V-550 UV/vis spectrophotometer and on a PerkinElmer LS-65 fluorometer, respectively. The molar absorptivity has been calculated applying the Beer-Lambert relationship to three independent measurements. Fluorescence spectra were measured using 1 nm steps and 0.5–1 s dwell time. Right angle detection was used. All the measurements were carried out at 22 °C in quartz cuvettes with path length of 1 cm. The fluorescence spectra were measured in air-equilibrated solutions absorbing less than 0.1 at all wavelengths to avoid inner filter effects and reabsorption of emission.

Confocal Microscopy. *T. brucei* parasites were incubated with 5 μM NDI compounds in 0.5 mL of each respective medium for 30 and 150 min at 37 °C and 100% of humidity. Then the parasites were fixed with paraformaldehyde 4% for 30 min, washed twice in cold phosphate buffered saline (PBS), and processed by microscope observation. Images were acquired using a Leica SP5 confocal microscope (exciting at 488 nm and detecting the emission between 540 and 650 nm), while the images were deconvoluted using Huygens Professional image processing software from Scientific Volume Imaging (<http://www.svi.nl>). The merge of the images were made with Fiji software (<https://fiji.sc/>).

■ ASSOCIATED CONTENT

📄 Supporting Information

The Supporting Information is available free of charge on the ACS Publications website at DOI: 10.1021/acs.jmedchem.7b01672.

DNA sequences used in the present study; PQS density found per chromosome of each parasite examined; CD spectra of EBR1 in the absence and presence of different concentrations of Na⁺; CD experiments with EBR1mut sequence; imino region of NMR spectra for EBR1 at different temperatures; characterization of EBR1-FT sequence; FRET-melting stabilization induced by compounds **6** and **7** on EBR1-FT G-quadruplex; absorption and emission spectra of **6** and **7** in water; zebrafish embryo graphs of concentration–mortality response (PDF)

Molecular formula strings and associated biological data (CSV)

■ AUTHOR INFORMATION

Corresponding Authors

*J.M.P.-V.: phone, +34-958181685; e-mail, josepv@ipb.csic.es.

*J.C.M.: phone, +34-958181644; e-mail, jcmorales@ipb.csic.es.

ORCID

Mauro Freccero: 0000-0002-7438-1526

Jean-Louis Mergny: 0000-0003-3043-8401

Juan Carlos Morales: 0000-0003-2400-405X

Notes

The authors declare no competing financial interest.

■ ACKNOWLEDGMENTS

This work was supported by the Spanish Ministerio de Economía y Competitividad (Grants CTQ2012-35360, CTQ2015-64275-P, and SAF2016-80228-R), Junta de Andalucía (Grant BIO1786), Worldwide Cancer Research Foundation (Grant 16-0290), Italian Association for Cancer Research (AIRC, Grant IG2013-14708), Agence Nationale de la Recherche (ANR Quarndiem, Grant ANR-12-BSV8-0008-01), the SYMBIT project (Reg. No. CZ.02.1.01/0.0/0.0/15_003/0000477) financed by the ERDF, and FEDER funds from the EU are gratefully acknowledged. M.A.-R. and M.M.-G. thank Ministerio de Educación, Cultura y Deporte for a FPU and a FPI predoctoral fellowship, respectively. E.B.-R. is a student of the pharmacy Ph.D. program of the University of Granada (Spain).

■ ABBREVIATIONS USED

PQS, putative G-quadruplex forming sequence; carb-NDI, carbohydrate conjugated naphthalene diimide; hTel, human telomerase DNA sequence; VSG, variable surface glycoprotein; ORF, open reading frames; GLUT, glucose transporter; CD, circular dichroism; TDS, thermal difference spectroscopy; IDS, isothermal difference spectroscopy; FRET, Förster resonance energy transfer; SI, selectivity index; NDI, naphthalene diimide

■ REFERENCES

- (1) (a) Huppert, J. L.; Bugaut, A.; Kumari, S.; Balasubramanian, S. G-quadruplexes: the beginning and end of UTRs. *Nucleic Acids Res.* **2008**, *36* (19), 6260–6268. (b) Huppert, J. L. Four-stranded nucleic acids: structure, function and targeting of G-quadruplexes. *Chem. Soc. Rev.* **2008**, *37* (7), 1375–1384. (c) Balasubramanian, S.; Neidle, S. G-quadruplex nucleic acids as therapeutic targets. *Curr. Opin. Chem. Biol.* **2009**, *13* (3), 345–353. (d) Neidle, S. The structures of quadruplex nucleic acids and their drug complexes. *Curr. Struct. Biol.* **2009**, *19* (3), 239–250. (e) Bedrat, A.; Lacroix, L.; Mergny, J. L. Re-evaluation of G-quadruplex propensity with G4Hunter. *Nucleic Acids Res.* **2016**, *44* (4), 1746–1759.
- (2) (a) Chambers, V. S.; Marsico, G.; Boutell, J. M.; Di Antonio, M.; Smith, G. P.; Balasubramanian, S. High-throughput sequencing of DNA G-quadruplex structures in the human genome. *Nat. Biotechnol.* **2015**, *33* (8), 877–881. (b) Huppert, J. L.; Balasubramanian, S. Prevalence of quadruplexes in the human genome. *Nucleic Acids Res.* **2005**, *33* (9), 2908–2916. (c) Kwok, C. K.; Merrick, C. J. G-Quadruplexes: prediction, characterization, and biological application. *Trends Biotechnol.* **2017**, *35* (10), 997–1013.
- (3) Rodriguez, R.; Miller, K. M.; Forment, J. V.; Bradshaw, C. R.; Nikan, M.; Britton, S.; Oelschlaegel, T.; Xhemalce, B.; Balasubramanian, S.; Jackson, S. P. Small-molecule-induced DNA damage identifies alternative DNA structures in human genes. *Nat. Chem. Biol.* **2012**, *8* (3), 301–310.
- (4) (a) Krusselbrink, E.; Guryev, V.; Brouwer, K.; Pontier, D. B.; Cuppen, E.; Tijsterman, M. Mutagenic capacity of endogenous G4 DNA underlies genome instability in FANCD1-defective *C. elegans*. *Curr. Biol.* **2008**, *18* (12), 900–905. (b) Koole, W.; van Schendel, R.; Karambelas, A. E.; van Heteren, J. T.; Okihara, K. L.; Tijsterman, M. A Polymerase Theta-dependent repair pathway suppresses extensive genomic instability at endogenous G4 DNA sites. *Nat. Commun.* **2014**, *5*, 3216. (c) Castillo Bosch, P.; Segura-Bayona, S.; Koole, W.; van Heteren, J. T.; Dewar, J. M.; Tijsterman, M.; Knipscheer, P. FANCD1 promotes DNA synthesis through G-quadruplex structures. *EMBO J.* **2014**, *33* (21), 2521–2533. (d) Ohnmacht, S. A.; Neidle, S. Small-molecule quadruplex-targeted drug discovery. *Bioorg. Med. Chem. Lett.* **2014**, *24* (12), 2602–2612. (e) Mendoza, O.; Bourdoncle, A.; Boule, J.

- B.; Brosh, R. M., Jr.; Mergny, J. L. G-quadruplexes and helicases. *Nucleic Acids Res.* **2016**, *44* (5), 1989–2006.
- (5) Sarkies, P.; Reams, C.; Simpson, L. J.; Sale, J. E. Epigenetic instability due to defective replication of structured DNA. *Mol. Cell* **2010**, *40* (5), 703–713.
- (6) Verma, A.; Halder, K.; Halder, R.; Yadav, V. K.; Rawal, P.; Thakur, R. K.; Mohd, F.; Sharma, A.; Chowdhury, S. Genome-wide computational and expression analyses reveal G-quadruplex DNA motifs as conserved cis-regulatory elements in human and related species. *J. Med. Chem.* **2008**, *51* (18), S641–S649.
- (7) (a) Hershman, S. G.; Chen, Q.; Lee, J. Y.; Kozak, M. L.; Yue, P.; Wang, L. S.; Johnson, F. B. Genomic distribution and functional analyses of potential G-quadruplex-forming sequences in *Saccharomyces cerevisiae*. *Nucleic Acids Res.* **2008**, *36* (1), 144–156. (b) Johnson, J. E.; Smith, J. S.; Kozak, M. L.; Johnson, F. B. In vivo veritas: Using yeast to probe the biological functions of G-quadruplexes. *Biochimie* **2008**, *90* (8), 1250–1263.
- (8) (a) Rawal, P.; Kumarasetti, V. B.; Ravindran, J.; Kumar, N.; Halder, K.; Sharma, R.; Mukerji, M.; Das, S. K.; Chowdhury, S. Genome-wide prediction of G4 DNA as regulatory motifs: role in *Escherichia coli* global regulation. *Genome Res.* **2006**, *16* (5), 644–655. (b) Wieland, M.; Hartig, J. S. Investigation of mRNA quadruplex formation in *Escherichia coli*. *Nat. Protoc.* **2009**, *4* (11), 1632–1640.
- (9) (a) Perrone, R.; Nadai, M.; Frasson, I.; Poe, J. A.; Butovskaya, E.; Smithgall, T. E.; Palumbo, M.; Palu, G.; Richter, S. N. A dynamic G-quadruplex region regulates the HIV-1 long terminal repeat promoter. *J. Med. Chem.* **2013**, *56* (16), 6521–6530. (b) Rajendran, A.; Endo, M.; Hidaka, K.; Tran, P. L.; Mergny, J. L.; Gorelick, R. J.; Sugiyama, H. HIV-1 nucleocapsid proteins as molecular chaperones for tetramolecular antiparallel G-quadruplex formation. *J. Am. Chem. Soc.* **2013**, *135* (49), 18575–18585. (c) Amrane, S.; Kerkour, A.; Bedrat, A.; Vialet, B.; Andreola, M. L.; Mergny, J. L. Topology of a DNA G-quadruplex structure formed in the HIV-1 promoter: a potential target for anti-HIV drug development. *J. Am. Chem. Soc.* **2014**, *136* (14), 5249–5252. (d) Artusi, S.; Nadai, M.; Perrone, R.; Biasolo, M. A.; Palu, G.; Flamand, L.; Calistri, A.; Richter, S. N. The Herpes Simplex Virus-1 genome contains multiple clusters of repeated G-quadruplex: implications for the antiviral activity of a G-quadruplex ligand. *Antiviral Res.* **2015**, *118*, 123–131.
- (10) Harris, L. M.; Merrick, C. J. G-quadruplexes in pathogens: a common route to virulence control? *PLoS Pathog.* **2015**, *11* (2), e1004562.
- (11) Gardner, M. J.; Hall, N.; Fung, E.; White, O.; Berriman, M.; Hyman, R. W.; Carlton, J. M.; Pain, A.; Nelson, K. E.; Bowman, S.; Paulsen, I. T.; James, K.; Eisen, J. A.; Rutherford, K.; Salzberg, S. L.; Craig, A.; Kyes, S.; Chan, M. S.; Nene, V.; Shallom, S. J.; Suh, B.; Peterson, J.; Angiuoli, S.; Pertea, M.; Allen, J.; Selengut, J.; Haft, D.; Mather, M. W.; Vaidya, A. B.; Martin, D. M.; Fairlamb, A. H.; Fraunholz, M. J.; Roos, D. S.; Ralph, S. A.; McFadden, G. I.; Cummings, L. M.; Subramanian, G. M.; Mungall, C.; Venter, J. C.; Carucci, D. J.; Hoffman, S. L.; Newbold, C.; Davis, R. W.; Fraser, C. M.; Barrell, B. Genome sequence of the human malaria parasite *Plasmodium falciparum*. *Nature* **2002**, *419* (6906), 498–511.
- (12) (a) Stanton, A.; Harris, L. M.; Graham, G.; Merrick, C. J. Recombination events among virulence genes in malaria parasites are associated with G-quadruplex-forming DNA motifs. *BMC Genomics* **2016**, *17* (1), 859. (b) Smargiasso, N.; Gabelica, V.; Damblon, C.; Rosu, F.; De Pauw, E.; Teulade-Fichou, M. P.; Rowe, J. A.; Claessens, A. Putative DNA G-quadruplex formation within the promoters of *Plasmodium falciparum* var genes. *BMC Genomics* **2009**, *10*, 362.
- (13) Bottius, E.; Bakhshis, N.; Scherf, A. *Plasmodium falciparum* telomerase: de novo telomere addition to telomeric and nontelomeric sequences and role in chromosome healing. *Mol. Cell. Biol.* **1998**, *18* (2), 919–925.
- (14) Dore, E.; Pace, T.; Ponzi, M.; Scotti, R.; Frontali, C. Homologous telomeric sequences are present in different species of the genus *Plasmodium*. *Mol. Biochem. Parasitol.* **1986**, *21* (2), 121–127.
- (15) (a) Duraisingh, M. T.; Voss, T. S.; Marty, A. J.; Duffy, M. F.; Good, R. T.; Thompson, J. K.; Freitas-Junior, L. H.; Scherf, A.; Crabb, B. S.; Cowman, A. F. Heterochromatin silencing and locus repositioning linked to regulation of virulence genes in *Plasmodium falciparum*. *Cell* **2005**, *121* (1), 13–24. (b) Freitas-Junior, L. H.; Hernandez-Rivas, R.; Ralph, S. A.; Montiel-Condado, D.; Ruvalcaba-Salazar, O. K.; Rojas-Meza, A. P.; Mancio-Silva, L.; Leal-Silvestre, R. J.; Gontijo, A. M.; Shorte, S.; Scherf, A. Telomeric heterochromatin propagation and histone acetylation control mutually exclusive expression of antigenic variation genes in malaria parasites. *Cell* **2005**, *121* (1), 25–36.
- (16) Claessens, A.; Hamilton, W. L.; Kekre, M.; Otto, T. D.; Faizullahoy, A.; Rayner, J. C.; Kwiatkowski, D. Generation of antigenic diversity in *Plasmodium falciparum* by structured rearrangement of Var genes during mitosis. *PLoS Genet.* **2014**, *10* (12), e1004812.
- (17) Scherf, A.; Hernandez-Rivas, R.; Buffet, P.; Bottius, E.; Benatar, C.; Pouvell, B.; Gysin, J.; Lanzer, M. Antigenic variation in malaria: in situ switching, relaxed and mutually exclusive transcription of var genes during intra-erythrocytic development in *Plasmodium falciparum*. *EMBO J.* **1998**, *17* (18), 5418–5426.
- (18) (a) Blackburn, E. H.; Challoner, P. B. Identification of a telomeric DNA sequence in *Trypanosoma brucei*. *Cell* **1984**, *36* (2), 447–457. (b) Van der Ploeg, L. H.; Liu, A. Y.; Borst, P. Structure of the growing telomeres of *Trypanosoma*. *Cell* **1984**, *36* (2), 459–468.
- (19) (a) Lanzer, M.; Fischer, K.; Le Blancq, S. M. Parasitism and chromosome dynamics in protozoan parasites: is there a connection? *Mol. Biochem. Parasitol.* **1995**, *70* (1–2), 1–8. (b) Crozatier, M.; Van der Ploeg, L. H.; Johnson, P. J.; Gommers-Ampt, J.; Borst, P. Structure of a telomeric expression site for variant specific surface antigens in *Trypanosoma brucei*. *Mol. Biochem. Parasitol.* **1990**, *42* (1), 1–12.
- (20) Glover, L.; Alford, S.; Horn, D. DNA break site at fragile subtelomeres determines probability and mechanism of antigenic variation in African trypanosomes. *PLoS Pathog.* **2013**, *9* (3), e1003260.
- (21) (a) Borst, P.; Greaves, D. R. Programmed gene rearrangements altering gene expression. *Science* **1987**, *235* (4789), 658–67. (b) Devlin, R.; Marques, C. A.; McCulloch, R. Does DNA replication direct locus-specific recombination during host immune evasion by antigenic variation in the African trypanosome? *Curr. Genet.* **2017**, *63* (3), 441–449.
- (22) Benne, R.; Van den Burg, J.; Brakenhoff, J. P.; Sloof, P.; Van Boom, J. H.; Tromp, M. C. Major transcript of the frameshifted *coxII* gene from trypanosome mitochondria contains four nucleotides that are not encoded in the DNA. *Cell* **1986**, *46* (6), 819–826.
- (23) Leeder, W. M.; Hummel, N. F.; Goring, H. U. Multiple G-quartet structures in pre-edited mRNAs suggest evolutionary driving force for RNA editing in trypanosomes. *Sci. Rep.* **2016**, *6*, 29810.
- (24) Cullen, D. R.; Mocerino, M. A Brief review of drug discovery research for human African Trypanosomiasis. *Curr. Med. Chem.* **2017**, *24* (7), 701–717.
- (25) Balasubramanian, S.; Hurley, L. H.; Neidle, S. Targeting G-quadruplexes in gene promoters: a novel anticancer strategy? *Nat. Rev. Drug Discovery* **2011**, *10* (4), 261–275.
- (26) (a) Davis, J. T. G-quartets 40 years later: from 5'-GMP to molecular biology and supramolecular chemistry. *Angew. Chem., Int. Ed.* **2004**, *43* (6), 668–698. (b) Maji, B.; Bhattacharya, S. Advances in the molecular design of potential anticancer agents via targeting of human telomeric DNA. *Chem. Commun.* **2014**, *50* (49), 6422–6438. (c) Xiong, Y.-X.; Huang, Z.-S.; Tan, J.-H. Targeting G-quadruplex nucleic acids with heterocyclic alkaloids and their derivatives. *Eur. J. Med. Chem.* **2015**, *97*, 538–551.
- (27) (a) Métifiot, M.; Amrane, S.; Mergny, J.-L.; Andreola, M.-L. Anticancer molecule AS1411 exhibits low nanomolar antiviral activity against HIV-1. *Biochimie* **2015**, *118*, 173–175. (b) Perrone, R.; Doria, F.; Butovskaya, E.; Frasson, I.; Botti, S.; Scalabrin, M.; Lago, S.; Grande, V.; Nadai, M.; Freccero, M.; Richter, S. N. Synthesis, binding and antiviral properties of potent core-extended naphthalene diimides targeting the HIV-1 long terminal repeat promoter G-quadruplexes. *J.*

- Med. Chem.* **2015**, *58* (24), 9639–9652. (c) Biswas, B.; Kandpal, M.; Vivekanandan, P. A G-quadruplex motif in an envelope gene promoter regulates transcription and virion secretion in HBV genotype B. *Nucleic Acids Res.* **2017**, *45* (19), 11268–11280.
- (28) De Cian, A.; Grellier, P.; Mouray, E.; Depoix, D.; Bertrand, H.; Monchaud, D.; Teulade-Fichou, M. P.; Mergny, J. L.; Alberti, P. Plasmodium telomeric sequences: structure, stability and quadruplex targeting by small compounds. *ChemBioChem* **2008**, *9* (16), 2730–2739.
- (29) Guillon, J.; Cohen, A.; Gueddouda, N. M.; Das, R. N.; Moreau, S.; Ronga, L.; Savrimoutou, S.; Basmaciyan, L.; Monnier, A.; Monget, M.; Rubio, S.; Garnerin, T.; Azas, N.; Mergny, J. L.; Mullie, C.; Sonnet, P. Design, synthesis and antimalarial activity of novel bis[N-[(pyrrolo[1,2-a]quinoxalin-4-yl)benzyl]-3-aminopropyl]amine derivatives. *J. Enzyme Inhib. Med. Chem.* **2017**, *32* (1), 547–563.
- (30) Calvo, E. P.; Wasserman, M. G-Quadruplex ligands: Potent inhibitors of telomerase activity and cell proliferation in Plasmodium falciparum. *Mol. Biochem. Parasitol.* **2016**, *207* (1), 33–38.
- (31) Arevalo-Ruiz, M.; Doria, F.; Belmonte-Reche, E.; De Rache, A.; Campos-Salinas, J.; Lucas, R.; Falomir, E.; Carda, M.; Perez-Victoria, J. M.; Mergny, J. L.; Freccero, M.; Morales, J. C. Synthesis, binding properties, and differences in cell uptake of G-quadruplex ligands based on carbohydrate naphthalene diimide conjugates. *Chem. - Eur. J.* **2017**, *23* (9), 2157–2164.
- (32) (a) Calvaresi, E. C.; Hergenrother, P. J. Glucose conjugation for the specific targeting and treatment of cancer. *Chem. Sci.* **2013**, *4* (6), 2319–2333. (b) Pohl, J.; Bertram, B.; Hilgard, P.; Nowrousian, M. R.; Stuben, J.; Wiessler, M. D-19575- a sugar-linked isophosphoramidate mustard derivative exploiting transmembrane glucose transport. *Cancer Chemother. Pharmacol.* **1995**, *35* (5), 364–370. (c) Liu, P.; Lu, Y.; Gao, X.; Liu, R.; Zhang-Negrerie, D.; Shi, Y.; Wang, Y.; Wang, S.; Gao, Q. Highly water-soluble platinum(II) complexes as GLUT substrates for targeted therapy: improved anticancer efficacy and transporter-mediated cytotoxic properties. *Chem. Commun.* **2013**, *49* (24), 2421–2423.
- (33) Burchmore, R. J.; Landfear, S. M. Differential regulation of multiple glucose transporter genes in Leishmania mexicana. *J. Biol. Chem.* **1998**, *273* (44), 29118–29126.
- (34) Rodriguez-Contreras, D.; Feng, X.; Keeney, K. M.; Bouwer, H. G. A.; Landfear, S. M. Phenotypic characterization of a glucose transporter null mutant in Leishmania mexicana. *Mol. Biochem. Parasitol.* **2007**, *153* (1), 9–18.
- (35) (a) Feng, X.; Rodriguez-Contreras, D.; Buffalo, C.; Bouwer, H. G. A.; Kruvand, E.; Beverley, S. M.; Landfear, S. M. Amplification of an alternate transporter gene suppresses the avirulent phenotype of glucose transporter null mutants in Leishmania mexicana. *Mol. Microbiol.* **2009**, *71* (2), 369–381. (b) Rodriguez-Contreras, D.; Landfear, S. M. Metabolic Changes in Glucose Transporter-deficient Leishmania mexicana and Parasite Virulence. *J. Biol. Chem.* **2006**, *281*, 20068–20076.
- (36) Woodrow, C. J.; Penny, J. I.; Krishna, S. Intraerythrocytic Plasmodium falciparum expresses a high affinity facilitative hexose transporter. *J. Biol. Chem.* **1999**, *274* (11), 7272–7277.
- (37) Barrett, M. P.; Tetaud, E.; Seyfang, A.; Bringaud, F.; Baltz, T. Trypanosome glucose transporters. *Mol. Biochem. Parasitol.* **1998**, *91* (1), 195–205.
- (38) Kikin, O.; D'Antonio, L.; Bagga, P. S. QGRS Mapper: a web-based server for predicting G-quadruplexes in nucleotide sequences. *Nucleic Acids Res.* **2006**, *34* (Web Server), W676–W682.
- (39) Karsisiotis, A. I.; Hessari, N. M.; Novellino, E.; Spada, G. P.; Randazzo, A.; Webba da Silva, M. Topological characterization of nucleic acid G-quadruplexes by UV absorption and circular dichroism. *Angew. Chem., Int. Ed.* **2011**, *50* (45), 10645–8.
- (40) (a) Diveshkumar, K. V.; Sakrikar, S.; Harikrishna, S.; Dhamodharan, V.; Pradeepkumar, P. I. Targeting promoter G-quadruplex DNAs by indenopyrimidine-based ligands. *ChemMedChem* **2014**, *9* (12), 2754–2765. (b) Perrone, R.; Nadai, M.; Poe, J. A.; Frasson, I.; Palumbo, M.; Palu, G.; Smithgall, T. E.; Richter, S. N. Formation of a unique cluster of G-quadruplex structures in the HIV-1 Nef coding region: implications for antiviral activity. *PLoS One* **2013**, *8* (8), e73121.
- (41) Mergny, J. L.; Li, J.; Lacroix, L.; Amrane, S.; Chaires, J. B. Thermal difference spectra: a specific signature for nucleic acid structures. *Nucleic Acids Res.* **2005**, *33* (16), e138.
- (42) Mergny, J. L.; Phan, A. T.; Lacroix, L. Following G-quartet formation by UV-spectroscopy. *FEBS Lett.* **1998**, *435* (1), 74–78.
- (43) Feigon, J.; Koshlap, K. M.; Smith, F. W. ¹H NMR spectroscopy of DNA triplexes and quadruplexes. *Methods Enzymol.* **1995**, *261*, 225–255.
- (44) Sipes, N. S.; Padilla, S.; Knudsen, T. B. Zebrafish: as an integrative model for twenty-first century toxicity testing. *Birth Defects Res., Part C* **2011**, *93* (3), 256–267.
- (45) Busquet, F.; Strecker, R.; Rawlings, J. M.; Belanger, S. E.; Braunbeck, T.; Carr, G. J.; Cenijn, P.; Fochtman, P.; Gourmelon, A.; Hubler, N.; Kleensang, A.; Knobel, M.; Kussatz, C.; Legler, J.; Lillicrap, A.; Martinez-Jeronimo, F.; Polleichtner, C.; Rzodeccko, H.; Salinas, E.; Schneider, K. E.; Scholz, S.; van den Brandhof, E. J.; van der Ven, L. T.; Walter-Rohde, S.; Weigt, S.; Witters, H.; Halder, M. OECD validation study to assess intra- and inter-laboratory reproducibility of the zebrafish embryo toxicity test for acute aquatic toxicity testing. *Regul. Toxicol. Pharmacol.* **2014**, *69* (3), 496–511.
- (46) (a) Ledoux, A.; St-Gelais, A.; Cieciewicz, E.; Jansen, O.; Bordignon, A.; Illien, B.; Di Giovanni, N.; Marvilliers, A.; Hoareau, F.; Pendeville, H.; Quetin-Leclercq, J.; Frederich, M. Antimalarial activities of alkyl cyclohexenone derivatives isolated from the leaves of Poupertia borbonica. *J. Nat. Prod.* **2017**, *80* (6), 1750–1757. (b) Teijeiro-Valino, C.; Yebra-Pimentel, E.; Guerra-Varela, J.; Csaba, N.; Alonso, M. J.; Sanchez, L. Assessment of the permeability and toxicity of polymeric nanocapsules using the zebrafish model. *Nanomedicine* **2017**, *12* (17), 2069–2082.
- (47) Ali, S.; van Mil, H. G. J.; Richardson, M. K. Large-scale assessment of the zebrafish embryo as a possible predictive model in toxicity testing. *PLoS One* **2011**, *6* (6), e21076.
- (48) Carvalho, L.; Martinez-Garcia, M.; Perez-Victoria, I.; Manzano, J. I.; Yardley, V.; Gamarro, F.; Perez-Victoria, J. M. The oral antimalarial drug tafenoquine shows activity against Trypanosoma brucei. *Antimicrob. Agents Chemother.* **2015**, *59* (10), 6151–6160.
- (49) Raz, B.; Iten, M.; Grether-Buhler, Y.; Kaminsky, R.; Brun, R. The Alamar Blue assay to determine drug sensitivity of African trypanosomes (T.b. rhodesiense and T.b. gambiense) in vitro. *Acta Trop.* **1997**, *68* (2), 139–147.
- (50) Perez-Victoria, J. M.; Bavchvarov, B. I.; Torrecillas, I. R.; Martinez-Garcia, M.; Lopez-Martin, C.; Campillo, M.; Castanys, S.; Gamarro, F. Sitamaquine overcomes ABC-mediated resistance to miltefosine and antimony in Leishmania. *Antimicrob. Agents Chemother.* **2011**, *55* (8), 3838–3844.
- (51) Mosmann, T. Rapid colorimetric assay for cellular growth and survival: application to proliferation and cytotoxicity assays. *J. Immunol. Methods* **1983**, *65* (1–2), 55–63.
- (52) Desjardins, R. E.; Canfield, C. J.; Haynes, J. D.; Chulay, J. D. Quantitative assessment of antimalarial activity in vitro by a semiautomated microdilution technique. *Antimicrob. Agents Chemother.* **1979**, *16* (6), 710–718.
- (53) At 24 h coagulated eggs were removed from the well to avoid contamination of E3 medium due to tissue decomposition.
- (54) If negative control cumulative mortality is greater than 20%, the experiment was not considered significant and had to be repeated.

3.3. Tyrosol and hydroxytyrosol derivatives as antitrypanosomal and antileishmanial agents.

Reference:

E. Belmonte-Reche, M. Martínez-García, P. Peñalver, V. Gómez-Pérez, R. Lucas, F. Gamarro, J. M. Pérez-Victoria, J. C. Morales, *European Journal of Medicinal Chemistry* **2016**, *119*, 132–140.

DOI:

[10.1016/j.ejmech.2016.04.047](https://doi.org/10.1016/j.ejmech.2016.04.047)

Supporting information:

<https://ars.els-cdn.com/content/image/1-s2.0-S0223523416303403-mmc1.docx>

Tyrosol and hydroxytyrosol derivatives as antitrypanosomal and antileishmanial agents

Efres Belmonte-Reche ^a, Marta Martínez-García ^a, Pablo Peñalver ^{a,b}, Verónica Gómez-Pérez ^a, Ricardo Lucas ^{a,b}, Francisco Gamarro ^a, José María Pérez-Victoria ^{a,*}, Juan Carlos Morales ^{a,b,*}

^a Department of Biochemistry and Molecular Pharmacology, Institute of Parasitology and Biomedicine López-Neyra, CSIC, Avda. del Conocimiento, 17, 18016 Armilla-Granada, Spain;

^b Department of Bioorganic Chemistry, Institute of Chemical Research, CSIC – University of Seville, Avda. Americo Vespucio, 49, 41092 Sevilla, Spain

Corresponding author: José María Pérez-Victoria (josepv@ipb.csic.es)

Juan Carlos Morales (jcmorales@ipb.csic.es)

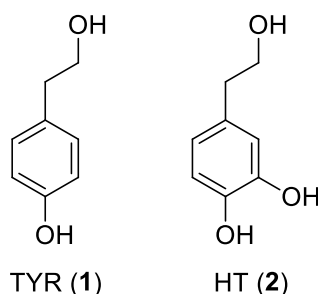
1. Introduction

Infectious diseases caused by protozoan parasites affect millions of people around the world, especially in tropical and subtropical areas. Among them, leishmaniasis (caused by different species of *Leishmania*) is a major global health problem with around 12 million people infected and causing 1-2 million new cases every year. *Trypanosoma brucei*, transmitted by the tsetse fly, is responsible for sleeping sickness in humans and preclude the development of productive livestock and agricultural activity based on domesticated animals where it causes Nagana.[1-2] For these reasons, this parasite is considered to be one of the major root causes of hunger and poverty in sub-Saharan Africa. Current treatments for both diseases present important drawbacks such as high toxicity, increased resistance and variability on their efficacy depending on the different strain of the parasite. Thus, the development of new antiparasitic therapies continues to be necessary.

Natural products have been tested for decades to find new antitrypanosomal and antileishmanial agents. Among them, several phenolics and polyphenols have shown relevant activity. For example, flavonoids such as 7,8-dihydroxyflavone, 3-hydroxyflavone and rhamnetin showed low micromolar IC₅₀ values for *Trypanosoma brucei rhodesiense* and others such as luteolin and quercetin also displayed low micromolar IC₅₀s for *Leishmania donovani*[3]. In fact, quercetin glycosides present in the aqueous extract of *Kalanchoe pinnata* were active by oral administration in experimental cutaneous and visceral leishmaniasis infections produced *in vivo*[4-5].

Tyrosol (TYR, **1**) and hydroxytyrosol (HT, **2**) (Figure 1) are natural phenolic antioxidants present in olives and olive oil. They have shown a diverse biological activity such as antibacterial[6-7], antiviral[8], anti-inflammatory[9-12], neuroprotective[13] and anticancer activity,[14] inhibition of human LDL oxidation[15] and prevention of platelet aggregation[16]. Recently, Moradi-Afrapoli *et al.* reported medium activity of TYR against *Trypanosoma brucei rhodesiense* ($IC_{50} > 15\mu M$)[17]. To the best of our knowledge, HT has not been examined for activity against *T. brucei*. Though, moderate antileishmanial activity was reported for HT against both, promastigotes of *L. infantum*, *L. donovani*, and *L. major*, and against *L. donovani* amastigotes that parasitize J774A.1 macrophages[18].

Figure 1.



The preparation of chemically-modified natural products to improve their antiparasitic activity is still a very active source of potential new drugs. This is the case of chalcone[19] or caracaine acid derivatives[20], or the preparation of hybrids such as *Cinchona* alkaloids with bile acids[21] or caffeine-based chalcones[22]. Tyrosol and hydroxytyrosol derivatives have also been synthesized in order to improve the antioxidant and biological properties of the parent compounds. Hydroxytyrosol fatty acid esters increased the protection of proteins and lipids against oxidation caused by peroxyl radicals in a brain homogenate as an *ex vivo* model[23]. Similarly, hydroxytyrosol acetate was able to reduce the metabolic imbalance induced by a high-cholesterol diet in rats to a higher extent than HT[24]. Finally, HT alkyl ether derivatives, more stable under biological conditions than HT, have been reported to exert antiproliferative[25], neuroprotective[26-27], antiplatelet and anti-inflammatory effects[28] that are greater than those of HT.

Due to the improved biological activity found for several HT derivatives with respect to HT itself, we decided to investigate the antitrypanosomal and antileishmanial activity of a series of TYR and HT derivatives. We prepared a series of tyrosol and hydroxytyrosol fatty acid esters together with three metabolites of HT and TYR, tyrosol sulfate, tyrosol glucuronate and

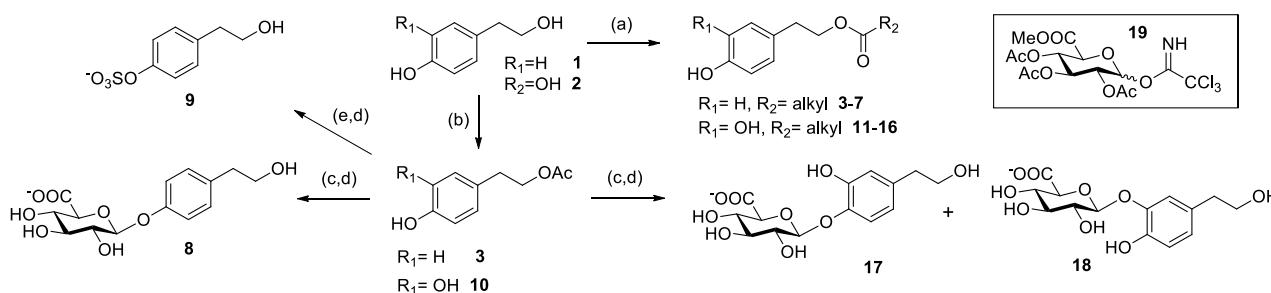
hydroxytyrosol glucuronate for a first *in vitro* screening. Later, we synthesized a focused library of compounds to explore structure-activity relevance varying the number of phenolic OH groups, the type of chemical bond between the phenolic ring and the alkyl chain, and the length of the alkyl chain.

2. Results and Discussion

2.1. Chemistry

Tyrosol and hydroxytyrosol fatty acid esters (**3-7** and **11-16**, respectively) were synthesized by enzymatic acylation using Novozym 435 and the corresponding vinyl acyl donor in t-butyl methyl ether as reported previously[29-31] (Scheme 1). Tyrosol and hydroxytyrosol glucuronates **8** and **17, 18** were prepared by glycosylation of the acetyl protected TYR or HT derivatives (**3** and **10**, respectively). We used the acetyl protected trichloroacetimidate glucuronosyl derivative **19** as glycosyl donor and boron trifluoride etherate as the catalyst in the glycosylation step. Final acetyl deprotection yielded glucuronate derivatives **8** and **17,18** as described previously[32]. TYR sulfate **9** was prepared following a similar strategy to the one used for the glucuronate derivative. Sulfation of tyrosol acetate **3** was carried out with $\text{SO}_3 \cdot \text{NMe}_3$ as sulfating reagent, NEt_3 as base, and acetonitrile as solvent at 100 °C under microwave radiation. The reaction afforded the sulfated TYR derivative in good yield. Final acyl deprotection and reverse phase purification gave TYR sulfate **9**.

Scheme 1

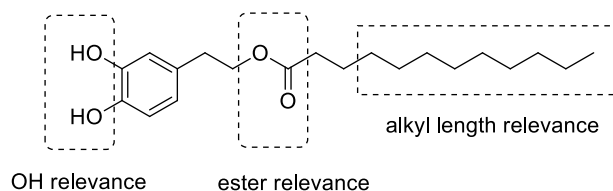


Reagents and conditions: (a) Vinyl alkyl ester, Novozym435, tBuOMe, 60°C; (b) EtOAc, Novozym435, 60°C; (c) **19**, $\text{BF}_3 \cdot \text{OEt}_2$, CH_2Cl_2 ; (d) Na_2CO_3 , MeOH, H_2O ; (e) $\text{SO}_3 \cdot \text{NMe}_3$, TEA, CH_3CN , 100°C, 20 min, MW

We identified hydroxytyrosol decanoate ester **13** and hydroxytyrosol dodecanoate ester **14** as relevant hit compounds against *T.brucei* (see below, Table 2) after carrying out the first *in vitro* screening on *T. brucei* and *L. donovani*. We decided then to perform structure-activity studies on **13** and **14** by changing the phenolic hydroxyl groups, the type of chemical bond between the

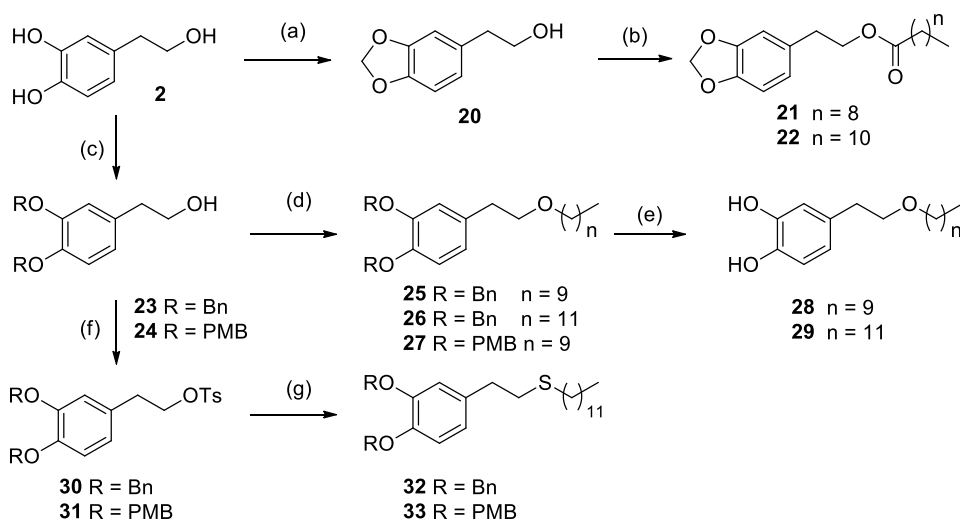
phenolic ring and the alkyl chain, and the length of the alkyl chain (Figure 2) in order to improve its biological activity.

Figure 2



We synthesized a hydroxyl protected version of compound **14** by formation of the acetal derivative **22** and also a shorter version with a decanoate alkyl chain, compound **21** (Scheme 2). The cyclic acetal intermediate **20** was obtained by reaction of HT with CH_2Cl_2 in basic conditions and then acylated using the enzymatic conditions used previously for HT yielding the desired compounds. The ether analogue of **14**, compound **29**, was prepared as reported previously[33] by benzyl protection of the phenolic groups, alkylation with 1-iodododecane under basic conditions and final hydrogenation. The HT ether decanoate derivative **28** was prepared following the same procedure. We also prepared the p-methoxybenzyl (PMB) protected HT derivative **24** trying to improve the yields of the route. However, deprotection with trifluoroacetic acid of the ether intermediate **27** was unsuccessful. The synthesis of the thioether analogue of **14** was attempted next. Tosylation of derivatives **23** and **24** was followed by nucleophilic displacement with 1-dodecanethiol producing the protected thioether derivatives **32** and **33** with moderate yields. Neither hydrogenation nor reaction under strong acidic conditions yielded the final thioether deprotected products.

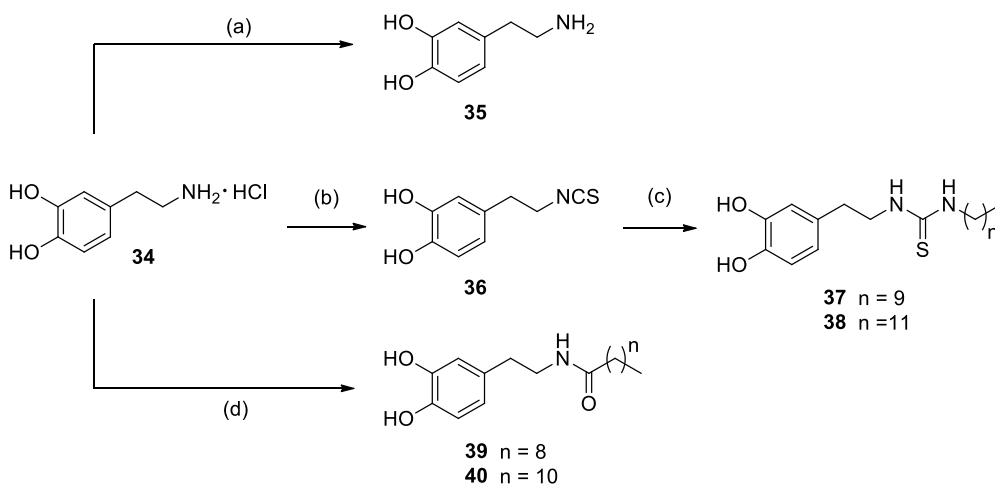
Scheme 2



Reagents and conditions: (a) CH_2Cl_2 , K_2CO_3 , DMF, Reflux; (b) Vinyl alkyl ester, Novozym435, tBuOMe; (c) BrBn or PMBBr, K_2CO_3 , Acetone, Reflux; (d) $\text{I}(\text{CH}_2)_n\text{CH}_3$, KOH, DMSO, 50 °C; (e) H_2 , Pd, 4 atm, THF; (f) TsCl, TEA, DCM, 0 °C; (g) $\text{HS}(\text{CH}_2)_{11}\text{CH}_3$, K_2CO_3 , THF.

Dopamine hydrochloride was the starting material for the synthesis of the amide and thiourea analogues of **13** and **14** (compounds **37-40**) (Scheme 3). Dopamine was also synthesized to compare its activity with HT. The thiourea derivatives were synthesized by reaction of the isothiocyanate intermediate **36** with the corresponding primary alkylamine to obtain the products in moderate yields. The amide analogues of **13** and **14** were prepared by reaction of dopamine hydrochloride with the corresponding fatty acids using HATU as the coupling reagent.

Scheme 3



Reagents and conditions: (a) KOH, MeOH; (b) CS_2 , TEA, MeOH, THF; (c) $\text{H}_2\text{N}(\text{CH}_2)_n\text{CH}_3$, TEA, Pyridine; (d) $\text{CH}_3(\text{CH}_2)_n\text{COOH}$, HATU, TEA, THF.

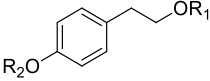
2.2. Biological evaluation

The *in vitro* antiparasitic activities of TYR, HT and their derivatives **3-18** were evaluated against *T. brucei brucei* and against axenic amastigotes of *L. donovani*. Those compounds exhibiting over 40% inhibition of axenic amastigotes at 20 μM were also evaluated on intracellular amastigotes of *L. donovani*. The cytotoxicity of these compounds was also evaluated against a human non-tumoral lung cell line (MRC-5). Suramin and amphotericin B were used as positive drug controls for *T. brucei* and *L. donovani*, respectively. Selectivity indices (SI) were calculated according to the formula: $\text{IC}_{50}(\text{MRC-5}) / \text{IC}_{50}(\text{parasite})$. The activity gain (AG) of each compound with respect to the reference compound (TYR or HT) was calculated according to the formulas: $\text{IC}_{50}(\text{TYR}) / \text{IC}_{50}(\text{compound})$ and $\text{IC}_{50}(\text{HT}) / \text{IC}_{50}(\text{compound})$.

Table 1 presents the antiparasitic and cytotoxic data for TYR and its derivatives **3-9**. IC_{50} values against *T. brucei* ranged from 10 to 62.7 μM and selectivity indices from 1.5 to 5. None of the TYR derivatives improved the activity of TYR itself as can be observed from the AG values. In the case of *L. donovani*, compounds **4** and **5** showed inhibition over 40% of axenic amastigotes at 20 μM concentration. These two derivatives were evaluated on intracellular amastigotes and showed IC_{50} values $>10 \mu\text{M}$. Aissa *et al.*[34] measured antileishmanial activity against *L. major* and *L. infantum* parasite species for tyrosol fatty acid esters from C2 to C18 chain length. They found the best IC_{50} values for medium chain tyrosyl derivatives **5-7** (e.g. tyrosol decanoate **6**: 65 and 132 μM , against *L. major* and *L. infantum*, respectively). The authors proposed this effect could be due to the surfactant activity reported for these medium chain tyrosyl fatty acid esters.[35]

When HT and its derivatives **10-18** were evaluated against *T. brucei* (Table 2), compounds **13-16** showed IC_{50} s in the low micromolar range (0.36-2.43 μM). Remarkably, hydroxytyrosol decanoate **13** and hydroxytyrosol dodecanoate **14** displayed a high selectivity index (118 and 101, respectively) and a large increase in activity with respect to HT (AG values of 79 and 132, respectively). A length of the alkyl chain around 10 to 12 carbons seems to be the optimum on this series. When these compounds were examined against axenic amastigotes of *L. donovani*, three of them (compounds **11-13**) exhibited over 40% inhibition at 20 μM concentration. When they were evaluated on intracellular amastigotes, the best IC_{50} value was displayed by hydroxytyrosol decanoate **13** (8.44 μM). Kyriazis *et al.*[18] had previously reported IC_{50} data for hydroxytyrosol of 393 μM against *L. donovani* and in the same range for *L. infantum* and *L. major*. We have observed that the addition of a fatty acid ester group to HT improves its activity with respect to HT against *L. donovani* although only to IC_{50} s in the low micromolar range.

Table 1. Cytotoxic, trypanocidal and leishmanicidal activities of tyrosol derivatives.

Compounds			<i>T.brucei</i> S-16				<i>L.donovani</i>			
	R ₁	R ₂	Cytotoxicity MRC-5 IC ₅₀ (μM)	IC ₅₀ (μM)	SI	AG	Axenic amastigotes % inhib. (20μM)	Intracellular amastigotes IC ₅₀ (μM)	SI	AG
TYR (1)	H	H	>500	>10	> 5	--	50	>10	5	--
3	COCH ₃	H	113.6 ± 11.3	79.4 ± 23.1	1.4	0.13	28	n.d.	--	--
4	CO(CH ₂) ₄ CH ₃	H	166.4 ± 0.6	59.1 ± 2.3	2.8	0.16	44	>10	16.6	1
5	CO(CH ₂) ₆ CH ₃	H	133.0 ± 9.8	56.8 ± 8.3	2.3	0.22	46	>10	13.3	1
6	CO(CH ₂) ₈ CH ₃	H	171.5 ± 15.7	81.4 ± 19.3	2.1	0.16	34	n.d.	--	--
7	CO(CH ₂) ₁₀ CH ₃	H	67.2 ± 0.2	16.2 ± 3.8	4.1	0.52	32	n.d.	--	--
8	H	GlcAc	110.2 ± 14.4	61.5 ± 23.8	1.8	0.17	36	n.d.	--	--
9	H	SO ₃ ⁻ K ⁺	106.4 ± 17.2	41.6 ± 12.6	2.6	0.16	36	n.d.	--	--
Suramin			--	0.038 ± 0.003				--		
Eflornitin			--	0.026 ± 0.002				--		
Amphotericin B			--	--				0.10 ± 0.01		

Experiments on *L. donovani* were carried out in axenic amastigotes and intracellular amastigotes.

SI= Selectivity Index (IC₅₀ MRC-5 / IC₅₀ parasite); AG= Activity gain (IC₅₀ tyrosol / IC₅₀ compound)

Table 2. Cytotoxic, trypanocidal and leishmanicidal activities of hydroxytyrosol derivatives.

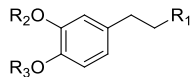
Compounds	Chemical structure		Cytotoxicity MRC-5	<i>T.brucei</i> S-16			<i>L.donovani</i>			
	R ₁	R ₂ , R ₃	IC ₅₀ (μM)	IC ₅₀ (μM)	SI	AG	Axenic amastigotes % inhib. (20μM)	Intracellular amastigotes IC ₅₀ (μM)	SI	AG
HT (2)	H	H, H	>50	47.5 ± 16.9	> 1	--	0	n.d.	--	--
10	COCH ₃	H, H	>50	43.4 ± 14.0	> 1	1	48	>10	--	--
11	CO(CH ₂) ₂ CH ₃	H, H	71.5 ± 15.5	9.4 ± 1.4	8	5	48	>10	7.1	--
12	CO(CH ₂) ₆ CH ₃	H, H	103.5 ± 15.2	9.6 ± 0.8	11	5	45	>10	10.3	--
13	CO(CH ₂) ₈ CH ₃	H, H	71.1 ± 6.9	0.6 ± 0.24	118	79	54	8.44 ± 1.6	8.4	--
14	CO(CH ₂) ₁₀ CH ₃	H, H	38.1 ± 2.4	0.36 ± 0.01	106	132	56	>10	--	--
15	CO(CH ₂) ₁₂ CH ₃	H, H	> 50	2.29 ± 0.48	> 22	21	53	>10	--	--
16	CO(CH ₂) ₁₄ CH ₃	H, H	> 50	2.43 ± 0.33	> 21	20	52	>10	--	--
17-18	H	GlcAc, H	118.8 ± 21.5	62.3 ± 16.8	2	0.8	31	n.d.	--	--

Experiments on *L. donovani* were carried out in axenic amastigotes and intracellular amastigotes.

SI= Selectivity Index (IC₅₀ MRC-5 / IC₅₀ parasite); AG= Activity gain (IC₅₀ hydroxytyrosol / IC₅₀ compound)

After performing this first *in vitro* screening on *T. brucei* and *L. donovani* for TYR, HT and their derivatives **3-18**, we decided to focus our efforts only on new compounds against *T. brucei*. We carried out a structural-activity study of analogues of hydroxytyrosol fatty acid esters **13** and **14** (Table 3) in order to probe the relevance of the phenolic hydroxyl groups, the type of chemical bond between the phenolic ring and the length of the alkyl chain.

Table 3. Cytotoxic and trypanocidal activities of hydroxytyrosol derivatives **19-40**.

Compounds			Cytotoxicity			
	R ₁	R ₂ , R ₃	MRC-5 IC ₅₀ (μM)	<i>T. brucei</i> S-16		
				IC ₅₀ (μM)	SI	AG
21	OCO(CH ₂) ₈ CH ₃	-CH ₂ -	>50	>10 (n=2)	> 5	> 5
22	OCO(CH ₂) ₁₀ CH ₃	-CH ₂ -	>50	>10 (n=3)	> 5	> 5
25	O(CH ₂) ₉ CH ₃	Bn, Bn	>50	>10 (n=3)	> 5	> 5
27	O(CH ₂) ₉ CH ₃	PMB, PMB	>50	>10 (n=2)	> 5	> 5
28	O(CH ₂) ₉ CH ₃	H, H	>50	1.29 ± 0.21	> 38	37
29	O(CH ₂) ₁₁ CH ₃	H, H	13.19 ± 2.90	0.63 ± 0.07	21	75
32	S(CH ₂) ₁₁ CH ₃	Bn, Bn	>50	>10 (n=2)	> 5	5
33	S(CH ₂) ₁₁ CH ₃	PMB, PMB	>50	>10 (n=2)	> 5	5
35	NH ₂	H, H	68.9 ± 15.11	>10 (n=2)	7	5
36	NCS	H, H	21.13 ± 8.78	9.87 ± 1.02	2	5
37	NHSNH(CH ₂) ₈ CH ₃	H, H	24.8	0.74 ± 0.36	33	64
38	NHSNH(CH ₂) ₁₀ CH ₃	H, H	2.96 ± 1.20	0.77 ± 0.28	4	62
39	NHCO(CH ₂) ₈ CH ₃	H, H	>50	>10 (n=4)	> 5	5
40	NHCO(CH ₂) ₁₀ CH ₃	H, H	>50	8.74 ± 1,15	> 5	5

SI= Selectivity Index (IC₅₀ MRC-5 / IC₅₀ *T. brucei*); AG= Activity gain (IC₅₀ hydroxytyrosol / IC₅₀ compound)

We found that the phenolic hydroxyl groups seem to be essential for activity against *T. brucei* since changing them to a methylene acetal (compounds **21** and **22**) or protecting them with benzyl or p-methoxybenzyl groups (compounds **25**, **27**, **32** and **33**) increased their IC₅₀ values (> 10 μM) with respect to those of **13** and **14**. The type of bond linking the alkyl chain to the HT scaffold on these compounds (ester, ether or thioether) appears to be much less important for their activity. When both phenolic hydroxyl groups and the medium size alkyl chain still remain as part of the structure of the compounds, the functional group connecting them seems to be less relevant. Actually, the hydroxytyrosol ether analogues **28** and **29**, and the thiourea analogues **37** and **38**

showed similar IC_{50} values (0.63 to 1.29 μM) to those of the ester derivatives **13** and **14**. In contrast, the amide derivatives **39** and **40** presented slightly worse antitrypanosomal activity (>10 and 8.74 μM , respectively) than the ester derivatives. However, none of the new compounds displayed better selectivity index than compounds **13** and **14** and their activity gain with respect to HT was lower too. Finally, the length of the alkyl chain seems optimum at 10-12 carbon atoms independently of the bond connecting it to the HT scaffold. Only a two-fold difference is observed for the ester and ether derivatives with decyl and dodecyl chains.

Hydroxytyrosol decanoate **13** and hydroxytyrosol dodecanoate **14** possess relevant surfactant properties, even better than medium chain tyrosyl fatty acid esters.[35] So, it could be argued that **13** and **14** are acting as nonspecific detergents disrupting the parasite's membrane. Another possibility is they could be inhibiting fatty acid biosynthesis, through inhibition of FabG, FabI or FabZ enzymes. The structural similarity of **13** and **14** with *trans*-2-hexadecenoyl-(*N*-acetylcysteamine)-thioester, a FabI inhibitor,[36-37] or with 2-, 5-, 6-, and 9-hexadecynoic acids (HDAs), inhibitors of FabG, FabI and FabZ of *P.falciparum*,[38] could be pointing to these potential therapeutic targets. In both cases, the inhibitors possess long alkyl chains (13 to 16 atoms in length) together with one or two groups at the end of the compound capable of accepting or donating hydrogen bonds resembling the scaffolds of compounds **13** and **14**.

3. Conclusions

We have examined the trypanocidal and leishmanicidal activities of several tyrosol and hydroxytyrosol fatty acid esters together with three of TYR and HT metabolites. We found notable IC_{50} values against *T. brucei* for HT decanoate ester **13** and HT dodecanoate ester **14** (0.6 and 0.36 μM , respectively) and against *L. donovani* for **14** (8.44 μM). We synthesized several analogues of **13** and **14** to investigate structure-activity relationship in *T. brucei*. We observed that the di-ortho phenolic ring and the medium size alkyl chain are essential for activity but the nature of the chemical bond among them is not so relevant.

4. Experimental Section

4.1. General

All chemicals were used without further purification, unless otherwise noted. All reactions were monitored by TLC on precoated Silica-Gel 60 plates F254, and detected by heating with 5% sulfuric acid in ethanol or Mostain (500 ml of 10% H_2SO_4 , 25g of $(\text{NH}_4)_6\text{Mo}_7\text{O}_{24}\cdot 4\text{H}_2\text{O}$, 1g $\text{Ce}(\text{SO}_4)_2\cdot 4\text{H}_2\text{O}$). Products were purified by flash chromatography with Silica gel 60 (200-400 mesh). Low resolution mass spectra were obtained on an ESI/ion trap mass spectrometer. High

resolution mass spectra were obtained on an ESI/quadrupole mass spectrometer. NMR spectra were recorded on a 300, 400 or 500 MHz [300 or 400 MHz (^1H), 75 or 100 (^{13}C)] NMR spectrometers, at room temperature for solutions in CDCl_3 , D_2O or CD_3OD . Chemical shifts are referred to the solvent signal. 2D experiments (COSY, TOCSY, ROESY, and HMQC) were done when necessary to assign the new compounds. Chemical shifts are in ppm. Data were processed using manufacturer software, raw data were multiplied by shifted exponential window function prior to Fourier transform, and the baseline was corrected using polynomial fitting.

4.2. Synthesis

Preparation of 2-(benzo[d][1,3]dioxol-5-yl)ethyl decanoate (21)

To a solution of **20**[39] (45 mg, 0.271 mmol) in *tert*-butyl methyl ether (3 ml), vinyl decanoate (0.061 ml, 0.271 mmol) and *Candida antarctica lipase* (Novozym 435, 200 mg) were added. The reaction was stirred by an orbital shaker for 24h at 55 °C and then the enzyme was separated and washed. The solvent was concentrated and purified by silica-gel flash column chromatography using a mixture of hexane/ethyl acetate, 9:1 (v/v). Evaporation of the solvents yielded 18.6 mg of the pure product as a white solid (Yield = 22%; R_f = 0.67 (Hexane/ethyl acetate, 4:1)). ^1H NMR (300 MHz, CDCl_3) δ = 6.77 – 6.47 (m, 3H, CH_{arom}), 5.86 (s, 2H, OCH_2O), 4.16 (t, J = 7.0 Hz, 2H, CH_2O), 2.77 (t, J = 6.9 Hz, 2H, $\text{CH}_2\text{CH}_2\text{O}$), 2.21 (t, J = 7.5 Hz, 2H, CH_2COO), 1.51 (d, J = 6.2 Hz, 2H, $\text{CH}_2\text{CH}_2\text{COO}$), 1.19 (s, 12H, CH_2), 0.81 (t, J = 5.4 Hz, 3H, CH_3); ^{13}C NMR (75 MHz, CDCl_3) δ = 174.0 (COO), 147.9 ($\text{C}^3_{\text{ipsoO}}$), 146.4 ($\text{C}^4_{\text{ipsoO}}$), 131.9 (C^1_{ipso}), 122.0 (C^6_{arom}), 109.6 (C^2_{arom}), 108.5 (C^5_{arom}), 101.1 (OCH_2O), 65.1 (C_1), 35.1 (C_2), 34.6 (CH_2COO), 32.1 (CH_2), 29.7 (CH_2), 29.5 (CH_2), 29.4 (CH_2), 25.2 (CH_2), 22.9 (CH_2), 14.4 (CH_3); ESI-HRMS [$\text{M} + \text{Na}$] calcd for $\text{C}_{19}\text{H}_{28}\text{O}_4$ 343.1885, found 343.1875.

Preparation of 2-(benzo[d][1,3]dioxol-5-yl)ethyl dodecanoate (22)

Following the same procedure used to prepare compound **21**, with vinyl dodecanoate (0.075 ml, 0.289 mmol) as the acylating agent, afforded 71.5 mg as a white solid (Yield = 71%; R_f = 0.65 (Hexane/ethyl acetate, 4:1)). ^1H NMR (300 MHz, CDCl_3) δ = 6.72 – 6.53 (m, 3H, CH_{arom}), 5.86 (s, 2H, OCH_2O), 4.16 (t, J = 7.0 Hz, 2H, CH_2O), 2.77 (t, J = 7.0 Hz, 2H, $\text{CH}_2\text{CH}_2\text{O}$), 2.21 (t, J = 7.5 Hz, 2H, CH_2COO), 1.58 – 1.47 (m, 2H, $\text{CH}_2\text{CH}_2\text{COO}$), 1.19 (s, 16H, CH_2), 0.81 (t, J = 6.6 Hz, 3H, CH_3); ^{13}C NMR (75 MHz, CDCl_3) δ = 174.0 (COO), 147.9 ($\text{C}^3_{\text{ipsoO}}$), 146.4 ($\text{C}^4_{\text{ipsoO}}$), 131.9 (C^1_{ipso}), 122.0 (C^6_{arom}), 109.6 (C^2_{arom}), 108.5 (C^5_{arom}), 101.1 (OCH_2O), 65.1 (C_1), 35.1 (C_2), 34.6 (CH_2COO), 32.2 (CH_2), 29.9 (CH_2), 29.7 (CH_2), 29.6 (CH_2), 29.5 (CH_2), 29.4 (CH_2), 25.2 (CH_2), 22.9 (CH_2), 14.4 (CH_3); ESI-HRMS [$\text{M} + \text{Na}$] calcd for $\text{C}_{21}\text{H}_{32}\text{O}_4$ 371.2198, found 371.2204.

Preparation of 2-(3,4-bis(benzyloxy)phenyl)ethan-1-ol (23)

Benzyl bromide (1.62 ml, 13.62 mmol) was added to a mechanically stirred degassed suspension of hydroxytyrosol (1 g, 6.49 mmol) and potassium carbonate (3.59 g, 25.9 mmol) in dry acetone (20 ml) and the resulting mixture was refluxed for 12 h. The reaction was then filtered through a celite © pad and purified by silica-gel flash chromatography column (hexane/ethyl acetate, 3:1 (v/v) as solvents) obtaining 1.68 g of the desired product as a white solid (Yield = 77%; R_f = 0.16 (hexane: ethyl acetate, 3:1)). The spectroscopic data coincide with the previous report[33].

Preparation of 2-(3,4-bis(4-methoxybenzyloxy)phenyl)ethan-1-ol (24)

Following the same procedure used to prepare compound **23**, with hydroxytyrosol (175 mg, 1.135 mmol), potassium carbonate (377 mg, 2.72 mmol) and 4-methoxybenzyl chloride (0.339 ml, 2.497 mmol) in DMF (2 ml), afforded 249.5 mg of the pure product as a white solid (yield = 56%; R_f = 0.35 (Hexane/ethyl acetate, 2:1)). Solvent purification mixture: Hexane/ethyl acetate, 4:1 (v/v). $^1\text{H NMR}$ (500 MHz, CDCl_3) δ = 7.23 (dd, J = 8.7, 2.0 Hz, 4H, H_{PMB}), 6.76 (dd, J = 8.5, 1.8 Hz 5H, H_{PMB} and $\text{H}'2$), 6.70 (d, J = 1.9 Hz, 1H, $\text{H}'5$), 6.61 (dd, J = 8.1, 2.0 Hz, 2H, $\text{H}'6$), 4.94 (s, 2H, $\text{CH}_2^{\text{PMB}}\text{O}$), 4.93 (s, 2H $\text{CH}_2^{\text{PMB}}\text{O}$), 3.69 (s, 3H, CH_3O), 3.69 (s, 3H, CH_3O), 3.66 (t, J = 6.4 Hz, 2H, CH_2OH), 2.64 (t, J = 6.5 Hz, 2H, $\text{CH}_2\text{CH}_2\text{OH}$); $^{13}\text{C NMR}$ (75 MHz, CDCl_3) δ = 159.3 (C_{ipso}), 149.1 (C_{ipso}), 147.9 (C_{ipso}), 131.8 (C_{ipso}), 129.5 (C_{ipso}), 129.4 (C_{ipso}), 129.1 ($\text{C}_{\text{arom}}^{\text{PMB}}$), 129.0 ($\text{C}_{\text{arom}}^{\text{PMB}}$), 121.9 (C_{arom}^6), 116.5 (C_{arom}^2), 115.8 (C_{arom}^5), 113.8 ($\text{C}_{\text{arom}}^{\text{PMB}}$), 71.4 ($\text{C}_{\text{H}_2\text{O}}^{\text{PMB}}$), 71.2 ($\text{C}_{\text{H}_2\text{O}}^{\text{PMB}}$), 63.7 (CH_2OH), 55.3 (CH_3O), 38.7 ($\text{CH}_2\text{CH}_2\text{OH}$); ESI-HRMS $[\text{M} + \text{Na}]$ calcd for $\text{C}_{24}\text{H}_{26}\text{O}_5$ 417.1678, found 417.1658.

Preparation of 1,2-bis((4, 4'-methoxybenzyl)oxy)-4-(2-(decyloxy)ethyl)benzene (27)

Compound **24** (50 mg, 0.127 mmol) and potassium hydroxide (49.8 mg, 0.887 mmol) were added to DMSO (2 ml) in a round-bottomed flask. 1-Iododecane (0.081 ml, 0.380 mmol) was then added and the reaction was heated to 50 °C and stirred overnight. The reaction mixture was diluted with hydrochloric acid (5%, 25 mL) and extracted with CH_2Cl_2 (3 x 25 mL). The combined organic layers were then dried with MgSO_4 , filtered and concentrated. The crude was purified by silica-gel flash column chromatography eluting with hexane/ethyl acetate, 3:1 (v/v) obtaining 40.5 mg of the pure product as a white solid (Yield = 60%; R_f = 0.8 (hexane/ethyl acetate, 2:1)). $^1\text{H NMR}$ (300 MHz, CDCl_3) δ = 7.27 (dd, J = 8.5, 4.7 Hz, 4H, H_{PMB}), 6.84 – 6.73 (m, 6H, H_{PMB} , $\text{H}'2$ and $\text{H}'5$), 6.68 – 6.61 (m, 1H, $\text{H}'6$), 4.97 (s, 2H, $\text{CH}_2^{\text{PMB}}\text{O}$), 4.95 (s, 2H, $\text{CH}_2^{\text{PMB}}\text{O}$), 3.73 (s, 3H, CH_3O), 3.72 (s, 3H, CH_3O), 3.48 (t, J = 7.3 Hz, 2H, CH_2O), 3.33 (t, J = 6.7 Hz, 2H, CH_2O), 2.70 (t, J = 7.2 Hz, 2H, $\text{CH}_2\text{CH}_2\text{O}$), 1.49 (dd, J = 13.5, 6.8 Hz, 2H, $\text{CH}_2\text{C}_{\text{ipso}}$), 1.18 (s, 16H, CH_2), 0.80 (t, J = 6.6 Hz, 3H, CH_3CH_2); $^{13}\text{C NMR}$ (126 MHz, CDCl_3) δ = 159.3 (C_{ipso}), 159.2 (C_{ipso}), 149.0 (C_{ipso}), 147.6 (C_{ipso}), 132.6 (C_{ipso}), 129.6 (C_{ipso}), 129.5 (C_{ipso}), 129.1

(C^{PMB}_{arom}), 129.0 (C^{PMB}_{arom}), 121.7 (C⁶_{arom}), 116.4 (C²_{arom}), 115.7 (C⁵_{arom}), 113.8 (C^{PMB}_{arom}), 113.8 (C^{PMB}_{arom}), 71.9 (CH₂O), 71.4 (CH₂O), 71.2 (CH₂O), 71.1 (CH₂O), 55.3 (CH₃O), 35.9 (CH₂), 31.9 (CH₂), 29.8 (CH₂), 29.6 (CH₂), 29.6 (CH₂), 29.5 (CH₂), 29.3 (CH₂), 26.2 (CH₂), 22.7 (CH₂), 14.1 (CH₃CH₂); ESI-HRMS [M + Na] calcd for C₃₄H₄₆O₅ 557.3243, found 557.3237.

Preparation of 3,4-bis(benzyloxy)phenethyl 4-methylbenzenesulfonate (30)

Tosyl chloride (0.855 g, 4.49 mmol) was dissolved in CH₂Cl₂ (1.5 ml) in a 10 mL flask under argon atmosphere. Compound **23** (1 g, 2.99 mmol) and triethylamine (1.250 ml, 8.97 mmol) were dissolved in CH₂Cl₂ (1.5 ml) in a second 10 mL flask under argon atmosphere and then cooled to 0 °C. The tosyl chloride solution was added at a rate of 0.75 mL/h (time = 2h) whilst stirring and the reaction was then left to react for another 21h at room temperature. The reaction mixture was then washed with water (3 x 20mL) and the organic phases were combined, concentrated and purified by silica gel column eluting with hexane/ethyl acetate, 3:1 (v/v) to give a yellow oil (Yield = 98%). ¹H NMR (300 MHz, CDCl₃) δ = 7.71 (d, *J* = 8.2 Hz, 2H, H^{Ts}), 7.48 (d, *J* = 7.0 Hz, 4H, H^{Bn}), 7.39 (dd, *J* = 16.2, 8.5 Hz, 6H, H^{Bn}), 7.30 (d, *J* = 8.1 Hz, 2H, H^{Ts}), 6.87 (d, *J* = 8.1 Hz, 1H, H^{HT}), 6.75 (s, 1H, H²), 6.67 (d, *J* = 8.1 Hz, 1H, H^{HT}), 5.14 (d, *J* = 15.3 Hz, 4H, CH₂O^{Bn}), 4.19 (t, *J* = 7.0 Hz, 2H, CH₂O), 2.89 (t, *J* = 7.9 Hz, 2H, CH₂CH₂O), 2.44 (s, 3H, CH₃); ¹³C NMR (75 MHz, CDCl₃) δ = 149.2 (C_{ipso}), 148.2 (C_{ipso}), 144.9 (C_{ipso}), 137.6 (C_{ipso}), 137.4 (C_{ipso}), 133.3 (C_{ipso}), 130.0 (C_{ipso}), 129.8 (C_{arom}), 128.7 (C_{arom}), 128.1 (C_{arom}), 127.6 (C_{arom}), 127.5 (C_{arom}), 122.1 (C_{arom}), 116.1 (C_{arom}), 115.5 (C_{arom}), 71.6 (CH₂O), 71.6 (CH₂O), 71.0 (CH₂O), 35.1 (CH₂CH₂O), 21.9 (CH₃); ESI-HRMS [M + Na] calcd for C₂₉H₂₈O₅S 511.1555, found 511.1561.

Preparation of 3,4-bis((4-methoxybenzyl)oxy)phenethyl 4-methylbenzenesulfonate (31)

Following the same procedure used to prepare compound **30**, with compound **24** (200 mg, 0.507 mmol) as starting material, tosyl chloride (145 mg, 0.761 mmol) and triethylamine (0.212 ml, 1.521 mmol) in 3 ml of DCM, afforded 184 mg of pure product as a yellow oil (Yield = 66%, R_f = 0.46 (hexane/ethyl acetate/Acetone, 4:2:1)). ¹H NMR (300 MHz, CDCl₃) δ = 7.52 (d, *J* = 8.2 Hz, 2H, H^{Ts}), 7.20 (d, *J* = 7.3 Hz, 4H, H^{PMB}), 7.10 (d, *J* = 8.0 Hz, 2H, H^{Ts}), 6.74 (dd, *J* = 8.6, 2.9 Hz, 4H, H^{PMB}), 6.68 (d, *J* = 8.2 Hz, 1H, H⁵), 6.57 (s, 1H, H²), 6.48 (d, *J* = 8.1 Hz, 1H, H⁶), 4.88 (s, 2H, CH₂O^{PMB}), 4.84 (s, 2H, CH₂O^{PMB}), 4.01 (t, *J* = 6.9 Hz, 2H, CH₂O), 3.64 (s, 3H, OCH₃), 3.63 (s, 3H, OCH₃), 2.69 (t, *J* = 6.9 Hz, 2H, CH₂CH₂O), 2.24 (s, 3H, CH₃); ¹³C NMR (75 MHz, CDCl₃) δ = 159.6 (C_{ipso}), 159.6 (C_{ipso}), 149.4 (C_{ipso}), 148.3 (C_{ipso}), 145.0 (C_{ipso}), 133.2 (C_{ipso}), 130.1 (C_{ipso}), 129.8 (C_{ipso}), 129.7 (C_{ipso}), 129.6 (C_{arom}), 129.4 (C_{arom}), 129.3 (C_{arom}), 128.1 (C_{arom}), 122.1 (C_{arom}), 116.4 (C_{arom}), 115.8 (C_{arom}), 114.1 (C_{arom}), 71.5 (CH₂O), 71.4 (CH₂O), 71.1 (CH₂O), 55.5 (CH₃O), 35.1 (CH₃O), 21.9 (CH₃); ESI-HRMS [M + Na] calcd for C₃₁H₃₂O₇S 571.1766, found 571.1771.

Preparation of (3,4-bis(benzyloxy)phenethyl)(dodecyl)sulfane (32)

To a mechanically stirred two socket flask under argon atmosphere was potassium carbonate (141 mg, 1.025 mmol) suspended in acetonitrile (5 ml) and heated to reflux. In a second and third flask under argon atmosphere was dodecane-1-thiol (0.054 ml, 0.225 mmol) dissolved in acetonitrile (1 ml) and compound **30** (100 mg, 0.205 mmol) dissolved in acetonitrile (2 ml), respectively. The second and third flask solutions were simultaneously added to the refluxing two socket flask and left to react for 48 h. The reaction product was then filtered, concentrated and purified by silica-gel flash chromatography column using a mixture of hexane/ethyl acetate, 9:1 (v/v) as solvents to obtain 50 mg of the desired product as a yellow oil (Yield = 47 %, $R_f = 0.83$ (Hexane: ethyl acetate – 4:1)). $^1\text{H NMR}$ (300 MHz, CDCl_3) δ 7.37 (dd, $J = 8.0, 2.4$ Hz, 4H, H^{Bn}), 7.26 (dtd, $J = 8.6, 6.7, 1.8$ Hz, 6H, H^{Bn}), 6.79 (d, $J = 8.2$ Hz, 1H, $\text{H}'5$), 6.73 (d, $J = 1.9$ Hz, 1H, $\text{H}'2$), 6.64 (dd, $J = 8.1, 1.9$ Hz, 1H, $\text{H}'6$), 5.07 (s, 2H, CH_2O), 5.05 (s, 2H, CH_2O), 2.74 – 2.64 (m, 2H, CH_2S), 2.64 – 2.55 (m, 2H, CH_2S), 2.46 – 2.34 (m, 2H, $\text{C}_{\text{ipso}}\text{CH}_2\text{CH}_2$), 1.52 – 1.45 (m, 2H, $\text{CH}_2\text{CH}_2\text{S}$), 1.18 (s, 18H, CH_2), 0.80 (t, $J = 6.6$ Hz, 3H, CH_3); $^{13}\text{C NMR}$ (75 MHz, CDCl_3) $\delta = 149.3$ (C_{ipso}), 147.8 (C_{ipso}), 137.7 (C_{ipso}), 137.6 (C_{ipso}), 134.5 (C_{ipso}), 128.7 (C^{Bn}), 128.0 (C^{Bn}), 128.0 (C^{Bn}), 127.6 (C^{Bn}), 127.6 (C^{Bn}), 121.6 (C^6_{arom}), 116.0 (C^2_{arom}), 115.5 (C^5_{arom}), 71.7 (OCH_2), 71.7 (OCH_2), 36.2 (SCH_2), 34.0 (SCH_2), 32.6 (CH_2), 32.2 (CH_2), 29.9 (CH_2), 29.9 (CH_2), 29.8 (CH_2), 29.6 (CH_2), 29.5 (CH_2), 29.2 (CH_2), 23.0 (CH_2), 14.4 (CH_3). ESI-HRMS [$\text{M} + \text{H}$] calcd for $\text{C}_{34}\text{H}_{46}\text{O}_2\text{S}$ 519.3297, found 519.3295.

Preparation of (3,4-bis((4-methoxybenzyl)oxy)phenethyl)(dodecyl)sulfane (33)

Following the same procedure used to prepare compound **32**, with compound **31** (100 mg, 0.182 mmol), potassium carbonate (126 mg, 0.911 mmol) and dodecane-1-thiol (0.048 ml, 0.2 mmol), afforded 97 mg of pure product as a yellow oil (Yield = 92 %, $R_f = 0.3$ (Hexane: ethyl acetate, 6:1)). $^1\text{H NMR}$ (300 MHz, CDCl_3) δ 7.26 (dd, $J = 8.4, 4.6$ Hz, 4H, H^{PMB}), 6.86 – 6.75 (m, 5H, H^{PMB} and $\text{H}'5$), 6.72 (d, $J = 1.5$ Hz, 1H, $\text{H}'2$), 6.63 (d, $J = 8.1$ Hz, 1H, $\text{H}'6$), 4.97 (s, 2H, CH_2O), 4.95 (s, 2H, CH_2O), 3.72 (s, 3H, CH_3O), 3.72 (s, 3H, CH_3O), 2.75 – 2.65 (m, 2H, CH_2S), 2.65 – 2.56 (m, 2H, CH_2S), 2.42 (t, $J = 7.4$ Hz, 2H, $\text{C}_{\text{ipso}}\text{CH}_2\text{CH}_2$), 1.57 – 1.42 (m, 2H, $\text{CH}_2\text{CH}_2\text{S}$), 1.18 (s, 18H, CH_2), 0.80 (t, $J = 6.5$ Hz, 3H, CH_3); $^{13}\text{C NMR}$ (75 MHz, CDCl_3) $\delta = 159.6$ (C_{ipso}), 159.5 (C_{ipso}), 149.3 (C_{ipso}), 147.9 (C_{ipso}), 134.5 (C_{ipso}), 129.8 (C_{ipso}), 129.7 (C_{ipso}), 129.4 (C_{arom}), 129.3 (C_{arom}), 121.6 (C_{arom}), 116.3 (C_{arom}), 115.9 (C_{arom}), 114.1 (C_{arom}), 71.6 (CH_2O), 71.6 (CH_2O), 55.5 (CH_3O), 36.2 (SCH_2), 34.1 (SCH_2), 32.6 (CH_2), 32.2 (CH_2), 30.0 (CH_2), 29.9 (CH_2), 29.9 (CH_2), 29.8 (CH_2), 29.6 (CH_2), 29.6 (CH_2), 29.2 (CH_2), 23.0 (CH_2), 14.4 (CH_3); ESI-HRMS [$\text{M} + \text{H}$] calcd for $\text{C}_{36}\text{H}_{50}\text{O}_4\text{S}$ 579.3508, found 579.3486.

Preparation of 4-(2-isothiocyanatoethyl)benzene-1,2-diol (36)

Triethylamine (1.617 ml, 11.60 mmol) was added to a stirring suspension of dopamine hydrochloride **34** (2 g, 10.55 mmol) in THF (26 ml). Methanol (20.80 ml) was slowly added to dissolve the dopamine hydrochloride, forming a clear solution. Carbon disulfide (3.17 ml, 52.7 mmol) was added to the mixture which was stirred for 1 h at 28 °C under argon atmosphere. The yellowish reaction mixture was cooled to 0°C and hydrogen peroxide (0.942 ml, 30% in water) was added drop wise (30%). The solution was immediately acidified with concentrated hydrochloric acid and then concentrated *in vacuo*. The resulting mixture was filtered and rinsed with water. The filtrate was extracted with ethyl acetate and the combined organic layers were dried over MgSO₄, filtered, and concentrated affording 740 mg of crude product as an oil (Yield = 36%). The spectroscopic data coincide with the previous report[40-41].

Preparation of 1-(3,4-dihydroxyphenethyl)-3-decylthiourea (37)

Compound **36** (355.7 mg, 1.822 mmol) and decan-1-amine (0.364 ml, 1.820 mmol) were dissolved in pyridine (10 ml) to give a yellow solution. The reaction was stirred for 3 h and triethylamine (0.254 ml, 1.822 mmol) was then added. The reaction was stirred for 1 h and then concentrated, diluted with 20 mL of hydrochloric acid (5%) and extracted with ethyl acetate (3 x 20 mL). The combined organic phases were concentrated and purified via silica-gel flash column chromatography while eluting with hexane/ethyl acetate, 2:1 (v/v) to give 338 mg of the pure product as a yellow solid (Yield = 53% R_f = 0.2 (hexane/ethyl acetate - 2:1)). ¹H NMR (300 MHz, CDCl₃) δ = 6.72 (d, *J* = 8.1 Hz, 2H, C²_{arom} and C⁵_{arom}), 6.56 (d, *J* = 7.9 Hz, 1H, C⁶_{arom}), 3.64 (t, *J* = 7.1 Hz, 2H, CH₂N), 3.39 (m, 2H, CH₂N), 2.74 (t, *J* = 7.1 Hz, 2H, CH₂C_{ipso}), 1.55 (t, 2H, CH₂CH₂N), 1.31 (s, 16H, CH₂), 0.91 (t, *J* = 6.7 Hz, 3H, CH₃); ¹³C NMR (75 MHz, CDCl₃) δ = 202.0 (NCN), 145.1 (C⁴_{arom}), 143.6 (C³_{arom}), 130.8 (C¹_{arom}), 120.0 (C⁶_{arom}), 115.8 (C²_{arom} or C⁵_{arom}), 115.3 (C²_{arom} or C⁵_{arom}), 34.6 (CH₂), 32.0 (CH₂), 29.6 (CH₂), 29.3 (CH₂), 26.9 (CH₂), 22.6 (CH₂), 13.4 (CH₃); ESI-HRMS [M + H] calcd for C₁₉H₃₂N₂O₂S 353.2252, found 353.2263.

Preparation of 1-(3,4-dihydroxyphenethyl)-3-dodecylthiourea (38)

Following the same procedure used to prepare compound **37**, from dodecan-1-amine (0.42 mL, 1.822 mmol), afforded 392.7 mg of the pure product as a yellow solid (Yield = 57% R_f = 0.5 (hexane/ethyl acetate - 1:1)). ¹H NMR (300 MHz, CDCl₃) δ = 6.68 (d, *J* = 8.0 Hz, 2H, C²_{arom} and C⁵_{arom}), 6.53 (dd, *J* = 8.0, 2.0 Hz, 1H, C⁶_{arom}), 3.61 (s, 2H, CH₂N), 3.30 (dt, *J* = 3.2, 1.6 Hz, 2H, CH₂N), 2.71 (t, *J* = 7.2 Hz, 2H, CH₂C_{ipso}), 1.56 – 1.46 (m, 2H, CH₂CH₂N), 1.29 (s, 18H, CH₂), 0.89 (t, *J* = 6.2 Hz, 3H, CH₃); ¹³C NMR (75 MHz, CDCl₃) δ = 196.0 (NHCNH), 146.3 (C⁴_{arom}), 144.5 (C³_{arom}), 131.9 (C¹_{arom}), 121.1 (C⁶_{arom}), 116.9 (C²_{arom} or C⁵_{arom}), 116.4 (C²_{arom} or C⁵_{arom}), 35.7 (CH₂), 35.7 (CH₂), 33.1 (CH₂), 30.7 (CH₂), 30.4 (CH₂), 28.0 (CH₂), 23.7 (CH₂), 14.4 (CH₃); ESI-HRMS [M + H] calcd for C₂₁H₃₆N₂O₂S 381.2576, found 381.2563.

4.3. Biological assays.

4.3.1. In vitro antitrypanosomal activity

Bloodstream forms (BSF) of *T. brucei brucei* 'single marker' S427 (S16) were grown at 37 °C, 5% CO₂ in HMI-9 medium supplemented with 10% (heat-inactivated fetal bovine serum, hiFBS). Drug susceptibility assay was performed as described in (Carvalho L et al, 2015). Briefly, parasites (1×10^4 BSF per mL) were incubated in 96-well plates with increasing concentration of drugs/compounds for 72 h at 37 °C, 5% CO₂ in culture medium. Cell proliferation was determined using the alamarBlue® assay[42]. The Alamar Blue assay to determine drug sensitivity of African trypanosomes (*T.b. rhodesiense* and *T.b. gambiense*) in vitro. Fluorescence was recorded with an Infinite® F200 microplate reader (Tecan Austria GmbH, Austria) equipped with 550 and 590 nm filters for excitation and emission wavelengths, respectively.

4.3.2. In vitro antileishmanial activity

The experiments of drug susceptibility on *L. donovani* were carried out in axenic amastigotes and intracellular amastigotes. Axenic *L. donovani* MHOM/ET/67/HU3 amastigote parasites were grown in Schneider medium supplemented with 20% hiFBS, pH 5.4 at 37 °C and 5% CO₂. 10^6 axenic amastigotes/ml in a 96-well plate were incubated with increasing concentrations of compounds for 72 h at 37 °C, followed by a resazurin-based assay, as described.[43] Additionally, we use intracellular amastigotes of a *L. donovani* (MHOM/ET/67/HU3) line with luciferase gene integrated into the parasite genome.[44] The susceptibility of intracellular *L. donovani* amastigotes to synthesized compounds was determined using the Luciferase Assay System Kit (Promega, Madison, Wis.) as previously described.[43] Briefly, macrophage-differentiated-THP-1 cells were plated at a density of 3×10^4 macrophages/well in 96-well white polystyrene microplates and were infected at a macrophage/parasite ratio of 1:10 with late-stage promastigotes. Infected cell cultures were incubated at different compound concentrations in RPMI 1640 medium plus 10% hiFBS at 37 °C with 5% CO₂ for 72 h and then lysed. Luminescence intensity was measured as indicative of the intracellular parasite growth, according to the instructions of the supplier.

4.3.3. Cytotoxicity assay

Human myelomonocytic cell line THP-1 were grown at 37 °C and 5% CO₂ in RPMI-1640 supplemented with 10% hiFBS, 2 mM glutamate, 100 U/mL penicillin and 100 µg/mL streptomycin. 3×10^4 cells/well in 96-well plates were differentiated to macrophages with 20 ng/mL of PMA treatment for 48 h followed by 24 h of culture in fresh medium.[43] MRC-5 cells, a SV-40 transformed human fetal lung fibroblast cell line, were maintained

at 37 °C and 5% CO₂ in DMEM supplemented with 10% hiFBS, 100 U/mL penicillin and 100 µg/mL streptomycin. Cells were harvested by treatment with 0.05% (w/v) trypsin plus 0.48 mM EDTA for 5 min, diluted to 4 x 10⁴ cell/ml in 96-well plates and incubated at 37 °C and 5% CO₂ before toxicity assay.[43] Cellular toxicity of all compounds was determined using the colorimetric MTT-based assay after incubation at 37 °C for 72 h in the presence of increasing concentrations of compounds.[43] The results are expressed as EC₅₀ values, as the concentration of compound that reduce cell growth by 50% versus untreated control cells.

Acknowledgements

We gratefully acknowledge to Junta de Andalucía (Grant No. FQM-7316 (JCM), BIO-1786 (JMPV), CTS-7282 (FG)) and Spanish Ministry of Economy and Competitiveness (Grant No. SAF2011-28215 (JMPV) and SAF2012-34267 (FG)) for financial support.

References

3.4. Alkylated resveratrol prodrugs and metabolites as potential therapeutics for neurodegenerative diseases.

Reference:

P. Peñalver, E. Belmonte-Reche, N. Adán, M. Caro, M. L. Mateos-Martín, M. Delgado, E. González-Rey, J. C. Morales, *European Journal of Medicinal Chemistry* **2018**, *146*,123-138.

DOI:

[10.1016/j.ejmech.2018.01.037](https://doi.org/10.1016/j.ejmech.2018.01.037)

Supporting information:

<https://ars.els-cdn.com/content/image/1-s2.0-S0223523418300503-mmc1.pdf>

Alkylated resveratrol prodrugs and metabolites as potential therapeutics for neurodegenerative diseases

Pablo Peñalver,# Efres Belmonte-Reche,# Norma Adán, Marta Caro, María Luisa Mateos-Martín, Mario Delgado, Elena González-Rey* and Juan Carlos Morales*

Affiliations

Department of Biochemistry and Molecular Pharmacology and Department of Cellular Biology and Immunology, Instituto de Parasitología y Biomedicina López Neyra, CSIC, PTS Granada, Avda. del Conocimiento, 17, 18016 Armilla, Granada, Spain.

Author Contributions

P.P. and E.B-R. contributed equally.

Corresponding Authors

*E.G.-R.: phone, +34-958181670; e-mail: elenag@ipb.csic.es

*J.C.M: phone, +34-958181644; e-mail: jcmorales@ipb.csic.es

KEYWORDS

Resveratrol, neuroprotection, inflammation, prodrug, zebra fish, neurodegenerative diseases

1. Introduction

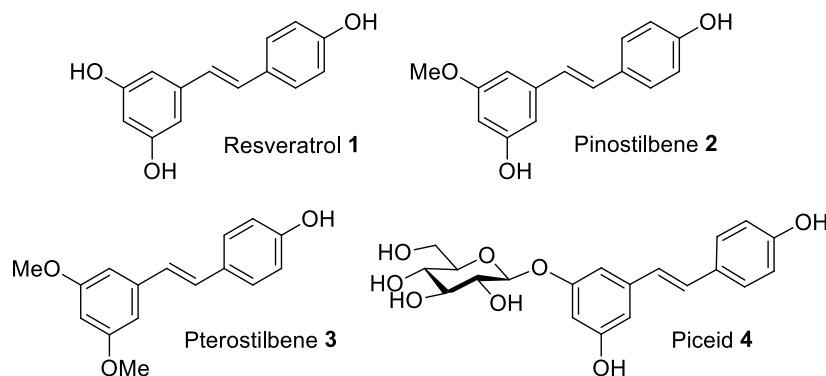
Neurodegenerative diseases are the result of progressive loss of neurons and neuronal connections in the central nervous system (CNS) which normally lead to cognition and motor dysfunction. Despite the differences in clinical manifestations of Alzheimer's disease (AD), Parkinson's disease (PD), Huntington's disease (HD), multiple sclerosis (MS) and amyotrophic lateral sclerosis (ALS), among others, the pathological processes appear similar, suggesting common neurodegenerative pathways [1]. Mitochondrial malfunction and oxidative stress [2-4] together with the activation of innate immune responses leading to inflammation [5] are known to play a major role in the pathophysiology of neurodegenerative diseases.

A huge effort is being made to obtain drugs to prevent, treat or cure neurodegenerative diseases. The majority of drug discovery programs are based on a 'one-target-one-disease' approach that has not been successful up to now. Thus, alternative approaches such as 'multi-target' strategies have been proposed [6-9]. The main aim is to modulate simultaneously different targets involved in the disease with just a single drug. Natural products have been proposed as sources of multi-targeted lead compounds with proven biological efficacy and safety [8, 10]. In fact, they can be considered as pre-optimized leads for additional structural optimization by improving their bioactivity and/or their pharmacokinetic properties.

Resveratrol **1** (Figure 1) is a natural product with a stilbene scaffold that has shown antiplatelet [11], antitumor [12, 13], anti-inflammatory [14] and neuroprotective activities [15-17]. Its bioactivity comes from direct interactions of resveratrol with multiple molecular targets involved on inflammation, cell cycle arrest, cell signaling, metabolism and posttranslational modification [18, 19]. Resveratrol has shown promising results as treatment of neurodegenerative diseases and thus, has reached clinical trials for AD [20, 21], PD and recently for HD (clinicaltrials.gov). When patients with mild-moderate Alzheimer's disease were treated with resveratrol (1 g by mouth twice daily), declines in cerebrospinal fluid A β 40 levels and activities of daily living scores were attenuated. However, high amounts of resveratrol need to be

administered due to its low bioavailability. These results indicate that resveratrol could be considered a lead compound that needs optimization.

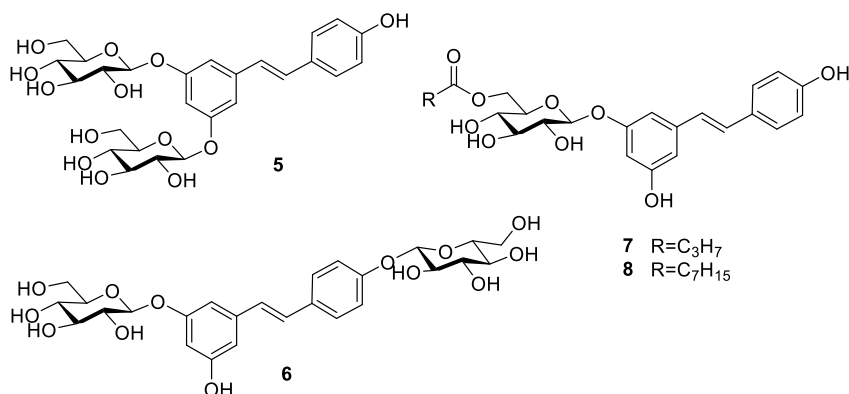
Fig. 1. Resveratrol and related natural products



Two simple natural resveratrol derivatives pinostilbene **2** and pterostilbene **3** (Figure 1) have shown improved neuroprotective capacity with respect to resveratrol. Pinostilbene **2** was reported to exert a potent neuroprotective effect in SH-SY5Y neuroblastoma cells with a wider effective concentration than resveratrol [22]. Low doses of pterostilbene **3** improved significantly radial arm water maze function in SAMP8 mice, a model of AD, together with positive modulation of inflammation and cellular stress whereas resveratrol showed no effect [23]. These results have inspired several groups to prepare *O*-alkylated and *C*-alkylated resveratrol derivatives and to examine their *in vitro* neuroprotective potential. Villalonga-Barber *et al.* [24] reported that 3',5'-*C*-alkylated-resveratrol derivatives were 100-fold more potent than resveratrol modulating oxidative stress on glutamate-challenged HT22 hippocampal neurons. Puksasook *et al.* [25] found that 4-prenylresveratrol exhibited better anti-A β aggregation activity than resveratrol and similar anti-BACE inhibitory activity. Other modifications on resveratrol such as imine resveratrol derivatives, [26] resveratrol tacrine hybrids [27] and resveratrol clioquinol hybrids [28] have also been explored as neuroprotective agents.

Due to the low bioavailability, rapid metabolism and low water solubility of resveratrol, several resveratrol prodrugs have been prepared [29, 30]. Our group previously reported a series of resveratrol glucosylated and acylated prodrugs (Figure 2) and evaluated their anti-inflammatory activity. Compounds **7** and **8** were capable of decreasing colon inflammation in a mouse dextran sulfate sodium model to a much higher extent than resveratrol [31]. Surprisingly, piceid **4** (Figure 1) and resveratrol lipoconjugates [32] are the only resveratrol prodrugs that have been examined as neuroprotective drugs. Piceid, was able to protect the brain on an ischemic stroke animal model, possibly by up-regulating the expression of Gli1, Ptch1 and SOD1 and down-regulating the expression of NF- κ B [33].

Fig. 2. Resveratrol prodrugs prepared previously.



In this work, our aim was to combine two strategies in the same molecule to optimize resveratrol, i.e. structural optimization through the synthesis of alkylated resveratrol derivatives to increase efficacy and the improvement of bioavailability through the preparation of their prodrugs (Figure 3, Table 1). We have also added resveratrol sulfate metabolites to our approach since metabolites of several drugs have shown to be more active than the drugs themselves, as in the case of morphine-6-glucuronide [34]. Cytotoxicity, neuroprotective capacity and anti-inflammatory activity of alkylated resveratrol derivatives **11-25** were first evaluated *in vitro* in

order to optimize the resveratrol scaffold. Then, prodrugs and metabolites of the best alkylated derivatives were synthesized and their toxicity and neuroprotection capacity was evaluated on zebrafish. Finally, the best resveratrol derivative, compound **8**, was investigated as potential treatment for neurodegeneration using a preclinical model for Huntington's disease. We have chosen this disease because it is a hereditary and degenerative brain disorder (characterized by behavioural, cognitive and motor dysfunctions), for which there is no cure or treatments which can slow down its progression. New approaches in order to develop new therapeutics are strongly needed.

Fig. 3. Strategy for the design of novel resveratrol derivatives, metabolites and prodrugs.

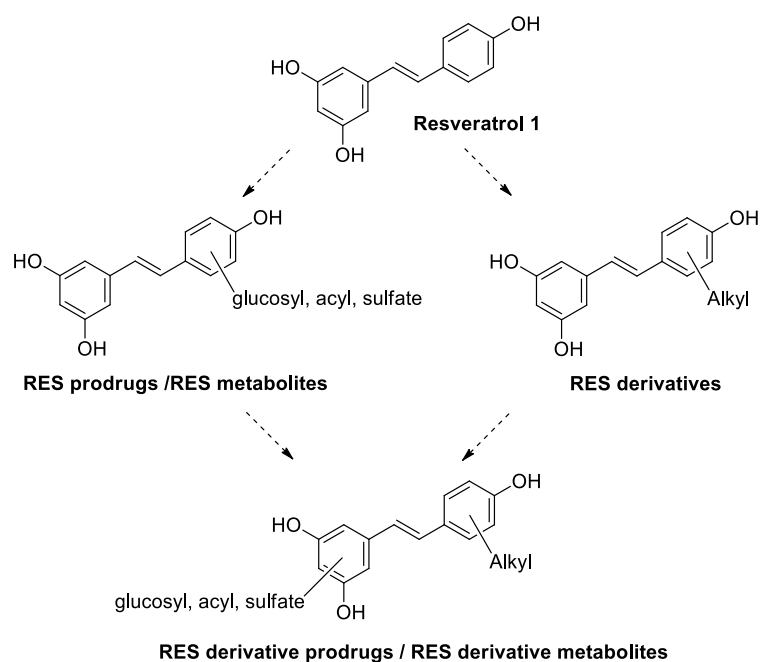
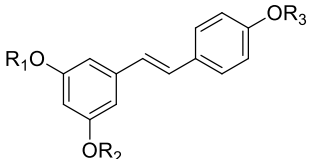
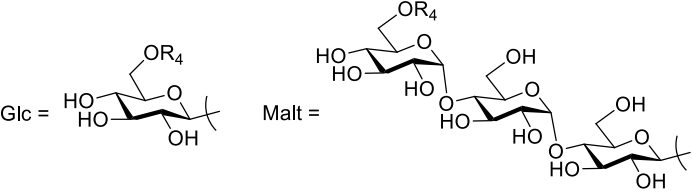


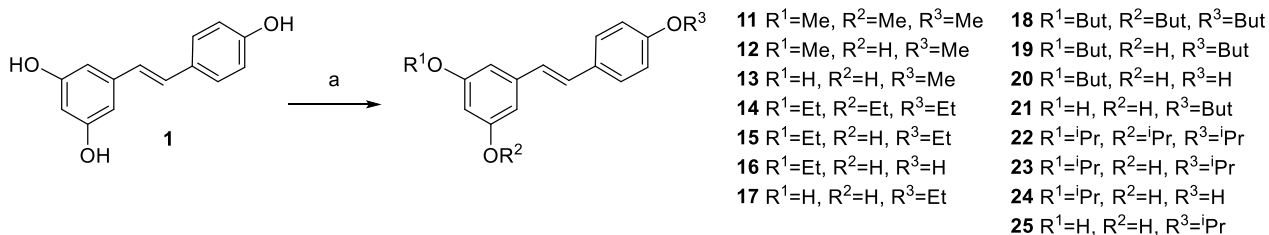
Table 1. Resveratrol derivatives examined in this work.

									
Comp.	R ₁	R ₂	R ₃	R ₄	Comp.	R ₁	R ₂	R ₃	R ₄
<i>RES prodrugs</i>					24	iPr	H	H	-
5	Glc	Glc	H	H	25	H	H	iPr	-
6	Glc	H	Glc	H	<i>Butyl RES prodrugs</i>				
7	Glc	H	H	COC ₃ H ₇	26	But	Glc	But	H
8	Glc	H	H	COC ₇ H ₁₅	27	But	Glc	Glc	H
<i>RES metabolites</i>					28	Glc	Glc	But	H
9	SO ₃ ⁻	H	H	-	<i>Butyl RES metabolites</i>				
10	SO ₃ ⁻	H	SO ₃ ⁻	-	29	But	SO ₃ ⁻	But	-
<i>Alkylated RES</i>					30	But	SO ₃ ⁻	SO ₃ ⁻	-
11	Me	Me	Me	-	31	SO ₃ ⁻	SO ₃ ⁻	But	-
12	Me	H	Me	-	<i>Methyl RES prodrugs</i>				
13	H	H	Me	-	32	Me	Glc	Me	H
14	Et	Et	Et	-	33	Glc	Glc	Me	H
15	Et	H	Et	-	34	Me	Me	Glc	H
16	Et	H	H	-	35	Me	Glc	Me	COC ₇ H ₁₅
17	H	H	Et	-	36	Glc	Glc	Me	COC ₇ H ₁₅
18	But	But	But	-	37	Me	Me	Glc	COC ₇ H ₁₅
19	But	H	But	-	38	Me	Glc	Me	COC ₃ H ₇
20	But	H	H	-	39	Me	Me	Glc	COC ₃ H ₇
21	H	H	But	-	40	Me	Me	Malt	H
22	iPr	iPr	iPr	-	41	Me	Me	Malt	COC ₇ H ₁₅
23	iPr	H	iPr	-					

2. Chemistry

Resveratrol glucosylated prodrugs **5** and **6** were synthesized by chemical glycosylation of TBDMS-protected resveratrol derivatives using a peracylated trichloroacetimidate donor, and posterior one-step deprotection with NaOH in MeOH/THF, as previously reported [31]. Piceid acylated prodrugs **7** and **8** were prepared by enzymatic acylation of piceid **4** using *Thermomyces lanuginosus* lipase immobilized on granulated silica (Lipozyme TL IM). The reactions were carried out in tert-butyl alcohol with the corresponding fatty acid vinyl esters to obtain high yields of the acylated compounds (92-97%) [31]. Resveratrol sulfate metabolites **9** and **10** were prepared following the procedure described by Hoshino *et al.* [35] with an improved purification methodology reported by our group.[36] Briefly, TBDMS-protected resveratrol derivatives were treated with $\text{SO}_3 \cdot \text{NMe}_3$ and NEt_3 in acetonitrile under microwave irradiation. The crude was first purified by LH-20 chromatography, then desilylated with KF in MeOH and finally purified by reversed-phase chromatography.

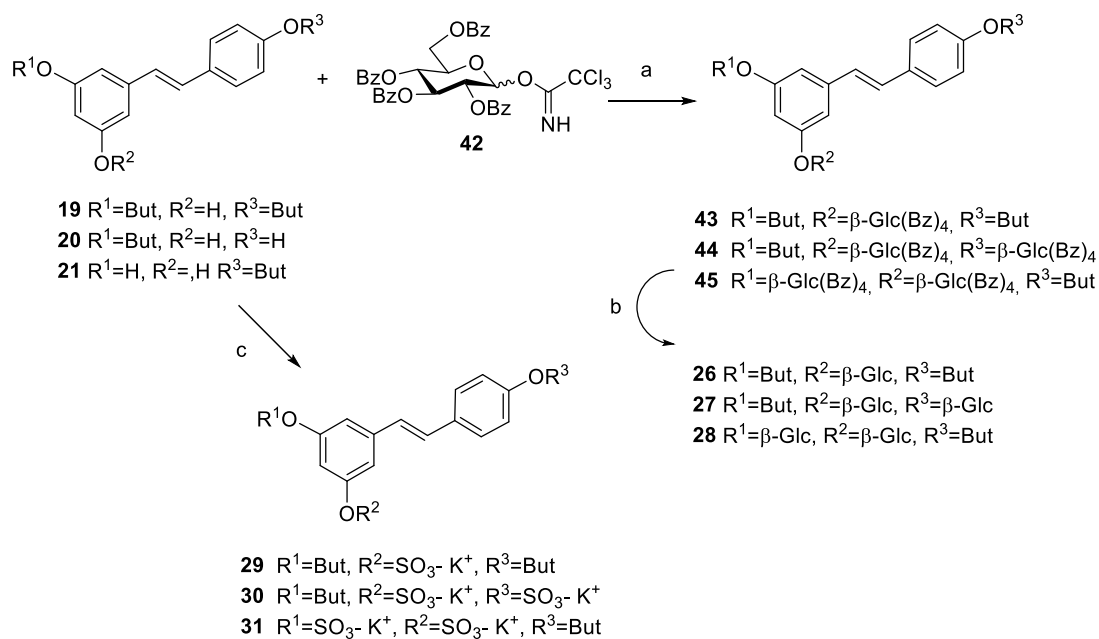
Methyl, ethyl, isopropyl and butyl resveratrol derivatives were synthesized by random alkylation in DMF using potassium carbonate and the corresponding 1-iodoalkane (Scheme 1) [25, 37]. Subsequent chromatographic separation afforded mono-, di- and trialkyl resveratrol derivatives **11-25** although several derivatives such as pterostilbene (**3**) could not be isolated under the chromatographic conditions used. Compound characterization was easily carried out using NMR spectroscopy due to the differences in symmetry between the mono-substituted regioisomers and the same applies to the di-substituted regioisomers.



Scheme 1. Synthesis of alkylated resveratrol derivatives **11-25**. Reagents and conditions: (a)

MeI or EtI or BuI or iPrI, K₂CO₃, DMF.

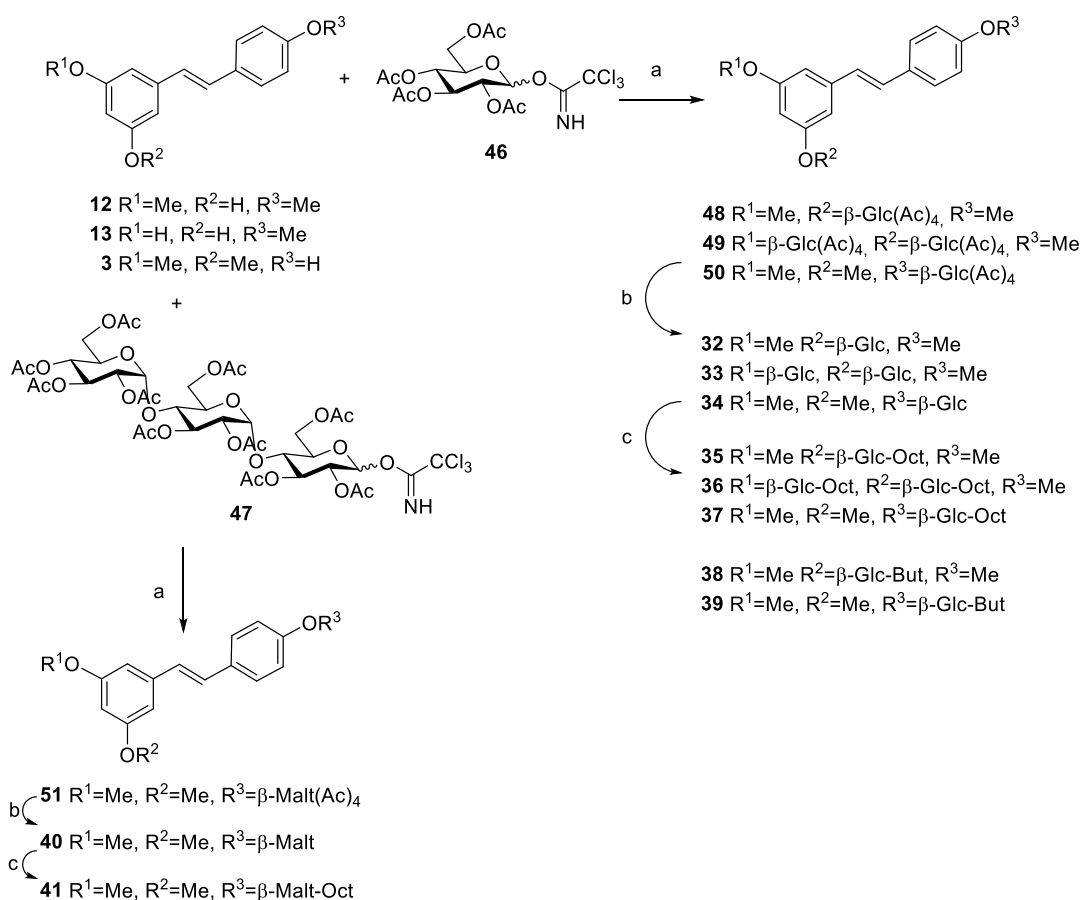
Since butyl resveratrol derivatives **18-21** showed the best overall *in vitro* neuroprotective activity and lowest cytotoxicity among the alkylated derivatives examined (see below), we decided to prepare their glucosylated prodrugs **26-28** and sulfate metabolites **29-31** for further investigation. Reaction of a peracylated glucosyl trichloroacetimidate donor with the corresponding butyl resveratrol derivatives and posterior basic deprotection with NaOMe in MeOH (Scheme 2) resulted on compounds **26-28**. Sulfation of butyl resveratrol derivatives was carried out using the same conditions described above for the silyl resveratrol derivatives and compounds **29-31** were obtained (Scheme 2).



Scheme 2. Synthesis of butylated resveratrol prodrugs and metabolites **26-31**. Reagents and conditions: (a) BF₃·Et₂O, CH₂Cl₂; (b) NaOMe/MeOH; (c) SO₃·NMe₃, TEA, CH₃CN, 100°C, 20 min, MW.

Since pterostilbene (3,5-dimethyl resveratrol) **3** has been reported to exert better neuroprotective and anti-inflammatory activity than resveratrol [23, 38], and the methyl resveratrol derivatives **11-13** were the second best family of alkylated derivatives on *in vitro* neuroprotection studies (see below), we decided to prepare several methyl resveratrol prodrugs **32-41**. Methyl resveratrol glucosylated derivatives **32-34** and **40** were prepared from the corresponding methyl resveratrol derivatives by reaction with peracylated glucosyl or maltotriosyl trichloroacetimidate donors and posterior basic deprotection with NaOMe in MeOH (Scheme 3). Since resveratrol sulfate metabolites showed high toxicity on the zebra fish embryo acute toxicity assay (see below), we decided to prepare acylated derivatives of methyl glucosyl resveratrol derivatives instead. Moreover, the butanoyl or octanoyl fatty acids could be adding an intrinsic anti-inflammatory effect (see below). Thus, enzymatic acylation of compounds **32-34**

and **40** was carried out with Lipozyme TL IM and butyric or octanoic acid vinyl esters to obtain compounds **35-39** and **41** (Scheme 3).



Scheme 3. Synthesis of methylated resveratrol prodrugs **32-41**. Reagents and conditions: (a)

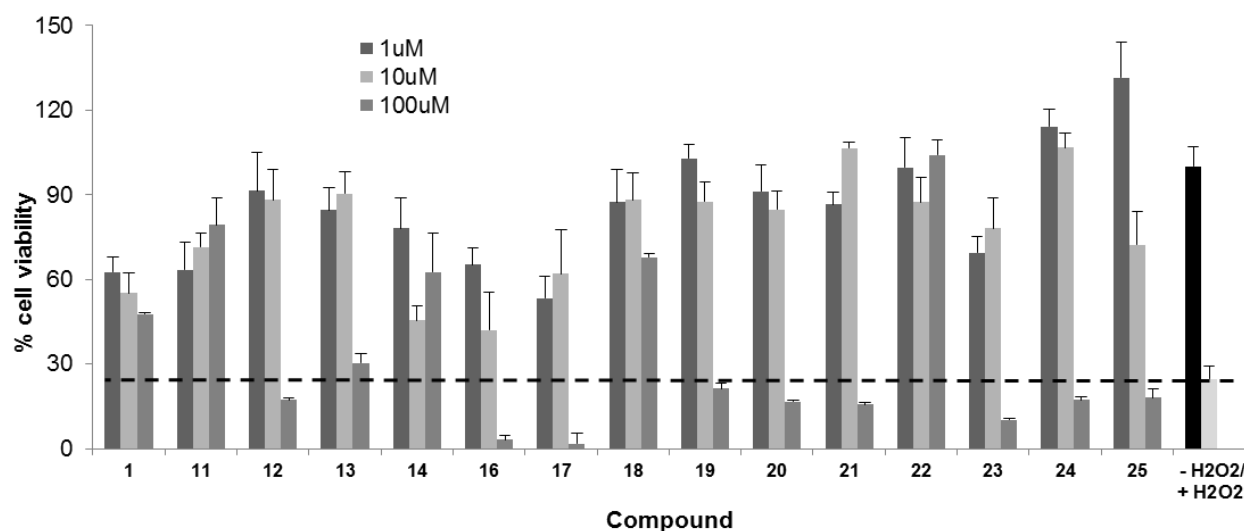
BF₃·Et₂O, CH₂Cl₂; (b) NaOMe/MeOH; (c) Lipozyme TL IM, vinyl fatty acid ester, 55 °C, 18h.

3. Results and discussion

3.1. Screening for neuroprotection against oxidative stress

To test if the alkylated modifications on resveratrol had any effect on its reported neuroprotective capacity [39], we evaluated viability of SH-SY5Y neuroblastoma cells after oxidative stress challenge with hydrogen peroxide in the presence or absence of the prepared alkylated resveratrol derivatives **11-25** [40]. We previously determined their cytotoxic effects at 10 μ M concentration on SH-SY5Y cells (Fig. S1) and found none of the compounds were toxic at the examined concentration. All alkylated resveratrol compounds **11-25** investigated counteracted to some extent oxidative damage on neuroblastoma cells produced by hydrogen peroxide at 1 and 10 μ M concentration. Methylated and butylated resveratrol derivatives, **11-13** and **18-21** respectively, showed a recovery up to 80-100% cell viability whereas resveratrol **1** only recovered up to 55% cell viability. These results are in accordance with previously reported results on the capacity to reduce oxidative stress of methylated resveratrol derivatives [22] and other alkylated derivatives [25] on similar cellular systems. At 100 μ M concentration several alkylated derivatives (**12**, **16**, **17**, **19-21** and **23-25**) showed no neuroprotection possibly due to their toxicity at higher concentrations as it could be deduced from toxicity data in zebra fish embryo (see below).

Fig. 4. Neuroprotective activity of alkylated resveratrol derivatives **11-25** on hydrogen peroxide-treated SH-SY5Y cells. Cell viability was evaluated in SH-SY5Y cells after 24h of hydrogen peroxide incubation (100 μ M) in combination with the compounds at 1, 10, and 100 μ M. Dashed line: reference value for viability found on the H₂O₂ control without compounds; black bar: control SH-SY5Y cell viability; white bar: SH-SY5Y cell viability after hydrogen peroxide incubation. Each bar represents mean \pm standard deviation of at least two different experiments run in quadruplicate.

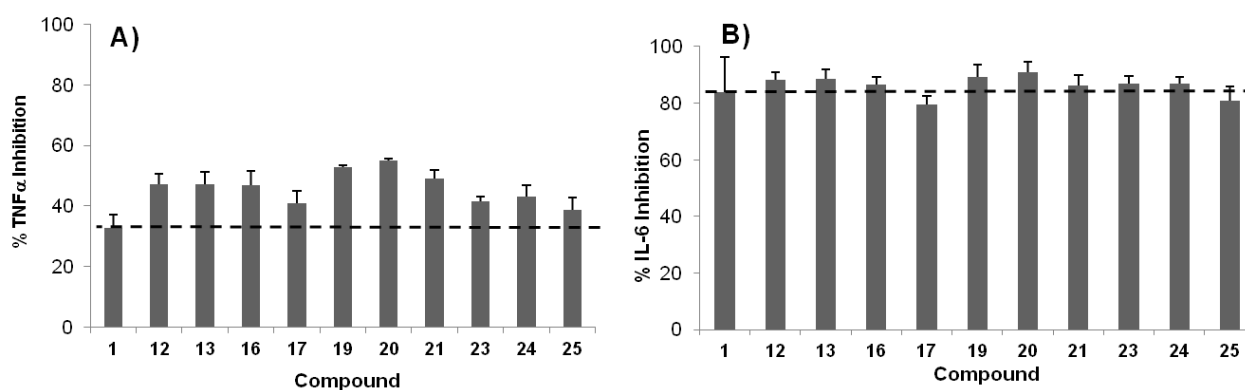


3.2. Screening for inhibitory activity against LPS-induced TNF- α and IL-6 release

Resveratrol has been reported to decrease inflammation by inhibiting the induced production of pro-inflammatory cytokines, such as TNF- α , IL-1 β , IL-6, IL-8 and matrix metalloproteinases MMP-2, MMP-3, MMP-9 and MMP-13, both on *in vitro* and on *in vivo* models [41-43]. We measured two inflammatory markers (TNF- α and IL-6) on lipopolysaccharide (LPS)-stimulated RAW 264.7 macrophage cells in the presence or absence of the alkylated resveratrol derivatives prepared. Peralkylated resveratrol derivatives were discarded due to their high hydrophobicity and no possibility of further modification. We found that the selected alkylated resveratrol compounds showed a higher inhibition of TNF- α production than resveratrol, except for 4'-

ethylresveratrol **17** and 4'-isopropylresveratrol **25** (Figure 5A). The levels of IL-6 produced were similar for resveratrol and all the investigated alkylated derivatives (Figure 5B).

Fig. 5. Anti-inflammatory profile of alkylated resveratrol derivatives in RAW macrophages. TNF- α (A) and IL-6 (B) production was determined in RAW cells after 24h of LPS incubation (100 ng/ml) in combination with the compounds at 10 μ M concentration. Data are shown as percentage of cytokine inhibition and they were normalized using the values corresponding to LPS and basal- production in RAW cells as reference values for maximal and minimum cytokine production, respectively. Dashed line: reference values for anti-inflammatory activity exerted by unmodified resveratrol **1**. Each bar represents mean \pm standard deviation of at least two different experiments run in quadruplicate.



3.3. Assessment of acute toxicity on zebra fish

To screen compound toxicity on zebra fish is a cost-effective model due to the high fecundity, rapid embryonic development and high homology to mammalian species of zebrafish [44]. Moreover, the embryo is preferred to adult fish because it is predicted that early life stages feel less pain and distress than adult fish. Fast acute toxicity was measured by incubation of zebrafish embryos with increasing concentration of each compound and cumulative mortality/toxicity was

observed after 96 hpf (hours post fertilization) [45]. It is important to note that cumulative mortality/toxicity is due to both developmental impact and organotoxicity.

In vivo toxicity on zebrafish embryo was measured for representative compounds of each family of resveratrol derivatives under study, alkylated resveratrol derivatives **11-25** and their corresponding synthesized prodrugs and metabolites **26-41**. We also measured toxicity for several resveratrol prodrugs **5-8**, metabolites **9-10** and resveratrol **1** itself. Table 2 and Figure S3 show NOEC, LOEC and LC₅₀ values for acute toxicity on zebrafish embryos. We observed that alkylated resveratrol derivatives **16**, **20** and **24** were quite toxic with LC₅₀ values from 11 to 13 µM whereas methylated resveratrol derivative **13** and pterostilbene **3** were slightly less toxic with LC₅₀ values of 32 and 36 µM, respectively. Addition of a sulfate group to the butyl resveratrol structure as in compound **30** did not improve toxicity (10 µM). In contrast, adding a glucose unit to the butyl resveratrol structure as in compounds **27** and **28** resulted in less toxic derivatives.

In the case of the methylated resveratrol derivatives, their modification with glucosyl or glucosyl-acyl groups (compounds **34-41**) resulted in similar toxicity to the parent compounds with LC₅₀ values from 29-45 µM. The exceptions were compounds **36** (8 µM) and **40** (379 µM). The least toxic compounds of the entire series were resveratrol **1** itself together with resveratrol prodrugs piceid **4**, diglucosyl resveratrol derivatives **5** and **6**, piceid butyrate **7**, piceid octanoate **8** and 4'-*O*-maltotriosyl pterostilbene **40**.

Table 2. NOEC, LOEC and LC₅₀ values for acute toxicity on zebra fish embryos for resveratrol prodrugs, metabolites and derivatives.

Compound	NOEC (μM)	LOEC (μM)	LC ₅₀ (μM)
1	1000	>1000	>1000
3	10	100	36
4	100	1000	114
<i>RES prodrugs</i>			
5	1000	>1000	>1000
6	1000	>1000	>1000
7	100	1000	315
8	1	10	138
<i>RES metabolites</i>			
9	10	100	29
10	0.1	1	17
<i>Alkylated RES</i>			
13	10	100	32
16	1	10	13
20	0.1	1	11
24	0.1	1	11
<i>Butylated RES prodrugs</i>			
27	10	100	35
28	10	100	21
<i>Butylated RES metabolites</i>			
30	0.1	1	10
<i>Methylated RES prodrugs</i>			
34	10	100	29
35	10	100	32
36	1	10	8
37	10	100	45
38	10	100	32
39	10	100	44
40	10	100	379
41	10	100	38

LC₅₀ (median lethal dose), calculated by fitting sigmoidal curve to mortality data ($y = \text{Bot} + (\text{Top} - \text{Bot}) / (1 + 10^{-(k \cdot (x_0 - \text{Log}(C)))})$). Bot, minimum mortality; Top, maximum mortality; k, curve slope; x₀, LC₅₀ estimated. NOEC (No observed effect concentration, with mortality score > 20% assumed as the effect). LOEC (Lowest observed effect concentration, with mortality score > 20% assumed as the effect). Negative control: 0.1% DMSO, in three replicates.

Positive controls: 4-Diethylaminobenzaldehyde (DEAB) at 5 different concentrations (0.1 μ M, 1 μ M, 10 μ M, 100 μ M, 1mM). DEAB is a competitive inhibitor of aldehyde dehydrogenases known to generate toxic and teratogenic effects.

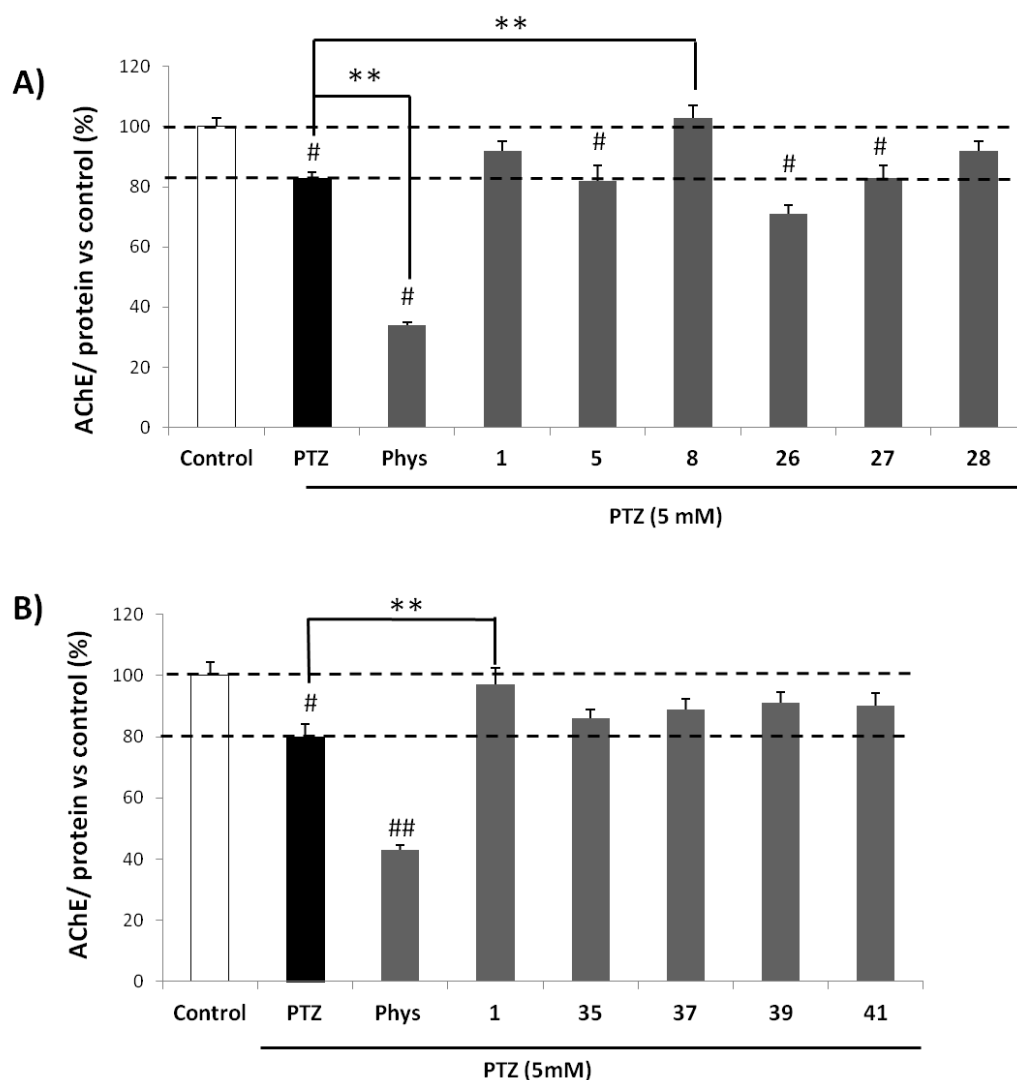
3.4. Assessment of neuroprotective activity on zebra fish

Pentylentetrazole (PTZ) is a competitive GABA antagonist which acts blocking Cl⁻ anion conductance and the formation of inhibitory postsynaptic potentials [46]. In zebra fish, PTZ acts as a pro-convulsant agent that blocks the GABAergic inhibitory synaptic transmission [47]. PTZ has been used previously in rats to induce neurodegeneration associated to an increase of damaged neurons, oxidative stress and neuroinflammation [48-51]. We measured acetylcholinesterase (AChE) activity on PTZ challenged zebra fish embryo since acetylcholine is a neurotransmitter involved in movement control and an important modulator of cognitive functions such as learning and memory [52]. Therefore, appropriate levels of AChE reflect a healthy neuronal state. Five days post fertilization (dpf) zebra fish larvae were pre-incubated with each of the resveratrol derivatives for 1h. Then, media was changed and larvae were co-incubated with PTZ and each of the resveratrol derivatives for 6h. Finally, larvae were processed to measure AChE activity under each condition. A group treated with physostigmine (Phys), a commercial inhibitor of the enzyme AChE, was included as positive control.

In a first assay we examined two prodrugs, 3,5-diglucosyl-resveratrol **5** and piceid octanoate **8** and the three butylated resveratrol glucosylated prodrugs **26-28** together with control resveratrol **1**. Butylated resveratrol sulfate metabolites were not included due to their toxicity on zebrafish embryo. We found that AChE activity of resveratrol-3-*O*-(6'-*O*-octanoyl)- β -D-glucopyranoside **8** group was fully recovered even over 100% (Figure 6A). In fact, its AChE activity was higher than the one found for resveratrol (92%) and for the other resveratrol prodrugs in this series. In a second assay we evaluated a series of methylated resveratrol prodrugs (**35**, **37**, **39** and **41**) to check the possible relevance of the methyl group position, the number of glucosyl groups and the optimum fatty acid group (Figure 6B). In this second assay all the compounds examined possessed a fatty acid chain because the results on the first assay pointed to their possible relevant role in

neuroprotection. We found the methyl resveratrol prodrugs examined were capable of partially recovering from PTZ damage but none of them showed higher AChE activity than resveratrol.

Fig. 6. Acetylcholinesterase (AChE) activity of resveratrol derivatives. The percentage of AChE (mU) enzyme activity normalized to total protein (μg) vs control (considered as 100%) is shown. A) Series of resveratrol glucosylated prodrugs and the butyl resveratrol prodrugs examined: B) Series of methyl resveratrol prodrugs examined. Resveratrol was used as internal control. PTZ is pentylenetetrazole and Phys is physostigmine. Two independent experiments were carried out with ten replicates of each experimental condition. Each bar represents mean \pm standard error of the mean (SEM). ANOVA statistics were carried out followed by Dunnett's test with multiple comparisons. It is considered significant when #P<0.05, ##P<0.01 respect to the control; **P<0.01 respect to the Control + PTZ.



We observed in our neuroprotective assay in zebra fish that 3,5-*O*-di- β -D-glucopyranosyl resveratrol **5**, a similar prodrug to resveratrol-3-*O*-(6'-*O*-octanoyl)- β -D-glucopyranoside **8** failed to prevent AChE activity loss. This result indicates that the octanoyl chain could be playing a key active role. Short and medium chain fatty acids have been reported to possess anti-inflammatory activity[53] and octanoic acid was capable of partly restoring mitochondrial respiration on starved human endothelial cells and monocytes under inflammatory conditions [54]. Octanoic acid is the main component of medium chain triglycerides (MCT), and diets with a carbohydrate-reduction and an increase in MCT intake, constitute an alternative for the treatment of drug-resistant epilepsy in children [55, 56]. Moreover, octanoic acid induces neurite outgrowth in PC12 neuronal cells and shows a maximum effect in comparison with shorter or longer fatty acids [57]. Growth of neurite processes from the cell body is a critical step in neuronal development. Kamata

et al. [57] suggested that the mechanism responsible is related with the activation of p38 mitogen-activated protein kinase (MAPK) and the extracellular signal-regulated kinase (ERK). This scenario, where the medium chain fatty acid and resveratrol would be playing a role side-by-side, indicates that compound **8** could indeed be a double-drug. Other double-drugs have been reported earlier as antimalarial [58], anti-HIV [59] or as antiproliferative agents [60].

Taking together, these results indicate that piceid octanoate **8** appeared to be one of the most effective resveratrol derivatives on neuroprotection. Therefore, we decided to evaluate its protective effect in a preclinical model of neurodegeneration.

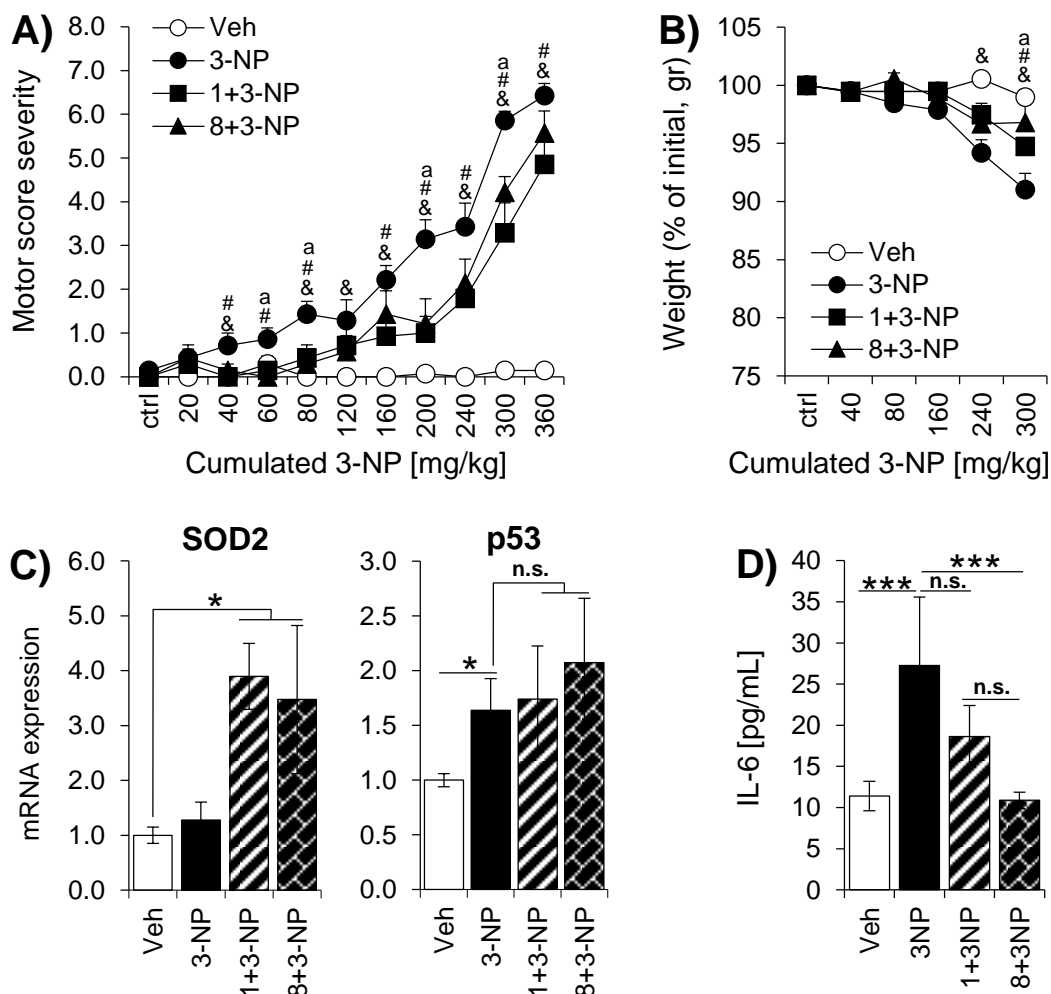
3.5. Neuroprotective activity on a 3-nitropropionic acid mice model

3-Nitropropionic acid (3-NP) is an irreversible inactivator of the succinate dehydrogenase and an inducer of mitochondrial dysfunction, which leads to an energy deprivation and oxidative stress exacerbation that promotes neuronal damage. 3-NP-induced neurodegeneration results in a striking preferential damage of striatum [61-63], the mainly anatomical region affected in Huntington's disease (HD). HD is a mortal progressive disorder caused by a dominant inherited expansion of CAG repeats in the Huntington gene. HD is characterized by neurological and systemic manifestations including cognitive, psychiatric and motor defects which are accompanied and even preceded in time by an increment of circulating pro-inflammatory cytokines (*i.e.* IL-6, TNF- α) [64, 65]. A plethora of evidences shows that 3-NP chronically administrated in rodents and primates can replicate key abnormalities underlying HD pathogenesis, including molecular alterations dependent of mitochondrial dysfunction (energetic deficit, oxidant species accumulation) as well as clinical (motor and cognitive) signs [61, 63, 66, 67] supporting the potential utility of the 3-NP intoxication model in HD studies [68, 69].

To analyze the neuroprotective and immune actions exerted by compound **8**, we used the 3-NP intoxication model (as described in the experimental section). Mice were given increasing

amounts of the toxin accompanied by the administration of compound **8** or resveratrol **1** which was used as reference.

Fig. 7. Evaluation of the activity of compound **8** in a 3-NP-induced neurodegeneration animal model. Mice were treated with vehicle (Veh), 3-NP, 3-NP plus resveratrol (**1**) or 3-NP plus compound **8**, and semi-quantitative motor-deficits (score from 0 to 8) (**A**) and body weight changes (relative to initial weight) (**B**) were evaluated at different time points (n = 7 mice). $^{\&}P < 0.05$ 3-NP vs. veh, $^{\#}P < 0.05$ 3-NP vs. 1+3-NP, $^aP < 0.05$ 3-NP vs. 8+3-NP. At the end of experiment, (**C**) SOD2 and p53 mRNA levels in whole brain-derived samples were determined by qRT-PCR (n = 4-7 mice) and (**D**) serum IL-6 levels detected were assayed by ELISA (n = 6-7 mice). Results represent mean \pm SEM. $^*P < 0.05$, $^{***}P < 0.005$, n.s.: non-significant.



We found an increment of the motor deficit-score scale and the weight loss in response to increasing doses of 3-NP (Figure 7A-B). Furthermore, administration of compound **8** had a protective effect similar to resveratrol on ameliorating loss of both motor coordination (Figure 7A) and weight induced by toxin (Figure 7B). To evaluate the mechanisms of action of compound **8** on molecular hallmarks of HD such as oxidative stress, neuronal death, and pro-inflammatory cytokines overproduction, we measured the expression of SOD2 and p53, as well as the serum circulating level of IL-6 (Figure 7C-D). 3-NP increased the expression of the proapoptotic p53 but neither resveratrol nor compound **8** counteracted its effect. However, we found that although 3-NP did not appear to modify the basal level of SOD2, both resveratrol and compound **8** induced in a similar way the overexpression of SOD2, an indicative result of their antioxidant capacity (Figure 7C). In addition, 3-NP administration replicated the pro-inflammatory phenotype of HD leading an increase of circulating IL-6 production. Interestingly, IL-6 stimulation was efficiently counteracted by compound **8**, while resveratrol produced a slight but not significant amelioration (Figure 7D). All together these results show that compound **8** could exert neuroprotective actions accompanied by antioxidant and anti-inflammatory effects *in vivo* as good as, or even better than resveratrol itself, making of compound **8** a promising candidate for the therapeutic treatment of neurodegenerative diseases such as HD.

4. Conclusions

In this study, we have combined two approaches for lead optimization of resveratrol for neurodegenerative diseases, structural optimization through the synthesis of resveratrol derivatives to improve its efficacy and an improvement in bioavailability through the preparation of their glucosylated and acylated prodrugs. We have designed and prepared resveratrol prodrugs, alkylated resveratrol derivatives and alkylated resveratrol prodrugs, together with sulfate metabolites of some of these resveratrol derivatives. Methylated and butylated resveratrol derivatives showed better neuroprotective and anti-inflammatory activity than resveratrol in the initial *in vitro* drug screening. When we examined toxicity in animals using a zebra fish embryo

model, we observed that alkylated resveratrol derivatives were highly toxic whereas their glycosylated prodrugs showed lower toxicity. When we investigated neuroprotection activity on zebra fish on a pentylenetetrazole challenged zebra fish, resveratrol-3-*O*-(6'-*O*-octanoyl)- β -D-glucopyranoside **8** displayed better neuroprotective activity than resveratrol. Methylated and butylated resveratrol prodrugs also could partially recover zebra fish embryo from neuronal damage although to a lower extent than resveratrol. We cannot rule out whether the intrinsic toxicity of the alkylated resveratrol derivatives are preventing a better recovery from the PTZ damage. We also observed that resveratrol-3-*O*-(6'-*O*-octanoyl)- β -D-glucopyranoside **8** was capable of ameliorating the onset and reducing the severity of HD-like symptoms induced by 3-nitropropionic acid in mice, used as a model of HD. Compound **8** improved mice locomotor activity and prevented weight loss in a similar way to resveratrol. Whereas their antioxidant effect seems to be comparable as revealed by SOD2 expression levels in brain tissue, the anti-inflammatory activity of compound **8** appears to be better than that of resveratrol as indicated by the circulating levels of IL-6. Finally, the octanoic acid chain within the structure of compound **8** could be playing an active role on inflammation and neuronal development what suggests **8** could be acting as a double-drug.

5. Experimental section

5.1. Chemistry

All solvents and chemicals were used as purchased without further purification. All reactions were monitored by TLC on precoated silica gel 60 plates F₂₅₄ (Merck) and detected by heating after staining with H₂SO₄:EtOH (1:9, v/v), anisaldehyde (450 ml ethanol, 25 ml anisaldehyde, 25 ml H₂SO₄ and 1 ml AcOH) or Mostain (500 ml of 10% H₂SO₄, 25g of (NH₄)₆Mo₇O₂₄•4H₂O, 1g Ce(SO₄)₂•4H₂O). Products were purified by flash chromatography with silica gel 60 (200-400 mesh). Eluents are indicated for each particular case. NMR spectra were recorded on Bruker Advance 300, 400 or 500 MHz [300, 400 or 500 MHz (¹H), 75, 101 or 126 (¹³C)] NMR spectrometers, at room temperature for solutions in CDCl₃, or CD₃OD. Chemical shifts are

referred to the solvent signal. 2D experiments (COSY, TOCSY, ROESY, and HMQC) were done when necessary to assign the new compounds. Chemical shifts are in ppm. Low resolution mass spectra were obtained on an ESI/ion trap mass spectrometer. High resolution mass spectra (HRMS) were obtained on an ESI/quadrupole mass spectrometer (WATERS, ACQUITY H CLASS). If necessary, the purity was determined by high performance liquid chromatography (HPLC). Purity of all final compounds was 95% or higher. The instrument used for chromatographic separation was a Waters Acquity UPLCTM H-class system (Waters, Manchester, UK). The column was an Acquity UPLC^R BEH C18 (2.1 x 100 mm, 1.7 μ M). A QDA single quadrupole mass spectrometer (Waters) equipped with an orthogonal Z-sprayTM electrospray ionization (ESI) source was used for metabolites detection. Empower 3 software was used for instrument control, peak detection and integration.

5.1.1. General procedure for etherification. Resveratrol (1 eq.) and potassium carbonate (2 eq.) were added to DMF (2.85 ml/mmol of resveratrol) under agitation in a round-bottomed flask. 1-Iodoalkane (1-1.5 eq) was added dropwise and reaction was stirred for 6 h at room temperature. The reaction mixture was filtered, diluted with water and extracted with ethyl acetate (3 x 20 mL). The combined organic layers were dried with MgSO₄ and the mixture filtered, concentrated. The crude was purified by flash column chromatography using different hexane/ethyl acetate mixtures.

5.1.1.1. Preparation of butylated resveratrol derivatives (18-21). Following the general procedure and starting from resveratrol (513 mg, 2.25 mmol) and 1-iodobutane (0.38 mL, 3.37 mmol) the reaction yielded **18-21** after purification with flash chromatography whilst eluting with a gradient concentration of hexane:ethyl acetate (8:1 to 1:1).

5.1.1.1.1. (E)-1-(3,5-dibutoxyphenyl)-2-(4-butoxyphenyl)ethene (18). Yield=16%; R_f = 0.9 (Hexane/ethyl acetate, 2:1). Compound characterization in accordance to literature [70].

5.1.1.1.2. (*E*)-1-(3-butoxy-5-hydroxyphenyl)-2-(4-butoxyphenyl)ethene (**19**). Yield=31%; Rf = 0.6 (Hexane/ ethyl acetate, 2:1). ¹H NMR (400 MHz, CDCl₃) δ = 7.44 (d, *J* = 8.7 Hz, 2H), 7.02 (d, *J* = 16.3 Hz, 1H), 6.97 – 6.82 (m, 3H), 6.74 – 6.63 (m, 1H), 6.63 – 6.54 (m, 1H), 6.35 (t, *J* = 2.2 Hz, 1H), 4.04 – 3.94 (m, 4H), 1.89 – 1.76 (m, 4H), 1.60 – 1.43 (m, 4H), 1.08 – 0.94 (m, 6H). ¹³C NMR (101 MHz, CDCl₃) δ = 160.64, 158.97, 156.84, 140.02, 129.76, 128.90, 127.83, 126.17, 115.70, 114.77, 105.61, 105.38, 105.00, 101.12, 67.86, 31.33, 19.28, 13.89; ESI-HRMS [M + H] calcd for C₂₂H₂₈O₃ 341.2111, found 341.2104.

5.1.1.1.3. (*E*)-1-(3-butoxy-5-hydroxyphenyl)-2-(4-hydroxyphenyl)ethene (**20**). Yield=13%; Rf = 0.25 (Hexane/ ethyl acetate, 2:1). ¹H NMR (400 MHz, CD₃OD) δ = 7.38 (d, *J* = 8.3 Hz, 2H), 7.01 (d, *J* = 16.3 Hz, 1H), 6.86 (d, *J* = 16.3 Hz, 1H), 6.79 (d, *J* = 8.3 Hz, 2H), 6.57 (s, 2H), 6.27 (s, 1H), 3.95 (t, *J* = 6.4 Hz, 2H), 1.81 – 1.69 (m, 2H), 1.51 (dd, *J* = 14.9, 7.4 Hz, 2H), 1.00 (t, *J* = 7.4 Hz, 3H). ¹³C NMR (101 MHz, CD₃OD) δ = 160.58, 158.22, 157.00, 139.91, 129.02, 128.27, 127.51, 125.62, 115.12, 105.16, 103.76, 100.57, 67.30, 31.20, 18.96, 12.87; ESI-HRMS [M + H] calcd for C₁₈H₂₀O₃ 285.1485, found 285.1480.

5.1.1.1.4. (*E*)-1-(3,5-dihydroxyphenyl)-2-(4-butoxyphenyl)ethene (**21**). Yield=35%; Rf = 0.3 (Hexane/ethyl acetate, 2:1). ¹H NMR (400 MHz, CD₃OD) δ = 7.40 (d, *J* = 8.4 Hz, 2H), 6.99 (d, *J* = 16.3 Hz, 1H), 6.90 – 6.81 (m, 3H), 6.51 (s, 2H), 6.23 (s, 1H), 3.92 (t, *J* = 6.4 Hz, 2H), 1.77 – 1.65 (m, 2H), 1.48 (dd, *J* = 15.0, 7.5 Hz, 2H), 0.97 (t, *J* = 7.4 Hz, 3H). ¹³C NMR (101 MHz, CD₃OD) δ = 158.90, 158.28, 139.87, 129.91, 127.85, 127.36, 126.24, 114.33, 104.56, 101.43, 67.39, 31.14, 18.93, 12.87; ESI-HRMS [M + H] calcd for C₁₈H₂₀O₃ 285.1485, found 285.1484.

5.1.1.2. Preparation of isopropylated resveratrol derivatives (22-25). Following the general procedure and starting from resveratrol (529 mg, 2.32 mmol) and 2-iodopropane (0.23 mL, 2.32 mmol) the reaction yielded **22-25** after purification with flash chromatography whilst eluting with a gradient concentration of hexane:ethyl acetate (8:1 to 2:1).

5.1.1.2.1. (*E*)-1-(3,5-di-isopropoxyphenyl)-2-(4-isopropoxyphenyl)ethene (**22**). Yield=2%; Rf = 0.8 (Hexane/ ethyl acetate, 2:1). Compound characterization in accordance to literature [71].

5.1.1.2.2. (*E*)-1-(3-isopropoxy-5-hydroxyphenyl)-2-(4-isopropoxyphenyl)ethene (**23**). Yield=15%; Rf = 0.5 (Hexane/ethyl acetate, 2:1). ¹H NMR (400 MHz, CDCl₃) δ = 7.39 (d, *J* = 8.4 Hz, 2H), 7.00 (d, *J* = 16.3 Hz, 1H), 6.91 – 6.77 (m, 3H), 6.58 (s, 1H), 6.56 (s, 1H), 6.28 (s, 1H), 4.62 – 4.41 (m, 2H), 1.28 (dd, *J* = 8.5, 6.4 Hz, 12H). ¹³C NMR (101 MHz, CDCl₃) δ = 159.31, 157.64, 156.89, 140.07, 129.82, 128.86, 127.89, 126.23, 116.16, 106.91, 105.66, 102.37, 70.21, 22.11, 22.07; ESI-HRMS [M - H] calcd for C₂₀H₂₄O₃ 311.1647, found 311.1633.

5.1.1.2.3. (*E*)-1-(3-isopropoxy-5-hydroxyphenyl)-2-(4-hydroxyphenyl)ethene (**24**). Yield=12%; Rf = 0.15 (Hexane/ethyl acetate, 2:1). ¹H NMR (400 MHz, CD₃OD) δ = 7.36 (d, *J* = 8.5 Hz, 2H), 6.99 (d, *J* = 16.2 Hz, 1H), 6.89 – 6.75 (m, 3H), 6.56 (s, 2H), 6.56 (s, 1H), 6.29 (s, 1H), 4.46 (dt, *J* = 12.0, 6.0 Hz, 1H), 1.24 (d, *J* = 6.1 Hz, 6H). ¹³C NMR (101 MHz, CD₃OD) δ = 158.26, 157.55, 139.99, 129.89, 128.01, 127.50, 126.27, 115.79, 104.77, 101.56, 69.75, 21; ESI-HRMS [M + H] calcd for C₁₇H₁₈O₃ 09271.1329, found 271.1323.

5.1.1.2.4. (*E*)-1-(3,5-dihydroxyphenyl)-2-(4-isopropoxyphenyl)ethene (**25**). Yield=33%; Rf = 0.4 (Hexane/ethyl acetate, 1:1). ¹H NMR (400 MHz, CD₃OD) δ = 7.38 (d, *J* = 8.4 Hz, 2H), 7.00 (d, *J* = 16.3 Hz, 1H), 6.85 (d, *J* = 16.3 Hz, 1H), 6.80 (d, *J* = 8.4 Hz, 2H), 6.58 (s, 1H), 6.56 (s, 1H), 6.28 (s, 1H), 4.56 (dt, *J* = 12.0, 6.0 Hz, 1H), 1.31 (d, *J* = 6.0 Hz, 6H). ¹³C NMR (101 MHz, CD₃OD) δ = 159.22, 158.25, 156.98, 139.98, 129.05, 128.29, 127.54, 125.65, 115.16, 105.40, 105.23, 102.03, 69.64, 21.10; ESI-HRMS [M + H] calcd for C₁₇H₁₈O₃ 271.1329, found 271.1331.

5.1.2.1. *General Procedure for glycosylation.* 2,3,4,6-tetra-*O*-benzoyl- α/β -*D*-glucopyranosyl trichloro acetimidate **42**⁵³ (1 mmol) was dissolved in anhydrous CH₂Cl₂ (15 mL) in a 50 mL round-bottomed flask under argon atmosphere. Butylated resveratrol derivative (0.33 mmol) and boron trifluoride diethyl etherate (0.033 mmol) were added to the stirring solution and after 30

min, the reaction was stopped with triethylamine (5 mL) and concentrated. The crude product was purified by flash column chromatography using different hexane/ethyl acetate mixtures with 1% TEA.

5.1.2.1. *(E)-1-(3-butoxy-5-(2,3,4,6-tetra-O-benzoyl-β-D-glucopyranosyloxy)phenyl)-2-(4-butoxyphenyl) ethene (43)*. Following the general procedure and starting from 3,4'-di-*O*-butyl-resveratrol **19**, the reaction yielded **43** after purification with flash chromatography whilst eluting with a gradient concentration of hexane:ethyl acetate (6:1). Yield=95%; Rf = 0.6 (Hexane/ethyl acetate, 2:1). ¹H NMR (300 MHz, CDCl₃) δ = 7.93 (d, *J* = 7.4 Hz, 1H), 7.90 – 7.77 (m, 5H), 7.75 (d, *J* = 8.3 Hz, 2H), 7.36 (d, *J* = 7.4 Hz, 1H), 7.32 – 7.24 (m, 3H), 7.17 (dd, *J* = 16.9, 8.6 Hz, 8H), 7.09 (d, *J* = 3.7 Hz, 2H), 6.83 (d, *J* = 16.2 Hz, 1H), 6.76 – 6.57 (m, 3H, CH), 6.51 (s, 1H), 6.42 (s, 1H), 6.35 (s, 1H), 6.05 – 5.85 (m, 1H), 5.79 – 5.59 (m, 2H), 5.50 – 5.37 (m, 1H), 4.66 – 4.47 (m, 1H), 4.47 – 4.33 (m, 1H), 4.33 – 4.20 (m, 1H), 3.79 (t, *J* = 6.5 Hz, 2H), 3.68 (t, *J* = 5.5 Hz, 2H), 1.66 – 1.54 (m, 2H), 1.49 (dd, *J* = 14.4, 6.6 Hz, 2H), 1.40 – 1.15 (m, 4H), 0.88 – 0.67 (m, 6H); ¹³C NMR (75 MHz, CDCl₃) δ = 166.49, 166.36, 166.12, 165.99, 165.91, 165.60, 165.51, 163.92, 160.73, 159.38, 158.55, 140.29, 133.87, 133.68, 133.56, 133.45, 130.28, 130.11, 130.00, 129.80, 129.76, 129.54, 129.37, 129.06, 129.03, 129.00, 128.78, 128.71, 128.67, 128.21, 126.16, 117.69, 115.00, 107.92, 107.46, 103.30, 99.90, 92.47, 89.13, 73.21, 72.90, 72.17, 70.74, 69.99, 68.64, 68.02, 63.70, 62.55, 31.60, 31.50, 31.28, 30.02, 19.55, 19.50, 14.19, 14.17; ESI-HRMS [M + H] calcd for C₅₆H₅₄O₁₂ 919.3694, found 919.3720.

5.1.2.2. *(E)-1-(3-butoxy-5-(2,3,4,6-tetra-O-benzoyl-β-D-glucopyranosyloxy)phenyl)-2-(4-(2,3,4,6-tetra-O-benzoyl-β-D-glucopyranosyloxy)phenyl)ethene (44)*. Following the general procedure and starting from 3-*O*-butyl-resveratrol **20** (0.33 mmol), the reaction yielded **44** after purification with flash chromatography whilst eluting with a gradient concentration of hexane:ethyl acetate (4:1). Yield = 88%; Rf = 0.3 (Hexane/ethyl acetate, 2:1). ¹H NMR (300 MHz, CDCl₃) δ = 7.92 (d, *J* = 7.7 Hz, 2H), 7.85 (t, *J* = 8.6 Hz, 10H), 7.76 (d, *J* = 7.6 Hz, 4H), 7.39 – 7.12 (m, 24H), 7.07 (d, *J* = 8.6 Hz, 2H), 6.86 (d, *J* = 8.6 Hz, 2H), 6.77 (d, *J* = 16.2 Hz, 1H), 6.67 – 6.54 (m, 3H, CH), 6.38 (s, 1H), 5.95 (t, *J* = 9.5 Hz, 2H), 5.75 (dd, *J* = 13.3, 5.5 Hz, 2H),

5.66 (dd, $J = 12.4, 6.4$ Hz, 2H), 5.43 (d, $J = 7.6$ Hz, 1H), 5.37 (d, $J = 7.7$ Hz, 1H), 5.12 (s, 1H), 4.62 (t, $J = 9.1$ Hz, 2H), 4.54 – 4.38 (m, 3H), 4.34 – 4.22 (m, 2H), 3.73 (t, $J = 5.7$ Hz, 2H), 1.61 – 1.49 (m, 2H), 1.30 (dd, $J = 14.9, 7.4$ Hz, 2H), 0.81 (t, $J = 7.4$ Hz, 3H); ^{13}C NMR (75 MHz, CDCl_3) $\delta = 171.40, 166.42, 166.28, 166.05, 165.55, 160.70, 158.50, 156.80, 139.84, 133.83, 133.65, 130.05, 129.93, 129.35, 128.96, 128.70, 128.63, 128.03, 117.62, 108.06, 107.61, 99.78, 73.08, 72.94, 72.02, 69.89, 68.09, 63.49, 60.65, 53.75, 31.46, 30.19, 29.91, 21.28, 19.45, 14.46, 14.11$; ESI-HRMS [$\text{M} + \text{Na}$] calcd for $\text{C}_{86}\text{H}_{72}\text{O}_{21}$ 1463.4464, found 1463.4453.

5.1.2.3. *(E)-1-(3,5-di-(2,3,4,6-tetra-O-benzoyl- β -D-glucopyranosyloxy)phenyl)-2-(4-butoxy)phenyl ethene (45)*. Following the general procedure and starting from 4'-*O*-butylresveratrol **21** (0.33 mmol), the reaction yielded **45** after purification with flash chromatography whilst eluting with a gradient concentration of hexane:ethyl acetate (4:1). Yield = 87%; $R_f = 0.3$ (Hexane/ethyl acetate, 2:1). ^1H NMR (300 MHz, CDCl_3) $\delta = 7.84$ (dd, $J = 13.3, 7.5$ Hz, 12H), 7.74 (d, $J = 7.5$ Hz, 4H), 7.40 – 7.08 (m, 27H), 6.74 (dd, $J = 17.5, 11.8$ Hz, 4H), 6.60 – 6.42 (m, 2H), 5.90 (t, $J = 9.5$ Hz, 2H), 5.65 (dd, $J = 19.6, 9.6$ Hz, 4H), 5.29 (s, 1H), 5.26 (s, 1H), 4.56 (d, $J = 9.7$ Hz, 2H), 4.41 (dd, $J = 12.0, 5.7$ Hz, 2H), 4.21 – 4.05 (m, 2H), 3.82 (t, $J = 6.5$ Hz, 2H), 1.60 (dd, $J = 14.4, 6.5$ Hz, 2H), 1.34 (dd, $J = 14.9, 7.4$ Hz, 2H), 0.82 (t, $J = 7.4$ Hz, 3H); ^{13}C NMR (75 MHz, CDCl_3) $\delta = 171.40, 166.45, 166.06, 165.54, 165.29, 159.47, 158.33, 140.81, 133.82, 133.64, 133.46, 130.13, 130.02, 129.66, 129.50, 129.38, 129.00, 128.76, 128.72, 128.64, 128.29, 125.34, 114.92, 110.33, 99.68, 73.02, 72.71, 72.05, 70.01, 68.01, 63.56, 60.66, 31.56, 29.98, 21.29, 19.51, 14.47, 14.15$; ESI-HRMS [$\text{M} + \text{Na}$] calcd for $\text{C}_{86}\text{H}_{72}\text{O}_{21}$ 1463.4464, found 1463.4445.

5.1.3. *General Procedure for benzoyl deprotection*. Butyl perbenzoylated glucopyranosyl resveratrol derivative (0.35 mmol) was dissolved in CH_2Cl_2 (5 mL) in a 25 mL round-bottomed flask to give a yellow solution. A solution of 25% sodium methoxide in methanol (5 mL) was added and left under stirring for 5 h. CH_2Cl_2 (20 mL) was then added and extracted with water (10 mL x 3). The aqueous phase was neutralized with IR-120 H^+ and concentrated. In the case of

derivative **45**, the organic phase was concentrated and purified by flash column gel chromatography eluting with Hexane:EtOAc (1:3).

5.1.3.1. (*E*)-1-(3-butoxy-5-(β -D-glucopyranosyloxy)phenyl)-2-(4-butoxyphenyl)ethene (**26**). Yield = 63%, white solid; ^1H NMR (300 MHz, CDCl_3) δ = 7.44 (d, J = 8.7 Hz, 2H), 7.07 (d, J = 16.4 Hz, 1H), 6.92 (d, J = 16.4 Hz, 1H), 6.91 – 6.85 (m, 3H), 6.72 (s, 1H), 6.58 (s, 1H), 4.91 (d, J = 7.2 Hz, 1H), 3.97 (q, J = 6.5 Hz, 4H), 3.93 (dd, J = 12.2, 1.8 Hz, 2H), 3.71 (dd, J = 12.0, 6.1 Hz), 3.54 – 3.44 (m, 2H), 3.39 (d, J = 9.0 Hz, 1H), 1.81 – 1.70 (m, 4H), 1.56 – 1.45 (m, 4H), 0.99 (td, J = 7.4, 3.2 Hz, 6H); ^{13}C NMR (75 MHz, CDCl_3) δ = 160.34, 159.05, 159.00, 139.83, 129.82, 128.59, 127.47, 127.31, 125.83, 116.52, 114.28, 106.56, 106.48, 102.18, 101.18, 76.90, 76.63, 73.58, 70.16, 67.45, 67.35, 61.23, 31.14, 31.12, 18.93, 18.90, 12.83, 12.81; ESI-HRMS [$\text{M} + \text{H}$] calcd for $\text{C}_{28}\text{H}_{38}\text{O}_8$ 503.2632, found 503.2645.

5.1.3.2 (*E*)-1-(3-butoxy-5-(β -D-glucopyranosyloxy)phenyl)-2-(β -D-glucopyranosyloxy)phenyl)ethene (**27**). Yield = 62%, white solid; ^1H NMR (300 MHz, CDCl_3) δ = 8.01 (d, J = 7.4 Hz, 1H), 7.47 (d, J = 7.4 Hz, 1H), 7.45 (d, J = 7.3 Hz, 1H), 7.10 (d, J = 16.3 Hz, 1H), 6.95 (s, 1H), 6.88 (d, J = 8.3 Hz, 2H), 6.76 (s, 1H), 6.66 (s, 1H), 4.94 (d, J = 6.3 Hz, 2H), 4.01 – 3.94 (m, 2H), 3.94 – 3.70 (m, 4H), 3.70 – 3.60 (m, 2H), 3.59 – 3.51 (m, 2H), 3.50 – 3.44 (m, 2H), 3.37 (d, J = 9.4 Hz, 2H), 1.80 – 1.68 (m, 2H), 1.57 – 1.42 (m, 2H), 0.98 (t, J = 7.3 Hz, 3H); ^{13}C NMR (75 MHz, CDCl_3) δ = 168.54, 159.17, 158.87, 140.01, 132.74, 129.40, 129.01, 128.16, 127.62, 125.6, 114.40, 108.50, 103.70, 100.94, 76.95, 76.71, 73.63, 70.35, 67.47, 61.44, 61.33, 31.22, 19.01, 12.90; ESI-HRMS [$\text{M} + \text{Na}$] calcd for $\text{C}_{30}\text{H}_{40}\text{O}_{13}$ 631.2367, found 631.2421.

5.1.3.3. (*E*)-1-(3,5-di-(β -D-glucopyranosyloxy)phenyl)-2-(4-butoxy)phenyl)ethene (**28**). Yield = 71%, white solid; ^1H NMR (300 MHz, CDCl_3) δ = δ = 8.03 – 8.02 (m, 1H), 8.01 (d, J = 1.3 Hz, 1H), 7.58 (ddd, J = 7.0, 2.5, 1.3 Hz, 1H), 7.47 – 7.43 (m, 2H), 7.11 – 7.07 (m, 1H), 6.98 – 6.91 (m, 1H, m, 1H), 6.74 (s, 1H), 6.59 (s, 1H), 4.94 (s, 2H), 4.01 – 3.88 (m, 4H), 3.94 – 3.88 (m, 2H), 3.75 – 3.70 (m, 2H), 3.56 – 3.39 (m, 6H), 1.73 (tt, J = 13.5, 6.8 Hz, 2H), 1.50 (td, J = 14.9, 7.5 Hz, 2H), 0.98 (t, J = 7.4 Hz, 3H); ^{13}C NMR (75 MHz, CDCl_3) δ = 168.54, 160.34, 158.99, 157.32, 132.70, 130.43, 129.32, 128.08, 127.41, 116.53, 114.36, 101.09, 100.74, 76.83, 76.68, 76.50,

73.57, 73.50, 70.16, 69.98, 67.51, 61.21, 61.10, 31.11, 18.93, 12.87; ESI-HRMS [M + Na] calcd for C₃₀H₄₀O₁₃ 631.2367, found 631.2366.

5.1.4. General Procedure for sulfation. Butylated resveratrol derivative (1.4 mmol) and sulfur trioxide trimethylamine complex (14 mmol) were dissolved in anhydrous acetonitrile (10 mL) in a 25 mL round-bottomed flask. Triethylamine (28 mmol) was then added. The reaction was carried out under agitation in a microwave reactor (150 W, 60 °C, 1 h). After completion the mixture was filtered and concentrated. The product was resuspended in 2-propanol, filtered and purified by flash column gel chromatography eluting with Hexane:EtOAc (1:1).

5.1.4.1 Potassium (E)-3-(4-butoxystyryl)-5-butoxyphenyl sulfate (29). Yield=66%, dark yellow oil, Eluents = Hexane:AcOEt (1:1), ¹H NMR (300 MHz, CD₃OD) δ = 7.27 (d, *J* = 8.7 Hz, 2H), 6.96 – 6.85 (m, 2H), 6.76 (d, *J* = 16.4 Hz, 1H), 6.69 (d, *J* = 8.4 Hz, 3H), 6.61 (d, *J* = 1.9 Hz, 1H), 3.83 – 3.72 (m, 4H), 1.61 – 1.47 (m, 4H), 1.30 (dt, *J* = 14.6, 7.3 Hz, 4H), 0.79 (td, *J* = 7.3, 5.3 Hz, 6H); ¹³C NMR (75 MHz, CD₃OD) δ = 187.82, 160.35, 159.40, 154.06, 139.91, 129.83, 129.23, 127.94, 125.70, 114.70, 111.13, 108.94, 106.78, 67.88, 67.68, 31.41, 19.25, 19.23, 13.25; ESI-HRMS [M + Na] calcd for C₂₂H₂₇O₆ 419.1521, found 419.1528.

5.1.4.2. Dipotassium (E)-5-(4-butoxystyryl)phenyl-1,3-disulfate (30). Yield=24%, yellow oil; R_f = 0.6 (Hexane:AcOEt - 1:1) , Column eluents = Hexane:AcOEt (1:1); ¹H NMR (300 MHz, CDCl₃) δ = 7.31 (d, *J* = 8.6 Hz, 2H), 6.96 (d, *J* = 16.5 Hz, 1H), 6.80 (d, *J* = 16.5 Hz, 1H), 6.76 (d, *J* = 8.6 Hz, 2H), 6.56 (s, 1H), 6.52 (s, 1H), 6.25 (s, 1H), 3.86 (t, *J* = 6.4 Hz, 2H), 1.73 – 1.58 (m, 2H), 1.48 – 1.36 (m, 2H), 0.91 (t, *J* = 7.3 Hz, 3H). ¹³C NMR (75 MHz, CDCl₃) δ = 188.77, 172.99, 161.76, 159.33, 158.10, 141.11, 130.25, 129.52, 128.81, 126.89, 116.39, 106.43, 105.11, 101.88, 68.54, 32.41, 20.20, 14.21; ESI-HRMS [M + H] calcd for C₁₈H₁₈O₉ S₂ 443.0470, found 443.0461.

5.1.4.3. Dipotassium (E)-3-(4-sulphate-styryl)-5-butoxyphenyl sulfate (31). Yield=32%, yellow oil; R_f = 0.65 (Hexane:AcOEt - 1:1), Eluents = Hexane:AcOEt (1:1); ¹H NMR (300 MHz,

CD₃OD) δ = 7.31 (d, J = 8.3 Hz, 2H), 6.96 (d, J = 16.2 Hz, 1H), 6.80 (d, J = 16.2 Hz, 1H), 6.76 (d, J = 8.0 Hz, 2H), 6.56 (s, 1H), 6.52 (s, 1H), 6.25 (s, 1H), 3.85 (t, J = 5.7 Hz, 2H), 1.68-1.61 (m, 2H), 1.52 – 1.33 (m, 2H), 0.91 (t, J = 7.2 Hz, 3H). ¹³C NMR (75 MHz, CD₃OD) δ = 187.82, 160.85, 158.58, 157.39, 140.05, 129.15, 128.60, 127.90, 125.79, 115.50, 105.42, 100.91, 100.88, 67.60, 31.46, 19.25, 13.21; ESI-HRMS [M + H] calcd for C₁₈H₁₈O₉ S₂ 443.0470, found 443.0476.

5.1.5. *Preparation of methylated resveratrol prodrugs (32-41). General Procedure for glycosylation.* 2,3,4,6-tetra-*O*-acetyl- α/β -D-glucopyranosyl trichloroacetimidate **46** [72] or per-*O*-acetyl- α/β -D-maltopyranosyl trichloroacetimidate **47** [73] (1 mmol) was dissolved in anhydrous CH₂Cl₂ (10 mL) in a 50 mL round-bottomed flask under argon atmosphere. Methylated resveratrol derivative (0.33 mmol) and boron trifluoride diethyl etherate (0.033 mmol) were added to the stirring solution. After 30 min the reaction was stopped with triethylamine (5 mL) and concentrated. The crude product was purified by flash column chromatography using different hexane/ethyl acetate mixtures with 1% TEA.

5.1.5.1. *(E)-1-(3-methoxy-5-(2,3,4,6-tetra-*O*-acetyl- β -D-glucopyranosyloxy)phenyl)-2-(4'-methoxyphenyl) ethene (48).* Following the general procedure and starting from 3,4'-di-*O*-methyl-resveratrol **12**, the reaction yielded **48** after purification with flash chromatography whilst eluting with a gradient concentration of hexane:ethyl acetate (4:1 to 1:2). Yield= 97%; ¹H NMR (400 MHz, CDCl₃) δ ppm : 7.36 (d, J = 8.7 Hz, 2H), 6.96 (d, J = 16.2 Hz, 1H), 6.81 (dd, J = 12.6, 6.7 Hz, 3H), 6.67 (d, J = 6.3 Hz, 2H), 6.39 (s, 1H), 5.23 (dt, J = 16.9, 9.4 Hz, 2H), 5.11 – 5.01 (m, 2H), 4.20 (dd, J = 12.2, 5.9 Hz, 1H), 4.07 – 3.98 (m, 1H), 3.81 (ddd, J = 9.1, 5.4, 2.0 Hz, 14H), 3.73 (d, J = 3.0 Hz, 6H), 2.00 – 1.95 (m, 12H); ¹³C NMR (101 MHz, CDCl₃): δ = 170.48, 170.07, 169.35, 169.24, 160.80, 159.48, 158.02, 139.89, 129.55, 129.17, 127.80, 125.92, 117.05, 114.13, 107.11, 106.36, 102.32, 98.77, 72.69, 71.93, 71.12, 68.39, 62.05, 55.31, 55.21, 55.18, 20.53, 20.50, 20.49, 20.46. HRMS (ES⁺) Calcd. for C₃₀H₃₄O₁₂Na: (M+Na) 609.1948, found; 609.1970.

5.1.5.2. *(E)-1-(3,5-di-(2,3,4,6-tetra-*O*-acetyl- β -D-glucopyranosyloxy)phenyl)-2-(4'-methoxyphenyl)ethene (49).* Following the general procedure and starting from 5-*O*-methyl-resveratrol

13, the reaction yielded **49** after purification with flash chromatography whilst eluting with a gradient concentration of hexane:ethyl acetate (2:1). Yield: 80%, Rf = 0.2 (4:1 – Hexane:EtOAc). ¹H NMR (300 MHz, CDCl₃) δ 7.36 (d, *J* = 8.6 Hz, 2H), 6.96 (d, *J* = 16.2 Hz, 1H), 6.90 – 6.79 (m, 3H), 6.66 (d, *J* = 3.9 Hz, 2H), 6.39 (s, 1H), 5.29 – 5.16 (m, 2H), 5.16 – 5.03 (m, 4H), 4.29 – 4.12 (m, 3H), 4.12 – 3.99 (m, 4H), 3.89 – 3.79 (m, 1H), 3.75 (s, 3H), 2.02 – 1.92 (m, 24H). ¹³C NMR (75 MHz, CDCl₃) δ 171.46, 170.93, 170.49, 169.66, 161.10, 159.76, 158.28, 140.23, 129.86, 129.52, 128.09, 126.21, 114.43, 107.38, 106.67, 102.64, 99.09, 72.98, 72.27, 71.42, 68.67, 62.36, 60.65, 55.69, 55.55, 21.28, 20.92, 20.83, 20.79, 14.42. TOF MS ES+ Calculated Mass [M + Na]: 925.2742, Expected Mass [M + Na]: 925.2747

5.1.5.3. (*E*)-1-(3-methoxy-4'-(2,3,4,6-tetra-*O*-acetyl-β-*D*-glucopyranosyloxy)phenyl)-2-(5-methoxyphenyl) ethene (**50**). Following the general procedure and starting from 3,5-di-*O*-methyl-resveratrol (pterostilbene, **3**), the reaction yielded **50** after purification with flash chromatography whilst eluting with a gradient concentration of hexane:ethyl acetate (4:1 to 1:2). Yield= 96%; ¹H NMR (400 MHz, CD₃OD) δ ppm : 7.49 – 7.42 (m, 2H), 7.07 (d, *J* = 16.3 Hz, 1H), 7.00 – 6.92 (m, 3H), 6.67 (d, *J* = 2.2 Hz, 2H), 6.36 (s, 1H), 5.39 – 5.30 (m, 1H), 5.24 (dd, *J* = 7.8, 2.7 Hz, 1H), 5.14 (dd, *J* = 9.3, 8.1 Hz, 1H), 5.12 – 5.03 (m, 1H), 4.27 (dd, *J* = 12.3, 5.3 Hz, 1H), 4.11 – 4.03 (m, 1H), 4.03 – 3.93 (m, 1H), 3.77 (d, *J* = 1.6 Hz, 6H), 2.00 (dd, *J* = 13.0, 6.4 Hz, 12H); ¹³C NMR (101 MHz, CD₃OD): δ = 170.81, 170.15, 169.81, 169.66, 161.08, 156.38, 139.45, 132.43, 127.83, 127.42, 116.57, 104.06, 99.33, 98.20, 72.72, 71.56, 71.29, 68.30, 61.67, 54.35, 19.21, 19.13, 19.11, 13.02; HRMS (ES⁺) Calcd. for C₃₀H₃₅O₁₂: (M+H) 587.2129, found; 587.2112.

5.1.5.4. (*E*)-1-(3-methoxy-4'-(*per-O*-acetyl-β-*D*-maltopyranosyloxy)phenyl)-2-(5-methoxyphenyl)ethene (**51**). Following the general procedure and starting from 3,5-di-*O*-methyl-resveratrol (Pterostilbene, **3**), the reaction yielded **51** after purification with flash chromatography whilst eluting with a gradient concentration of hexane:ethyl acetate (3:2 to 1:3). Yield= 41%; ¹H NMR (400 MHz, CDCl₃): 7.39 (dt, *J* = 7.0, 1.6 Hz, 2H), 7.03 – 6.83 (m, 4H), 6.60 (t, *J* = 2.2 Hz, 2H), 6.37 – 6.30 (m, 1H), 5.42 – 5.21 (m, 6H), 5.14 – 4.96 (m, 3H), 4.80 (dtd, *J* = 8.3, 4.4, 2.0 Hz, 1H), 4.75 – 4.64 (m, 1H), 4.41 (ddd, *J* = 12.4, 5.5, 2.8 Hz, 2H), 4.10 – 3.93 (m, 4H), 3.89 (q, *J* = 9.1, 7.1 Hz, 4H), 3.77 (q, *J* = 1.8 Hz, 6H), 2.14 – 1.92 (m, 30H); ¹³C NMR (101 MHz, CDCl₃):

δ = 170.98, 170.48, 170.41, 170.32, 170.28, 170.00, 169.75, 169.61, 169.55, 169.34, 160.92, 156.25, 139.27, 132.42, 128.17, 127.80, 127.69, 117.10, 104.41, 99.84, 98.26, 95.81, 95.65, 75.13, 73.82, 72.57, 72.20, 71.94, 71.67, 71.63, 70.42, 70.01, 69.31, 68.96, 68.50, 68.43, 67.88, 62.95, 62.38, 61.37, 60.28, 55.27, 20.94, 20.82, 20.80, 20.76, 20.73, 20.70, 20.58, 20.55, 20.50, 20.47, 20.41, 14.12; HRMS (ES⁺) Calcd. for C₅₄H₆₆O₂₈Na: (M+Na) 1185.3638, found; 1185.3632.

5.1.6. *General Procedure for acetyl deprotection.* Methyl peracetylated glucopyranosyl- or maltopyranosyl- resveratrol derivative (0.75 mmol) was dissolved in methanol (10 mL) in a 25 mL round-bottomed flask. A solution of 25% sodium methoxide in methanol (0.5 mL) was added slowly and left under stirring at room temperature for 1 h. The solution was filtered first through IR-120 H⁺ to neutralize it, filtered through celite to remove salt excess and finally concentrated.

5.1.6.1. *(E)-1-(3-methoxy-5-(β -D-glucopyranosyloxy)phenyl)-2-(4'-methoxyphenyl)ethene (32).* Following the general procedure and starting from **48**, the reaction yielded **32** (98%), which characterization was in accordance to the literature [74].

5.1.6.2. *(E)-1-(5-methoxy-3-(β -D-glucopyranosyloxy)phenyl)-2-(4'-(β -D-glucopyranosyloxy)phenyl)ethene (33).* Following the general procedure and starting from **49** after purification with flash chromatography whilst eluting with a gradient concentration of ethyl acetate: methanol (20:1- 5:1) the reaction yielded **33**. Yield: 82%, R_f = 0.1 (20:1 - EtOAc:MeOH). Compound **33** characterization was in accordance to the literature [75].

5.1.6.3. *(E)-1-(3-methoxy-4'-(β -D-glucopyranosyloxy)phenyl)-2-(5-methoxyphenyl)ethene (34).* Following the general procedure and starting from **50**, compound **34** was afforded (100%). Characterization was in accordance to the literature [76].

5.1.6.4. *(E)-1-(3-methoxy-4'-(*per-O*-acetyl- β -D-maltopyranosyloxy)phenyl)-2-(5-methoxyphenyl)ethene (40).* Following the general deprotection procedure and starting from **51**, the reaction yielded **40** as a white solid. Yield= 96%; ¹H NMR (400 MHz, CD₃OD) δ ppm : 7.47 – 7.37 (m, 2H), 7.08 – 6.87 (m, 4H), 6.64 (t, *J* = 1.8 Hz, 2H), 6.38 – 6.31 (m, 1H), 5.25 – 5.12 (m,

2H), 4.94 (d, $J = 7.7$ Hz, 1H), 3.95 – 3.79 (m, 7H), 3.75 (d, $J = 1.5$ Hz, 6H), 3.72 – 3.58 (m, 5H), 3.58 – 3.42 (m, 6H); ^{13}C NMR (101 MHz, CD_3OD): $\delta = 161.02, 157.18, 139.58, 131.67, 128.13, 127.39, 126.97, 116.55, 104.06, 101.44, 101.36, 101.23, 100.56, 99.29, 79.86, 79.46, 78.88, 76.21, 75.25, 73.68, 73.58, 73.33, 73.08, 72.78, 72.34, 71.95, 70.07, 61.33, 60.81, 60.65, 54.46, 54.45, 48.55, 48.53$; HRMS (ES^+) Calcd. for $\text{C}_{34}\text{H}_{46}\text{O}_{18}\text{Na}$: (M+Na) 765.2582, found; 765.2584.

5.1.7. *General procedure for esterification.* Starting material (1 eq.) and vinyl ester (3 eq.) were dissolved in *t*-BuOH (10ml) in a round-bottomed flask. Lipozyme[®] TL IM was then added to the solution (same mass of enzyme than that of starting material) and reaction was stirred overnight at 55°C in an orbital shaker. The reaction mixture was filtered to remove the enzyme and the crude was purified by flash column chromatography using different hexane/ethyl acetate/ methanol mixtures.

5.1.7.1. *(E)-1-(3-methoxy-5-(6-O-octanoyl- β -D-glucopyranosyloxy)phenyl)-2-(4'-methoxyphenyl)ethene (35).* Following the general procedure and starting from **32**, the reaction yielded compound **35**. The crude was purified by flash column chromatography (hexane: ethyl acetate from 1:20 to 0:100 and then ethyl acetate: methanol 50:1) to afford **35** (21%); ^1H NMR (400 MHz, CD_3OD) δ ppm : 7.46 (d, $J = 8.8$ Hz, 2H), 7.13 – 6.83 (m, 5H), 6.77 – 6.63 (m, 1H), 6.54 (t, $J = 2.2$ Hz, 1H), 4.94 – 4.90 (m, 1H), 4.44 (td, $J = 11.3, 10.8, 2.2$ Hz, 1H), 4.23 (td, $J = 11.9, 7.3$ Hz, 1H), 3.83 – 3.78 (m, 6H), 3.71 (ddd, $J = 10.0, 7.6, 2.2$ Hz, 1H), 3.56 – 3.44 (m, 2H), 3.42 – 3.33 (m, 1H), 2.27 (t, $J = 7.4$ Hz, 2H), 1.60 (dq, $J = 10.3, 7.1, 6.0$ Hz, 2H), 1.31 (m, 8H), 0.95 – 0.86 (t, $J = 13.8, 6.7$ Hz, 3H); ^{13}C NMR (101 MHz, CD_3OD): 176.25, 173.95, 160.84, 159.55, 158.77, 139.73, 129.83, 128.58, 127.48, 126.01, 116.60, 113.76, 106.41, 105.69, 102.11, 100.66, 76.46, 73.95, 73.40, 70.59, 63.52, 54.45, 54.34, 33.57, 31.45, 28.80, 28.69, 24.69, 22.25, 13.03; HRMS (ES^+) Calcd. for $\text{C}_{30}\text{H}_{40}\text{O}_9\text{Na}$: (M+Na) 567.2570, found; 567.2547.

5.1.7.2. *(E)-1-(3,5-di-(6-O-octanoyl- β -D-glucopyranosyloxy)phenyl)-2-(4'-methoxyphenyl)ethene (36).* Following the general procedure and starting from **33** after purification with flash chromatography whilst eluting with a gradient concentration of ethyl acetate: methanol (5:1-

2:1) the reaction yielded compound **36**. Yield: 18%, R_f = 0.3 (4:1 - EtOAc:MeOH); ¹H NMR (500 MHz, CD₃OD) δ 7.51 – 7.44 (m, 2H), 7.18 (d, *J* = 5.0 Hz, 1H), 7.12 (d, *J* = 15.5 Hz, 1H), 6.98 (d, *J* = 6.0 Hz, 1H), 6.95 – 6.89 (m, 2H), 6.72 (s, 1H), 6.67 (s, 1H), 4.95 (d, *J* = 7.1 Hz, 1H), 4.82 (dd, *J* = 12.6, 6.3 Hz, 2H), 4.47 (dd, *J* = 21.7, 9.4 Hz, 2H), 4.26 – 4.15 (m, 3H), 3.80 (s, 3H), 3.68 (dd, *J* = 12.7, 6.1 Hz, 2H), 3.49 (dd, *J* = 5.5, 2.6 Hz, 2H), 3.42 – 3.36 (m, 2H), 1.62 – 1.58 (m, 4H), 1.39 – 1.26 (m, 20H), 0.91 (t, *J* = 7.0 Hz, 6H). ¹³C NMR (126 MHz, CD₃OD) δ 176.32, 174.01, 173.89, 159.68, 158.76, 158.53, 128.85, 127.55, 113.83, 113.77, 107.80, 100.43, 96.79, 92.55, 76.52, 73.94, 73.52, 73.36, 72.37, 72.03, 70.60, 70.24, 69.26, 63.54, 61.39, 54.37, 33.62, 31.49, 28.83, 28.73, 24.72, 22.28, 13.06. HRMS (ES⁺) Calcd. for C₄₃H₆₂O₁₅ (M+Na) 841.3986, found 841.3993.

5.1.7.3. (*E*)-1-(3-methoxy-4'-(6-*O*-octanoyl-β-*D*-glucopyranosyloxy)phenyl)-2-(5-methoxyphenyl)ethene (**37**). Following the general procedure and starting from **34**, compound **37** was afforded (61%). The crude was purified by flash column chromatography (hexane: ethyl acetate from 1:20 to 0:100 and then ethyl acetate: methanol 50:1); ¹H NMR (400 MHz, CD₃OD) δ (d, *J* = 8.1 Hz, 2H), 7.16 – 6.87 (m, 4H), 6.66 (s, 2H), 6.36 (s, 1H), 4.89 (d, *J* = 5.8 Hz, 1H), 4.40 (d, *J* = 11.8 Hz, 1H), 4.22 (dd, *J* = 11.8, 7.1 Hz, 1H), 3.78 (s, 6H), 3.62 (dt, *J* = 15.3, 7.9 Hz, 1H), 3.52 – 3.41 (m, 2H), 3.38 – 3.31 (m, 1H), 2.28 (dt, *J* = 21.6, 7.5 Hz, 2H), 1.56 (h, *J* = 8.2 Hz, 2H), 1.27 (m, 8H), 0.84 (dt, *J* = 28.5, 6.5 Hz, 3H); ¹³C NMR (101 MHz, CD₃OD): δ = 176.3, 173.9, 161.1, 157.1, 139.5, 131.7, 128.0, 127.2, 127.0, 116.6, 104.0, 100.6, 99.2, 76.4, 74.0, 73.4, 70.4, 63.2, 54.3, 33.7, 33.5, 31.5, 31.4, 28.8, 28.75, 28.7, 24.7, 22.3, 22.2, 13.0. HRMS (ES⁺) Calcd. for C₃₀H₄₀O₉: (M+H) 545.2751, found; 545.2728.

5.1.7.4. (*E*)-1-(3-methoxy-5-(6-*O*-butanoyl-β-*D*-glucopyranosyloxy)phenyl)-2-(4'-methoxyphenyl)ethene (**38**). Following the general procedure and starting from **32**, the reaction yielded compound **38**. The crude was purified by flash column chromatography (hexane: ethyl acetate from 1:20 to 0:100 and then ethyl acetate: methanol 50:1) to afford **38** (20%); ¹H NMR (600 MHz, CD₃OD) δ 7.48 – 7.42 (m, 2H), 7.08 (d, *J* = 16.3 Hz, 1H), 6.96 – 6.88 (m, 3H), 6.84 (t, *J* = 1.7 Hz, 1H), 6.77 – 6.74 (m, 1H), 6.54 (t, *J* = 2.2 Hz, 1H), 4.91 (d, *J* = 7.1 Hz, 1H), 4.44 (td, *J* = 12.3, 2.2 Hz, 1H), 4.22 (ddd, *J* = 17.0, 11.9, 7.1 Hz, 1H), 3.81 – 3.78 (m, 6H), 3.73 – 3.63

(m, 1H), 3.52 – 3.43 (m, 2H), 3.40 – 3.32 (m, 1H), 2.26 (t, $J = 7.5$ Hz, 2H), 1.53 (h, $J = 7.4$ Hz, 2H), 0.80 (t, $J = 7.4$ Hz, 3H); ^{13}C NMR (151 MHz, CD_3OD): δ 173.8, 161.08, 160.89, 159.58, 158.77, 139.81, 129.86, 128.61, 127.47, 125.97, 113.74, 106.57, 105.50, 103.99, 102.09, 100.70, 76.45, 74.01, 73.43, 70.52, 63.43, 54.44, 54.33, 35.47, 17.94, 12.44; HRMS (ES^+) Calcd. for $\text{C}_{26}\text{H}_{33}\text{O}_9$: (M+H) 489.2125, found; 489.2108.

5.7.1.5. *(E)*-1-(3-methoxy-4'-(6-*O*-butanoyl- β -*D*-glucopyranosyloxy)-butyrate)phenyl)-2-(5-methoxyphenyl) ethene (**39**). Following the general esterification procedure and starting from **34** compound **39** was obtained. The crude was purified by flash column chromatography (hexane: ethyl acetate from 1:20 to 0:100 and then ethyl acetate: methanol 50:1) to afford compound **39** (159 mg, 56%); ^1H NMR (400 MHz, CD_3OD) δ ppm : 7.56 – 7.35 (m, 2H), 7.13 – 7.04 (m, 3H), 6.97 (d, $J = 16.3$ Hz, 1H), 6.69 (d, $J = 2.2$ Hz, 2H), 6.39 (t, $J = 2.2$ Hz, 1H), 4.98 – 4.88 (m, 1H), 4.47 (dd, $J = 11.9, 2.2$ Hz, 1H), 4.27 (dd, $J = 11.9, 6.8$ Hz, 1H), 4.12 (q, $J = 7.1$ Hz, 1H), 3.83 (s, 6H), 3.75 – 3.61 (m, 1H), 3.56 – 3.50 (m, 1H), 3.45 – 3.36 (m, 1H), 2.35 (t, $J = 7.4$ Hz, 2H), 1.65 (h, $J = 7.3$ Hz, 2H), 0.96 (t, $J = 7.4$ Hz, 3H); ^{13}C NMR (101 MHz, CD_3OD): $\delta = 173.8, 171.7, 161.0, 157.1, 139.5, 131.8, 128.1, 127.3, 127.1, 116.7, 104.1, 100.7, 99.4, 78.0, 77.7, 77.4, 76.4, 74.0, 73.3, 70.3, 63.3, 60.2, 54.6, 35.7, 18.1, 12.8$. HRMS (ES^+) Calcd. for $\text{C}_{26}\text{H}_{33}\text{O}_9$: (M+H) 489.2125, found; 489.2108.

5.7.1.6. *(E)*-1-(3-methoxy-4'-(6,6',6''-*O*-trioctanoyl- β -*D*-maltopyranosyloxy)phenyl)-2-(5-methoxyphenyl) ethene (**41**). Following the general deprotection procedure and starting from **40**, the reaction yielded compound **41** as a white solid. Yield= 9%; ^1H NMR (500 MHz, CD_3OD) δ ppm : 7.53 – 7.47 (m, 2H), 7.15 – 6.94 (m, 4H), 6.70 (d, $J = 2.3$ Hz, 2H), 6.39 (t, $J = 2.0$ Hz, 1H), 5.35 – 5.09 (m, 2H), 5.08 – 4.90 (m, 1H), 4.02 (d, $J = 5.7$ Hz, 1H), 3.89 (m, 6H), 3.81 (s, 6H), 3.71 – 3.57 (m, 5H), 3.57 – 3.40 (m, 6H), 2.10 – 1.94 (m, 2H), 1.72 – 1.54 (m, 2H), 1.43 – 1.24 (m, 8H), 0.98 – 0.85 (m, 3H); ^{13}C NMR (126 MHz, CD_3OD): $\delta = 174.09, 161.10, 157.30, 139.62, 131.75, 128.07, 127.29, 126.97, 116.53, 103.97, 101.74, 101.27, 100.67, 99.25, 96.69, 80.72, 79.52, 76.26, 75.36, 73.61, 73.52, 73.11, 72.81, 72.30, 72.08, 70.93, 70.75, 70.23, 70.07, 68.54,$

66.27, 63.51, 62.05, 54.72, 54.36, 33.51, 33.34, 31.47, 28.78, 28.69, 24.61, 13.01; HRMS (ES⁺)
Calcd. for C₄₂H₆₀O₁₉Na: (M+Na) 891.3627, found; 891.3636.

5.2. Biological evaluation

5.2.1. *Cell cultures.* SH-S5Y5 neurons were cultured in collagen-pretreated petri-dishes with DMEM-F12 medium supplemented with Penicillin/Streptomycin and 10 % inactivated fetal bovine serum (iFBS). RAW 264.7 macrophages were cultured in DMEM high glucose medium supplemented with Penicillin/Streptomycin and 10 % iFBS.

5.2.2. *Cell viability assays.* Neuron assays were done in collagen-pretreated 96 well plates by seeding 2×10^4 neurons per well in a 100 μ L volume and with 24 h of incubation time before compound addition. Macrophage assays were done in 96 well plates by seeding 2.5×10^4 macrophages per well in a 100 μ L volume with 4 h of incubation time before compound addition. 10, 1 and 0.1 mM DMSO stocks of the tested compounds were prepared. 1:100 dilutions of each stock in cell culture media were carried out upon addition of the compounds to the well plate. Thus, the final compound concentrations in the plate were 100, 10 and 1 μ M respectively, whereas the DMSO percentage in each well was 1%. Cell viability was evaluated 24 hours after compound addition by mitochondrial MTT assay, according to manufacturer. Averages and standard deviations of at least two experiments in quadruplicate were calculated.

5.2.3. *Neuroprotective assay.* Neurons were cultured and plated as described in the cell viability assay. Tested compounds were added at different concentrations (1, 10 and 100 μ M dissolved in cell culture media with 1% DMSO) and after 10 min incubation 100 μ M of hydrogen peroxide was added. Final DMSO percentage in each well was adjusted to 1% DMSO. Cell viability was evaluated 24 hours after compound addition by mitochondrial MTT assay, according to manufacturer. Averages and standard deviations of at least two experiments in quadruplicate were

calculated. Neuron recovery was calculated by normalizing the results from H₂O₂-neuron viability to the H₂O₂ positive control.

5.2.4. Cytokine Production studies. To determine cytokine production, 5×10^5 RAW 264.7 macrophages were seeded in 24-well plates (in 0.5 ml). Compounds (10 μ M) were then added and macrophages were either stimulated or not by adding LPS (1 μ g/ml) to the medium. After 24 hr, levels of IL-6 and TNF- α in the supernatants were determined by ELISA using capture/biotinylated detection antibodies from BD PharMingen and PreproTech [77, 78]. A minimum of two independent sets of experiments and three replicates per experiment were carried out. All data are expressed as mean \pm SEM.

5.2.5. Zebra fish toxicity assay. This assay was subcontracted to Zeclinics (Barcelona, Spain). Fertilized embryos of zebrafish (*Danio rerio* – strain AB) were harvested 3 hours post fertilization and grouped into wells (20 embryos per well) in E3 medium with the desired compounds in gradient concentrations (5 different concentrations, from 0.1 μ M to 1 mM). They were further incubated at 28.5 °C for 93 more hours and then LC50 values (median lethal dose) were calculated by fitting sigmoidal curve to mortality data ($y = \text{Bot} + (\text{Top}-\text{Bot}) / (1 + 10^{-(k \cdot (x_0 - \text{Log}(C)))})$). Bot, minimum mortality; Top, maximum mortality; k, curve slope; x_0 , LC50 estimated. Negative controls were 0.1% of DMSO and as positive controls 4-diethylaminobenzaldehyde (DEAB) at 5 different concentrations (from 0.1 μ M to 1 mM).

5.2.6. PTZ neuroprotection assay. This assay was subcontracted to Neuron Bio (Granada, Spain). Fertilized embryos of zebrafish (*Danio rerio* – strain AB) were seeded into a Petri dish with 50 mL of dilution water until they reached larva state (5 days post fertilization). After verification of no abnormalities, five larvae per well were transferred into a 24 well plate and ten replicates of each experimental condition were carried out. Two independent experiments were performed.

Pretreatment: larvae were incubated for 1h at 26 °C in a volume of 2 mL of dilution water containing 0.1% DMSO (control and control+PTZ groups), the positive control group (Phys) included physostigmine (20µM) and the groups with each compound to be examined included 10µM of the compound. After this pretreatment, media was changed and larvae were incubated for 6h at 26 °C with Phys (20µM) or each compound (10µM) in combination with a final concentration of 5 mM PTZ. Then, larvae were examined and their overall status was normal, without visible abnormalities and with normal behavior. Finally, in order to determine the levels of AChE activity, the larvae were mechanically homogenized and the samples centrifuged to obtain the supernatant, which was then directly tested. AChE activity was measured following methodology by Ellman et al [79]. Total protein was quantified using BCA methodology in order to normalize the obtained enzymatic values. Lastly, the negative control values were considered to be the 100% values. A statistical analysis was carried out using the Dunnett multiple comparison test (One-way ANOVA) with the GraphPad Prism program.

5.2.7. *Mice*. C57BL/6 mice 12 weeks old were obtained from Charles River and housed under standard conditions (12h light/dark cycle) with access to food and water *ad libitum*. Animals were handled and habituated to the experimenters one week before any behavioral assessment. All experiments with animals were performed in accordance with the European ethical guidelines and approved by the Animal Care Unit Committee from the Institute of Parasitology and Biomedicine Lopez-Neyra - Consejo Superior de Investigaciones Científicas. Procedures were designed to minimize the number of animals used and their suffering.

5.2.8. *3-Nitropropionic acid intoxication*. 3-nitropropionic acid (3-NP, Sigma) was prepared and administered as previously indicated with minor modifications [80-82]. 3-NP was dissolved in distilled water final pH 7.4, filtered (0.22 µm, Millipore), protected from light and kept at 4° C until use. Resveratrol (compound **1**) and compound **8** were dissolved in an aqueous solution containing 13% (2-hydroxypropyl)-β-cyclodextrin (average MW ≈1380) and 2% Tween-80. 28 animals were grouped as follow for treatment administration: vehicle (veh, n=7), 3-NP (n=7),

resveratrol (compound **1**) + 3-NP (1+3-NP, n=7), and compound **8** + 3-NP (8+3-NP, n=7). For 3-NP intoxication, animals received twice daily i.p. injections (8:00 am: 6:00 pm) 10 h apart with the next regimen 4x20 mg/kg, 4x40 mg/kg, 2x60 mg/kg (cumulated dose: 360 mg/kg in 5 days) (Figure S4). Resveratrol (5.5 mg/kg [38.75 μ M]) and compound **8** (12.46 mg/kg [38.75 μ M]) were injected only and immediately before the morning dose of 3-NP. All treatments were administered in a volume of \approx 100 μ L and always after behavioral evaluations.

5.2.9. Behavioral assessment. Mice were weighed and then behavioral semi-quantitative assessments were carried out. Evaluations (weight and behavioral register) were performed just before injections, excepting the last one, performed three hours after the final 3-NP injection (60 mg/kg). Clinical semi-quantitative motor symptoms assessment was based on a previously reported motor scale with minor modification.[80, 82] Included items were: global locomotor activity, hindlimb claspings, hindlimb dystonia and truncal dystonia, each rated on a three levels scale of severity (0-absent, 1-slight to moderate and 2-severe) resulting in a total score ranging from 0 to 8.

5.2.10. Tissue collection. At the end of the experiment and at least three hours after any animal manipulation, mice were sacrificed in a CO₂ chamber and blood and brain tissue were immediately collected. Blood was centrifuged for serum recovering, and collected serum samples were stored at -20 °C from obtaining until the analysis of interleukin-6 (IL-6) content. Brains were frozen in liquid nitrogen and subsequently processed to qRT-PCR assay.

5.2.11. IL-6 detection. IL-6 content in serums from healthy or 3-NP treated mice was measured by a sandwich ELISA. In brief, a 96-well ELISA plate was coated overnight at 4°C with IL-6 capture antibody in 0.1 M phosphate buffer pH 9.0. The plate was washed and blocked with 0.1 M PBS containing 10% fetal bovine serum at room temperature for 3h. Then, serum samples or

different concentrations of the recombinant IL-6 were added and incubated overnight at 4° C, followed by a 2 h period incubation with biotinylated secondary antibody at RT. Finally, avidin peroxidase (Sigma) was added followed by the ABTS substrate addition at RT, and plate was protected from light until color development. Three washing buffer (0.1 M PBS plus 0.05% Tween-20) washes were applied between steps. Absorbance was obtained in a reader plate at 405 nM, and amount of IL-6 was calculated from the standard curve.

5.2.12. qRT-PCR. RNA was isolated from brain tissues using Tripure (Roche) accordingly the manufacturer's indications. Total RNA (1 µg) was reverse transcribed in a 20 µL volume using the reagents supplied in the synthesis cDNA kit (*Thermo Scientific RevertAid First Strand KI622*, Vilnius, Lithuania). 20 ng cDNA (2 µL) were amplified by real-time PCR using SensyFast and sequences of specific primers including: iNOS, Nitric oxide synthetase 2; CAT, catalase; SOD2, dismutase duperoxide; p53, and GAPDH (Glyceraldehyde 3-phosphate dehydrogenase) as housekeeping [see Table 1]. All PCR reaction was carried out in a Bio-Rad CFX equipment (Bio-Rad). Thermal cycling profile consisted of a preincubation step at 94°C for 5 min, followed by 40 cycles of denaturation (94°C, 30 sec), annealing (temperature adjusted for each gene (Table S1), 30 sec), and extension (72°C, 30 sec).

5.2.13. Statistical analysis. Data analysis was performed using the Sigma Stat 3.5 (Systat Software Inc.) and the GraphPad 5 (GraphPad Software, Inc.) software. In case of normal distribution and/or equal variance data, statistical differences were determined by two-tails Student's t test for a 2-groups comparison, or by One-way ANOVA followed by Bonferroni's post-Hoc test to compare more than three groups. Data with nonparametric distribution were evaluated for differences by Mann Whitney's or Kruskal-Wallis followed by Dunn's post-Hoc test when two or more than three groups were compared, respectively. $P < 0.05$ was considered statistically significant.

Acknowledgements

This work was supported by the Junta de Andalucía (FQM-7316), Spanish Ministerio de Economía y Competitividad grant SAF2014-58354-R and FEDER funds from the EU are gratefully acknowledged. PPP's work was supported by Junta de Andalucía (FQM-7316). EBR is a student of the Pharmacy PhD program of the University of Granada (Spain). NA's work was supported by a Juan de la Cierva Fellowship from the Spanish Ministerio de Economía y Competitividad.

Appendix A. Supplementary data

Supplementary data related to this article can be found at:

References

- [1] E. Radi, P. Formichi, C. Battisti, A. Federico, Apoptosis and oxidative stress in neurodegenerative diseases, *J Alzheimers Dis*, 42 Suppl 3 (2014) S125-152.
- [2] M.T. Lin, M.F. Beal, Mitochondrial dysfunction and oxidative stress in neurodegenerative diseases, *Nature*, 443 (2006) 787-795.
- [3] A.H. Bhat, K.B. Dar, S. Anees, M.A. Zargar, A. Masood, M.A. Sofi, S.A. Ganie, Oxidative stress, mitochondrial dysfunction and neurodegenerative diseases; a mechanistic insight, *Biomed Pharmacother*, 74 (2015) 101-110.
- [4] A. Federico, E. Cardaioli, P. Da Pozzo, P. Formichi, G.N. Gallus, E. Radi, Mitochondria, oxidative stress and neurodegeneration, *J Neurol Sci*, 322 (2012) 254-262.
- [5] S. Amor, L.A. Peferoen, D.Y. Vogel, M. Breur, P. van der Valk, D. Baker, J.M. van Noort, Inflammation in neurodegenerative diseases--an update, *Immunology*, 142 (2014) 151-166.
- [6] R. Morphy, Z. Rankovic, Designed multiple ligands. An emerging drug discovery paradigm, *J Med Chem*, 48 (2005) 6523-6543.
- [7] G.R. Zimmermann, J. Lehar, C.T. Keith, Multi-target therapeutics: when the whole is greater than the sum of the parts, *Drug Discov Today*, 12 (2007) 34-42.
- [8] A. Koeberle, O. Werz, Multi-target approach for natural products in inflammation, *Drug Discov Today*, 19 (2014) 1871-1882.
- [9] M.G. Katselou, A.N. Matralis, A.P. Kourounakis, Multi-Target Drug Design Approaches for Multifactorial Diseases: From Neurodegenerative to Cardiovascular Applications, *Curr. Med. Chem.*, 21 (2014) 2743-2787.
- [10] X. Chen, M. Decker, Multi-Target Compounds Acting in the Central Nervous System Designed From Natural Products, *Curr. Med. Chem.*, 20 (2013) 1673-1685.

- [11] B.N. Zordoky, I.M. Robertson, J.R. Dyck, Preclinical and clinical evidence for the role of resveratrol in the treatment of cardiovascular diseases, *Biochim Biophys Acta*, 1852 (2015) 1155-1177.
- [12] J.A. Baur, D.A. Sinclair, Therapeutic potential of resveratrol: the in vivo evidence, *Nat Rev Drug Discov*, 5 (2006) 493-506.
- [13] M. Jang, L. Cai, G.O. Udeani, K.V. Slowing, C.F. Thomas, C.W. Beecher, H.H. Fong, N.R. Farnsworth, A.D. Kinghorn, R.G. Mehta, R.C. Moon, J.M. Pezzuto, Cancer chemopreventive activity of resveratrol, a natural product derived from grapes, *Science*, 275 (1997) 218-220.
- [14] N. Elmali, O. Baysal, A. Harma, I. Esenkaya, B. Mizrak, Effects of Resveratrol in Inflammatory Arthritis, *Inflammation*, 30 (2007) 1-6.
- [15] M.S. Lopez, R.J. Dempsey, R. Vemuganti, Resveratrol neuroprotection in stroke and traumatic CNS injury, *Neurochem Int*, 89 (2015) 75-82.
- [16] S. Bastianetto, C. Menard, R. Quirion, Neuroprotective action of resveratrol, *Biochim Biophys Acta*, 1852 (2015) 1195-1201.
- [17] N. Singh, M. Agrawal, S. Dore, Neuroprotective properties and mechanisms of resveratrol in in vitro and in vivo experimental cerebral stroke models, *ACS Chem Neurosci*, 4 (2013) 1151-1162.
- [18] R.G. Britton, C. Koor, K. Brown, Direct molecular targets of resveratrol: identifying key interactions to unlock complex mechanisms, *Ann N Y Acad Sci*, 1348 (2015) 124-133.
- [19] S.S. Kulkarni, C. Canto, The molecular targets of resveratrol, *Biochim Biophys Acta*, 1852 (2015) 1114-1123.
- [20] R.S. Turner, R.G. Thomas, S. Craft, C.H. van Dyck, J. Mintzer, B.A. Reynolds, J.B. Brewer, R.A. Rissman, R. Raman, P.S. Aisen, A randomized, double-blind, placebo-controlled trial of resveratrol for Alzheimer disease, *Neurology*, 85 (2015) 1383-1391.
- [21] C. Moussa, M. Hebron, X. Huang, J. Ahn, R.A. Rissman, P.S. Aisen, R.S. Turner, Resveratrol regulates neuro-inflammation and induces adaptive immunity in Alzheimer's disease, *J Neuroinflammation*, 14 (2017) 1.
- [22] J. Chao, H. Li, K.W. Cheng, M.S. Yu, R.C. Chang, M. Wang, Protective effects of pinostilbene, a resveratrol methylated derivative, against 6-hydroxydopamine-induced neurotoxicity in SH-SY5Y cells, *J Nutr Biochem*, 21 (2010) 482-489.
- [23] J. Chang, A. Rimando, M. Pallas, A. Camins, D. Porquet, J. Reeves, B. Shukitt-Hale, M.A. Smith, J.A. Joseph, G. Casadesus, Low-dose pterostilbene, but not resveratrol, is a potent neuromodulator in aging and Alzheimer's disease, *Neurobiol Aging*, 33 (2012) 2062-2071.
- [24] C. Villalonga-Barber, A.K. Meligova, X. Alexi, B.R. Steele, C.E. Kouzinou, C.G. Screttas, E.S. Katsanou, M. Micha-Screttas, M.N. Alexis, New hydroxystilbenoid derivatives endowed with neuroprotective activity and devoid of interference with estrogen and aryl hydrocarbon receptor-mediated transcription, *Bioorg Med Chem*, 19 (2011) 339-351.
- [25] T. Puksasook, S. Kimura, S. Tadtong, J. Jiaranaikulwanitch, J. Pratuangdejkul, W. Kitphati, K. Suwanborirux, N. Saito, V. Nukoolkarn, Semisynthesis and biological evaluation of prenylated resveratrol derivatives as multi-targeted agents for Alzheimer's disease, *J Nat Med*, (2017).
- [26] S.Y. Li, X.B. Wang, L.Y. Kong, Design, synthesis and biological evaluation of imine resveratrol derivatives as multi-targeted agents against Alzheimer's disease, *Eur J Med Chem*, 71 (2014) 36-45.
- [27] J. Jerabek, E. Uliassi, L. Guidotti, J. Korabecny, O. Soukup, V. Sepsova, M. Hrabnova, K. Kuca, M. Bartolini, L.E. Pena-Altamira, S. Petralla, B. Monti, M. Roberti, M.L. Bolognesi,

- Tacrine-resveratrol fused hybrids as multi-target-directed ligands against Alzheimer's disease, *Eur J Med Chem*, 127 (2017) 250-262.
- [28] C. Lu, Y. Guo, J. Yan, Z. Luo, H.B. Luo, M. Yan, L. Huang, X. Li, Design, synthesis, and evaluation of multitarget-directed resveratrol derivatives for the treatment of Alzheimer's disease, *J Med Chem*, 56 (2013) 5843-5859.
- [29] L. Biasutto, A. Mattarei, N. Sassi, M. Azzolini, M. Romio, C. Paradisi, M. Zoratti, Improving the efficacy of plant polyphenols, *Anticancer Agents Med Chem*, 14 (2014) 1332-1342.
- [30] L. Biasutto, A. Mattarei, M. Azzolini, M. La Spina, N. Sassi, M. Romio, C. Paradisi, M. Zoratti, Resveratrol derivatives as a pharmacological tool, *Ann N Y Acad Sci*, 1403 (2017) 27-37.
- [31] M. Larrosa, J. Tome-Carneiro, M.J. Yanez-Gascon, D. Alcantara, M.V. Selma, D. Beltran, M.T. Garcia-Conesa, C. Urban, R. Lucas, F. Tomas-Barberan, J.C. Morales, J.C. Espin, Preventive oral treatment with resveratrol pro-prodrugs drastically reduce colon inflammation in rodents, *J Med Chem*, 53 (2010) 7365-7376.
- [32] R. Chillemi, N. Cardullo, V. Greco, G. Malfa, B. Tomasello, S. Sciuto, Synthesis of amphiphilic resveratrol lipoconjugates and evaluation of their anticancer activity towards neuroblastoma SH-SY5Y cell line, *Eur J Med Chem*, 96 (2015) 467-481.
- [33] H. Ji, X. Zhang, Y. Du, H. Liu, S. Li, L. Li, Polydatin modulates inflammation by decreasing NF-kappaB activation and oxidative stress by increasing Gli1, Ptch1, SOD1 expression and ameliorates blood-brain barrier permeability for its neuroprotective effect in pMCAO rat brain, *Brain Res Bull*, 87 (2012) 50-59.
- [34] R. Osborne, S. Joel, D. Trew, M. Slevin, Analgesic activity of morphine-6-glucuronide, *Lancet*, 1 (1988) 828.
- [35] J. Hoshino, E.J. Park, T.P. Kondratyuk, L. Marler, J.M. Pezzuto, R.B. van Breemen, S. Mo, Y. Li, M. Cushman, Selective synthesis and biological evaluation of sulfate-conjugated resveratrol metabolites, *J Med Chem*, 53 (2010) 5033-5043.
- [36] E. Falomir, R. Lucas, P. Penalver, R. Marti-Centelles, A. Dupont, A. Zafra-Gomez, M. Carda, J.C. Morales, Cytotoxic, Antiangiogenic and Antitelomerase Activity of Glucosyl- and Acyl- Resveratrol Prodrugs and Resveratrol Sulfate Metabolites, *Chembiochem*, 17 (2016) 1343-1348.
- [37] F. Orsini, L. Verotta, M. Lecchi, R. Restano, G. Curia, E. Redaelli, E. Wanke, Resveratrol Derivatives and Their Role as Potassium Channels Modulators, *J. Nat. Prod.*, 67 (2004) 421-426.
- [38] S.M. Poulouse, N. Thangthaeng, M.G. Miller, B. Shukitt-Hale, Effects of pterostilbene and resveratrol on brain and behavior, *Neurochem. Int.*, 89 (2015) 227-233.
- [39] N. Singh, M. Agrawal, S. Doré, Neuroprotective Properties and Mechanisms of Resveratrol in in Vitro and in Vivo Experimental Cerebral Stroke Models, *ACS Chem. Neurosci.*, 4 (2013) 1151-1162.
- [40] E.R. Whitemore, D.T. Loo, J.A. Watt, C.W. Cotman, A detailed analysis of hydrogen peroxide-induced cell death in primary neuronal culture, *Neuroscience*, 67 (1995) 921-932.
- [41] M. Dvorakova, P. Landa, Anti-inflammatory activity of natural stilbenoids: A review, *Pharmacol. Res.*, 124 (2017) 126-145.
- [42] M. Venigalla, S. Sonogo, E. Gyengesi, M.J. Sharman, G. Munch, Novel promising therapeutics against chronic neuroinflammation and neurodegeneration in Alzheimer's disease, *Neurochem Int*, 95 (2016) 63-74.
- [43] J. Renaud, M.G. Martinoli, Resveratrol as a protective molecule for neuroinflammation: a review of mechanisms, *Curr Pharm Biotechnol*, 15 (2014) 318-329.

- [44] N.S. Sipes, S. Padilla, T.B. Knudsen, Zebrafish: as an integrative model for twenty-first century toxicity testing, *Birth Defects Res C Embryo Today*, 93 (2011) 256-267.
- [45] F. Busquet, R. Strecker, J.M. Rawlings, S.E. Belanger, T. Braunbeck, G.J. Carr, P. Cenijn, P. Fochtman, A. Gourmelon, N. Hubler, A. Kleensang, M. Knobel, C. Kussatz, J. Legler, A. Lillicrap, F. Martinez-Jeronimo, C. Polleichtner, H. Rzodeczko, E. Salinas, K.E. Schneider, S. Scholz, E.J. van den Brandhof, L.T. van der Ven, S. Walter-Rohde, S. Weigt, H. Witters, M. Halder, OECD validation study to assess intra- and inter-laboratory reproducibility of the zebrafish embryo toxicity test for acute aquatic toxicity testing, *Regul Toxicol Pharmacol*, 69 (2014) 496-511.
- [46] R.L. Macdonald, J.L. Barker, Specific antagonism of GABA-mediated postsynaptic inhibition in cultured mammalian spinal cord neurons: a common mode of convulsant action, *Neurology*, 28 (1978) 325-330.
- [47] R.Q. Huang, C.L. Bell-Horner, M.I. Dibas, D.F. Covey, J.A. Drewe, G.H. Dillon, Pentylentetrazole-induced inhibition of recombinant gamma-aminobutyric acid type A (GABA(A)) receptors: mechanism and site of action, *J Pharmacol Exp Ther*, 298 (2001) 986-995.
- [48] T.V. Pavlova, A.A. Yakovlev, M.Y. Stepanichev, N.V. Gulyaeva, Pentylentetrazol kindling in rats: Is neurodegeneration associated with manifestations of convulsive activity?, *Neurosci Behav Physiol*, 36 (2006) 741-748.
- [49] T. Pavlova, M. Stepanichev, N. Gulyaeva, Pentylentetrazole kindling induces neuronal cyclin B1 expression in rat hippocampus, *Neurosci Lett*, 392 (2006) 154-158.
- [50] J.H. Park, H. Cho, H. Kim, K. Kim, Repeated brief epileptic seizures by pentylentetrazole cause neurodegeneration and promote neurogenesis in discrete brain regions of freely moving adult rats, *Neuroscience*, 140 (2006) 673-684.
- [51] T.P. Kalantaripour, S. Esmaili-Mahani, V. Sheibani, M. Asadi-Shekaari, H. Pasban-Aliabadi, Anticonvulsant and neuroprotective effects of apelin-13 on pentylentetrazole-induced seizures in male rats, *Biomed Pharmacother*, 84 (2016) 258-263.
- [52] M.E. Hasselmo, M. Sarter, Modes and models of forebrain cholinergic neuromodulation of cognition, *Neuropsychopharmacology*, 36 (2011) 52-73.
- [53] A. Hoshimoto, Y. Suzuki, T. Katsuno, H. Nakajima, Y. Saito, Caprylic acid and medium-chain triglycerides inhibit IL-8 gene transcription in Caco-2 cells: comparison with the potent histone deacetylase inhibitor trichostatin A, *Br J Pharmacol*, 136 (2002) 280-286.
- [54] M. Hecker, N. Sommer, H. Voigtmann, O. Pak, A. Mohr, M. Wolf, I. Vadasz, S. Herold, N. Weissmann, R.E. Morty, W. Seeger, K. Mayer, Impact of short- and medium-chain fatty acids on mitochondrial function in severe inflammation, *JPEN J Parenter Enteral Nutr*, 38 (2014) 587-594.
- [55] P.R. Huttenlocher, A.J. Wilbourn, J.M. Signore, Medium-chain triglycerides as a therapy for intractable childhood epilepsy, *Neurology*, 21 (1971) 1097-1103.
- [56] M.A. Sills, W.I. Forsythe, D. Haidukewych, A. MacDonald, M. Robinson, The medium chain triglyceride diet and intractable epilepsy, *Arch Dis Child*, 61 (1986) 1168-1172.
- [57] Y. Kamata, H. Shiraga, A. Tai, Y. Kawamoto, E. Gohda, Induction of neurite outgrowth in PC12 cells by the medium-chain fatty acid octanoic acid, *Neuroscience*, 146 (2007) 1073-1081.
- [58] E. Davioud-Charvet, S. Delarue, C. Biot, B. Schwöbel, C.C. Boehme, A. Müssigbrodt, L. Maes, C. Sergheraert, P. Grellier, R.H. Schirmer, K. Becker, A Prodrug Form of a Plasmodium falciparum Glutathione Reductase Inhibitor Conjugated with a 4-Anilinoquinoline, *J Med Chem*, 44 (2001) 4268-4276.

- [59] Y. Younis, R. Hunter, C.I. Muhanji, I. Hale, R. Singh, C.M. Bailey, T.J. Sullivan, K.S. Anderson, [d4U]-Spacer-[HI-236] double-drug inhibitors of HIV-1 reverse-transcriptase, *Bioorg. Med. Chem.*, 18 (2010) 4661-4673.
- [60] R.A. Smith, H. Yuan, R. Weissleder, L.C. Cantley, L. Josephson, A Wortmannin–Cetuximab as a Double Drug, *Bioconjug Chem*, 20 (2009) 2185-2189.
- [61] M. Garcia, P. Vanhoutte, C. Pages, M.J. Besson, E. Brouillet, J. Caboche, The mitochondrial toxin 3-nitropropionic acid induces striatal neurodegeneration via a c-Jun N-terminal kinase/c-Jun module, *J Neurosci*, 22 (2002) 2174-2184.
- [62] E. Brouillet, M.C. Guyot, V. Mittoux, S. Altairac, F. Conde, S. Palfi, P. Hantraye, Partial inhibition of brain succinate dehydrogenase by 3-nitropropionic acid is sufficient to initiate striatal degeneration in rat, *J Neurochem*, 70 (1998) 794-805.
- [63] E. Brouillet, C. Jacquard, N. Bizat, D. Blum, 3-Nitropropionic acid: a mitochondrial toxin to uncover physiopathological mechanisms underlying striatal degeneration in Huntington's disease, *J Neurochem*, 95 (2005) 1521-1540.
- [64] M. Bjorkqvist, E.J. Wild, J. Thiele, A. Silvestroni, R. Andre, N. Lahiri, E. Raibon, R.V. Lee, C.L. Benn, D. Soulet, A. Magnusson, B. Woodman, C. Landles, M.A. Pouladi, M.R. Hayden, A. Khalili-Shirazi, M.W. Lowdell, P. Brundin, G.P. Bates, B.R. Leavitt, T. Moller, S.J. Tabrizi, A novel pathogenic pathway of immune activation detectable before clinical onset in Huntington's disease, *J Exp Med*, 205 (2008) 1869-1877.
- [65] K.H. Chang, Y.R. Wu, Y.C. Chen, C.M. Chen, Plasma inflammatory biomarkers for Huntington's disease patients and mouse model, *Brain Behav Immun*, 44 (2015) 121-127.
- [66] M.F. Beal, E. Brouillet, B.G. Jenkins, R.J. Ferrante, N.W. Kowall, J.M. Miller, E. Storey, R. Srivastava, B.R. Rosen, B.T. Hyman, Neurochemical and histologic characterization of striatal excitotoxic lesions produced by the mitochondrial toxin 3-nitropropionic acid, *J Neurosci*, 13 (1993) 4181-4192.
- [67] A. Hariharan, S. Shetty, T. Shirole, A.G. Jagtap, Potential of protease inhibitor in 3-nitropropionic acid induced Huntington's disease like symptoms: mitochondrial dysfunction and neurodegeneration, *Neurotoxicology*, 45 (2014) 139-148.
- [68] C.V. Borlongan, T.K. Koutouzis, P.R. Sanberg, 3-Nitropropionic acid animal model and Huntington's disease, *Neurosci Biobehav Rev*, 21 (1997) 289-293.
- [69] M.A. La Fontaine, J.W. Geddes, A. Banks, D.A. Butterfield, 3-nitropropionic acid induced in vivo protein oxidation in striatal and cortical synaptosomes: insights into Huntington's disease, *Brain Res*, 858 (2000) 356-362.
- [70] Q. Liu, C. Kim, Y. Jo, S. Kim, B. Hwang, M. Lee, Synthesis and Biological Evaluation of Resveratrol Derivatives as Melanogenesis Inhibitors, *Molecules*, 20 (2015) 16933.
- [71] G. Solladié, Y. Pasturel-Jacopé, J. Maignan, A re-investigation of resveratrol synthesis by Perkins reaction. Application to the synthesis of aryl cinnamic acids, *Tetrahedron*, 59 (2003) 3315-3321.
- [72] U. Huchel, P. Tiwari, R.R. Schmidt, N-Aryl-O-glycosyl Haloacetimidates as Glycosyl Donors, *J. Carbohydr. Chem.*, 29 (2010) 61-75.
- [73] T.K. Ritter, K.-K.T. Mong, H. Liu, T. Nakatani, C.-H. Wong, A Programmable One-Pot Oligosaccharide Synthesis for Diversifying the Sugar Domains of Natural Products: A Case Study of Vancomycin, *Angew Chem Int Ed*, 42 (2003) 4657-4660.
- [74] A.M. Nyemba, T.N. Mpondo, S.F. Kimbu, J.D. Connolly, Stilbene glycosides from *Guibourtia tessmannii*, *Phytochemistry*, 39 (1995) 895-898.

- [75] L.-M. Dai, J. Tang, H.-L. Li, Y.-H. Shen, C.-Y. Peng, W.-D. Zhang, A new stilbene glycoside from the n-butanol fraction of *Veratrum dahuricum*, *Chem Nat Compd*, 2009 v.45 no.3 (2009) pp. 325-329.
- [76] C.S. Mizuno, K.K. Schrader, A.M. Rimando, Algicidal Activity of Stilbene Analogues, *J Agric Food Chem*, 56 (2008) 9140-9145.
- [77] E. Gonzalez-Rey, P. Anderson, M.A. Gonzalez, L. Rico, D. Buscher, M. Delgado, Human adult stem cells derived from adipose tissue protect against experimental colitis and sepsis, *Gut*, 58 (2009) 929-939.
- [78] S. Sanchez, T. Barger, L. Zhou, M. Hale, D. Mytych, S. Gupta, S.J. Swanson, F. Civoli, Strategy to confirm the presence of anti-erythropoietin neutralizing antibodies in human serum, *J Pharm Biomed Anal*, 55 (2011) 1265-1274.
- [79] G.L. Ellman, K.D. Courtney, V. Andres, Jr., R.M. Feather-Stone, A new and rapid colorimetric determination of acetylcholinesterase activity, *Biochem Pharmacol*, 7 (1961) 88-95.
- [80] E. Diguët, P.O. Fernagut, X. Wei, Y. Du, R. Rouland, C. Gross, E. Bezard, F. Tison, Deleterious effects of minocycline in animal models of Parkinson's disease and Huntington's disease, *Eur J Neurosci*, 19 (2004) 3266-3276.
- [81] L.W. Chen, L.Y. Horng, C.L. Wu, H.C. Sung, R.T. Wu, Activating mitochondrial regulator PGC-1 α expression by astrocytic NGF is a therapeutic strategy for Huntington's disease, *Neuropharmacology*, 63 (2012) 719-732.
- [82] P.O. Fernagut, E. Diguët, N. Stefanova, M. Biran, G.K. Wenning, P. Canioni, B. Bioulac, F. Tison, Subacute systemic 3-nitropropionic acid intoxication induces a distinct motor disorder in adult C57Bl/6 mice: behavioural and histopathological characterisation, *Neuroscience*, 114 (2002) 1005-1017.

4. Conclusions

- I. New carbohydrate conjugates of NDI G4 ligands have been synthesized and characterized.
- II. New glycosyl- and alkyl- derivatives of RES, Tyr and HT have been synthesized and characterized.
- III. A new and highly frequent PQS (EBR1) was discovered in the genome of *Trypanosoma brucei* and then validated as a G4. *Leishmania major* and *Plasmodium falciparum* also presented several G4s in their genome including the hTel sequence.
- IV. The carb-NDI conjugates showed binding to different G4 topologies -including EBR1- but no significant differences were observed among them and with the aglycone NDI.
- V. The carb-NDI conjugates showed excellent *in vitro* anti-proliferative and antiparasitic activity.
- VI. The carb-NDI conjugates cellular uptake in tumoral cells was at least partially mediated by GLUT4 transporters and less efficient than for the aglycone NDI.
- VII. The carb-NDI conjugates were located in the nucleus of tumoral and non-tumoral cells and also in the nucleus and kinetoplast of *Trypanosoma brucei*.
- VIII. Several methylated and butylated RES derivatives showed better neuroprotective and anti-inflammatory activity than RES *in vitro*.
- IX. 3-O-(6'-O-octanoyl)- β -D-glucopyranoside resveratrol (compound **8** in *Eur. J. Med. Chem.* 2018, 146, 123-138) displayed better neuroprotective activity than RES in zebra fish on pentylenetetrazole challenged and in a HD murine model.
- X. HT decanoate and dodecanoate esters (compounds **13** and **14** in *Eur. J. Med. Chem.* 2016, 119, 132-140) displayed significant IC₅₀ values against *Trypanosoma brucei* (0.6 and 0.36 μ M, respectively).

5. Tools developed

Several tools were created to facilitate and expedite treatment of all the data obtained in this thesis. These include several informatic algorithms written in R statistical programming language.

5.1. High-resolution mass finder

Chemical synthesis is extenuatingly ungrateful. It is very typical for reactions which theoretically transform into a desired product to yield secondary products. These unwanted side molecules -which sometimes are the only results- need to be identified or directly dismissed. When the identification path is desired, the two common options to start with are NMR or mass spectrometry (MS). NMR usually requires previous purification of the crude so the fastest method is generally MS, which however requires knowing the chemical formulas which coincide with the obtained masses. To do so, the only accessible option to those that don't have access to specific software is drawing the possible structures in an attempt to find the such mass. This, at the least, is a terribly tedious and time-consuming process.

To speed up the process, a code in R was developed to fetch all viable options for a specific mass inside a specific mass range. The result is a list, size-dependent on the range, which gives the actual possibilities within the element range determined by the user.

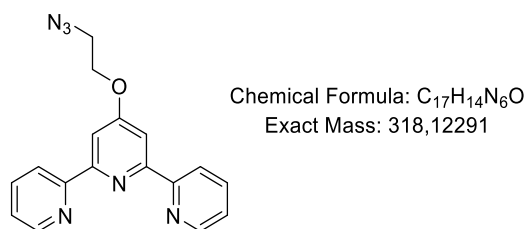
The developed code needs only three things, which are:

- I. The mass to be determined
- II. The range of the mass to show as acceptable
- III. The number of each element which are acceptable

The code will construct an initial table of results by combining all the possibilities of the elements and calculating their exact mass. These results will then be filtered in a second table with those chemical formulas which fit inside the range of the determined mass. The code will also give the difference and absolute difference against the mass and it will order the results to further simplify the search.

An example is shown here for the synthesis of 4'-(2-azidoethoxy)-2,2':6',2''-terpyridine (Figure 32).

Figure 32: Structure and properties of the problem reaction product.



Unexpectedly, the unknown mass of 249.0913 was obtained by HRMS when analyzing the reaction results. To discover that specific mass, the High-resolution mass finder code was executed with the following variables:

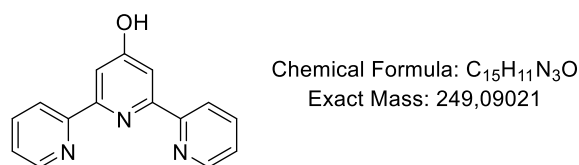
1. *Determined Mass* = 249.0903
2. *Range* = 0.005
3. *Element range*: H = 5 to 40, C = 10 to 40, N = 1 to 10, O = 0 to 3, Na = 0 to 1.

Which resulted in the first table of 89280 rows with all the possible element combinations. However, only 5 fell inside of the desired range within the determined mass. These were:

	Exact Mass	Abs. Difference	Molecular Formula
1	249,0902	0,000088	C15H11N3O1
2	249,0889	0,001431	C13H9N6
3	249,0878	0,002493	C13H12N3O1Na1
4	249,0865	0,003836	C11H10N6Na1
5	249,0862	0,00411	C10H11N5O3

The first and nearest option to the problem mass resulted to fit with the chemical formula of 4'-hydroxy-2,2':6,2''-terpyridine (Figure 33). To confirm this hypothesis however, further characterization experiments are required.

Figure 33: Structure and properties of the possible reaction product.



5.2. Cellular viability analyzer

The analysis of the raw data for any cellular viability assays (either the MTT or the Resazurin assays) is not trivial. Theoretically, once with this data -and only if cell count is sufficient to avoid inherent discreteness of the results- a sigmoidal dose-response model must be fitted to extrapolate the tested compounds IC_{50} . This of course must be done after applying the transformations given by the corresponding controls which will also validate the experiment. The main problem is that there are no free programs which can fit this dose-response curve to the data. Additionally, these pay-to-use programs usually need to receive the data already transformed into dose-response columns (for example, SigmaPlot or Origin) which means that the original data must first be processed elsewhere (usually in Excel, which is also extremely time consuming) and then analyzed with the corresponding dedicated program. Once the IC_{50} of the compounds is obtained, it is usually saved into an Excel-based library of results and the rest of data is neglected. However, for any future verification or validation of such results, this process must be repeated and the structure of the raw data must be known, which is not always the case.

In order to avoid wasting hours a code in R was developed to automate this process. It directly transforms the raw data into a vector constituted by the IC_{50} values of the tested compounds and 2 very clear images of the results.

The first step to run the code is reading the raw results. Then several variables must be delimited which will organize the raw data into the different controls, and the viability of the cells under the gradient concentration of the examined compounds. These variables are:

Category	Name	Variable name	Comment
Experimental data	Cellular line	<i>Linea</i>	As a string
	Time (h)	<i>Tiempo</i>	As a number
Location of Controls	Negative Control	<i>XCNeg</i>	Location as columns and rows in the raw data
	Positive Control	<i>XCPos</i>	
	Media (blanc) control	<i>XN</i>	
Compound data	Names	<i>Nombres</i>	As a vector of characters
	Initial concentrations	<i>CCis</i>	As a vector of strings
	Concentration units	<i>Units</i>	As a vector of strings
	1/Dilution factor	<i>FD</i>	As a vector of numbers
	Direction of dilutions	<i>Izquierda</i>	As a logical value

The code will start by calculating the means and standard deviations of all the controls as well as that the control means obey: $XN \approx XCNeg < XCPos$. If so, it will continue to calculate the

concentration of each compound along the plate. Afterwards it will extract the readings of each compounds and transform them into its viability using the formula:

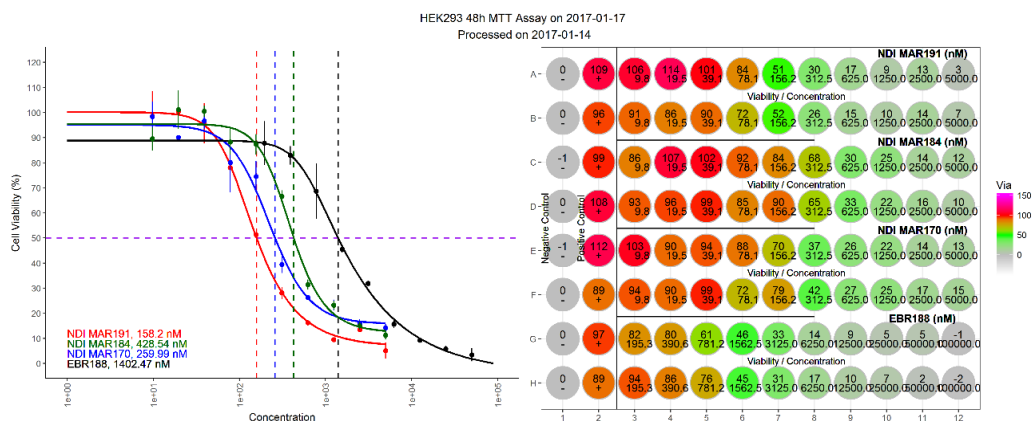
Equation 1: Viability calculation

$$Viability (\%) = \frac{mean(Data) - mean(XN)}{mean(XCPos) - mean(XN)}$$

Finally, it will construct two graphs using the R package ggplot2. The first graph is also dependent of the package drc which will construct the sigmoidal-fit curves for each compound and give the corresponding IC₅₀ with its units. The second graph is the representation of the actual well plate, organized between controls and compounds evaluated. Each well is given two numbers, the first one being the cellular viability calculated for that well, and the second one the compound concentration. To give extra visibility, the wells are colored with a scale of colors depending on the well viability, being red 100 % (as the mean of XCPos), green 50 % (as IC₅₀ value) and grey as 0 % (as the mean of XCNeg). To improve the results, it is possible to eliminate anomalous data values due to odd errors and re-evaluate the data.

An example of the result of this code is shown for the raw data (absorbance) of a MTT-based 96 well plate evaluating 4 compounds viability effect on HEK-293 cells (Figure 34).

Figure 34: MTT results of 4 compounds using an cellular viability analyzer.



Using this method of analyses allows fast and easy evaluation of compounds, as well as homogeneous methodology. Additionally, it allows to save all data obtained easily with minimum effort.

6. Bibliography

- [1] I. Kola, J. Landis, *Nat. Rev. Drug Discov.* **2004**, *3*, 711–716.
- [2] R. Macarron, M. N. Banks, D. Bojanic, D. J. Burns, D. A. Cirovic, T. Garyantes, D. V. S. Green, R. P. Hertzberg, W. P. Janzen, J. W. Paslay, et al., *Nat. Rev. Drug Discov.* **2011**, *10*, 188–195.
- [3] E. S. Lander, *Nature* **2011**, *470*, 187–197.
- [4] S. M. Paul, D. S. Mytelka, C. T. Dunwiddie, C. C. Persinger, B. H. Munos, S. R. Lindborg, A. L. Schacht, *Nat. Rev. Drug Discov.* **2010**, DOI 10.1038/nrd3078.
- [5] S. Morgan, P. Grootendorst, J. Lexchin, C. Cunningham, D. Greyson, *Health Policy* **2011**, *100*, 4–17.
- [6] M. Dickson, J. P. Gagnon, *Nat. Rev. Drug Discov.* **2004**, *3*, 417–429.
- [7] R. Mullin, *Sci. Am.* **2014**.
- [8] D. C. Swinney, J. Anthony, *Nat. Rev. Drug Discov.* **2011**, *10*, 507–519.
- [9] P. Imming, C. Sinning, A. Meyer, *Nat. Rev. Drug Discov.* **2006**, *5*, 821–834.
- [10] A. L. Hopkins, C. R. Groom, *Nat. Rev. Drug Discov.* **2002**, *1*, 727–730.
- [11] A. P. Russ, S. Lampel, *Drug Discov. Today* **2005**, *10*, 1607–1610.
- [12] W. F. An, N. Tolliday, *Mol. Biotechnol.* **2010**, *45*, 180–186.
- [13] J. A. Lee, S. Chu, F. S. Willard, K. L. Cox, R. J. Sells Galvin, R. B. Peery, S. E. Oliver, J. Oler, T. D. Meredith, S. A. Heidler, et al., *J. Biomol. Screen.* **2011**, *16*, 588–602.
- [14] www.emolecule.com, accessed January 2018
- [15] C. A. Lipinski, *Drug Discov. Today Technol.* **2004**, *1*, 337–341.
- [16] D. J. Huggins, A. R. Venkitaraman, D. R. Spring, *ACS Chem. Biol.* **2011**, *6*, 208–217.
- [17] M. M. Morente, L. Cereceda, M. J. Artiga, in *Manag. Chem. Biol. Samples Screen. Appl.* (Eds.: M. Wigglesworth, T. Wood), Wiley-VCH Verlag GmbH & Co. KGaA, Weinheim, Germany, **2012**, pp. 351–366.
- [18] M. A. Clark, R. A. Acharya, C. C. Arico-Muendel, S. L. Belyanskaya, D. R. Benjamin, N. R. Carlson, P. A. Centrella, C. H. Chiu, S. P. Creaser, J. W. Cuzzo, et al., *Nat. Chem. Biol.* **2009**, *5*, 647–654.
- [19] C. W. Murray, D. C. Rees, *Nat. Chem.* **2009**, *1*, 187–192.
- [20] P. A. Johnston, *Curr. Opin. Chem. Biol.* **2011**, *15*, 174–182.
- [21] J. Bajorath, *F1000Research* **2014**, DOI 10.12688/f1000research.5426.1.
- [22] N. Plundrich, M. A. Lila, E. Foegeding, S. Laster, *F1000Research* **2017**, *6*, 254.
- [23] L. Romero, J. M. Vela, in *Methods Princ. Med. Chem.* (Eds.: J.M. Vela, R. Maldonado, M. Hamon), Wiley-VCH Verlag GmbH & Co. KGaA, Weinheim, Germany, **2014**, pp. 27–58.
- [24] G. Moroy, V. Y. Martiny, P. Vayer, B. O. Villoutreix, M. A. Miteva, *Drug Discov. Today* **2012**, *17*, 44–55.
- [25] D. Stepensky, *Clin. Pharmacokinet.* **2013**, *52*, 415–431.
- [26] C. Nieto-Draghi, G. Fayet, B. Creton, X. Rozanska, P. Rotureau, J.-C. de Hemptinne, P. Ungerer, B. Rousseau, C. Adamo, *Chem. Rev.* **2015**, *115*, 13093–13164.
- [27] A. B. Raies, V. B. Bajic, *Wiley Interdiscip. Rev. Comput. Mol. Sci.* **2016**, *6*, 147–172.

- [28] J. Pohl, B. Bertram, P. Hilgard, M. R. Nowrousian, J. Stüben, M. Wiessler, *Cancer Chemother. Pharmacol.* **1995**, *35*, 364–370.
- [29] E. Hounsell, in *Encycl. Biophys.* (Ed.: G.C.K. Roberts), Springer Berlin Heidelberg, Berlin, Heidelberg, **2013**, pp. 931–932.
- [30] G. L. Kellett, *Diabetes* **2012**, *61*, e4–e4.
- [31] F. Reimann, A. M. Habib, G. Tolhurst, H. E. Parker, G. J. Rogers, F. M. Gribble, *Cell Metab.* **2008**, *8*, 532–539.
- [32] E. Ferrannini, A. Solini, *Nat. Rev. Endocrinol.* **2012**, *8*, 495–502.
- [33] A. Carruthers, J. DeZutter, A. Ganguly, S. U. Devaskar, *Am. J. Physiol. Endocrinol. Metab.* **2009**, *297*, E836–848.
- [34] F. R. Gorga, G. E. Lienhard, *Biochemistry (Mosc.)* **1982**, *21*, 1905–1908.
- [35] L. Koranyi, R. E. Bourey, D. James, M. Mueckler, F. T. Fiedorek, M. A. Permutt, *Mol. Cell. Neurosci.* **1991**, *2*, 244–252.
- [36] L. Pellerin, G. Bonvento, J. Y. Chatton, K. Pierre, P. J. Magistretti, *Diabetes Nutr. Metab.* **2002**, *15*, 268–273; discussion 273.
- [37] D. Wang, J. M. Pascual, H. Yang, K. Engelstad, X. Mao, J. Cheng, J. Yoo, J. L. Noebels, D. C. De Vivo, *Hum. Mol. Genet.* **2006**, *15*, 1169–1179.
- [38] K. H. Moley, M. M.-Y. Chi, C. M. Knudson, S. J. Korsmeyer, M. M. Mueckler, *Nat. Med.* **1998**, *4*, 1421–1424.
- [39] M. Younes, L. V. Lechago, J. R. Somoano, M. Mosharaf, J. Lechago, *Cancer Res.* **1996**, *56*, 1164–1167.
- [40] M. Uldry, M. Ibberson, M. Hosokawa, B. Thorens, *FEBS Lett.* **2002**, *524*, 199–203.
- [41] B. Thorens, Z. Q. Cheng, D. Brown, H. F. Lodish, *Am. J. Physiol.* **1990**, *259*, C279–285.
- [42] N. Marty, M. Dallaporta, M. Foretz, M. Emery, D. Tarussio, I. Bady, C. Binnert, F. Beermann, B. Thorens, *J. Clin. Invest.* **2005**, *115*, 3545–3553.
- [43] A. R. Manolescu, R. Augustin, K. Moley, C. Cheeseman, *Mol. Membr. Biol.* **2007**, *24*, 455–463.
- [44] I. A. Simpson, D. Dwyer, D. Malide, K. H. Moley, A. Travis, S. J. Vannucci, *Am. J. Physiol. Endocrinol. Metab.* **2008**, *295*, E242–253.
- [45] C. Barron, E. Tsiani, T. Tsakiridis, *BMC Proc.* **2012**, *6*, P4.
- [46] M. Larance, G. Ramm, D. E. James, *Mol. Endocrinol. Baltim. Md* **2008**, *22*, 226–233.
- [47] B. B. Kahn, *Diabetes* **1996**, *45*, 1644–1654.
- [48] Y. Schlein, *Parasitol. Today Pers. Ed* **1986**, *2*, 175–177.
- [49] R. J. Burchmore, M. P. Barrett, *Int. J. Parasitol.* **2001**, *31*, 1311–1320.
- [50] M. J. McConville, D. de Souza, E. Saunders, V. A. Likic, T. Naderer, *Trends Parasitol.* **2007**, *23*, 368–375.
- [51] T. Naderer, M. J. McConville, *Cell. Microbiol.* **2008**, *10*, 301–308.
- [52] R. J. Burchmore, S. M. Landfear, *J. Biol. Chem.* **1998**, *273*, 29118–29126.
- [53] D. Rodriguez-Contreras, X. Feng, K. M. Keeney, H. G. A. Bouwer, S. M. Landfear, *Mol. Biochem. Parasitol.* **2007**, *153*, 9–18.
- [54] D. Zilberstein, D. M. Dwyer, *Mol. Biochem. Parasitol.* **1984**, *12*, 327–336.
- [55] D. Zilberstein, D. M. Dwyer, *Proc. Natl. Acad. Sci. U. S. A.* **1985**, *82*, 1716–1720.

- [56] R. J. Burchmore, D. T. Hart, *Mol. Biochem. Parasitol.* **1995**, *74*, 77–86.
- [57] X. Feng, D. Rodriguez-Contreras, C. Buffalo, H. G. A. Bouwer, E. Kruvand, S. M. Beverley, S. M. Landfear, *Mol. Microbiol.* **2009**, *71*, 369–381.
- [58] D. Rodríguez-Contreras, S. M. Landfear, *J. Biol. Chem.* **2006**, *281*, 20068–20076.
- [59] S. A. Desai, D. J. Krogstad, E. W. McCleskey, *Nature* **1993**, *362*, 643–646.
- [60] C. J. Woodrow, J. I. Penny, S. Krishna, *J. Biol. Chem.* **1999**, *274*, 7272–7277.
- [61] M. P. Barrett, E. Tetaud, A. Seyfang, F. Bringaud, T. Baltz, *Mol. Biochem. Parasitol.* **1998**, *91*, 195–205.
- [62] M. P. Barrett, E. Tetaud, A. Seyfang, F. Bringaud, T. Baltz, *Biochem. J.* **1995**, *312* (Pt 3), 687–691.
- [63] D. Voet, J. G. Voet, C. W. Pratt, *Fundamentals of Biochemistry: Life at the Molecular Level*, Wiley, Hoboken, N.J, **2006**.
- [64] P. P. Hsu, D. M. Sabatini, *Cell* **2008**, *134*, 703–707.
- [65] R. J. DeBerardinis, J. J. Lum, G. Hatzivassiliou, C. B. Thompson, *Cell Metab.* **2008**, *7*, 11–20.
- [66] R. J. Shaw, M. Kosmatka, N. Bardeesy, R. L. Hurley, L. A. Witters, R. A. DePinho, L. C. Cantley, *Proc. Natl. Acad. Sci. U. S. A.* **2004**, *101*, 3329–3335.
- [67] R. J. DeBerardinis, A. Mancuso, E. Daikhin, I. Nissim, M. Yudkoff, S. Wehrli, C. B. Thompson, *Proc. Natl. Acad. Sci. U. S. A.* **2007**, *104*, 19345–19350.
- [68] H. R. Christofk, M. G. Vander Heiden, M. H. Harris, A. Ramanathan, R. E. Gerszten, R. Wei, M. D. Fleming, S. L. Schreiber, L. C. Cantley, *Nature* **2008**, *452*, 230–233.
- [69] H. Kondoh, M. E. Lleonart, J. Gil, J. Wang, P. Degan, G. Peters, D. Martinez, A. Carnero, D. Beach, *Cancer Res.* **2005**, *65*, 177–185.
- [70] O. Warburg, *Science* **1956**, *123*, 309–314.
- [71] E. C. Calvaresi, P. J. Hergenrother, *Chem. Sci.* **2013**, *4*, 2319.
- [72] C. Granchi, S. Fortunato, F. Minutolo, *Med Chem Commun* **2016**, *7*, 1716–1729.
- [73] J. A. Engelman, L. Chen, X. Tan, K. Crosby, A. R. Guimaraes, R. Upadhyay, M. Maira, K. McNamara, S. A. Perera, Y. Song, et al., *Nat. Med.* **2008**, *14*, 1351–1356.
- [74] R. L. Elstrom, D. E. Bauer, M. Buzzai, R. Karnauskas, M. H. Harris, D. R. Plas, H. Zhuang, R. M. Cinalli, A. Alavi, C. M. Rudin, et al., *Cancer Res.* **2004**, *64*, 3892–3899.
- [75] J. T. Powers, S. Hong, C. N. Mayhew, P. M. Rogers, E. S. Knudsen, D. G. Johnson, *Mol. Cancer Res. MCR* **2004**, *2*, 203–214.
- [76] H. R. Christofk, M. G. Vander Heiden, M. H. Harris, A. Ramanathan, R. E. Gerszten, R. Wei, M. D. Fleming, S. L. Schreiber, L. C. Cantley, *Nature* **2008**, *452*, 230–233.
- [77] H. R. Christofk, M. G. Vander Heiden, N. Wu, J. M. Asara, L. C. Cantley, *Nature* **2008**, *452*, 181–186.
- [78] V. R. Fantin, J. St-Pierre, P. Leder, *Cancer Cell* **2006**, *9*, 425–434.
- [79] S. Gottschalk, N. Anderson, C. Hainz, S. G. Eckhardt, N. J. Serkova, *Clin. Cancer Res. Off. J. Am. Assoc. Cancer Res.* **2004**, *10*, 6661–6668.
- [80] K. B. Nolop, C. G. Rhodes, L. H. Brudin, R. P. Beaney, T. Krausz, T. Jones, J. M. Hughes, *Cancer* **1987**, *60*, 2682–2689.
- [81] G. L. Semenza, *Nat. Rev. Cancer* **2003**, *3*, 721–732.

- [82] C. Chen, N. Pore, A. Behrooz, F. Ismail-Beigi, A. Maity, *J. Biol. Chem.* **2001**, 276, 9519–9525.
- [83] S. Pavlides, D. Whitaker-Menezes, R. Castello-Cros, N. Flomenberg, A. K. Witkiewicz, P. G. Frank, M. C. Casimiro, C. Wang, P. Fortina, S. Addya, et al., *Cell Cycle Georget. Tex* **2009**, 8, 3984–4001.
- [84] T. Joet, U. Eckstein-Ludwig, C. Morin, S. Krishna, *Proc. Natl. Acad. Sci. U. S. A.* **2003**, 100, 7476–7479.
- [85] B. M. Bakker, H. V. Westerhoff, F. R. Opperdoes, P. A. Michels, *Mol. Biochem. Parasitol.* **2000**, 106, 1–10.
- [86] H. K. Bayele, *Parasitol. Res.* **2001**, 87, 911–914.
- [87] L. Azema, S. Claustre, I. Alric, C. Blonski, M. Willson, J. Perié, T. Baltz, E. Tetaud, F. Bringaud, D. Cottem, et al., *Biochem. Pharmacol.* **2004**, 67, 459–467.
- [88] R. Boutron-Charlard, *Ann. Chim. Phys.* **1830**, 44, 352–382.
- [89] M. Bellis, *ThoughtCo.* **n.d.**
- [90] S. Lotito, B. Frei, *Free Radic. Biol. Med.* **2006**, 41, 1727–1746.
- [91] V. Izzi, L. Masuelli, I. Tresoldi, P. Sacchetti, A. Modesti, F. Galvano, R. Bei, *Front. Biosci. Landmark Ed.* **2012**, 17, 2396–2418.
- [92] R. M. van Dam, N. Naidoo, R. Landberg, *Curr. Opin. Lipidol.* **2013**, 24, 25–33.
- [93] B. B. Simpson, M. Conner-Ogorzaly, *Economic Botany: Plants in Our World*, McGraw-Hill, Boston, **2001**.
- [94] C. Martin, *Diet and Nutrition in Dementia and Cognitive Decline*, Elsevier, Boston, MA, **2014**.
- [95] V. R. Preedy, Ed. , *Handbook of Nutrition, Diet, and the Eye*, Elsevier/AP, Amsterdam ; Boston, **2014**.
- [96] M. Usman Mirza, A. H. Mirza, N.-H. Ghori, saba ferdous, *Drug Des. Devel. Ther.* **2014**, 187.
- [97] J. F. Fisher, A. W. Harrison, G. L. Bundy, K. F. Wilkinson, B. D. Rush, M. J. Ruwart, *J. Med. Chem.* **1991**, 34, 3140–3143.
- [98] Y. Henin, C. Gouyette, O. Schwartz, J. C. Debouzy, J. M. Neumann, T. Huynh-Dinh, *J. Med. Chem.* **1991**, 34, 1830–1837.
- [99] A. Namane, C. Gouyette, M. P. Fillion, G. Fillion, T. Huynh-Dinh, *J. Med. Chem.* **1992**, 35, 3039–3044.
- [100] J. Stüben, R. Port, B. Bertram, U. Bollow, W. E. Hull, M. Schaper, J. Pohl, M. Wiessler, *Cancer Chemother. Pharmacol.* **1996**, 38, 355–365.
- [101] H. M. M. Arafa, *Eur. J. Pharmacol.* **2009**, 616, 58–63.
- [102] E. Briasoulis, I. Judson, N. Pavlidis, P. Beale, J. Wanders, Y. Groot, G. Veerman, M. Schuessler, G. Niebch, K. Siamopoulos, et al., *J. Clin. Oncol. Off. J. Am. Soc. Clin. Oncol.* **2000**, 18, 3535–3544.
- [103] E. Briasoulis, N. Pavlidis, C. Terret, J. Bauer, W. Fiedler, P. Schöffski, J. L. Raoul, D. Hess, R. Selvais, D. Lacombe, et al., *Eur. J. Cancer Oxf. Engl. 1990* **2003**, 39, 2334–2340.
- [104] G. Giaccone, E. F. Smit, M. de Jonge, E. Dansin, E. Briasoulis, A. Ardizzoni, J.-Y. Douillard, D. Spaeth, D. Lacombe, B. Baron, et al., *Eur. J. Cancer Oxf. Engl. 1990* **2004**, 40, 667–672.

- [105] T. E. Ciuleanu, A. V. Pavlovsky, G. Bodoky, A. M. Garin, V. K. Langmuir, S. Kroll, G. T. Tidmarsh, *Eur. J. Cancer Oxf. Engl. 1990* **2009**, *45*, 1589–1596.
- [106] Y.-S. Lin, R. Tungpradit, S. Sinchaikul, F.-M. An, D.-Z. Liu, S. Phutrakul, S.-T. Chen, *J. Med. Chem.* **2008**, *51*, 7428–7441.
- [107] D.-Z. Liu, S. Sinchaikul, P. V. G. Reddy, M.-Y. Chang, S.-T. Chen, *Bioorg. Med. Chem. Lett.* **2007**, *17*, 617–620.
- [108] T. Halmos, M. Santarromana, K. Antonakis, D. Scherman, *Eur. J. Pharmacol.* **1996**, *318*, 477–484.
- [109] R. D. Goff, J. S. Thorson, *J. Med. Chem.* **2010**, *53*, 8129–8139.
- [110] E. Miot-Noirault, B. Reux, E. Debiton, J.-C. Madelmont, J.-M. Chezal, P. Coudert, V. Weber, *Invest. New Drugs* **2011**, *29*, 424–433.
- [111] S. J. Bensinger, H. R. Christofk, *Semin. Cell Dev. Biol.* **2012**, *23*, 352–361.
- [112] K. Beaumont, R. Webster, I. Gardner, K. Dack, *Curr. Drug Metab.* **2003**, *4*, 461–485.
- [113] F. Kratz, *J. Control. Release Off. J. Control. Release Soc.* **2008**, *132*, 171–183.
- [114] A. Varshney, P. Sen, E. Ahmad, M. Rehan, N. Subbarao, R. H. Khan, *Chirality* **2010**, *22*, 77–87.
- [115] T. Murakami, W. Wijagkanalan, M. Hashida, K. Tsuchida, *Nanomed.* **2010**, *5*, 867–879.
- [116] A. J. Zurita, P. Troncoso, M. Cardó-Vila, C. J. Logothetis, R. Pasqualini, W. Arap, *Cancer Res.* **2004**, *64*, 435–439.
- [117] M. Nikanjam, E. A. Blakely, K. A. Bjornstad, X. Shu, T. F. Budinger, T. M. Forte, *Int. J. Pharm.* **2007**, *328*, 86–94.
- [118] L. A. Stoddart, N. J. Smith, G. Milligan, *Pharmacol. Rev.* **2008**, *60*, 405–417.
- [119] A. P. Davenport, S. P. H. Alexander, J. L. Sharman, A. J. Pawson, H. E. Benson, A. E. Monaghan, W. C. Liew, C. P. Mpamhanga, T. I. Bonner, R. R. Neubig, et al., *Pharmacol. Rev.* **2013**, *65*, 967–986.
- [120] A. J. Brown, S. M. Goldsworthy, A. A. Barnes, M. M. Eilert, L. Tcheang, D. Daniels, A. I. Muir, M. J. Wigglesworth, I. Kinghorn, N. J. Fraser, et al., *J. Biol. Chem.* **2003**, *278*, 11312–11319.
- [121] S. R. Smith, P. W. F. Wilson, *J. Clin. Endocrinol. Metab.* **2006**, *91*, 2506–2508.
- [122] J. C. McNelis, Y. S. Lee, R. Mayoral, R. van der Kant, A. M. F. Johnson, J. Wollam, J. M. Olefsky, *Diabetes* **2015**, *64*, 3203.
- [123] S. J. Paulsen, L. K. Larsen, G. Hansen, S. Chelur, P. J. Larsen, N. Vrang, *PLoS ONE* **2014**, *9*, e88227.
- [124] D. Y. Oh, S. Talukdar, E. J. Bae, T. Imamura, H. Morinaga, W. Fan, P. Li, W. J. Lu, S. M. Watkins, J. M. Olefsky, *Cell* **2010**, *142*, 687–698.
- [125] D. Y. Oh, E. Walenta, T. E. Akiyama, W. S. Lagakos, D. Lackey, A. R. Pessentheiner, R. Sasik, N. Hah, T. J. Chi, J. M. Cox, et al., *Nat. Med.* **2014**, *20*, 942–947.
- [126] M. Z. Khan, L. He, *Neuropharmacology* **2017**, *113*, 639–651.
- [127] L. B. Bindels, P. Porporato, E. M. Dewulf, J. Verrax, A. M. Neyrinck, J. C. Martin, K. P. Scott, P. Buc Calderon, O. Feron, G. G. Muccioli, et al., *Br. J. Cancer* **2012**, *107*, 1337–1344.
- [128] Y. Tang, Y. Chen, H. Jiang, G. T. Robbins, D. Nie, *Int. J. Cancer* **2011**, *128*, 847–856.
- [129] T. Yonezawa, Y. Kobayashi, Y. Obara, *Cell. Signal.* **2007**, *19*, 185–193.

- [130] P. Yaqoob, *Annu. Rev. Nutr.* **2009**, 29, 257–282.
- [131] F. H. Epstein, R. A. Lewis, K. F. Austen, R. J. Soberman, *N. Engl. J. Med.* **1990**, 323, 645–655.
- [132] S. L. Tilley, T. M. Coffman, B. H. Koller, *J. Clin. Invest.* **2001**, 108, 15–23.
- [133] C. N. Serhan, C. B. Clish, J. Brannon, S. P. Colgan, N. Chiang, K. Gronert, *J. Exp. Med.* **2000**, 192, 1197–1204.
- [134] C. N. Serhan, S. Hong, K. Gronert, S. P. Colgan, P. R. Devchand, G. Mirick, R.-L. Moussignac, *J. Exp. Med.* **2002**, 196, 1025–1037.
- [135] C. N. Serhan, N. Chiang, T. E. Van Dyke, *Nat. Rev. Immunol.* **2008**, 8, 349–361.
- [136] A. Szanto, L. Nagy, *Immunobiology* **2008**, 213, 789–803.
- [137] V. J. Stella, *J. Pharm. Sci.* **2010**, 99, 4755–4765.
- [138] J. Rautio, in *Methods Princ. Med. Chem.* (Ed.: J. Rautio), Wiley-VCH Verlag GmbH & Co. KGaA, Weinheim, Germany, **2011**, pp. 1–30.
- [139] H. van de Waterbeemd, D. A. Smith, K. Beaumont, D. K. Walker, *J. Med. Chem.* **2001**, 44, 1313–1333.
- [140] B. Testa, *Biochem. Pharmacol.* **2004**, 68, 2097–2106.
- [141] V. J. Stella, K. W. Nti-Addae, *Adv. Drug Deliv. Rev.* **2007**, 59, 677–694.
- [142] O. Helen Chan, B. H. Stewart, *Drug Discov. Today* **1996**, 1, 461–473.
- [143] M. D. Taylor, *Adv. Drug Deliv. Rev.* **1996**, 19, 131–148.
- [144] J. D. Unadkat, M. Rowland, *Drug Metab. Dispos. Biol. Fate Chem.* **1985**, 13, 503–509.
- [145] K. M. Huttunen, H. Raunio, J. Rautio, *Pharmacol. Rev.* **2011**, 63, 750–771.
- [146] S. Majumdar, S. Duvvuri, A. K. Mitra, *Adv. Drug Deliv. Rev.* **2004**, 56, 1437–1452.
- [147] P. D. Dobson, D. B. Kell, *Nat. Rev. Drug Discov.* **2008**, 7, 205–220.
- [148] D. N. Cruz, *Expert Opin. Pharmacother.* **2000**, 1, 835–840.
- [149] M. Tsuda, *J. Pharmacol. Exp. Ther.* **2006**, 318, 455–460.
- [150] G. E. Granero, G. L. Amidon, *Int. J. Pharm.* **2006**, 317, 14–18.
- [151] S.-P. Khor, A. Hsu, *Curr. Clin. Pharmacol.* **2007**, 2, 234–243.
- [152] L.-å Svensson, A. Tunek, *Drug Metab. Rev.* **1988**, 19, 165–194.
- [153] P. Ettmayer, G. L. Amidon, B. Clement, B. Testa, *J. Med. Chem.* **2004**, 47, 2393–2404.
- [154] C. Lin, G. Sunkara, J. B. Cannon, V. Ranade, *Am. J. Ther.* **2012**, 19, 33–43.
- [155] W. A. Denny, *Eur. J. Med. Chem.* **2001**, 36, 577–595.
- [156] S. Burge, G. N. Parkinson, P. Hazel, A. K. Todd, S. Neidle, *Nucleic Acids Res.* **2006**, 34, 5402–5415.
- [157] K. Hoogsteen, *Acta Crystallogr.* **1963**, 16, 907–916.
- [158] T. J. Pinnavaia, C. L. Marshall, C. M. Mettler, C. L. Fisk, H. T. Miles, E. D. Becker, *J. Am. Chem. Soc.* **1978**, 100, 3625–3627.
- [159] A. Wong, G. Wu, *J. Am. Chem. Soc.* **2003**, 125, 13895–13905.
- [160] J. L. Huppert, *Nucleic Acids Res.* **2005**, 33, 2908–2916.
- [161] E. Besnard, A. Babled, L. Lapasset, O. Milhavet, H. Parrinello, C. Dantec, J.-M. Marin, J.-M. Lemaitre, *Nat. Struct. Mol. Biol.* **2012**, 19, 837–844.

- [162] A. Bugaut, S. Balasubramanian, *Nucleic Acids Res.* **2012**, *40*, 4727–4741.
- [163] C. B. Harley, A. B. Futcher, C. W. Greider, *Nature* **1990**, *345*, 458–460.
- [164] C. W. Greider, E. H. Blackburn, *Cell* **1985**, *43*, 405–413.
- [165] J. S. Smith, Q. Chen, L. A. Yatsunyk, J. M. Nicoludis, M. S. Garcia, R. Kranaster, S. Balasubramanian, D. Monchaud, M.-P. Teulade-Fichou, L. Abramowitz, et al., *Nat. Struct. Mol. Biol.* **2011**, *18*, 478–485.
- [166] T. de Lange, *Cold Spring Harb. Symp. Quant. Biol.* **2010**, *75*, 167–177.
- [167] A. J. Zaug, E. R. Podell, T. R. Cech, *Proc. Natl. Acad. Sci.* **2005**, *102*, 10864–10869.
- [168] J. Eddy, *Nucleic Acids Res.* **2006**, *34*, 3887–3896.
- [169] J. L. Huppert, S. Balasubramanian, *Nucleic Acids Res.* **2006**, *35*, 406–413.
- [170] J. A. Smestad, L. J. Maher, *BMC Med. Genet.* **2015**, *16*, DOI 10.1186/s12881-015-0236-4.
- [171] J. E. Johnson, K. Cao, P. Ryvkin, L.-S. Wang, F. B. Johnson, *Nucleic Acids Res.* **2010**, *38*, 1114–1122.
- [172] G. H. Nguyen, W. Tang, A. I. Robles, R. P. Beyer, L. T. Gray, J. A. Welsh, A. J. Schetter, K. Kumamoto, X. W. Wang, I. D. Hickson, et al., *Proc. Natl. Acad. Sci.* **2014**, *111*, 9905–9910.
- [173] W. Huang, P. J. Smaldino, Q. Zhang, L. D. Miller, P. Cao, K. Stadelman, M. Wan, B. Giri, M. Lei, Y. Nagamine, et al., *Nucleic Acids Res.* **2012**, *40*, 1033–1049.
- [174] L. T. Gray, A. C. Vallur, J. Eddy, N. Maizels, *Nat. Chem. Biol.* **2014**, *10*, 313–318.
- [175] J. A. Capra, K. Paeschke, M. Singh, V. A. Zakian, *PLoS Comput. Biol.* **2010**, *6*, e1000861.
- [176] I. T. Holder, J. S. Hartig, *Chem. Biol.* **2014**, *21*, 1511–1521.
- [177] P. Rawal, *Genome Res.* **2006**, *16*, 644–655.
- [178] S. Artusi, M. Nadai, R. Perrone, M. A. Biasolo, G. Palù, L. Flamand, A. Calistri, S. N. Richter, *Antiviral Res.* **2015**, *118*, 123–131.
- [179] K. Tlučková, M. Marušič, P. Tóthová, L. Bauer, P. Šket, J. Plavec, V. Víglašky, *Biochemistry (Mosc.)* **2013**, *52*, 7207–7216.
- [180] J. Norseen, F. B. Johnson, P. M. Lieberman, *J. Virol.* **2009**, *83*, 10336–10346.
- [181] D. Bhartiya, V. Chawla, S. Ghosh, R. Shankar, N. Kumar, *Genomics* **2016**, *108*, 224–231.
- [182] A. Stanton, L. M. Harris, G. Graham, C. J. Merrick, *BMC Genomics* **2016**, *17*, DOI 10.1186/s12864-016-3183-3.
- [183] N. W. Kim, M. A. Piatyszek, K. R. Prowse, C. B. Harley, M. D. West, P. L. Ho, G. M. Coviello, W. E. Wright, S. L. Weinrich, J. W. Shay, *Science* **1994**, *266*, 2011–2015.
- [184] H. Han, L. H. Hurley, *Trends Pharmacol. Sci.* **2000**, *21*, 136–142.
- [185] A. Siddiqui-Jain, C. L. Grand, D. J. Bearss, L. H. Hurley, *Proc. Natl. Acad. Sci.* **2002**, *99*, 11593–11598.
- [186] S. Rankin, A. P. Reszka, J. Huppert, M. Zloh, G. N. Parkinson, A. K. Todd, S. Ladame, S. Balasubramanian, S. Neidle, *J. Am. Chem. Soc.* **2005**, *127*, 10584–10589.
- [187] H. Fernando, A. P. Reszka, J. Huppert, S. Ladame, S. Rankin, A. R. Venkitaraman, S. Neidle, S. Balasubramanian, *Biochemistry (Mosc.)* **2006**, *45*, 7854–7860.
- [188] R. De Armond, S. Wood, D. Sun, L. H. Hurley, S. W. Ebbinghaus, *Biochemistry (Mosc.)* **2005**, *44*, 16341–16350.

- [189] C. M. Lombardo, S. J. Welsh, S. J. Strauss, A. G. Dale, A. K. Todd, R. Nanjunda, W. D. Wilson, S. Neidle, *Bioorg. Med. Chem. Lett.* **2012**, 22, 5984–5988.
- [190] J. Dai, D. Chen, R. A. Jones, L. H. Hurley, D. Yang, *Nucleic Acids Res.* **2006**, 34, 5133–5144.
- [191] P. Agrawal, E. Hatzakis, K. Guo, M. Carver, D. Yang, *Nucleic Acids Res.* **2013**, 41, 10584–10592.
- [192] K. Guo, A. Pourpak, K. Beetz-Rogers, V. Gokhale, D. Sun, L. H. Hurley, *J. Am. Chem. Soc.* **2007**, 129, 10220–10228.
- [193] S. Cogoi, M. Paramasivam, B. Spolaore, L. E. Xodo, *Nucleic Acids Res.* **2008**, 36, 3765–3780.
- [194] A. Membrino, S. Cogoi, E. B. Pedersen, L. E. Xodo, *PLoS ONE* **2011**, 6, e24421.
- [195] S. A. Ohnmacht, M. Micco, V. Petrucci, A. K. Todd, A. P. Reszka, M. Gunaratnam, M. A. Carvalho, M. Zloh, S. Neidle, *Bioorg. Med. Chem. Lett.* **2012**, 22, 5930–5935.
- [196] D. Wei, A. K. Todd, M. Zloh, M. Gunaratnam, G. N. Parkinson, S. Neidle, *J. Am. Chem. Soc.* **2013**, 135, 19319–19329.
- [197] T. Mitchell, A. Ramos-Montoya, M. Di Antonio, P. Murat, S. Ohnmacht, M. Micco, S. Jurmeister, L. Fryer, S. Balasubramanian, S. Neidle, et al., *Biochemistry (Mosc.)* **2013**, 52, 1429–1436.
- [198] J. Yan, X. Zhao, B. Liu, Y. Yuan, Y. Guan, *Mol. Carcinog.* **2016**, 55, 897–909.
- [199] S. Basu, *Nucleic Acids Res.* **1997**, 25, 1327–1332.
- [200] T. Simonsson, P. Pecinka, M. Kubista, *Nucleic Acids Res.* **1998**, 26, 1167–1172.
- [201] S. A. Ohnmacht, S. Neidle, *Bioorg. Med. Chem. Lett.* **2014**, 24, 2602–2612.
- [202] S. Neidle, 6th G4thring in Prague, **2016**.
- [203] M. Franceschin, *Eur. J. Org. Chem.* **2009**, 2009, 2225–2238.
- [204] J. Seenisamy, S. Bashyam, V. Gokhale, H. Vankayalapati, D. Sun, A. Siddiqui-Jain, N. Streiner, K. Shin-ya, E. White, W. D. Wilson, et al., *J. Am. Chem. Soc.* **2005**, 127, 2944–2959.
- [205] D. Gomez, N. Aouali, A. Renaud, C. Douarre, K. Shin-Ya, J. Tazi, S. Martinez, C. Trentesaux, H. Morjani, J.-F. Riou, *Cancer Res.* **2003**, 63, 6149–6153.
- [206] H.-S. Huang, C.-L. Chou, C.-L. Guo, C.-L. Yuan, Y.-C. Lu, F.-Y. Shieh, J.-J. Lin, *Bioorg. Med. Chem.* **2005**, 13, 1435–1444.
- [207] R. J. Harrison, S. M. Gowan, L. R. Kelland, S. Neidle, *Bioorg. Med. Chem. Lett.* **1999**, 9, 2463–2468.
- [208] M. Read, R. J. Harrison, B. Romagnoli, F. A. Tanius, S. H. Gowan, A. P. Reszka, W. D. Wilson, L. R. Kelland, S. Neidle, *Proc. Natl. Acad. Sci.* **2001**, 98, 4844–4849.
- [209] S. M. Gowan, J. R. Harrison, L. Patterson, M. Valenti, M. A. Read, S. Neidle, L. R. Kelland, *Mol. Pharmacol.* **2002**, 61, 1154–1162.
- [210] C. M. Incles, C. M. Schultes, H. Kempfski, H. Koehler, L. R. Kelland, S. Neidle, *Mol. Cancer Ther.* **2004**, 3, 1201–1206.
- [211] A. M. Burger, *Cancer Res.* **2005**, 65, 1489–1496.
- [212] N. H. Campbell, G. N. Parkinson, A. P. Reszka, S. Neidle, *J. Am. Chem. Soc.* **2008**, 130, 6722–6724.

- [213] M.-P. Teulade-Fichou, C. Carrasco, L. Guittat, C. Bailly, P. Alberti, J.-L. Mergny, A. David, J.-M. Lehn, W. D. Wilson, *J. Am. Chem. Soc.* **2003**, *125*, 4732–4740.
- [214] K. Jantos, R. Rodriguez, S. Ladame, P. S. Shirude, S. Balasubramanian, *J. Am. Chem. Soc.* **2006**, *128*, 13662–13663.
- [215] P. S. Shirude, E. R. Gillies, S. Ladame, F. Godde, K. Shin-ya, I. Huc, S. Balasubramanian, *J. Am. Chem. Soc.* **2007**, *129*, 11890–11891.
- [216] R. Rodriguez, S. Müller, J. A. Yeoman, C. Trentesaux, J.-F. Riou, S. Balasubramanian, *J. Am. Chem. Soc.* **2008**, *130*, 15758–15759.
- [217] D. Monchaud, P. Yang, L. Lacroix, M.-P. Teulade-Fichou, J.-L. Mergny, *Angew. Chem. Int. Ed.* **2008**, *47*, 4858–4861.
- [218] J. E. Reed, S. Neidle, R. Vilar, *Chem. Commun.* **2007**, 4366.
- [219] R. T. Wheelhouse, D. Sun, H. Han, F. X. Han, L. H. Hurley, *J. Am. Chem. Soc.* **1998**, *120*, 3261–3262.
- [220] G. W. Collie, R. Promontorio, S. M. Hampel, M. Micco, S. Neidle, G. N. Parkinson, *J. Am. Chem. Soc.* **2012**, *134*, 2723–2731.
- [221] M. Micco, G. W. Collie, A. G. Dale, S. A. Ohnmacht, I. Pazitna, M. Gunaratnam, A. P. Reszka, S. Neidle, *J. Med. Chem.* **2013**, *56*, 2959–2974.
- [222] S. Erten, Y. Posokhov, S. Alp, S. Icli, *Dyes Pigments* **2005**, *64*, 171–178.
- [223] F. Doria, I. Manet, V. Grande, S. Monti, M. Freccero, *J. Org. Chem.* **2013**, *78*, 8065–8073.
- [224] F. Würthner, S. Ahmed, C. Thalacker, T. Debaerdemaeker, *Chem. - Eur. J.* **2002**, *8*, 4742–4750.
- [225] A. Fin, I. Petkova, D. A. Doval, N. Sakai, E. Vauthey, S. Matile, *Org. Biomol. Chem.* **2011**, *9*, 8246.
- [226] S. Takenaka, K. Yamashita, M. Takagi, Y. Uto, H. Kondo, *Anal. Chem.* **2000**, *72*, 1334–1341.
- [227] S. J. Langford, M. J. Latter, C. P. Woodward, *Photochem. Photobiol.* **2006**, *82*, 1530.
- [228] S. Bhosale, *Science* **2006**, *313*, 84–86.
- [229] H. Tanaka, S. Litvinchuk, D.-H. Tran, G. Bollot, J. Mareda, N. Sakai, S. Matile, *J. Am. Chem. Soc.* **2006**, *128*, 16000–16001.
- [230] V. Gorteau, G. Bollot, J. Mareda, A. Perez-Velasco, S. Matile, *J. Am. Chem. Soc.* **2006**, *128*, 14788–14789.
- [231] S. V. Bhosale, C. H. Jani, S. J. Langford, *Chem Soc Rev* **2008**, *37*, 331–342.
- [232] J. L. Sessler, C. T. Brown, D. O'Connor, S. L. Springs, R. Wang, M. Sathiosatham, T. Hirose, *J. Org. Chem.* **1998**, *63*, 7370–7374.
- [233] F. Cuenca, O. Greciano, M. Gunaratnam, S. Haider, D. Munnur, R. Nanjunda, W. D. Wilson, S. Neidle, *Bioorg. Med. Chem. Lett.* **2008**, *18*, 1668–1673.
- [234] C. Sissi, L. Lucatello, A. Paul Krapcho, D. J. Maloney, M. B. Boxer, M. V. Camarasa, G. Pezzoni, E. Menta, M. Palumbo, *Bioorg. Med. Chem.* **2007**, *15*, 555–562.
- [235] A. Milelli, V. Tumiatti, M. Micco, M. Rosini, G. Zuccari, L. Raffaghello, G. Bianchi, V. Pistoia, J. Fernando Díaz, B. Pera, et al., *Eur. J. Med. Chem.* **2012**, *57*, 417–428.
- [236] S. M. Hampel, A. Sidibe, M. Gunaratnam, J.-F. Riou, S. Neidle, *Bioorg. Med. Chem. Lett.* **2010**, *20*, 6459–6463.

- [237] S. M. Hampel, A. Pepe, K. M. Greulich-Bode, S. V. Malhotra, A. P. Reszka, S. Veith, P. Boukamp, S. Neidle, *Mol. Pharmacol.* **2013**, *83*, 470–480.
- [238] S. Mpima, S. A. Ohnmacht, M. Barletta, J. Husby, L. C. Pett, M. Gunaratnam, S. T. Hilton, S. Neidle, *Bioorg. Med. Chem.* **2013**, *21*, 6162–6170.
- [239] M. Gunaratnam, M. de la Fuente, S. M. Hampel, A. K. Todd, A. P. Reszka, A. Schätzlein, S. Neidle, *Bioorg. Med. Chem.* **2011**, *19*, 7151–7157.
- [240] S. A. Ohnmacht, C. Marchetti, M. Gunaratnam, R. J. Besser, S. M. Haider, G. Di Vita, H. L. Lowe, M. Mellinas-Gomez, S. Diocou, M. Robson, et al., *Sci. Rep.* **2015**, *5*, 11385.
- [241] F. Ortega-García, J. Peragón, *J. Sci. Food Agric.* **2010**, *90*, 2295–2300.
- [242] M. Servili, B. Sordini, S. Esposito, S. Urbani, G. Veneziani, I. Di Maio, R. Selvaggini, A. Taticchi, *Antioxidants* **2013**, *3*, 1–23.
- [243] B. Bayram, B. Ozcelik, G. Schultheiss, J. Frank, G. Rimbach, *Food Chem.* **2013**, *138*, 1663–1669.
- [244] Z. Piñeiro, E. Cantos-Villar, M. Palma, B. Puertas, *J. Agric. Food Chem.* **2011**, *59*, 11683–11689.
- [245] A. Carrasco-Pancorbo, L. Cerretani, A. Bendini, A. Segura-Carretero, M. Del Carlo, T. Gallina-Toschi, G. Lercker, D. Compagnone, A. Fernández-Gutiérrez, *J. Agric. Food Chem.* **2005**, *53*, 8918–8925.
- [246] H. J. Forman, K. J. A. Davies, F. Ursini, *Free Radic. Biol. Med.* **2014**, *66*, 24–35.
- [247] C. Manna, P. Galletti, G. Maisto, V. Cucciolla, S. D'Angelo, V. Zappia, *FEBS Lett.* **2000**, *470*, 341–344.
- [248] E. Miró-Casas, M.-I. Covas, M. Fitó, M. Farré-Albadalejo, J. Marrugat, R. de la Torre, *Eur. J. Clin. Nutr.* **2003**, *57*, 186–190.
- [249] D. Caruso, F. Visioli, R. Patelli, C. Galli, G. Galli, *Metabolism.* **2001**, *50*, 1426–1428.
- [250] S. D'Angelo, C. Manna, V. Migliardi, O. Mazzoni, P. Morrica, G. Capasso, G. Pontoni, P. Galletti, V. Zappia, *Drug Metab. Dispos. Biol. Fate Chem.* **2001**, *29*, 1492–1498.
- [251] M.-C. López de las Hazas, L. Rubió, A. Kotronoulas, R. de la Torre, R. Solà, M.-J. Motilva, *Mol. Nutr. Food Res.* **2015**, *59*, 1395–1399.
- [252] O. Khymenets, M. Farré, M. Pujadas, E. Ortiz, J. Joglar, M. I. Covas, R. de la Torre, *Food Chem.* **2011**, *126*, 306–314.
- [253] K. L. Tuck, P. J. Hayball, I. Stupans, *J. Agric. Food Chem.* **2002**, *50*, 2404–2409.
- [254] A. Kotronoulas, N. Pizarro, A. Serra, P. Robledo, J. Joglar, L. Rubió, Á. Hernaéz, C. Tormos, M. J. Motilva, M. Fitó, et al., *Pharmacol. Res.* **2013**, *77*, 47–56.
- [255] C. Manna, F. Della Ragione, V. Cucciolla, A. Borriello, S. D'Angelo, P. Galletti, V. Zappia, *Adv. Exp. Med. Biol.* **1999**, *472*, 115–130.
- [256] S. Granados-Principal, J. L. Quiles, C. L. Ramirez-Tortosa, J. Ochoa-Herrera, P. Perez-Lopez, M. Pulido-Moran, M. Ramirez-Tortosa, *Mol. Nutr. Food Res.* **2012**, *56*, 733–740.
- [257] R. E. Zwane, A. Parker, T. Kudanga, L. M. Davids, S. G. Burton, *J. Agric. Food Chem.* **2012**, *60*, 11509–11517.
- [258] M. Deiana, O. I. Aruoma, M. L. Bianchi, J. P. Spencer, H. Kaur, B. Halliwell, R. Aeschbach, S. Banni, M. A. Dessi, F. P. Corongiu, *Free Radic. Biol. Med.* **1999**, *26*, 762–769.
- [259] X. Zou, Z. Feng, Y. Li, Y. Wang, K. Wertz, P. Weber, Y. Fu, J. Liu, *J. Nutr. Biochem.* **2012**, *23*, 994–1006.

- [260] H. Zrelli, M. Matsuoka, S. Kitazaki, M. Araki, M. Kusunoki, M. Zarrouk, H. Miyazaki, *J. Agric. Food Chem.* **2011**, *59*, 4473–4482.
- [261] H. Zrelli, M. Matsuoka, S. Kitazaki, M. Zarrouk, H. Miyazaki, *Eur. J. Pharmacol.* **2011**, *660*, 275–282.
- [262] H. Zrelli, M. Matsuka, M. Araki, M. Zarrouk, H. Miyazaki, *Planta Med.* **2011**, *77*, 1680–1686.
- [263] T. Hashimoto, M. Ibi, K. Matsuno, S. Nakashima, T. Tanigawa, T. Yoshikawa, C. Yabe-Nishimura, *Free Radic. Biol. Med.* **2004**, *36*, 555–564.
- [264] L. Zhu, Z. Liu, Z. Feng, J. Hao, W. Shen, X. Li, L. Sun, E. Sharman, Y. Wang, K. Wertz, et al., *J. Nutr. Biochem.* **2010**, *21*, 1089–1098.
- [265] E. H. Sarsour, M. G. Kumar, A. L. Kalen, M. Goswami, G. R. Buettner, P. C. Goswami, *AGE* **2012**, *34*, 95–109.
- [266] C. Giovannini, E. Straface, D. Modesti, E. Coni, A. Cantafora, M. De Vincenzi, W. Malorni, R. Masella, *J. Nutr.* **1999**, *129*, 1269–1277.
- [267] S. Schaffer, M. Podstawa, F. Visioli, P. Bogani, W. E. Müller, G. P. Eckert, *J. Agric. Food Chem.* **2007**, *55*, 5043–5049.
- [268] J. Muñoz-Marín, J. P. De La Cruz, A. Guerrero, I. López-Leiva, J. A. López-Villodres, J. J. Reyes, J. L. Espartero, A. Madrona, M. T. Labajos, J. A. González-Correa, *J. Agric. Food Chem.* **2012**, *60*, 7659–7664.
- [269] J. A. González-Correa, M. D. Navas, J. A. Lopez-Villodres, M. Trujillo, J. L. Espartero, J. P. De La Cruz, *Neurosci. Lett.* **2008**, *446*, 143–146.
- [270] T. Hu, X.-W. He, J.-G. Jiang, X.-L. Xu, *J. Agric. Food Chem.* **2014**, *62*, 1449–1455.
- [271] M. González-Santiago, E. Martín-Bautista, J. J. Carrero, J. Fonollá, L. Baró, M. V. Bartolomé, P. Gil-Loyzaga, E. López-Huertas, *Atherosclerosis* **2006**, *188*, 35–42.
- [272] F. Warleta, C. S. Quesada, M. Campos, Y. Allouche, G. Beltrán, J. J. Gaforio, *Nutrients* **2011**, *3*, 839–857.
- [273] H. Poudyal, F. Campbell, L. Brown, *J. Nutr.* **2010**, *140*, 946–953.
- [274] H. Jemai, I. Fki, M. Bouaziz, Z. Bouallagui, A. El Feki, H. Isoda, S. Sayadi, *J. Agric. Food Chem.* **2008**, *56*, 2630–2636.
- [275] H. Jemai, M. Bouaziz, I. Fki, A. El Feki, S. Sayadi, *Chem. Biol. Interact.* **2008**, *176*, 88–98.
- [276] S. Cicerale, L. Lucas, R. Keast, *Int. J. Mol. Sci.* **2010**, *11*, 458–479.
- [277] S. M. Samuel, M. Thirunavukkarasu, S. V. Penumathsa, D. Paul, N. Maulik, *J. Agric. Food Chem.* **2008**, *56*, 9692–9698.
- [278] A. Camargo, J. Ruano, J. M. Fernandez, L. D. Parnell, A. Jimenez, M. Santos-Gonzalez, C. Marin, P. Perez-Martinez, M. Uceda, J. Lopez-Miranda, et al., *BMC Genomics* **2010**, *11*, 253.
- [279] X. Zhang, J. Cao, L. Jiang, L. Zhong, *Biol. Pharm. Bull.* **2009**, *32*, 578–582.
- [280] X. Zhang, J. Cao, L. Zhong, *Naunyn. Schmiedebergs Arch. Pharmacol.* **2009**, *379*, 581–586.
- [281] A. Procopio, S. Alcaro, M. Nardi, M. Oliverio, F. Ortuso, P. Sacchetta, D. Pieragostino, G. Sindona, *J. Agric. Food Chem.* **2009**, *57*, 11161–11167.
- [282] H. Rafehi, K. Ververis, T. C. Karagiannis, *J. Diet. Suppl.* **2012**, *9*, 96–109.

- [283] H. Rafehi, A. J. Smith, A. Balcerczyk, M. Ziemann, J. Ooi, S. J. Loveridge, E. K. Baker, A. El-Osta, T. C. Karagiannis, *Genes Nutr.* **2012**, *7*, 343–355.
- [284] R. Quirantes-Piné, M. Herranz-López, L. Funes, I. Borrás-Linares, V. Micol, A. Segura-Carretero, A. Fernández-Gutiérrez, *Phytomedicine Int. J. Phytother. Phytopharm.* **2013**, *20*, 1112–1118.
- [285] C. Guichard, E. Pedruzzi, M. Fay, J.-C. Marie, F. Braut-Boucher, F. Daniel, A. Grodet, M.-A. Gougerot-Pocidaló, E. Chastre, L. Kotelevets, et al., *Carcinogenesis* **2006**, *27*, 1812–1827.
- [286] G. Bisignano, A. Tomaino, R. Lo Cascio, G. Crisafi, N. Uccella, A. Saija, *J. Pharm. Pharmacol.* **1999**, *51*, 971–974.
- [287] J. D. Kyriazis, N. Aligiannis, P. Polychronopoulos, A.-L. Skaltsounis, E. Dotsika, *Phytomedicine* **2013**, *20*, 275–281.
- [288] E. Medina, A. de Castro, C. Romero, M. Brenes, *J. Agric. Food Chem.* **2006**, *54*, 4954–4961.
- [289] N. Zoric, I. Horvat, N. Kopjar, A. Vucemilovic, D. Kremer, S. Tomic, I. Kosalec, *Curr. Drug Targets* **2013**, *14*, 992–998.
- [290] R. Mateos, G. Pereira-Caro, S. Saha, R. Cert, M. Redondo-Horcajo, L. Bravo, P. A. Kroon, *Food Chem.* **2011**, *125*, 865–872.
- [291] S. Grasso, L. Siracusa, C. Spatafora, M. Renis, C. Tringali, *Bioorganic Chem.* **2007**, *35*, 137–152.
- [292] Z. Bouallagui, M. Bouaziz, S. Lassoued, J. M. Engasser, M. Ghouli, S. Sayadi, *Appl. Biochem. Biotechnol.* **2011**, *163*, 592–599.
- [293] R. Bernini, F. Crisante, M. Barontini, D. Tofani, V. Balducci, A. Gambacorta, *J. Agric. Food Chem.* **2012**, *60*, 7408–7416.
- [294] A. Guerrero, J. P. De la Cruz, J. Muñoz-Marín, J. A. López-Villodres, A. Madrona, J. L. Espartero, J. A. González-Correa, *Food Chem.* **2012**, *134*, 2176–2183.
- [295] D. Tofani, V. Balducci, T. Gasperi, S. Incerpi, A. Gambacorta, *J. Agric. Food Chem.* **2010**, *58*, 5292–5299.
- [296] R. Bernini, F. Crisante, N. Merendino, R. Molinari, M. C. Soldatelli, F. Velotti, *Eur. J. Med. Chem.* **2011**, *46*, 439–446.
- [297] G. Pereira-Caro, B. Sarriá, A. Madrona, J. L. Espartero, L. Goya, L. Bravo, R. Mateos, *J. Agric. Food Chem.* **2011**, *59*, 5964–5976.
- [298] J. M. Calderón-Montaña, A. Madrona, E. Burgos-Morón, M. L. Orta, S. Mateos, J. L. Espartero, M. López-Lázaro, *J. Agric. Food Chem.* **2013**, *61*, 5046–5053.
- [299] G. Pereira-Caro, R. Mateos, M. H. Traka, J. R. Bacon, R. Bongaerts, B. Sarriá, L. Bravo, P. A. Kroon, *Food Chem.* **2013**, *138*, 1172–1182.
- [300] M. Takaoka, *NIPPON KAGAKU KAISHI* **1939**, *60*, 1261–1264.
- [301] J. A. Baur, D. A. Sinclair, *Nat. Rev. Drug Discov.* **2006**, *5*, 493–506.
- [302] M. M. Lyons, C. Yu, R. B. Toma, S. Y. Cho, W. Reiboldt, J. Lee, R. B. van Breemen, *J. Agric. Food Chem.* **2003**, *51*, 5867–5870.
- [303] G. J. Soleas, E. P. Diamandis, D. M. Goldberg, *Clin. Biochem.* **1997**, *30*, 91–113.
- [304] L. Frémont, *Life Sci.* **2000**, *66*, 663–673.
- [305] F. Sparvoli, C. Martin, A. Scienza, G. Gavazzi, C. Tonelli, *Plant Mol. Biol.* **1994**, *24*, 743–755.

- [306] E. H. Siemann, L. L. Creasy, *Am. J. Enol. Vitic.* **1992**, *43*, 49.
- [307] J.-F. Marier, *J. Pharmacol. Exp. Ther.* **2002**, *302*, 369–373.
- [308] M. Asensi, I. Medina, A. Ortega, J. Carretero, M. C. Baño, E. Obrador, J. M. Estrela, *Free Radic. Biol. Med.* **2002**, *33*, 387–398.
- [309] T. Walle, *Drug Metab. Dispos.* **2004**, *32*, 1377–1382.
- [310] L. D. Williams, G. A. Burdock, J. A. Edwards, M. Beck, J. Bausch, *Food Chem. Toxicol.* **2009**, *47*, 2170–2182.
- [311] M. Vaz-da-Silva, A. I. Loureiro, A. Falcao, T. Nunes, J.-F. Rocha, C. Fernandes-Lopes, E. Soares, L. Wright, L. Almeida, P. Soares-da-Silva, *Int. J. Clin. Pharmacol. Ther.* **2008**, *46*, 564–570.
- [312] D. J. Boocock, G. E. S. Faust, K. R. Patel, A. M. Schinas, V. A. Brown, M. P. Ducharme, T. D. Booth, J. A. Crowell, M. Perloff, A. J. Gescher, et al., *Cancer Epidemiol. Biomarkers Prev.* **2007**, *16*, 1246–1252.
- [313] C. Iuga, J. R. Alvarez-Idaboy, N. Russo, *J. Org. Chem.* **2012**, *77*, 3868–3877.
- [314] A. Galtieri, E. Tellone, S. Ficarra, A. Russo, E. Bellocco, D. Barreca, R. Scatena, G. Laganà, U. Leuzzi, B. Giardina, *Biol. Chem.* **2010**, *391*, DOI 10.1515/bc.2010.100.
- [315] E. Tellone, A. Galtieri, A. Russo, S. Ficarra, *Neural Regen. Res.* **2016**, *11*, 86.
- [316] S. Pervaiz, *FASEB J.* **2003**, *17*, 1975–1985.
- [317] E. N. Frankel, A. L. Waterhouse, J. E. Kinsella, *Lancet Lond. Engl.* **1993**, *341*, 1103–1104.
- [318] E. Savaskan, G. Olivieri, F. Meier, E. Seifritz, A. Wirz-Justice, F. Müller-Spahn, *Gerontology* **2003**, *49*, 380–383.
- [319] G.-C. Yen, P.-D. Duh, C.-W. Lin, *Free Radic. Res.* **2003**, *37*, 509–514.
- [320] C. A. de la Lastra, I. Villegas, *Biochem. Soc. Trans.* **2007**, *35*, 1156–1160.
- [321] Y. Bai, Q.-Q. Mao, J. Qin, X.-Y. Zheng, Y.-B. Wang, K. Yang, H.-F. Shen, L.-P. Xie, *Cancer Sci.* **2010**, *101*, 488–493.
- [322] J. K. Kundu, K.-S. Chun, S. O. Kim, Y.-J. Surh, *BioFactors* **2004**, *21*, 33–39.
- [323] P. Parekh, L. Motiwale, N. Naik, K. V. K. Rao, *Exp. Toxicol. Pathol.* **2011**, *63*, 167–173.
- [324] M. Lagouge, C. Argmann, Z. Gerhart-Hines, H. Meziane, C. Lerin, F. Daussin, N. Messadeq, J. Milne, P. Lambert, P. Elliott, et al., *Cell* **2006**, *127*, 1109–1122.
- [325] S. Nemoto, M. M. Fergusson, T. Finkel, *J. Biol. Chem.* **2005**, *280*, 16456–16460.
- [326] C. Cantó, Z. Gerhart-Hines, J. N. Feige, M. Lagouge, L. Noriega, J. C. Milne, P. J. Elliott, P. Puigserver, J. Auwerx, *Nature* **2009**, *458*, 1056–1060.
- [327] B. J. Wilson, A. M. Tremblay, G. Deblois, G. Sylvain-Drolet, V. Giguère, *Mol. Endocrinol.* **2010**, *24*, 1349–1358.
- [328] T. Lawrence, *Cold Spring Harb. Perspect. Biol.* **2009**, *1*, a001651–a001651.
- [329] K. T. Howitz, K. J. Bitterman, H. Y. Cohen, D. W. Lamming, S. Lavu, J. G. Wood, R. E. Zipkin, P. Chung, A. Kisielewski, L.-L. Zhang, et al., *Nature* **2003**, *425*, 191–196.
- [330] D. R. Valenzano, E. Terzibasi, T. Genade, A. Cattaneo, L. Domenici, A. Cellerino, *Curr. Biol.* **2006**, *16*, 296–300.
- [331] J. G. Wood, B. Rogina, S. Lavu, K. Howitz, S. L. Helfand, M. Tatar, D. Sinclair, *Nature* **2004**, *430*, 686–689.
- [332] L. M. Vieira de Almeida, C. C. Piñeiro, M. C. Leite, G. Brolese, F. Tramontina, A. M. Feoli, C. Gottfried, C.-A. Gonçalves, *Cell. Mol. Neurobiol.* **2007**, *27*, 661–668.

- [333] M. Yáñez, L. Galán, J. Matías-Guiu, A. Vela, A. Guerrero, A. G. García, *Brain Res.* **2011**, *1423*, 77–86.
- [334] F. Orallo, *Curr. Med. Chem.* **2008**, *15*, 1887–1898.
- [335] A. V. Witte, L. Kerti, D. S. Margulies, A. Floel, *J. Neurosci.* **2014**, *34*, 7862–7870.
- [336] D. O. Kennedy, E. L. Wightman, J. L. Reay, G. Lietz, E. J. Okello, A. Wilde, C. F. Haskell, *Am. J. Clin. Nutr.* **2010**, *91*, 1590–1597.
- [337] E. L. Wightman, J. L. Reay, C. F. Haskell, G. Williamson, T. P. Dew, D. O. Kennedy, *Br. J. Nutr.* **2014**, *112*, 203–213.
- [338] Fan, Jiang, Zhang, Bai, *Int. J. Vitam. Nutr. Res.* **2008**, *78*, 3–8.
- [339] M. Larrosa, J. Tomé-Carneiro, M. J. Yáñez-Gascón, D. Alcántara, M. V. Selma, D. Beltrán, M. T. García-Conesa, C. Urbán, R. Lucas, F. Tomás-Barberán, et al., *J. Med. Chem.* **2010**, *53*, 7365–7376.
- [340] H. I. Rocha-González, M. Ambriz-Tututi, V. Granados-Soto, *CNS Neurosci. Ther.* **2008**, *14*, 234–247.
- [341] P. Kumar, S. S. V. Padi, P. S. Naidu, A. Kumar, *Fundam. Clin. Pharmacol.* **2007**, *21*, 297–306.
- [342] X. Feng, N. Liang, D. Zhu, Q. Gao, L. Peng, H. Dong, Q. Yue, H. Liu, L. Bao, J. Zhang, et al., *PLoS ONE* **2013**, *8*, e59888.
- [343] J. Luo, A. Y. Nikolaev, S. Imai, D. Chen, F. Su, A. Shiloh, L. Guarente, W. Gu, *Cell* **2001**, *107*, 137–148.
- [344] H. Vaziri, S. K. Dessain, E. N. Eaton, S.-I. Imai, R. A. Frye, T. K. Pandita, L. Guarente, R. A. Weinberg, *Cell* **2001**, *107*, 149–159.
- [345] F. Caruso, J. Tanski, A. Villegas-Estrada, M. Rossi, *J. Agric. Food Chem.* **2004**, *52*, 7279–7285.
- [346] J. Chao, H. Li, K.-W. Cheng, M.-S. Yu, R. C.-C. Chang, M. Wang, *J. Nutr. Biochem.* **2010**, *21*, 482–489.
- [347] D. McCormack, D. McFadden, *Oxid. Med. Cell. Longev.* **2013**, *2013*, 1–15.
- [348] H. Liu, A. Dong, C. Gao, C. Tan, H. Liu, X. Zu, Y. Jiang, *Bioorg. Med. Chem.* **2008**, *16*, 10013–10021.
- [349] B.-F. Ruan, X.-F. Huang, H. Ding, C. Xu, H.-M. Ge, H.-L. Zhu, R.-X. Tan, *Chem. Biodivers.* **2006**, *3*, 975–981.
- [350] C. Mulakayala, B. Babajan, P. Madhusudana, C. M. Anuradha, R. M. Rao, R. P. Nune, S. K. Manna, N. Mulakayala, C. S. Kumar, *J. Mol. Graph. Model.* **2013**, *41*, 43–54.
- [351] H. Szaefer, M. Cichocki, V. Krajka-Kuźniak, T. Stefański, S. Sobiak, B. Licznerska, W. Baer-Dubowska, *Pharmacol. Rep.* **2014**, *66*, 732–740.
- [352] C. Lu, Y. Guo, J. Yan, Z. Luo, H.-B. Luo, M. Yan, L. Huang, X. Li, *J. Med. Chem.* **2013**, *56*, 5843–5859.
- [353] F. Minutolo, G. Sala, A. Bagnacani, S. Bertini, I. Carboni, G. Placanica, G. Prota, S. Rapposelli, N. Sacchi, M. Macchia, et al., *J. Med. Chem.* **2005**, *48*, 6783–6786.
- [354] Q. Liu, W. Jin, Y. Zhu, J. Zhou, M. Lu, Q. Zhang, *Steroids* **2012**, *77*, 419–423.
- [355] G. Chen, W. Shan, Y. Wu, L. Ren, J. Dong, Z. Ji, *Chem. Pharm. Bull. (Tokyo)* **2005**, *53*, 1587–1590.

Annex 1: Supplementary material of *Chem. Eur. J.* 2017.

CHEMISTRY

A European Journal

Supporting Information

Synthesis, Binding Properties, and Differences in Cell Uptake of G-Quadruplex Ligands Based on Carbohydrate Naphthalene Diimide Conjugates

Matilde Arévalo-Ruiz^{+, [a]} Filippo Doria^{+, [b]} Efres Belmonte-Reche,^[a] Aurore De Rache,^[c] Jenny Campos-Salinas,^[a] Ricardo Lucas,^[a] Eva Falomir,^[d] Miguel Carda,^[d] José María Pérez-Victoria,^[a] Jean-Louis Mergny,^[c] Mauro Freccero,^{*, [b]} and Juan Carlos Morales^{*, [a]}

chem_201604886_sm_miscellaneous_information.pdf

Table of Contents

Supplementary Experimental Procedure

Materials and General Procedures	Page S2
Synthesis of intermediates and final ligands	S3-9
Scheme S1	S3
Scheme S2	S9
Oligonucleotides	S10
FRET-melting assays	S11
Circular dichroism (CD) spectroscopy	S11
Cell Culture	S11
Cytotoxicity assay	S12
Flow cytometry	S12
NDI cell uptake quantification	S12
NDI cell uptake quantification in the presence of GLUT inhibitors	S13
Confocal microscopy	S13

Supplementary Figures, Table and Data:

Figure S1. FRET-melting study	S14
Figure S2. CD spectra of compounds 1 , 4 , 6 and 7	S15
Figure S3. Cell uptake of compounds 1 , 5 and 7 by flow cytometry	S16
Figure S3-S6. Flow Cytometry diagrams for compounds 1 , 5 and 7	S17-19
Figure S7. Inhibition experiments	S20
Figure S8-10. Confocal images of compounds 1 , 6 and 7	S21-23
HPLC purity data.	S24-28
¹ H- and ¹³ C-NMR spectra.	S29-42
Supplementary References	S43

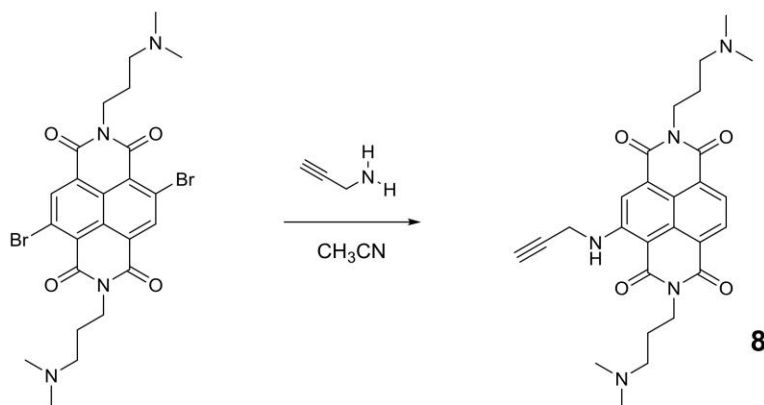
Supplemental Experimental Procedures

Materials and General Procedures.

Reagents, solvents and chemicals were purchased from Alfa Aesar, or Sigma-Aldrich and were used as supplied without further purification. TLC analysis was carried out on silica gel (Merck 60F-254) with visualization at 254 and 366 nm. HPLC analysis and purifications were performed using two different HPLC: Waters system combining a Delta 600 PUMP, a 2489 UV/VIS detector and Fraction Collector III (for preparative and analytical) and an Agilent system SERIES 1260 (for analytical). The analytical column was XSelect CSH Phenyl-Hexyl (150 x 4.6 mm) (Waters). The preparative column was XSelect CSH Prep Phenyl-Hexyl 5 μ m (150 x 30 mm) (Waters). Flows were 1 ml/min or 1.4 ml/min for analytical and 27 ml/min for preparative. For the analytical analysis were used the two following method A, B: (Aqueous solvent: 0.1% trifluoroacetic acid in water; Organic solvent: Acetonitrile; Method A= 1.4 ml/min, Gradient: 95% aqueous, gradually to 40% aqueous over 8 minutes and at the end an isocratic flow over 4 minutes; Method B= 1.4 ml/min, Gradient: 95% aqueous, gradually to 60% aqueous over 12 minutes and at the end an isocratic flow over 2 minutes). Preparative HPLC were performed using an upgrade of the analytical method. ¹H-, ¹³C-NMR spectra were recorded on a Bruker ADVANCE 300 and 400 MHz spectrometer.

Synthesis of intermediates and final ligands:**Synthesis of compound 8**

The di-bromo-substituted-NDI reported below has been synthesized according to the published procedure.^[13] For the following nucleophilic aromatic substitution (S_NAr) was performed an efficient protocol, in order to synthesized the ligand **8** as major product with good yield.

**Scheme S1.**

The dibromo-substituted-NDI in Scheme S1 (0.5 mmol) was dissolved into 40 ml of acetonitrile in a round bottom flask together with 1.5 mmol of propargylamine, the mixture was stirred at 70°C for 2 h under argon. The resulting red solution was concentrated under vacuum yielding a red solid. The crude product was analysed and purified by HPLC chromatography, ($\text{CH}_3\text{CN}:\text{H}_2\text{O}$ 0.1%TFA) according to analytical method A.

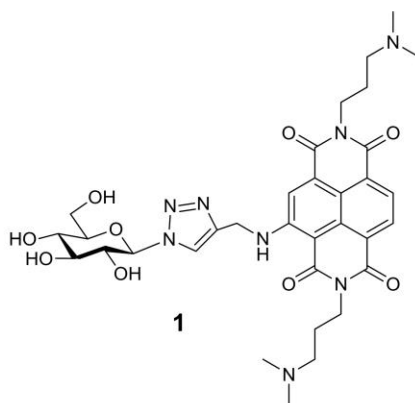
NDI-8 (Red Solid, Yield = 75%, Purity by HPLC analysis, 99.0% (R_t = 5.26 min) m.p.dec.>200°C); $^1\text{H-NMR}$ (300 MHz, Methanol- d_4) δ 8.48 (d, J = 7.8 Hz, 1H, H_{AR}), 8.22 (d, J = 7.8 Hz, 1H, H_{AR}), 8.20 (s, 1H, H_{AR}), 4.56 (s, 1H), 4.34-4.32 (m, 4H), 3.36 (bs, 4H), 3.31 (d, J = 15 Hz, 1H), 3.05 (s, 12H), 2.30 (bs, 2H).

$^{13}\text{C NMR}$ (75 MHz, Methanol- d_4) δ 167.2(CO), 164.7(CO), 164.4(CO), 164.2(CO), 152.9(C_{AR}), 132.2, 130.2, 128.9, 127.3, 125.9, 124.5, 120.9, 120.6, 101.6, 80.0, 74.9, 57.1, 57.0, 43.8, 39.0, 38.5, 33.6, 24.9.

Synthesis of compounds 1-6

General click coupling reactions.

To a suspension of azido-glyco-derivatives in 2 ml of tBuOH, a solution of (+)-sodium L-ascorbate (12 mg, 0.06 mmol), copper(II) sulfate pentahydrate (1.5 mg, 0.006 mmol) and NDI **8** (30 mg, 0.06 mmol) in 2 ml of H₂O was added in one portion. The heterogeneous mixture was stirred at r. t. under nitrogen atmosphere for 2 hrs. The resulting red solution was concentrated under vacuum and a red solid was obtained. The crude product was analysed and purified by HPLC chromatography, (CH₃CN:H₂O 0.1%TFA) according to analytical method B.

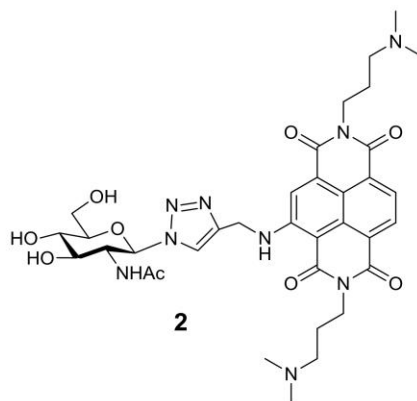


NDI-1: Red Solid, Yield = 97%, Purity by HPLC analysis, 99.8% (R_t = 6.69 min). m.p. > 275°C.

¹H-NMR (400 MHz, Methanol-d₄) δ 8.42 (d, J = 7.8 Hz, 1H, H_{AR}), 8.37 (s, 1H, H_{AR}), 8.22 (s, 1H, H_{AR}), 8.16 (d, J = 7.8 Hz, 1H, H_{AR}), 5.68 (d, J = 9.2 Hz, 1H, H₁), 4.94 (s, 2H, NHCH₂), 4.21 (t, J = 6.7 Hz, 4H, 2xCH₂N), 3.97 – 3.87 (m, 2H, H₂, H₆), 3.76 – 3.71 (m, 1H, H₆), 3.62 – 3.59 (m, 2H, H₅, H₃), 3.53 – 3.47 (m, 1H, H₄) 3.30 – 3.24 (m, 4H, 2xNCH₂), 2.95 (s, 6H, N(CH₃)₂), 2.94 (s, 6H, N(CH₃)₂), 2.24 – 3.17 (m, 4H, 2xCH₂).

¹³C-NMR (101 MHz, Methanol-d₄) δ 167.10(CO), 164.66(CO), 164.39(CO), 164.20(CO), 153.09(C_{AR}), 149.71(C_{AR}), 132.08(C_{AR}), 130.29(C_{AR}), 128.98(CH_{AR}), 127.30(C_{AR}), 125.53(C_{AR}), 124.36(CH_{AR}), 120.92(CH_{AR}), 120.57(CH_{AR}), 116.94(C_{AR}), 101.02(C_{AR}), 89.70(C₁), 81.24(C₃), 78.50(C₅), 74.14(C₂), 70.98(C₄), 62.38(C₆), 56.83(NCH₂), 56.76(NCH₂), 43.61(NCH₃), 39.56(NHCH₂), 38.12(CH₂N), 24.63(CH₂).

HRMS(ES⁺): Calcd. for C₃₃H₄₂N₈NaO₉(M+Na): 717.2972; found: 717.2963.

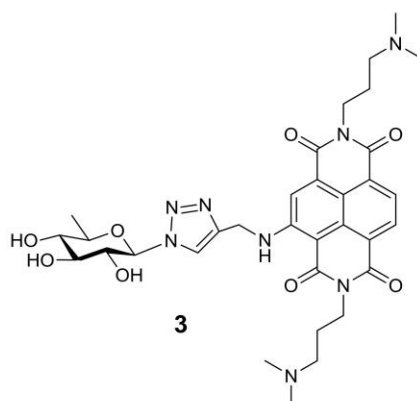


NDI-2: Red Solid, Yield = 95%, Purity by HPLC analysis, 100% (Rt = 4.83 min). m.p. > 275°C.

¹H-NMR (300 MHz, Methanol-d₄) δ 8.89 (s, 1H, NH), 8.70 (d, J = 7.8 Hz, 1H, H_{AR}), 8.45 (s, 1H, H_{AR}), 8.43 (d, J = 7.8 Hz, 1H, H_{AR}), 8.36 (s, 1H, H_{AR}), 5.88 (d, J = 9.7 Hz, 1H, H_I), 5.08 (s, 2H, 2xNHCH₂), 4.41 – 4.34 (m, 5H, 2xCH₂N, H₂), 4.0 (d, J = 11.9 Hz, 1H, H₅), 3.89 – 3.65 (m, 4H, H₃, H₄, H₆), 3.42 (bs, 4H, 2xNCH₂), 3.05 (s, 12H, 2xN(CH₃)₂), 2.34 – 2.29 (m, 4H, 2xCH₂), 1.78 (s, 3H, NHCOCH₃).

¹³C NMR (75 MHz, MeOD) δ 173.6(CO), 167.5(CO), 165.1 (CO), 164.8(CO), 164.5(CO), 153.5(C_{AR}), 145.5(C_{AR}), 132.4(C_{AR}), 130.7(C_{AR}), 129.4(CH_{AR}), 127.7(C_{AR}), 125.8(C_{AR}), 124.7(C_{AR}), 123.6(CH_{AR}), 121.2(CH_{AR}), 121.0(CH_{AR}), 101.5(C_{AR}), 88.7(C_I), 81.6, 76.1, 71.6, 62.6, 57.2, 57.1, 56.8, 43.9, 39.6, 38.9, 38.4, 24.9, 22.8(COCH₃).

HRMS(ES⁺): Calcd. for C₃₅H₄₅N₉NaO₉(M+Na): 758.3238; found: 758.3218.



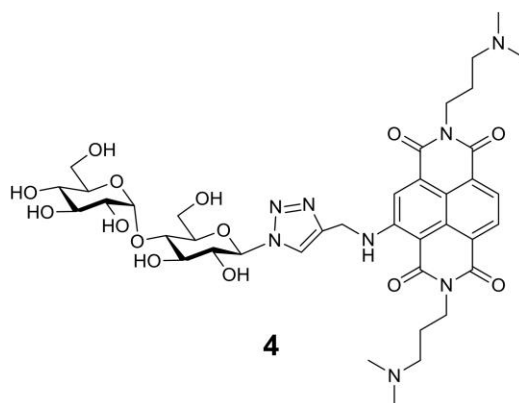
NDI-3: Red Solid, Yield = 98%, Purity by HPLC analysis, 97.6% (Rt = 7.14 min). m.p. > 275°C.

¹H-NMR (400 MHz, Methanol-d₄) δ 10.29 – 10.22 (m, 1H, NH), 8.36 – 8.29 (m, 2H, 2xH_{AR}), 8.12 – 8.03 (m, 2H, 2xH_{AR}), 5.66 (d, J = 9.0 Hz, 1H, H_I), 4.89 (s, 2H, NHCH₂), 4.17 (s, 4H, 2xCH₂N), 3.98 (t, J = 9.0 Hz, 1H, H₂), 3.65 (dd, J = 9.5, 5.8 Hz, 1H, H₅), 3.56 (t, J = 9.0 Hz, 1H,

H₃), 3.30 – 3.18 (m, 5H, 2xNCH₂, H₄), 2.97 (s, 6H, N(CH₃)₂), 2.95 (s, 6H, N(CH₃)₂), 2.21 – 2.16 (m, 4H, 2xCH₂), 1.32 (d, J = 5.8 Hz, 3H, 3xH₆).

¹³C-NMR (101 MHz, MeOD) δ 166.85(CO), 164.43(CO), 164.12(CO), 163.96(CO), 152.83(C_{AR}), 144.87(C_{AR}), 131.99(C_{AR}), 129.98(CH_{AR}), 128.67(C_{AR}), 127.00(C_{AR}), 125.44(C_{AR}), 124.07(CH_{AR}), 123.84(C_{AR}), 120.77(CH_{AR}), 120.22(CH_{AR}), 100.73(C_{AR}), 89.63(C₁), 78.28(C₃), 76.69(C₅), 76.51(C₄), 74.34(C₂), 56.80(CH₂-NCH₃), 56.73(CH₂-NCH₃), 43.63(NCH₃), 40.04(NHCH₂), 38.79(CH₂N), 38.22(CH₂N), 24.63(CH₂), 18.15(C₆).

HRMS(ES⁺): Calcd. for C₃₃H₄₂N₈NaO₈(M+Na): 701.3023; found 701.3007.

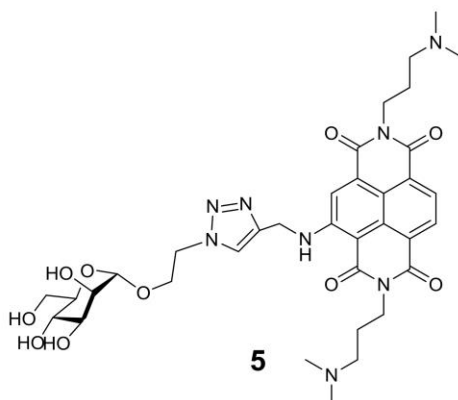


NDI-4: Red Solid, Yield = 87%, Purity by HPLC analysis, 99.3% (Rt = 6.61 min). m.p. > 275°C.

¹H-NMR (400 MHz, Methanol-d₄) δ 8.40 (s, 1H, H_{AR}), 8.27 (d, J = 7.8 Hz, 1H, H_{AR}), 8.08 (s, 1H, H_{AR}), 8.02 (d, J = 7.8 Hz, 1H, H_{AR}), 5.74 (d, J = 9.1 Hz, 1H, H_{1A}), 5.24 (d, J = 3.8 Hz, 1H, H_{1B}), 4.87 (s, 2H, 2xNHCH₂), 4.20 – 4.10 (m, 4H, 4xCH₂N), 4.03 (t, J = 9.2 Hz, 1H, H_{2A}), 3.94 – 3.80 (m, 4H, H_{61B}, H_{6'1B}, H_{61A}, H_{3A}), 3.80 – 3.60 (m, 5H, H_{3B}, H_{5B}, H_{4A}, H_{5A}, H_{6'1A}), 3.49 (dd, J = 9.7, 3.7 Hz, 1H, H_{2B}), 3.29 – 3.23 (m, 5H, H_{4B}, 4xNCH₂), 2.95 (s, 6H, NCH₃), 2.94 (s, 6H, NCH₃), 2.25 – 2.08 (m, 4H, 4xCH₂).

¹³C-NMR (101 MHz, MeOD) δ 166.84(CO), 164.42(CO), 164.11(CO), 163.98(CO), 152.84(C_{AR}), 147.78(C_{AR}), 132.03(C_{AR}), 129.99(C_{AR}), 128.67(CH_{AR}), 127.00(C_{AR}), 125.48(C_{AR}), 124.08(CH_{AR}), 124.02(C_{AR}), 120.83(CH_{AR}), 120.23(CH_{AR}), 102.98(C_{AR}), 100.73(C_{1B}), 89.52(C_{1A}), 80.49(C_{3B}), 79.69(C_{4A}), 78.24(C_{3A}), 75.06(C_{5B}), 74.95(C_{5A}), 74.12(C_{2B}), 73.79(C_{2A}), 71.55(C_{4B}), 62.79(C_{6A}), 61.85(C_{6B}), 56.80(NCH₂), 43.62(NCH₃), 39.40(NHCH₂), 38.75(CH₂N), 38.18(CH₂N), 24.59(CH₂).

HRMS(ES⁺): Calcd. for C₃₉H₅₂N₈NaO₁₄(M+Na): 879.3501; found: 879.3478.

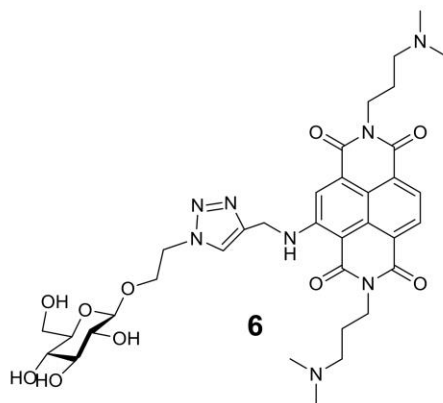


NDI-5: Red Solid, Yield = 93%, Purity by HPLC analysis, 96.9% (Rt = 6.73 min). m.p. > 275°C.

¹H-NMR (400 MHz, Methanol-d₄) δ 10.38(s, NH), 8.48 (d, J = 7.6 Hz, 1H, H_{AR}), 8.22 – 8.15 (m, 3H, 3xH_{AR}), 4.95 (s, 2H, NHCH₂), 4.83(H₁), 4.70 (s, 2H), 4.28 – 4.23 (m, 4H, 2xCH₂N), 4.15 – 4.12 (m, 1H, H₂), 3.88 – 3.86 (m, 1H, H₃), 3.70 – 3.50 (m, 5H, H₅, 2H₆, CH₂), 3.32 – 3.22 (m, 4H, 2xNCH₂), 3.19 – 3.18 (m, 1H, H₄), 2.95 (s, 12H, 2xN(CH₃)₂), 2.23 – 2.20 (m, 4H, 2xCH₂).

¹³C-NMR (101 MHz, MeOD) δ 167.21(CO), 164.78(CO), 164.48(CO), 164.30(CO), 153.15(C_{AR}), 132.08(C_{AR}), 130.7(C_{AR}), 130.43(C_{AR}), 129.12(CH_{AR}), 127.44(C_{AR}), 125.55(C_{AR}), 124.48(CH_{AR}), 120.78(CH_{AR}), 120.75(CH_{AR}), 120.70(C_{AR}), 101.61(C₁), 101.20(C_{AR}), 74.82(C₄), 72.48(C₆), 71.85(CH₂), 68.30(C₂), 66.84(C₃), 62.59(C₅), 56.81(NCH₂), 51.44(CH₂), 43.63(NCH₃), 39.41(NHCH₂), 38.67(CH₂N), 38.15(CH₂N), 24.70(CH₂).

HRMS(ES⁺): Calcd. For C₃₅H₄₆N₈NaO₁₀ (M+Na): 761.3235; found: 761.3259.



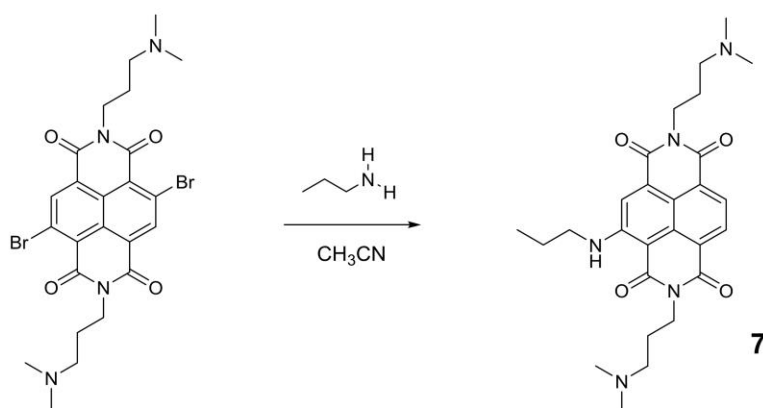
NDI-6: Red Solid, Yield = 91%, Purity by HPLC analysis, 99.2% ($R_t = 7.4$ min). m.p. $> 275^\circ\text{C}$.

$^1\text{H-NMR}$ (300 MHz, D_2O) δ 8.22 (d, $J = 7.6$ Hz, 1H, H_{AR}), 8.13 (s, 1H, H_{AR}), 7.97 (d, $J = 7.6$ Hz, 1H, H_{AR}), 7.87 (s, 1H, H_{AR}), 4.81 (s, 2H, NHCH_2), 4.64 (s, 2H), 4.28 (d, $J = 7.7$ Hz, 1H, H_1), 4.23-4.19 (m, 1H), 4.06 (bs, 4H, $2\times\text{CH}_2\text{N}$), 3.68 (d, $J = 12.3$ Hz, 1H), 3.47-3.40 (m, 1H), 3.29-3.19 (m, 6H, $2\times\text{NCH}_2$, OCH_2), 3.09 – 2.93 (m, 3H), 2.86 (s, 6H, $6\times\text{NCH}_3$), 2.85 (s, 6H, $6\times\text{NCH}_3$), 2.07 (bs, 4H, $2\times\text{CH}_2$).

$^{13}\text{C-NMR}$ (75 MHz, D_2O) δ 165.3(CO), 163.8(CO), 163.6(CO), 163.2(CO), 151.4(C_{AR}), 130.9(C_{AR}), 128.2(C_{AR}), 126.7(CH_{AR}), 125.2(C_{AR}), 124.9(C_{AR}), 124.8(C_{AR}), 124.5(CH_{AR}), 122.3(CH_{AR}), 119.7(CH_{AR}), 118.5(C_{AR}), 102.2(C_1), 99.3(C_{AR}), 75.7, 75.3, 72.9, 69.4, 67.8, 60.5, 55.2(NCH_2), 55.1(NCH_2), 50.4, 42.7(NCH_3), 37.9(NHCH_2), 37.6 (CH_2N), 37.0(CH_2N), 22.8(CH_2).

HRMS(ES^+): Calcd. for $\text{C}_{35}\text{H}_{47}\text{N}_8\text{O}_{10}$ (M^+): 739.3415; found: 739.3465.

Synthesis of compound 7:



Scheme S2.

The dibromo-substituted-NDI in Scheme S2 (0.5 mmol) was dissolved into 40 ml of acetonitrile in a round bottom flask together with 1.5 mmol of n-propylamine, the mixture was stirred at 70°C for 2 h under argon. The resulting red solution was concentrated under vacuum yielding a red solid. The crude product was analysed and purified by HPLC chromatography, (CH₃CN:H₂O 0.1%TFA) according to analytical method A.

NDI-7 (Red Solid, Yield = 68%, Purity by HPLC analysis, 100% (R_t = 5.65 min) m.p.dec.>200°C); ¹H-NMR (300 MHz, D₂O) δ 8.09 (d, J = 7.9 Hz, 1H, H_{AR}), 7.85 (d, J = 7.9 Hz, 1H, H_{AR}), 7.65 (s, 1H, H_{AR}), 4.07-3.98 (m, 4H), 3.37 (t, J = 2.2 Hz, 2H), 3.25-3.05 (m, 4H), 2.86 (s, 6H), 2.84 (s, 6H), 2.10-2.05 (m, 4H), 1.78-1.68 (m, 4H), 1.04 (t, J = 7.3 Hz, 3H).

¹³C NMR (75 MHz, D₂O) δ 165.1(CO), 163.6(CO), 163.3(CO), 163.0(CO), 151.8, 130.6, 128.3, 126.5, 124.9, 123.8, 121.6, 120.0, 118.1, 97.8, 55.1, 44.6, 44.4, 42.6, 37.6, 37.0, 22.6, 21.9, 10.6.

HRMS(ES⁺): Calcd. for C₂₇H₃₅N₅O₄Na (M+Na): 516.2587; found: 516.2577.

Oligonucleotides

All oligonucleotides (Table 1) were purchased from Eurogentec (Belgium) and used without further purification for FRET and CD experiments. NMR samples were purified by centrifugation on 5 kDa filters. Oligonucleotide stock solutions (around 500 μ M) were prepared in MilliQ water and stored at -20 °C. The exact stock concentrations were determined from the absorbance at 260 nm. For the FRET melting experiments, the compounds were solubilised either in DMSO or in MilliQ water at concentrations of 5 or 10 mM depending on the solubility of the compound. Identical results were obtained independently of the ligand solvent. For CD and NMR experiments were conducted using a 5 mM stock solution in deuterated-DMSO.

Table S1: DNA sequences used in the present study and closest corresponding reported structure types (various salt compositions, see references for details).

Short Name	Description	Sequence	Structure type	Method (PDB code)
25Ceb	Human minisatellite	FAM-AG ₃ TG ₃ TGTAAGTGTG ₃ TG ₃ -Tamra	Parallel quadruplex	NMR (2LPW ^[1])
myc	c-Myc promoter	FAM-TTGAG ₃ TG ₃ TAG ₃ TG ₃ TAA-Tamra	Parallel quadruplex	NMR (1XAV ^[2] , 2A5P ^[3])
Bom17	Bombyx telomere	FAM-G ₂ TTAG ₂ TTAG ₂ TTG ₂ -Tamra	Anti-parallel quadruplex	UV+CD +NMR ^[4]
21CTA	Human DNA telomere (variant)	FAM-G ₃ CTAG ₃ CTAG ₃ CTAG ₃ -Tamra	Anti-parallel quadruplex	NMR (2KM3 ^[5])
21g	Human DNA telomere	FAM-G ₃ TTAG ₃ TTAG ₃ TTAG ₃ -Tamra	Parallel quadruplex 3+1 quadruplex Anti-parallel quadruplex	X-ray (1KF1 ^[6]), NMR (2LD8 ^[7]) NMR (2GKU ^[8] , 2JSL ^[9] , 2JSM ^[9]) NMR (2KF8 ^[10] , 143D ^[11] , 2MBJ ^[12])
dx	Duplex	FAM-TATAGCTAT-hexaethyleneglycol-TATAGCTATA-Tamra		

FRET-melting assays

The ligand-induced thermal stabilisations ($\Delta T_{1/2}$) were determined from the difference between the temperature of mid-transition measured without and with 2 μM of ligand for a final oligonucleotide strand concentration of 0.2 μM . Three independent experiments were conducted on a Stratagene Mx3005P real-time PCR equipment using duplicate conditions in 96 well-plates. The excitation wavelength was set to 492 nm and the emission recorded at 516 nm. The temperature profile consisted in an initial stabilisation at 25 °C for 5 min followed by a 1°C by minute increase till 95 °C. The induced stabilisation was compared for a set of six sequences (Table 1) containing 5 G-quadruplexes and a hairpin duplex in 10 mM lithium cacodylate (pH 7.2) supplemented with 10 mM KCl and 90 mM LiCl. The evaluation of the selectivity of the ligands against duplexes was performed by competition assays using the self-complementary ds26 duplex (5'-CAA TCG GAT CGA ATT CGA TCC GAT TG-3') both in the same buffer and in cacodylate containing 100 mM NaCl. All DNA sequences were purchased from Eurogentec and dissolved in pure water to an approximate concentration of 500 μM . The exact concentration of the stock solutions were determined from the absorbance at 260 nm recorded on a Uvikon XS spectrophotometer. The stock solutions were stored at -20°C.

Circular dichroism (CD) spectroscopy

CD-spectra were recorded at 20°C on a Jasco J-815 equipped with a Peltier temperature controller. Each spectrum corresponds to the average of two scans measured in 1-cm path-length quartz cells at 100 nm min⁻¹ (bandwidth: 2 nm, data integration time: 1s). The molar-ratio samples were prepared at least 1 hour before the measurements. The oligonucleotide were pre-folded at 4 μM in 10 mM lithium cacodylate (pH 7.2) supplemented with 100 mM KCl. The ligand concentration was adapted to reach the desired ratio (between 1:0 and 1:10).

Cell Culture

MRC5 cells were maintained at 37 °C and 5 % CO₂ in 100% of humidity in low glucose DMEM (1 g/L) supplemented with 10% iFBS, 100 U/ml penicillin and 100 mg/ml streptomycin. HT29 and MCF7 cells were maintained at 37 °C and 5 % CO₂ in high glucose DMEM (4.5 g/L) supplemented with 10% iFBS, 100 U/ml penicillin and 100 mg/ml streptomycin.

Cytotoxicity assay

MCF7, HT29 and MRC5 cells were harvested by trypsinization (0.25%) and seeded in 96 well plates (5000 cells in 100 uL /well) in the presence of increasing concentrations of NDI-compounds. Cellular toxicity was determined using the colorimetric MTT-based assay after incubation at 37 ° C for 48 h (HT29 and MCF7) or 72 h (MRC5). The results are expressed as the concentration of compound that reduce cell growth by 50% versus untreated control cells (EC 50).

Flow cytometry

Determination of cell fluorescence by size and cell complexity (Forward Scatter and Side Scatter) was achieved by flow cytometry. 450,000 MCF7, HT29 and MRC5 cells were harvested by trypsinization and incubated in their medium (1.5mL) for different times at 4 °C and 37 °C. After supernatant removal and washing, the cells were analyzed on an FACScalibur flow cytometer (BD Biosciences, San Jose, CA) simultaneously using a 15mw-Argon and a 635nm diode lasers. Data obtained from detection of orange fluorescence at FL2 channel was organized with FlowJo (Tree Star, Ashland, OR), analyzed with R-Studio V.0.99.891 and represented with ggplot2 package V.1.0.1.

NDI cell uptake quantification

225,000 MCF7, HT29 and MRC5 cells were harvested by trypsinization and incubated with 5 uM of a NDI-Compound in 0.75 mL of medium for 2 h at 37 °C. After centrifugation, supernatant removal and washing, the cell pellet was re-suspended in 0.75 mL of SDS 0.4 % and homogenized. Fluorescence was detected with a TECAN infinite F200 fluorescence-intensity multiplate reader (excitation wavelength: 485 nm, emission wavelength: 535 nm). Fluorescence values were normalized via protein quantification assay using Pierce BCA test (ThermoFisher Scientific) and concentration values were extrapolated from a fluorescence – NDI-concentration calibration curve.

NDI cell uptake quantification in the presence of GLUT inhibitors

225,000 HT29 and MRC5 cells were harvested by trypsinization and preincubated in 0.75 mL of medium with 100 μ M of a Glut inhibitor (Fasentin, Genistein, Ritonavir, ZWB117 and Quercetin, Sigma Aldrich©) for 1 h at 37 °C. 5 μ M of a NDI-compound was then added and incubated for another 2 h at 37 °C. Sample treatment and NDI-uptake quantification was achieved following the previously mentioned NDI-uptake quantification protocol. Inhibition values were calculated using NDI-uptake in presence of the Glut inhibitor (A) and NDI-uptake values (B) as inhibitor-free controls using the formula: Inhibition (%) = (B-A)/B x 100.

Confocal microscopy

MRC5 and HT29 cells were incubated with 5 μ M of NDI compounds in 0.5 mL of each respective medium for 2 h at 37 °C and 100 % of humidity. Cells were washed seven times in 500 ml of cold phosphate-buffered saline (PBS), fixed and processed by microscope observation. Images were acquired using a Leica SP5 confocal microscope, while the images were deconvoluted using Huygens Professional image processing software from Scientific Volume Imaging (<http://www.svi.nl>). The merge of the images were made with Fiji software (<https://fiji.sc/>).

Figure S1. FRET-melting stabilization induced by the tested compounds (2 μ M) on G-quadruplexes of various topologies in 10 mM lithium cacodylate pH 7.2 containing 10 mM KCl and 90 mM LiCl.

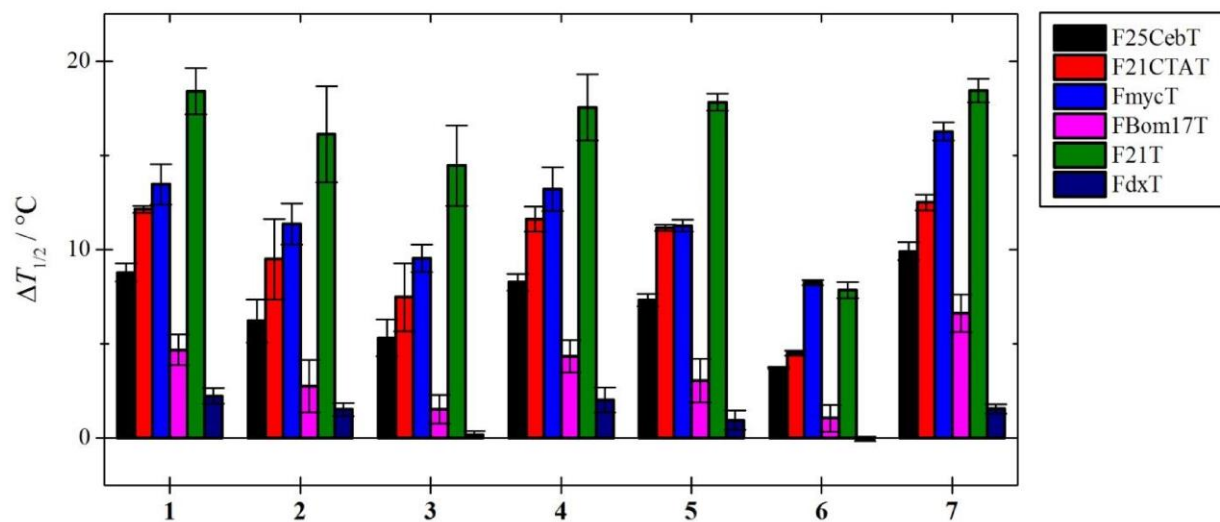


Figure S2. CD signatures of compounds (a) **1**, (b) **4**, (c) **6** and (d) **7** alone (40 μ M).

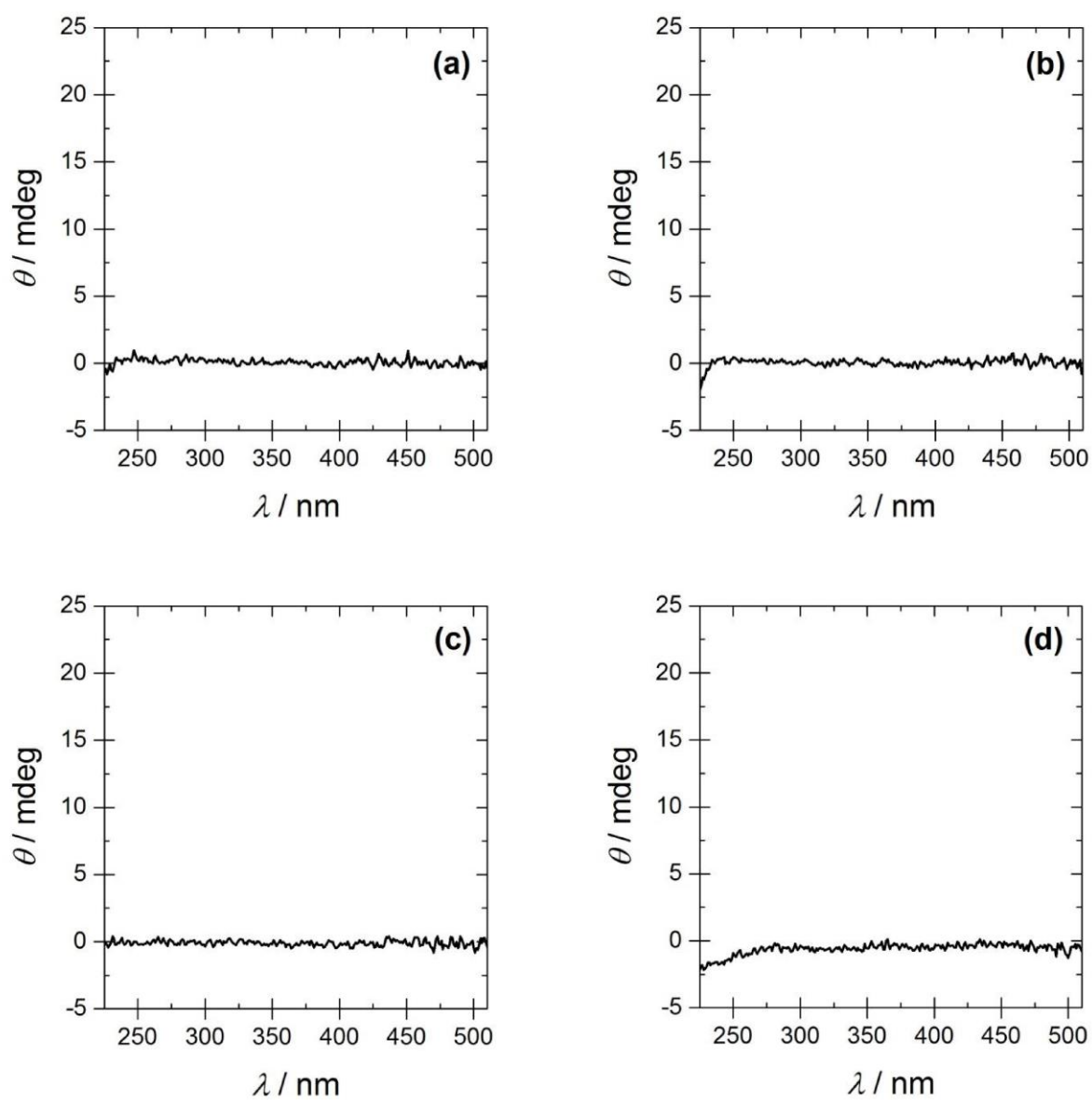


Figure S3. The mean fluorescence intensity of compound **1** (1 μ M, old compound NDI-506), compound **5** (1 μ M, old compound NDI-504) and compound **7** (1 μ M, old compound NDI-prop), incubated with various cancer and normal cell lines for 2 h measured by flow cytometry. Bars in red, temp= 4 $^{\circ}$ C; bars in blue, temp= 37 $^{\circ}$ C.

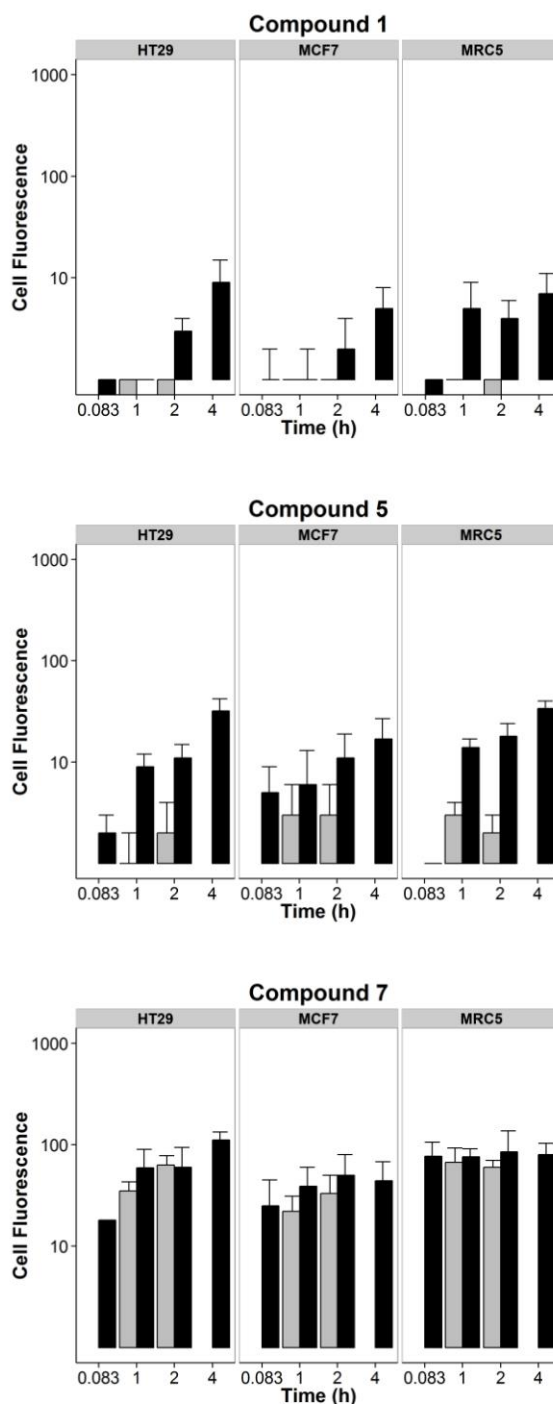


Figure S4. Flow cytometry diagrams of compound **1** (5 μ M, old compound NDI-506) incubated with various cancer and normal cell lines for 2 h measured by flow cytometry. Bars in red, temp= 4 $^{\circ}$ C; bars in blue, temp= 37 $^{\circ}$ C.

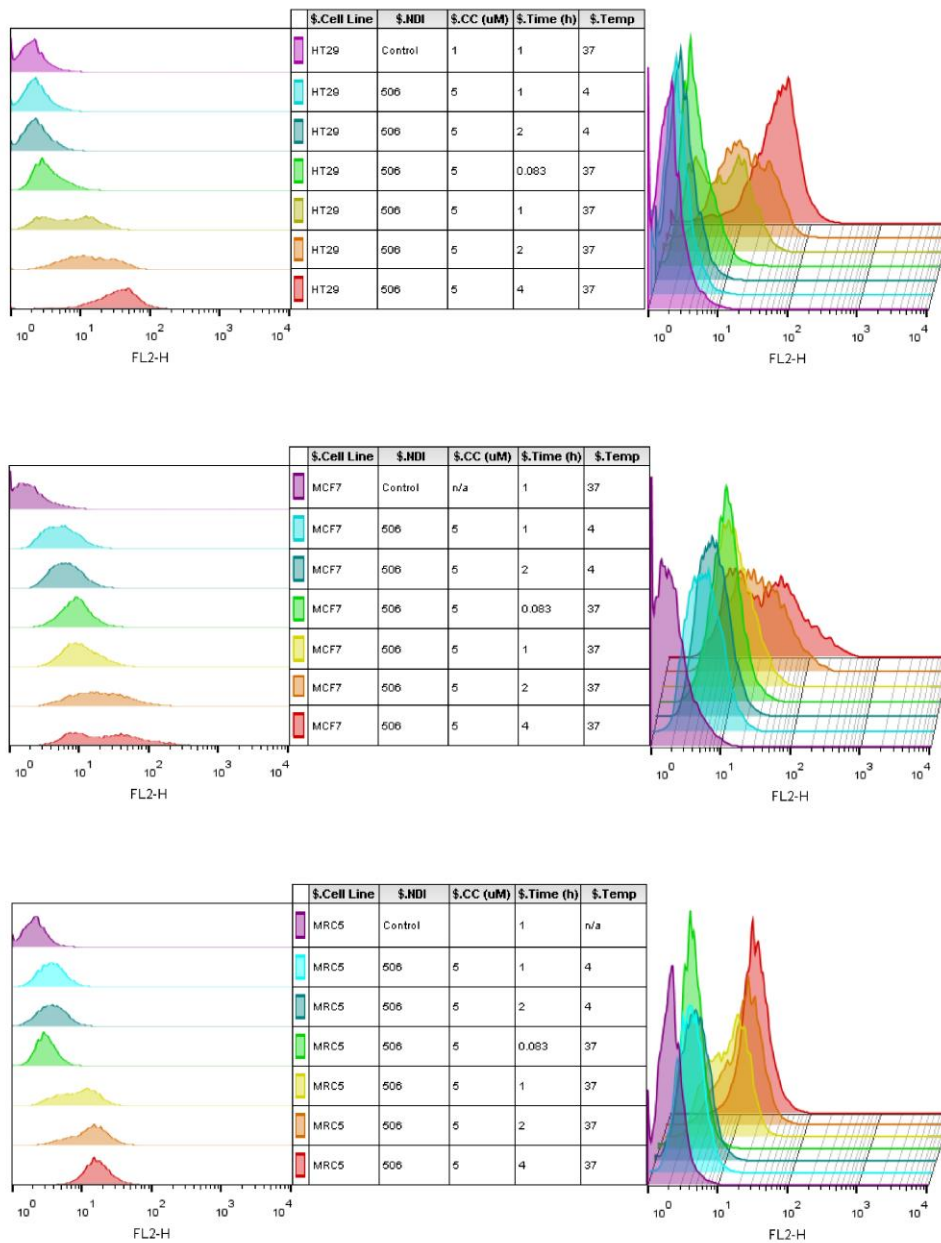


Figure S5. Flow cytometry diagrams of compound **5** (5 μ M, old compound NDI-504) incubated with various cancer and normal cell lines for 2 h measured by flow cytometry. Bars in red, temp= 4 $^{\circ}$ C; bars in blue, temp= 37 $^{\circ}$ C.

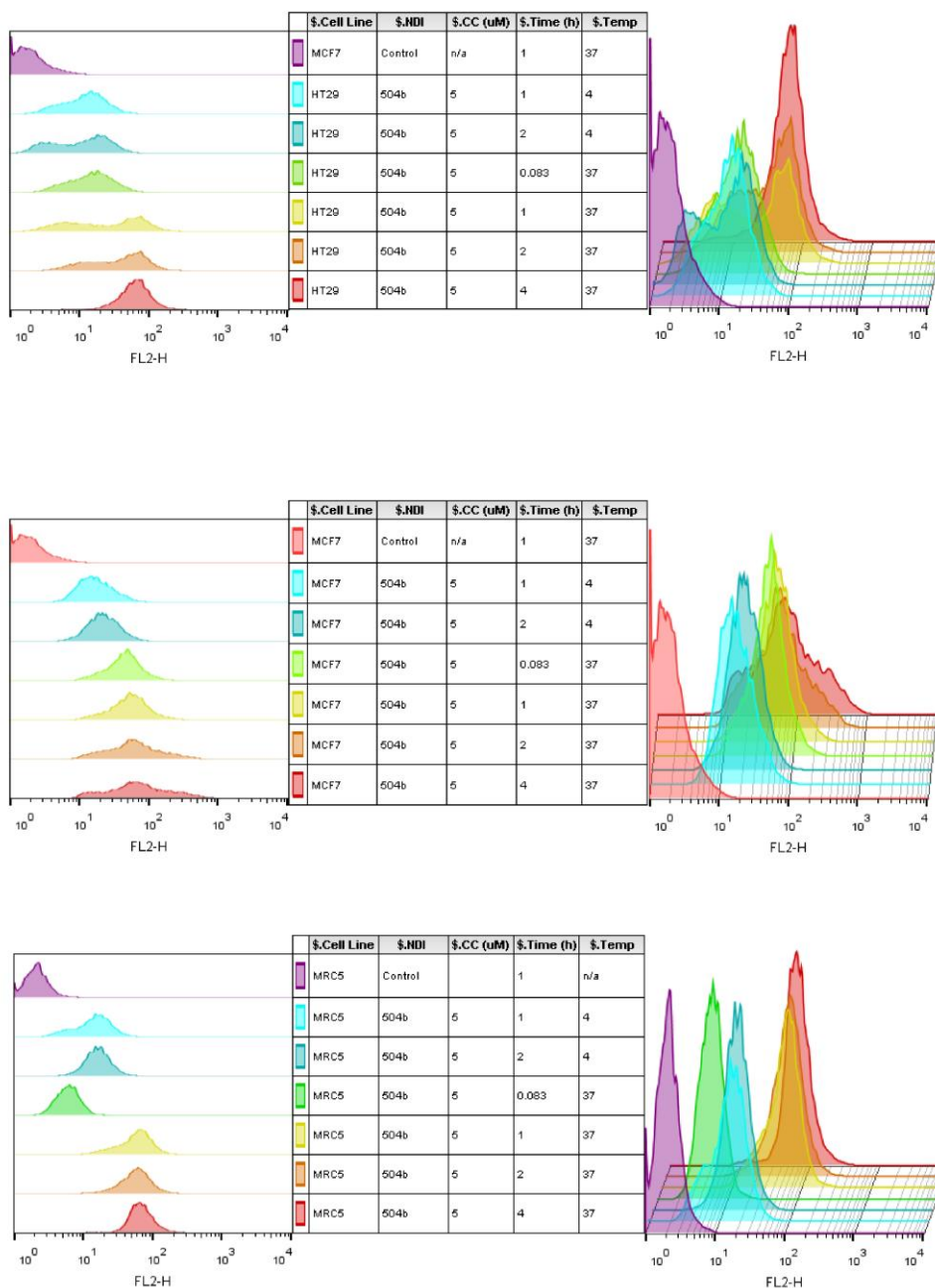


Figure S6. Flow cytometry diagrams of compound 7 (5 μ M, old compound NDI-prop), incubated with various cancer and normal cell lines for 2 h measured by flow cytometry. Bars in red, temp= 4 $^{\circ}$ C; bars in blue, temp= 37 $^{\circ}$ C.

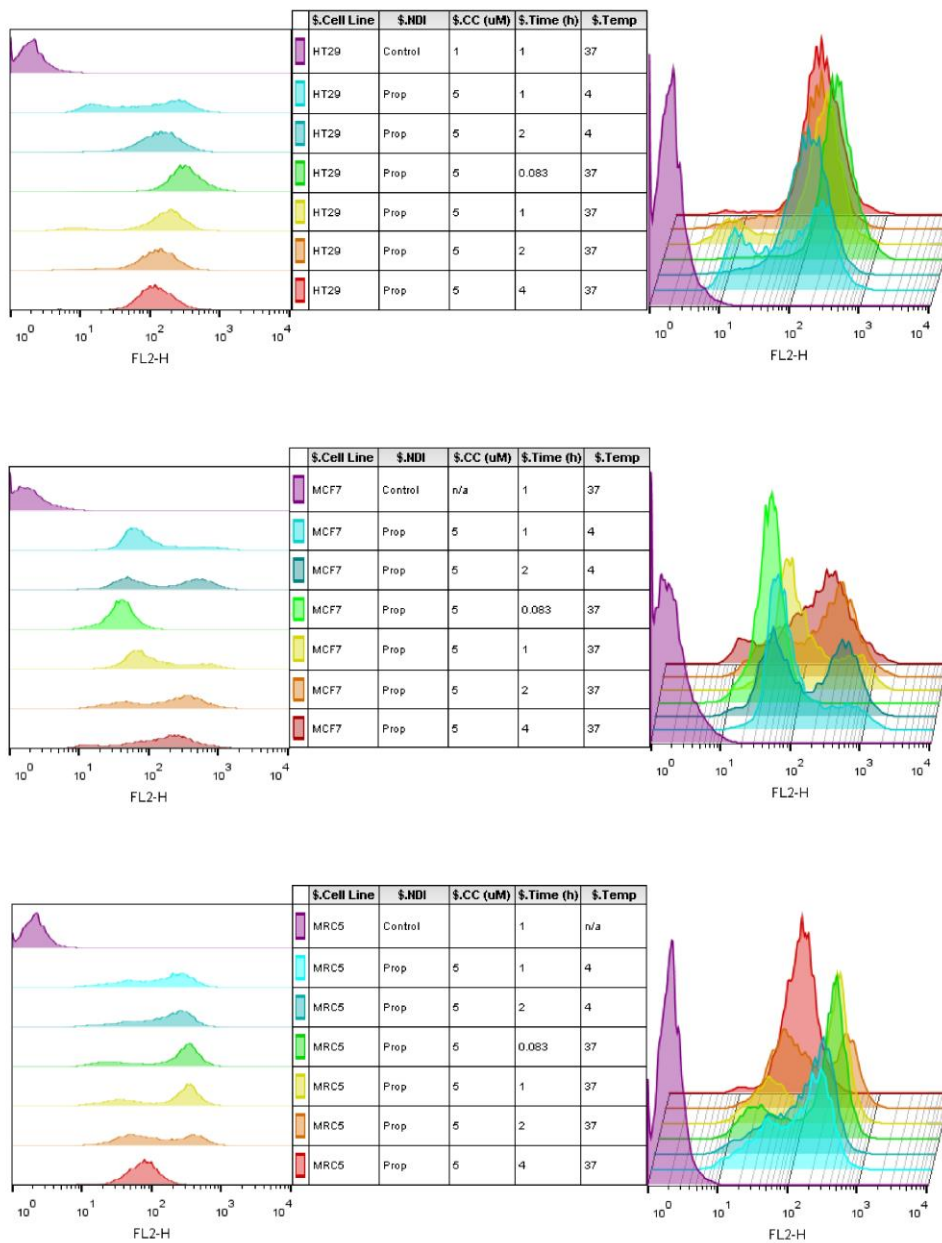


Figure S7. Cell uptake inhibition in MRC-5 non cancerous cells of β -glc-NDI **1**, α -man-NDI **5**, β -glcC2-NDI **6** and aglycone-NDI **7** in the presence of several GLUT inhibitors as measured by intracellular concentration using fluorescence spectroscopy. Concentration for each compound was 5 μ M and for the inhibitors were 100 μ M. Incubation time was 1h.

Inhibitor	Glut Target	MRC5-uptake Inhibition (%)				Inhibition (%)	
		Prop-NDI 7	glc-NDI 1	manC2-NDI 5	glcC2-NDI 6	% < 25	% > 40
ZWB117	Glut 1	○ 0	○ -11	○ -1	○ -11	○ Small	
Quercetin	Glut 1 & 4	○ 4	○ 9	● 37	○ -10	● Medium	
Genistein	Glut 1 & 4	○ 14	○ 17	● 28	○ 1	● High	
Ritonavir	Glut 4	○ -2	○ -7	○ 19	○ -24		

Graph with cell uptake inhibition percentage for β -glc-NDI **1**, α -man-NDI **5**, β -glcC2-NDI **6** and aglycone-NDI **7** in the presence of GLUT inhibitors shown on Figures 7 and S7.

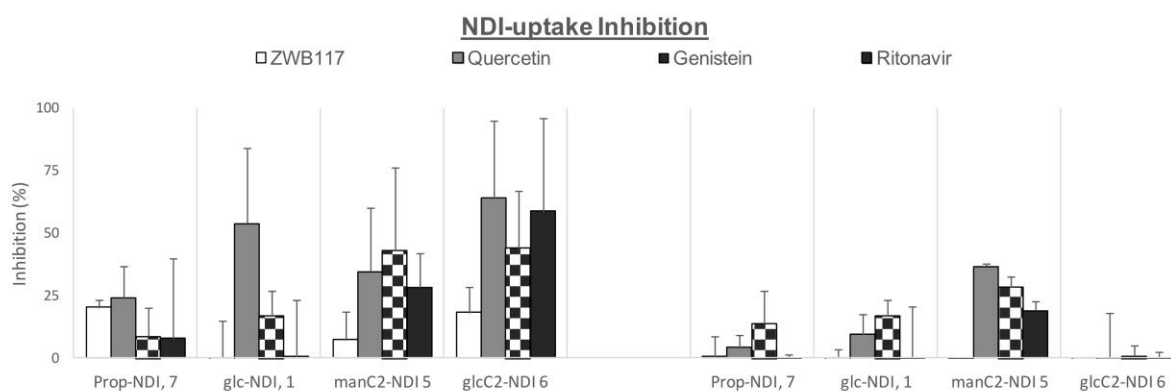


Figure S8. Confocal images of HT-29 and MRC-5 cells after co-incubation with β -glc-NDI **1** (5 μ M) for 5 min. HT-29 cells: a) fluorescence image of compound **1**; b) Transmitted light image; c) merged image; MRC-5 cells: d) fluorescence image of compound **1**; e) Transmitted light image; f) merged image.

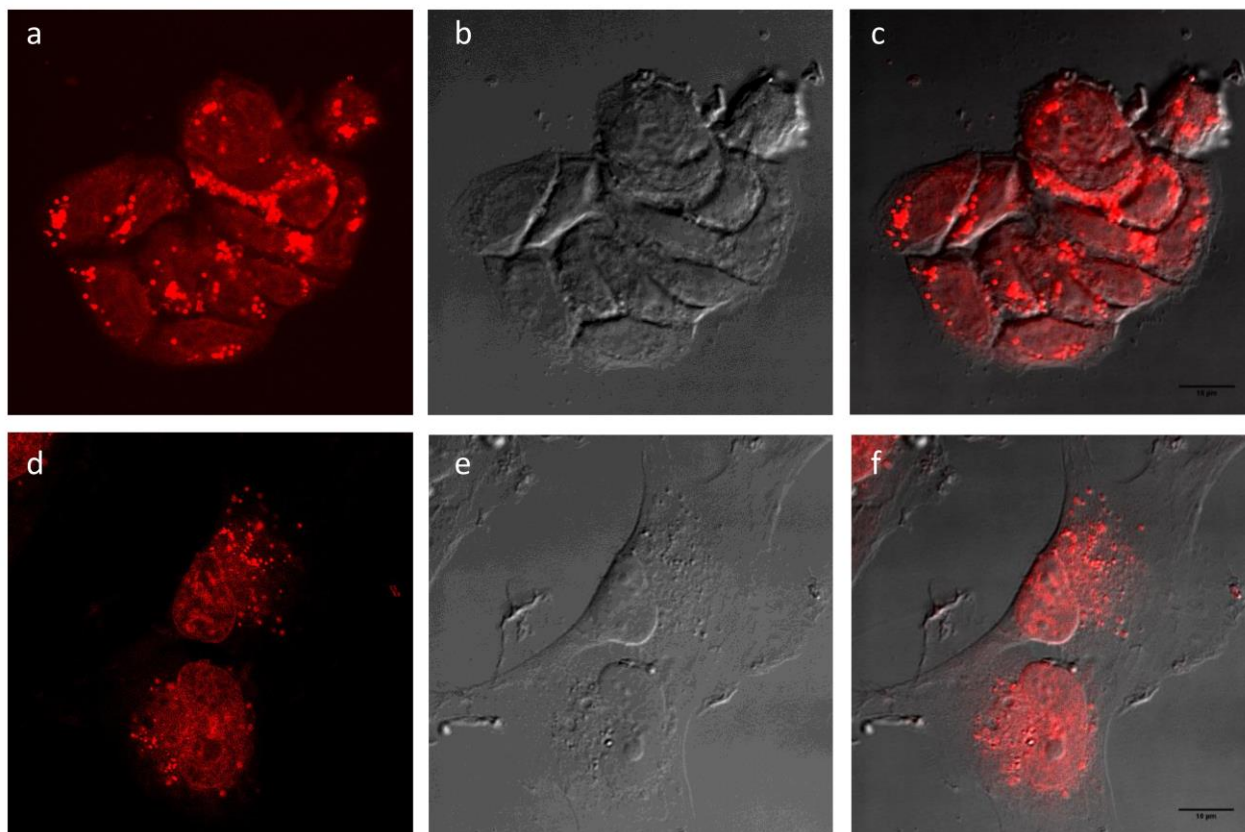


Figure S9. Confocal images of HT-29 and MRC-5 cells after co-incubation with β -glcC2-NDI **6** ($5 \mu\text{M}$ each) for 5 min. HT-29 cells: a) fluorescence image of compound **6**; b) Transmitted light image; c) merged image; MRC-5 cells: d) fluorescence image of compound **6**; e) Transmitted light image; f) merged image.

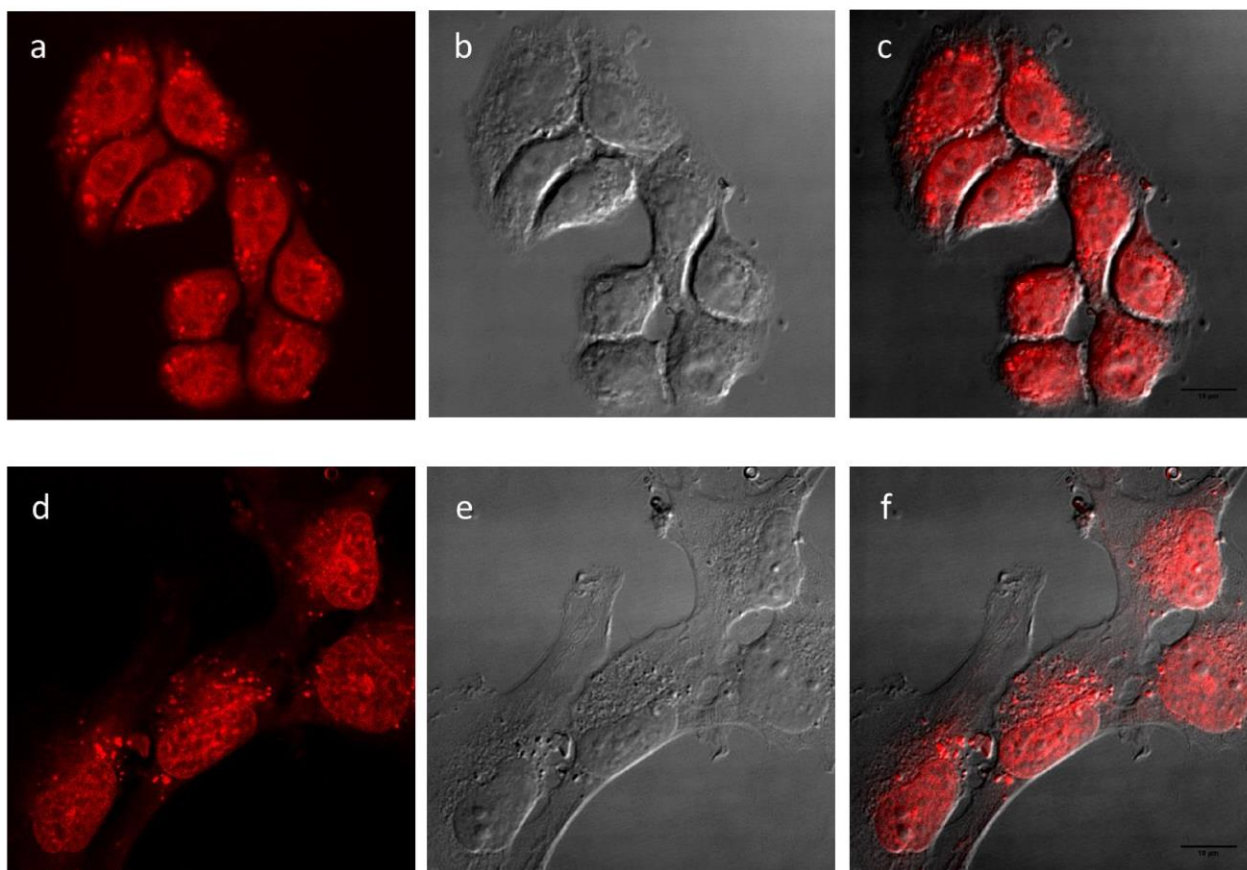
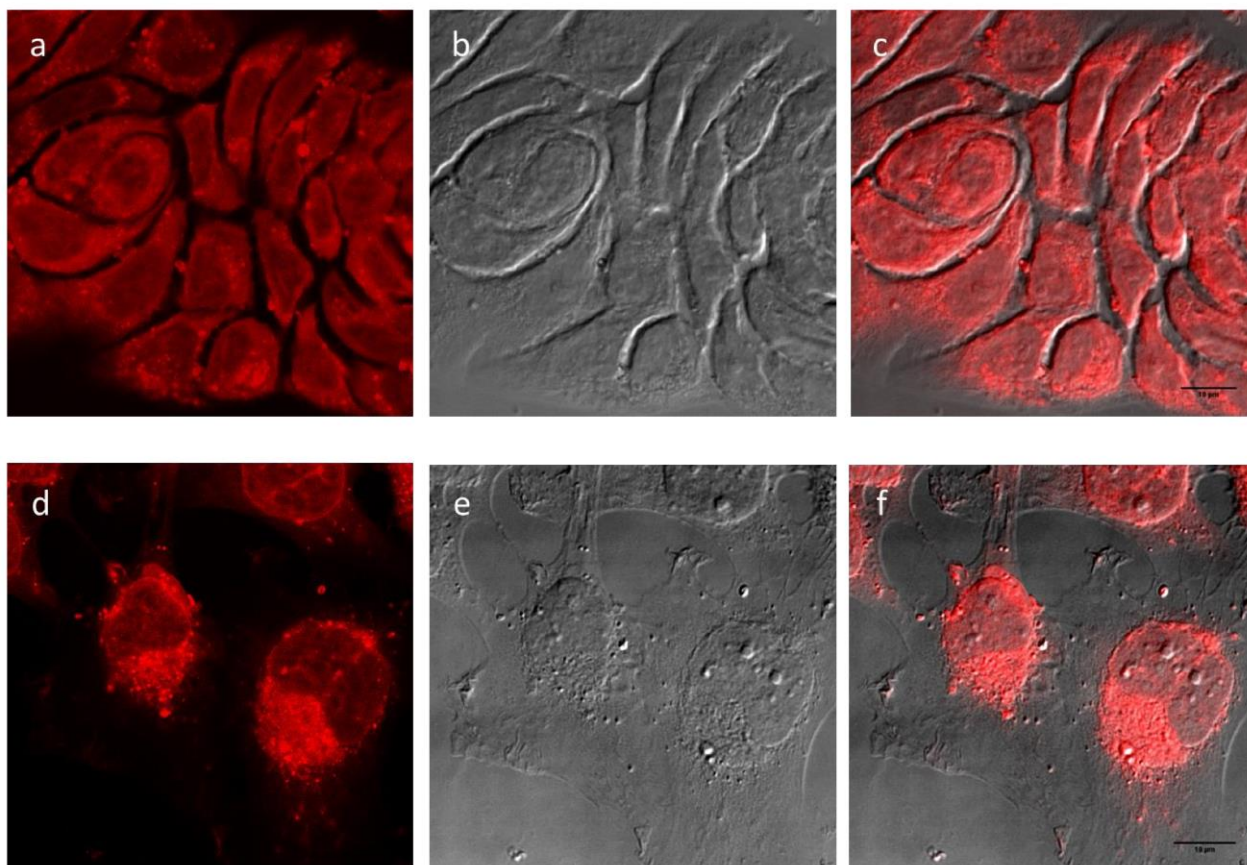


Figure S10. Confocal images of HT-29 and MRC-5 cells after co-incubation with aglycone-NDI 7 (5 μ M each) for 5 min. HT-29 cells: a) fluorescence image of compound 7; b) Transmitted light image; c) merged image; MRC-5 cells: d) fluorescence image of compound 7; e) Transmitted light image; f) merged image.



HPLC PURITY DATA

Analytical Method A

flow rate of 1 mL/min; loop 10 μ L; $\lambda_{\text{obs}} = 256$ nm

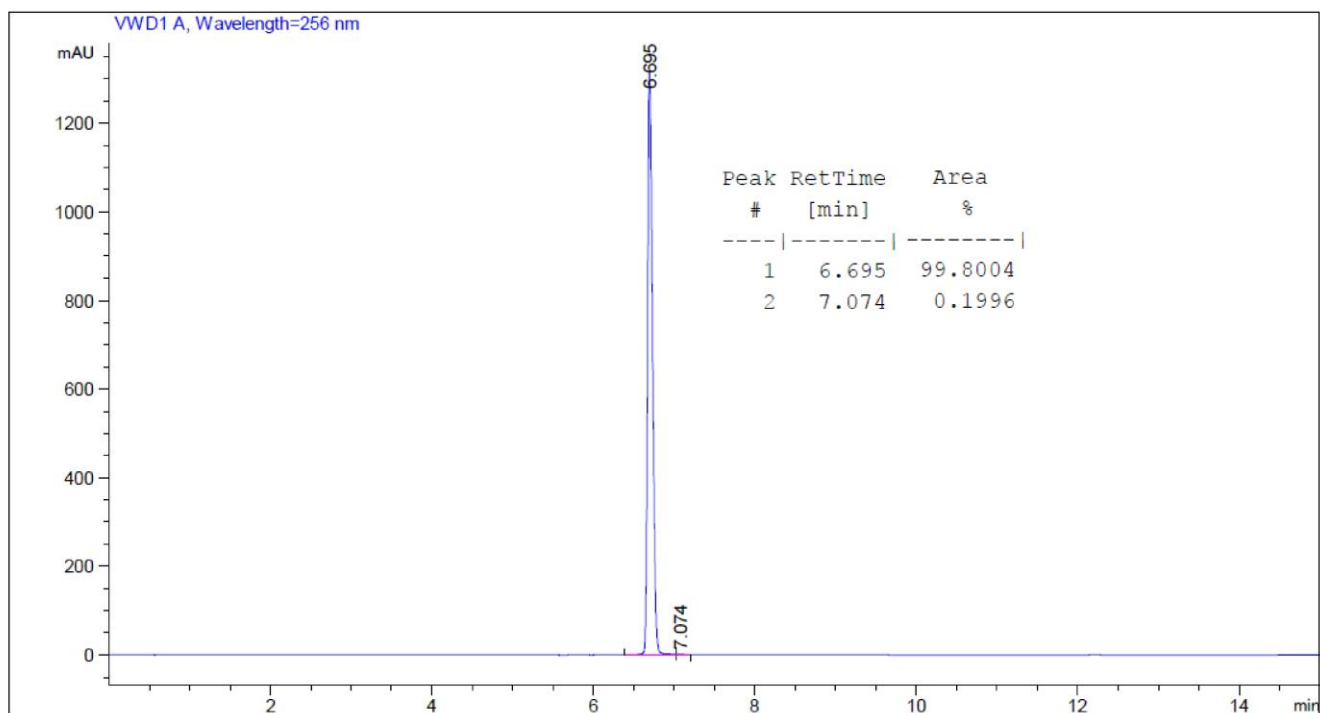
t (min)	H₂O 0.1% TFA	MeCN
0	95.0	5.0
2	95.0	5.0
8	40	60
12	40	60

Analytical Method B

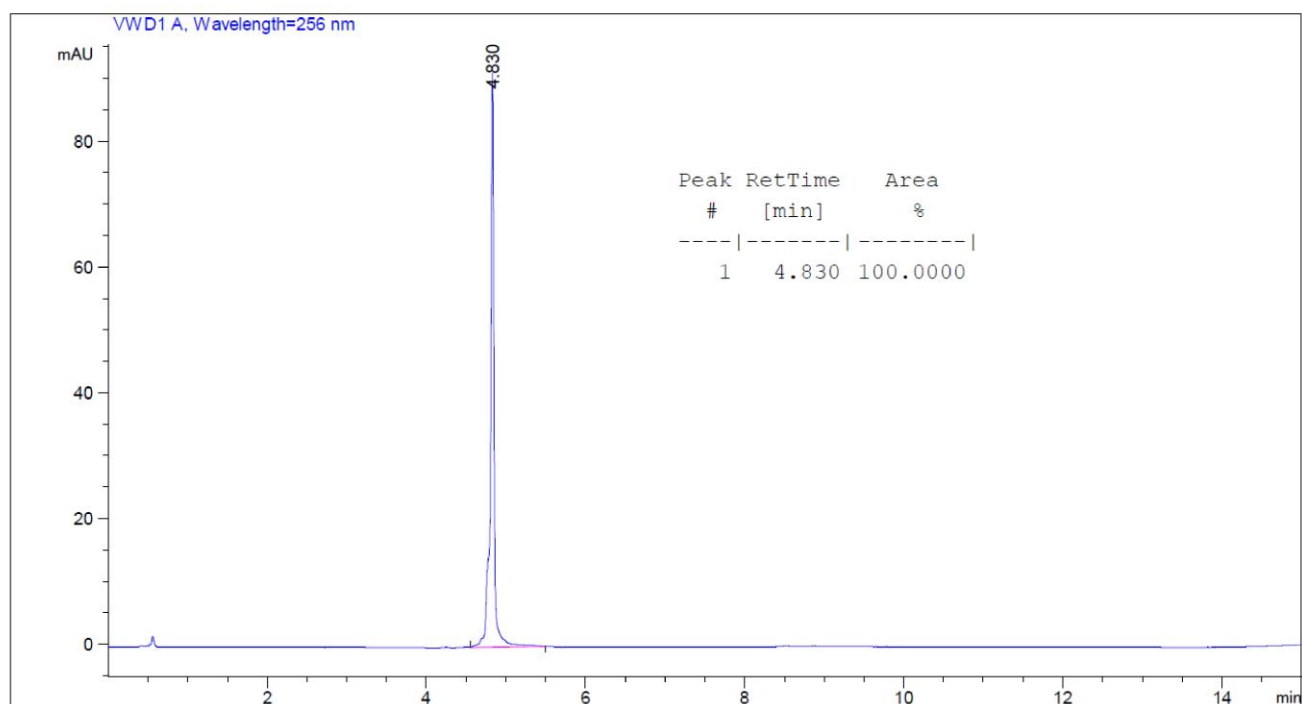
flow rate of 1 mL/min; loop 10 μ L; $\lambda_{\text{obs}} = 256$ nm

t (min)	H₂O 0.1% TFA	MeCN
0	95.0	5.0
2	95.0	5.0
12	60	40
14	60	40

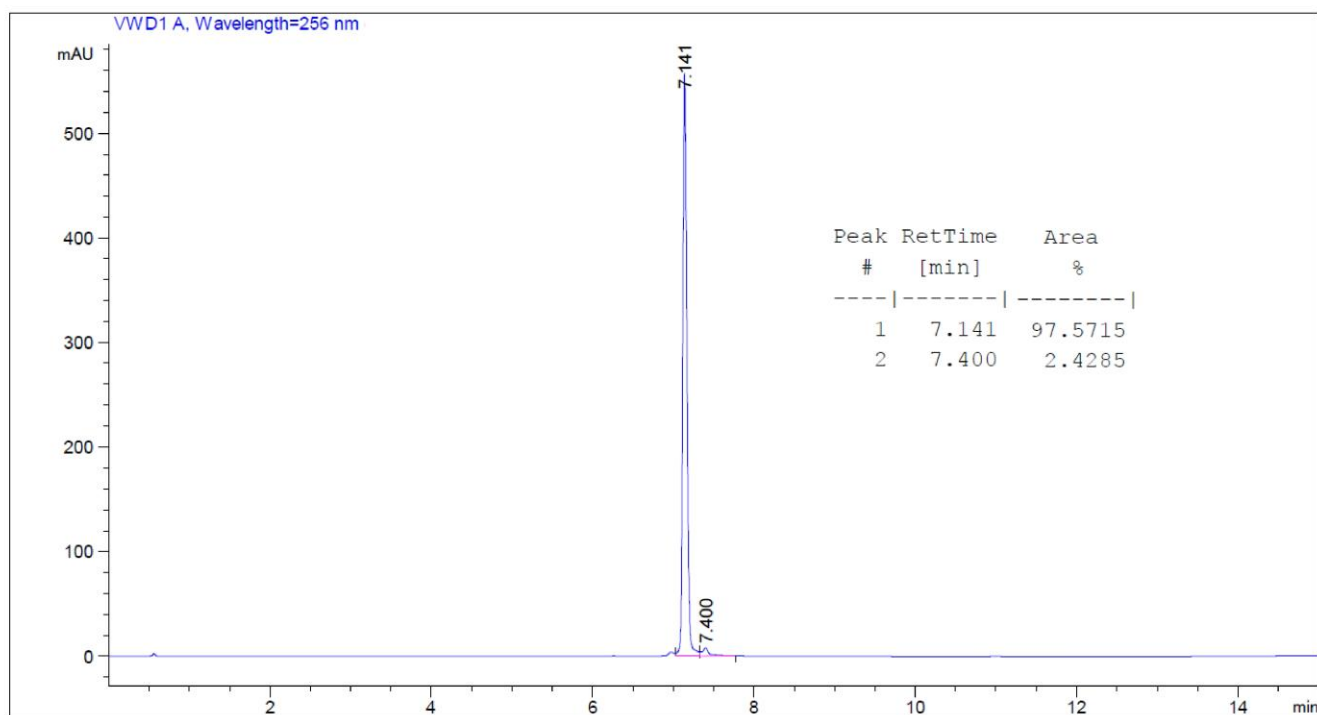
Compound 1: Method B



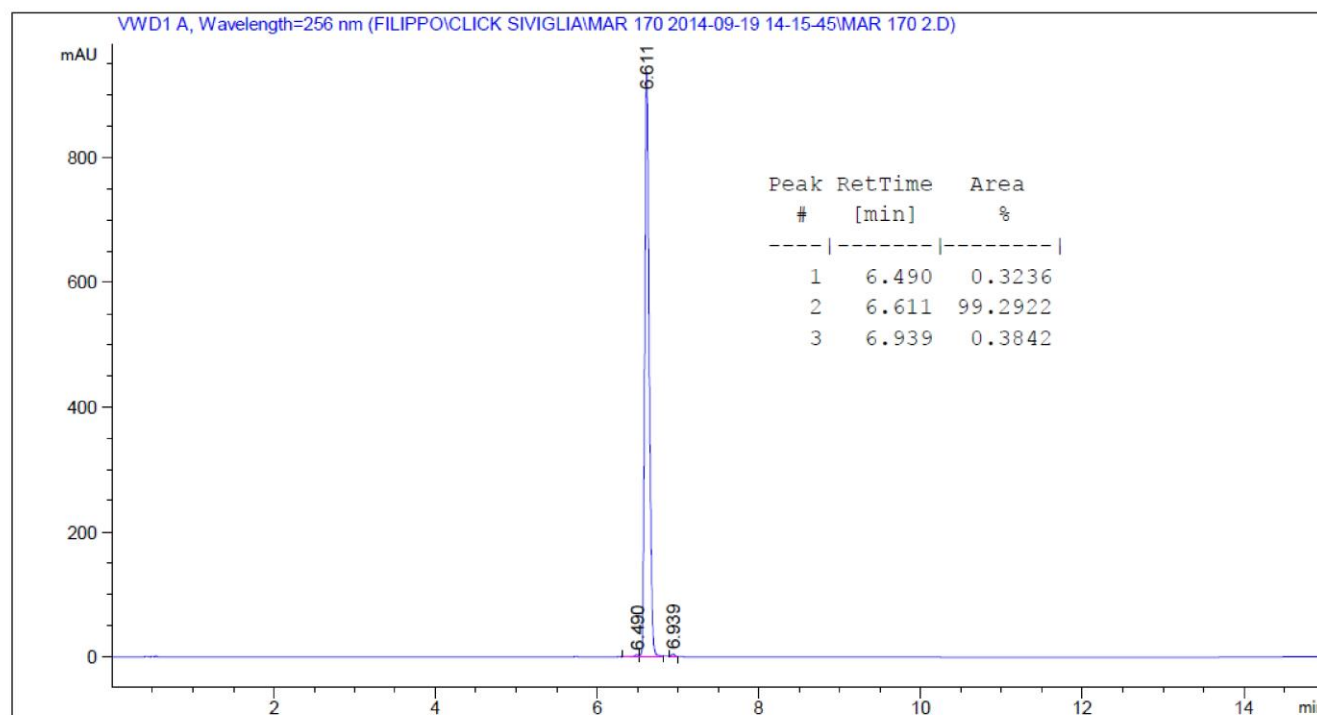
Compound 2: Method B



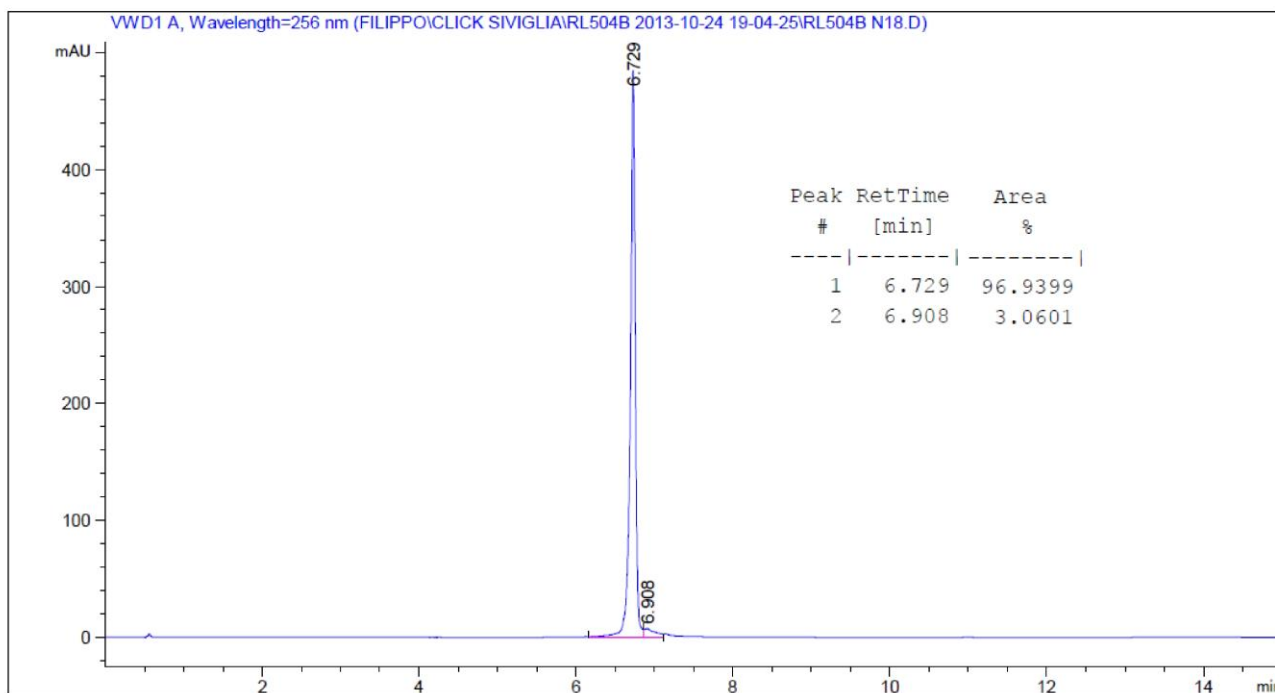
Compound 3: Method B



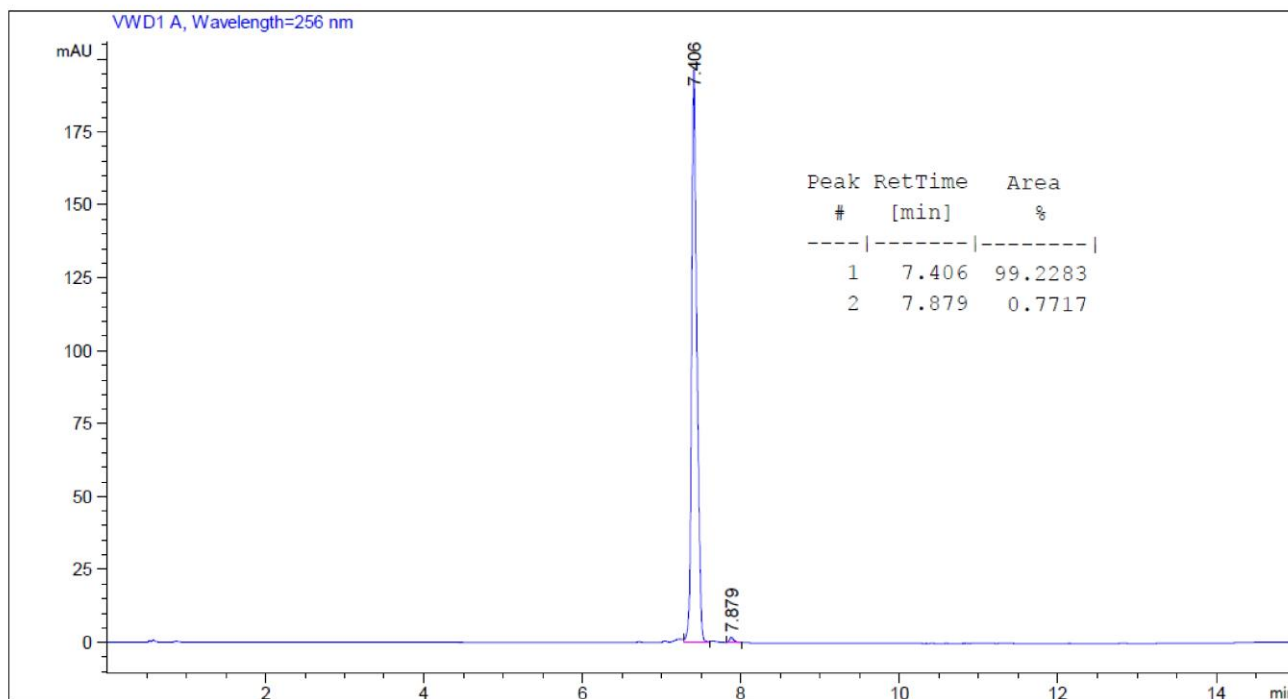
Compound 4: Method B



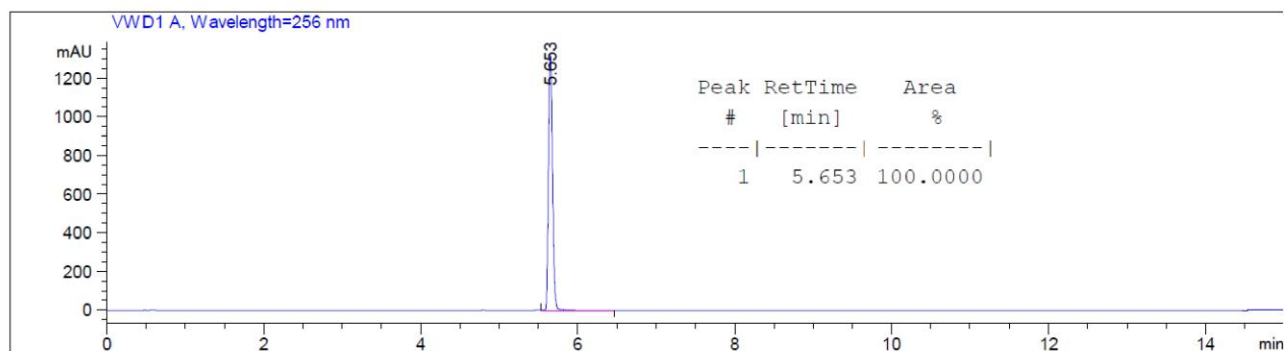
Compound 5: Method B



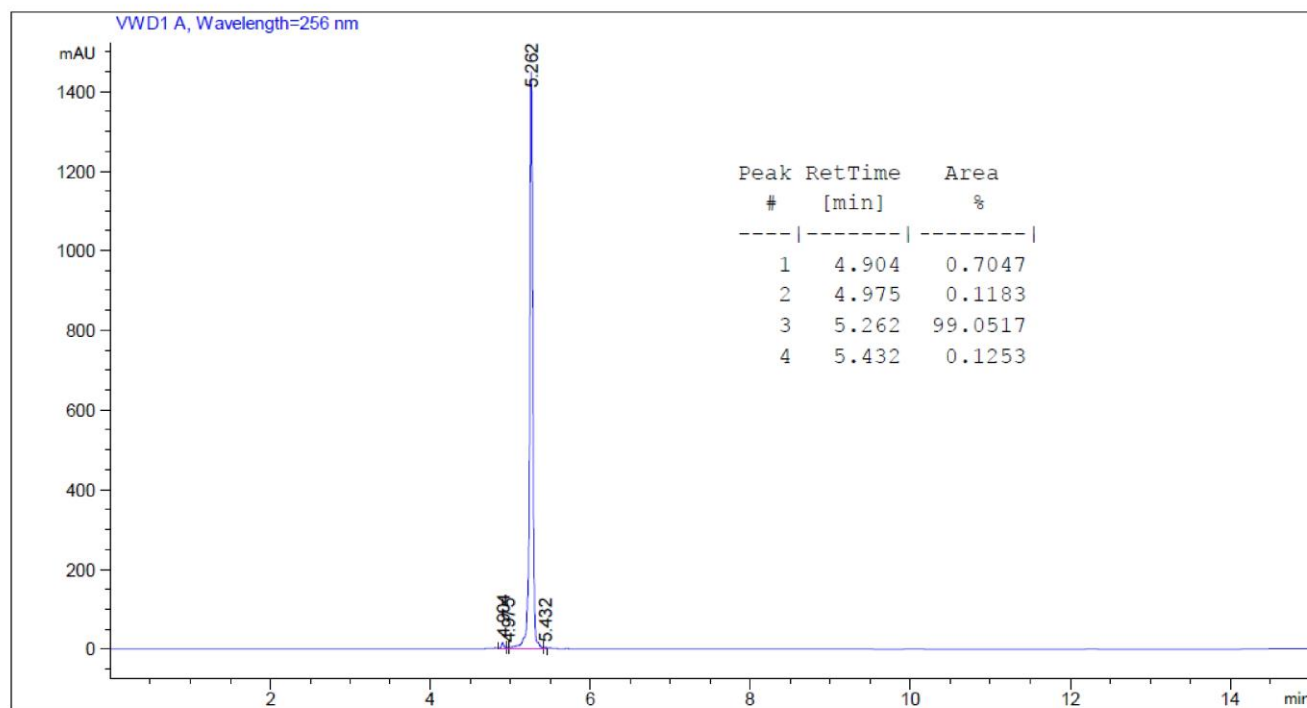
Compound 6: Method B



Compound 7: Method A

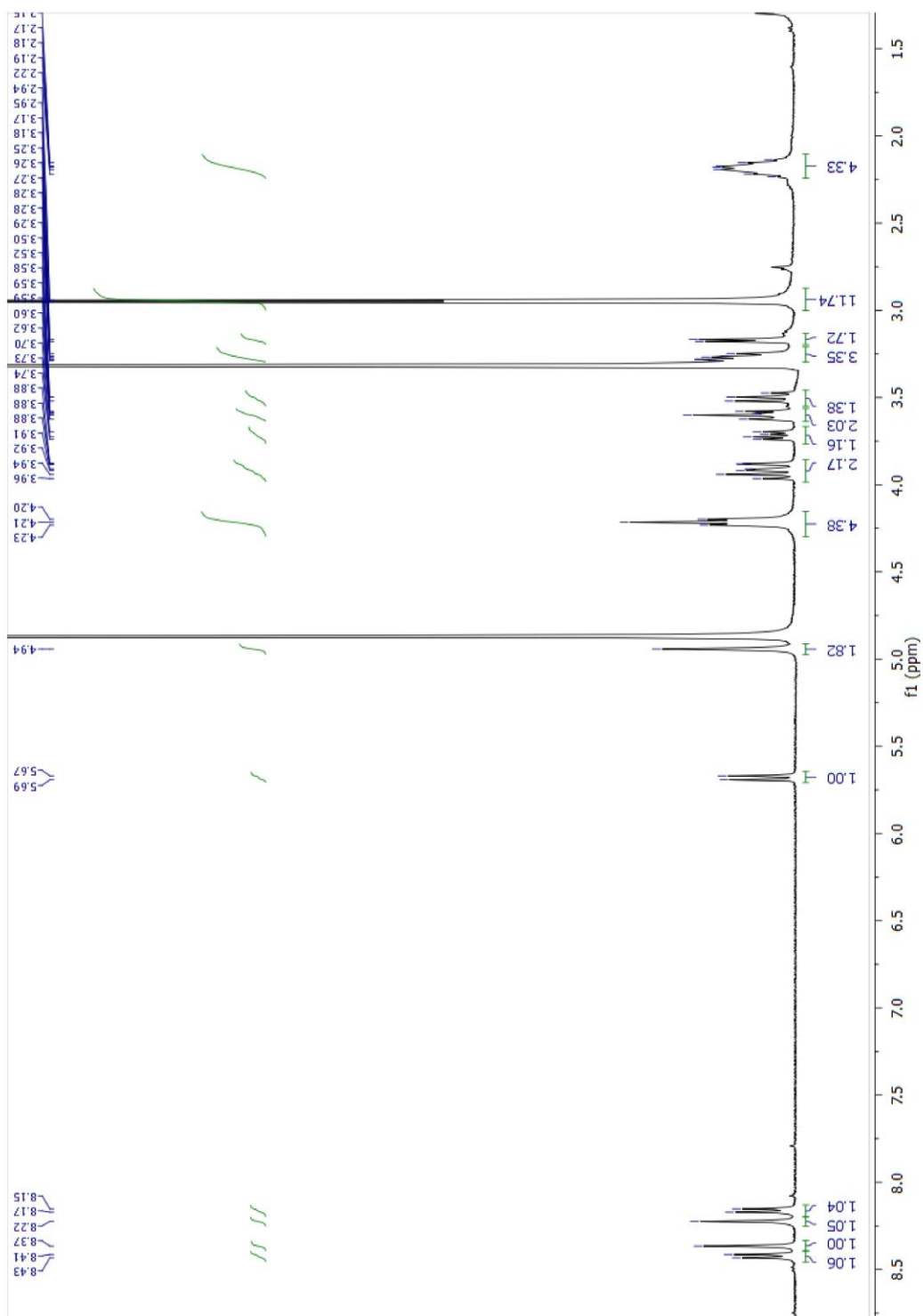


Compound 8: Method A

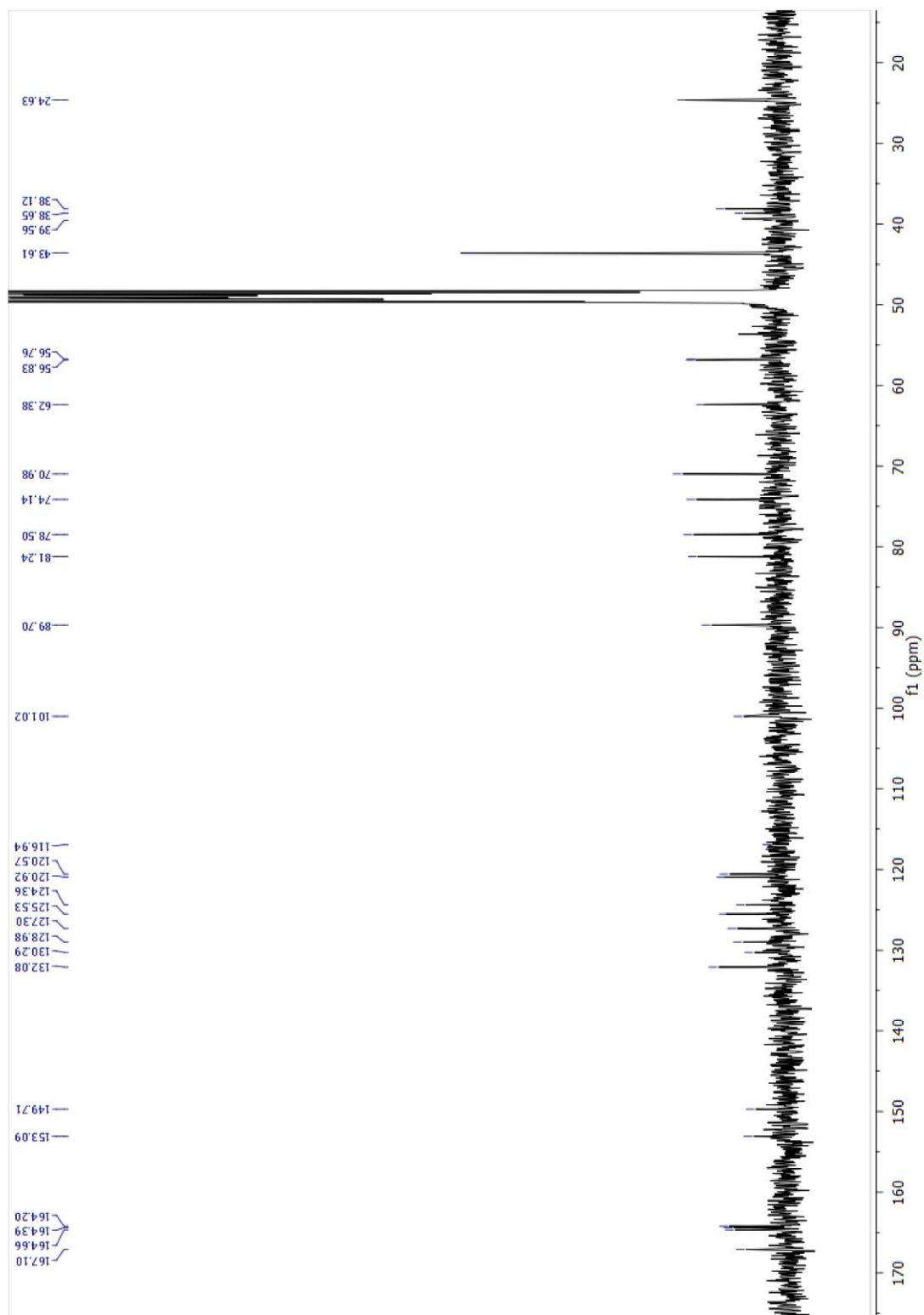


NMR Spectra:

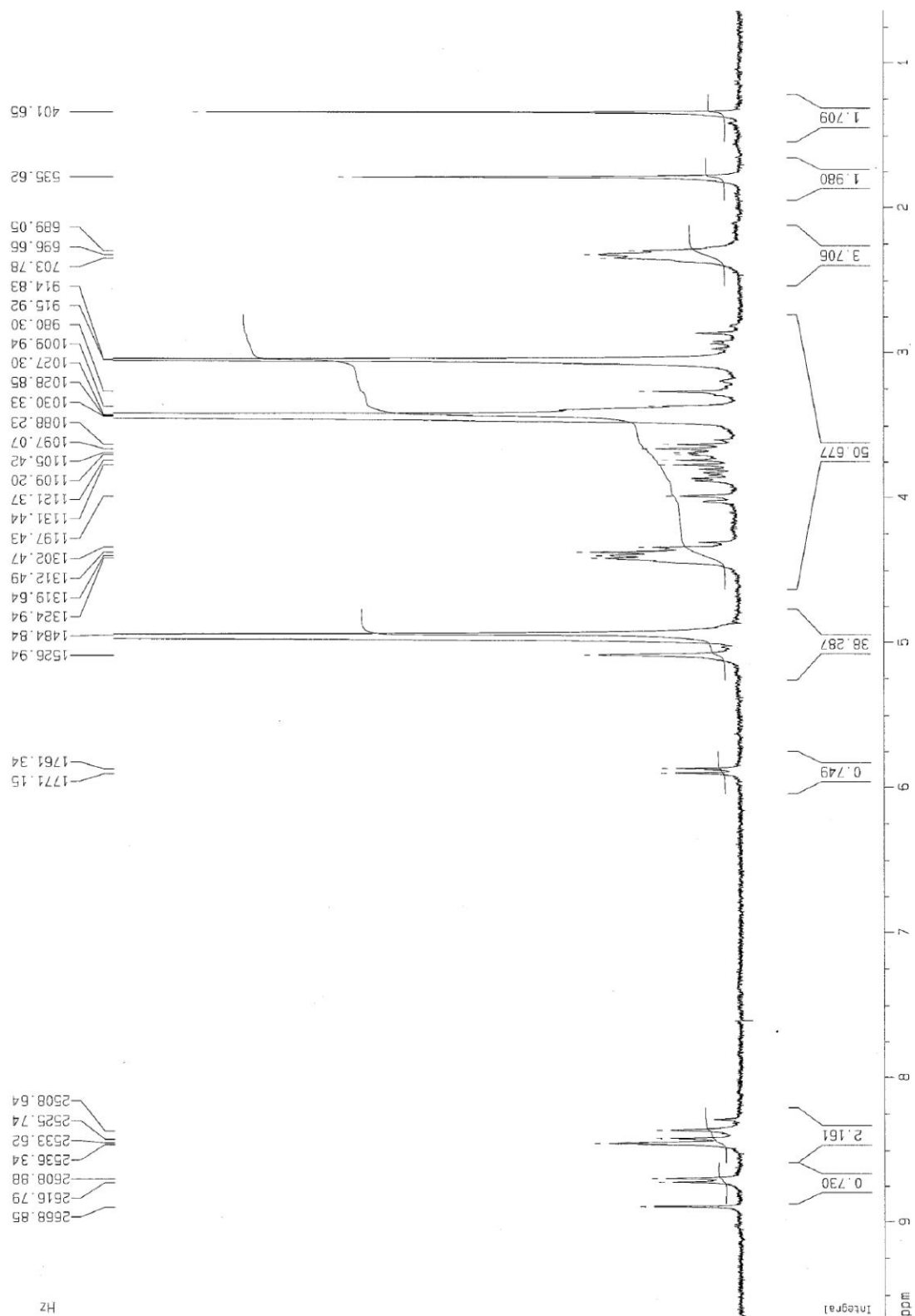
NDI- 1 (CD₃OD) ¹H NMR 400MHz

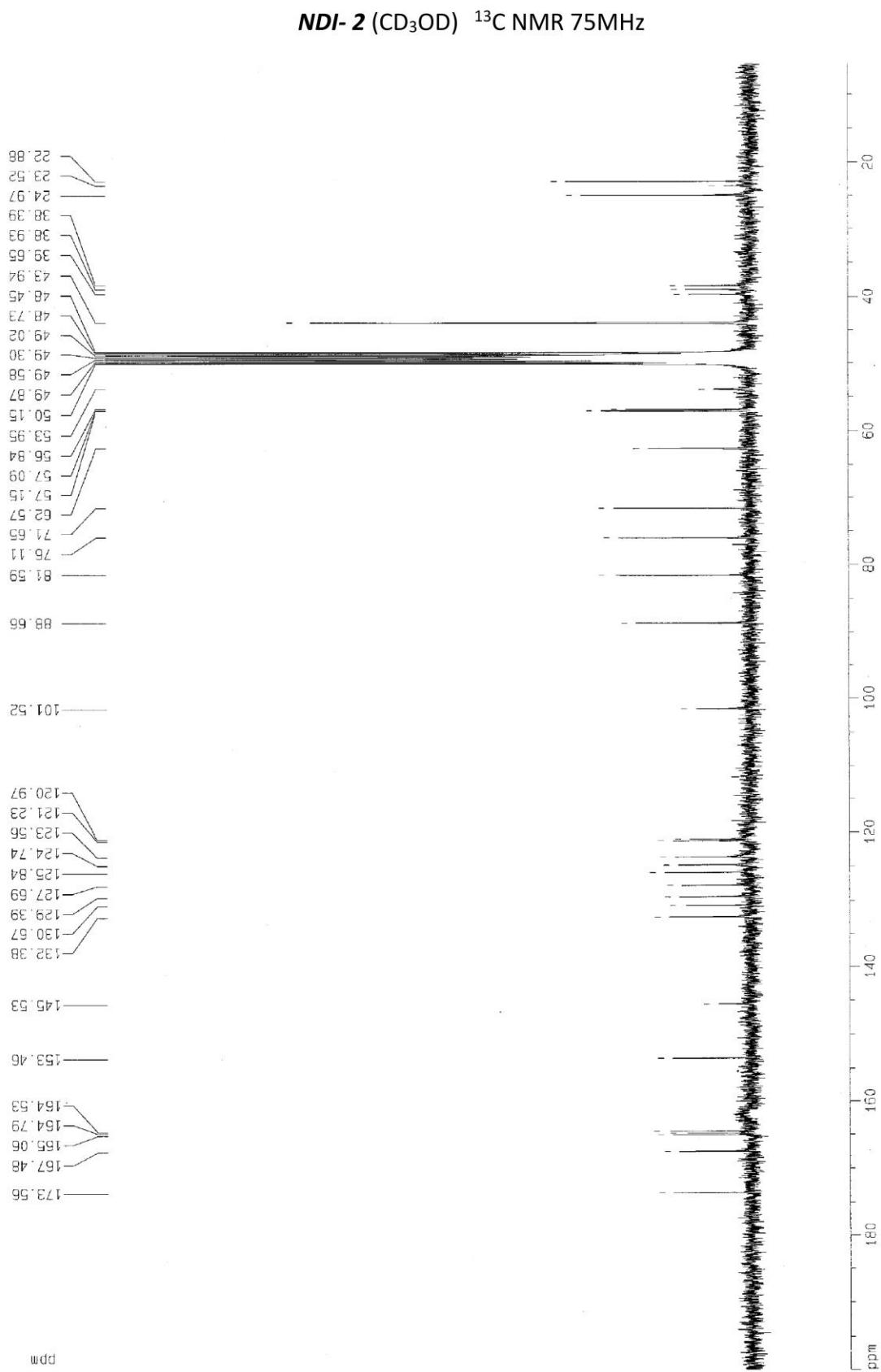


NDI- 1 (CD₃OD) ¹³C NMR 101MHz

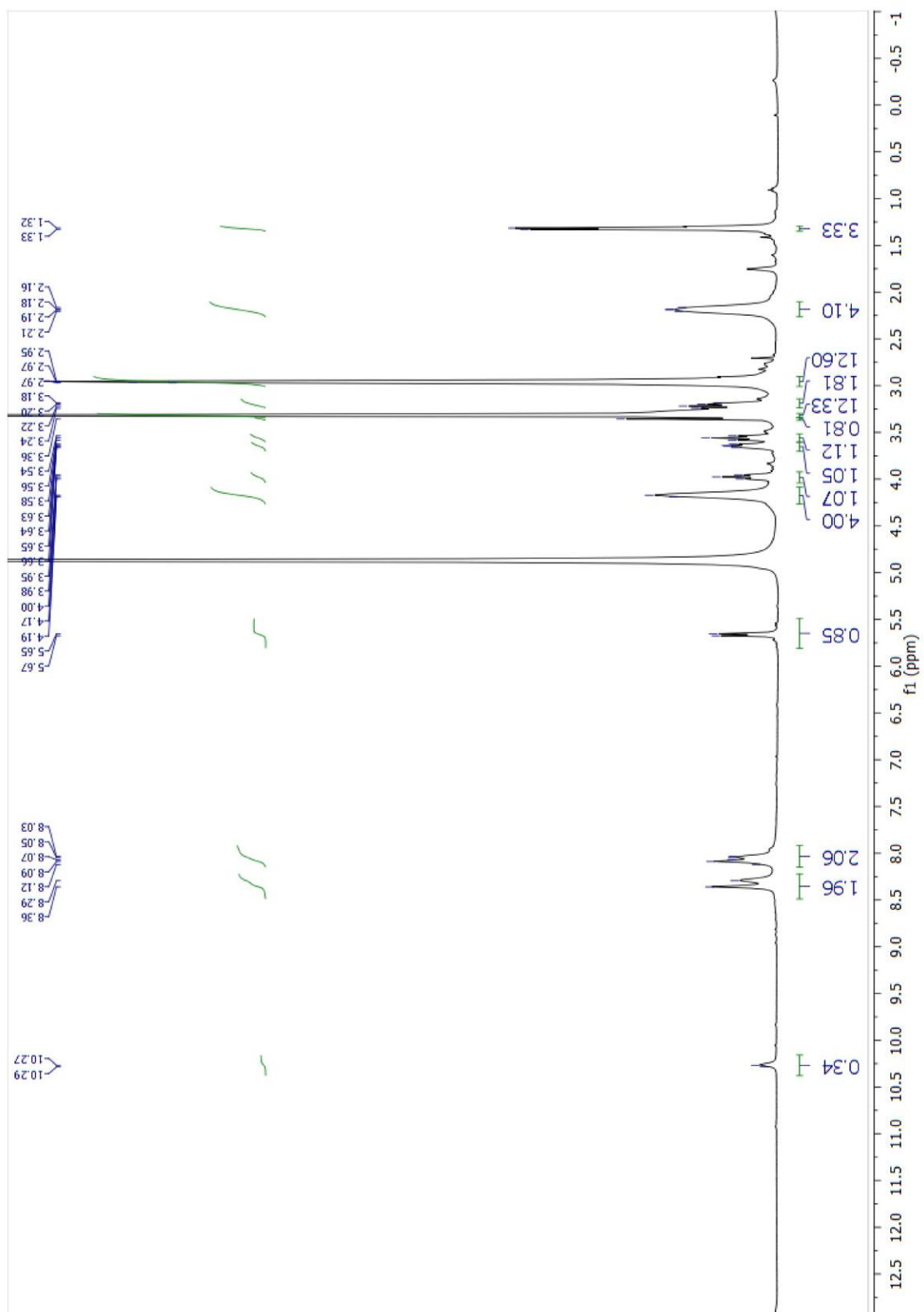


NDI-2 (CD₃OD) ¹H NMR 300MHz

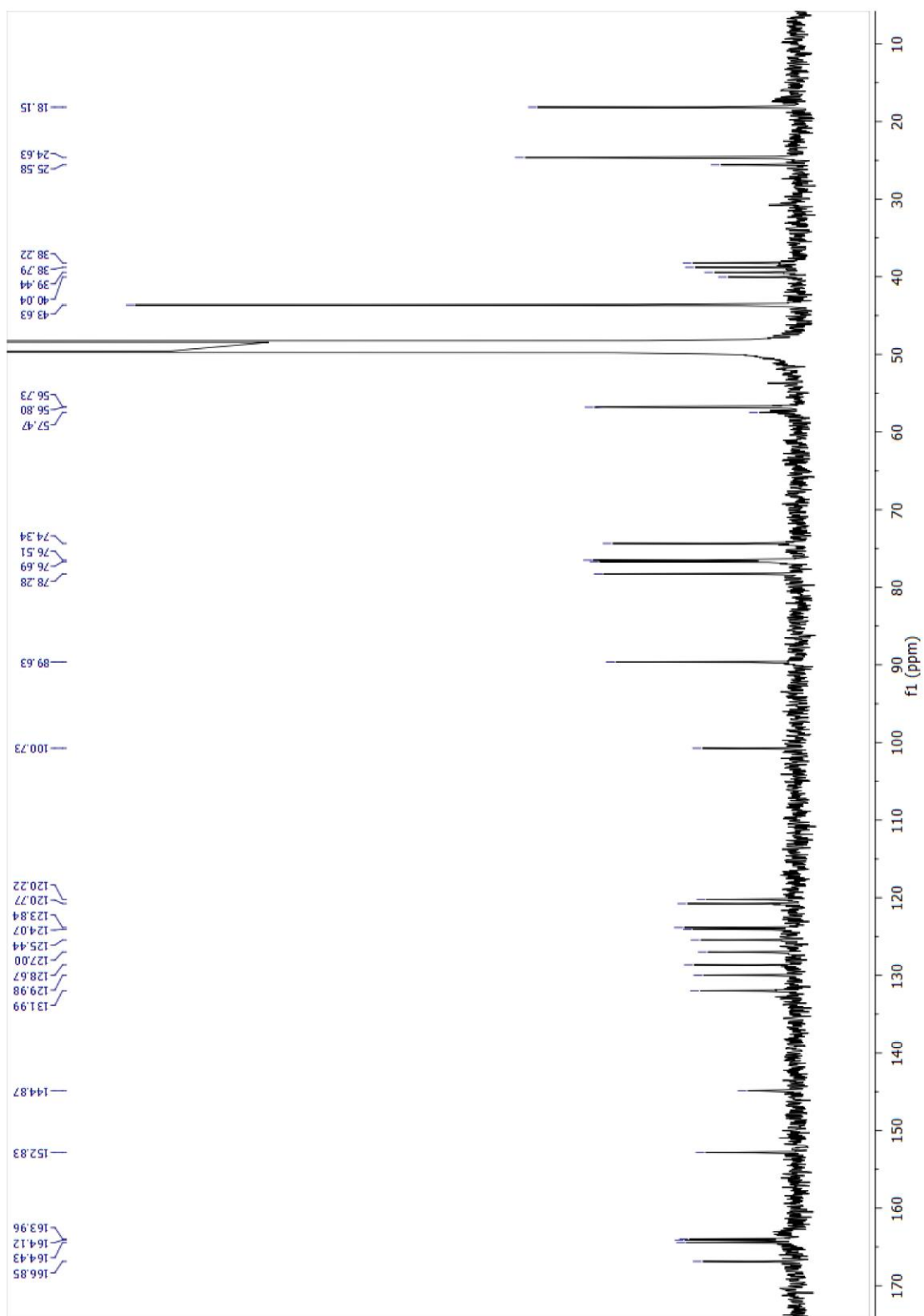




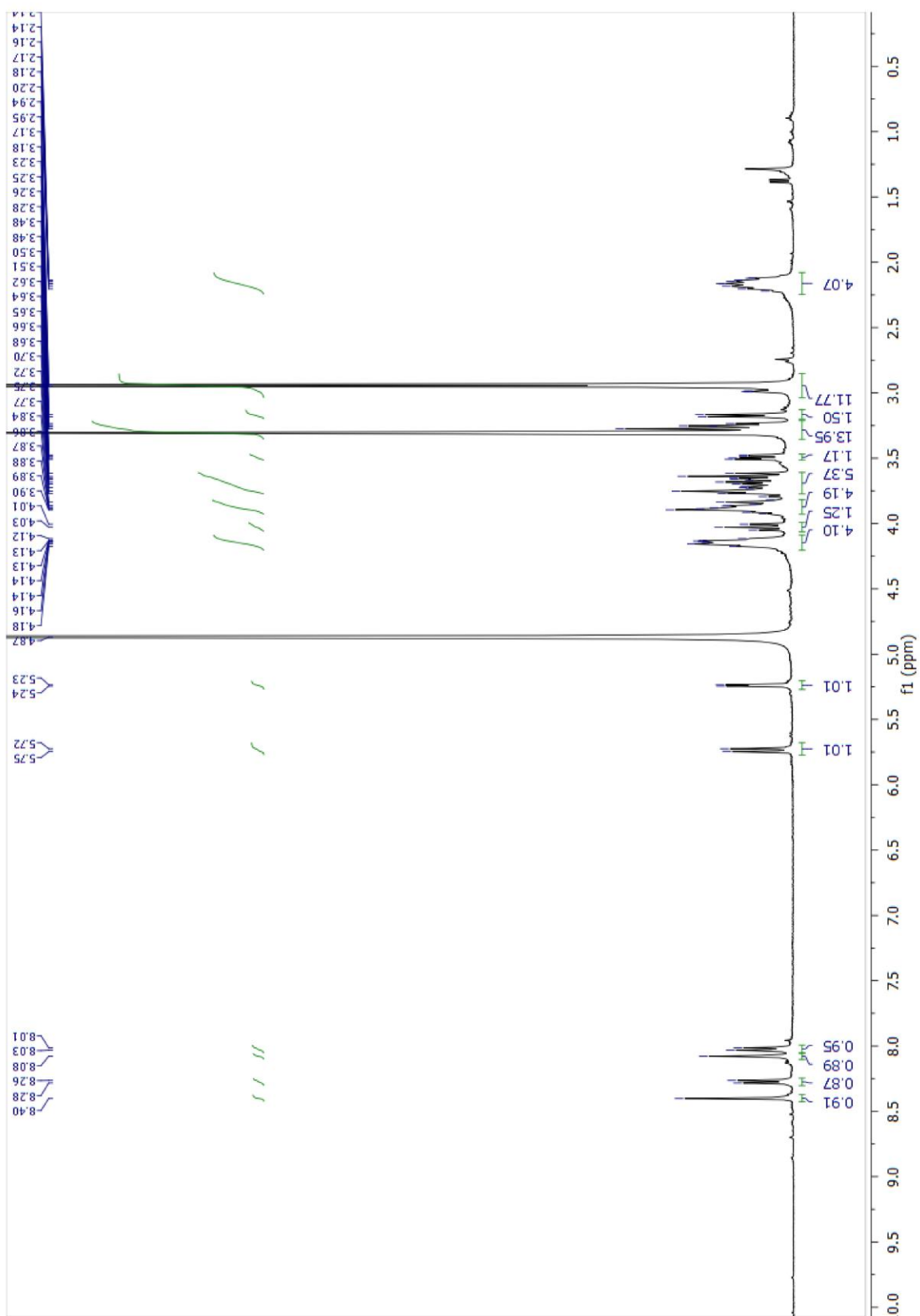
NDI-3 (CD₃OD) ¹H NMR 400MHz



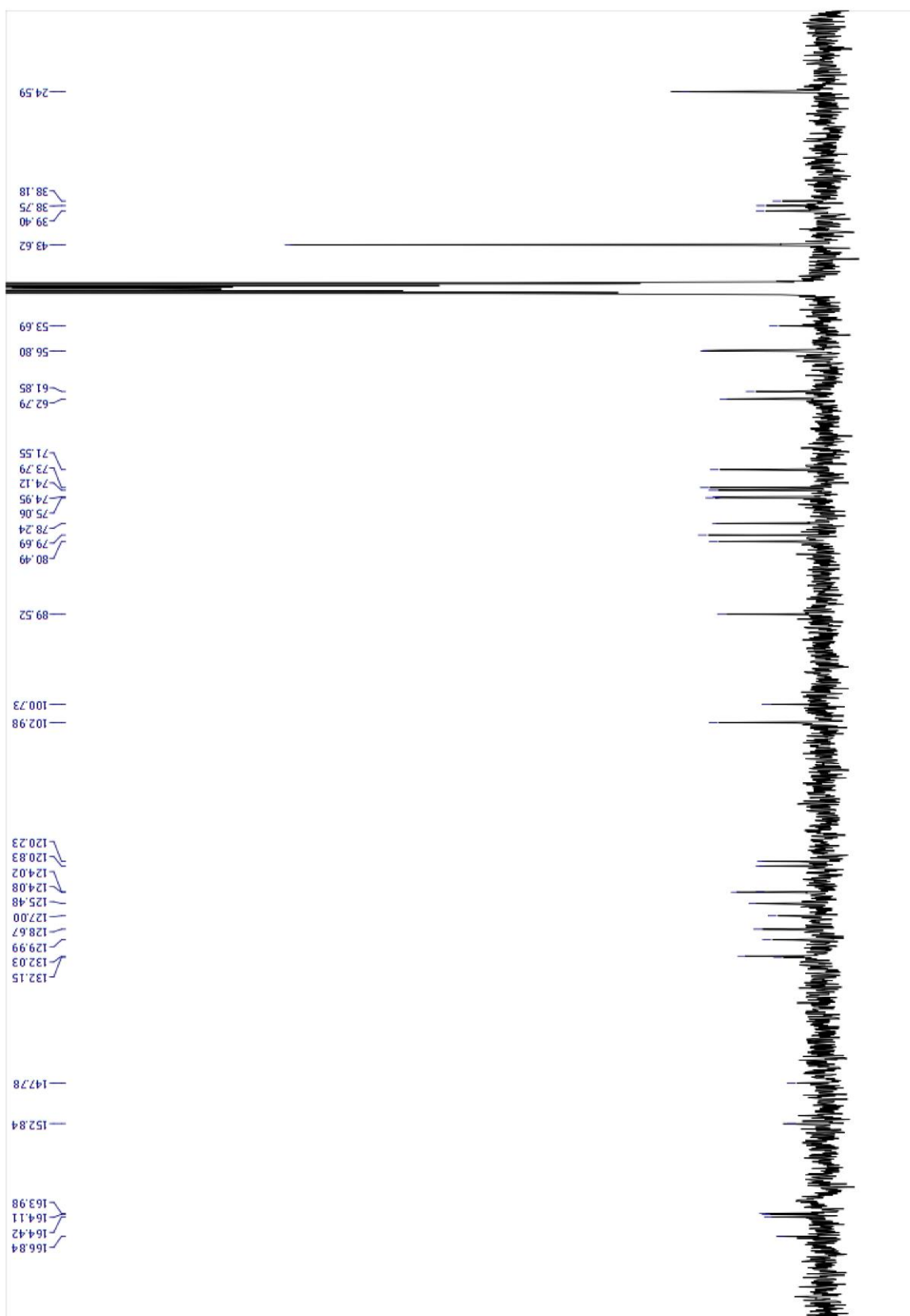
NDI-3 (CD₃OD) ¹³C NMR 101MHz



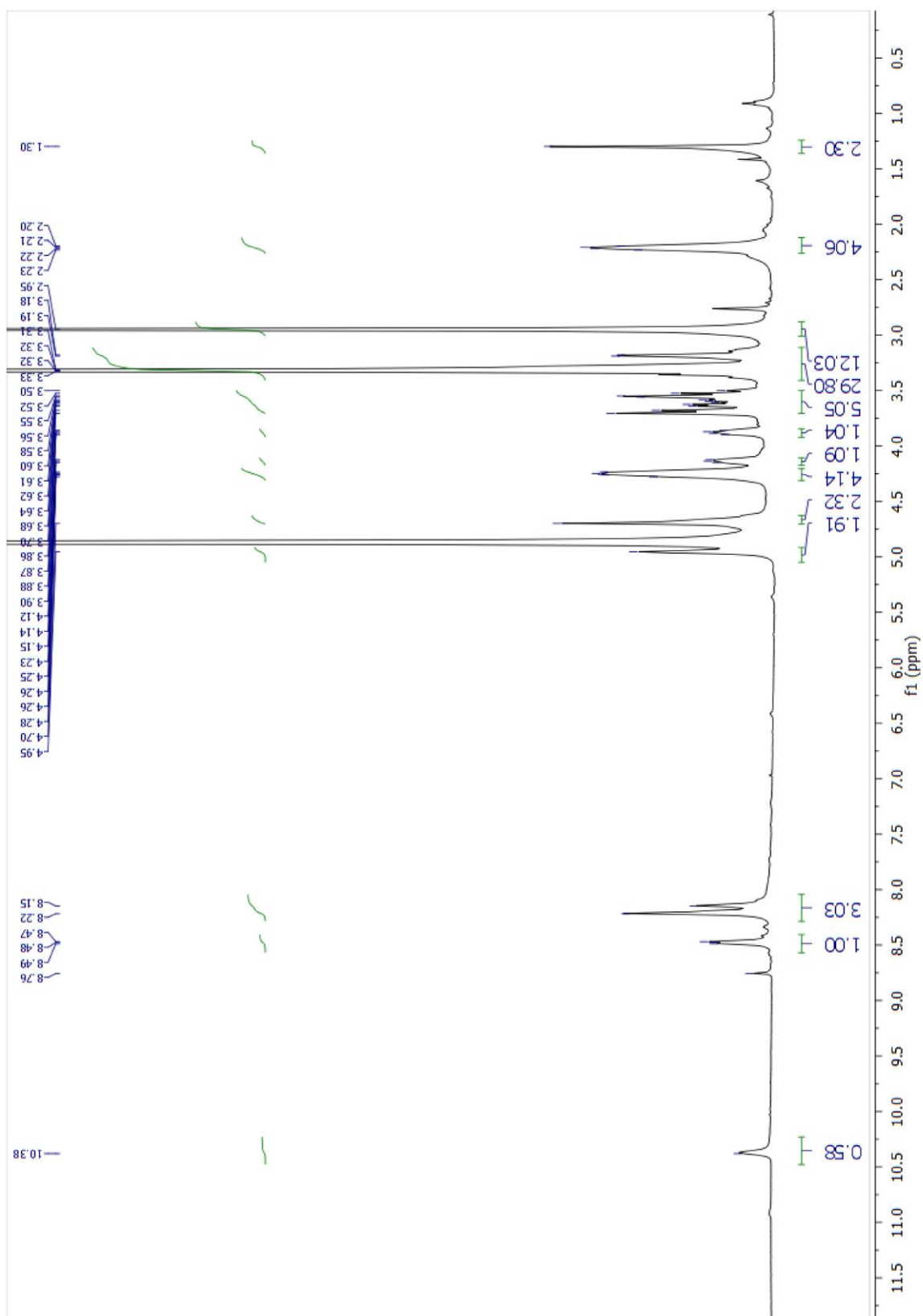
NDI-4 (CD₃OD) ¹H NMR 400MHz

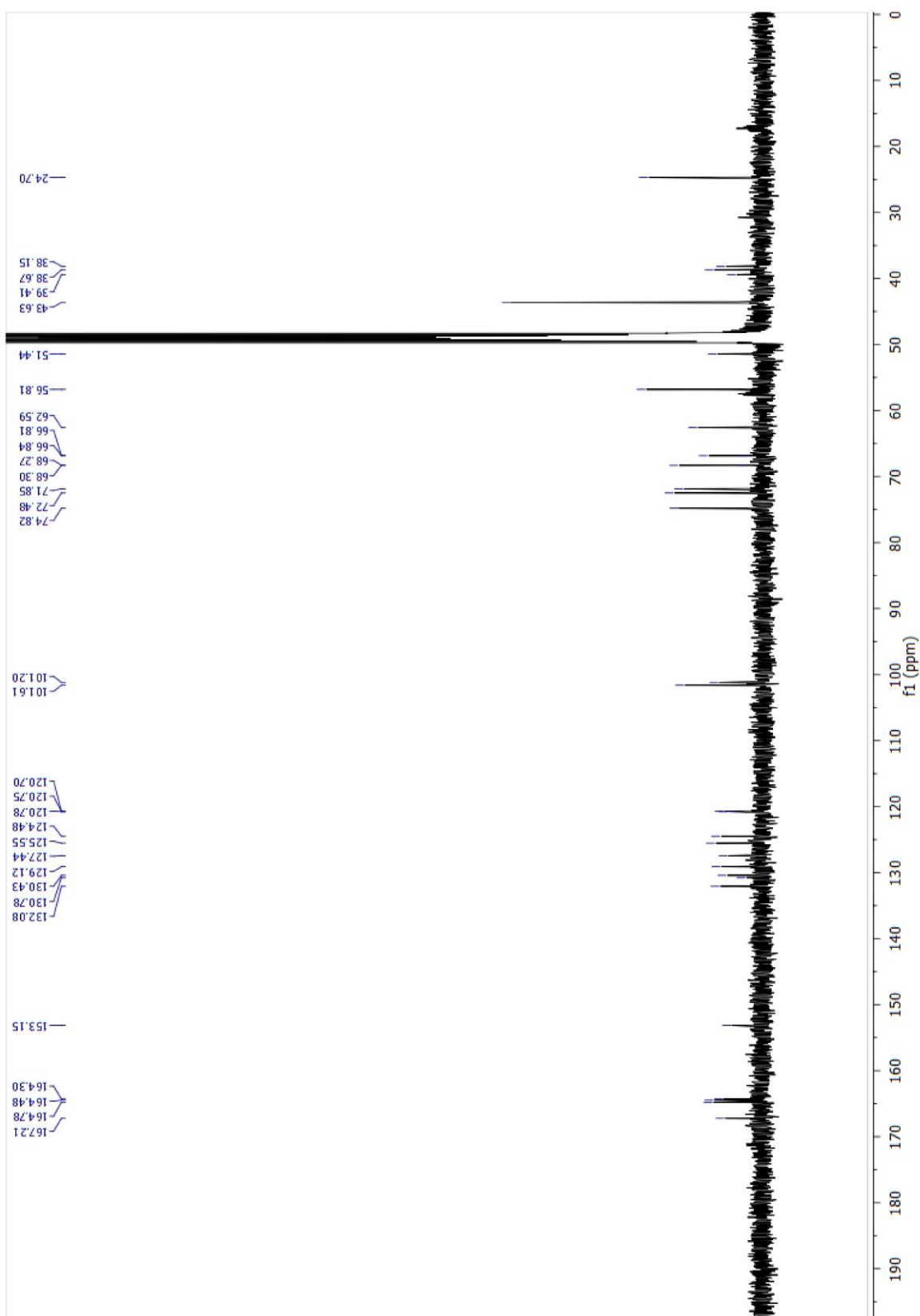


NDI- 4 (CD₃OD) ¹³C NMR 101MHz

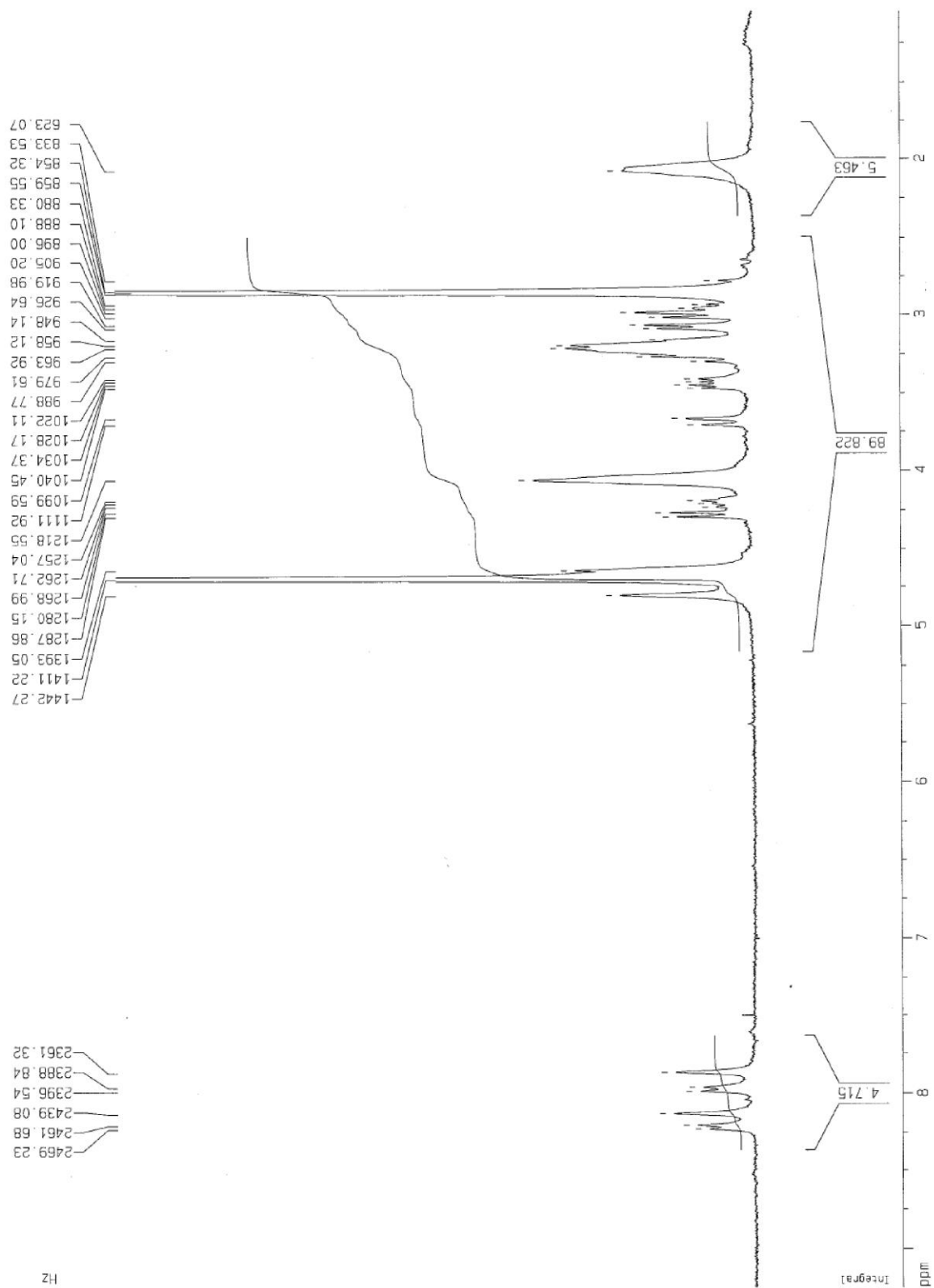


NDI-5 (CD₃OD) ¹H NMR 400MHz

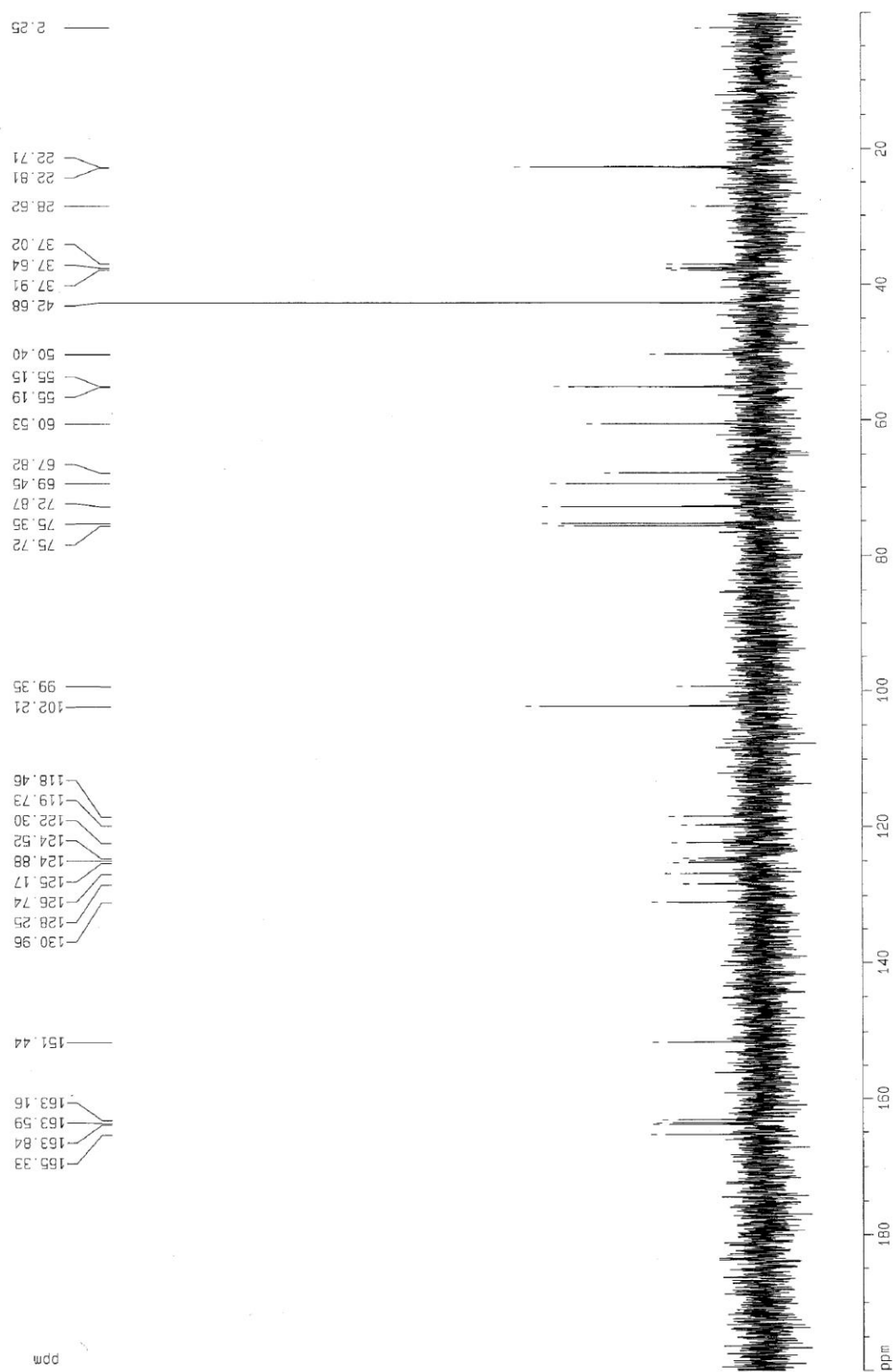


NDI-5 (CD₃OD) ¹³C NMR 101MHz

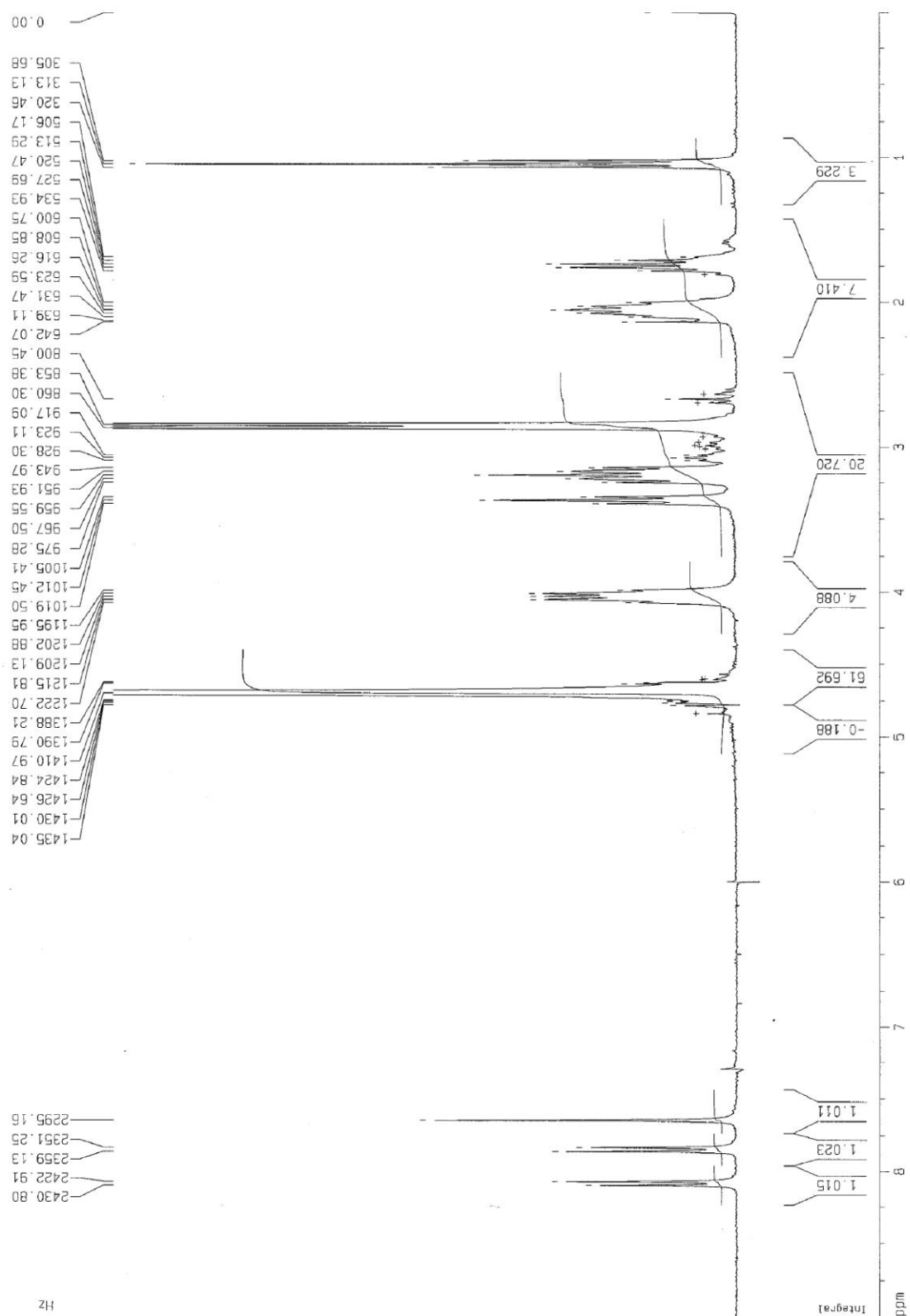
NDI-6 (D₂O) ¹H NMR 300MHz



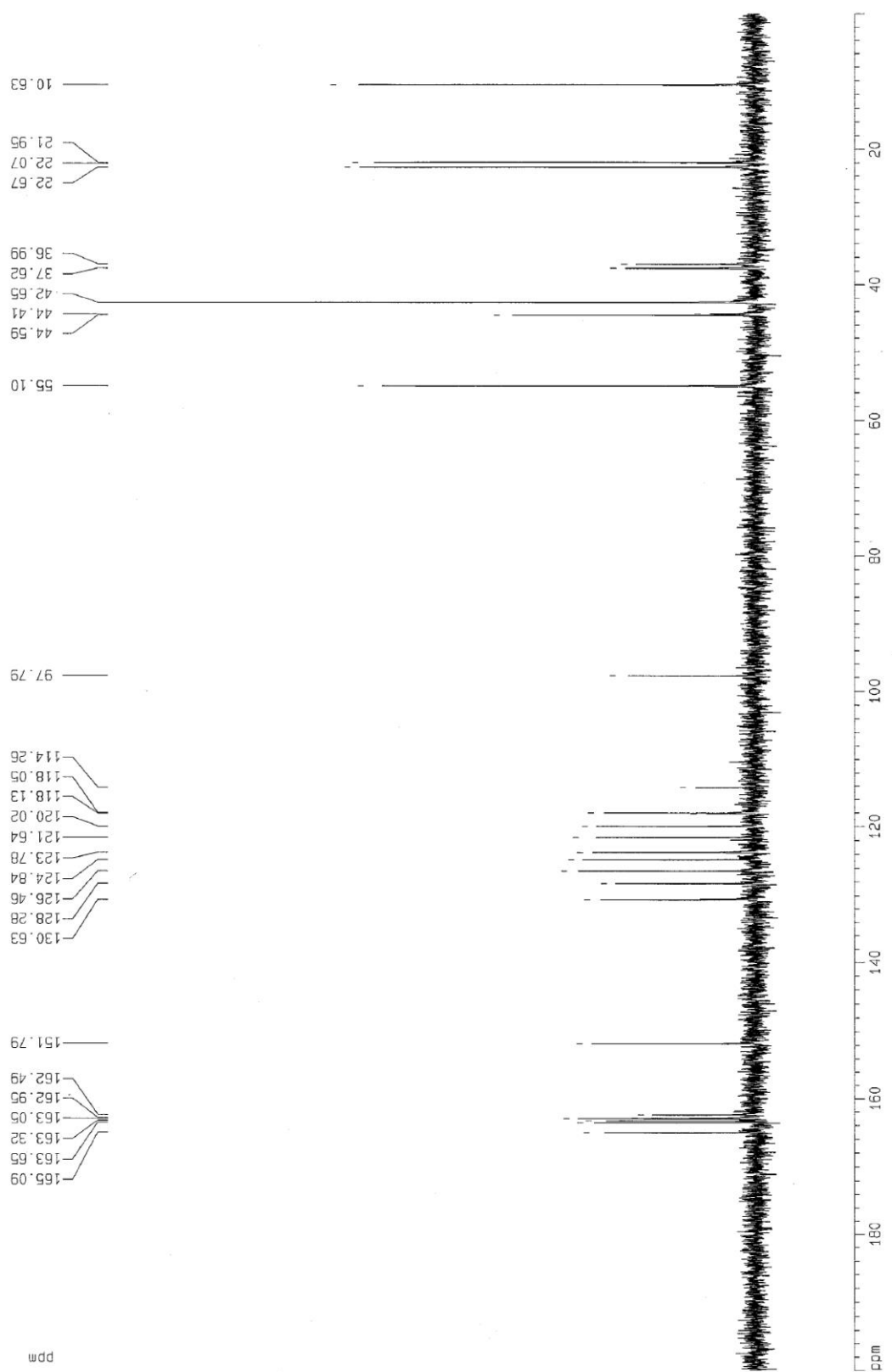
NDI-6 (D₂O) ¹³C NMR 75MHz



NDI-7 (D₂O) ¹H NMR 300MHz



NDI- 7 (D₂O) ¹³C NMR 75MHz



Supplementary References

- [1] S. Amrane, M. Adrian, B. Heddi, A. Serero, A. Nicolas, J.-L. Mergny, A. T. Phan, *J. Am. Chem. Soc.* **2012**, *134*, 5807-5816.
- [2] A. Ambrus, D. Chen, J. Dai, R. A. Jones, D. Yang, *Biochemistry* **2005**, *44*, 2048-2058.
- [3] A. T. Phan, V. Kuryavyi, H. Y. Gaw, D. J. Patel, *Nat. Chem. Biol.* **2005**, *1*, 167-173.
- [4] S. Amrane, R. W. L. Ang, Z. M. Tan, C. Li, J. K. C. Lim, J. M. W. Lim, K. W. Lim, A. T. Phan, *Nucleic Acids Res.* **2009**, *37*, 931-938.
- [5] K. W. Lim, P. Alberti, A. Guédin, L. Lacroix, J.-F. Riou, N. J. Royle, J.-L. Mergny, A. T. Phan, *Nucleic Acids Res.* **2009**, *37*, 6239-6248.
- [6] G. N. Parkinson, M. P. H. Lee, S. Neidle, *Nature* **2002**, *417*, 876-880.
- [7] B. Heddi, A. T. Phan, *J. Am. Chem. Soc.* **2011**, *133*, 9824-9833.
- [8] K. N. Luu, A. T. Phan, V. Kuryavyi, L. Lacroix, D. J. Patel, *J. Am. Chem. Soc.* **2006**, *128*, 9963-9970.
- [9] A. T. Phan, V. Kuryavyi, K. N. Luu, D. J. Patel, *Nucleic Acids Res.* **2007**, *35*, 6517-6525.
- [10] K. W. Lim, S. Amrane, S. Bouaziz, W. Xu, Y. Mu, D. J. Patel, K. N. Luu, A. T. Phan, *J. Am. Chem. Soc.* **2009**, *131*, 4301-4309.
- [11] Y. Wang, D. J. Patel, *Structure* **1993**, *1*, 263-282.
- [12] K. W. Lim, V. C. M. Ng, N. Martín-Pintado, B. Heddi, A. T. Phan, *Nucleic Acids Res.* **2013**, *41*, 10556-10562.
- [13] F. Doria, I. Manet, V. Grande, S. Monti, M. Freccero, *J. Org. Chem.* **2013**, *78*, 8065-8073.

Annex 2: Supplementary material of *J. Med. Chem.* 2018

G-quadruplex identification in the genome of protozoan parasites points to naphthalene diimide ligands as new antiparasitic agents

Efres Belmonte-Reche,[†] Marta Martínez-García,[†] Aurore Guédin,[‡] Michela Zuffo,^{||} Matilde Arévalo-Ruiz,[†] Filippo Doria,^{||} Jenny Campos-Salinas,[†] Marjorie Maynadier,[⊥] José Juan López-Rubio,[#] Mauro Freccero,^{||} Jean-Louis Mergny,^{‡,⊥} José María Pérez-Victoria,^{†,*} and Juan Carlos Morales^{†,*}

Contents.

Table S1. DNA sequences used in the present study.	S2
Table S2. PQS density found per chromosome of each parasite examined	S2
Figure S1. CD spectra of EBR1 in the absence and presence of different concentrations of Na ⁺ .	S3
Figure S2. CD experiments with EBR1mut sequence.	S3
Figure S3. Imino region of NMR spectra for EBR1 at different temperatures	S4
Figure S4. Characterization of EBR1-FT sequence. a) CD spectra in the absence and presence of different concentrations of K ⁺ . b) UV-monitored thermal denaturation experiment.	S5
Figure S5. FRET-melting stabilization induced by compounds 6 and 7 on EBR1-FT G-quadruplex	S6
Figure S6. Absorption and emission spectra of 6 and 7 in water.	S7
Figure S7. Zebra fish embryo graphs concentration-mortality response	S8

Table S1. DNA sequences used in the present study.

Short Name	Description	Sequence
EBR1	<i>T. brucei</i> genome	GGGCAGGGGGTGATGGGGAGGAGCCAGGG
EBR1-mut	--	AGGCATTAGGTGATAAAGAGTAGCCATGG
EBR1-FT	<i>T. brucei</i> genome	FAM-GGGCAGGGGGTGATGGGGAGGAGCCAGGG-Tamra

Table S2. PQS density found per chromosome of each parasite examined

<i>Leishmania major</i>			<i>Trypanosoma brucei</i>		
Chrom.	Hits	Density (□)	Chrom.	Hits	Density (□)
1	39	1,45	1	24	0,23
2	51	1,43	2	15	0,13
3	68	1,77	3	18	0,11
4	117	2,47	4	20	0,12
5	56	1,20	5	24	0,15
6	48	0,93	6	20	0,11
7	60	1,01	7	31	0,14
8	63	1,10	8	28	0,11
9	79	1,38	9	75	0,21
10	106	1,86	10	73	0,18
11	48	0,82	11	105	0,19
12	103	1,53			
13	137	2,10			
14	106	1,70			
15	99	1,57			
16	112	1,57			
17	179	2,61			
18	98	1,32			
19	33	0,47			
20	88	1,19			
21	122	1,58			
22	98	1,37			
23	97	1,26			
24	110	1,31			
25	173	1,90			
26	110	1,01			
27	101	0,89			
28	141	1,22			
29	121	1,00			
30	183	1,30			
31	225	1,52			
32	126	0,79			
33	144	0,91			
34	412	2,21			
35	314	1,50			
36	552	2,06			

<i>Plasmodium falciparum</i>		
Chrom.	Hits	Density (□)
1	13	0,20
2	19	0,20
3	144	1,35
4	21	0,17
5	16	0,12
6	42	0,30
7	16	0,11
8	23	0,16
9	23	0,15
10	26	0,15
11	35	0,17
12	5	0,02
13	70	0,24
14	13	0,04

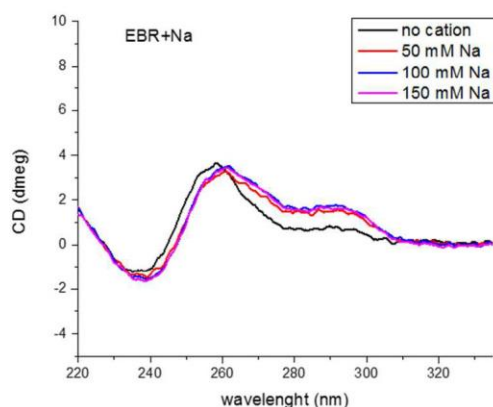
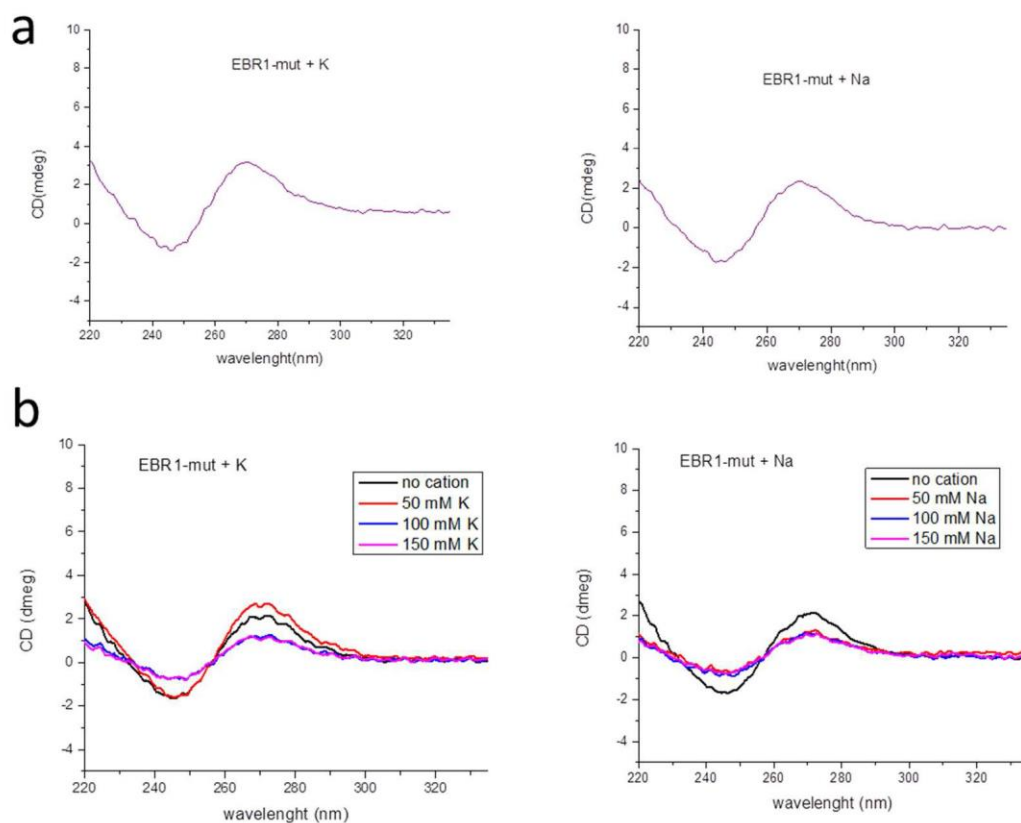
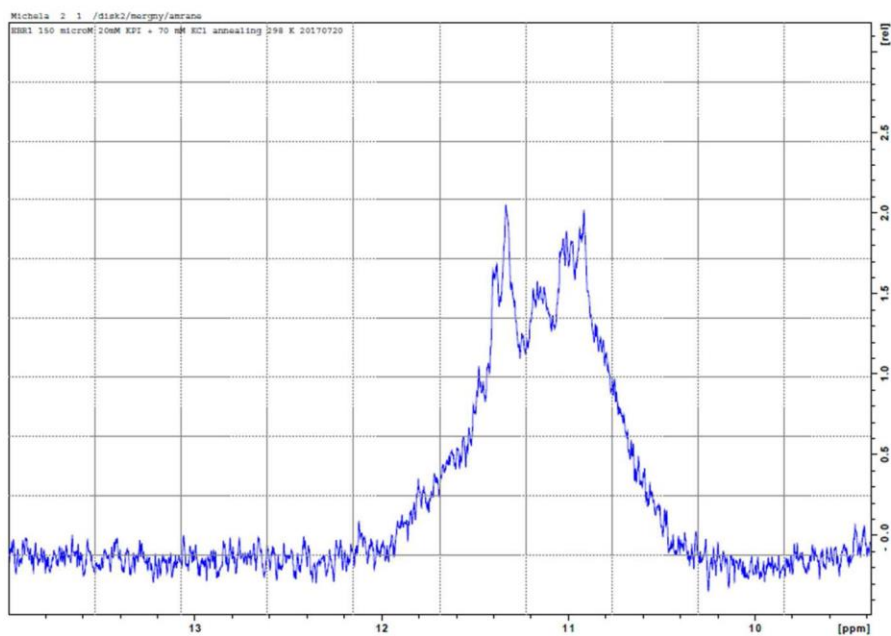
Figure S1. CD spectra of EBR1 in the absence and presence of different concentrations of Na⁺.**Figure S2.** CD experiments with EBR1-mut sequence (4 μM). a) CD spectra in 10 mM LiCaco pH 7.4 buffer supplemented with 100 mM KCl or NaCl. b) Titration experiments with increasing amounts of K⁺ or Na⁺ salts.

Figure S3. Imino region of NMR spectra for EBR1 (150 μ M) in 20 mM phosphate buffer 70 mM KCl, 10% deuterated water at different temperatures: a) 25 $^{\circ}$ C and b) 60 $^{\circ}$ C.

a)



b)

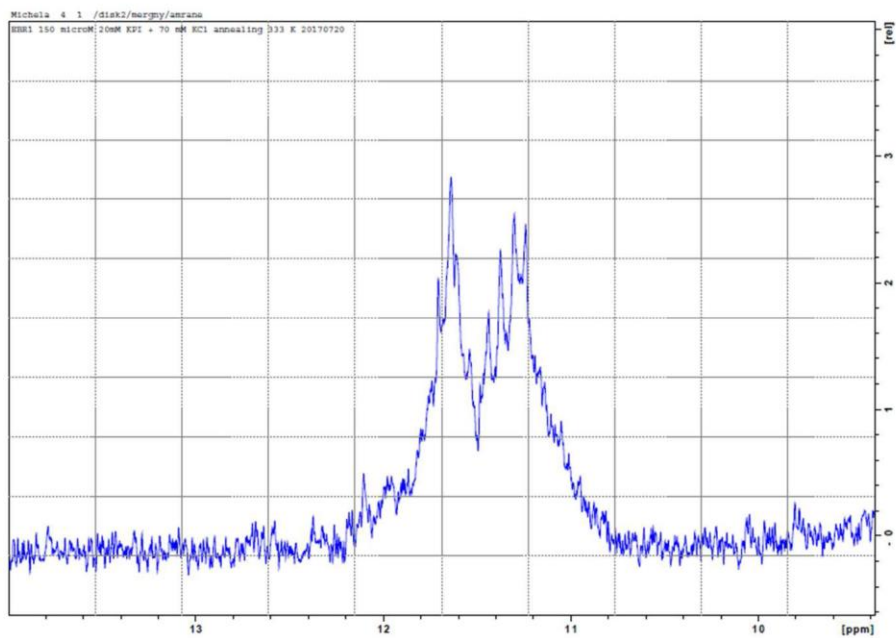


Figure S4. Characterization of EBR1-FT sequence at 4 μM . a) CD spectra in the absence and presence of different concentrations of K^+ . b) UV-monitored thermal denaturation experiment (100 mM KCl).

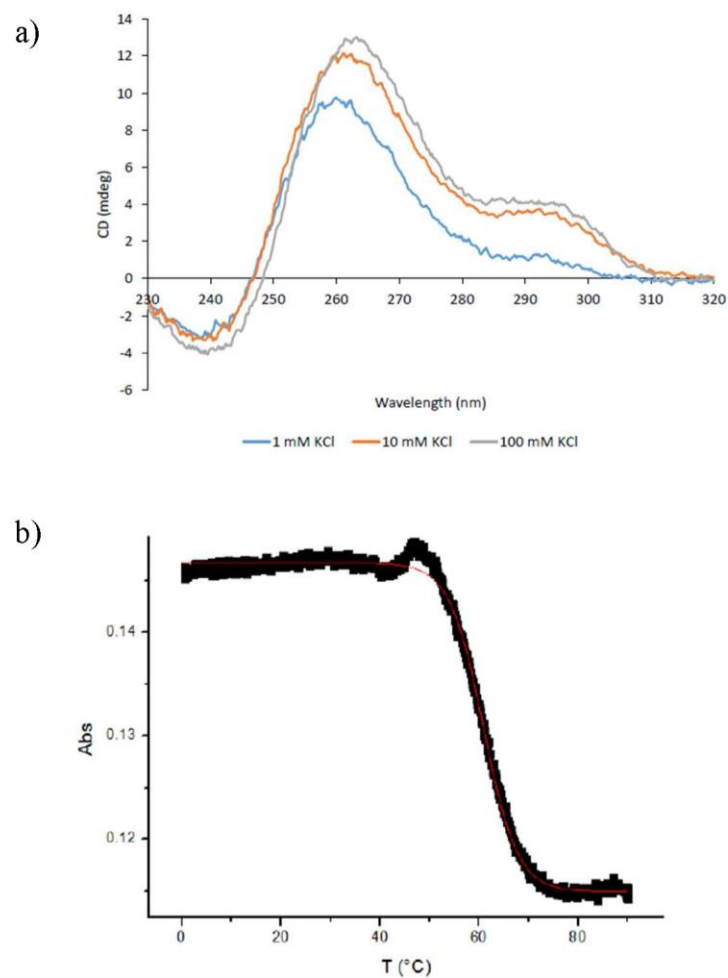


Figure S5. FRET-melting stabilization induced by compounds **6** (A, C) and **7** (B, D) at different concentrations (0.5, 1 and 2 μM) on EBR1-FT G-quadruplex (0.2 μM) in 10 mM lithium cacodylate pH 7.2 containing 10 mM KCl and 90 mM LiCl (A, B) or 50 mM KCl and 50 mM LiCl (C, D).

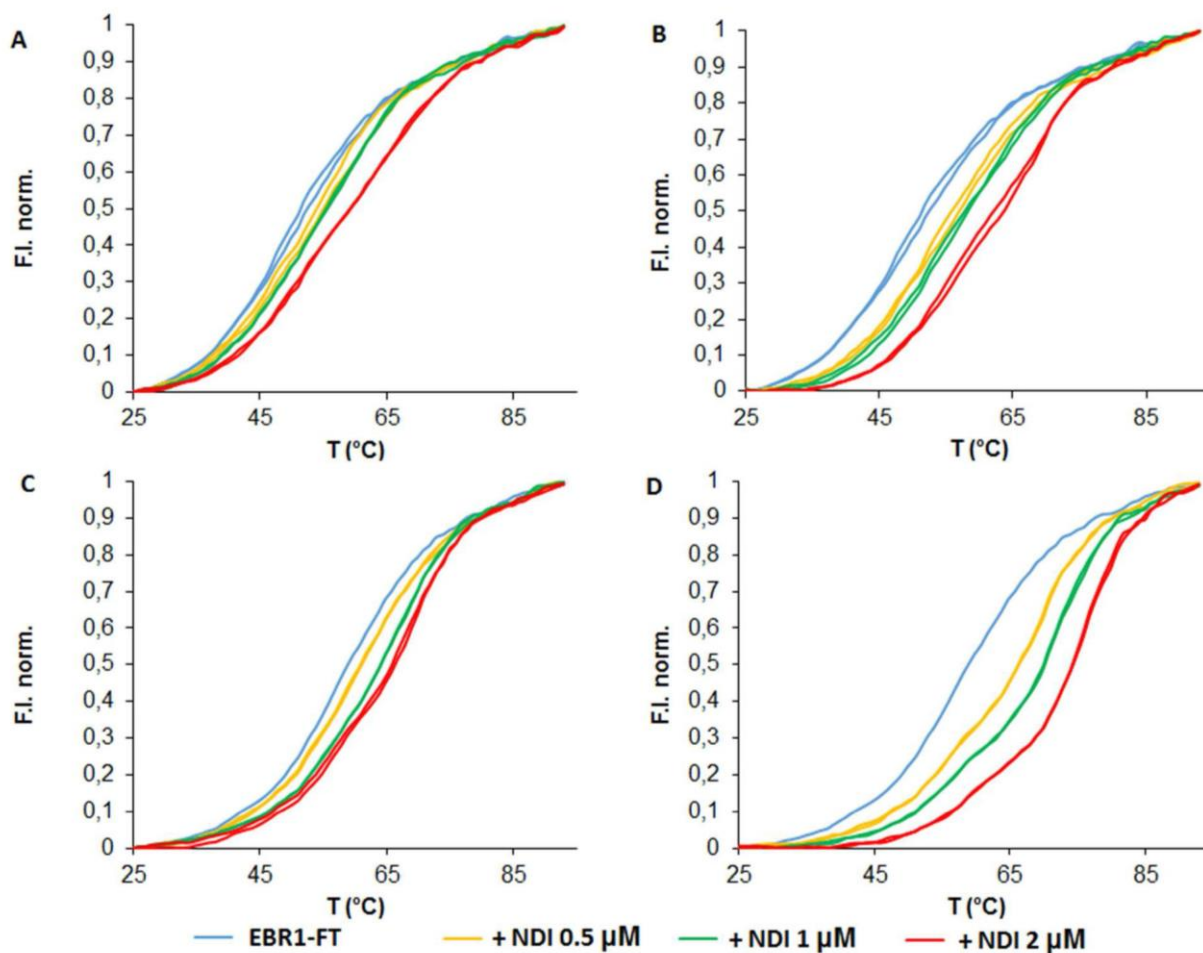
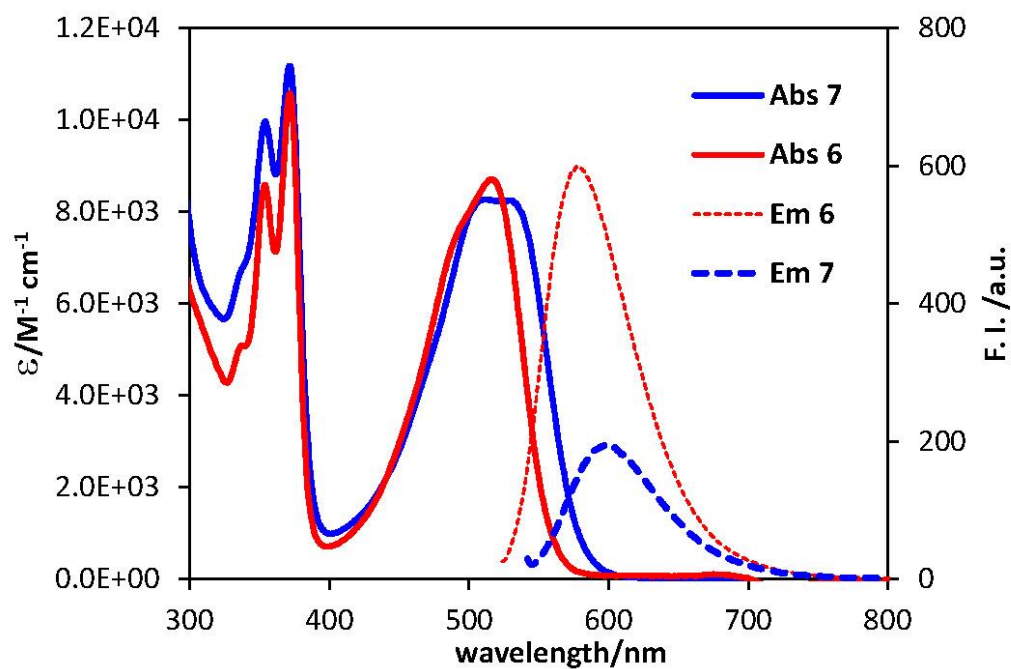
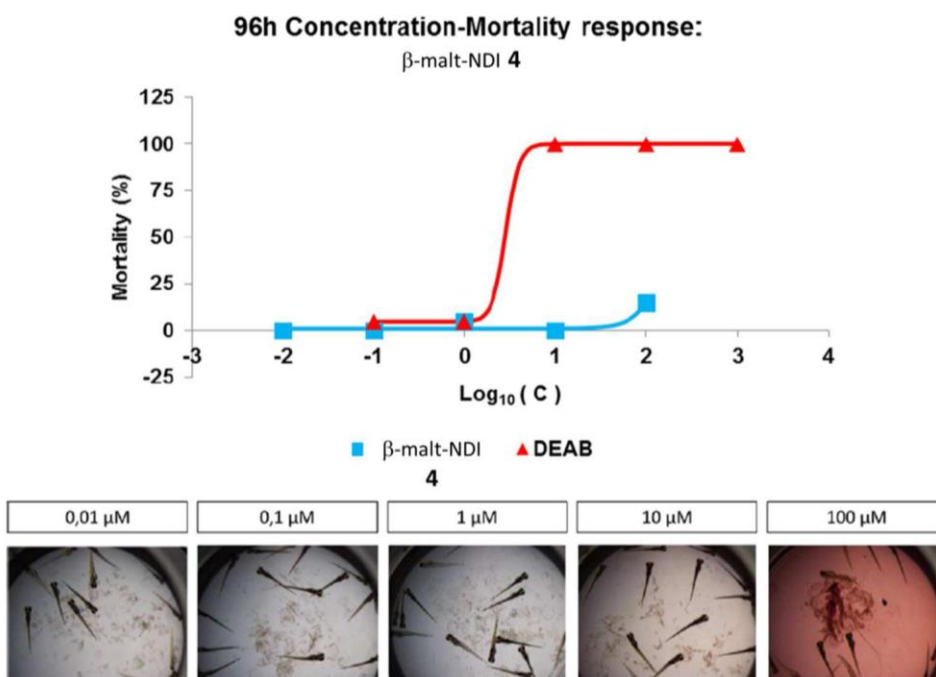
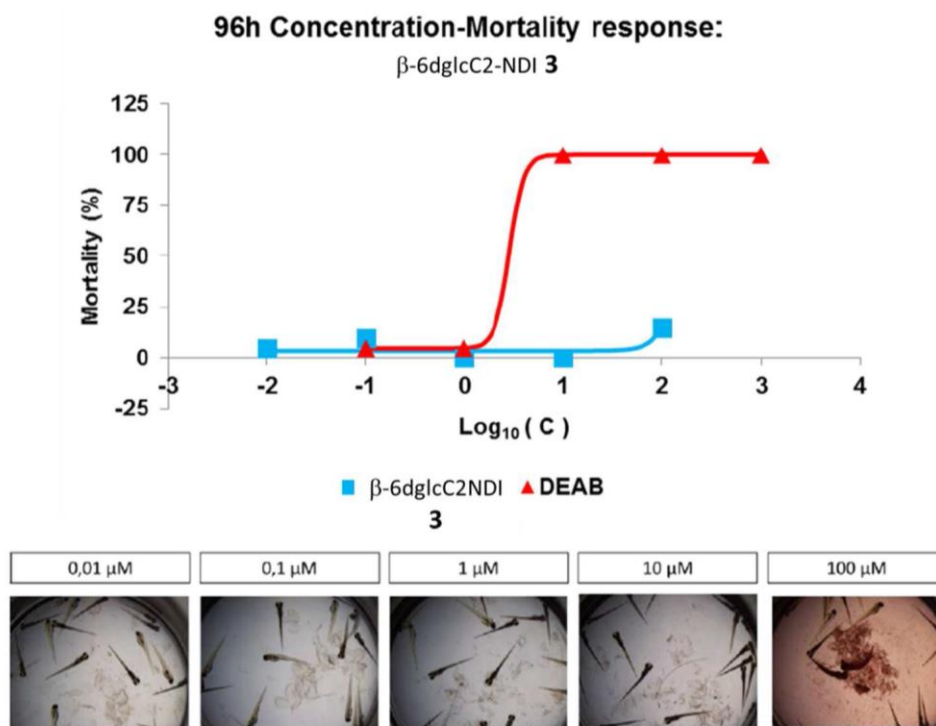
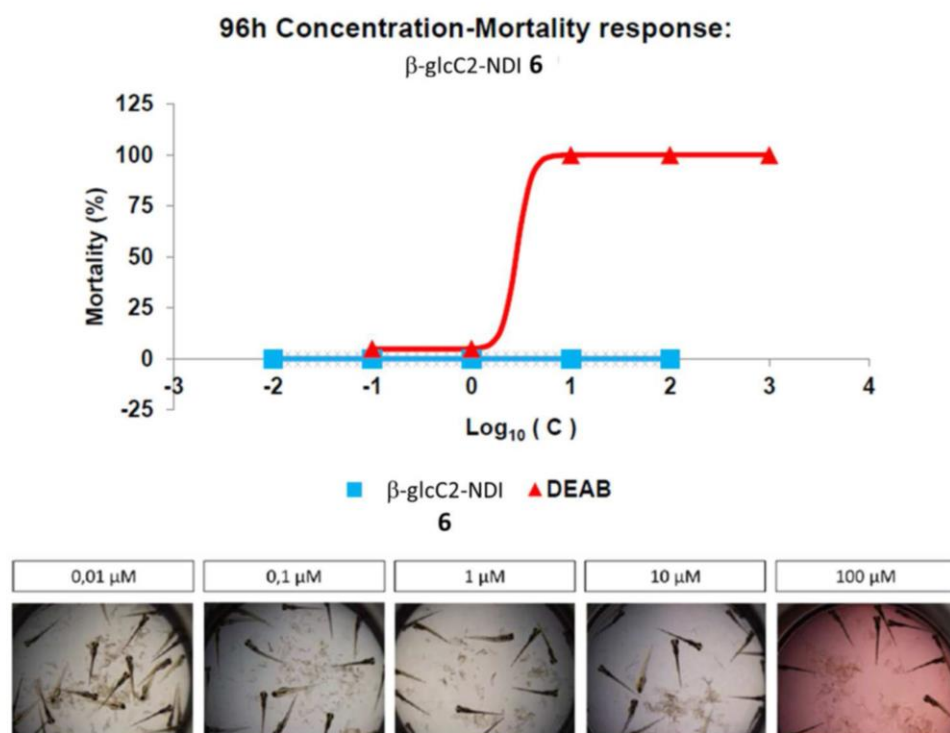
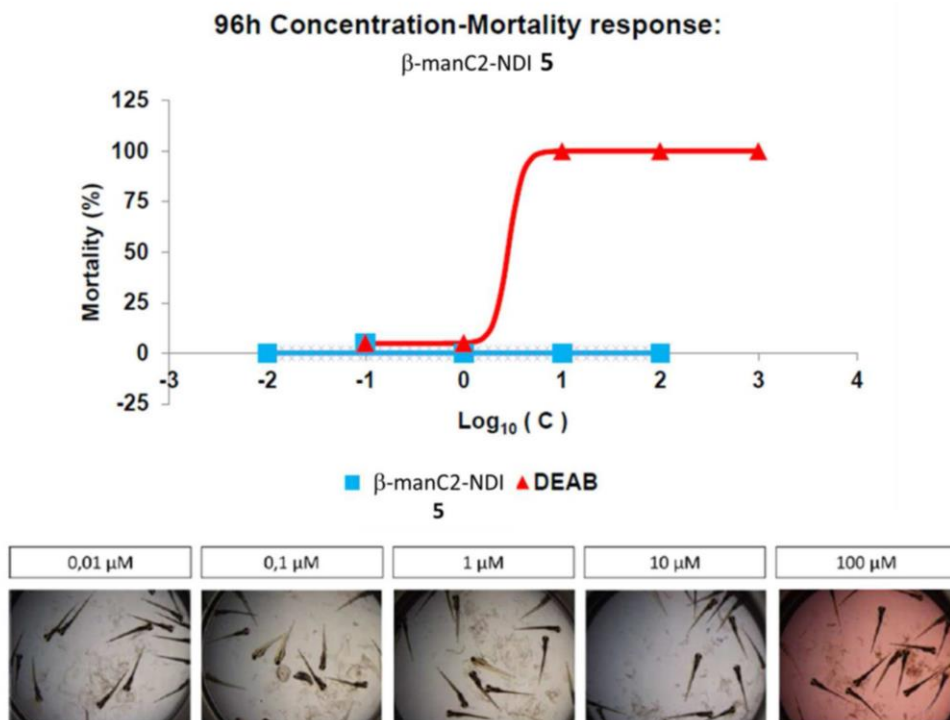
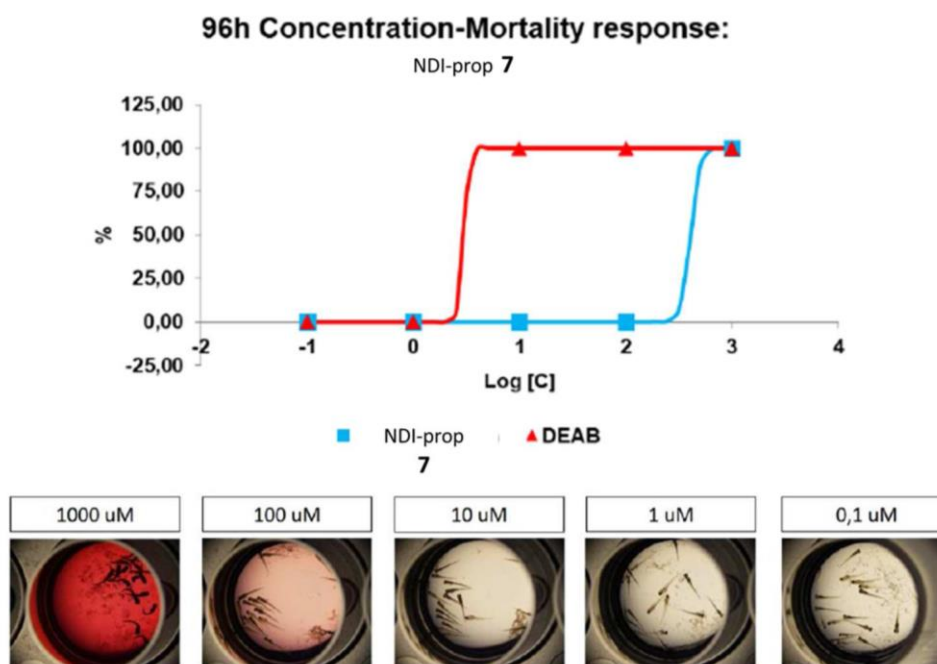


Figure S6. Absorption (continuous lines) and emission (dashed lines, $\lambda_{\text{exc}} = 500$ nm) spectra of 5×10^{-6} M solutions of **6** ($\lambda_{\text{exc}} = 517$ nm) and **7** ($\lambda_{\text{exc}} = 538$ nm) in water (pH 7.4, Tris-HCl buffer 1×10^{-3} M).









Annex 3: Supplementary material of *E. J. Med. Chem.* 2016

Tyrosol and hydroxytyrosol derivatives as antitrypanosomal and antileishmanial agents

Efres Belmonte-Reche, Marta Martínez-García, Pablo Peñalver, Verónica Gómez-Pérez, Ricardo Lucas, Francisco Gamarro, José María Pérez-Victoria*, Juan Carlos Morales*

Table of contents

Figures 1-10. ^1H - and ^{13}C -NMR spectra for compounds **21**, **22**, **24**, **27**, **30-33**, **37** and **38**.

Figure 1. $^1\text{H-NMR}$ and $^{13}\text{C-NMR}$ spectra for compound 21

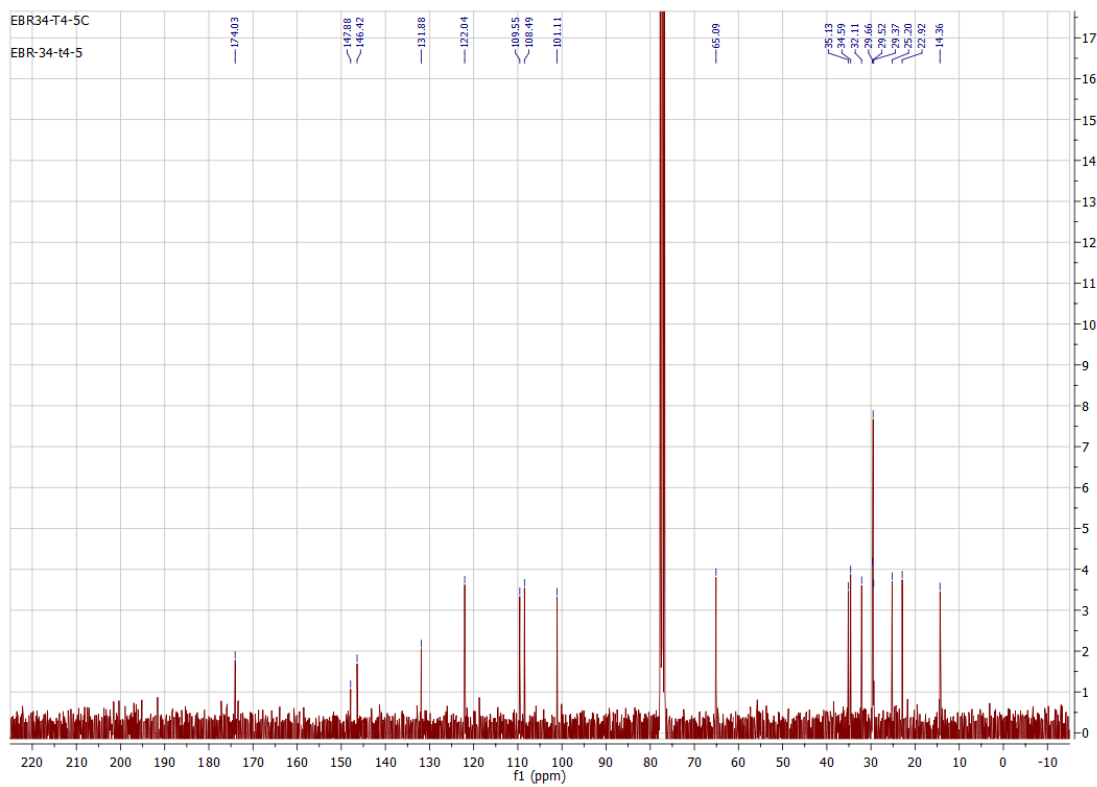
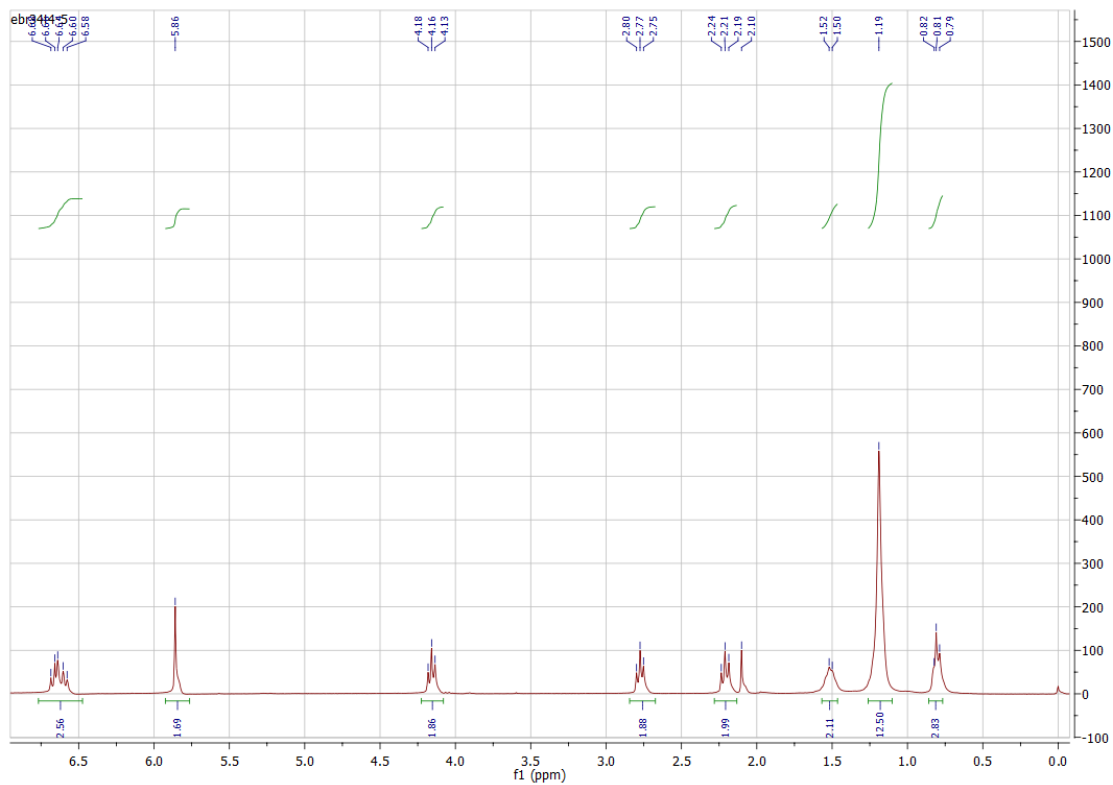
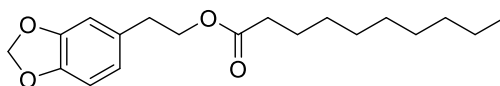


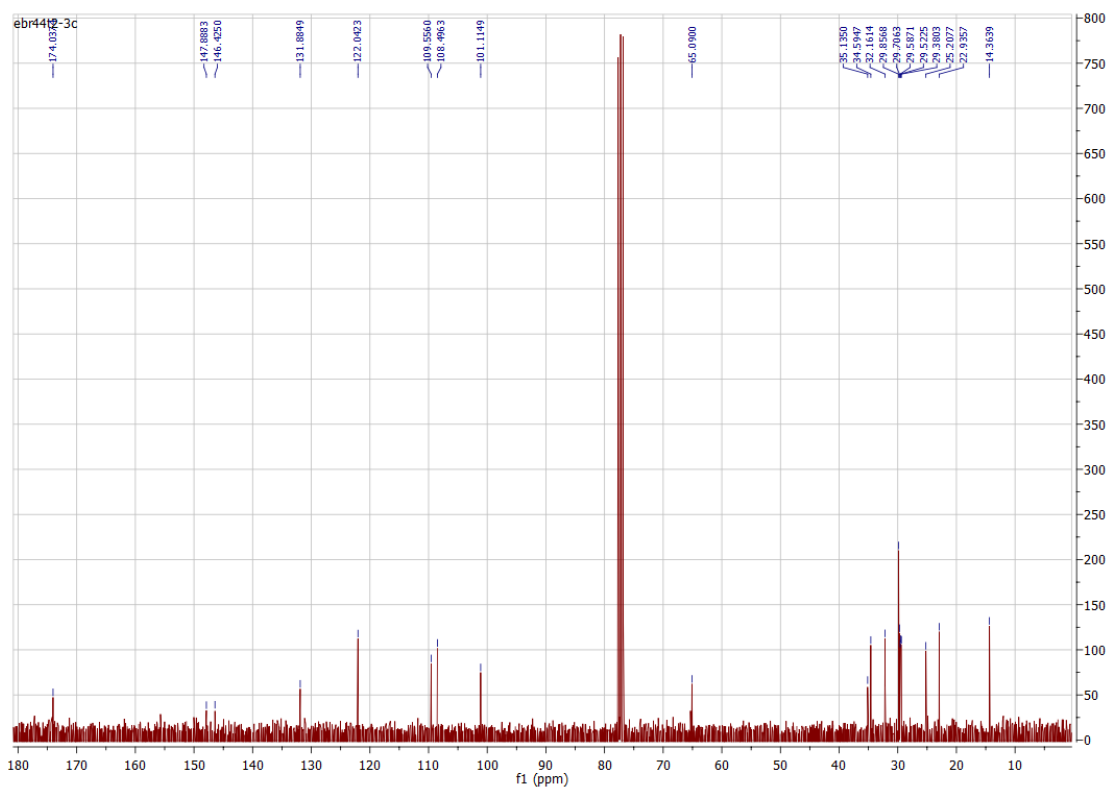
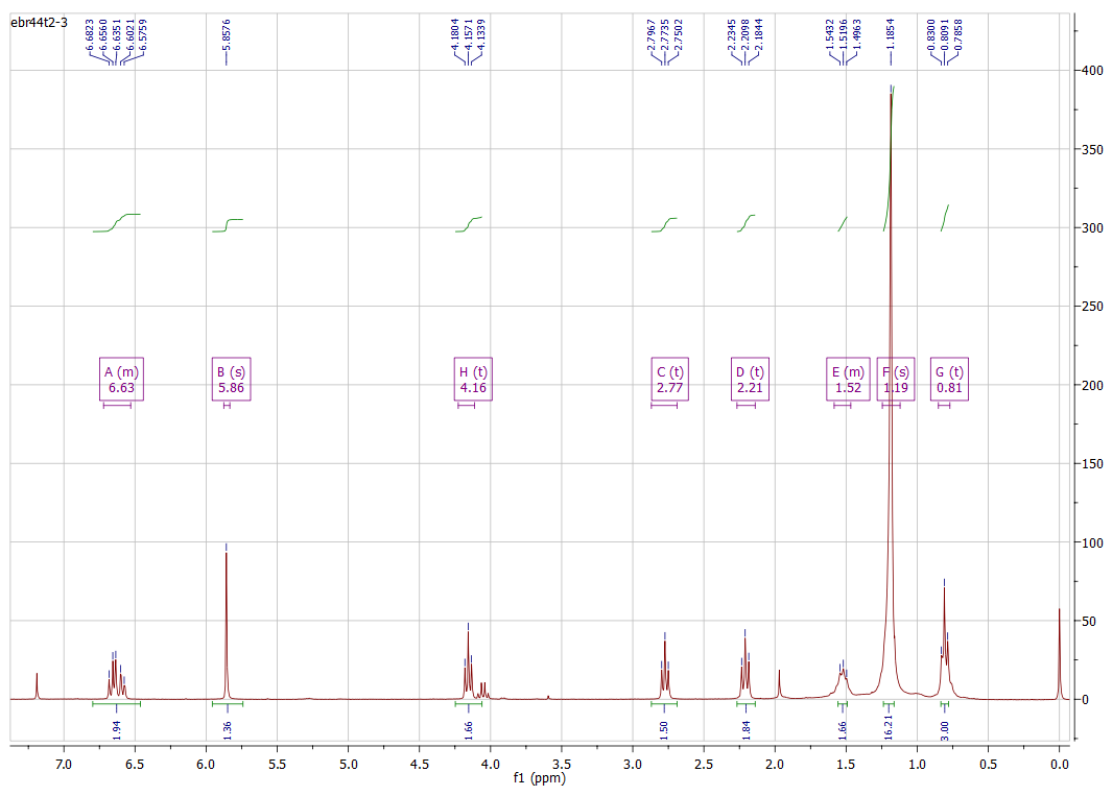
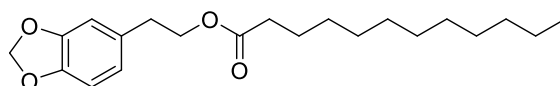
Figure 2. ^1H -NMR and ^{13}C -NMR spectra for compound **22**

Figure 3. ¹H-NMR and ¹³C-NMR spectra for compound 24

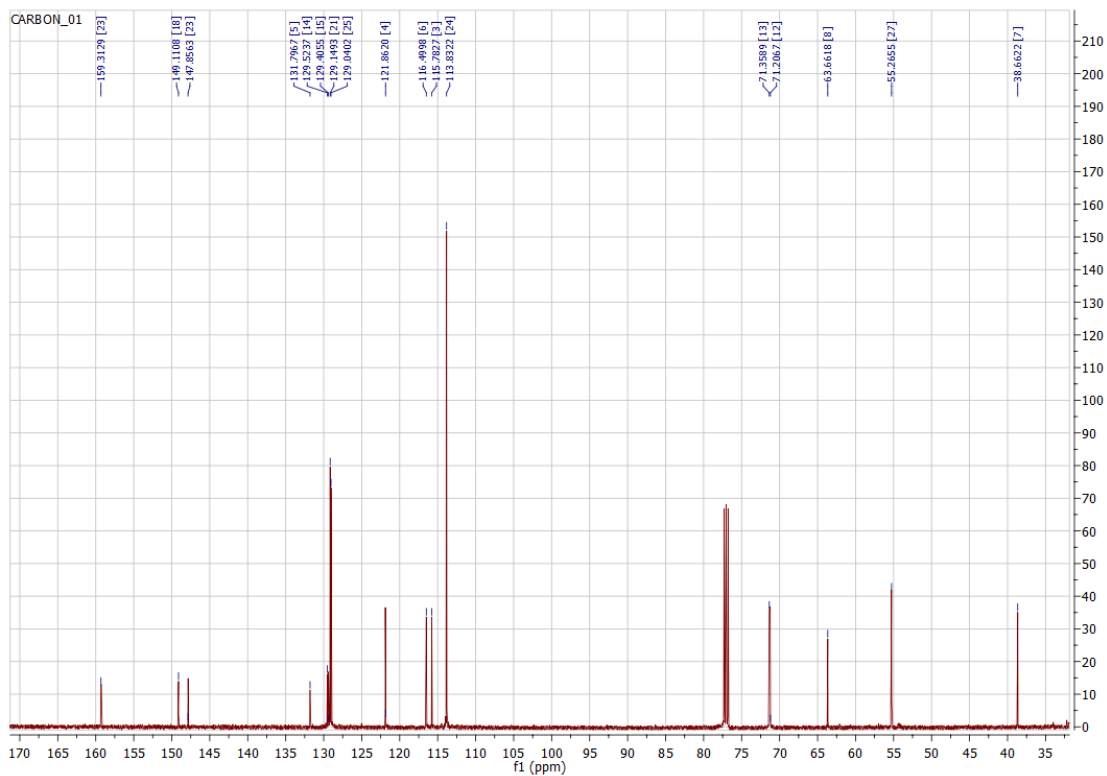
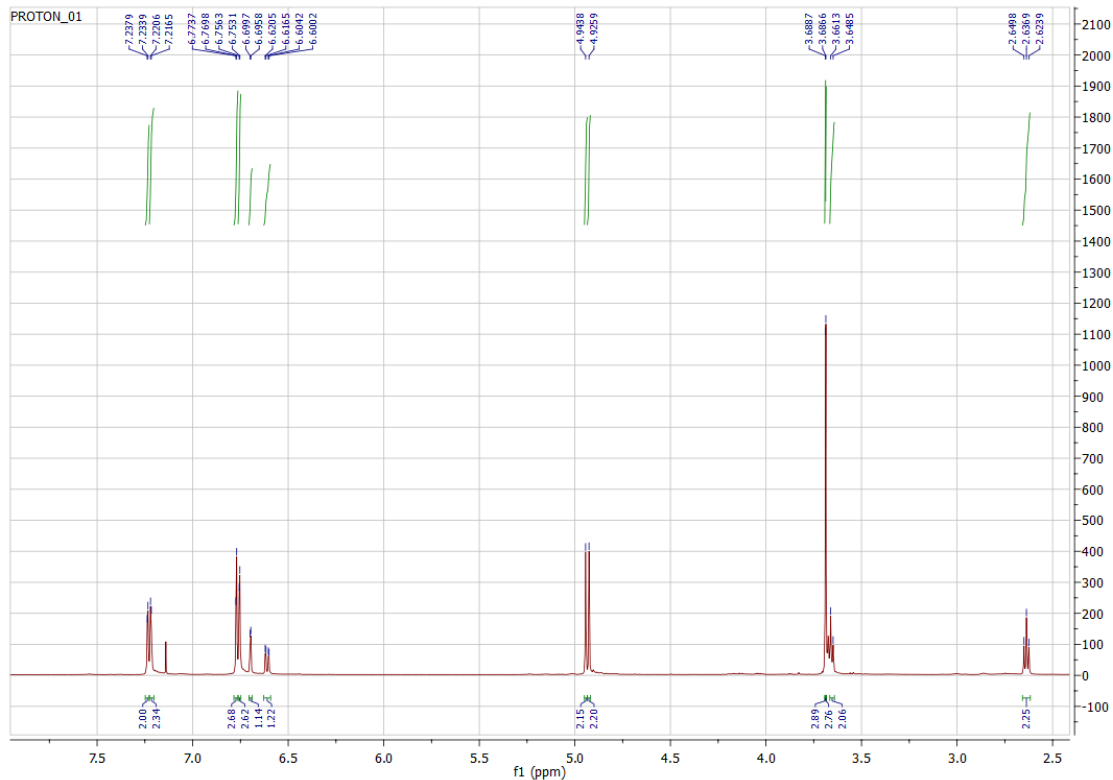
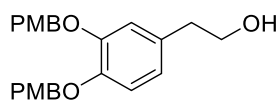


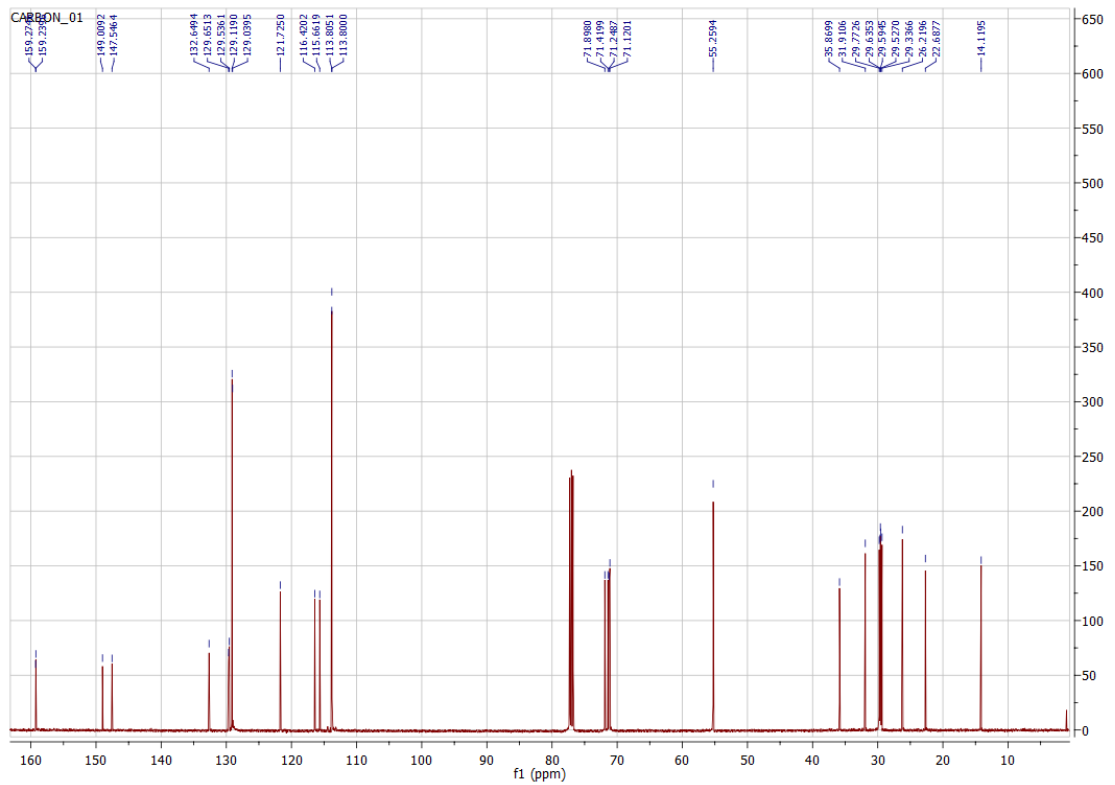
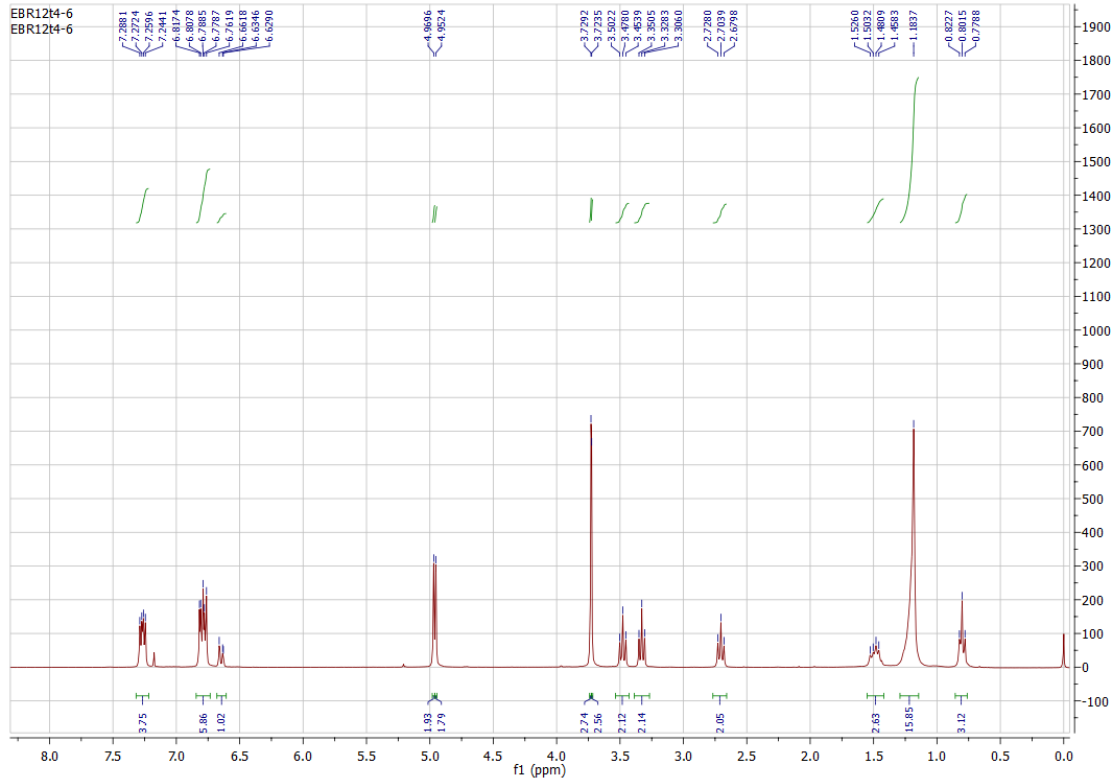
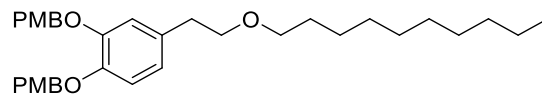
Figure 4. $^1\text{H-NMR}$ and $^{13}\text{C-NMR}$ spectra for compound **27**

Figure 5. ¹H-NMR and ¹³C-NMR spectra for compound 30

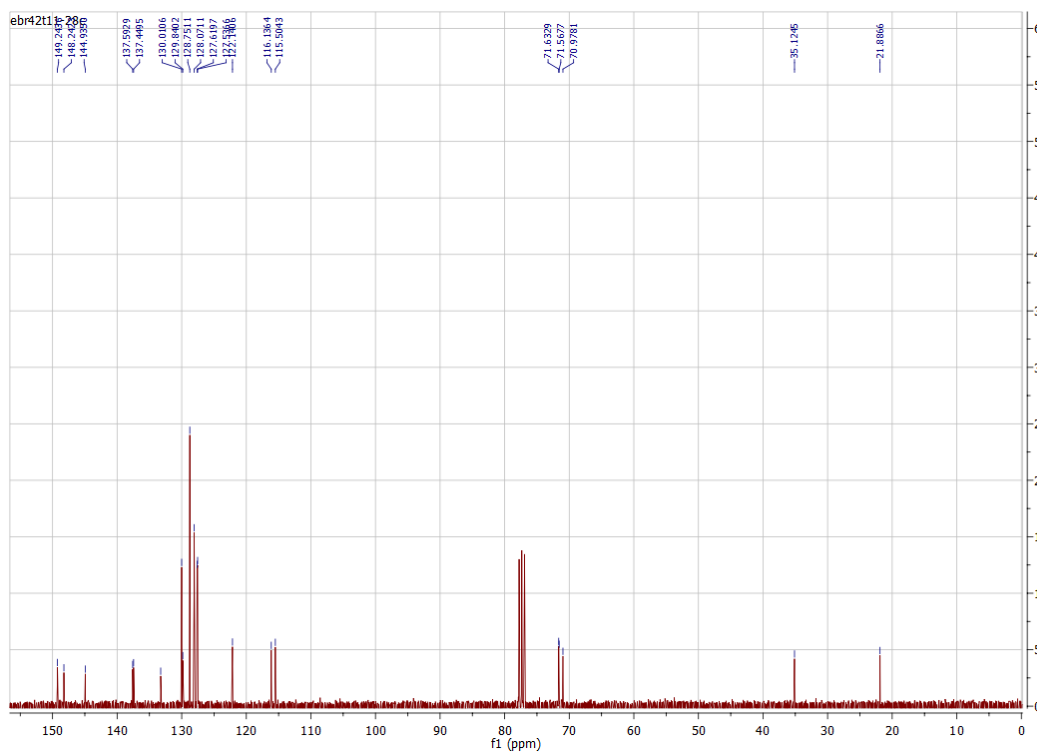
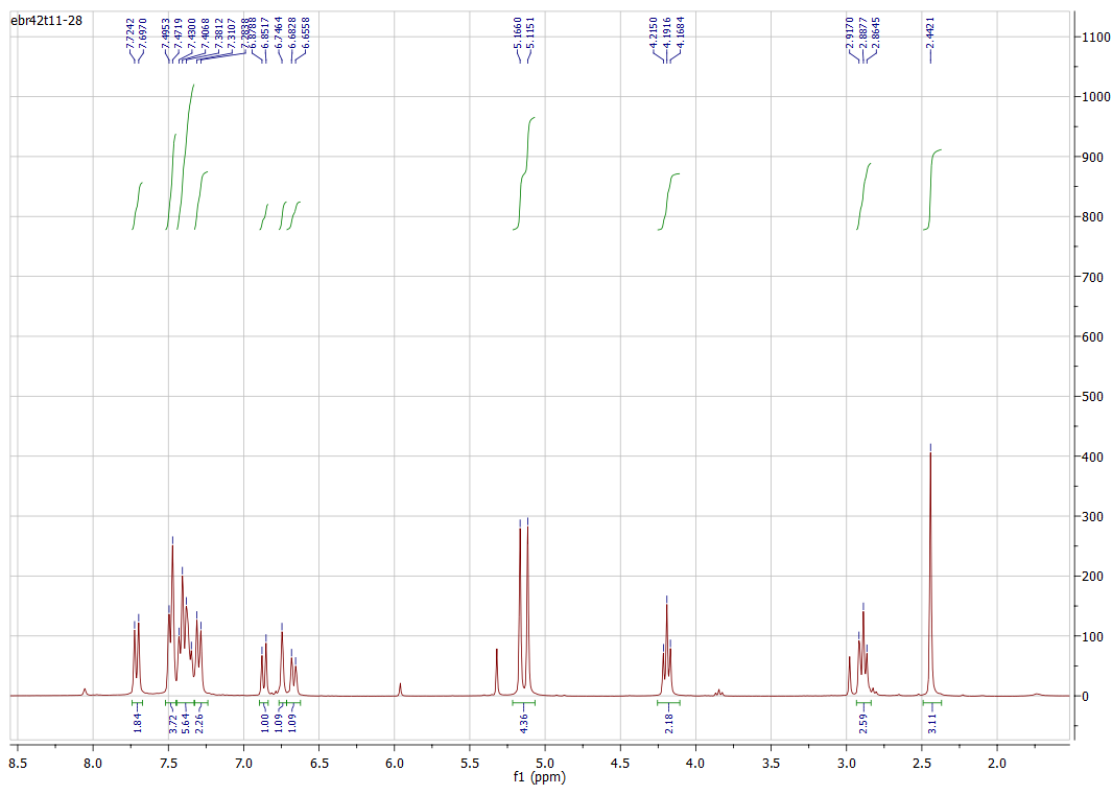
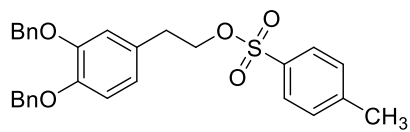


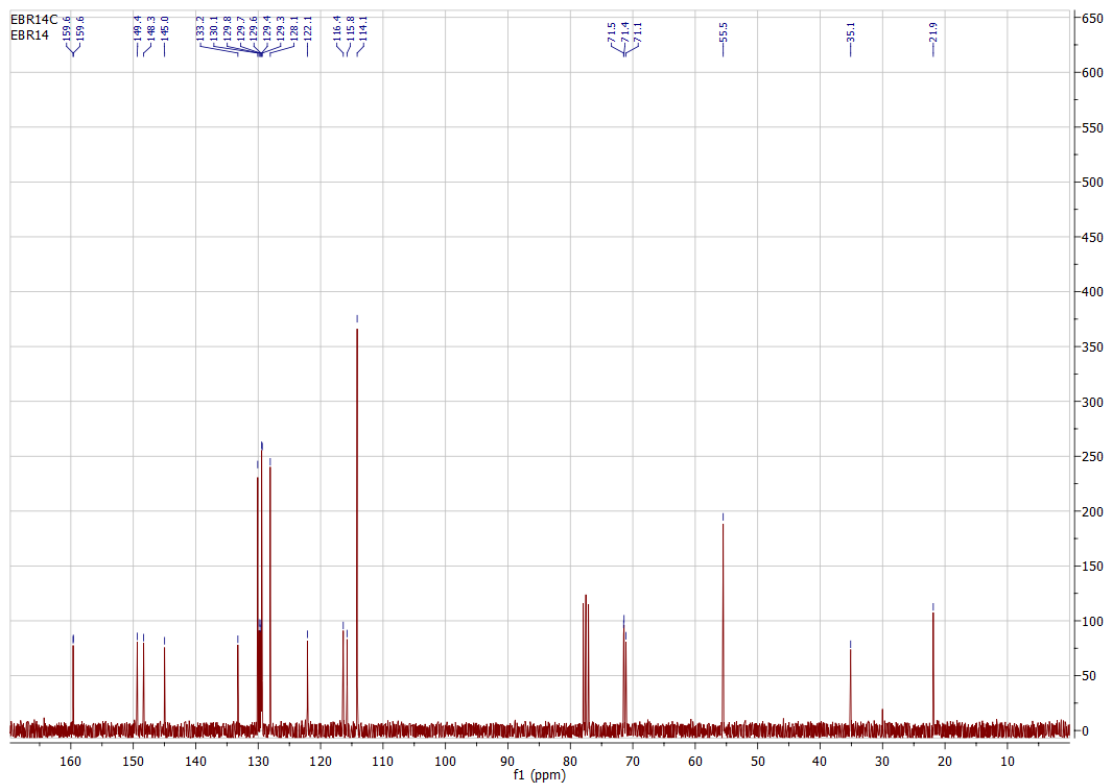
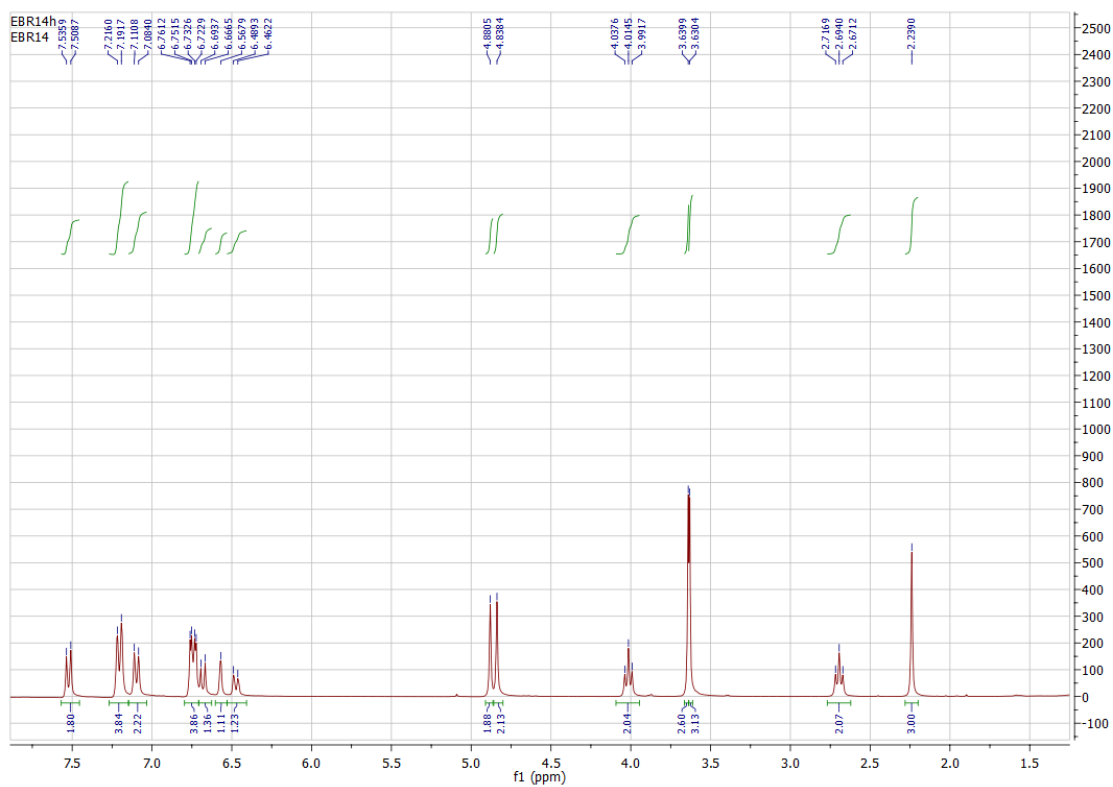
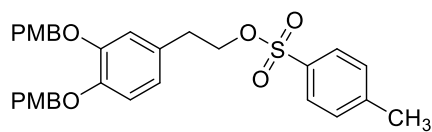
Figure 6. $^1\text{H-NMR}$ and $^{13}\text{C-NMR}$ spectra for compound **31**

Figure 7. ¹H-NMR and ¹³C-NMR spectra for compound 32

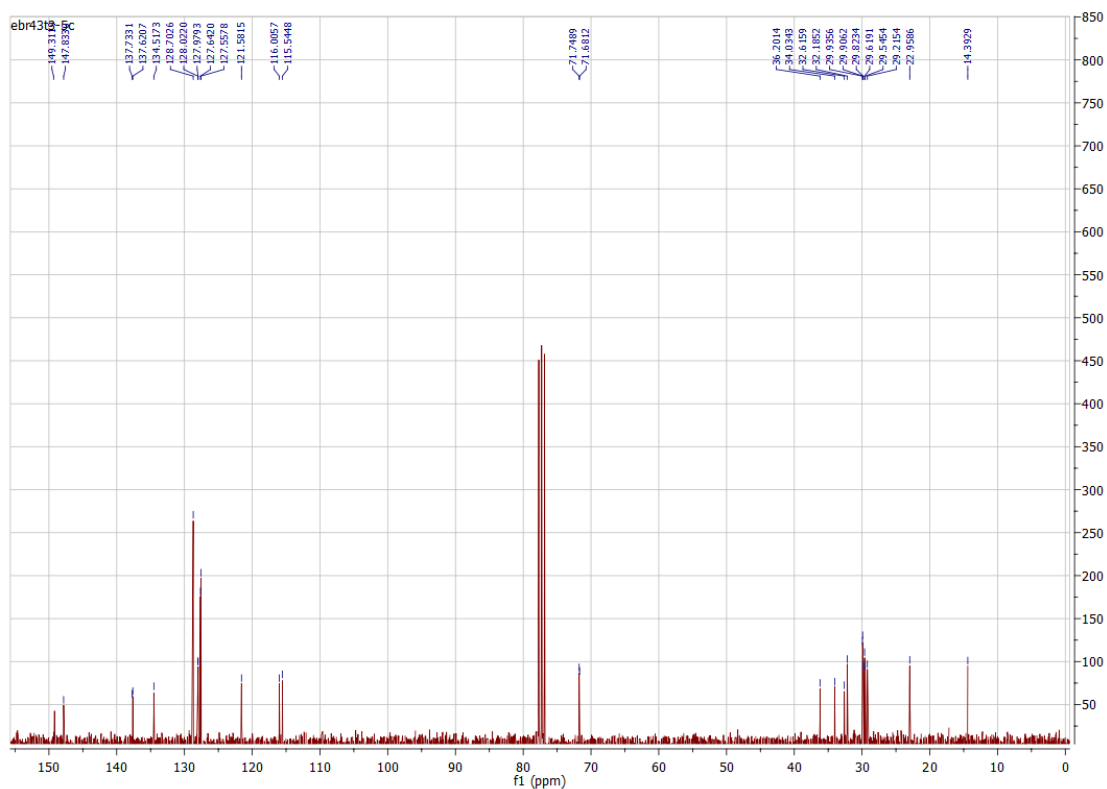
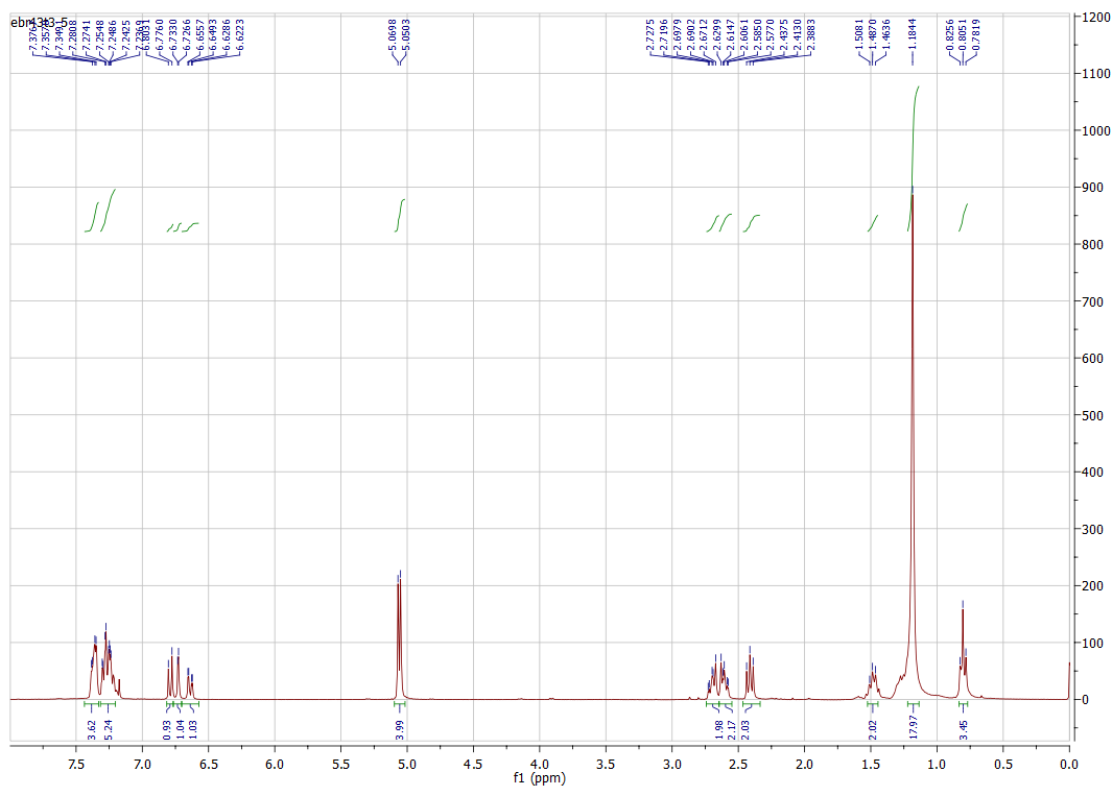
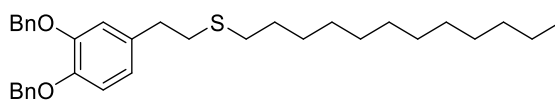


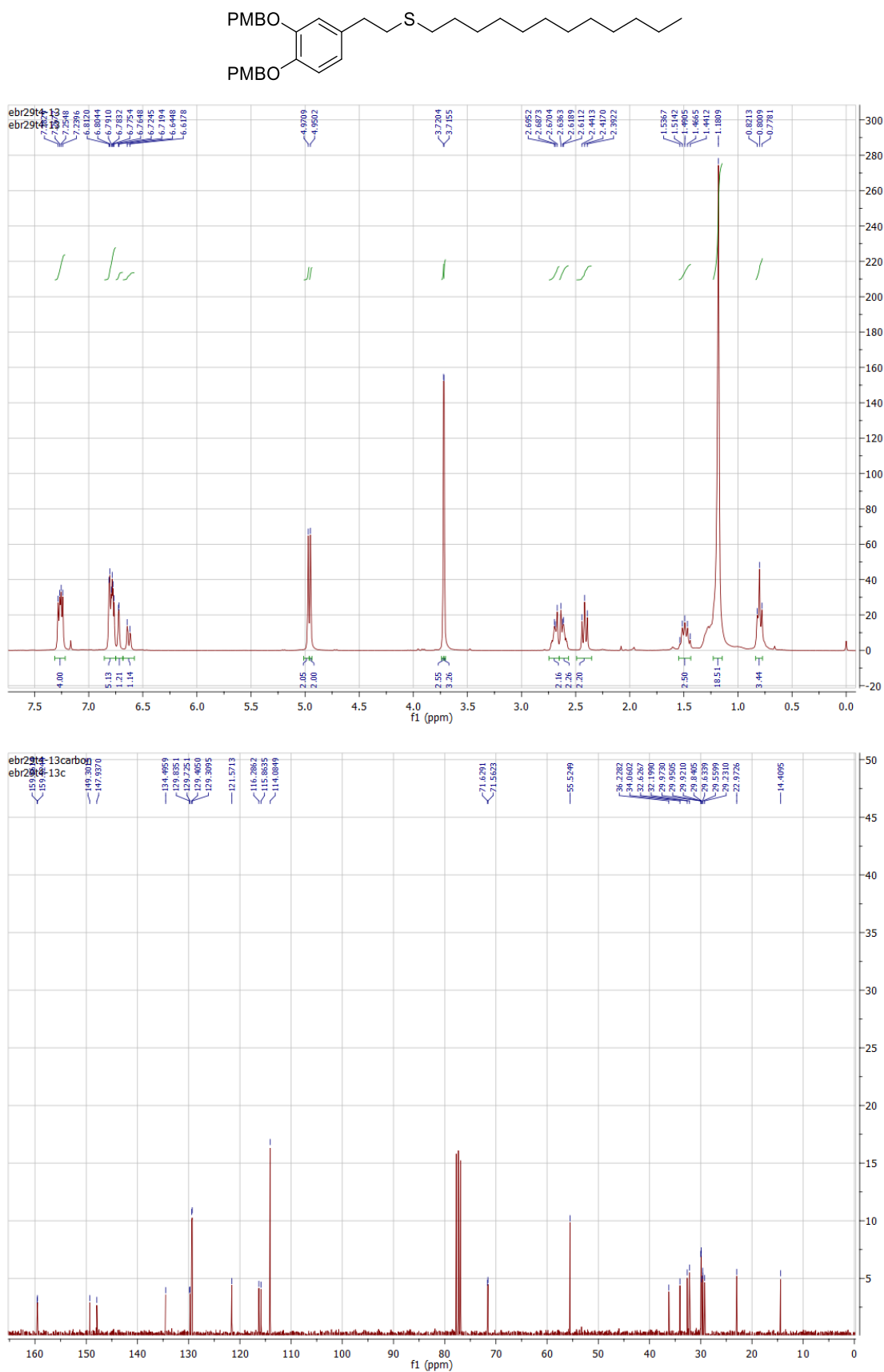
Figure 8. $^1\text{H-NMR}$ and $^{13}\text{C-NMR}$ spectra for compound 33

Figure 9. ¹H-NMR and ¹³C-NMR spectra for compound 37

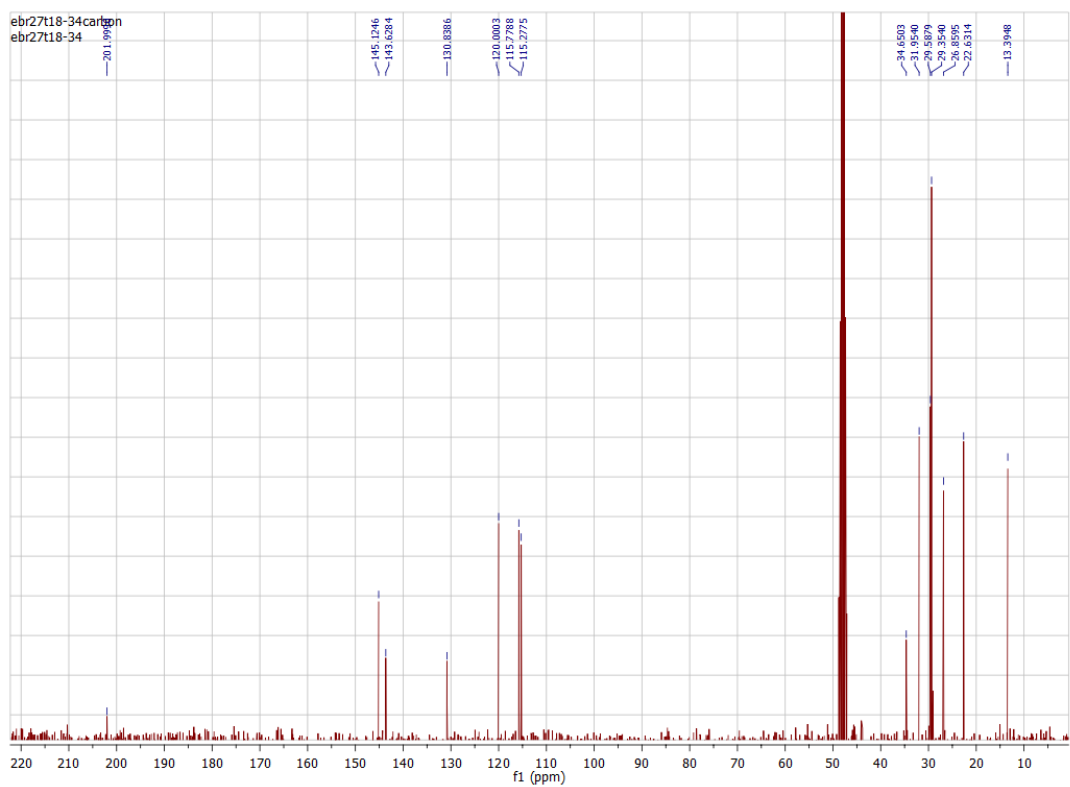
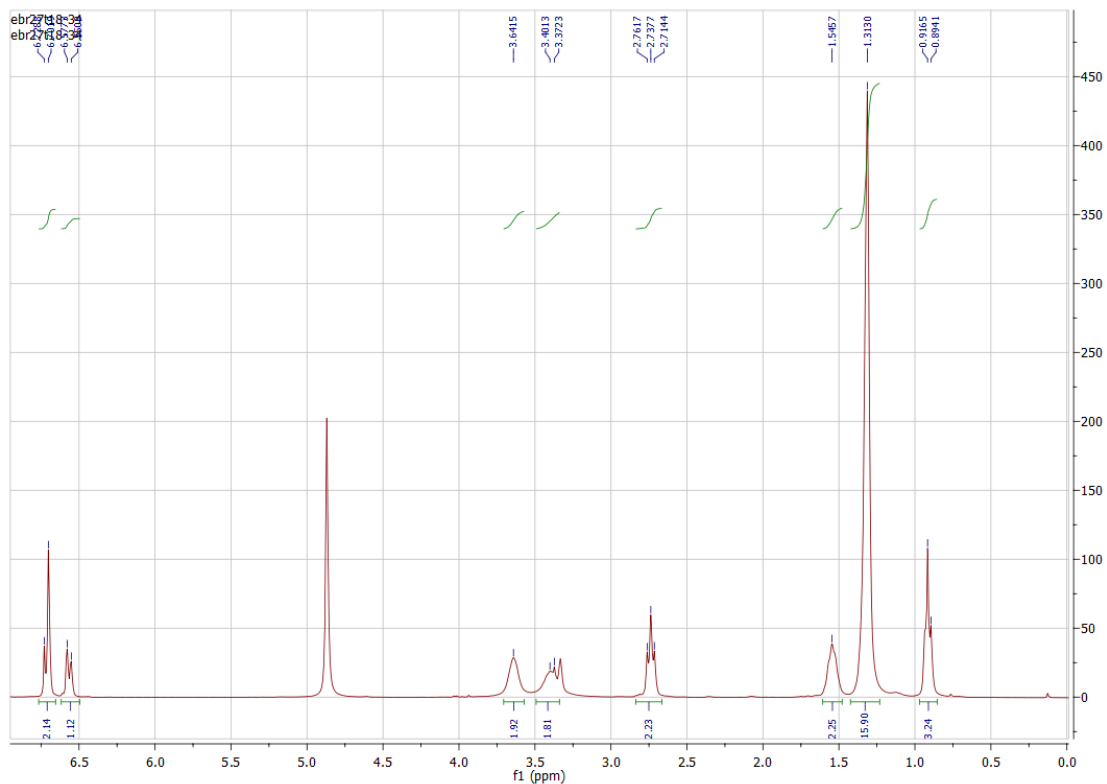
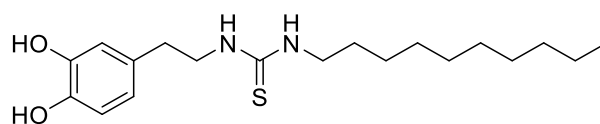
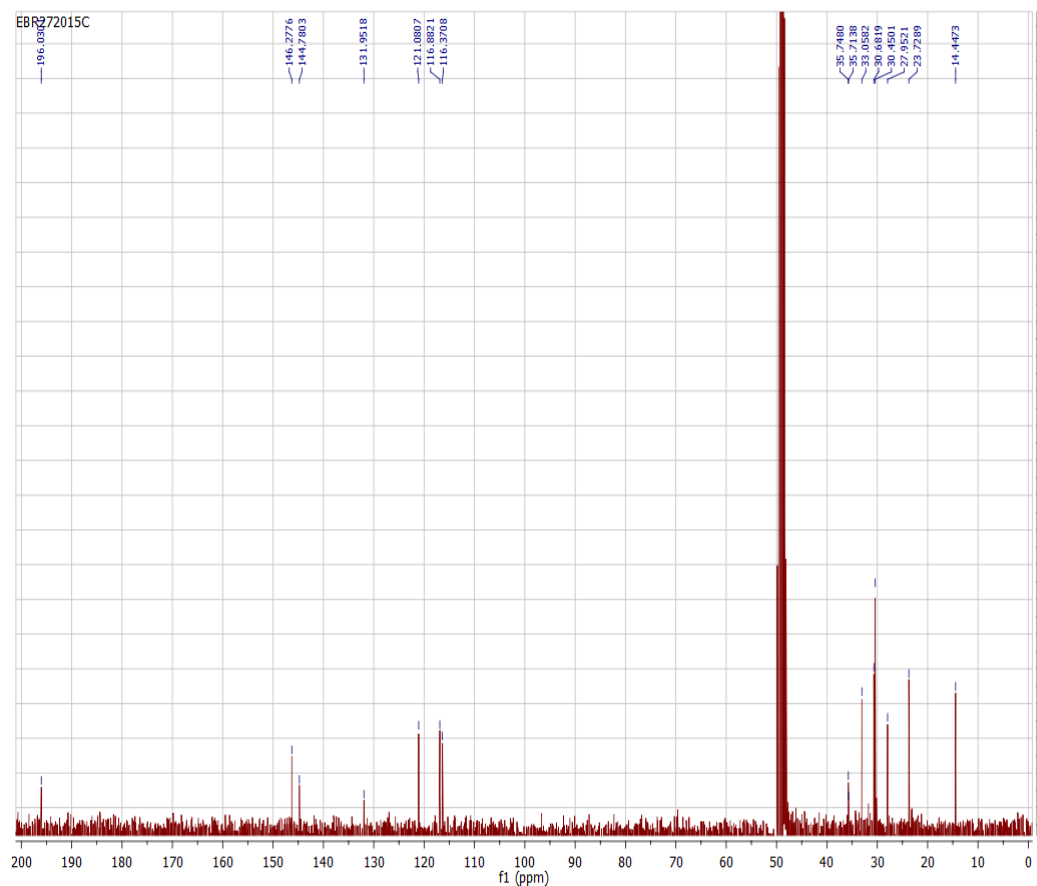
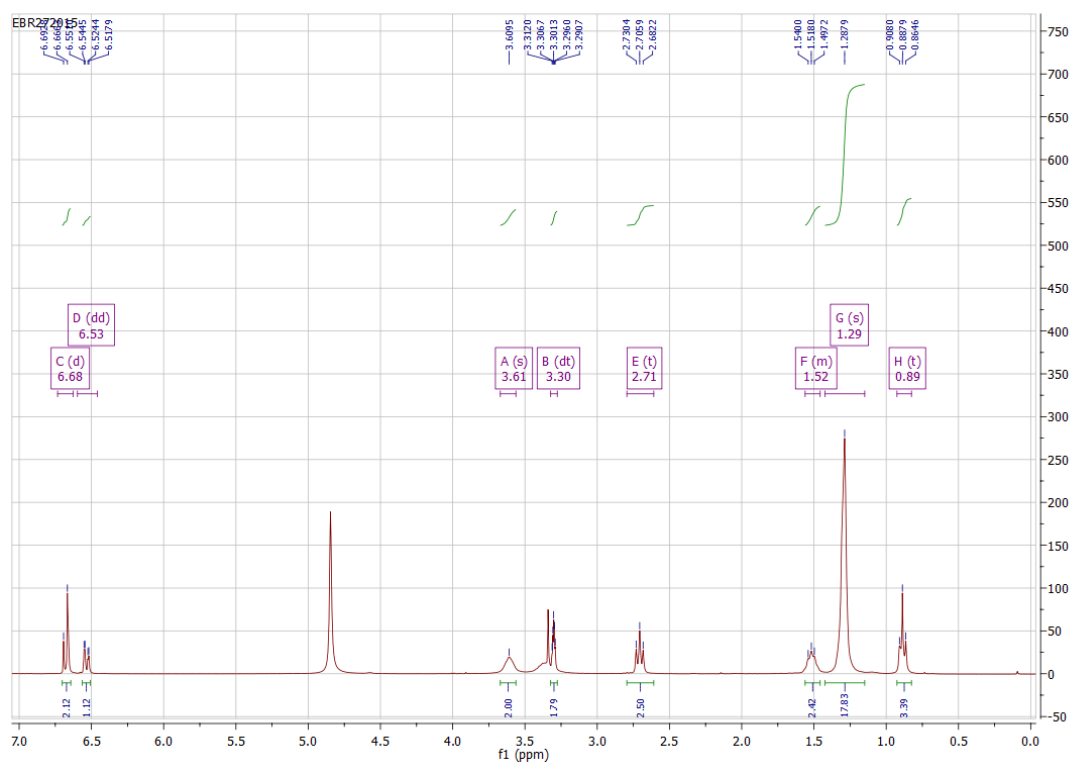
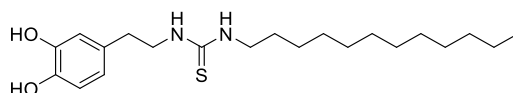


Figure 10. ^1H -NMR and ^{13}C -NMR spectra for compound 38

Annex 4: Supplementary material of *E. J. Med. Chem.* 2018

Alkyl resveratrol prodrugs and metabolites as potential therapeutics for neurodegenerative diseases

Pablo Peñalver, Efres Belmonte-Reche, Norma Adán, Marta Caro, María Luisa Mateos-Martín, Mario Delgado, Elena González-Rey* and Juan Carlos Morales*

Table of Contents.

¹H and ¹³C-NMR spectra of new resveratrol derivatives S2-S27

Supplementary Schemes Figures, Tables and Data:

Figure S1. Toxicity of alkyl resveratrol derivatives on SH-SY5Y neuroblastoma cells. S28

Figure S2. Toxicity of alkyl resveratrol derivatives on RAW 264.7 macrophage cells. S28

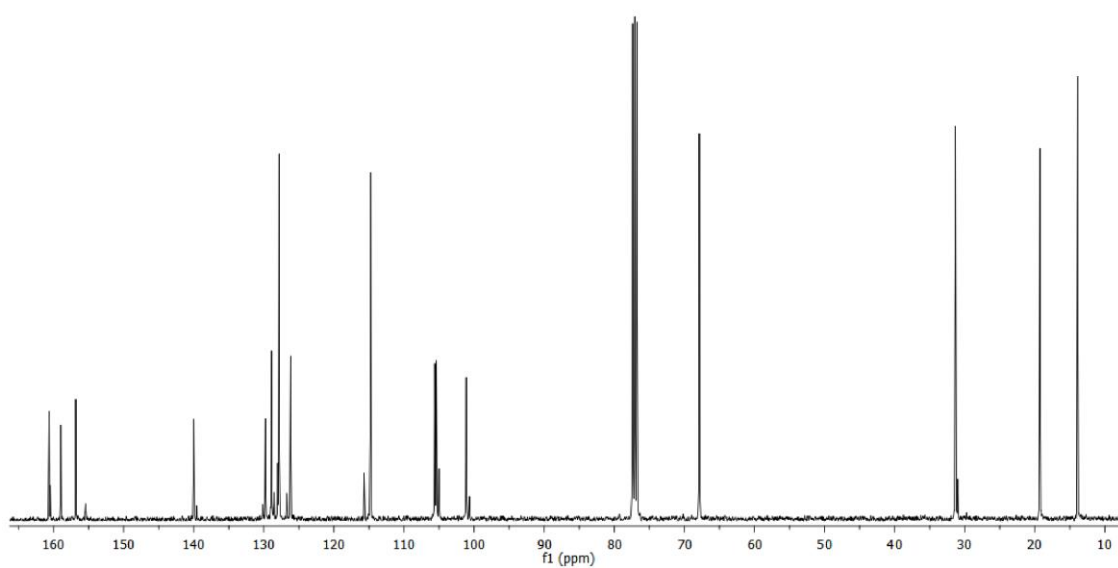
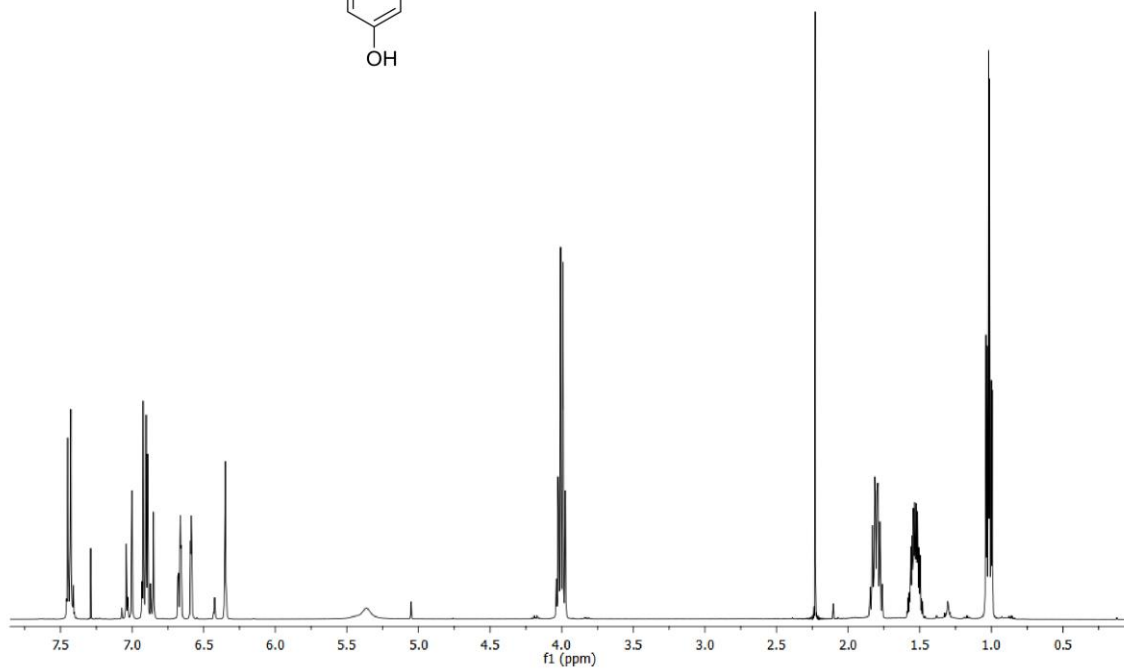
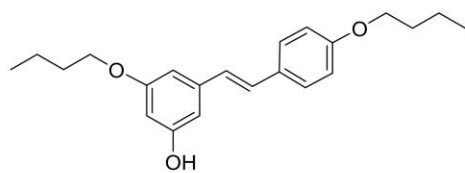
Figure S3. Acute toxicity test assay of representative resveratrol derivatives. S29

Figure S4. HD 3-NP mice model summary S30

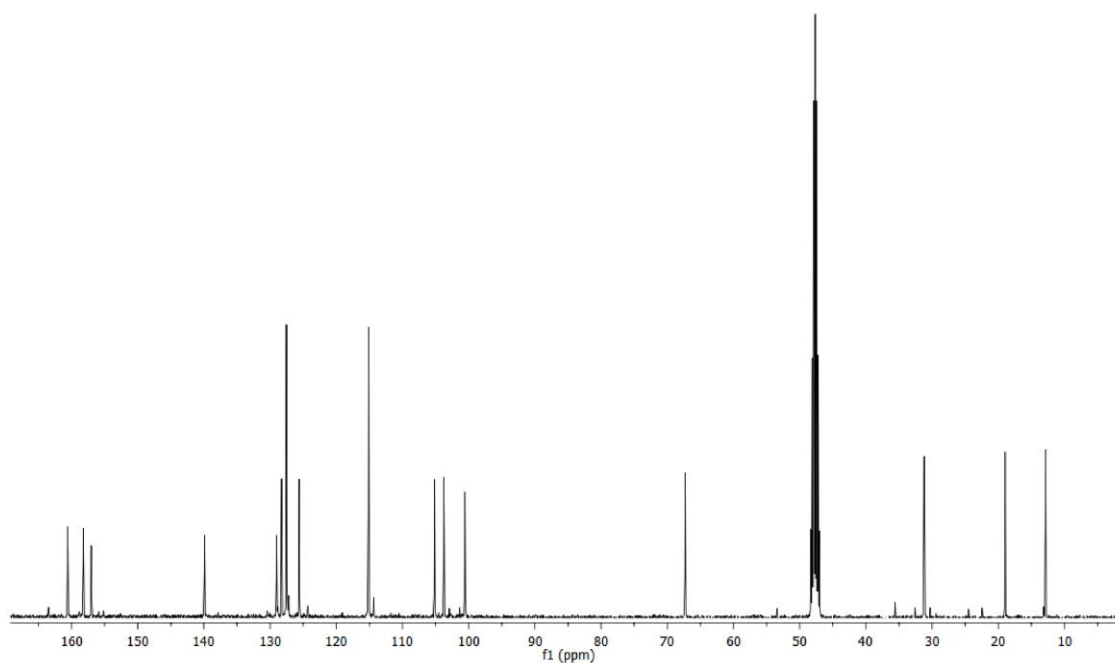
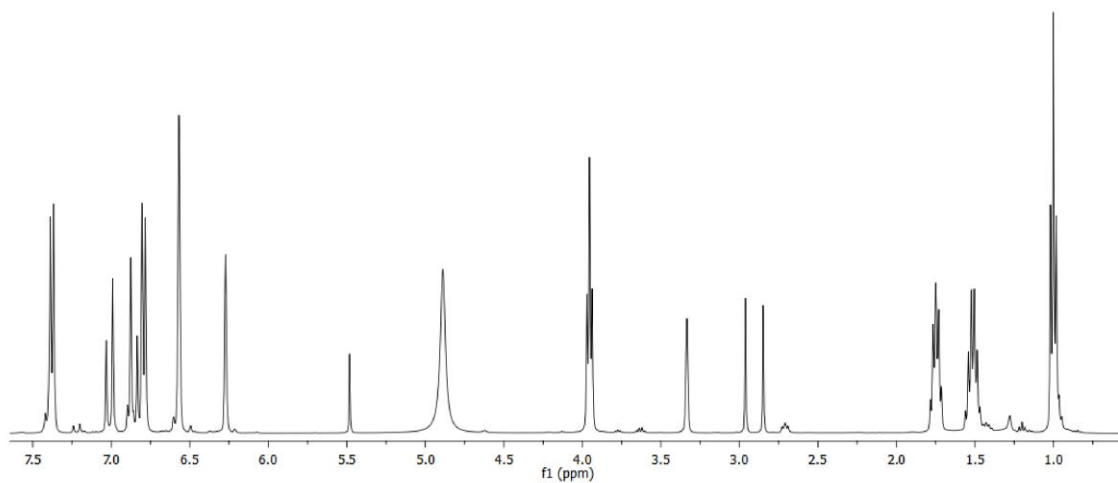
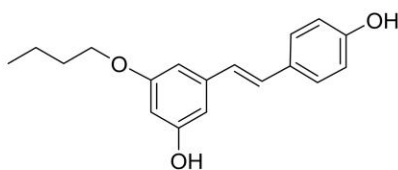
Table S1. Primers used in real-time PCR. S30

Alkylated resveratrol derivatives

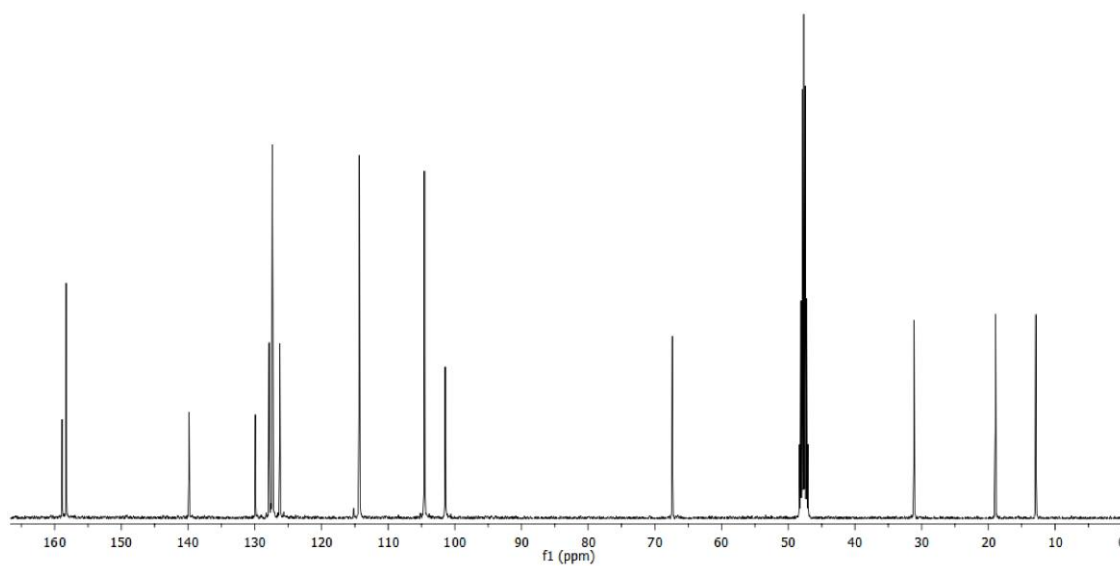
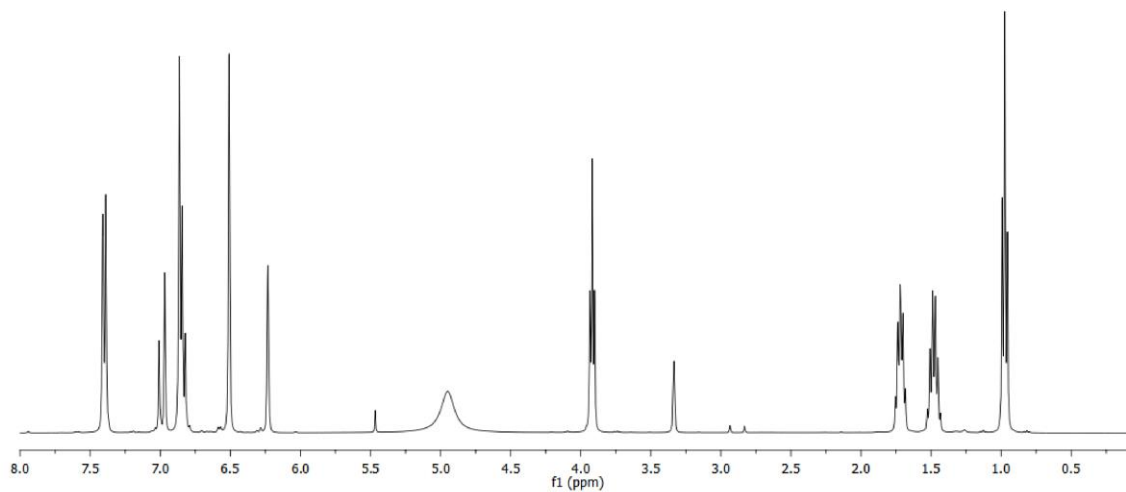
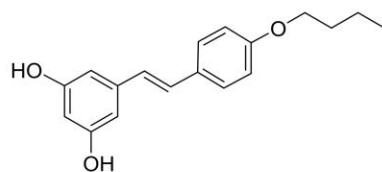
(E)-1-(3-butoxy-5-hydroxyphenyl)-2-(4-butoxyphenyl)ethane, 19.



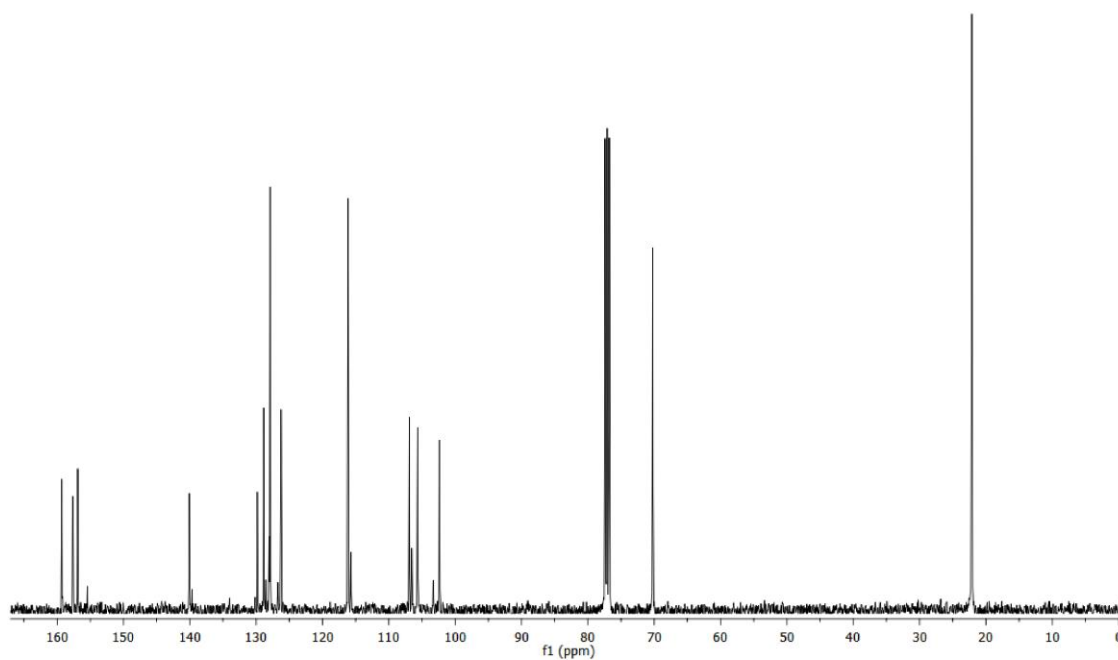
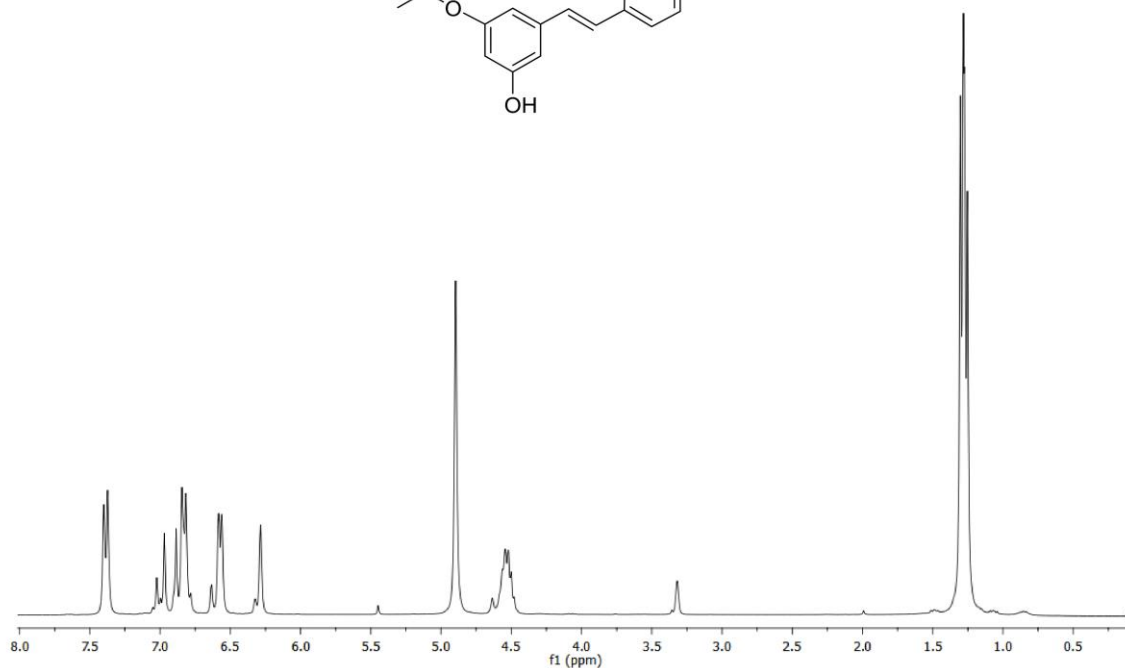
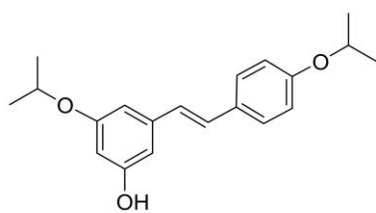
(E)-1-(3-butoxy-5-hydroxyphenyl)-2-(4-hydroxyphenyl)ethane, 20.



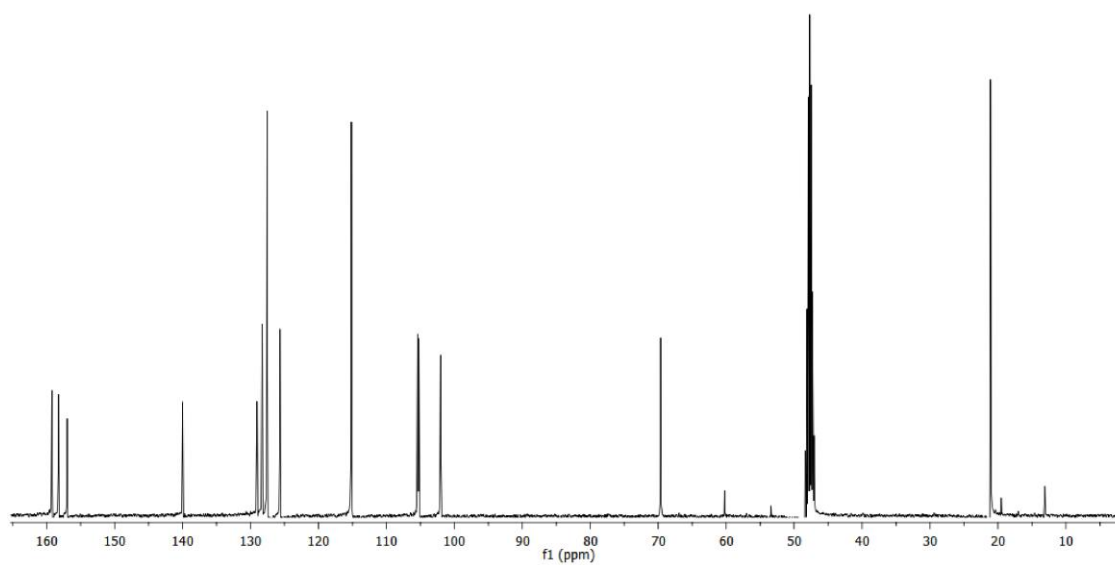
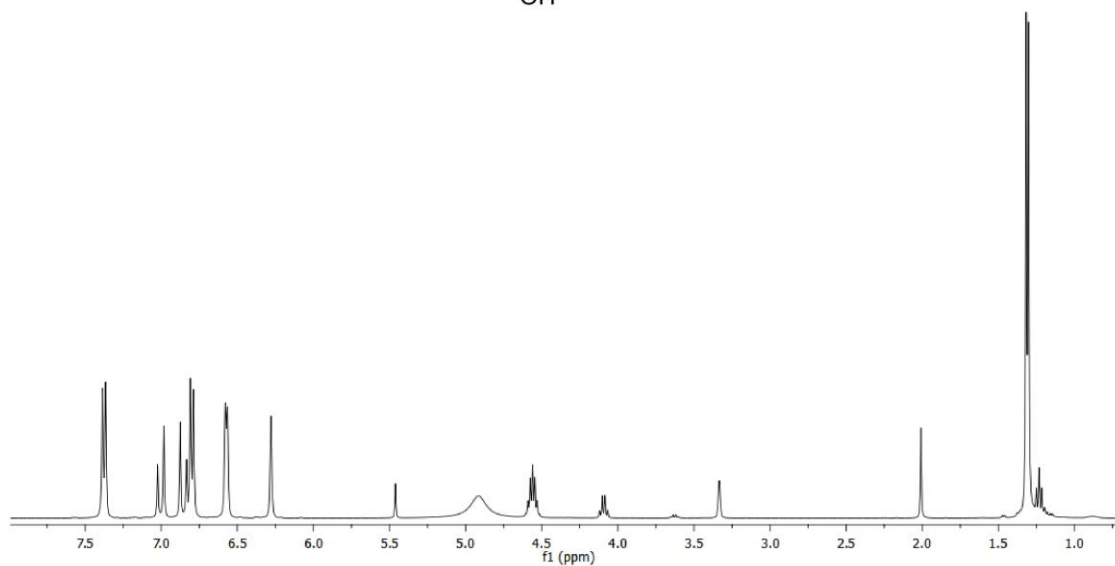
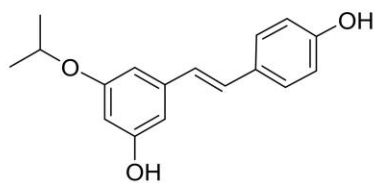
(E)-1-(3,5-dihydroxyphenyl)-2-(4-butoxyphenyl)ethane, 21.



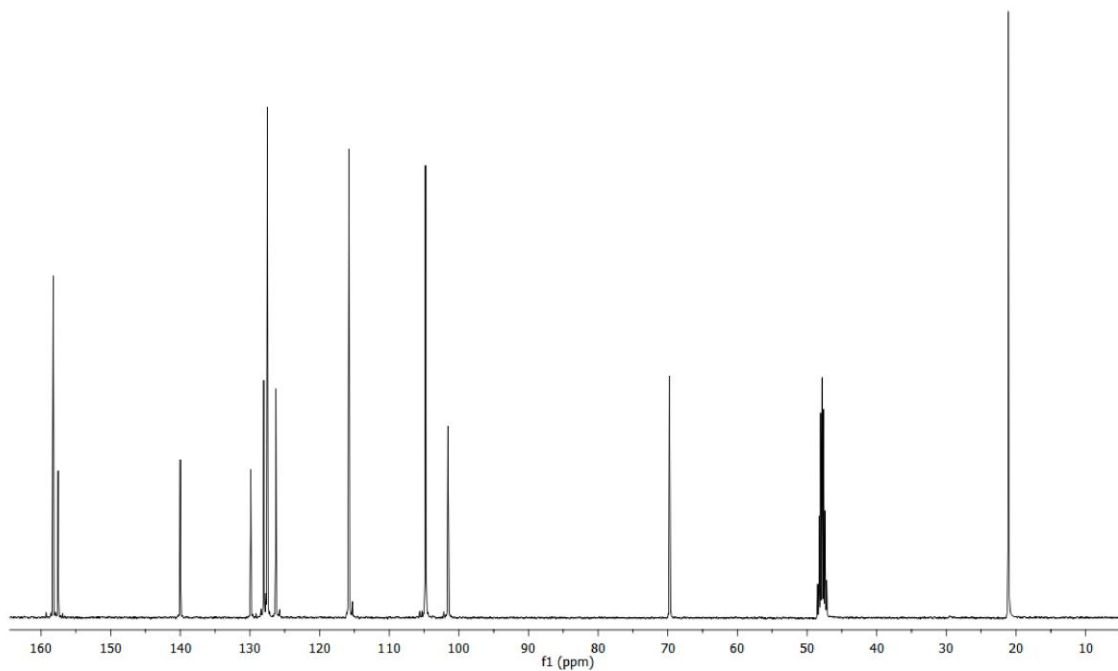
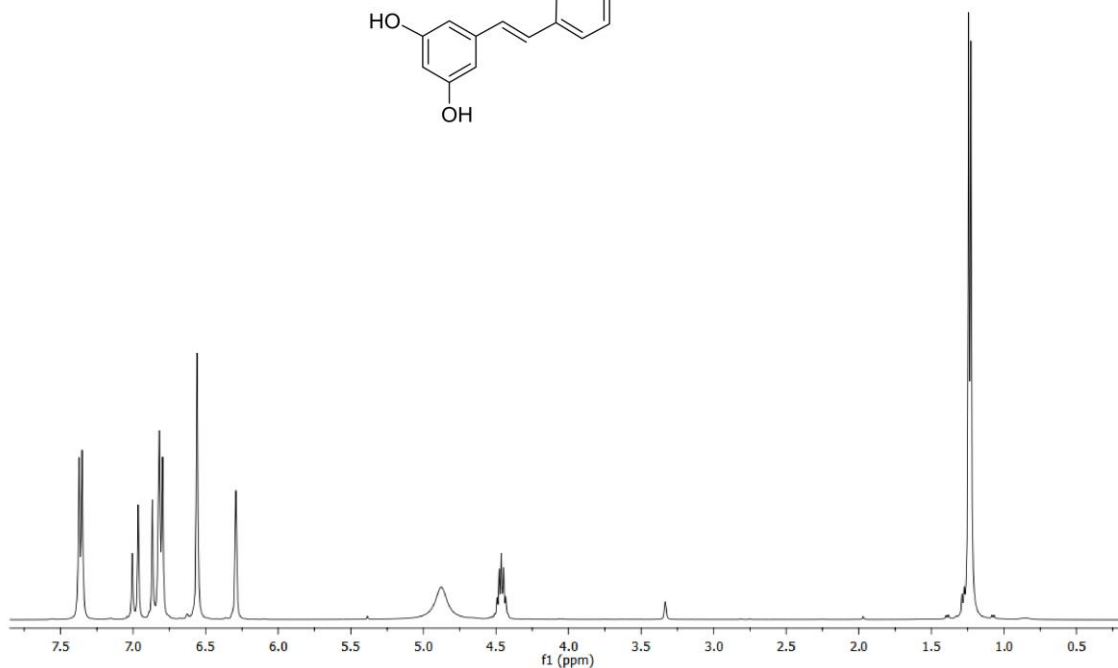
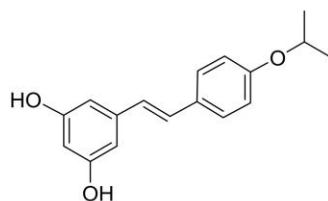
(E)-1-(3-isopropoxy-5-hydroxyphenyl)-2-(4-isopropoxyphenyl)ethane, 23.



(E)-1-(3-isopropoxy-5-hydroxyphenyl)-2-(4-hydroxyphenyl)ethane, 24.

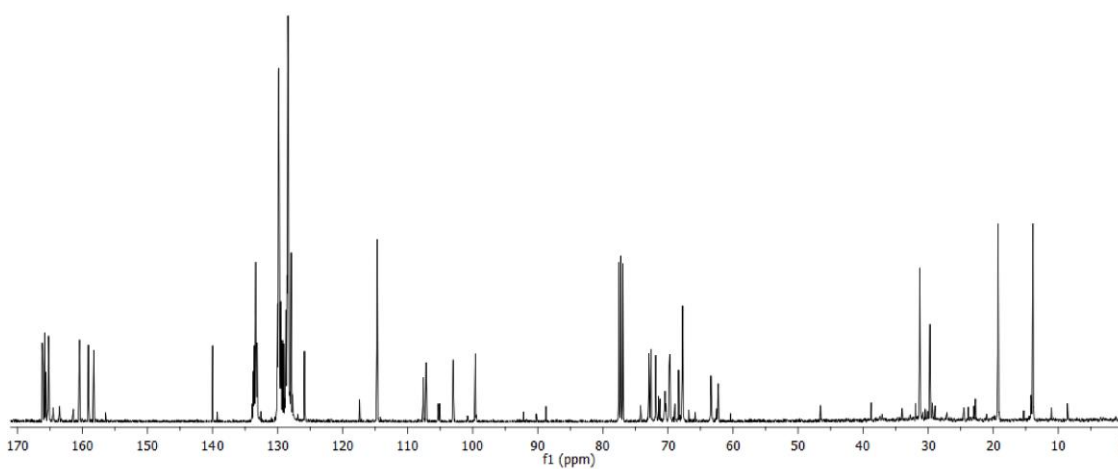
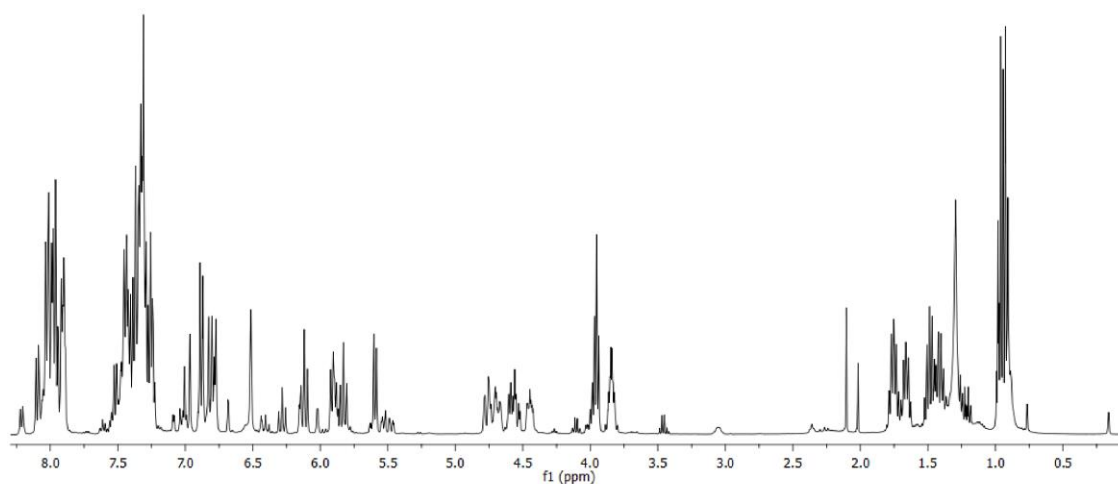
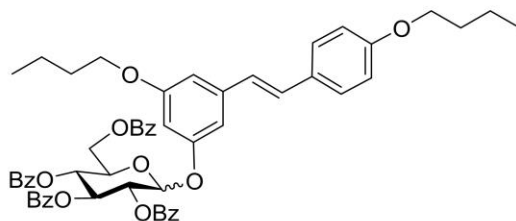


(E)-1-(3,5-dihydroxyphenyl)-2-(4-isopropoxyphenyl)ethane, 25.

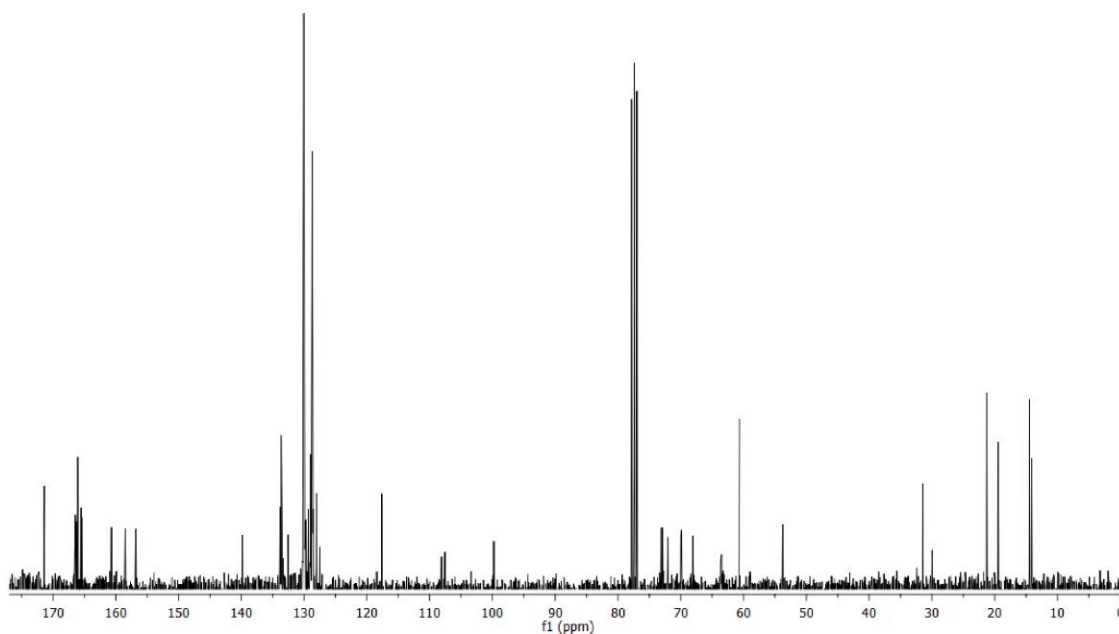
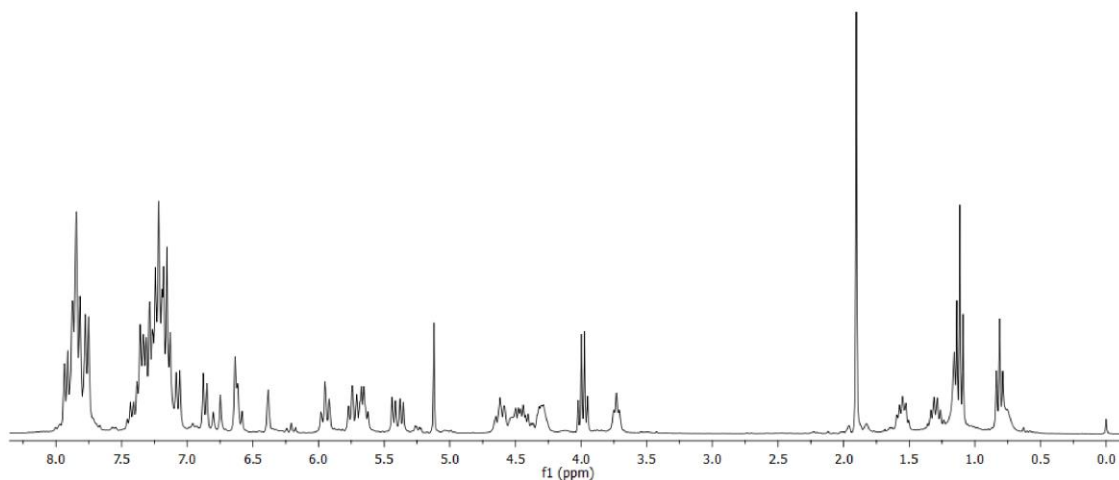
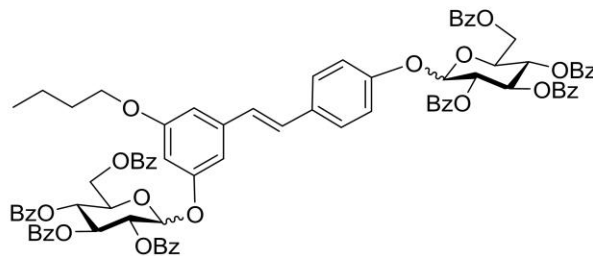


Butylated resveratrol prodrugs and metabolites (26-31) and intermediates

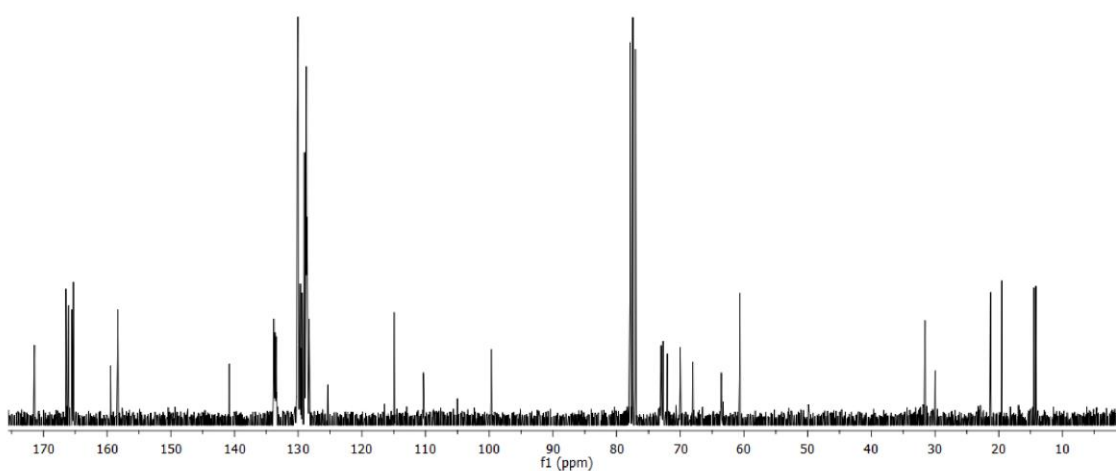
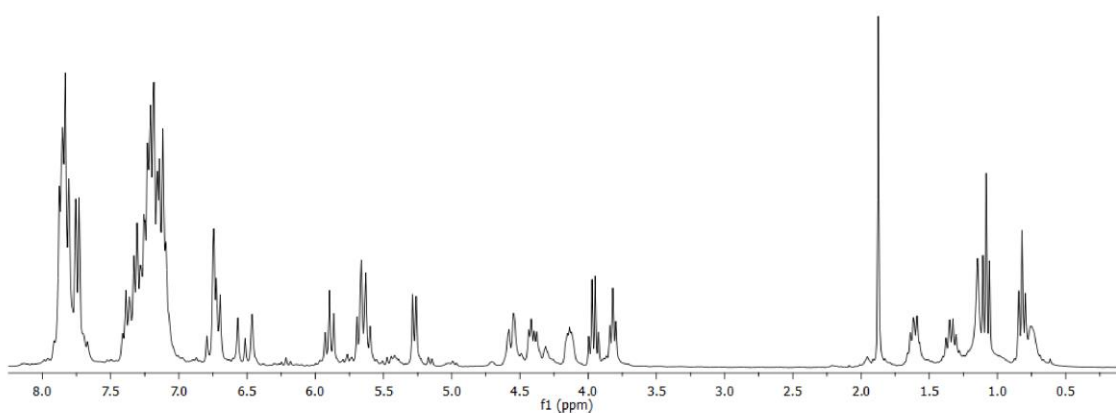
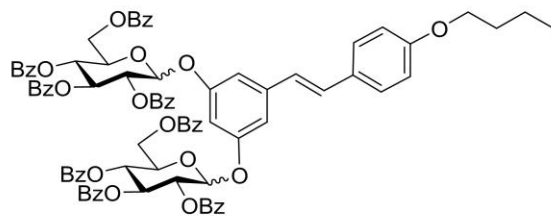
(E)-1-(3-butoxy-5-(2,3,4,6-tetra-O-benzoyl- β -D-glucopyranosyloxy)phenyl)-2-(4-butoxyphenyl)ethene (43)



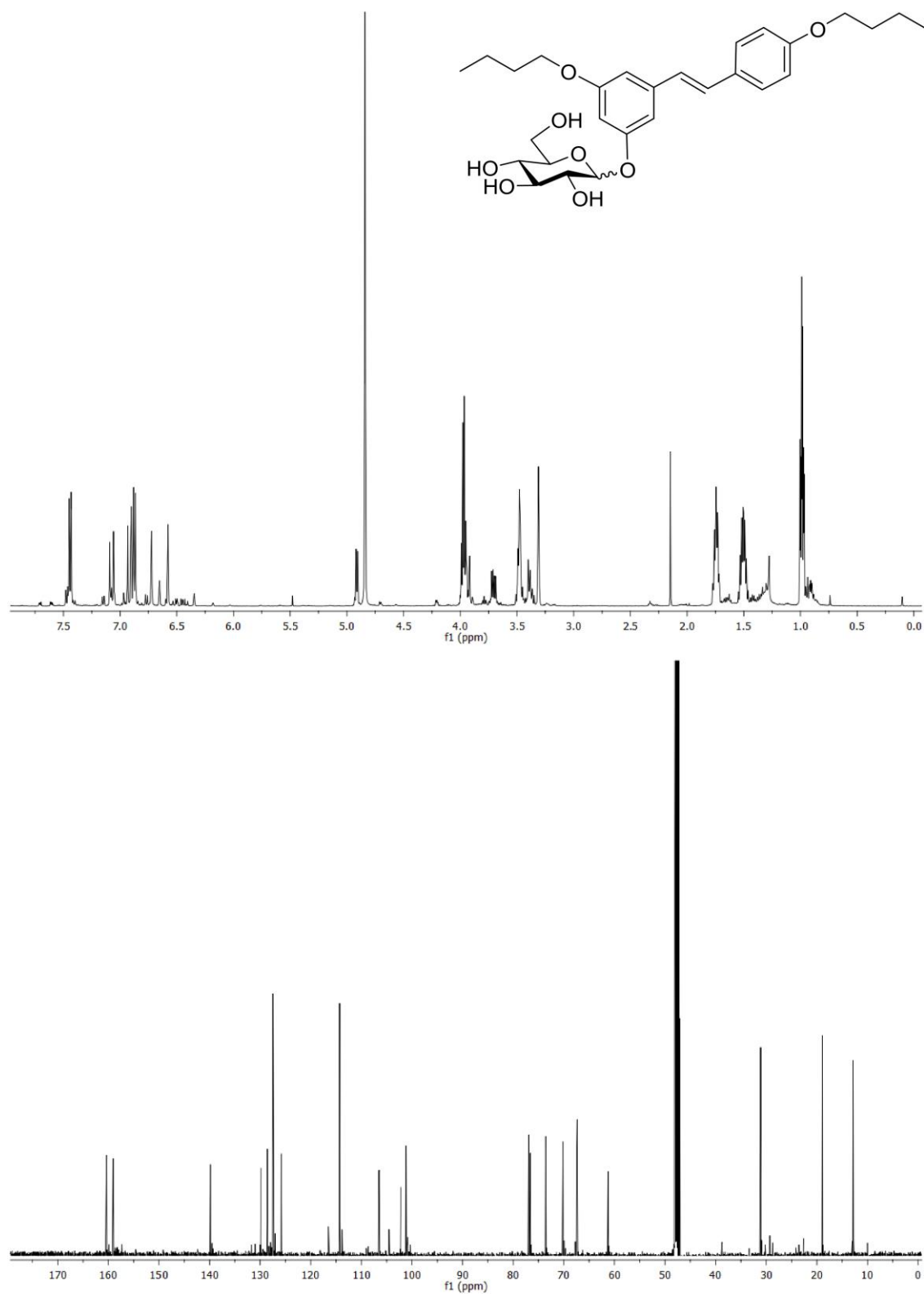
(E)-1-(3-butoxy-5-(2,3,4,6-tetra-O-benzoyl-β-D-glucopyranosyloxy)phenyl)-2-(4-(2,3,4,6-tetra-O-benzoyl-β-D-glucopyranosyloxy)phenyl)ethene (44).



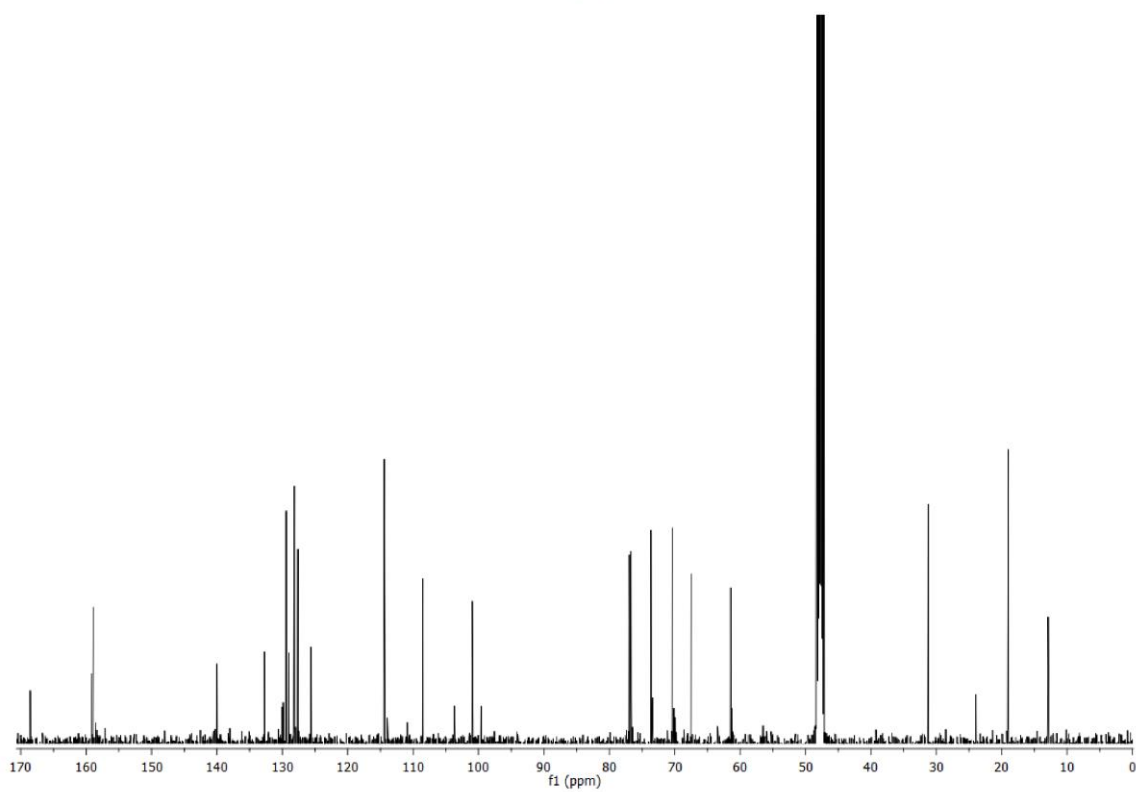
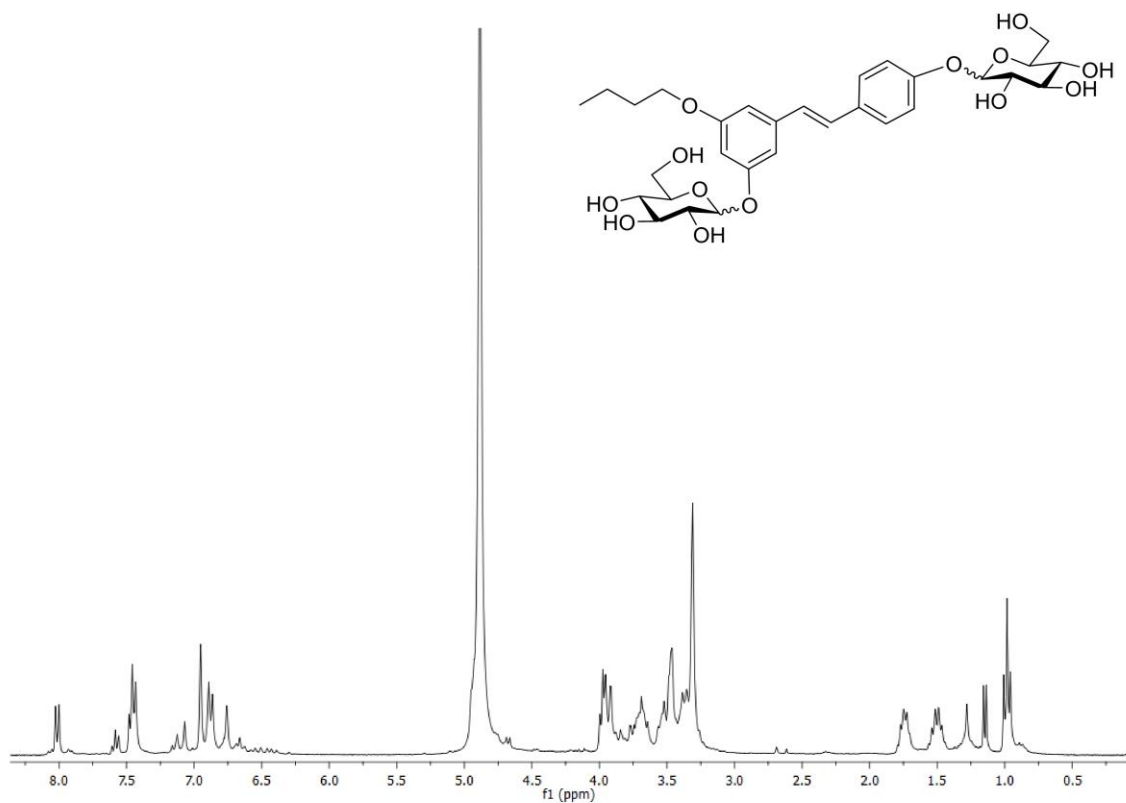
(E)-1-(3,5-di-(2,3,4,6-tetra-*O*-benzoyl- β -D-glucopyranosyloxy)phenyl)-2-(4-butoxy)phenylethene (45).



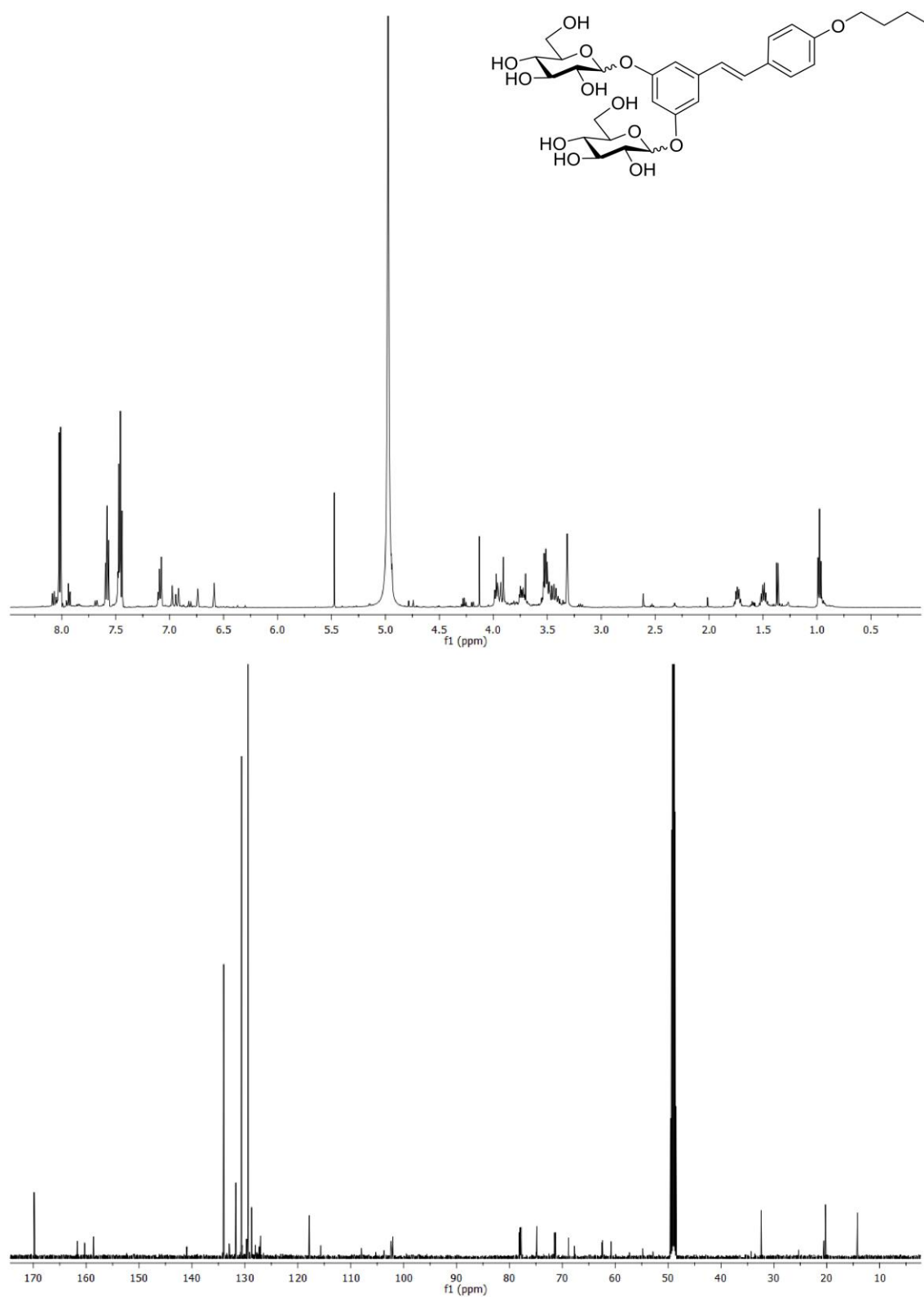
(E)-1-(3-butoxy-5-(β -D-glucopyranosyloxy)phenyl)-2-(4-butoxyphenyl)ethane, 26.



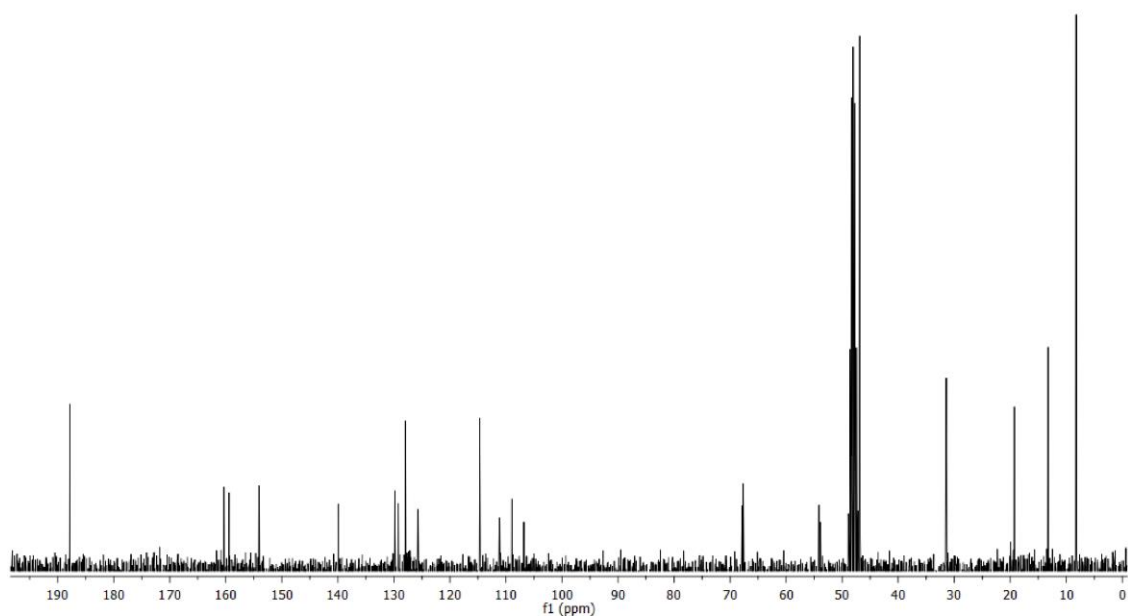
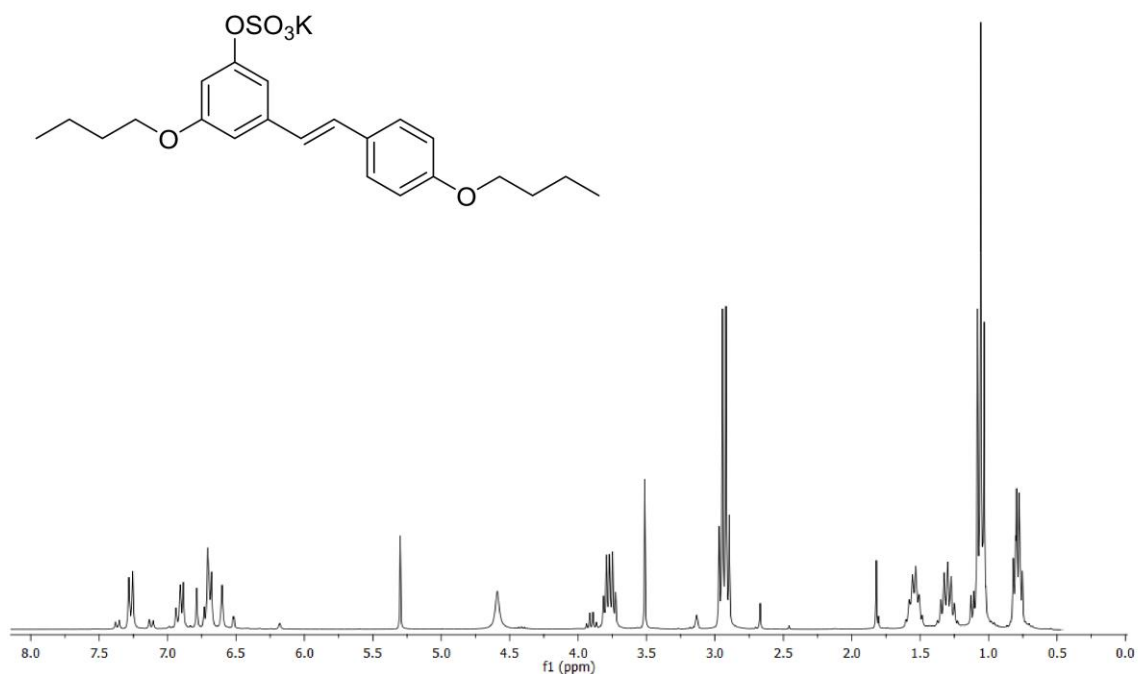
(E)-1-(3-butoxy-5-(β -D-glucopyranosyloxy)phenyl)-2-(β -D-glucopyranosyloxy)phenyl ethane, 27.



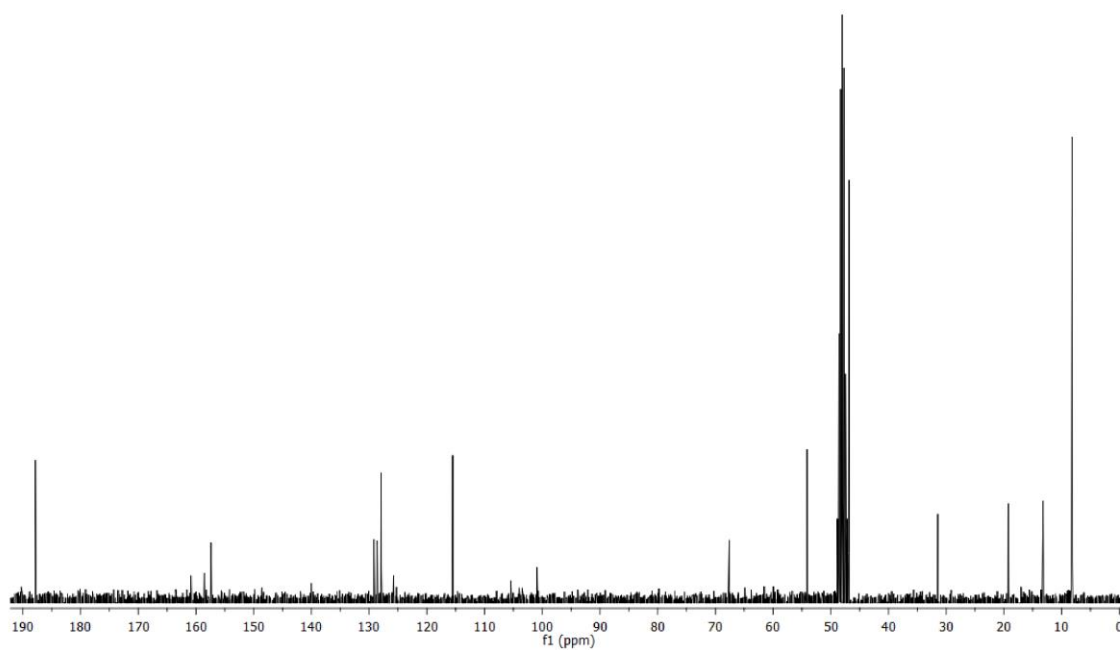
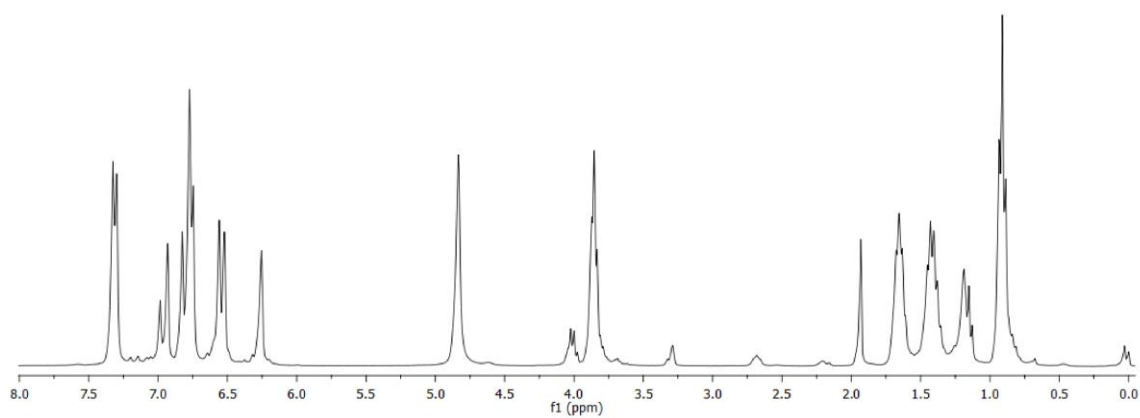
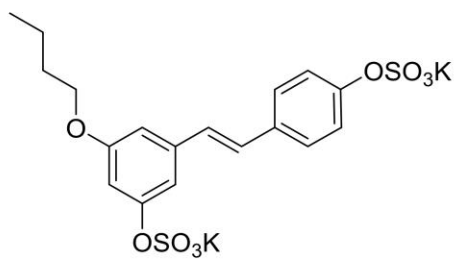
(E)-1-(3,5-di-(β-D-glucopyranosyloxy)phenyl)-2-(4-butoxy)phenylethane, 28.



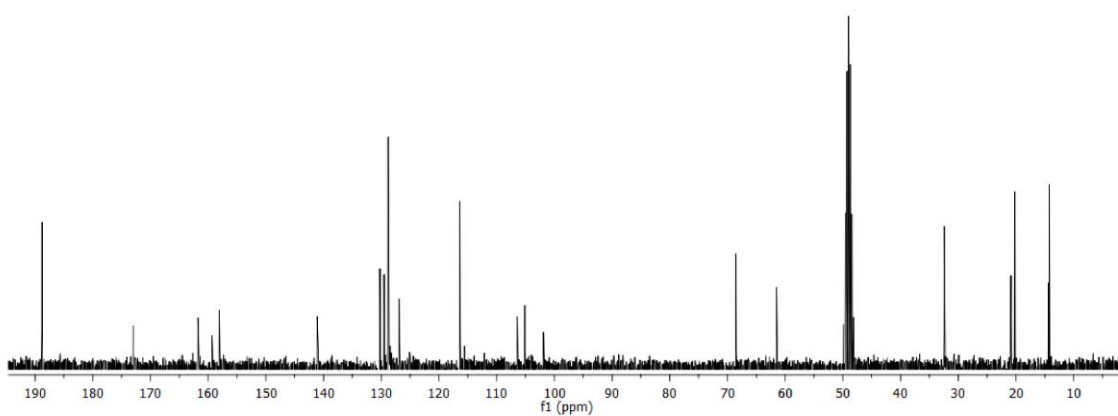
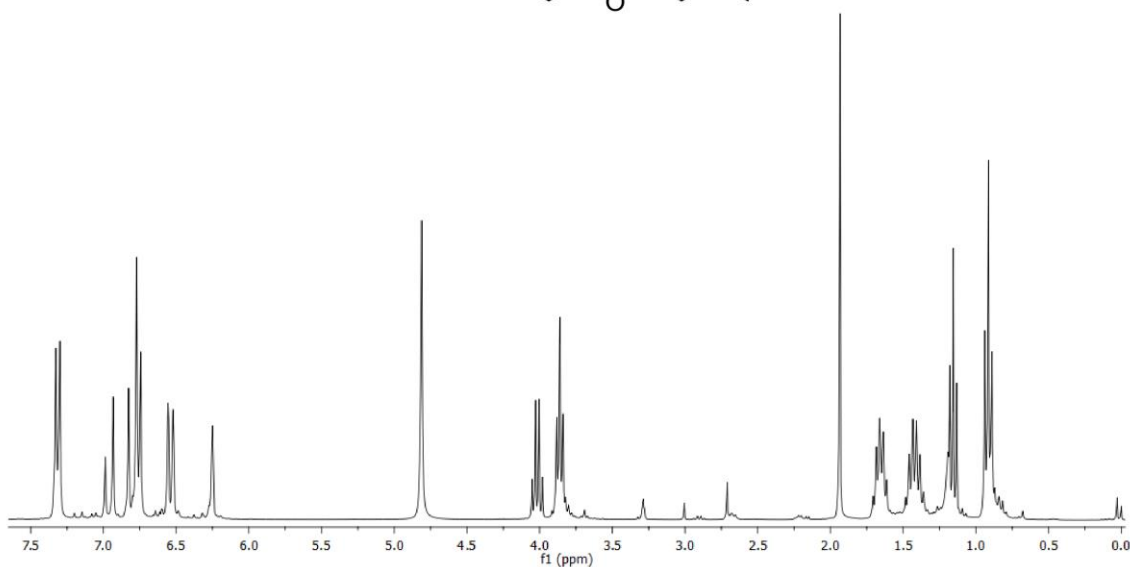
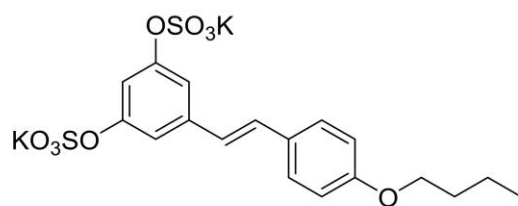
Potassium (*E*)-3-(4-butoxystyryl)-5-butoxyphenyl sulfate, 29.



Dipotassium (*E*)-5-(4-butoxystyryl)phenyl-1,3-disulfate, 30.

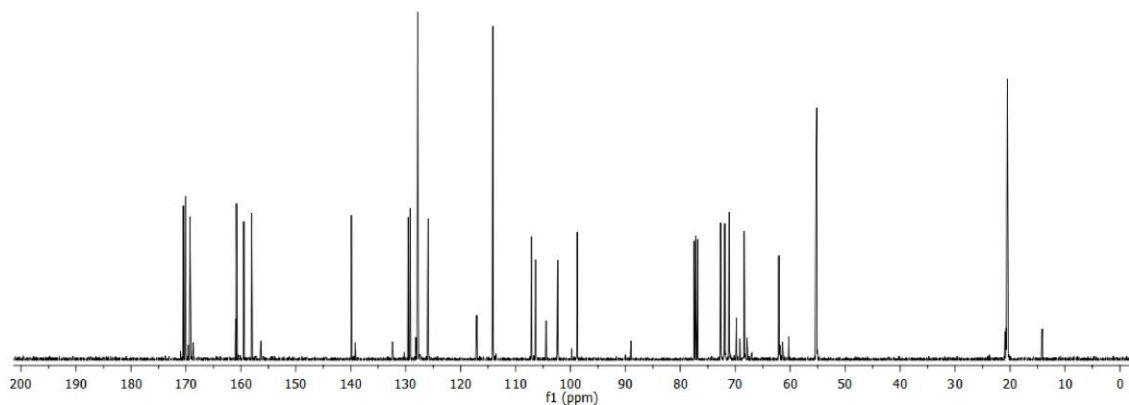
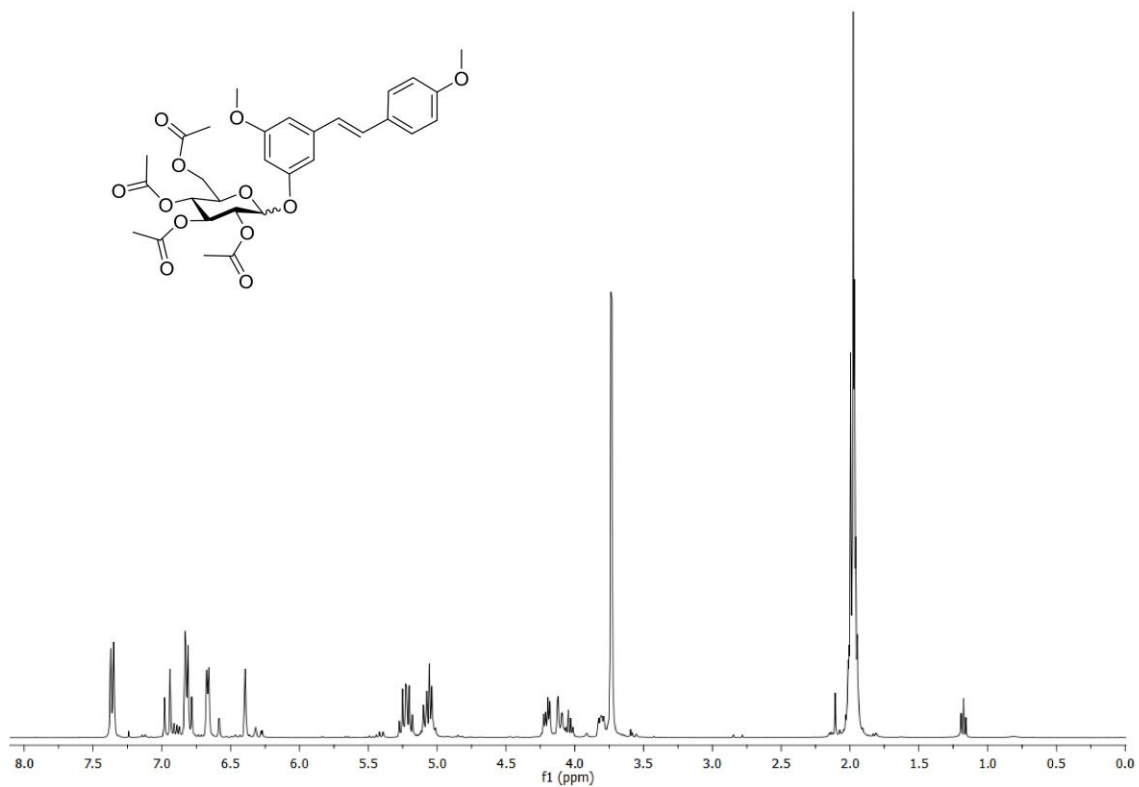


Dipotassium (*E*)-3-(4-sulphate-styryl)-5-butoxyphenyl sulfate, 31.

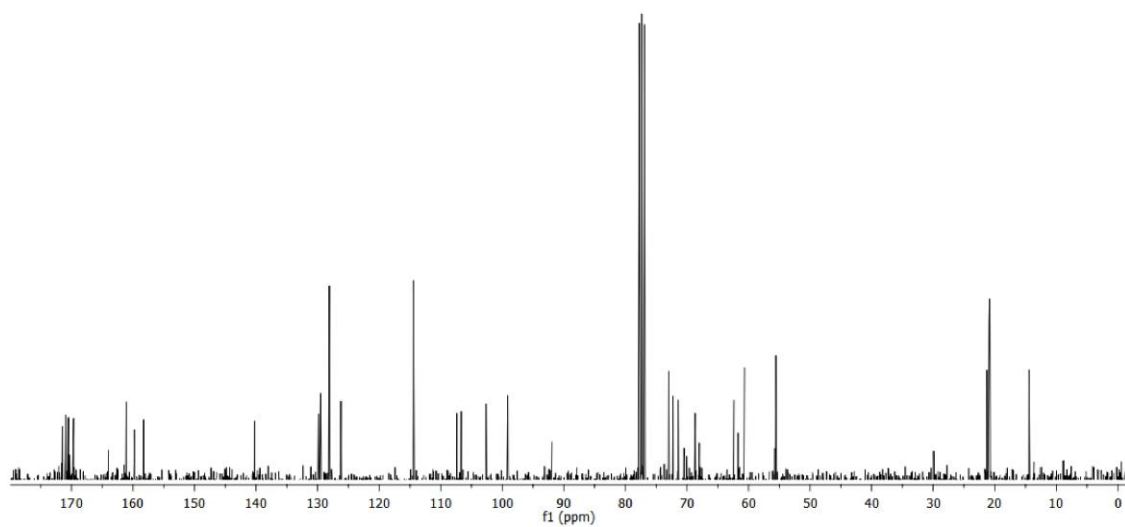
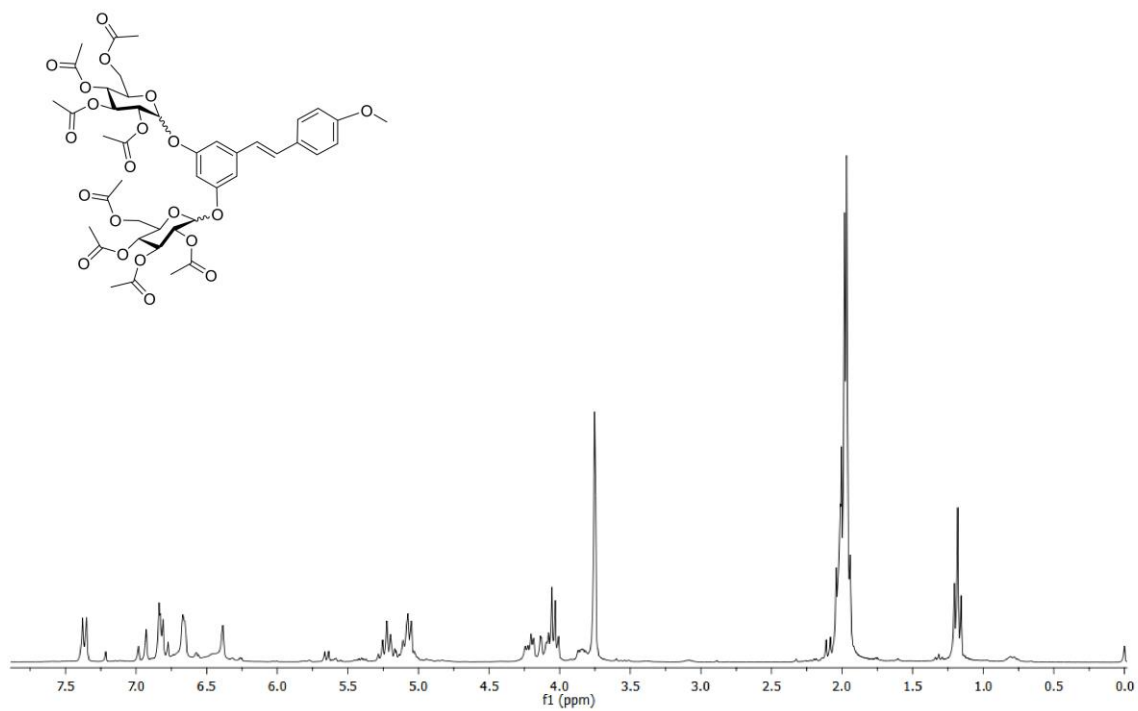


methylated resveratrol prodrugs (32-41) and intermediates

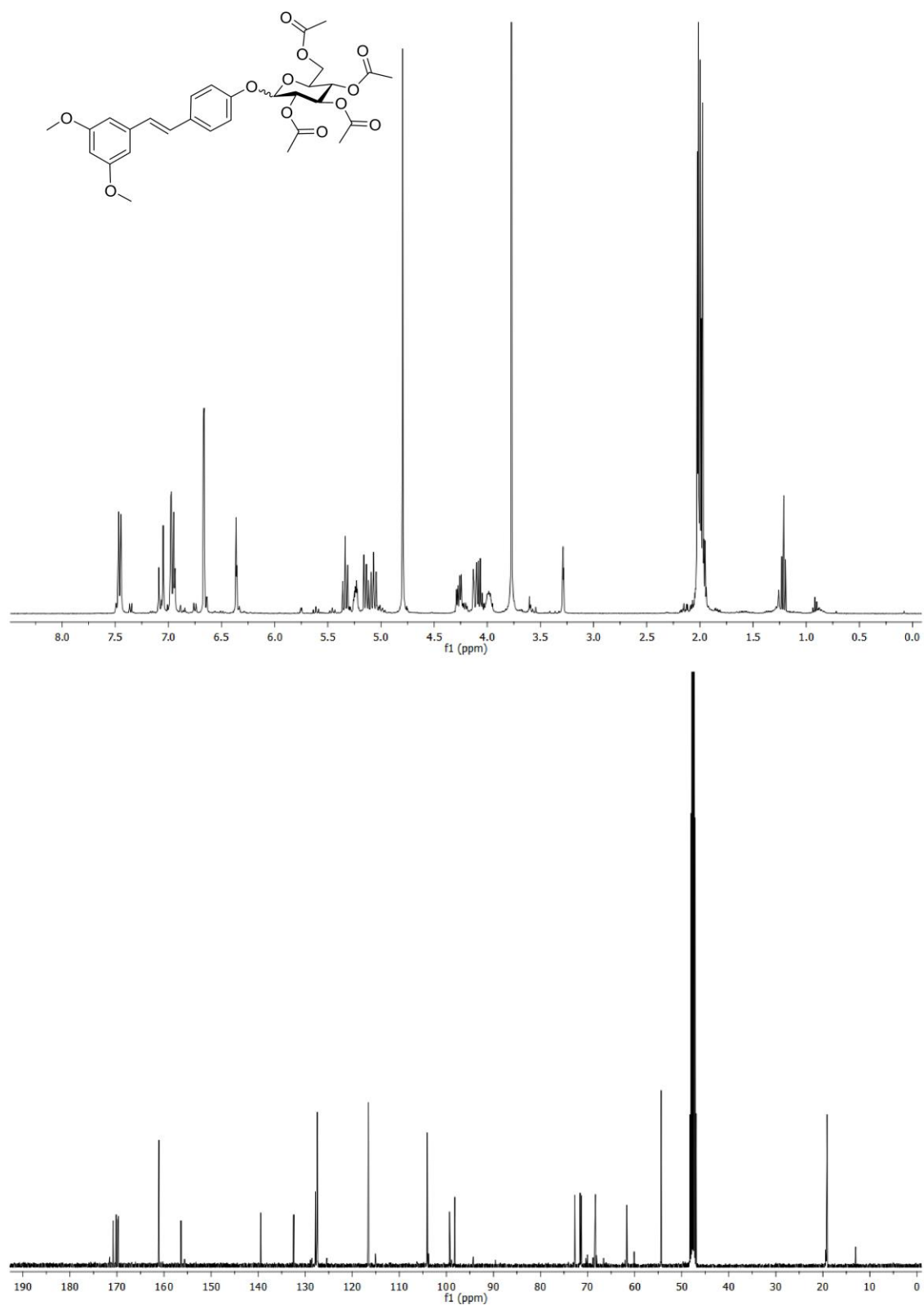
(E)-1-(3-methoxy-5-(2,3,4,6-tetra-O-acetyl- β -D-glucopyranosyloxy)phenyl)-2-(4'-methoxyphenyl)ethene, (48).



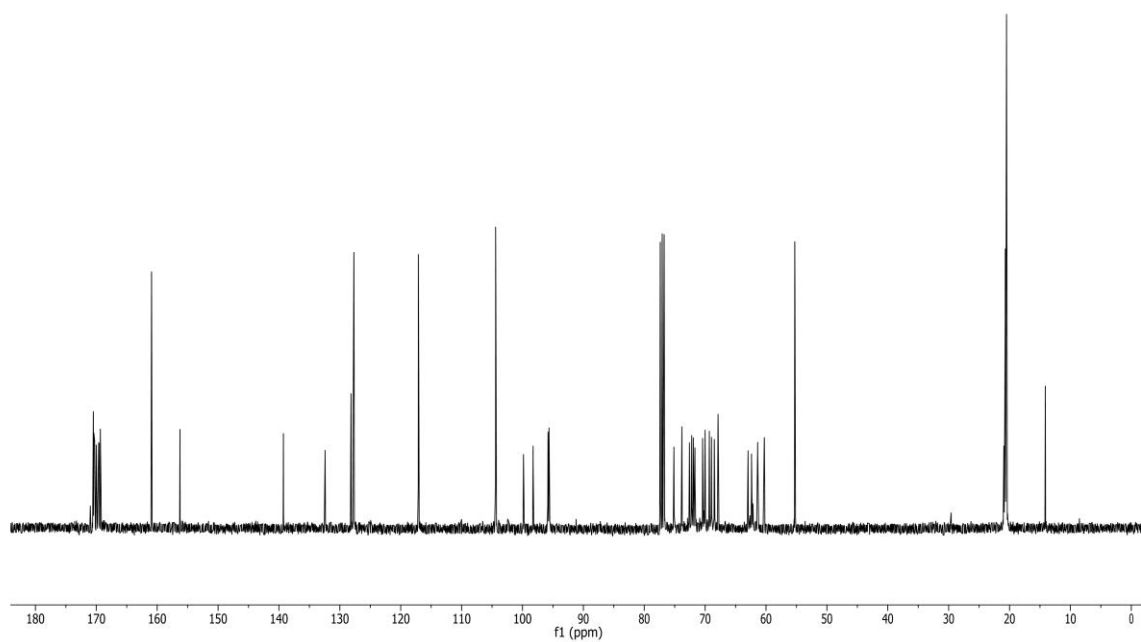
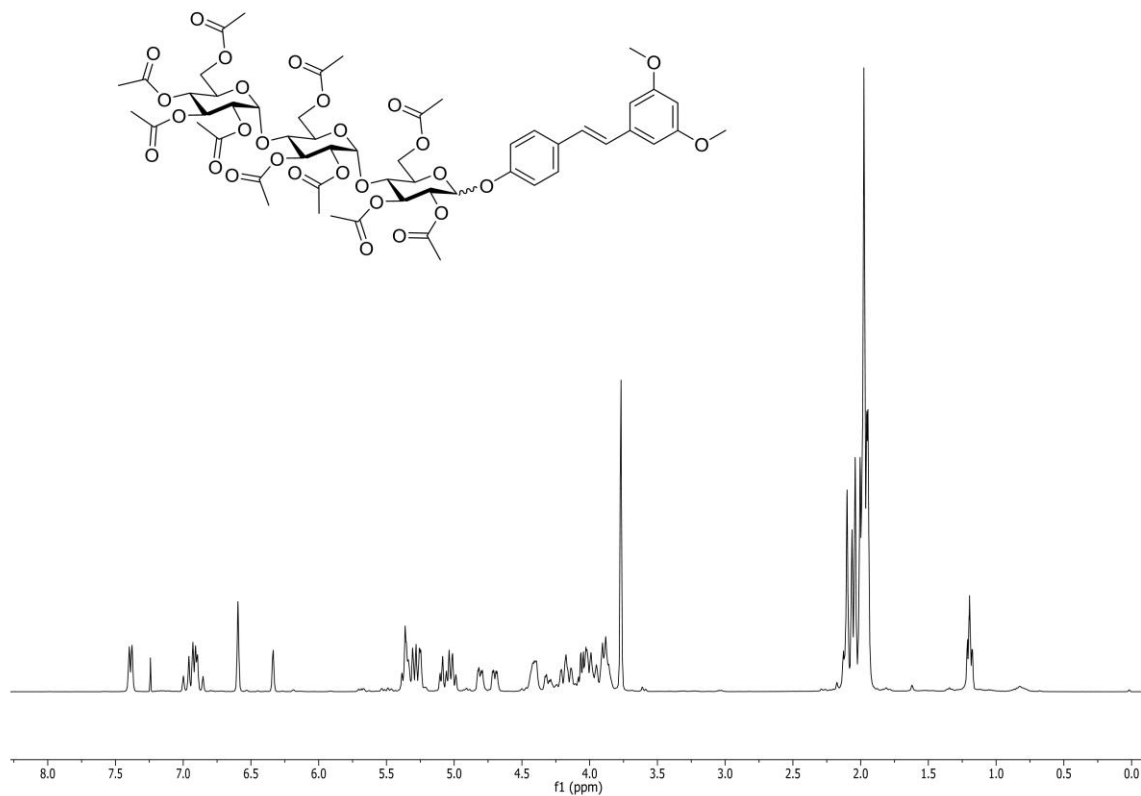
(E)-1-(3,5-di-(2,3,4,6-tetra-O-acetyl- β -D-glucopyranosyloxy)phenyl)-2-(4'-methoxyphenyl)ethene, (49).



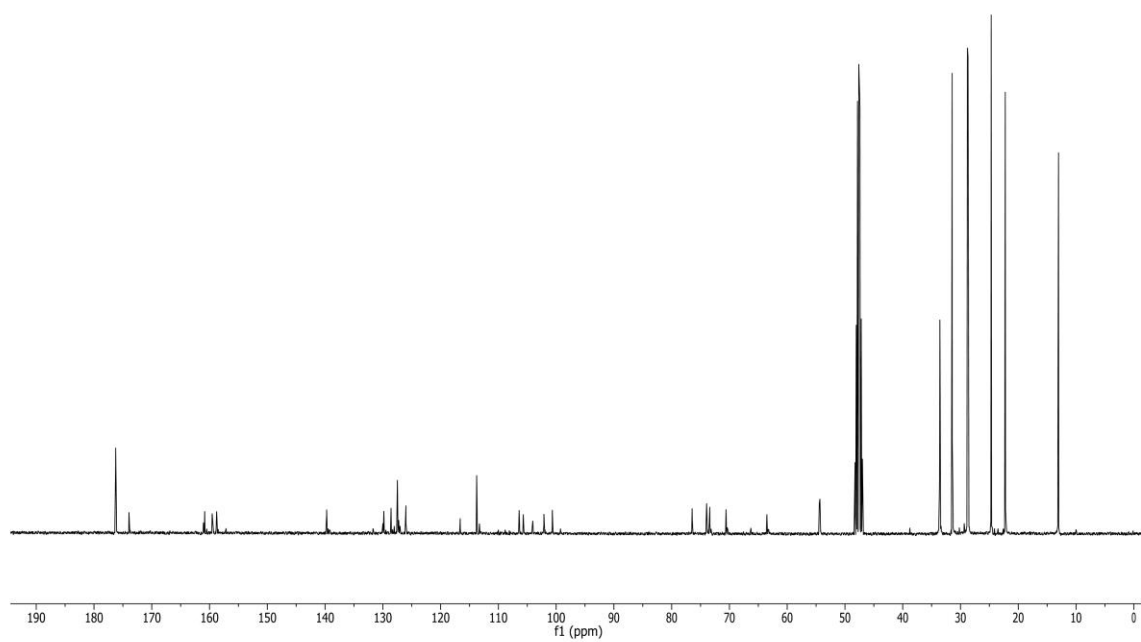
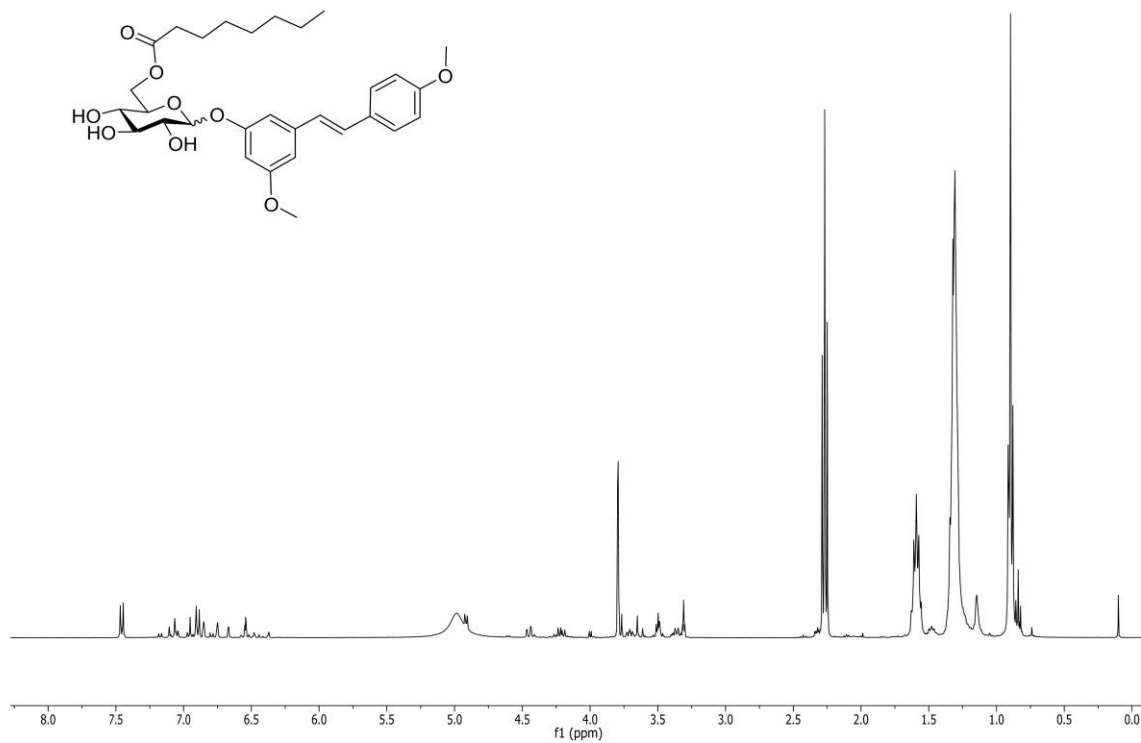
(E)-1-(3-methoxy-4'-(2,3,4,6-tetra-O-acetyl-β-D-glucopyranosyloxy)phenyl)-2-(5-methoxyphenyl)ethene, (50).



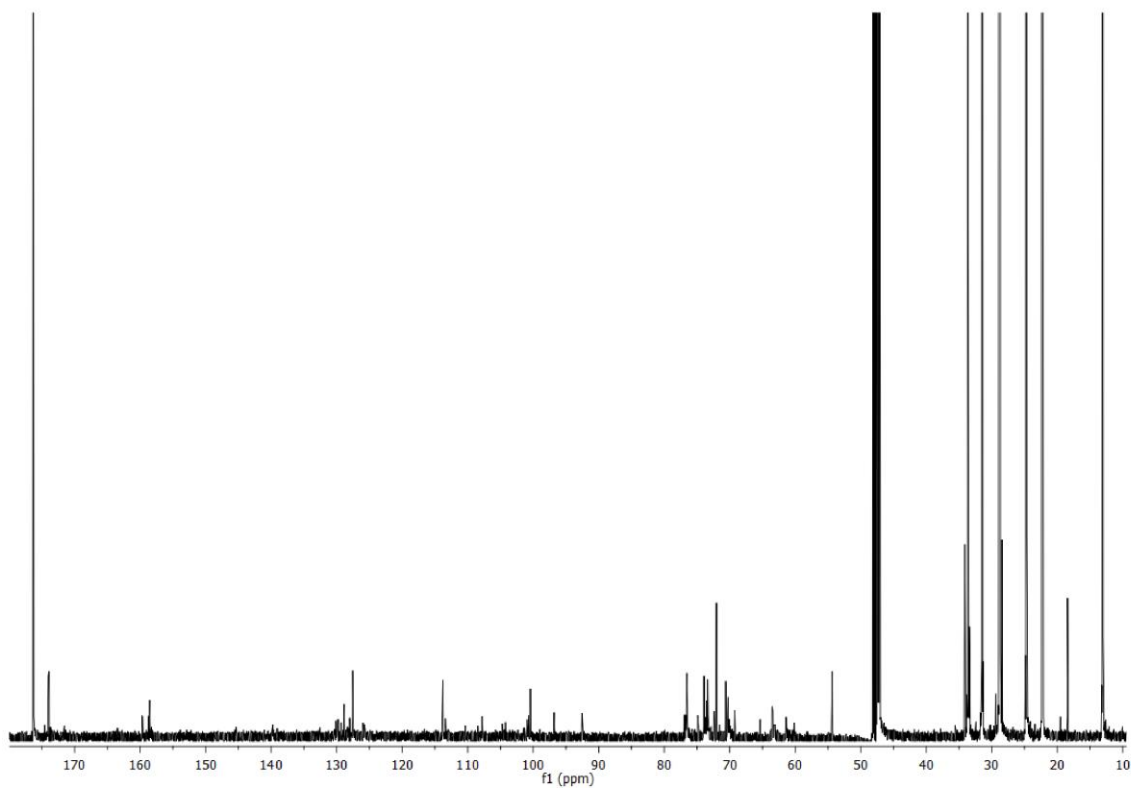
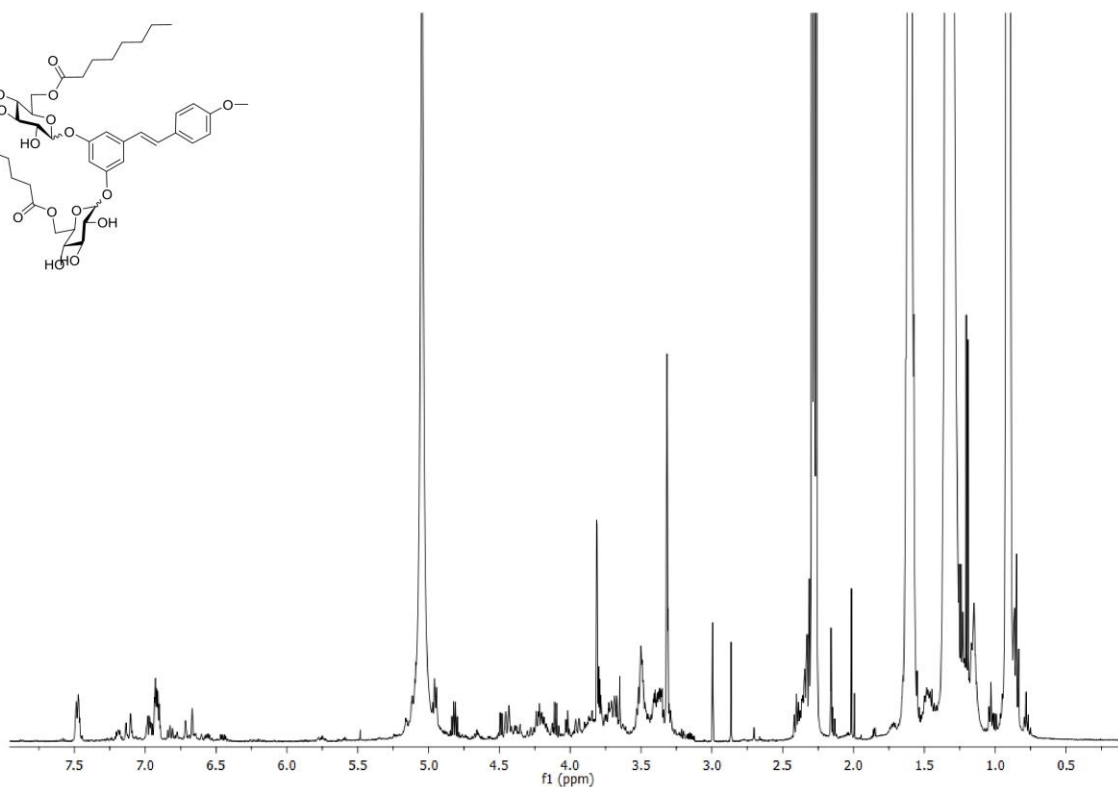
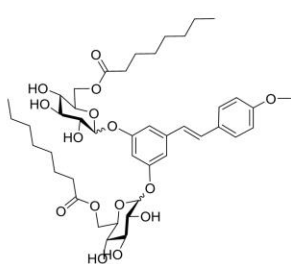
(E)-1-(3-methoxy-4'-(per-O-acetyl- β -D-maltopyranosyloxy)phenyl)-2-(5-methoxyphenyl)ethene, (51).



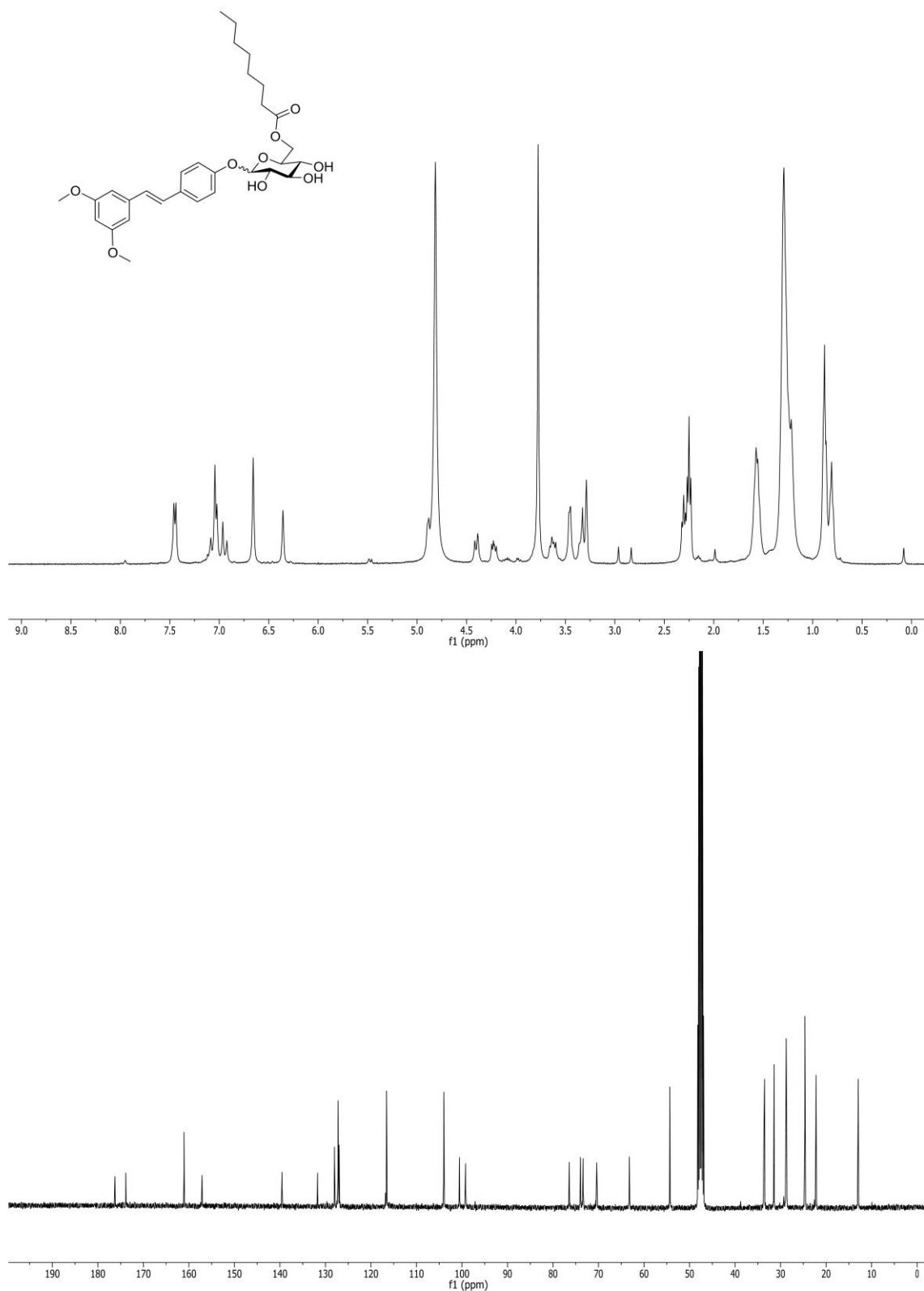
(E)-1-(3-methoxy-5-(β -D-glucopyranosyloxy-octanoate)phenyl)-2-(4'-methoxyphenyl)ethene, (35).



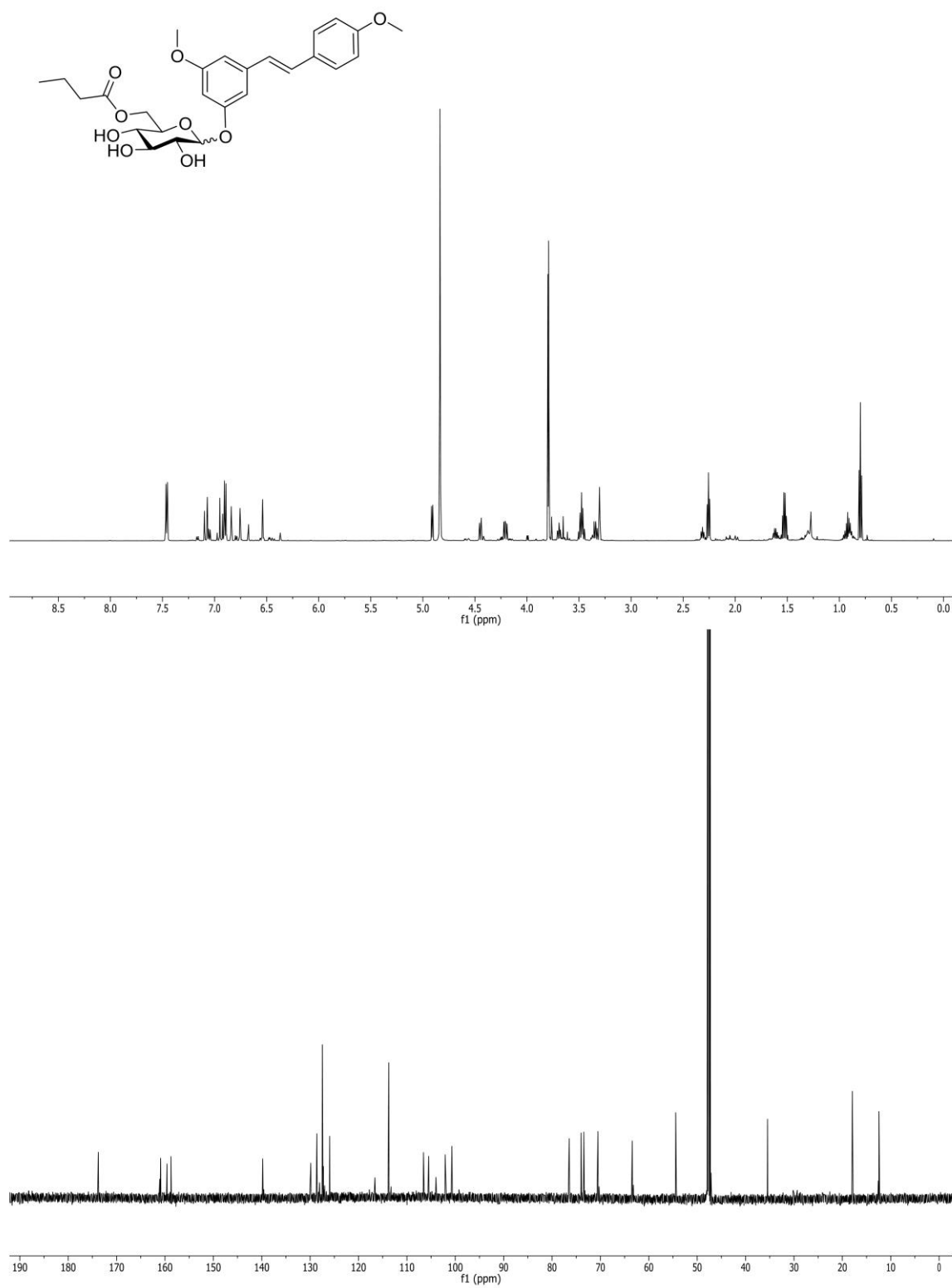
(E)-1-(3, 5-di-(6-O-octanoyl- β -D-glucopyranosyloxy)phenyl)-2-(4'-methoxy-phenyl)ethene, (36)



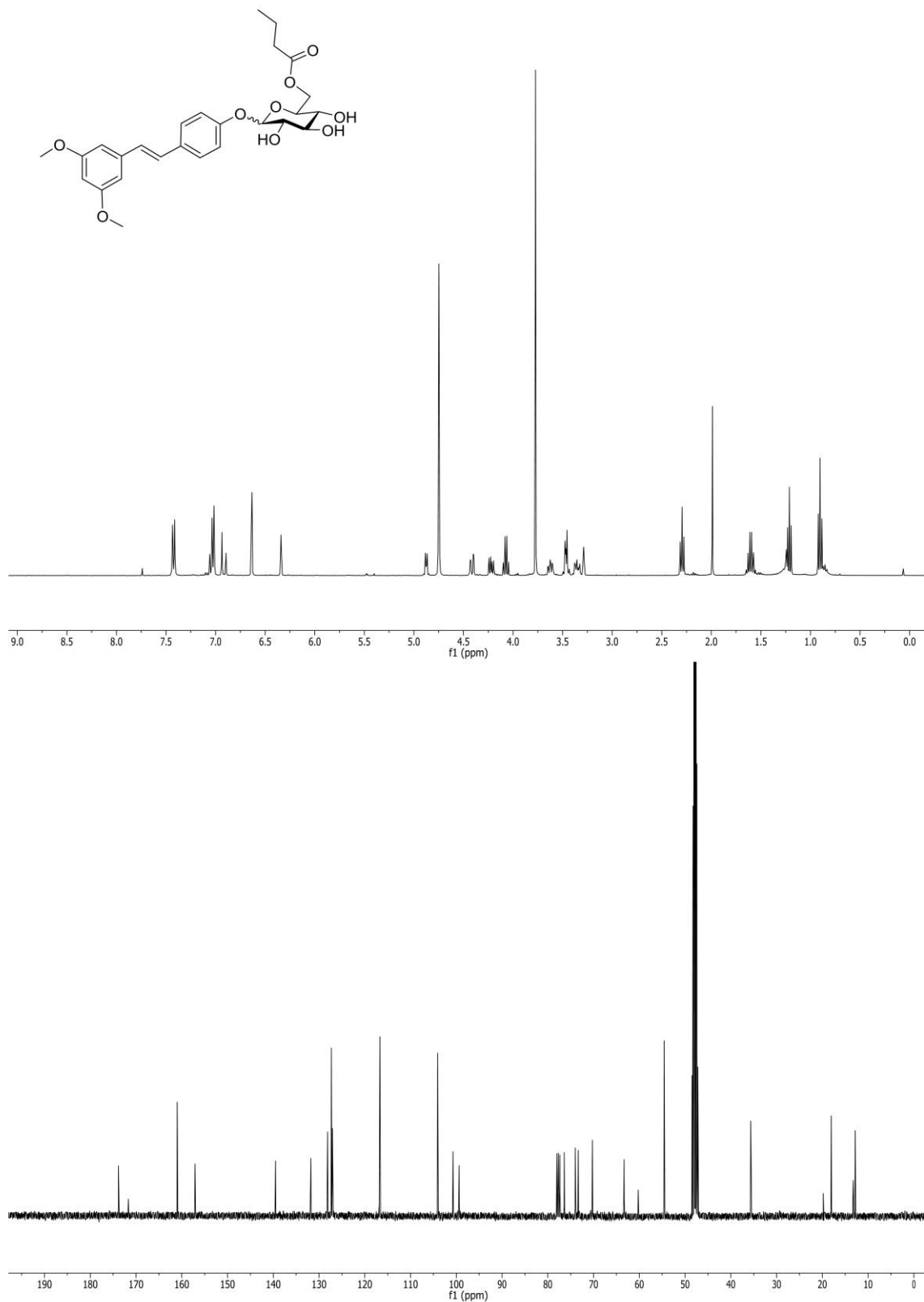
(E)-1-(3-methoxy-4'-(β-D-glucopyranosyloxy-octanoate)phenyl)-2-(5-methoxyphenyl)ethene, (37).



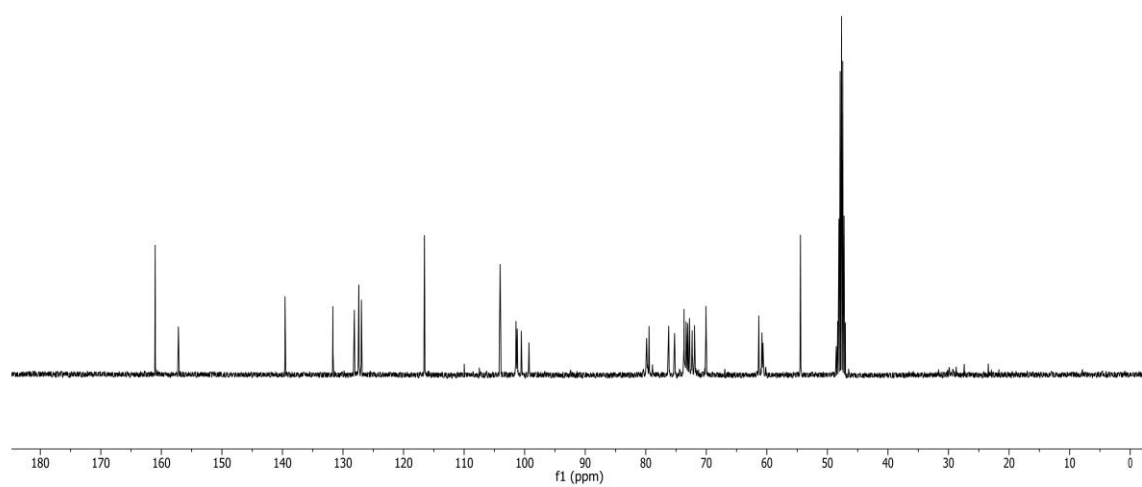
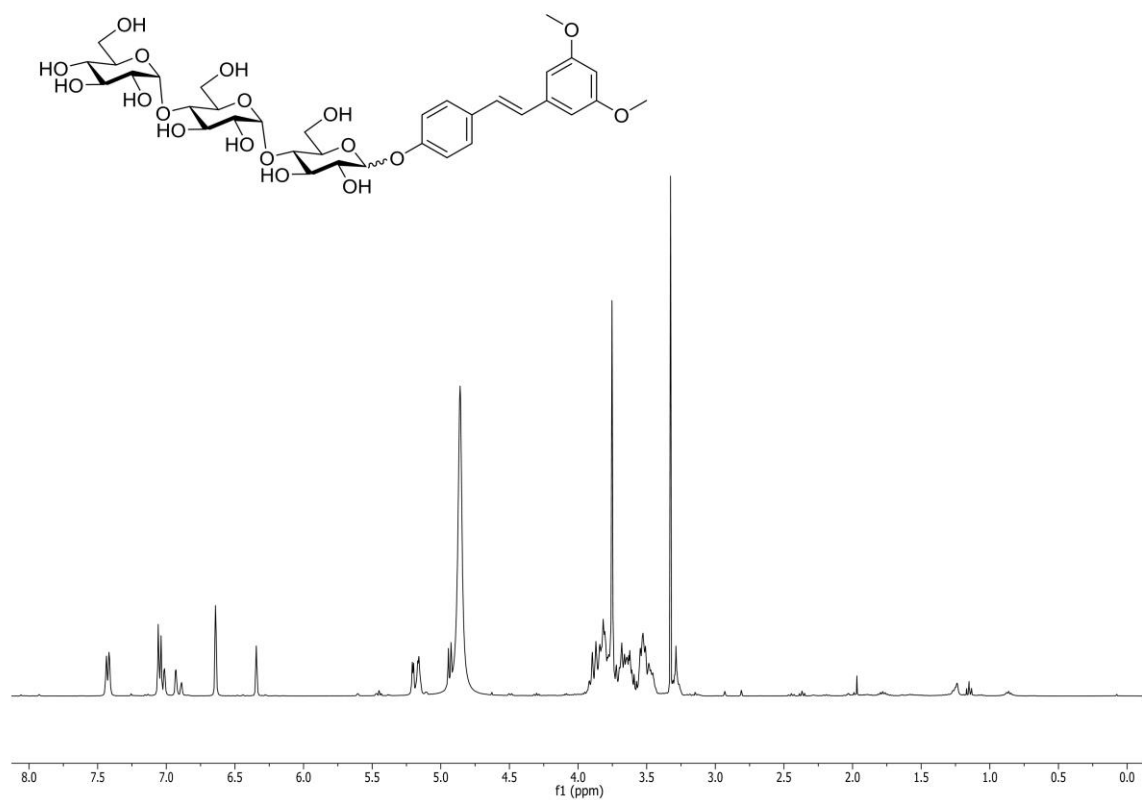
(E)-1-(3-methoxy-5-(β -D-glucopyranosyloxy-butyrato)phenyl)-2-(4'-methoxyphenyl)ethene, (38).



(E)-1-(3-methoxy-4'-(β-D-glucopyranosyloxy-butyrato)phenyl)-2-(5-methoxyphenyl)ethene, (39).



(E)-1-(3-methoxy-4'-(per-O-acetyl- β -D-maltopyranosyloxy)phenyl)-2-(5-methoxyphenyl)ethene, (40).



(E)-1-(3-methoxy-4'-(per-O-acetyl- β -D-maltopyranosyloxy-octanoate)phenyl)-2-(5-methoxyphenyl)ethene, (41).

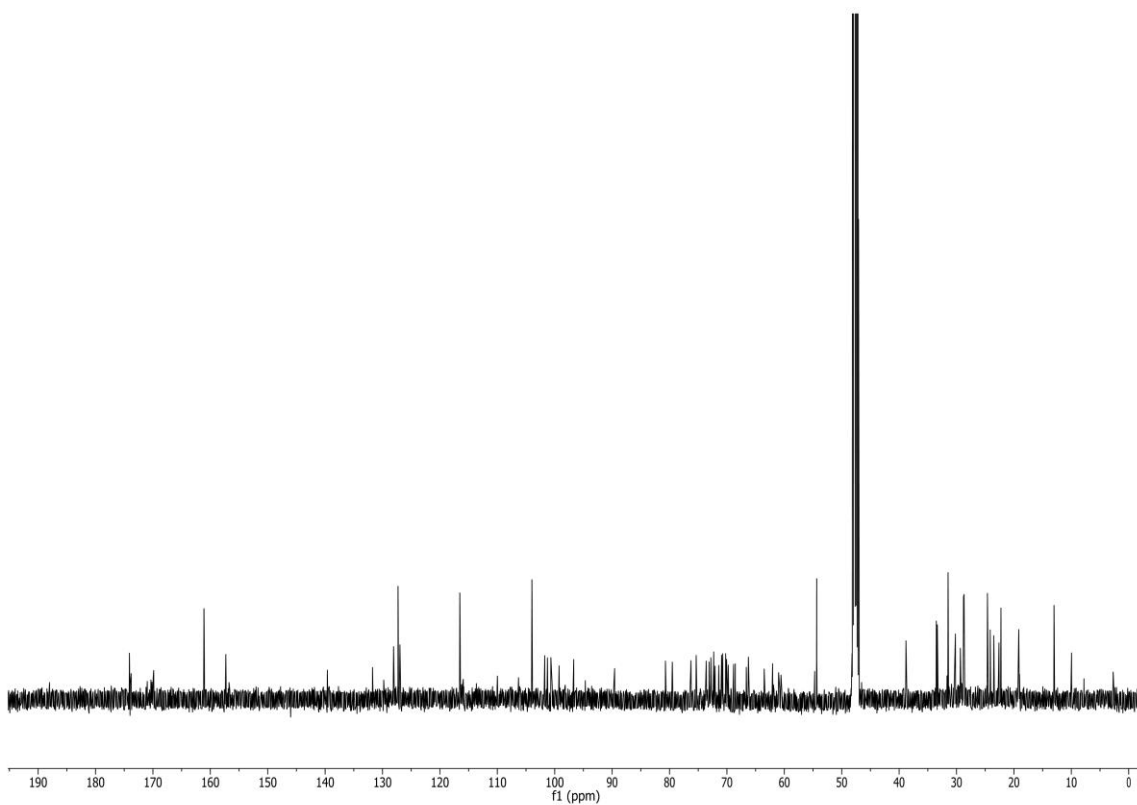
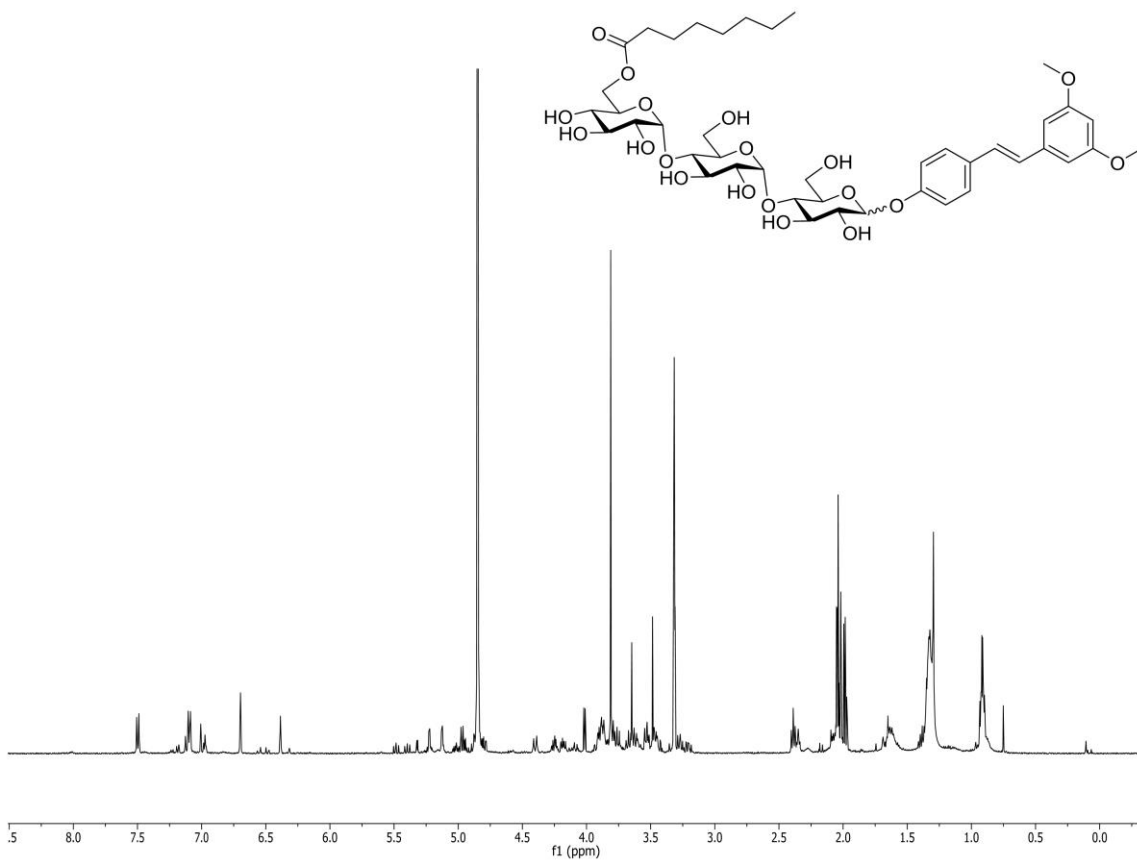


Figure S1. Toxicity of alkyl resveratrol derivatives (10 μ M) on SH-SY5Y neuroblastoma cells. Cell viability was evaluated in SH-SY5Y cells after 24h in combination with the compounds. Dashed line: reference value for viability found on control without compounds; Each bar represents mean \pm standard deviation.

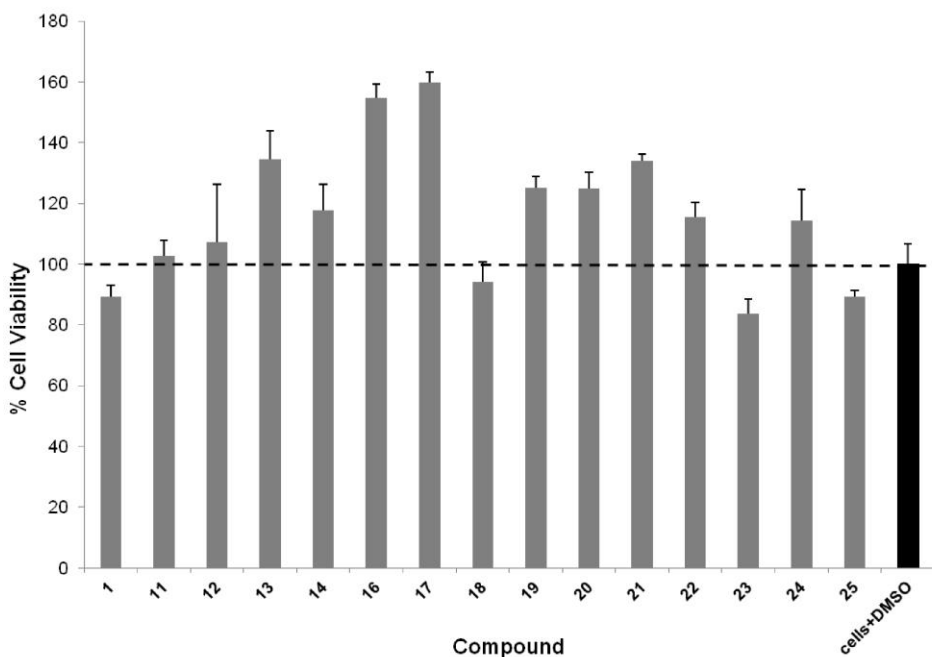


Figure S2. Toxicity of alkyl resveratrol derivatives (10 μ M) on RAW 264.7 macrophage cells. Cell viability was evaluated in RAW 264.7 macrophage cells after 24h in combination with the compounds. Dashed line: reference value for viability found on control without compounds; Each bar represents mean \pm standard deviation.

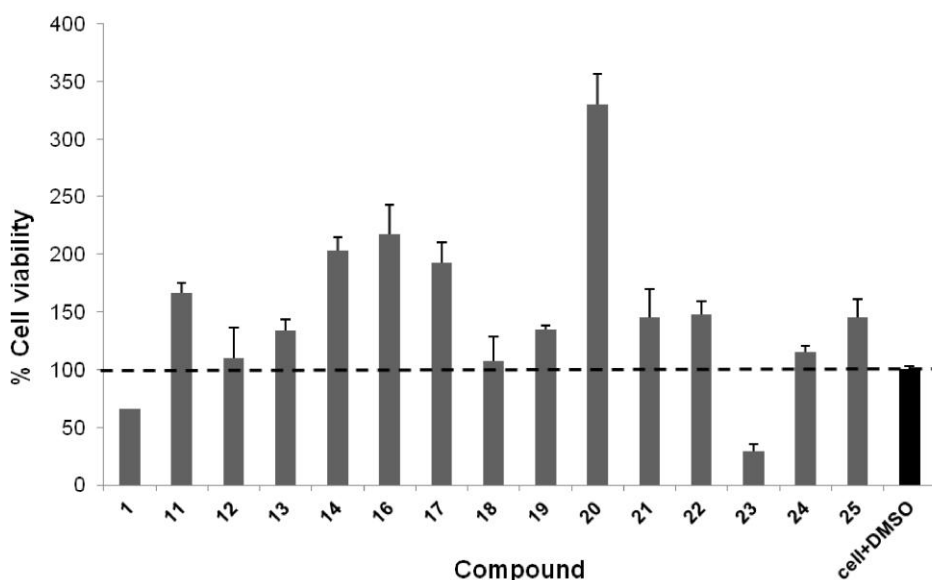
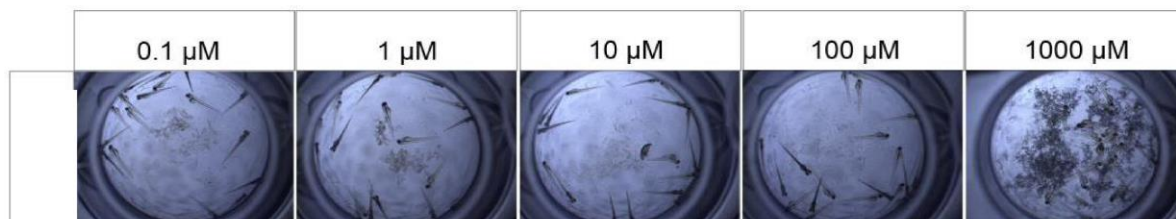


Figure S3. Acute toxicity test assay of representative resveratrol derivatives.

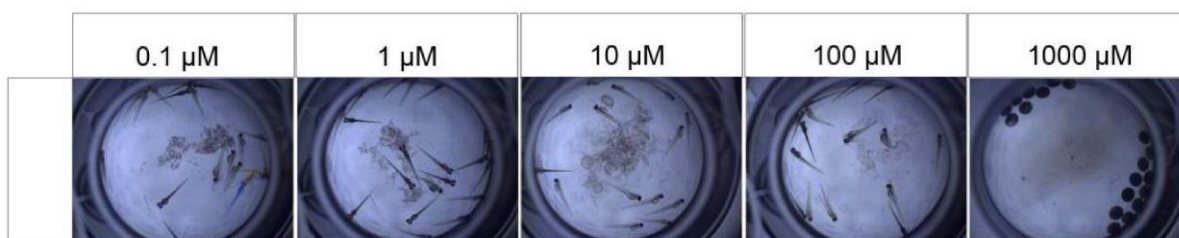
Resveratrol 1



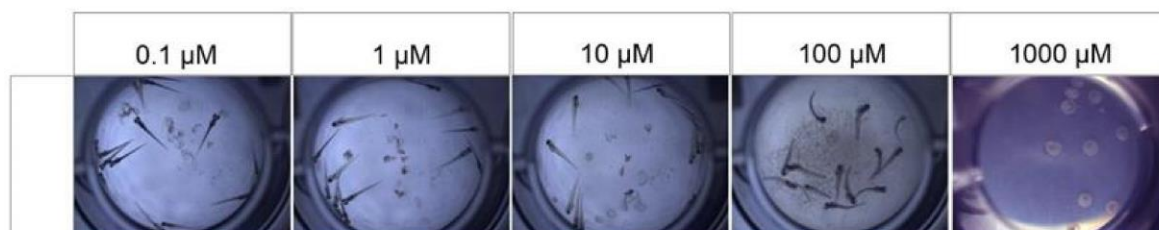
Compound 6



Compound 8



Compound 10



Compound 20

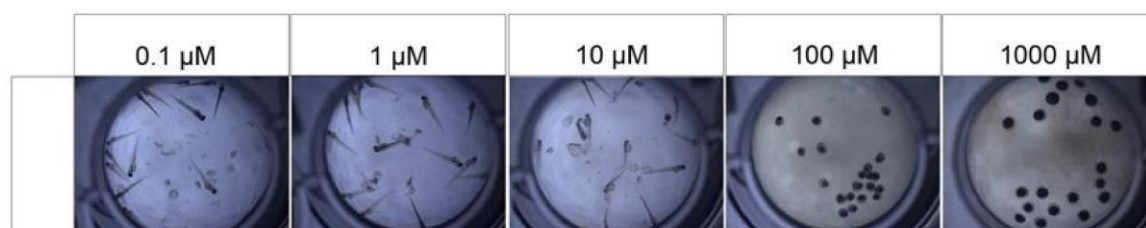


Figure S4. Design of HD 3-NP mice study

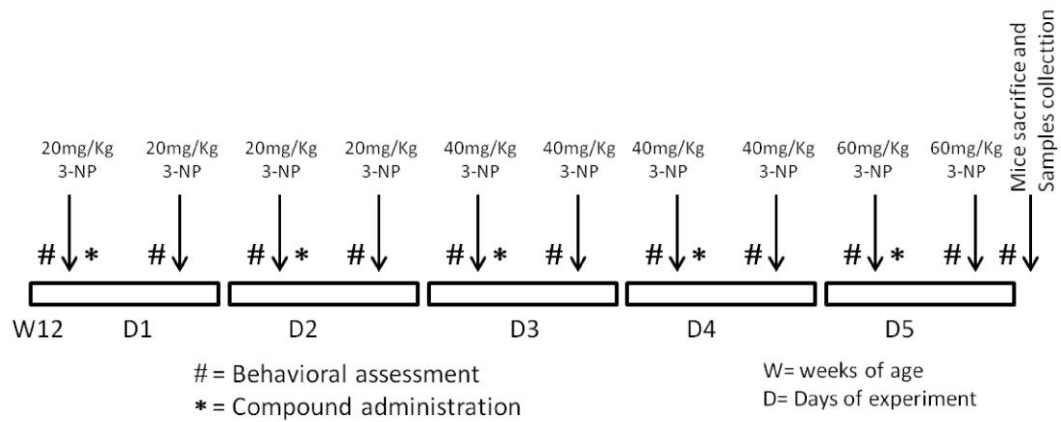


Table S1. Primers used in real-time PCR

Gene	Primer (5'-3')	Sequence	melt T
GAPDH	Forward	AACTTTGGCATTGTGGAAGG	
	Reverse	ACACATTGGGGGTAGGAACA	
iNOS	Forward	CTGCTGGTGGTGACAAGCACATT	58°C
	Reverse	ATGTCATGAGCAAAGGCGCAGAAC	
CAT	Forward	GGCATCAAAAACCTTGCCTGT	56°C
	Reverse	TGGGTCAAAAAGCCATCTGTT	
SOD2	Forward	ACACATTAACGCGCAGATCA	56°C
	Reverse	ATATGTCCCCCACCATTGAA	
P53	Forward	GAGTCACAGTCGGATATCAG	58°C
	Reverse	AGCAACAGATCGTCCATGCA	

